

Expanding the Scope of Available Iron-Based Catalysts for Suzuki-Miyaura Cross-Coupling Reactions Through Ligand Design and Mechanistic Investigation

Chet Chhawang Tyrol

A Dissertation

Submitted to the Faculty of

the Department of Chemistry

in Partial Fulfillment

of the Requirements for the Degree of

Doctor of Philosophy

Boston College

Morrissey College of Arts and Sciences Graduate School

June 2021

Expanding the Scope of Available Iron-Based Catalysts for Suzuki-Miyaura Cross-Coupling Reactions Through Ligand Design and Mechanistic Investigation

Chet Chhawang Tyrol

Advisor: Jeffery A. Byers

Abstract: This dissertation describes the design and logic that went into the development of Suzuki-Miyaura cross-coupling reactions catalyzed by iron-based complexes. Chapter 1 provides an overview into the field of iron cross-coupling and the comparison to state-of-the-art nickel-based systems. A combination of methodology development and mechanistic insight will be discussed. Chapter 2 describes the initial discovery and optimization of a Suzuki-Miyaura cross-coupling reaction between alkyl halides and unactivated arylboronic pinacol esters catalyzed by an iron cyanobis(oxazoline) complex. Chapter 3 discusses the extension of the catalytic system developed in Chapter 2 to an enantioselective reaction to afford chiral 1,1-diarylalkanes. The dissertation concludes with Chapter 4 which describes the development of a C(sp³)-C(sp³) Suzuki-Miyaura reaction catalyzed by a β -diketiminato iron complex. Ligand design and mechanistic studies are discussed here to provide insight into the mechanistic intricacies of the reaction and its effect on future reaction development.

Acknowledgements

Looking back over the past five years of graduate school, I can say with absolute confidence that I made the right decision to pursue a Ph.D. in chemistry. Before my time at Boston College, I first fell in love with chemistry in General Chemistry at Eckerd College. In this class, I met Professor Chris Schnabel who inspired me with his passion for chemistry and teaching. He provided endless help and guidance throughout my collegiate studies as a mentor and friend, and I will always be thankful for that. My time at Boston College has been an equally valuable experience. Working for Jeff has been such a wonderful experience and he has been an amazing mentor to me. His passion for chemistry is contagious and his equal concern for the wellbeing of his students makes him a top tier principal investigator. I have learned so many skills from him, both as a chemist and an individual. I would also like to acknowledge Dr. Liu and Dr. Hoveyda for taking the time to read my thesis and for being on my committee throughout my time at Boston College. I have learned a lot through our discussions and am very thankful for them pushing me to think more critically about my chemistry to become a better chemist.

The chemistry was by no means my only motivation to continue the degree. I have a fantastic network of family and friends who picked me up after a bad day in lab. My number one supporter is my mom. She has been a phone call or car ride away every time I needed help. She also fed me filet-mignon while I was up late into the night writing my thesis. For all these things and more I am grateful. Of course, to my father, sister and my new nephew, Hunter, who I cannot wait to play basketball with. Also, to my closest peers Michael, Alex, Miao, Matt and Nancy, you have been fantastic labmates who I will always

call friends. I would especially like to thank Michael for his incredible mentoring skills and friendship. I would also like to thank some of my other friends including Vincent, Paul, Sarah, Kendra, Bri, Grayson and Becca for always knowing how to make me laugh. And to Lisa who put up with my incredibly late hours in lab. I will always cherish my moments with you and wish you to be the best lawyer ever! Also, to some of the amazing professors I have had the pleasure of working with including Professor Wolfman and Professor Deak. I learned so much from them about teaching and they inspired me to become the best teacher I could.

As this chapter in my life closes, I am truly fortunate to have gotten this education and meet all the wonderful people along the way. I am very excited for the next steps in my life and am ready for my next journey.

Table of Contents:

Chapter 1. The Development and Mechanistic Underpinnings of Iron-Catalyzed Cross-Coupling Reactions with Comparison to State-of-the Art.....	1
1.1 Introduction.....	2
1.2 The Discovery and Early Development of Iron-Catalyzed Cross-Coupling	4
1.3 Kumada Cross-Coupling Reactions Mediated by Iron-Based Catalysts	5
1.3.1 C(sp ²)-Hybridized Grignard Nucleophile	5
1.3.1a C(sp ²)-Hybridized Electrophile	5
1.3.1b C(sp ³)-Hybridized Electrophile.....	8
1.3.2 C(sp ³)-Hybridized Grignard Nucleophile	20
1.3.2a C(sp ²)-Hybridized Electrophile	20
1.3.2b C(sp ³)-Hybridized Electrophile.....	28
1.4 Negishi Cross-Coupling Reactions Mediated by Iron-Based Catalysts	34
1.4.1 C(sp ²)-Hybridized Zinc-Based Nucleophile	35
1.4.1a C(sp ²)-Hybridized Electrophile	35
1.4.1b C(sp ³)-Hybridized Electrophile.....	36
1.4.2 C(sp ³)-Hybridized Zinc-Based Nucleophile	40
1.4.2a C(sp ³)-Hybridized Electrophile	40
1.5 Suzuki-Miyaura Cross-Coupling Reactions Mediated by Iron-Based Catalysts	42
1.5.1 C(sp ²)-Hybridized Boron-Based Nucleophile.....	42
1.5.1a C(sp ²)-Hybridized Electrophile	42
1.5.1b C(sp ³)-Hybridized Electrophile.....	44
1.5.2 C(sp ³)-Hybridized Boron-Based Nucleophile.....	48
1.5.2a C(sp ³)-Hybridized Electrophile	48
1.6 Conclusion	50
1.7 References.....	52
Chapter 2. Iron-Catalyzed Suzuki-Miyaura Crossed -Coupling Reactions Between Alkyl Halides and Unactivated Aryl Boronic Esters	74
2.1 Introduction.....	75
2.2 Overcoming Aggregation.....	78
2.3 Reaction Optimization	83
2.4 Substrate Scope Evaluation and Pharmaceutical Target.....	91
2.5 Mechanistic Experiments and Considerations	94
2.6 Conclusion:	100
2.7 Experimental:	101

2.8 References:.....	121
Chapter 3. Enantioconvergent Suzuki–Miyaura Cross-Coupling to Afford Enantioenriched 1,1-Diarylalkanes Using an Iron-Based Catalyst.....	130
3.1 Introduction.....	131
3.2 Approach Toward the Synthesis of Chiral 1,1-Diarylalkanes	132
3.3 Optimization of an Enantioselective Suzuki-Miyaura Reaction Using an Iron- Based Catalyst.....	136
3.4 Substrate Scope.....	141
3.5 Mechanistic Insights:	145
3.6 Conclusion:	151
3.7 Experimental:	152
3.8 References:.....	194
Chapter 4. Iron-Catalyzed Suzuki-Miyaura Cross-Coupling Reaction Between Unactivated Alkyl Halides and Alkyl Boranes	204
4.1 Introduction.....	205
4.2 Mechanistically Guided Ligand Design.....	209
Initial Discovery and Optimization of Reaction Parameters	211
4.3 Substrate Scope Evaluation.....	216
4.4 Elucidation of Mechanistic Features and the Catalytic Cycle	221
Conclusion	239
4.5 Experimental.....	241
4.6 References.....	276
Appendix A. Spectral Data.	287
Appendix A.1 Spectral Data for Chapter 2.....	287
Appendix A.2 Spectral Data for Chapter 3.....	291
Appendix A.3 Spectral Data for Chapter 4.....	306
Appendix B. X-Ray Crystallographic Data	326
Appendix B.1 X-Ray Crystallography Data from Chapter 1.....	326
Appendix B.1.1 Crystallographic Data for 2.8	326
Appendix B.2 X-Ray Crystallography Data from Chapter 4.....	340
Appendix B.2.1 Crystallographic Data for 4.11	340
Appendix B.2.2 Crystallographic Data for 4.5	352
Appendix B.2.3 Crystallographic Data for 4.49	363
Appendix B.2.4 Crystallographic Data for 4.55	374

ABBREVIATIONS:

ΔG	change in Gibbs free energy
ΔH	change in enthalpy
ΔS	change in entropy
ΔG^\ddagger	free energy activation energy
ΔH^\ddagger	enthalpic activation energy
ΔH^\ddagger	entropic activation energy
δ	chemical shift (NMR)
<i>J</i> -value	coupling constant
CV	cyclic voltammetry
$E_{1/2}$	half-wave potential or redox potential
brsm	based on recovered starting material
Å	angstrom
T	temperature
rt	room temperature
°C	degrees Celsius
solv	solvent
cat	catalyst
equiv.	equivalents(s)
conv.	conversion
h	hour
ee	enantiomeric excess

er	enantiomeric ratio
dr	diastereomeric ratio
thf	tetrahydrofuran
DME	dimethoxyethane
DMA	dimethylacetamide
1,2-DFB	1,2-difluorobenzene
Ph	phenyl
Ar	aryl
Bu	butyl
<i>t</i> Bu	<i>tert</i> -butyl
<i>i</i> Pr	<i>iso</i> -propyl
<i>i</i> Bu	<i>iso</i> -butyl
TBS	<i>tert</i> -butyldimethylsilyl
PMP	<i>para</i> -methoxyphenyl
dppe	bis(diphenylphosphinoethane)
NHC	<i>N</i> -heterocyclic carbenes
IMes	1,3-Bis(2,4,6-trimethylphenyl)-1,3-dihydro-2 <i>H</i> -imidazol-2-ylidene
SciOPP	spin-control-intended <i>ortho</i> -phenylene bisphosphine
BenzP*	1,2-bis(<i>tert</i> -butylmethylphosphino)benzene
QuinoxP*	2,3-bis(<i>tert</i> -butylmethylphosphino)quinoxaline
Bopa	bis(oxazolinyphenyl)amido
Box	bis(oxazoline)
CN-Box	cyanobis(oxazoline)

acac	acetylacetone
mes	mesityl
cod	cyclooctadiene
bipy	bipyridine
1,3,5-TMB	1,3,5-trimethoxybenzene
1,2,4-TMB	1,2,4-trimethoxybenzene
TMEDA	tetramethylethylene diamine
NMP	<i>N</i> -methylpyrrolidine
diglyme	bis(2-methoxyethyl) ether
pin	pinacol
9-BBN	9-borabicyclo(3.3.1)nonane
DG	directing group
r.d.s	rate-determining step
EN	electronegativity

Chapter 1. The Development and Mechanistic Underpinnings of Iron-Catalyzed Cross-Coupling Reactions with Comparison to State-of-the Art

1.1 Introduction

Over the past four decades, the development of metal-catalyzed cross-coupling methodologies have revolutionized the field of synthetic organic chemistry.¹ In particular, palladium-catalyzed cross-coupling reactions have become powerful and prominent tools for the reliable assembly of C(sp²)-C(sp²) bonds in natural products, pharmaceutically relevant compounds, and polymeric materials.² Despite the high efficiency and generality of these methods, the reliance on noble metals like palladium has raised concerns over the toxicity³ and the availability⁴ of the metal catalysts. Moreover, cross-coupling reactions between C(sp²)-C(sp²) centers make up a distinct majority of examples of catalytic systems based on noble metals,⁵ and the development of reactions involving C(sp³)-hybridized substrates remains an active area of research.⁶ The limited examples of C(sp³)-hybridized coupling partners is due in part to undesired side reactivity in the form of β -hydride elimination, which is not observed in palladium(II) aryl complexes that are common intermediates in C(sp²)-C(sp²) cross-coupling. In contrast, it is a commonly observed and facile pathway from the analogous palladium(II) alkyl complexes to yield palladium-alkene complexes.⁶ These aforementioned concerns with palladium-based catalysts are especially magnified in the pharmaceutical industry, where costs associated with removal of toxic metal salts and ligands affect implementation of these methodologies on a large scale.³ As a result of the overreliance in palladium cross-coupling reactions, flat molecules have become overrepresented among medicinally relevant compounds.⁷

Catalytic systems featuring the use of more abundant and less toxic first-row transition metals such as nickel,¹ iron and cobalt⁸ have shown remarkable promise for addressing these challenges.¹ In addition to economic and environmental advantages,

systems catalyzed by non-noble metals exhibit the ability to undergo one or two-electron redox events that enable access to different classes of substrates, including the aforementioned C(sp³)-hybridized substrates.^{6,9} Access to these single-electron processes allow these first-row transition metal catalysts to circumvent some of the difficulties experienced by palladium for these transformations. Over the past two decades, nickel-based systems have seen extraordinary levels of development for these type of cross-coupling reactions involving C(sp³)-hybridized substrates, proving to be highly valuable methodologies for formation of challenging carbon-carbon bonds.⁶ While nickel-catalyzed methods have demonstrated high synthetic value, nickel still poses some toxicity concerns similar to that of palladium.¹⁰ Due to this toxicity and often use of high catalyst loadings (5-20 mol%), nickel-based catalysts have largely been avoided in the pharmaceutical industry for use in large-scale syntheses of active pharmaceutical ingredients.³ Iron, also being a first-row transition metal, is an attractive alternative to nickel because of its non-toxic properties, high abundance in the earth's crust and efficient reactivity with both C(sp²) and C(sp³)-hybridized substrates (Figure 1.1).¹ For this reason, the development of iron-based catalysts for cross-coupling reactions continues to be an active area of research

Figure 1.1. Toxicities of some transition metals with figure regenerated from reference 2.

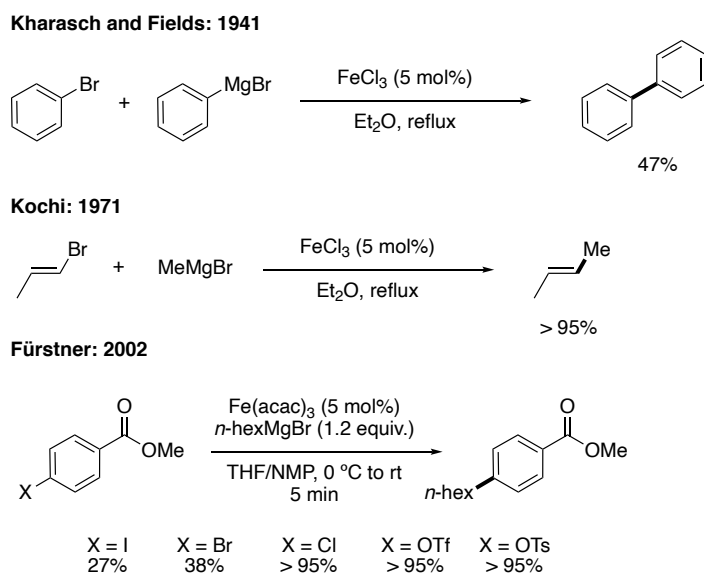
	Fe	Co	Ni	Cu
	Ru	Rh	Pd	Ag
Rating	Common Description		LD ₅₀ (single oral dose for rats) (mg/kg)	
3	Moderately Toxic		50-500	
4	Slightly Toxic		500-5000	
5	Practially non-toxic		5000-15000	
6	Relatively Harmless		>15000	

for many groups, and it is the subject of this chapter. Insight into recent methodology development will be discussed, comparisons will be made to state-of-the-art nickel-based systems to highlight the complementary reactivity offered by iron-based catalysts. Additionally, mechanistic proposals will be discussed for the most well studied systems.

1.2 The Discovery and Early Development of Iron-Catalyzed Cross-Coupling

While the field of palladium-catalyzed cross-coupling has advanced considerably over the past four decades,¹¹ it is interesting to note that iron-based systems predate those of palladium. In 1941, Kharasch and Fields reported the first iron-mediated cross-coupling reaction between aryl halides and aryl Grignard reagents using a simple iron salt (Scheme 1.1).¹² Further developments were made by Kochi in 1971, with the discovery of stereospecific couplings between alkenyl bromides and alkyl Grignard reagents catalyzed by iron halide salts.^{13,14} Despite this pioneering work, the field remained dormant for over 30 years, overshadowed by the success of palladium-based systems.¹⁵ It was not until the

Scheme 1.1. Early discoveries of iron-mediated cross-coupling.



early 2000s when iron-catalyzed cross-coupling enjoyed a renaissance, led by the work of Fürstner who demonstrated the utility of iron salts for cross-coupling and provided the first mechanistic studies aimed at studying these reactions.^{16–19} This work revitalized the field of cross-coupling reactions catalyzed by iron-based complexes, leading to major methodological and mechanistic developments that included Kumada, Negishi and Suzuki-Miyaura cross-coupling reactions.

1.3 Kumada Cross-Coupling Reactions Mediated by Iron-Based Catalysts

By far the most common types of cross-coupling reactions involving iron-based catalysts use organomagnesium reagents as the transmetalating agent. These reactions benefit from the high reactivity of the Grignard reagents, leading to rapid rates of transmetalation that display unusually good functional group tolerance.¹⁶ As a result of this high reactivity, reactions have been developed for the construction of many types of carbon-carbon bonds, including the use of C(sp²) and C(sp³)-hybridized organomagnesium nucleophiles^{1,20} and C(sp²) and C(sp³)-hybridized electrophiles.¹ In addition, there has been significant effort toward gaining a better mechanistic understanding of these iron-catalyzed Kumada cross-coupling reactions.²⁰ These reactions will be organized by hybridization of organomagnesium nucleophile followed by the corresponding electrophile.

1.3.1 C(sp²)-Hybridized Grignard Nucleophile

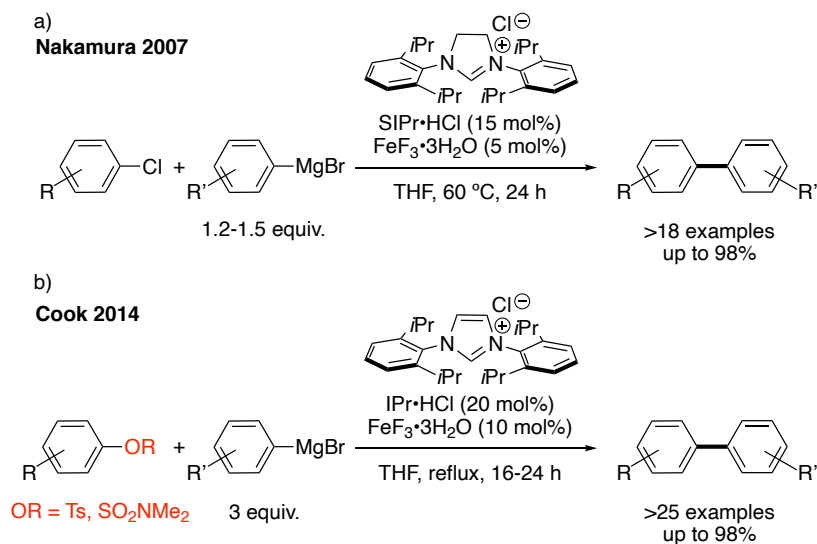
1.3.1a C(sp²)-Hybridized Electrophile

In comparison to palladium and nickel-based catalysts, iron-based catalysts are much less common for mediating C(sp²)-C(sp²) cross-coupling reactions. This dearth of examples using iron catalysis is a symptom of competitive homocoupling of the aryl

Grignard reagents, caused from over-transmetalation.^{17,21} To disfavor this homodimerization with iron-based catalysts, groups have tempered the reactivity of the organomagnesium reagents by using copper additives to form less reactive magnesium-derived organocopper reagents²² or by using more electron-deficient heteroaryl halides as electrophiles.¹⁶ However, in some cases it has been shown that small copper or palladium impurities have led to irreproducible results due to trace heavy metal catalysis.²³

Of the limited examples demonstrating this type of reactivity, one commonality is the use of *N*-heterocyclic carbene (NHC) ligands and monodentate, anionic ligands to help suppress homodimerization pathways. An example of this comes from the Nakamura group whose studies demonstrated the highly selective cross-coupling of aryl chlorides with aryl Grignard reagents catalyzed by iron(III) fluoride in the presence of an imidazolium salt (Scheme 1.2a).^{21,24} The role of the fluoride anion was found to be paramount to the success of the reaction and was hypothesized to suppress formation of a ferrate complex which could undergo unselective biaryl production.²¹ In a similar system to Nakamura's, the

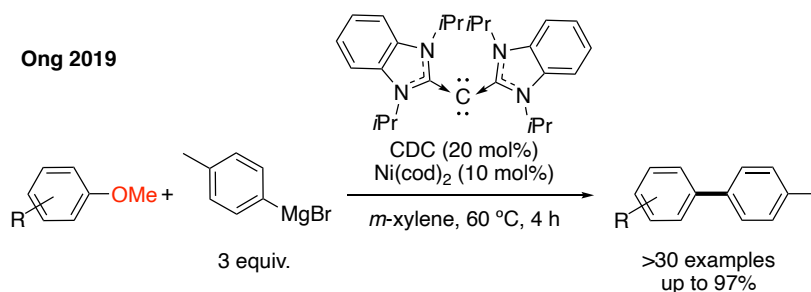
Scheme 1.2. Iron-mediated C(sp²)-C(sp²) cross-coupling reactions of a) aryl chlorides and b) C-O electrophiles.



Duong group were able to utilize bulky alkoxide additives to serve the same role as fluoride by suppressing ferrate formation.²⁵ Perhaps the most impressive reactivity comes from Cook and co-workers who demonstrated the cross-coupling of aryl sulfamate and aryl tosylate electrophiles with aryl Grignard reagents catalyzed by iron(III) fluoride and an imidazolium NHC precursor (Scheme 1.2b). This reaction is noteworthy because the use of C-O electrophiles avoids inherent issues associated with halide-containing electrophiles such as preparation, handling and disposal, which raises environmental concerns for the pharmaceutical industry.²⁶

In comparison, nickel-based systems have been known since the early reports by the groups of Kumada²⁷ and Corriu,²⁸ demonstrating the coupling of aryl halides with aryl Grignards. Since their original discovery, much recent work has focused on the use of C-O electrophiles. Ong and coworkers recently disclosed a system utilizing a carbodicarbene (CDC) nickel catalyst for the coupling of aryl ethers with *p*-tolylmagnesium bromide (Scheme 1.3).²⁹ This method showcases the unique reactivity of nickel-based catalysts through the activation of highly inert C-OMe ether bonds. This work is particularly noteworthy since it demonstrates access to a new electrophile class besides commonly used aryl halides.

Scheme 1.3. Nickel-mediated C(sp²)-C(sp²) cross-coupling reaction using aryl ethers as electrophiles

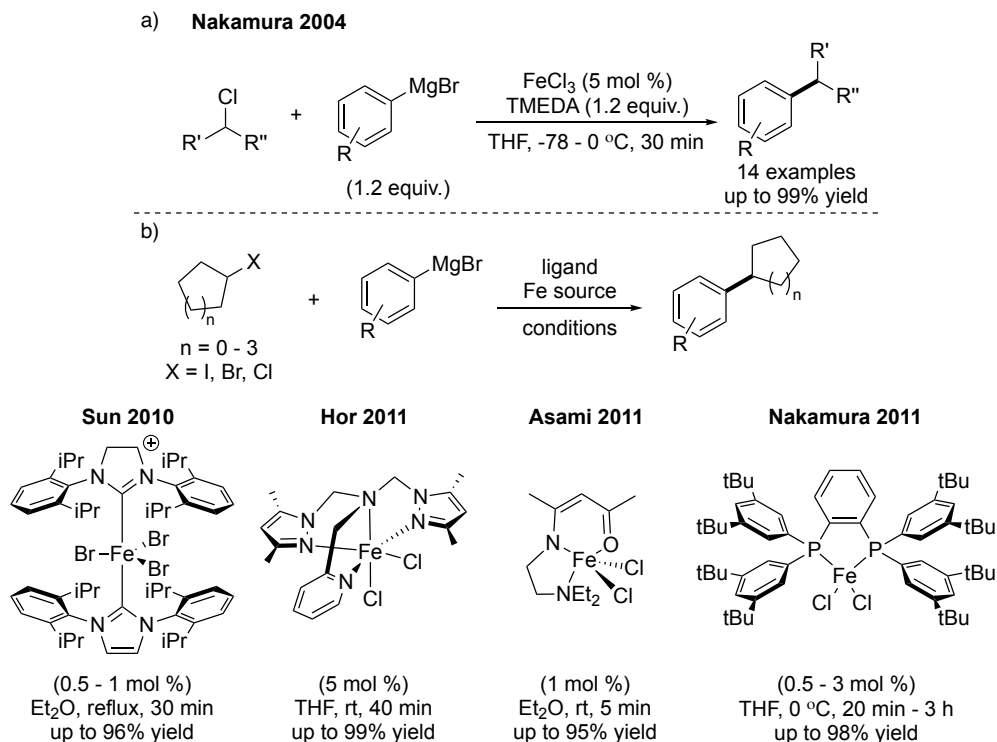


While the environmental benefits currently outweigh the synthetic benefits offered by iron-based systems for C(sp²)-C(sp²) cross-coupling reactions when compared to those of nickel, steps have been made in the right direction toward overcoming undesired homocoupling and promoting cross-coupling. Deeper understanding of the precise mechanism of action using fluoride additives will hopefully be used to help drive new and improved methodologies in this area of iron-catalyzed cross-coupling.

1.3.1b C(sp³)-Hybridized Electrophile

Within the past two decades, C(sp³)-C(sp²) Kumada-Tamao-Corriu cross-coupling reactions mediated by iron-based catalysts have seen substantial growth. In 2004, the Nakamura group demonstrated the first example of an iron-catalyzed Kumada cross-coupling reaction between acyclic and cyclic secondary alkyl halides and aryl Grignard reagents. The cross-coupling reactions developed by the Nakamura group could be catalyzed by iron salts in the presence of tetramethylethylenediamine (TMEDA) to suppress alkene formation (Scheme 1.4a).^{30,31} Since this time, many groups have turned their efforts to ligand design to develop more active iron catalysts and improve the generality and applicability of Kumada couplings catalyzed by iron-based systems. Among the ligand classes explored include NHC-ligands,³² amine-pyrazolyl tripodal ligands with labile pendant heteroaromatic rings,³³ tridentate β-aminoketonato ligands,³⁴ and ortho-phenylene-bisphosphine ligands (Scheme 1.4b).³⁵ A notable example from this list is the latter example by the Nakamura group who demonstrated that the bulky bisphosphine ligand SciOPP, or spin-control-intended *o*-phenylene bisphosphine) led to efficient coupling between cyclic and acyclic primary and secondary alkyl chlorides with aryl Grignard reagents.³⁵ Impressively, challenging coupling partners such as sterically

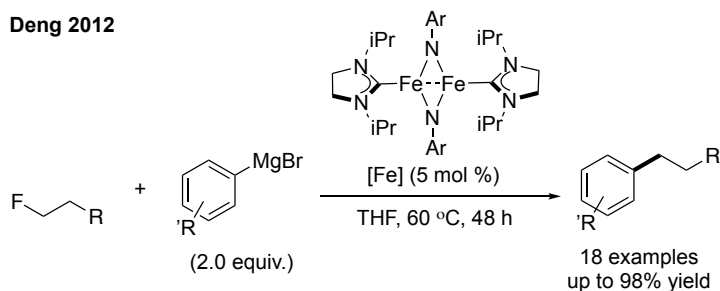
Scheme 1.4. a) First example of an iron-mediated C(sp³)-C(sp²) cross-coupling reaction. b) Ligand development leading to new reactivity.



hindered mesityl Grignard reagents and adamantyl chloride underwent efficient cross-coupling. However, the coupling of other tertiary alkyl halides was not demonstrated. Additionally, Fürstner and coworkers have also been able to demonstrate similar reactivity with the coupling of sterically encumbered aryl Grignard reagents with primary alkyl halides and tosylates using the bisphosphine ligand bis(diethylphosphino)ethane (depe).³⁶

Another exemplary case of ligand design driving reactivity comes from Deng and coworkers who demonstrated that alkyl fluorides, which are notoriously unreactive substrates for cross-coupling, could be activated using a dinuclear NHC iron complex (Scheme 1.5).³⁷ Despite being limited to primary alkyl fluorides, this report is highly promising for future reaction development.

Scheme 1.5. Iron-mediated C(sp³)-C(sp²) cross-coupling of alkyl fluorides.

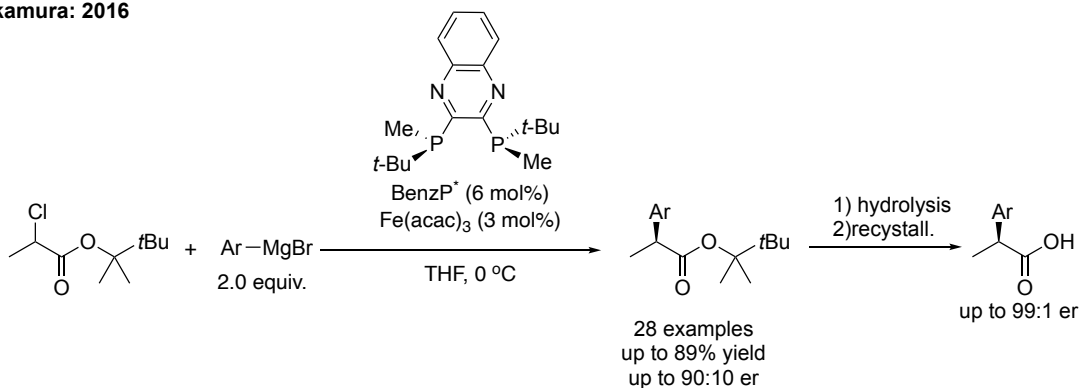


Enantioselective iron cross-coupling reactions remain very rare within the literature, particularly when compared with the abundance of systems seen with nickel-based systems.³⁸ The first reported example came from the Nakamura group who was able to develop an enantioselective Kumada cross-coupling reaction between α -haloesters and aryl Grignard reagents catalyzed by a chiral bisphosphine iron catalyst (Scheme 1.6).³⁹ In this system, the group was able to obtain high yields of cross-coupled product with up to 91:9 enantiomeric ratios (er), which could be further improved upon recrystallization to 99:1 er.

The pursuit for greater mechanistic insight into iron cross-coupling reactions has historically been a formidable challenge due to the challenges associated with characterizing paramagnetic iron species, air sensitivity of iron intermediates as well as

Scheme 1.6. Enantioselective iron-catalyzed C(sp²)-C(sp³) Kumada cross-coupling reaction between aryl Grignard reagents and α -haloesters.

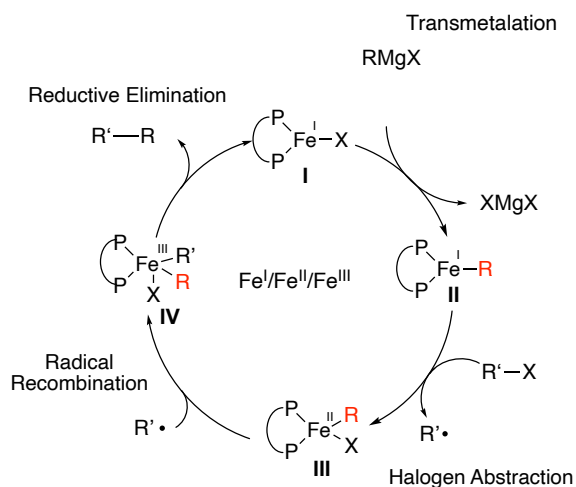
Nakamura: 2016



access to one and two-electron processes.⁴⁰ In addition, there remains an added layer of complexity since no one mechanism exists to unify all reactions in iron cross-coupling, being highly sensitive to reaction conditions and coupling partners. Despite these challenges, two prevailing mechanisms have surfaced for these iron-catalyzed C(sp³)-C(sp²) Kumada cross-couplings that rely on one-electron processes. The first mechanism involves an iron(I)/(II)/(III) cycle which is initiated by reduction of an iron(II) precatalyst by Grignard reagent to a catalytically active iron(I) halide species (**I**) (Scheme 1.7).⁴¹ Intermediate **I** can engage in transmetalation with the aryl Grignard reagent to yield **II**. Iron(II) aryl **II** can then engage in halogen abstraction, forming a carbon-centered radical and an iron(II) aryl-halide to form **III**. Species **III** can then undergo radical recombination to form an iron(III) species **IV**, followed by reductive elimination to furnish cross-coupled product and regenerate **I**.

This mechanism was first proposed by the Norrby⁴² and Bedford⁴³ groups. Norrby and coworkers carried out Hammett studies on Kumada cross-couplings between aryl Grignard reagents and benzylic bromides, which were consistent with a radical-based

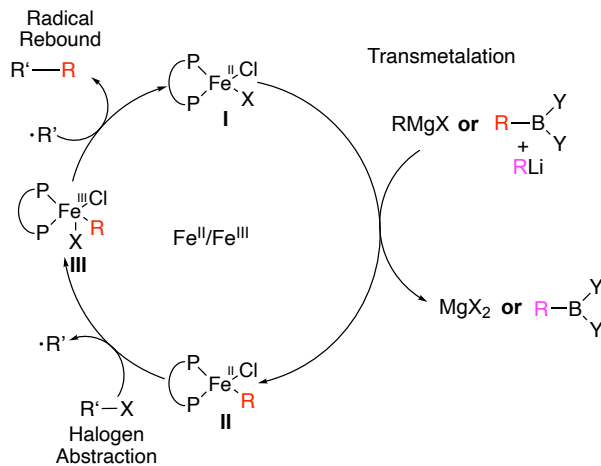
Scheme 1.7. Proposed Fe(I)/(II)/(III) cycle for iron cross-coupling reactions using bisphosphine ligands.



The carbon-centered radical can then escape the solvent cage and recombine with a different iron(II)monophenyl species **III**, formed from transmetalation with the aryl Grignard reagent. The newly formed iron(III) intermediate **IV** can then reductively eliminate to generate cross-coupled product and regenerate the iron(I) halide species **I**. In both cases, the enantiodetermining step was determined to be radical recombination to **IV**. As for the origin of enantioselectivity, the Nakamura group used energy decomposition analysis to determine that selectivity was induced from steric interactions between the ligand *tert*-butyl group and aryl ligand,⁴⁶ while the Gutierrez group determined a model for stereoinduction identifying key π -donor/acceptor and C-H \cdots π noncovalent interactions as enantiocontrol elements.⁴⁷ Despite the similar conclusions made by these two groups, there was no experimental evidence to support these claims.

The second proposed mechanism involves an Fe(II)/(III) cycle where iron(II) bis halide species **I** first undergoes transmetalation with the aryl Grignard reagent to form iron(II) aryl halide species **II** (Scheme 1.9). Iron intermediate **II** can then engage in halogen abstraction with the alkyl halide to form a carbon-centered radical and iron(III) species **III**.

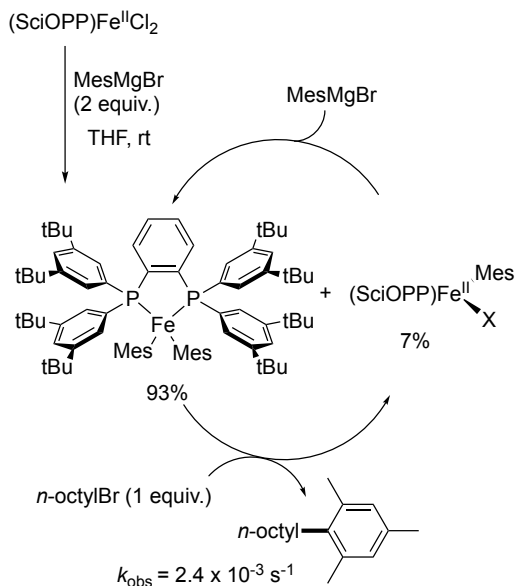
Scheme 1.9. Proposed Fe(II)/(III) cycle for iron cross-coupling reactions using bisphosphine ligands.



Intermediate **III** can then engage in a radical rebound process to deliver the cross-coupled product and regenerate **I**.

To probe this mechanism, the Neidig group carried out a rigorous spectroscopic study using a combination of *in situ* Mössbauer, EPR, MCD spectroscopies and DFT studies to investigate Nakamura's Kumada cross-coupling system between mesityl magnesium bromide and primary alkyl halides (Scheme 1.10).^{35,48} The findings of these studies identified (SciOPP)Fe(Mes)₂ as the active catalyst which provide an interesting contrast to TMEDA-ligated iron complexes that form Fe(Mes)₃⁻ in the presence of an excess mesityl magnesium Grignard.⁴³ The excess SciOPP ligand and slow addition of the Grignard reagent in the catalytic reaction were shown to suppress formation of the Fe(Mes)₃⁻, leading to a more active and selective catalyst. Additionally, crystallographic and computational analysis of (SciOPP)Fe(Mes)₂ and (SciOPP)FeBrMes revealed distorted

Scheme 1.10. Discovery of (SciOPP)FeMes₂ as the active species in Nakamura's Kumada cross-coupling reaction between MesMgBr and *n*-octylbromide.

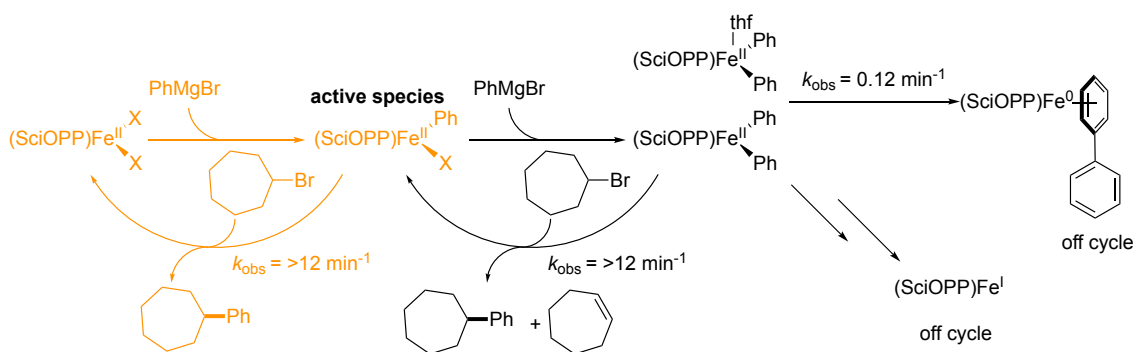


square planar and tetrahedral geometries respectively.⁴⁸ From the corresponding molecular

orbital diagrams, they found that only the former iron species had an unoccupied and low-lying frontier molecular orbital needed for substrate activation.

In a follow-up study, the Neidig group investigated the differences in iron speciation when using phenyl instead of bulkier mesityl Grignard reagents in a Kumada cross-coupling reaction developed by Nakamura's group (Scheme 1.11).⁴⁹ When analyzing reactions between (SciOPP)FeBr₂ and phenyl magnesium bromide by freeze-trapped *in situ* Mössbauer and EPR, they observed an *S* = ½ iron(I) species previously seen by Bedford. However, upon spin-counting it was found this Fe(I) accounted for 5% of iron in solution. Furthermore, when subjected to electrophile, the Fe(I) species is too slow to be catalytically relevant, suggesting it to be an off-cycle iron species. In the same study, the Neideg group was able to show monometalated species (SciOPP)FeBrPh to be the highly active and selective species during catalysis. While (SciOPP)FePh₂ was catalytically competent and displayed similar kinetic relevance to (SciOPP)FeBrPh, the former species was far less selective, forming phenylcycloheptane and cycloheptene in equal amounts. These results

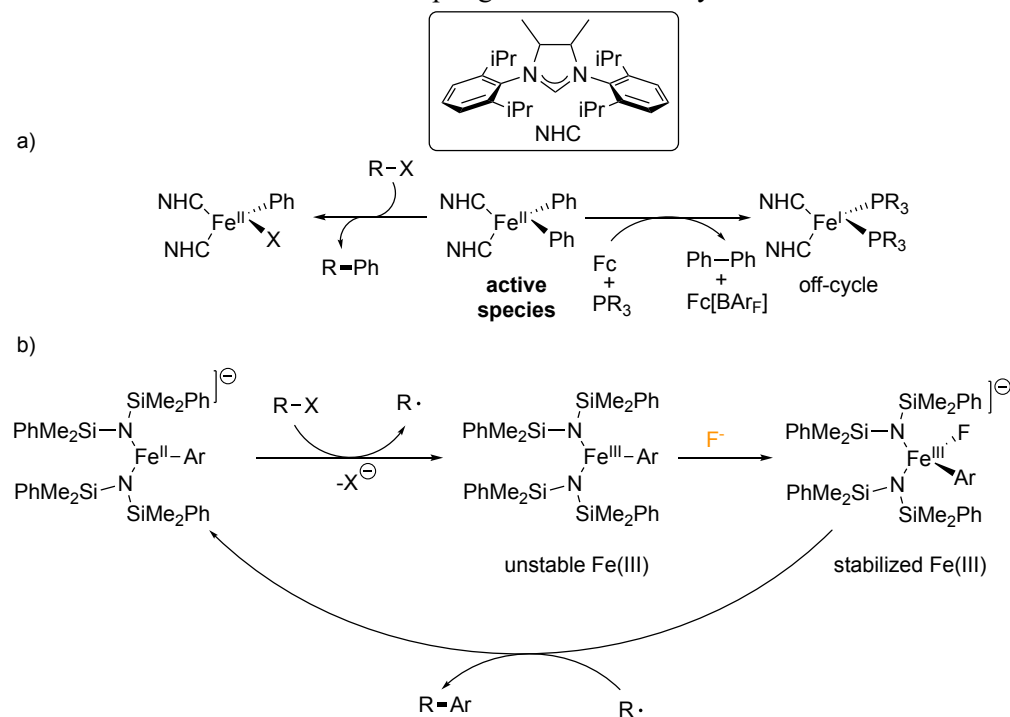
Scheme 1.11. Discovery of (SciOPP)FePhX as the active species in Nakamura's Kumada cross-coupling reaction between PhMgBr and cycloheptylbromide.



are supportive of the Fe(II)/(III) mechanistic cycles that have been proposed for iron-SciOPP catalyzed Kumada cross-coupling reactions.³⁵

In addition to mechanistic studies using bisphosphine-ligated iron complexes, other ligand systems that has been actively studied are *N*-heterocyclic carbenes (NHCs) and amido-based ligands. In a 2015 report by the Deng group, a four-coordinate (NHC)₂FePh₂ complex was shown to be stoichiometrically and catalytically competent for reactions with non-activated alkyl halides (Scheme 1.12a).⁵⁰ From these catalytic reactions using the iron(II) diphenyl complex, moderate yields of cross-coupled product was obtained in the presence of alkyl halide to furnish (NHC)₂FePhX, with significant production of alkene and alkane products. To test for a lower oxidation state mechanism, they were able to synthesize an iron(I) species from (NHC)₂FePh₂ using ferrocene as a reductant followed

Scheme 1.12. a) (NHC)₂FePh₂ and its catalytic activity for Kumada cross-couplings with alkyl halides. b) Importance of fluoride source in stabilizing an Fe(III)Ar intermediate in a Kumada cross-coupling reaction with alkyl halides.



by trapping with stabilizing phosphine ligands, however the complex demonstrated poor

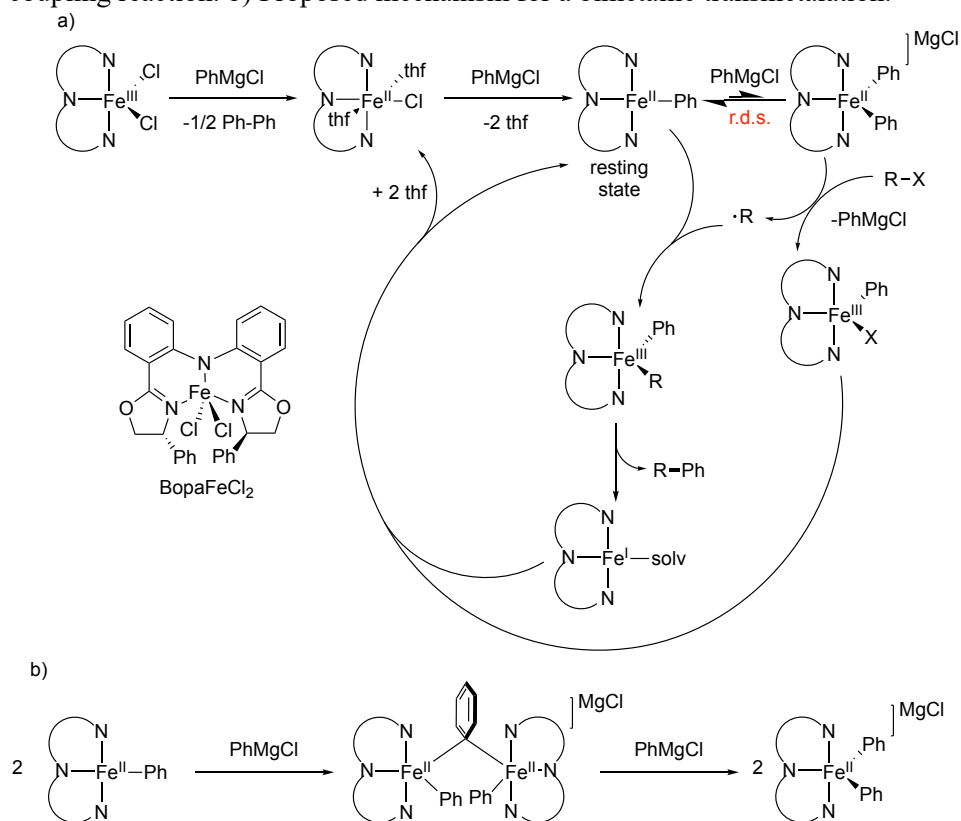
catalytic activity. From these results, they concluded the mechanism was more consistent with an iron(II)/(III) cycle and an $(\text{NHC})_2\text{FePh}_2$ active species.

Very recently, the Lefevre group was able to isolate a singly transmetalated $\text{Fe}(\text{NSiR}_2)_2\text{Ar}$ ferrate species using a bulky silylamide ligand framework (Scheme 1.12b).⁵¹ This work highlights a key theme in most iron-catalyzed Kumada cross-coupling reactions⁸; i.e., the degree of transmetalation, or number of transferred carbon fragments from the nucleophile, is critically important. The key findings of this work were the use of tetrabutylammonium difluorophenylsilicate as a fluoride source which acted to stabilize high-valent iron(III) species in order to suppress biaryl formation. This fluoride effect was first seen when carrying out reactions with electron-neutral Grignard reagents and validated by electrochemical investigation. In these cyclic voltammetry studies, they found changes in the reversibility of the oxidation peak and position of the reduction peak, indicative of a new fluoride-ligated iron(III) species. Upon introducing fluoride, the reduction potential lowered significantly from -0.52 V to -1.15 V vs Fc/Fc^+ , leading to a more stable Fe(III) species less prone to a second transmetalation event. From these studies, the authors conclude an Fe(II)/Fe(III) cycle proceeding through a radical rebound process seems most likely, although an Fe(I)/(II)/(III) cycle was not ruled out.

In addition to these commonly proposed monometallic mechanisms, Hu and coworkers suggested a bimetallic mechanism is operative in a Kumada cross-coupling reaction between aryl Grignard reagents and alkyl halides catalyzed by a bis(oxazolinyphenyl)amido (Bopa) pincer ligated iron complex (Scheme 1.13a).⁵² Performing kinetic studies, they found the reaction to be second order in catalyst, first order in Grignard and zero order in alkyl iodide, which suggested a bimetallic transmetalation to

be the rate-determining step (Scheme 1.13b). In addition, radical clock studies and stereochemical probes suggested the intermediacy of a carbon-centered radical. To rule out a radical rebound mechanism, they discovered a linear correlation between catalyst loading and ratio of uncyclized to cyclized product using an alkenyl radical clock. These results are more consistent with the carbon-centered radical escaping the solvent cage and either recombining with the original or new iron species since a radical rebound would be insensitive to catalyst loading.⁵² Furthermore, the Hu group was able to show that the

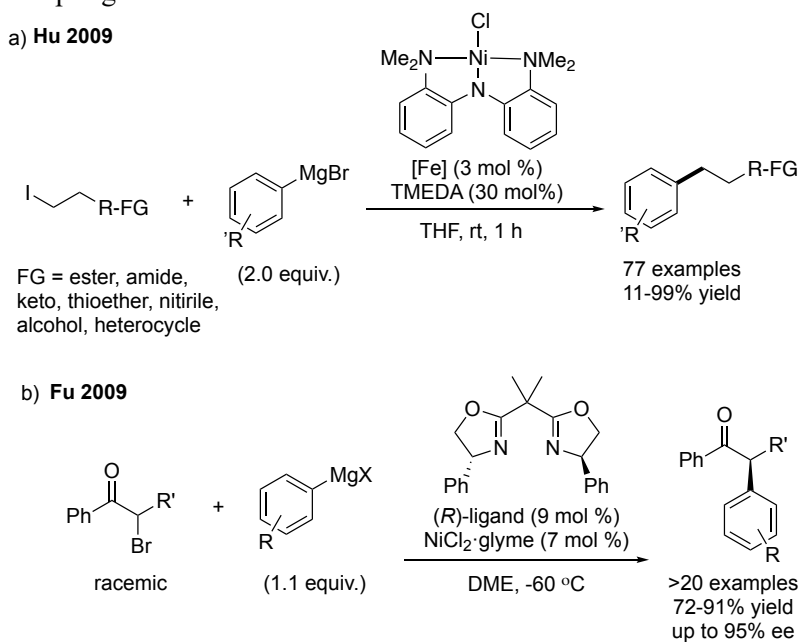
Scheme 1.13. a) Bimetallic mechanism for a BopaFeCl₂ catalyzed Kumada cross-coupling reaction. b) Proposed mechanism for a bimetallic transmetalation.



(Bopa)FePhX species is not kinetically relevant while the (Bopa)Fe(Ph)₂⁻ ferrate species is both catalytically competent and kinetically relevant.

Compared to iron, nickel-based systems have developed at a much slower rate for C(sp³)-C(sp²), with most systems being limited to primary alkyl halides and very few examples employing secondary alkyl halides. One notable example was developed in 2009 by Hu and coworkers who developed the first general Kumada cross-coupling between nonactivated alkyl halides and aryl and heteroaryl Grignard reagents catalyzed by a nickel pincer complex (Scheme 1.14a).⁵³ This system demonstrated exceptional functional group tolerance (esters, amides, nitriles, alcohols, etc.) but examples were limited to primary alkyl iodides or bromocyclohexane with little to no product formation using other secondary alkyl halides. The same year, the Fu group demonstrated the first enantioselective Kumada cross-coupling reaction.⁵⁴ This reaction was catalyzed by a nickel bis(oxazoline) complex to couple α -bromo esters with aryl Grignard reagents and showcased moderate to excellent

Scheme 1.14. a) Nickel-mediated C(sp³)-C(sp²) cross-coupling of alkyl iodides showcasing a wide functional group tolerance. b) First example of an enantioselective C(sp³)-C(sp²) Kumada cross-coupling.



selectivities as well as good functional group tolerance (esters, nitriles, acetals, thiophenes, *N*-Boc indoles, etc) (Scheme 1.14b).

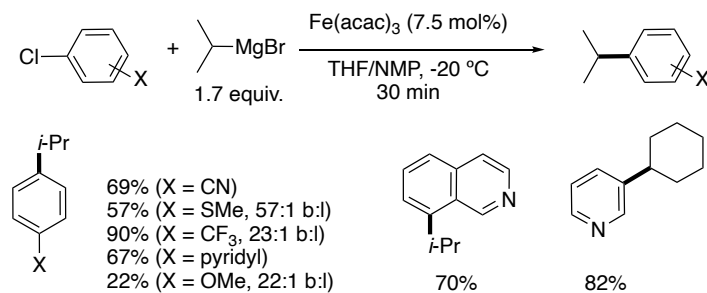
From comparison of these systems, iron-based systems currently demonstrate multiple advantages over nickel for C(sp³)-C(sp²) Kumada cross-couplings. These advantages include access to 2° and 3° alkyl halides, 1° alkyl fluorides as well as the development of enantioselective reactions. In addition, there has been significant effort into understanding mechanistic features of these reactions which has historically been a formidable challenge due to the difficulties associated with characterizing paramagnetic iron speciation, air sensitivity of iron intermediates as well as access to one and two-electron processes.⁴⁰ Nickel-based systems certainly show exceptional functional-group tolerance and demonstrate the ability to develop stereoselective variants, but reports remain uncommon with much room for improvement.

1.3.2 C(sp³)-Hybridized Grignard Nucleophile

1.3.2a C(sp²)-Hybridized Electrophile

Examples of iron-catalyzed C(sp²)-C(sp³) Kumada-Tamao-Corriu cross-coupling reactions between aryl halides and alkyl Grignard reagents has been known since Kochi's work in 1971 (Scheme 1.15a)^{13,14} as well as the discovery of an effective NMP cosolvent.⁵⁵ Insight into the role of NMP was elegantly determined by the Neidig group, through a combination of spectroscopic tools, to stabilize catalytically active iron ferrates through magnesium coordination.⁵⁶ In 2002, Fürstner and coworkers demonstrated the utility and unusual activity of iron salts for these type of cross-couplings (Scheme 1.6).¹⁶⁻¹⁹ The unique properties of these iron-based catalysts complemented that of palladium and nickel-based catalysts with preference for aryl chlorides and tosylates over bromides and iodides

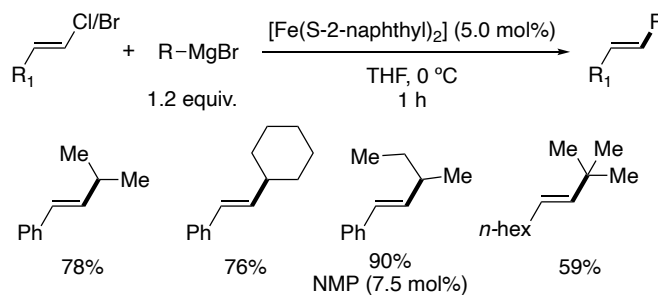
Scheme 1.16. The coupling of aryl and heteroaryl chlorides with *i*-PrMgCl using Fe(acac)₃.



tolerance and proceeded smoothly with electron-deficient arenes but was sluggish with electron-rich arene electrophiles. Percy's cross-coupling system most notably displayed little to no branched product, showing for the first time a system that precluded chain-walking events. However, no comments were made on how the system precluded generating branched products. Additionally, the reaction manifold was general for coupling some secondary Grignard reagents such as isopropyl magnesium bromide and cyclohexyl magnesium bromide with heteroaryl chlorides.

The use of secondary Grignard reagents is common for Kumada cross-couplings using iron-based catalysts, yet there is a dearth of examples utilizing tertiary alkyl Grignards.^{14,55} One notable example by the Cahiez group demonstrates iron thiolate complexes to be efficient catalysts for the stereoretentive coupling of alkenyl chlorides and

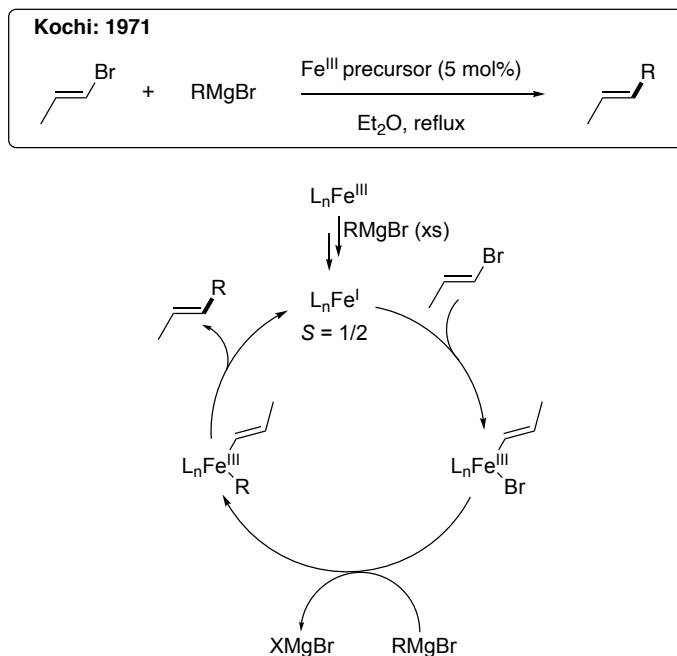
Scheme 1.17. The coupling of alkenyl chloride and bromides with secondary and tertiary alkyl Grignard reagents catalyzed by a bis-iron-thiolate complex.



bromides with primary, secondary and tertiary alkyl Grignard reagents (Scheme 1.17). The substrate scope was shown to be broad with respect to unfunctionalized primary and secondary alkyl Grignard nucleophiles while *t*BuMgCl yielded reduced yields of cross-coupled product yet demonstrated no isomerized product. This rare example demonstrates the utility and need for ligand design, since most reactions of this type are simple iron salts.

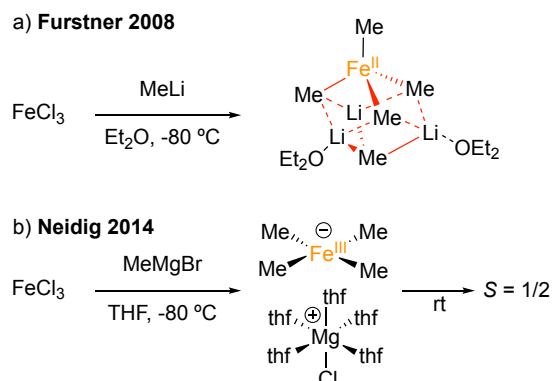
As shown in the examples above, simple ferric iron salts have proven to be effective precatalysts for a wide number of cross-couplings between alkyl Grignard reagents and aryl or alkenyl halides.¹ In 1971, the Kochi group pursued to identify the active iron species in the newly discovered stereospecific coupling of methyl magnesium bromide and alkenyl bromides.^{67,68} In these reports, they observed a broad $S = \frac{1}{2}$ signal by EPR and production of ethane when subjecting ferric salts to alkylmagnesium halide nucleophiles, suggestive of an iron(I) active species. From these studies, Kochi proposed a mechanism where the Grignard reagent first served as the reducing agent to reduce the iron(III) precatalyst to an active iron(I) species (Scheme 1.18). The reactive iron(I) intermediate then undergoes two-electron oxidative addition with the alkenyl bromide followed by transmetalation with the alkyl Grignard reagent and reductive elimination to furnish the cross-coupled product. While these findings were only suggestive of an iron(I) active species, Fürstner and coworkers were the first to provide structural evidence of a possible active iron species characterized as a homoleptic tetramethyliron(II) ferrate species formed upon reduction of an iron(III) precursor to an iron(II) species with methyl lithium (Scheme 1.19a).¹⁸ However, the work by Fürstner was not done under catalytically relevant conditions nor accounted for the iron(I) species seen by Kochi. Furthermore, reactivity of this iron cluster was not demonstrated with alkenyl halides but only with activated aryl electrophiles.

Scheme 1.18. Early mechanistic investigations by Kochi.



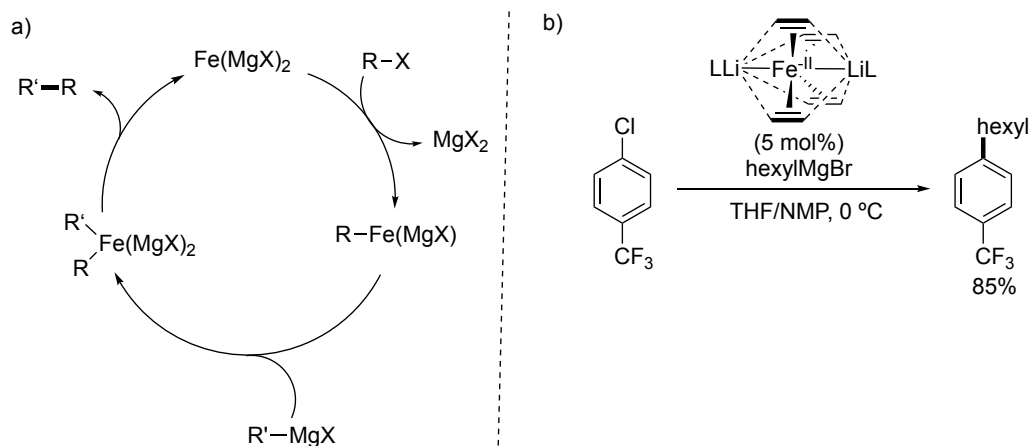
More recently, the Neidig group have isolated and characterized a novel homoleptic tetramethyliron(III) ferrate complex formed from reacting ferric chloride with methyl magnesium bromide under catalytically relevant conditions (Scheme 1.19b).⁶⁹ Through freeze-trapped *in situ* EPR spectroscopy studies, they were able to identify and isolate an intermediate spin $S = 3/2$ iron(III) species, which upon warming and generation of ethane undergoes clean formation to the $S = 1/2$ species originally observed by Kochi. Furthermore, when the thermally sensitive $S = 3/2$ iron(III) species was subjected to an alkenyl bromide no reaction occurred, which further corroborated Kochi's findings. While the exact nature of the iron(I) species remains unclear from this study, these findings are highly supportive of this *in situ* generated species being the catalytically competent and kinetically relevant species during catalysis.

Scheme 1.19. Homoleptic iron ferrate complexes formed by a) ferric chloride and methyl lithium and b) ferric chloride and methyl magnesium bromide.



In addition to an iron(I)/(III) cycle, lower valent mechanisms have been proposed for these types of cross-coupling reactions, including a notable iron(-II)/(0) catalytic cycle (Scheme 1.20a).¹⁶ This mechanism, first proposed by the Fürstner group, was based upon intriguing results when carrying out cross-coupling reactions between aryl chlorides and alkyl magnesium bromide reagents.¹⁸ From these studies, they discovered only Grignard reagents which could undergo β -hydride elimination could undergo cross-coupling, which was consistent in light of prior work by Bogdanovic who suggested ethyl Grignard reagents

Scheme 1.20. a) Proposed Fe(-II)/(0) cycle. b) Catalytic competency of a discrete Fe(-II) precatalyst.



led to reduced iron clusters of the formal composition $[\text{Fe}(\text{MgX}_2)_2]_n$ or $[\text{Fe}(\text{MgX})_2]_n$.^{70,71} To support these claims, Fürstner and coworkers synthesized a variety of Fe(-II) olefin complexes which were highly active for cross-coupling with aryl and allyl halides (Scheme 1.20b).¹⁸ However, iron catalysts in higher oxidation states were also catalytically competent. Thus, the unambiguous assignment of the kinetically relevant catalytic cycle is still a formidable challenge.

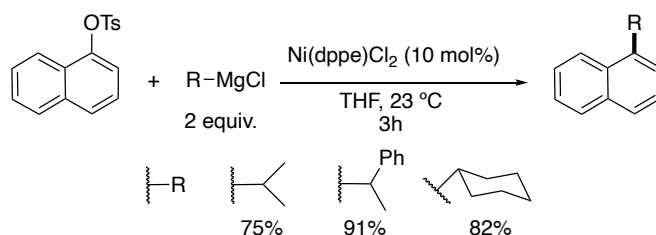
By comparison, nickel-catalyzed cross-couplings between aryl or alkenyl halides and primary alkyl Grignard reagents have been known since the early 1970s beginning with the seminal work of Kumada and coworkers.^{27,72} Within the past two decades, there has been steady advancement in this field to increase the breadth of substrates and functional groups with the use of a range of aryl halides, particularly aryl fluorides, and primary alkyl Grignards.⁷³⁻⁷⁶ While primary Grignard reagents perform well in these reactions, secondary and tertiary Grignard reagents are more challenging substrates due to the formation of isomerized linear products from chain-walking events. To this end, recent work has been dedicated toward developing more general catalytic systems tolerating secondary and tertiary Grignard reagents as well as using less reactive and abundant aryl and vinyl pseudohalides.

The Szostak group recently reported the coupling of aryl tosylates with primary and secondary alkyl Grignard reagents using a diphenylphosphinoethane (dppe) nickel chloride complex (Scheme 1.21). C-O electrophiles for C(sp²)-C(sp³) couplings remain rare,⁷⁶⁻⁷⁸ particularly with secondary alkyl Grignard reagents, with no reported examples utilizing an aryl tosylate. The group found the reaction to be broad for a range of electronically disparate arenes as well as primary Grignard reagents. A range of secondary Grignard

reagents were suitable under the reaction conditions with no isomerization events taking place; the use of isopropyl and 1-phenylethyl magnesium chloride resulted in high yields of product and no linear product.

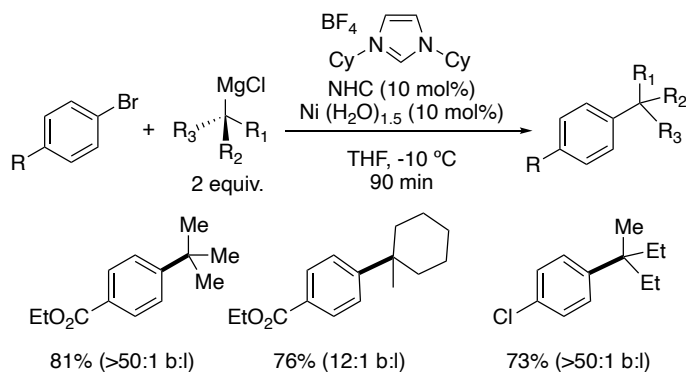
The construction of quaternary centers has been demonstrated in a select few of reactions with the use of tertiary Grignard reagents. Groups such as Biscoe and Glorius have found *N*-heterocyclic carbenes (NHCs) as supporting ligands highly effective for

Scheme 1.21. The coupling of 1-naphthyl tosylates with secondary alkyl Grignard reagents using Ni(dppe)Cl₂.



these couplings using aryl bromides (Scheme 1.22).^{79,80} The Biscoe group's reaction is particularly impactful to the synthesis of quaternary centers as chain-walking events are minimized with the ratio of branched to linear being >30:1 for most substrates. Additionally, the Tang group recently discovered a ligand-free reaction using aryl bromides that displayed good suppression of chain-walking with an average ratio of

Scheme 1.22. The coupling of aryl bromides with tertiary Grignard reagents catalyzed by a nickel NHC complex.



branched to linear product to be 15:1.⁸¹ Despite these major achievements, these reactions continue to remain nontrivial due to variable amounts of chain-walking events in most cases leading to inseparable isomeric products.⁸²

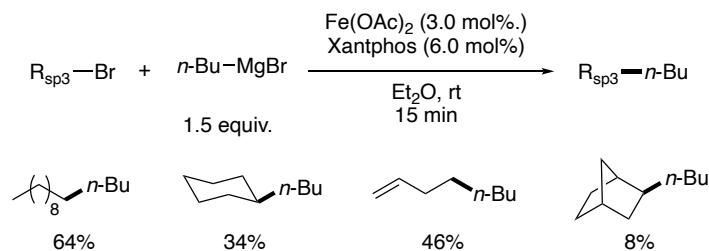
From these C(sp²)-C(sp³) cross-coupling examples, it is evident that iron-based catalysts benefit from higher reactivity than nickel-based systems, being able to preferentially activate aryl chlorides and tosylates over more reactive aryl bromides and iodides and do so with rapid efficiency. In addition, iron-based systems show less evidence of isomeric products from chain-walking events when using secondary or tertiary Grignard reagents. Conversely, nickel-based systems commonly produce isomeric products, which are difficult to separate by column chromatography. However, nickel-based catalysts do exhibit a wider variety of catalytic systems utilizing tertiary alkyl Grignard reagents, despite also generating some amounts of inseparable isomeric products.

1.3.2b C(sp³)-Hybridized Electrophile

Despite the expansive number of iron-catalyzed couplings between aryl halides and alkyl Grignard reagents, iron-catalyzed C(sp³)-C(sp³) cross-couplings using Grignard reagents are exceedingly rare.⁸³⁻⁸⁵ It was not until 2007 when the Chai group reported the first C(sp³)-C(sp³) Kumada cross-coupling reaction. In this reaction, primary and secondary alkyl bromides and primary alkyl Grignard reagents were coupled using an iron-Xantphos complex (Scheme 1.23).⁸⁶ The reaction proceeded with moderate to good yields of coupled product, displaying low levels of functional group tolerance (nitriles and esters are tolerated).

To further improve substrate scope and functional group tolerance, the Cardenas group developed an Fe(OAc)₂/IMes (IMes, 1,3-Bis(2,4,6-trimethylphenyl)-1,3-dihydro-2H-

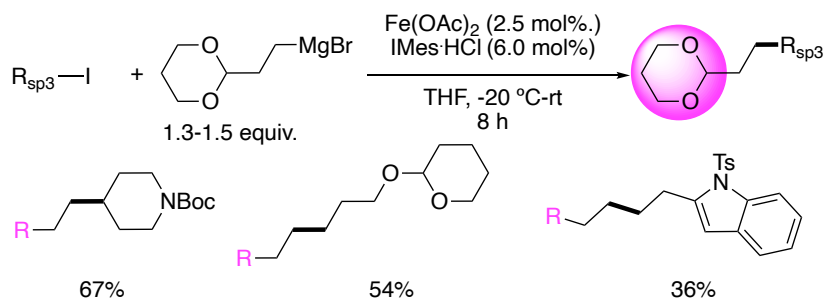
Scheme 1.23. The coupling of primary and secondary alkyl bromides with *n*-BuMgBr in the presence of an iron Xantphos catalyst.



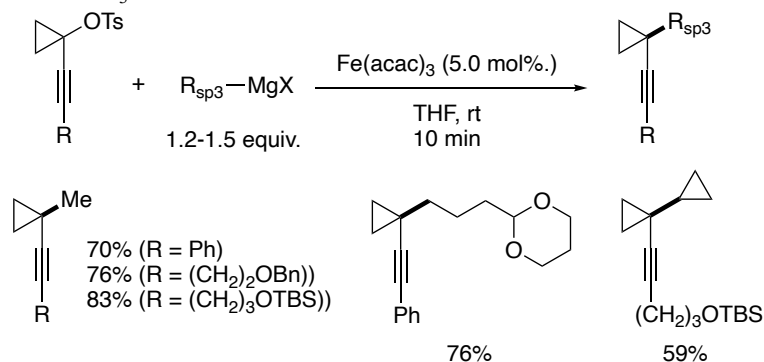
imidazol-2-ylidene) catalyst for the coupling of primary and secondary alkyl iodides and a primary Grignard reagent containing a pendant acetal group.⁸⁷ The reaction proceeded with good to excellent yields of cross-coupled product and tolerated a variety of functional groups such as esters, pyrans, piperidines and tosyl-protected indoles (Scheme 1.24). Critical to this reaction was an acetal containing Grignard reagent, which was shown by the Neideg group to coordinate to the iron center in order to disfavor β -hydride elimination.⁸⁸

Cross-coupling of secondary and tertiary electrophiles with alkyl Grignard reagents remains a formidable challenge. To address some of these issues, the Fürstner group recently developed a system for the coupling of 1-alkynylcyclopropyl tosylates with primary and secondary alkyl Grignard reagents catalyzed by $\text{Fe}(\text{acac})_3$ (Scheme 1.25).⁸⁹

Scheme 1.24. The coupling of primary and secondary alkyl iodides with (1,3-dioxan-2-ylethyl)magnesium bromide in the presence of an iron IMes catalyst.



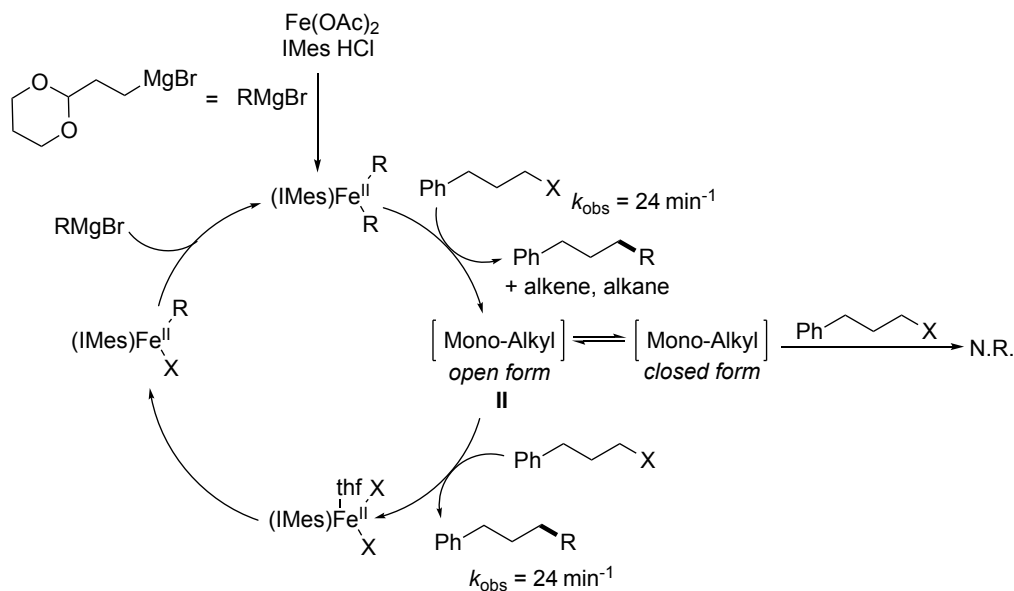
Scheme 1.25. Coupling between tertiary alkyl tosylates and primary Grignard reagents catalyzed by $\text{Fe}(\text{acac})_3$.



This reaction represented a significant advance in this field because now tertiary alkyl tosylates are suitable electrophiles, leading to a sterically crowded quaternary center. The reaction proceeded with good to excellent yields of cross-coupled product but displayed a limited functional group tolerance with only acetals and ethers being demonstrated. The reaction was also limited with respect to the secondary alkyl Grignard scope with cyclopropyl Grignard being the only example.

In addition to mechanistic studies of $\text{C}(\text{sp}^3)\text{-C}(\text{sp}^2)$ Kumada-based systems, there has also been some efforts to probe the mechanisms of $\text{C}(\text{sp}^3)\text{-C}(\text{sp}^3)$ cross-coupling reactions. The Neidig group carried out a recent study looking at the $\text{C}(\text{sp}^3)\text{-C}(\text{sp}^3)$ Kumada cross-coupling reaction developed by Cardenas between alkyl iodides and primary Grignard reagents containing acetal groups catalyzed by an NHC ligated iron complex (Schemes 1.24-1.26).^{87,88} Using *in situ* Mössbauer and EPR analysis as well as reactivity studies, they were able to determine that the doubly transmetalated iron species $(\text{IMes})\text{Fe}((1,3\text{-dioxan-2-yl})\text{ethyl})_2$ was the key active species while the mono-transmetalated species $(\text{IMes})\text{FeBr}((1,3\text{-dioxan-2-yl})\text{ethyl})$ exhibited no reactivity toward the electrophile. They found that $(\text{IMes})\text{Fe}((1,3\text{-dioxan-2-yl})\text{ethyl})_2$ underwent two rapid

Scheme 1.26. Mechanistic cycle for an C(sp³)-C(sp³) Kumada cross-coupling reaction catalyzed by and (IMes)Fe((1,3-dioxan-2-yl)ethyl)₂ active species.

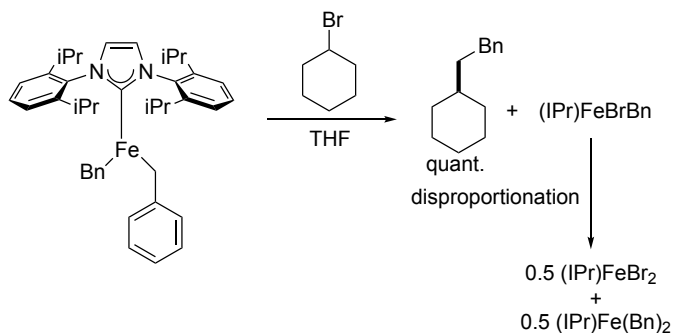


turnovers with electrophile at catalytically relevant rates ($k_{\text{obs}} = 24 \text{ min}^{-1}$). A putative mono-alkylated iron(II)-IMes intermediate **II** was highly selective for generation of cross-coupled product. Interestingly, the mono-alkylated iron(II)-IMes species formed during catalysis was distinct from (IMes)FeBr((1,3-dioxan-2-yl)ethyl) which they surmise was due to an open form of the complex where the acetal oxygen does not coordinate to iron. Importantly, they were able to determine that an EPR observable $S = \frac{1}{2}$ iron(I) species that was observed by Cardenas accounted for only 0.5% of all iron species in solution, and it was an off-cycle intermediate. In addition to reactivity studies, they were also able to gain insight from the crystal structures of the iron complexes which exhibited chelation from the acetal moiety of the nucleophile. This binding provides the catalyst with high resistance to β -hydride elimination which accounts for the low levels of alkene product seen during catalysis. From these results, the authors conclude the system to be most consistent with an iron(II)/(III) cycle.

The Tonzetich group were able to demonstrate the stoichiometric efficiency of NHC-ligated (IPr)Fe(Bn)₂ complexes with bromocyclohexane leading to clean formation of benzylcyclohexane and dimeric bridging (IPr)FeBr₂ species, formed from disproportionation of the (IPr)FeBrBn product (Scheme 1.27).⁹⁰ Radical clock studies were also carried out which demonstrated a linear correlation between linear/cyclic product and catalyst concentration, which was supportive of a radical-based mechanism where the carbon-centered radical escapes the solvent cage. Additionally, the group attempted the synthesis of an iron(III) species using I₂ as an oxidant so they could probe its reactivity and relevance in the catalytic cycle, but in all cases such reactions formed dimeric bridging (IPr)FeI₂ species. These findings are supportive of an Fe(II)/(III) cycle with (IPr)Fe(R)₂ being the active species able to perform halogen abstraction. However, they could not definitively rule out a mechanism involving an iron(I) species.

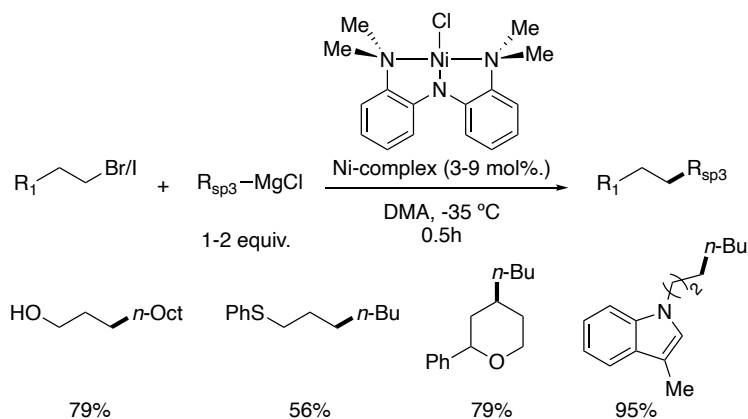
Nickel-based systems for C(sp³)-C(sp³) couplings in comparison have enjoyed a steady development since the first report by Kambe in 2002,⁹¹ showcasing increased functional group tolerance and use of pseudohalides in reactions between primary alkyl halides and primary Grignard reagents. However the use of secondary Grignards reagents remaining virtually unknown.⁹²⁻⁹⁵ A major advance came from the Hu group where they

Scheme 1.27. Stoichiometric reactions of an (IPr)Fe(Bn)₂ complex with bromocyclohexane.



demonstrated an unparalleled substrate scope in reactions between primary and secondary alkyl halides and primary Grignard reagents using a pincer amidobis(amine) nickel complex (Scheme 1.28).⁹⁶ A range of functional groups were tolerated such as nitriles, heteroaromatics, free alcohols, thiols, esters as well as many others. The reaction provided excellent yields for primary alkyl halides as well as cyclic alkyl halides with primary Grignard reagents while secondary Grignard reagents were absent from the substrate scope.

Scheme 1.28. The coupling of alkyl bromides and iodides with primary alkyl Grignard reagents in the presence of a pincer amidobis(amine) nickel complex

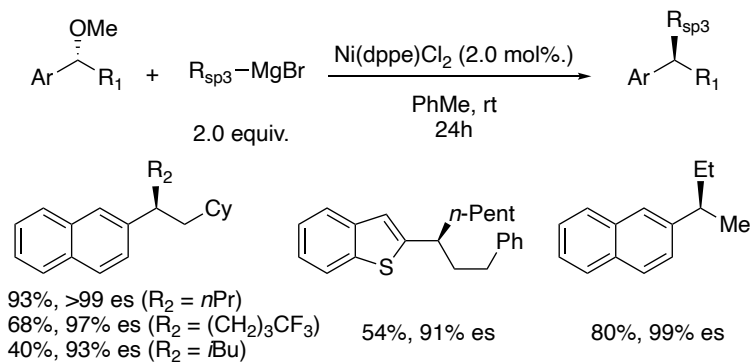


The ability to couple secondary alkyl halides is an important feature for cross-coupling reactions because the synthesis of enantioenriched molecules becomes possible. To this end, there have been limited reports demonstrating this type of reactivity for nickel-catalyzed alkyl-alkyl Kumada cross-couplings, none showing enantioselective examples.⁹⁷⁻⁹⁹ The Jarvo group has developed stereoinvertive reactions where an enantioenriched secondary benzylic ester undergoes stereospecific cross-coupling with methyl Grignard reagents catalyzed by an achiral nickel bis-phosphine complex (Scheme 1.29). In a particular instance the Jarvo group has demonstrated highly enantiospecific couplings between benzylic ethers containing a naphthyl ring with a range of primary alkyl

Grignard reagents catalyzed by Ni(dppe)Cl₂.¹⁰⁰ The reaction provided high yields and enantiospecificity of cross-coupled product in most instances but was limited in terms of functional group tolerance. Sterically encumbering primary Grignard reagents with β -branching led to low yields while secondary Grignard reagents were not reported, hinting at high levels of β -hydride elimination.

Nickel-based systems provide significant advantages in terms of functional-group tolerance and stereoselective reactions. However, iron-based systems have demonstrated

Scheme 1.29. Stereospecific cross-coupling of benzylic methyl ethers with primary alkyl Grignard reagents catalyzed by Ni(dppe)Cl₂.



remarkable reactivity with challenging tertiary tosylate electrophiles and provide some limited examples of secondary-secondary cross-couplings, which have not yet been demonstrated with analogous nickel-based systems. Furthermore, mechanistic studies have provided insight into these reactions which should help drive further reaction development.

1.4 Negishi Cross-Coupling Reactions Mediated by Iron-Based Catalysts

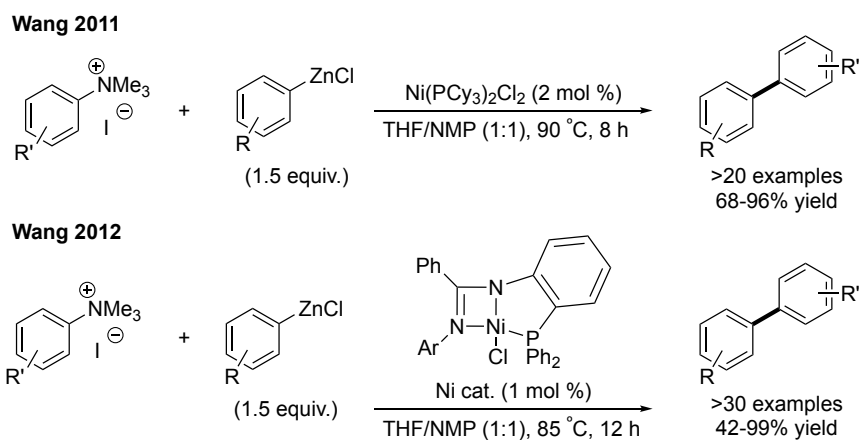
The second most common type of iron-catalyzed cross-couplings are Negishi reactions, which are characterized by employing organozinc reagents as the transmetalating agent. These reactions benefit from the mild reaction conditions as compared to Kumada systems, allowing for excellent functional group tolerance. Despite these reactivity

excellent yields and good functional group tolerance including esters, ketones and trifluoromethyl groups.

Nickel-based catalysts certainly provide advantages for these C(sp²)-C(sp²) cross-couplings reactions due to the lack of examples using iron-based catalysts. This type of general reactivity has yet to be realized using an iron-based system.

1.4.1b C(sp³)-Hybridized Electrophile

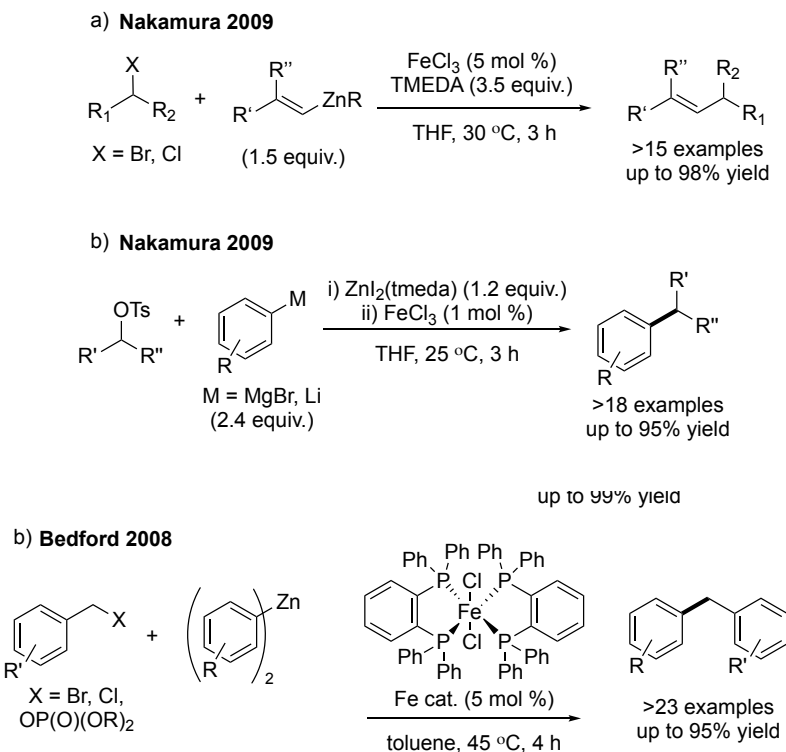
Scheme 1.31. Examples of nickel catalyzed C(sp²)-C(sp²) Negishi cross-coupling reactions.



Negishi cross-coupling reactions between alkyl electrophiles and aryl organozinc nucleophiles catalyzed by iron-based systems has seen substantial progress over the past 15 years. In 2005, Nakamura and co-workers reported the first C(sp³)-C(sp²) Negishi cross-coupling of catalyzed by iron salts (Scheme 1.32a).¹⁰⁷ A variety of diaryl and diheteroaryl organozinc nucleophiles were tolerated under these conditions, but secondary alkyl halides were limited to those in 6 or 7-membered rings. Bedford and co-workers expanded upon this discovery, demonstrating that iron-based catalysts supported by 1,2-bis(diphenylphosphino)benzene ligands enabled the coupling of benzylic halide and alkyl phosphate electrophiles with diarylzinc nucleophiles (Scheme 1.32b).¹⁰⁸ It is worth noting

that secondary benzylic halides were not tolerated under these reaction conditions, presumably due to greater steric encumbrance.

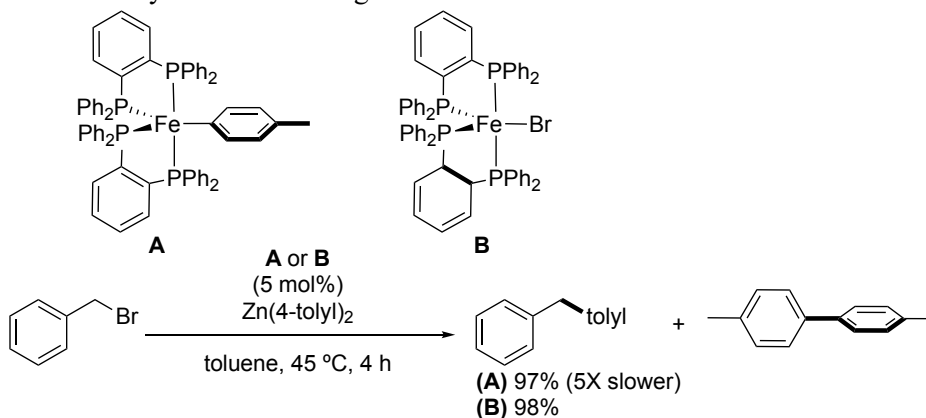
Scheme 1.33. a) The first example of an iron-catalyzed C(sp³)-C(sp²) Negishi cross-coupling using alkenylzinc reagents b) Use of alkyl tosylates as electrophiles.



Building upon their previous system, Nakamura and co-workers demonstrated that alkenylzinc reagents could be coupled to primary and secondary alkyl halides showcasing high stereospecificity of the electrophile in all cases (Scheme 1.33a).¹⁰⁹ This reaction also displayed high functional group tolerance, with nitriles, esters and carbamates remaining untouched in the cross-coupling reaction. In another example, the Nakamura group was able to show that the addition of magnesium salts to the original system enabled the successful coupling of secondary alkyl sulfonate electrophiles through *in situ* formation of the corresponding aryl zinc reagent and secondary alkyl iodide (Scheme 1.33b), further enhancing the scope of these reactions.¹¹⁰

In addition to methodology development, there has been increased interest in understanding the mechanism of these C(sp³)-C(sp²) Negishi cross-coupling reactions. The first example came from the Bedford group who wanted to determine if an iron(I) active species was the lowest kinetically reasonable oxidation state, as originally proposed by Kochi.¹¹¹ The reaction they studied was the Negishi coupling between benzylic bromides

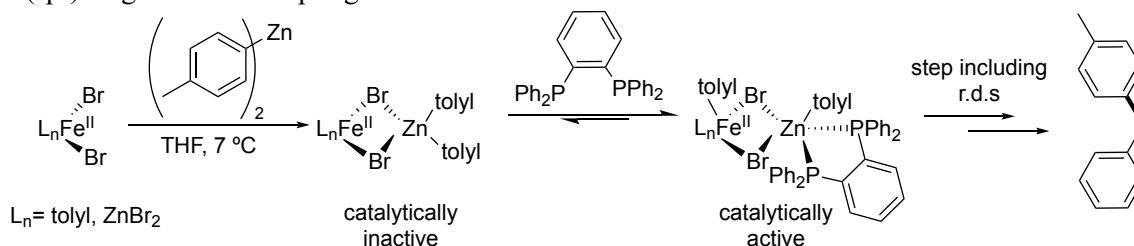
Scheme 1.34. Evidence and reactivity of Fe(I) intermediates in couplings between aryl nucleophiles and alkyl halides in a Negishi reaction.



and diaryl zinc reagents catalyzed by a bis(diphenylphosphino)benzene ligated iron dihalide complex (Scheme 1.34).¹¹² In this system, they observed formation of bitolyl products which they used as a proxy to measure the bulk oxidation state. From this method of measuring oxidation state, results were consistent with an iron(I) species. However, the Neidig group has shown this method to be misleading due to biaryl formation upon quenching the reaction.⁴⁹ Additionally, in this system, the Bedford group was able to synthesize discrete low-spin Fe(dppz)₂Ar and Fe(dppz)₂Br complexes which were both catalytically competent, however only the halide complex was kinetically relevant. From these results they conclude that the iron aryl complex was most likely an off-cycle species.

In a 2019 study, the Bedford group was able to determine the role of the phosphine ligand in an $C(sp^3)$ - $C(sp^2)$ Negishi cross-coupling reaction (Scheme 1.35).¹¹³ The Bedford group used time-resolved X-ray absorption fine structure spectroscopy (XAFS) to monitor

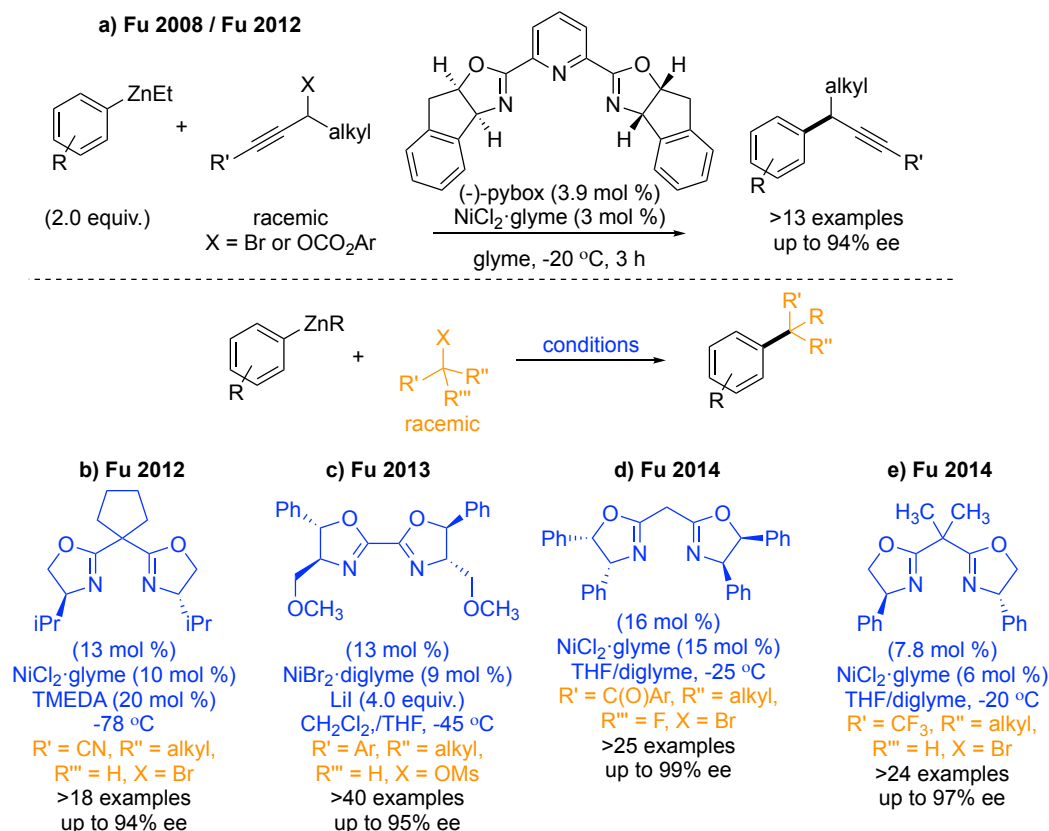
Scheme 1.35. Evidence of biphosphine ligands coordinating to zinc in iron-catalyzed $C(sp^3)$ - $C(sp^2)$ Negishi cross-coupling reactions.



the catalytic reactions to probe speciation. From these studies, they discovered the diphosphine ligand was mainly coordinated to zinc during turnover. Furthermore, combined stoichiometric and kinetic studies suggested the formation of a mixed Fe-Zn(dpbz) species prior to the later steps including the rate-determining step. These results were unexpected and challenged prior beliefs that the biphosphine ligands stayed coordinated to the iron center.

In comparison to iron, nickel-based systems have advanced at a considerable pace just within the last decade for $C(sp^3)$ - $C(sp^2)$ couplings, leading to an impressive arsenal of enantioselective reactions showcasing high selectivities. Fu and coworkers have been able to use ligand design to drive this new reactivity where propargylic halides and carbonates (Scheme 1.36a)¹¹⁴ could serve as substrates using nickel-complexes supported by a pyridine bis(oxazoline) ligand. Furthermore, secondary α -halonitriles (Scheme 1.36b),¹¹⁵ secondary benzylic mesylates (Scheme 1.36c),¹¹⁶ α,α -dihaloketones (Scheme 1.36d)¹¹⁷ and CF_3 -substituted secondary alkyl halides (Scheme 1.36e)¹¹⁸ could be accessed using a bis(oxazoline) ligand framework.

Scheme 1.36. Examples of enantioselective C(sp³)-C(sp²) Negishi cross-couplings catalyzed by nickel-based catalysts.



Like C(sp²)-C(sp²) cross-couplings, the synthetic advantages of using iron-based catalysts for these Negishi C(sp³)-C(sp²) reactions are not yet obvious, particularly with the overshadowing of nickel-based systems which have shown impressive reactivity. Future development of this field should provide more insight into the complementary reactivity of iron-based catalysts.

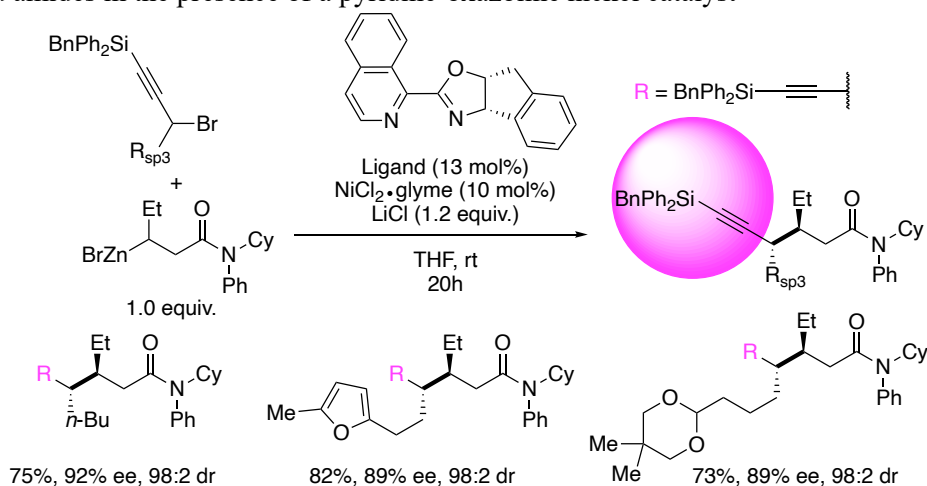
1.4.2 C(sp³)-Hybridized Zinc-Based Nucleophile

1.4.2a C(sp³)-Hybridized Electrophile

C(sp³)-C(sp³) couplings using an iron-based system are exceedingly rare with only one example reported in the literature. In this system, the Nakamura group was able to

develop a C(sp³)-C(sp³) Negishi-type coupling reaction between alkyl bromides and alkylaluminum reagents catalyzed by an iron bisphosphine catalyst.¹⁰² These reactions demonstrated high functional group tolerance (unprotected indoles, carboxylic acids, alcohols) due to the low basicity of the organoaluminum reagents and potassium fluoride additive. However, this reaction was limited to primary alkyl bromides since secondary alkyl bromides led to high amounts of alkene products.

Scheme 1.37. Doubly stereoconvergent coupling between propargyl bromides and secondary β -zincated amides in the presence of a pyridine-oxazoline nickel catalyst



In comparison, nickel-based systems have made significant progress toward utilizing both secondary alkyl halides^{119,120} and secondary alkyl¹²¹ zinc reagents as well the development of stereoconvergent reactions.^{122,123} To highlight these achievements, the Fu group recently reported a doubly enantioconvergent cross-coupling reaction between racemic β -zincated amide nucleophiles and racemic propargylic bromides catalyzed by a chiral pyridine-oxazoline nickel complex (Scheme 1.37).¹²⁴ The reaction was highly enantioselective (89-95% ee) and diastereoselective (>98:2 dr) as well as high yielding, tolerating a variety of functional groups such as ethers, acetals, alkynes and esters on either nucleophile or electrophile. The origin of enantioselectivity in the nucleophile was

hypothesized to originate from coordination of the amide oxygen to the nickel catalyst to differentiate between the two alkyl groups.

Nickel-based systems have seen tremendous growth in the area of C(sp³)-C(sp³) Negishi cross-coupling, leading to protocols for secondary-secondary couplings and doubly stereocovergent reactions. Currently, no advantages of using iron-based catalysts for these types of couplings are obvious due to the paucity of iron-based systems.

1.5 Suzuki-Miyaura Cross-Coupling Reactions Mediated by Iron-Based Catalysts

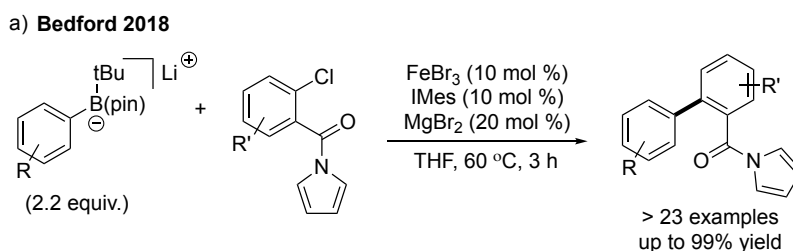
The iron-catalyzed Suzuki-Miyaura cross-coupling reaction is the least developed methodology of the three, being quoted by Nakamura and Bedford as “something of a ‘holy grail’ in coupling chemistry”.¹²⁵ This reaction is a particularly attractive method to form carbon-carbon bonds due to the ease of handling, non-toxic byproducts and high commercial availability of organoboron nucleophiles. However, since the organoboron nucleophiles provide higher stability, they also exhibit lower reactivity and consequently require a base additive.¹²⁶ Nevertheless, these reactions see frequent use in industrial applications⁷ and improved methods continue to be highly desirable. Akin to iron-catalyzed Negishi reactions, Suzuki-Miyaura reactions mediated by iron-based catalysts are rare and mainly limited to C(sp³)-C(sp²) couplings. Despite this lack of reactivity, there exists only one example of an C(sp²)-C(sp²) coupling,¹²⁷ a single example of an C(sp³)-C(sp³) coupling reaction¹²⁸ and no examples of C(sp²)-C(sp³) couplings.

1.5.1 C(sp²)-Hybridized Boron-Based Nucleophile

1.5.1a C(sp²)-Hybridized Electrophile

The iron-catalyzed C(sp²)-C(sp²) Suzuki-Miyaura cross-coupling reaction has remained elusive and problematic. Recently, Bedford and co-workers reported the first example, demonstrating the coupling of aryl halides with activated aryl boronic esters catalyzed by an iron-NHC system (Scheme 1.38).¹²⁷ To achieve this reactivity, the aryl halide had to be functionalized with an ortho-substituted *N*-pyrrole amide directing group. The authors propose that the pyrrole is necessary to participate in π -coordination to the iron center in order for the C-Cl bond to be in proper orientation for oxidative addition.

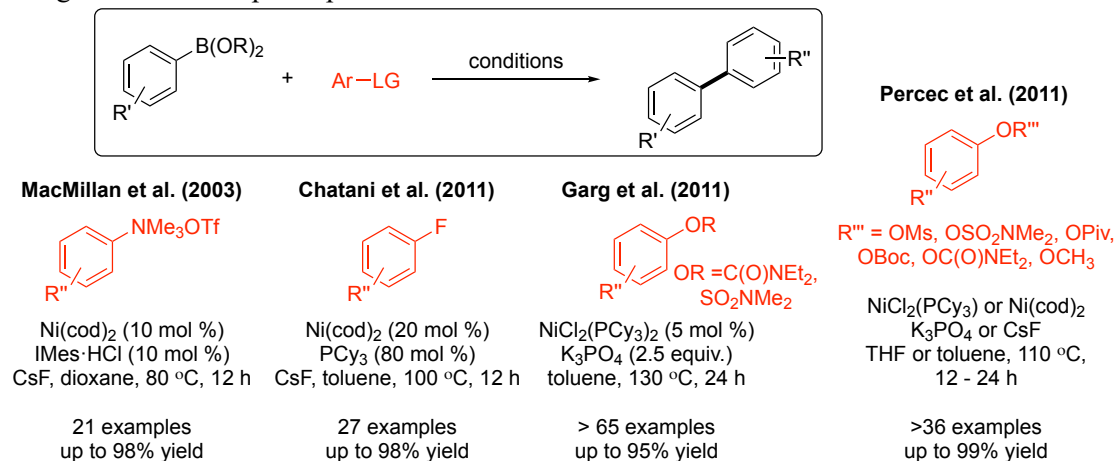
Scheme 1.38. Example of the first C(sp²)-C(sp²) Suzuki-Miyaura cross-coupling catalyzed by an iron-based catalyst.



Nickel-based systems have received significant attention for C(sp²)-C(sp²) Suzuki-Miyaura cross-couplings over the past two decades. Unique to these systems are the ability to activate a wide number of electrophiles, many of which are uncommonly used in noble-metal cross-coupling reactions. Some representative electrophiles that have been used by various groups include aryl trimethylammonium triflates,¹²⁹ aryl fluorides,¹³⁰ aryl carbamates and sulfamates¹³¹ and aryl ethers (Scheme 1.39).¹³² In a 2012 study by the Percec group, five distinct reaction conditions were reported for the coupling of aryl mesylates, aryl methyl ethers, and aryl sulfamates, pivalates, carbonates and carbamates with aryl boron nucleophiles.¹³³ They noted nickel(0) precatalysts demonstrated high selectivity toward C-O electrophiles while nickel(II) precatalysts were nonselective.

The pursuit of finding iron-based catalysts for effecting C(sp²)-C(sp²) Suzuki-Miyaura cross-coupling reactions remains an ongoing process. Nickel-based systems have a commanding advantage over those of iron. Furthermore, the ability of nickel-based catalysts to activate the relatively inert carbon-heteroatom bonds greatly expands the

Scheme 1.39. Examples of nickel-catalyzed C(sp²)-C(sp²) Suzuki-Miyaura cross-couplings using various electrophilic partners.

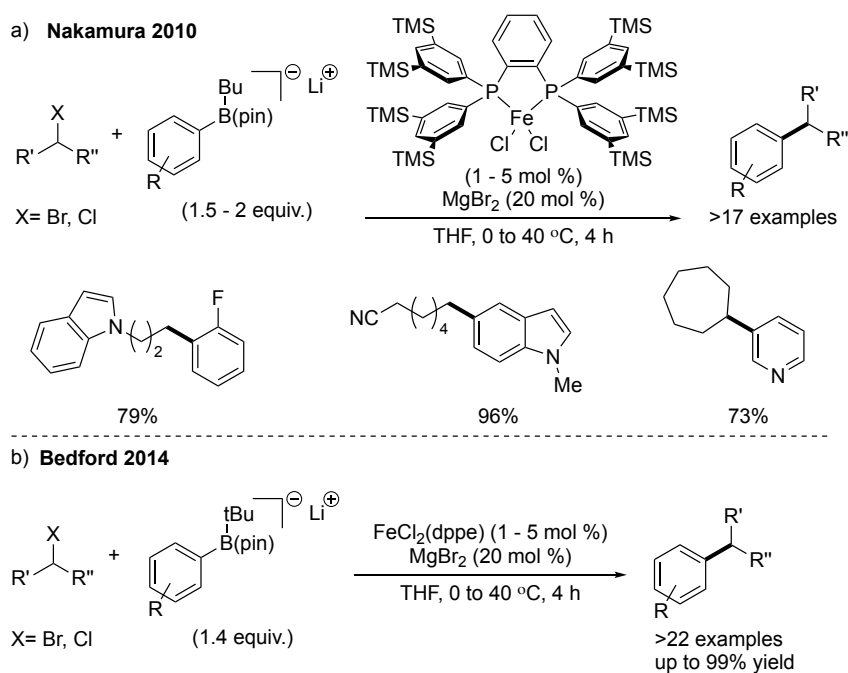


available substrate scope as well as providing complementary reactivity to established palladium catalysis.

1.5.1b C(sp³)-Hybridized Electrophile

Within the past decade, examples of Suzuki-Miyaura cross-coupling reactions of alkyl electrophiles and aryl organoboron nucleophiles catalyzed by iron-based complexes have garnered increased interest. Nakamura and co-workers were the first to report such a transformation in 2010. In this system, they successfully demonstrated the cross-coupling of preactivated arylboronic pinacol esters (B(pin)) with a variety of primary and secondary alkyl halide electrophiles, catalyzed by an iron(II) chloride complex supported by the bisphosphine ligand 3,5-TMS-SciOPP (Scheme 1.40a).¹³⁴ The aryl boronic ester was preactivated by *in situ* borate formation with alkyllithium reagents, and the reaction did not

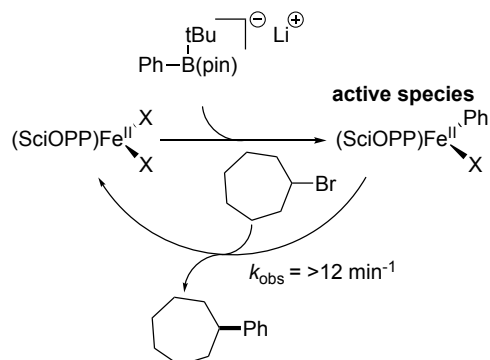
Scheme 1.40. Two examples demonstrating C(sp²)-C(sp²) Suzuki-Miyaura cross-coupling catalyzed by an iron-based catalyst. b) Example of the first C(sp³)-C(sp³) Suzuki-Miyaura cross-coupling catalyzed by an iron-based catalyst



take place in the absence of a MgBr₂ co-catalyst, which the authors propose accelerates the transmetalation between the borate and the iron catalyst. However with this magnesium additive, the authors cannot rule out a Kumada-type reaction. Rigorous spectroscopic analysis of this system by the Neidig group revealed upon spin-counting that iron(I) species accounted for less than 0.5% of the total iron in solution when using *tert*-butylphenyl borate as the nucleophile.⁴⁹ Furthermore, they revealed similar results to the Kumada system where (SciOPP)FeBrPh was the catalytically active and kinetically relative species for catalysis (Scheme 1.41).

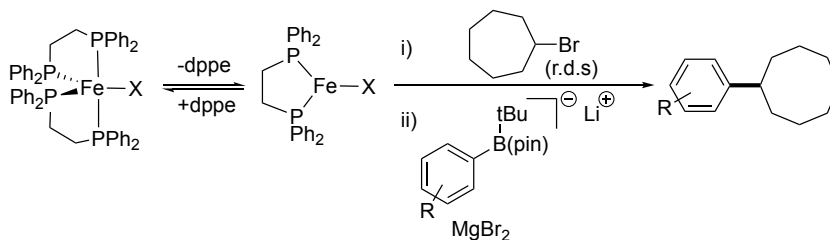
In 2014, Bedford and co-workers reported the cross-coupling reaction of preactivated aryl boronic acid pinacol esters (B(pin)) with a variety of primary and secondary alkyl halide electrophiles could be catalyzed by iron complexes supported by

Scheme 1.41. Discovery of (SciOPP)FePhX as the active species in Nakamura's Suzuki-Miyaura cross-coupling reaction between *tert*-butylphenyl borate and cycloheptylbromide.



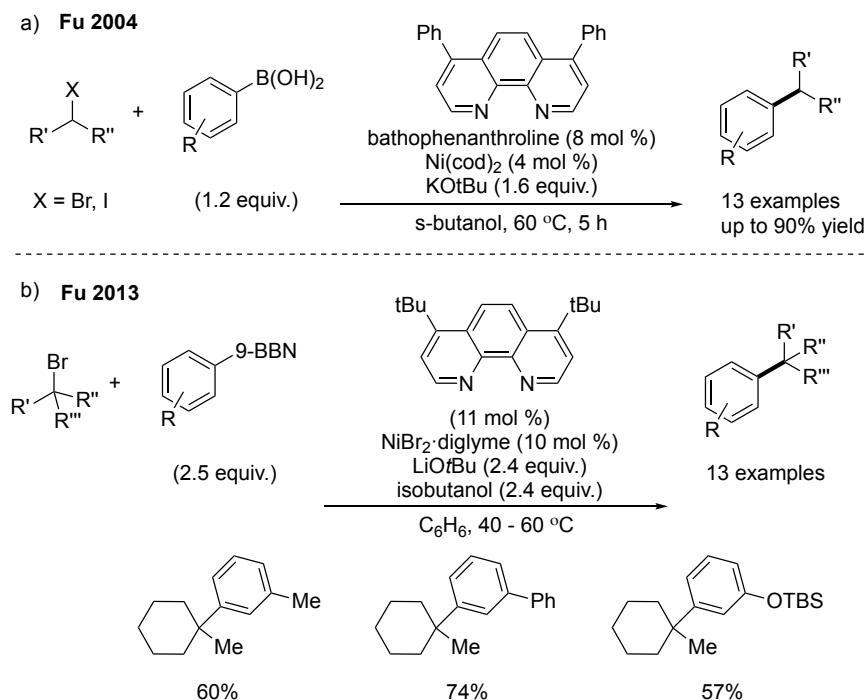
inexpensive and commercially available diphosphine ligands (dppe or dppp) (Scheme 1.40b).⁴¹ Like the system reported by Nakamura and co-workers, preactivation of the boronic ester with *tert*-butyllithium and the addition of MgBr₂ was required for the reaction to occur. Activated alkyl halides, including allyl and benzyl halides, were also shown to produce cross-coupled product in good yields. In this system, the Bedford group found further support for an Fe(I) species (Scheme 1.42). Carrying out *in situ* EPR analysis, they were able to reveal the presence of an iron(I) consistent with an Fe(dppe)₂X species. When kinetic studies were carried out, they found the active species to be Fe(dppe)X, formed from equilibration with Fe(dppe)₂X, which then undergoes rate-determining halogen abstraction with the alkyl halide. However, recent studies by the Neidig group question these results by demonstrating that iron(I) species are off-cycle in a similar reaction using the bisphosphine ligand SciOPP.⁴⁹

Scheme 1.42. Evidence and reactivity of Fe(I) intermediates in a Suzuki-Miyaura reaction.



In comparison to iron, nickel-based C(sp³)-C(sp²) couplings have received considerable amounts of attention, particularly from the pioneering work of the Fu group. Similar to palladium-based systems, Fu and coworkers were able to demonstrate the use of boronic acids as coupling partners which have practical advantages to boronic esters such as greater air stability and commercial availability. In this system, they were able to carry out coupling between arylboronic acids and unactivated secondary alkyl halides when using a bathophenanthroline-ligated nickel catalyst (Scheme 1.43a).¹³⁵ In another example, the Fu group was able to show the first example of a Suzuki-Miyaura cross-coupling reaction using a wide variety of tertiary alkyl halides (Scheme 1.43b).¹³⁶ However, nickel-based system required the use of a highly active organoborane nucleophile (9-BBN) and

Scheme 1.43. Nickel-catalyzed C(sp³)-C(sp²) Suzuki-Miyaura cross-coupling utilizing boronic acid nucleophiles. b) Suzuki arylations of tertiary electrophiles catalyzed by a nickel-based catalyst.



was limited to phenyl or meta-substituted aryl-(9-BBN) reagents with electron donating groups.

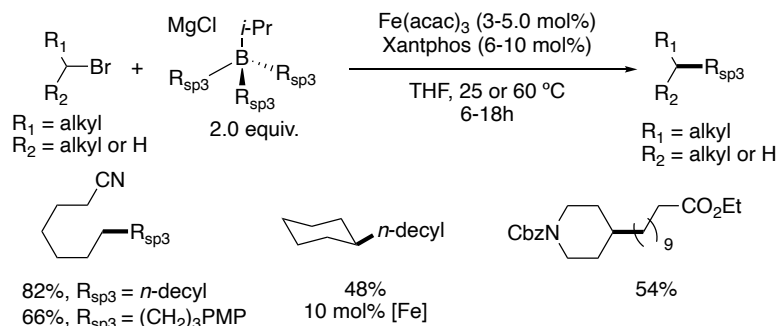
From a comparison of these methods, nickel-based systems showcase some clear advantages over those of iron. These include the use of air-stable boronic acids as coupling partners and the use of a wide variety of tertiary alkyl halides. In analogous iron-based systems, more reactive alkyl lithium activated arylboronic esters are needed as well as magnesium halide additives. The development of more iron-based systems are needed to identify the advantages of using an iron-based catalyst for these C(sp³)-C(sp²) Suzuki-Miyaura couplings.

1.5.2 C(sp³)-Hybridized Boron-Based Nucleophile

1.5.2a C(sp³)-Hybridized Electrophile

The only known report of an iron-catalyzed Suzuki-Miyaura C(sp³)-C(sp³) cross-coupling reaction comes from the Nakamura group.¹²⁸ This reaction, catalyzed by a Xantphos/Fe(acac)₃ system, demonstrated for the first time the coupling between primary and secondary alkyl bromides with primary trialkylboranes (Scheme 1.44). The transmetalation of the trialkylborane was facilitated by the use of *i*-PrMgCl and elevated temperatures. Although the reaction conditions were harsh, the substrate scope displayed moderate functional group tolerance particularly with nitriles, esters and carbamates. The reaction was general and high yielding for a variety of functionalized primary alkyl bromides but was limited in scope for secondary alkyl bromides; only bromocyclohexane

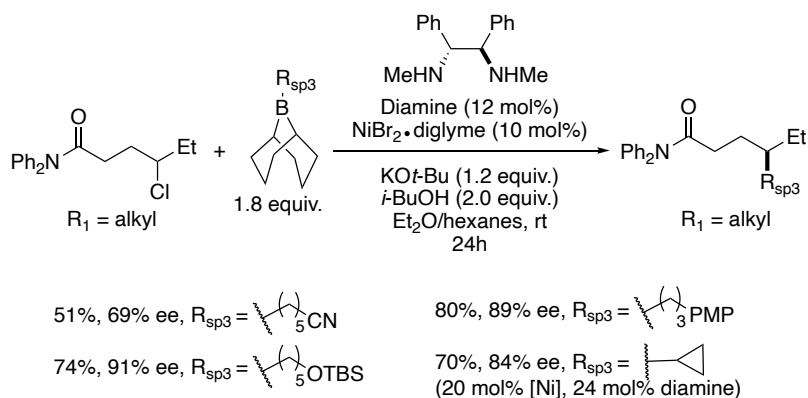
Scheme 1.44. Coupling of primary and secondary alkyl bromides with activated primary trialkyl boranes using a Xantphos/Fe(acac)₃ catalytic system.



and its derivatives provided acceptable to good yields. The utility of this method was demonstrated by the synthesis of long-chain ethyl ester fatty acid derivatives.

In comparison, the Fu group has singlehandedly advanced the field of nickel-catalyzed alkyl-alkyl Suzuki-Miyaura cross-couplings to huge lengths over the past two decades. Major accomplishments by this group were the development of enantioconvergent cross-coupling reactions utilizing unactivated alkyl halides with the use of a host of directing groups.^{137–139} A particularly impressive example was the γ -alkylation of γ -chloro-*N*-diphenylamides using a nickel-diamine catalyst and primary alkylboranes (Scheme 1.45).¹⁴⁰ The reaction tolerated a wide variety of functional groups on the

Scheme 1.45. Stereoconvergent coupling between γ -chloro amides and primary alkyl boranes using a *trans*-*N,N'*-dimethyl-1,2-diphenylethylenediamine nickel complex



alkylborane such as acetals, silyl-protected alcohols, ethers, *N*-protected indoles and nitriles, which proceeded with good yields and high enantioselectivities. Most notable from this catalytic system were the first and only known reports of coupling between unactivated secondary alkyl halides and an arylborane, arylboronic ester and secondary alkylborane which has expanded the available coupling partners significantly.

As a result of the significant developments made using nickel-based catalysts and the paucity of iron-based systems, there are clear advantages using nickel-based systems. The development of more iron-catalyzed Suzuki-Miyaura C(sp³)-C(sp³) cross-coupling reactions are needed to identify advantages or complementary reactivity to those of nickel.

1.6 Conclusion

Transition-metal catalyzed cross-coupling reactions have received significant attention within the last three decades for the incorporation of C(sp³)-hybridized centers.¹ These methodologies have proven to be extremely efficient and robust methods which provide high value for both academia and the pharmaceutical industry due to efforts to “escape flatland.” Despite the success of these methods, the field continues to be heavily dominated by nickel-based systems, which themselves have some synthetic limitations. Iron cross-coupling reactions provide an attractive alternative to nickel. The main advantages of iron-based systems, as identified by from this review, firstly include the higher reactivity of iron-based catalysts over nickel-based catalysts (Table 1.2). This higher reactivity led to iron-based systems utilizing less reactive aryl tosylates and chlorides as electrophiles in C(sp²)-C(sp³) Kumada cross-couplings¹⁴¹ and unactivated arylboronic esters in C(sp³)-C(sp²) cross-couplings using tertiary alkyl halides.¹⁴² An additional advantage of iron-based systems are that these catalysts are less prone to chain-walking

Scheme 1.46. Advantages and disadvantages of iron and nickel-based catalysts for cross-coupling reactions.

	Iron-Based Catalysts	Nickel-Based Catalysts
Advantages	<ul style="list-style-type: none">• More reactive catalysts• Less isomerization products	<ul style="list-style-type: none">• Many enantioselective systems• High functional group tolerance
Disadvantages	<ul style="list-style-type: none">• Many methodologies still need developing• Limited enantioselective systems	<ul style="list-style-type: none">• Less reactive catalysts• Inseparable isomeric products commonly form

than nickel-based systems, which commonly form inseparable isomeric products when using alkyl halide electrophiles.⁸²

Through the development of new iron-based systems, complementary reactivity to nickel-based systems can be identified and used to develop even better catalytic systems. Methodological gaps that should be addressed in the future, and which have been identified in this overview of the cross-coupling field, are such: the use of unactivated arylboronic esters as nucleophiles, tertiary coupling partners, C(sp³)-C(sp³) couplings and stereoselective reactions, particularly between two secondary coupling partners.

1.7 References

- (1) Jana, R.; Pathak, T. P.; Sigman, M. S. Advances in Transition Metal (Pd,Ni,Fe)-Catalyzed Cross-Coupling Reactions Using Alkyl-Organometallics as Reaction Partners. *Chem. Rev.* **2011**, *111*, 1417–1492. <https://doi.org/10.1021/cr100327p>.
- (2) Buskes, M. J., Blanco, M. Impact of Cross-Coupling Reactions in Drug Discovery and Development. *Molecules* **2020**, *25*, 3493.
- (3) Egorova, K. S.; Ananikov, V. P. Toxicity of Metal Compounds: Knowledge and Myths. *Organometallics* **2017**, *36*, 4071–4090. <https://doi.org/10.1021/acs.organomet.7b00605>.
- (4) Hunt, A. J.; Matharu, A. S.; King, A. H.; Clark, J. H. The Importance of Elemental Sustainability and Critical Element Recovery. *Green Chem.* **2015**, *17*, 1949–1950. <https://doi.org/10.1039/c5gc90019k>.
- (5) Martin, R.; Buchwald, S. L. Palladium-Catalyzed Suzuki-Miyaura Cross-Coupling Reactions Employing Dialkylbiaryl Phosphine Ligands. *Acc. Chem. Res.* **2008**, *41*, 1461–1473. <https://doi.org/10.1021/ar800036s>.
- (6) Choi, J.; Fu, G. C. Transition Metal-Catalyzed Alkyl-Alkyl Bond Formation: Another Dimension in Cross-Coupling Chemistry. *Science* **2017**, *356*, 559–564. <https://doi.org/10.1126/science.aaf7230>.
- (7) Brown, D. G.; Boström, J. Analysis of Past and Present Synthetic Methodologies on Medicinal Chemistry: Where Have All the New Reactions Gone? *J. Med. Chem.* **2016**, *59*, 4443–4458. <https://doi.org/10.1021/acs.jmedchem.5b01409>.
- (8) Kyne, S. H.; Lefèvre, G.; Ollivier, C.; Petit, M.; Ramis Cladera, V. A.; Fensterbank,

- L. Iron and Cobalt Catalysis: New Perspectives in Synthetic Radical Chemistry. *Chem. Soc. Rev.* **2020**, *49*, 8501–8542. <https://doi.org/10.1039/d0cs00969e>.
- (9) Fu, G. C. Transition-Metal Catalysis of Nucleophilic Substitution Reactions: A Radical Alternative to S_N1 and S_N2 Processes. *ACS Cent. Sci.* **2017**, *3*, 692–700. <https://doi.org/10.1021/acscentsci.7b00212>.
- (10) Egorova, K. S.; Ananikov, V. P. Which Metals Are Green for Catalysis? Comparison of the Toxicities of Ni, Cu, Fe, Pd, Pt, Rh, and Au Salts. *Angew. Chemie - Int. Ed.* **2016**, *55*, 12150–12162. <https://doi.org/10.1002/anie.201603777>.
- (11) Kambe, N.; Iwasaki, T.; Terao, J. Pd-Catalyzed Cross-Coupling Reactions of Alkyl Halides. *Chem. Soc. Rev.* **2011**, *40*, 4937–4947. <https://doi.org/10.1039/c1cs15129k>.
- (12) Kharasch, M. S.; Lambert, F. L. Factors Determining the Course and Mechanisms of Grignard Reactions. III. The Effect of Metallic Halides on the Reaction between Benzophenone and Methylmagnesium Bromide. *J. Am. Chem. Soc.* **1941**, *63*, 2315–2316.
- (13) Tamura, M.; Kochi, J. Vinylation of Grignard Reagents. Catalysis by Iron. *J. Am. Chem. Soc.* **1971**, *93*, 1487–1489. <https://doi.org/10.1021/ja00735a030>.
- (14) Neumann, S. M.; Kochi, J. K. Synthesis of Olefins. Cross Coupling of Alkenyl Halides and Grignard Reagents Catalyzed by Iron Complexes. *J. Org. Chem.* **1975**, *40*, 599–606. <https://doi.org/10.1021/jo00893a013>.
- (15) Johansson Seechurn, C. C. C.; Kitching, M. O.; Colacot, T. J.; Snieckus, V. Palladium-Catalyzed Cross-Coupling: A Historical Contextual Perspective to the 2010 Nobel Prize. *Angew. Chemie - Int. Ed.* **2012**, *51*, 5062–5085.

<https://doi.org/10.1002/anie.201107017>.

- (16) Fürstner, A.; Leitner, A.; Méndez, M.; Krause, H. Iron-Catalyzed Cross-Coupling Reactions. *J. Am. Chem. Soc.* **2002**, *124*, 13856–13863. <https://doi.org/10.1021/ja027190t>.
- (17) Fürstner, A.; Leitner, A.; Méndez, M.; Krause, H. Iron-Catalyzed Cross-Coupling Reactions Iron-Catalyzed Cross-Coupling Reactions. *Tetrahedron* **2002**, *124*, 13856–13863. <https://doi.org/10.1021/ja027190t>.
- (18) Fürstner, A.; Martin, R.; Krause, H.; Seidel, G.; Goddard, R.; Lehmann, C. W. Preparation, Structure, and Reactivity of Nonstabilized Organoiron Compounds. Implications for Iron-Catalyzed Cross Coupling Reactions. *J. Am. Chem. Soc.* **2008**, *130*, 8773–8787. <https://doi.org/10.1021/ja801466t>.
- (19) Scheiper, B.; Bonnekessel, M.; Krause, H.; Fürstner, A. Selective Iron-Catalyzed Cross-Coupling Reactions of Grignard Reagents with Enol Triflates, Acid Chlorides, and Dichloroarenes. *J. Org. Chem.* **2004**, *69*, 3943–3949. <https://doi.org/10.1021/jo0498866>.
- (20) Mako, T. L.; Byers, J. A. Recent Advances in Iron-Catalysed Cross Coupling Reactions and Their Mechanistic Underpinning. *Inorg. Chem. Front.* **2016**, *3*, 766–790. <https://doi.org/10.1039/c5qi00295h>.
- (21) Hatakeyama, T.; Nakamura, M. Iron-Catalyzed Selective Biaryl Coupling: Remarkable Suppression of Homocoupling by the Fluoride Anion. *J. Am. Chem. Soc.* **2007**, *129*, 9844–9845. <https://doi.org/10.1021/ja073084l>.
- (22) Sapountzis, I.; Lin, W.; Kofink, C. C.; Despotopoulou, C.; Knochel, P. Iron-Catalyzed Aryl-Aryl Cross-Couplings with Magnesium-Derived Copper Reagents.

Angew. Chemie - Int. Ed. **2005**, *44*, 1654–1658.
<https://doi.org/10.1002/anie.200462013>.

- (23) Thomé, I.; Nijs, A.; Bolm, C. Trace Metal Impurities in Catalysis. *Chem. Soc. Rev.* **2012**, *41*, 979–987. <https://doi.org/10.1039/c2cs15249e>.
- (24) Hatakeyama, T.; Hashimoto, S.; Ishizuka, K.; Nakamura, M. Highly Selective Biaryl Cross-Coupling Reactions between Aryl Halides and Aryl Grignard Reagents: A New Catalyst Combination of N-Heterocyclic Carbenes and Iron, Cobalt, and Nickel Fluorides. *J. Am. Chem. Soc.* **2009**, *131*, 11949–11963. <https://doi.org/10.1021/ja9039289>.
- (25) Chua, Y. Y.; Duong, H. A. Selective Kumada Biaryl Cross-Coupling Reaction Enabled by an Iron(III) Alkoxide-N-Heterocyclic Carbene Catalyst System. *Chem. Commun.* **2014**, *50*, 8424–8427. <https://doi.org/10.1039/c4cc02930e>.
- (26) Constable, D. J. C.; Dunn, P. J.; Hayler, J. D.; Humphrey, G. R.; Leazer, J. L.; Linderman, R. J.; Lorenz, K.; Manley, J.; Pearlman, B. A.; Wells, A.; et al. Key Green Chemistry Research Areas—a Perspective from Pharmaceutical Manufacturers. *Green Chem.* **2007**, *9*, 411–442. <https://doi.org/10.1039/b703488c>.
- (27) Tamao, K.; Sumitani, K.; Kumada, M. Selective Carbon-Carbon Bond Formation by Cross-Coupling of Grignard Reagents with Organic Halides. Catalysis by Nickel-Phosphine Complexes. *J. Am. Chem. Soc.* **1972**, *94*, 4374–4376. <https://doi.org/10.1021/ja00767a075>.
- (28) Corriu, R. J. P.; Masse, J. P. Activation of Grignard Reagents by Transition-Metal Complexes. A New and Simple Synthesis of Trans-Stilbenes and Polyphenyls. *J. Chem. Soc. Chem. Commun.* **1972**, *0*, 7062. <https://doi.org/10.1039/C3972000144a>.

- (29) Ambre, R.; Yang, H.; Chen, W. C.; Yap, G. P. A.; Jurca, T.; Ong, T. G. Nickel Carbodicarbene Catalyzes Kumada Cross-Coupling of Aryl Ethers with Grignard Reagents through C–O Bond Activation. *Eur. J. Inorg. Chem.* **2019**, *2019*, 3511–3517. <https://doi.org/10.1002/ejic.201900692>.
- (30) Nakamura, M.; Matsuo, K.; Ito, S.; Nakamura, E. Iron-Catalyzed Cross-Coupling of Primary and Secondary Alkyl Halides with Aryl Grignard Reagents. *J. Am. Chem. Soc.* **2004**, *126*, 3686–3687. <https://doi.org/10.1021/ja049744t>.
- (31) Nagano, T.; Hayashi, T. Iron-Catalyzed Grignard Cross-Coupling with Alkyl Halides Possessing β -Hydrogens. *Org. Lett.* **2004**, *6*, 1297–1299. <https://doi.org/10.1021/ol049779y>.
- (32) Gao, H. H.; Yan, C. H.; Tao, X. P.; Xia, Y.; Sun, H. M.; Shen, Q.; Zhang, Y. Synthesis of Anionic Iron(II) Complex Bearing an n-Heterocyclic Carbene Ligand and Its Catalysis for Aryl Grignard Cross-Coupling of Alkyl Halides. *Organometallics* **2010**, *29*, 4189–4192. <https://doi.org/10.1021/om100482w>.
- (33) Xue, F.; Zhao, J.; Hor, T. S. A. Iron(I) Complexes with Functionalized Amine-Pyrazolyl Tripodal Ligands in the Cross-Coupling of Aryl Grignard with Alkyl Halides. *Dalt. Trans.* **2011**, *40*, 8935. <https://doi.org/10.1039/c1dt10258c>.
- (34) Yamaguchi, Y.; Ando, H.; Nagaya, M.; Hinago, H.; Ito, T.; Asami, M. Synthesis of Iron(III) Complex Bearing Tridentate β -Aminoketonato Ligand: Application to Iron-Catalyzed Cross-Coupling Reaction of Arylmagnesium Bromides with Alkyl Halides. *Chem. Lett.* **2011**, *40*, 983–985. <https://doi.org/10.1246/cl.2011.983>.
- (35) Hatakeyama, T.; Fujiwara, Y. I.; Okada, Y.; Itoh, T.; Hashimoto, T.; Kawamura, S.; Ogata, K.; Takaya, H.; Nakamura, M. Kumada-Tamao-Corriu Coupling of Alkyl

- Halides Catalyzed by an Iron-Bisphosphine Complex. *Chem. Lett.* **2011**, *40*, 1030–1032. <https://doi.org/10.1246/cl.2011.1030>.
- (36) Sun, C. L.; Krause, H.; Fürstner, A. A Practical Procedure for Iron-Catalyzed Cross-Coupling Reactions of Sterically Hindered Aryl-Grignard Reagents with Primary Alkyl Halides. *Adv. Synth. Catal.* **2014**, *356*, 1281–1291. <https://doi.org/10.1002/adsc.201301089>.
- (37) Mo, Z.; Zhang, Q.; Deng, L. Dinuclear Iron Complex-Catalyzed Cross-Coupling of Primary Alkyl Fluorides with Aryl Grignard Reagents. *Organometallics* **2012**, *31*, 6518–6521. <https://doi.org/10.1021/om300722g>.
- (38) Liu, L.; Lee, W.; Yuan, M.; Acha, C.; Geherty, M. B.; Williams, B.; Gutierrez, O. Intra- and Intermolecular Fe-Catalyzed Dicarbofunctionalization of Vinyl Cyclopropanes. *Chem. Sci.* **2020**, *11*, 3146–3151. <https://doi.org/10.1039/D0SC00467G>.
- (39) Jin, M.; Adak, L.; Nakamura, M. Iron-Catalyzed Enantioselective Cross-Coupling Reactions of α -Chloroesters with Aryl Grignard Reagents. *J. Am. Chem. Soc.* **2015**, *137*, 7128–7134. <https://doi.org/10.1021/jacs.5b02277>.
- (40) Neidig, M. L.; Carpenter, S. H.; Curran, D. J.; Demuth, J. C.; Fleischauer, V. E.; Iannuzzi, T. E.; Neate, P. G. N.; Sears, J. D.; Wolford, N. J. Development and Evolution of Mechanistic Understanding in Iron-Catalyzed Cross-Coupling. *Acc. Chem. Res.* **2019**, *52*, 140–150. <https://doi.org/10.1021/acs.accounts.8b00519>.
- (41) Bedford, R. B.; Brenner, P. B.; Carter, E.; Carvell, T. W.; Cogswell, P. M.; Gallagher, T.; Harvey, J. N.; Murphy, D. M.; Neeve, E. C.; Nunn, J.; et al. Expedient Iron-Catalyzed Coupling of Alkyl, Benzyl and Allyl Halides with Arylboronic

Esters. *Chem. - A Eur. J.* **2014**, *20*, 7935–7938.
<https://doi.org/10.1002/chem.201402174>.

- (42) Hedström, A.; Izakian, Z.; Vreto, I.; Wallentin, C. J.; Norrby, P. O. On the Radical Nature of Iron-Catalyzed Cross-Coupling Reactions. *Chem. - A Eur. J.* **2015**, *21*, 5946–5953. <https://doi.org/10.1002/chem.201406096>.
- (43) Bedford, R. B.; Brenner, P. B.; Carter, E.; Cogswell, P. M.; Haddow, M. F.; Harvey, J. N.; Murphy, D. M.; Nunn, J.; Woodall, C. H. TMEDA in Iron-Catalyzed Kumada Coupling: Amine Adduct versus Homoleptic “Ate” Complex Formation. *Angew. Chemie - Int. Ed.* **2014**, *53*, 1804–1808. <https://doi.org/10.1002/anie.201308395>.
- (44) Lee, W.; Zhou, J.; Gutierrez, O. Mechanism of Nakamura’s Bisphosphine-Iron-Catalyzed Asymmetric C(Sp²)-C(Sp³) Cross-Coupling Reaction: The Role of Spin in Controlling Arylation Pathways. *J. Am. Chem. Soc.* **2017**, *139*, 16126–16133. <https://doi.org/10.1021/jacs.7b06377>.
- (45) Sharma, A. K.; Sameera, W. M. C.; Jin, M.; Adak, L.; Okuzono, C.; Iwamoto, T.; Kato, M.; Nakamura, M.; Morokuma, K. DFT and AFIR Study on the Mechanism and the Origin of Enantioselectivity in Iron-Catalyzed Cross-Coupling Reactions. *J. Am. Chem. Soc.* **2017**, *139*, 16117–16125. <https://doi.org/10.1021/jacs.7b05917>.
- (46) Sharma, A. K.; Sameera, W. M. C.; Jin, M.; Adak, L.; Okuzono, C.; Iwamoto, T.; Kato, M.; Nakamura, M.; Morokuma, K. DFT and AFIR Study on the Mechanism and the Origin of Enantioselectivity in Iron-Catalyzed Cross-Coupling Reactions. *J. Am. Chem. Soc.* **2017**, *139*, 16117–16125. <https://doi.org/10.1021/jacs.7b05917>.
- (47) Lee, W.; Zhou, J.; Gutierrez, O. Mechanism of Nakamura’s Bisphosphine-Iron-Catalyzed Asymmetric C(Sp²)-C(Sp³) Cross-Coupling Reaction: The Role of Spin

- in Controlling Arylation Pathways. *J. Am. Chem. Soc.* **2017**, *139*, 16126–16133. <https://doi.org/10.1021/jacs.7b06377>.
- (48) Daifuku, S. L.; Al-Afyouni, M. H.; Snyder, B. E. R.; Kneebone, J. L.; Neidig, M. L. Erratum: Combined Mössbauer, Magnetic Circular Dichroism, and Density Functional Theory Approach for Iron Cross-Coupling Catalysis: Electronic Structure, in Situ Formation, and Reactivity of Iron-Mesityl-Bisphosphines. *J. Am. Chem. Soc.* **2014**, *136*, 11847. <https://doi.org/10.1021/ja5076162>.
- (49) Daifuku, S. L.; Kneebone, J. L.; Snyder, B. E. R.; Neidig, M. L. Iron(II) Active Species in Iron-Bisphosphine Catalyzed Kumada and Suzuki-Miyaura Cross-Couplings of Phenyl Nucleophiles and Secondary Alkyl Halides. *J. Am. Chem. Soc.* **2015**, *137*, 11432–11444. <https://doi.org/10.1021/jacs.5b06648>.
- (50) Liu, Y.; Xiao, J.; Wang, L.; Song, Y.; Deng, L. Carbon-Carbon Bond Formation Reactivity of a Four-Coordinate NHC-Supported Iron(II) Phenyl Compound. *Organometallics* **2015**, *34*, 599–605. <https://doi.org/10.1021/om501061b>.
- (51) Rousseau, L.; Touati, N.; Binet, L.; Thu, P.; Lefe, G. Relevance of Single-Transmetalated Resting States in Iron-Mediated Cross-Couplings: Unexpected Role of σ -Donating Additives. *J. Am. Chem. Soc.* **2021**, *60*, 7991-7997. <https://doi.org/10.1021/acs.inorgchem.1c00518>.
- (52) Bauer, G.; Wodrich, M. D.; Scopelliti, R.; Hu, X. Iron Pincer Complexes as Catalysts and Intermediates in Alkyl-Aryl Kumada Coupling Reactions. *Organometallics* **2015**, *34*, 289–298. <https://doi.org/10.1021/om501122p>.
- (53) Vechorkin, O.; Proust, V.; Hu, X. Functional Group Tolerant Kumada-Corriu-Tamao Coupling of Nonactivated Alkyl Halides with Aryl and Heteroaryl

- Nucleophiles: Catalysis by a Nickel Pincer Complex Permits the Coupling of Functionalized Grignard Reagents. *J. Am. Chem. Soc.* **2009**, *131*, 9756–9766. <https://doi.org/10.1021/ja9027378>.
- (54) Lou, S.; Fu, G. C. Nickel/Bis(Oxazoline)-Catalyzed Asymmetric Kumada Reactions of Alkyl Electrophiles: Cross-Couplings of Racemic α -Bromoketones. *J. Am. Chem. Soc.* **2010**, *132*, 1264–1266. <https://doi.org/10.1021/ja909689t>.
- (55) Cahiez, G.; Avedissian, H. Highly Stereo and Chemoselective Iron-Catalyzed Alkenylation of Organomagnesium Compounds. *Synthesis*. **1998**, *8*, 1199–1205. <https://doi.org/10.1055/s-1998-2135>.
- (56) Muñoz, S. B.; Daifuku, S. L.; Sears, J. D.; Baker, T. M.; Carpenter, S. H.; Brennessel, W. W.; Neidig, M. L. The N-Methylpyrrolidone (NMP) Effect in Iron-Catalyzed Cross-Coupling with Simple Ferric Salts and MeMgBr. *Angew. Chemie - Int. Ed.* **2018**, *57*, 6496–6500. <https://doi.org/10.1002/anie.201802087>.
- (57) Gogsig, T. M.; Lindhardt, A. T.; Skrydstrup, T. Heteroaromatic Sulfonates and Phosphates as Electrophiles in Iron-Catalyzed Cross-Couplings. *Org. Lett.* **2009**, *11*, 4886–4888. <https://doi.org/10.1021/ol901975u>.
- (58) Gülak, S.; Gieshoff, T. N.; Von Wangelin, A. J. Olefin-Assisted Iron-Catalyzed Alkylation of Aryl Chlorides. *Adv. Synth. Catal.* **2013**, *355*, 2197–2202. <https://doi.org/10.1002/adsc.201300095>.
- (59) Gärtner, D.; Stein, A. L.; Grupe, S.; Arp, J.; Von Wangelin, A. J. Iron-Catalyzed Cross-Coupling of Alkenyl Acetates. *Angew. Chemie - Int. Ed.* **2015**, *54*, 10545–10549. <https://doi.org/10.1002/anie.201504524>.
- (60) Nishikado, H.; Nakatsuji, H.; Ueno, K.; Nagase, R.; Tanabe, Y. Mild, Efficient, and

- Robust Method for Stereocomplementary Iron-Catalyzed Cross-Coupling Using (*E*)- and (*Z*)-Enol Tosylates. *Synlett* **2010**, *14*, 2087–2092. <https://doi.org/10.1055/s-0030-1258131>.
- (61) Bisz, E.; Szostak, M. Iron-Catalyzed C(Sp²)-C(Sp³) Cross-Coupling of Aryl Chlorobenzoates with Alkyl Grignard Reagents. *Molecules* **2020**, *25*, 1–13. <https://doi.org/10.3390/molecules25010230>.
- (62) Agrawal, T.; Cook, S. P. Iron-Catalyzed Cross-Coupling Reactions of Alkyl Grignards with Aryl Sulfamates and Tosylates. *Org. Lett.* **2013**, *15*, 96–99. <https://doi.org/10.1021/ol303130j>.
- (63) Perry, M. C.; Gillett, A. N.; Law, T. C. An Unprecedented Iron-Catalyzed Cross-Coupling of Primary and Secondary Alkyl Grignard Reagents with Non-Activated Aryl Chlorides. *Tetrahedron Lett.* **2012**, *53*, 4436–4439. <https://doi.org/10.1016/j.tetlet.2012.06.048>.
- (64) Agata, R.; Iwamoto, T.; Nakagawa, N.; Isozaki, K.; Hatakeyama, T.; Takaya, H.; Nakamura, M. Iron Fluoride/N-Heterocyclic Carbene Catalyzed Cross Coupling between Deactivated Aryl Chlorides and Alkyl Grignard Reagents with or without β -Hydrogens. *Synth.* **2015**, *47*, 1733–1740. <https://doi.org/10.1055/s-0034-1380361>.
- (65) Li, Z.; Liu, L.; Sun, H. M.; Shen, Q.; Zhang, Y. Alkyl Grignard Cross-Coupling of Aryl Phosphates Catalyzed by New, Highly Active Ionic Iron(II) Complexes Containing a Phosphine Ligand and an Imidazolium Cation. *Dalt. Trans.* **2016**, *45*, 17739–17747. <https://doi.org/10.1039/c6dt02995g>.
- (66) Sanderson, J. N.; Dominey, A. P.; Percy, J. M. Iron-Catalyzed Isopropylation of

- Electron-Deficient Aryl and Heteroaryl Chlorides. *Adv. Synth. Catal.* **2017**, *359*, 1007–1017. <https://doi.org/10.1002/adsc.201601097>.
- (67) Kwan, C. L.; Kochi, J. K. Electron Spin Resonance Studies of the Reduction of Transition Metal Complexes with Grignard Reagents. 1. Dianion Radicals of β -Diketonates. *J. Am. Chem. Soc.* **1976**, *98*, 4903–4912. <https://doi.org/10.1021/ja00432a035>.
- (68) Smith, R. S.; Kochi, J. K. Mechanistic Studies of Iron Catalysis in the Cross Coupling of Alkenyl Halides and Grignard Reagents. *J. Org. Chem.* **1976**, *41*, 502–509. <https://doi.org/10.1021/jo00865a019>.
- (69) Al-Afyouni, M. H.; Fillman, K. L.; Brennessel, W. W.; Neidig, M. L. Isolation and Characterization of a Tetramethyliron(III) Ferrate: An Intermediate in the Reduction Pathway of Ferric Salts with MeMgBr. *J. Am. Chem. Soc.* **2014**, *136*, 15457–15460. <https://doi.org/10.1021/ja5080757>.
- (70) Aleandri, L. E.; Bogdanović, B.; Bons, P.; Durr, C.; Gaidies, A.; Hartwig, T.; Hockett, S. C.; Lagarden, M.; Wilczok, U.; Brand, R. A. Inorganic Grignard Reagents. Preparation and Their Application for the Synthesis of Highly Active Metals, Intermetallics, and Alloys. *Chem. Mater.* **1995**, *7*, 1153–1170. <https://doi.org/10.1021/cm00054a015>.
- (71) Bogdanovi, B.; Schwickardi, M. Transition Metal Catalyzed Preparation of Grignard Compounds. *Angew. Chemie - Int. Ed.* **2000**, *39*, 4610–4612. [https://doi.org/10.1002/1521-3773\(20001215\)39:24<4610::AID-ANIE4610>3.0.CO;2-O](https://doi.org/10.1002/1521-3773(20001215)39:24<4610::AID-ANIE4610>3.0.CO;2-O).
- (72) Tamao, K.; Kodama, S.; Nakajima, I.; Kumada, M.; Minato, A.; Suzuki, K. Nickel-

- Phosphine Complex-Catalyzed Grignard Coupling-II. Grignard Coupling of Heterocyclic Compounds. *Tetrahedron* **1982**, 38, 3347–3354. [https://doi.org/10.1016/0040-4020\(82\)80117-8](https://doi.org/10.1016/0040-4020(82)80117-8).
- (73) Wang, J. R.; Manabe, K. High Ortho Preference in Ni-Catalyzed Cross-Coupling of Halophenols with Alkyl Grignard Reagents. *Org. Lett.* **2009**, 11, 741–744. <https://doi.org/10.1021/ol802824b>.
- (74) Ho, Y. A.; Leiendecker, M.; Liu, X.; Wang, C.; Alandini, N.; Rueping, M. Nickel-Catalyzed Csp²-Csp³ Bond Formation via C-F Bond Activation. *Org. Lett.* **2018**, 20, 5644–5647. <https://doi.org/10.1021/acs.orglett.8b02351>.
- (75) Roques, N.; Saint-Jalmes, L. Efficient Access to 3-Alkyl-Trifluoromethylbenzenes Using Kumada's Coupling Reaction. *Tetrahedron Lett.* **2006**, 47, 3375–3378. <https://doi.org/10.1016/j.tetlet.2006.03.076>.
- (76) Guan, B. T.; Xiang, S. K.; Wu, T.; Sun, Z. P.; Wang, B. Q.; Zhao, K. Q.; Shi, Z. J. Methylation of Arenes via Ni-Catalyzed Aryl C-O/F Activation. *Chem. Commun.* **2008**, 2, 1437–1439. <https://doi.org/10.1039/b718998b>.
- (77) Tobisu, M.; Takahira, T.; Morioka, T.; Chatani, N. Nickel-Catalyzed Alkylative Cross-Coupling of Anisoles with Grignard Reagents via C-O Bond Activation. *J. Am. Chem. Soc.* **2016**, 138, 6711–6714. <https://doi.org/10.1021/jacs.6b03253>.
- (78) Busacca, C. A.; Eriksson, M. C.; Fiaschi, R. Cross Coupling of Vinyl Triflates and Alkyl Grignard Reagents Catalyzed by Nickel(0)-Complexes. *Tetrahedron Lett.* **1999**, 40, 3101–3104. [https://doi.org/10.1016/S0040-4039\(99\)00439-6](https://doi.org/10.1016/S0040-4039(99)00439-6).
- (79) Joshi-Pangu, A.; Wang, C. Y.; Biscoe, M. R. Nickel-Catalyzed Kumada Cross-Coupling Reactions of Tertiary Alkylmagnesium Halides and Aryl

- Bromides/Triflates. *J. Am. Chem. Soc.* **2011**, *133*, 8478–8481.
<https://doi.org/10.1021/ja202769t>.
- (80) Lohre, C.; Dröge, T.; Wang, C.; Glorius, F. Nickel-Catalyzed Cross-Coupling of Aryl Bromides with Tertiary Grignard Reagents Utilizing Donor-Functionalized N-Heterocyclic Carbenes (NHCs). *Chem. - A Eur. J.* **2011**, *17*, 6052–6055.
<https://doi.org/10.1002/chem.201100909>.
- (81) Wu, Z.; Si, T.; Xu, G.; Xu, B.; Tang, W. Ligand-Free Nickel-Catalyzed Kumada Couplings of Aryl Bromides with Tert-Butyl Grignard Reagents. *Chinese Chem. Lett.* **2019**, *30*, 597–600. <https://doi.org/10.1016/j.ccllet.2018.12.027>.
- (82) Joshi-Pangu, A.; Biscoe, M. R. The Use of Tertiary Alkylmagnesium Nucleophiles in Ni-Catalyzed Cross-Coupling Reactions. *Synlett* **2012**, *23*, 1103–1107.
<https://doi.org/10.1055/s-0031-1290765>.
- (83) Iwasaki, T.; Shimizu, R.; Imanishi, R.; Kuniyasu, H.; Kambe, N. Cross-Coupling Reaction of Alkyl Halides with Alkyl Grignard Reagents Catalyzed by Cp-Iron Complexes in the Presence of 1,3-Butadiene. *Chem. Lett.* **2018**, *47*, 763–766.
<https://doi.org/10.1246/cl.180201>.
- (84) Gartia, Y.; Pulla, S.; Ramidi, P.; Farris, C. C.; Nima, Z.; Jones, D. E.; Biris, A. S.; Ghosh, A. A Novel Iron Complex for Cross-Coupling Reactions of Multiple C-Cl Bonds in Polychlorinated Solvents with Grignard Reagents. *Catal. Letters* **2012**, *142*, 1397–1404. <https://doi.org/10.1007/s10562-012-0913-2>.
- (85) Domingo-Legarda, P.; Soler-Yanes, R.; Quirós-López, M. T.; Buñuel, E.; Cárdenas, D. J. Iron-Catalyzed Coupling of Propargyl Bromides and Alkyl Grignard Reagents. *European J. Org. Chem.* **2018**, *2018*, 4900–4904.

- <https://doi.org/10.1002/ejoc.201800849>.
- (86) Dongol, K. G.; Koh, H.; Sau, M.; Chai, C. L. L. Iron-Catalysed Sp³-Sp³ Cross-Coupling Reactions of Unactivated Alkyl Halides with Alkyl Grignard Reagents. *Adv. Synth. Catal.* **2007**, *349*, 1015–1018. <https://doi.org/10.1002/adsc.200600383>.
- (87) Guisán-Ceinos, M.; Tato, F.; Buñuel, E.; Calle, P.; Cárdenas, D. J. Fe-Catalysed Kumada-Type Alkyl-Alkyl Cross-Coupling. Evidence for the Intermediacy of Fe(i) Complexes. *Chem. Sci.* **2013**, *4*, 1098–1104. <https://doi.org/10.1039/c2sc21754f>.
- (88) Fleischauer, V. E.; Muñoz, S. B.; Neate, P. G. N.; Brennessel, W. W.; Neidig, M. L. NHC and Nucleophile Chelation Effects on Reactive Iron(II) Species in Alkyl-Alkyl Cross-Coupling. *Chem. Sci.* **2018**, *9*, 1878–1891. <https://doi.org/10.1039/c7sc04750a>.
- (89) Tindall, D. J.; Krause, H.; Fürstner, A. Iron-Catalyzed Cross-Coupling of 1-Alkynylcyclopropyl Tosylates and Related Substrates. *Adv. Synth. Catal.* **2016**, *358*, 2398–2403. <https://doi.org/10.1002/adsc.201600357>.
- (90) Przyojski, J. A.; Veggeberg, K. P.; Arman, H. D.; Tonzetich, Z. J. Mechanistic Studies of Catalytic Carbon-Carbon Cross-Coupling by Well-Defined Iron NHC Complexes. *ACS Catal.* **2015**, *5*, 5938–5946. <https://doi.org/10.1021/acscatal.5b01445>.
- (91) Terao, J.; Watanabe, H.; Ikumi, A.; Kuniyasu, H.; Kambe, N. Nickel-Catalyzed Cross-Coupling Reaction of Grignard Reagents with Alkyl Halides and Tosylates: Remarkable Effect of 1,3-Butadienes. *J. Am. Chem. Soc.* **2002**, *124*, 4222–4223. <https://doi.org/10.1021/ja025828v>.
- (92) Guan, B. T.; Xiang, S. K.; Wang, B. Q.; Sun, Z. P.; Wang, Y.; Zhao, K. Q.; Shi, Z.

- J. Direct Benzylic Alkylation via Ni-Catalyzed Selective Benzylic Sp³ C-O Activation. *J. Am. Chem. Soc.* **2008**, *130*, 3268–3269. <https://doi.org/10.1021/ja710944j>.
- (93) Soler-Yanes, R.; Guisán-Ceinos, M.; Buñuel, E.; Cárdenas, D. J. Nickel-Catalyzed Kumada Coupling of Benzyl Chlorides and Vinylogous Derivatives. *European J. Org. Chem.* **2014**, *2014*, 6625–6629. <https://doi.org/10.1002/ejoc.201403007>.
- (94) Singh, S. P.; Terao, J.; Kambe, N. Nickel-Catalyzed Cross-Coupling of Unactivated Alkyl Halides and Tosylate Carrying a Functional Group with Alkyl and Phenyl Grignard Reagents. *Tetrahedron Lett.* **2009**, *50*, 5644–5646. <https://doi.org/10.1016/j.tetlet.2009.07.094>.
- (95) Iwasaki, T.; Higashikawa, K.; Reddy, V. P.; Ho, W. W. S.; Fujimoto, Y.; Fukase, K.; Terao, J.; Kuniyasu, H.; Kambe, N. Nickel-Butadiene Catalytic System for the Cross-Coupling of Bromoalkanoic Acids with Alkyl Grignard Reagents: A Practical and Versatile Method for Preparing Fatty Acids. *Chem. - A Eur. J.* **2013**, *19*, 2956–2960. <https://doi.org/10.1002/chem.201204222>.
- (96) Vechorkin, O.; Hu, X. Nickel-Catalyzed Cross-Coupling of Non-Activated and Functionalized Alkyl Halides with Alkyl Grignard Reagents. *Angew. Chemie - Int. Ed.* **2009**, *48*, 2937–2940. <https://doi.org/10.1002/anie.200806138>.
- (97) Perez Garcia, P. M.; Di Franco, T.; Orsino, A.; Ren, P.; Hu, X. Nickel-Catalyzed Diastereoselective Alkyl-Alkyl Kumada Coupling Reactions. *Org. Lett.* **2012**, *14*, 4286–4289. <https://doi.org/10.1021/ol302067b>.
- (98) Taylor, B. L. H.; Swift, E. C.; Waetzig, J. D.; Jarvo, E. R. Stereospecific Nickel-Catalyzed Cross-Coupling Reactions of Alkyl Ethers: Enantioselective Synthesis of

- Diarylethanes. *J. Am. Chem. Soc.* **2011**, *133*, 389–391.
<https://doi.org/10.1021/ja108547u>.
- (99) Greene, M. A.; Yonova, I. M.; Williams, F. J.; Jarvo, E. R. Traceless Directing Group for Stereospecific Nickel-Catalyzed Alkyl-Alkyl Cross-Coupling Reactions. *Org. Lett.* **2012**, *14*, 4293–4296. <https://doi.org/10.1021/ol300891k>.
- (100) Yonova, I. M.; Johnson, A. G.; Osborne, C. A.; Moore, C. E.; Morrissette, N. S.; Jarvo, E. R. Stereospecific Nickel-Catalyzed Cross-Coupling Reactions of Alkyl Grignard Reagents and Identification of Selective Anti-Breast-Cancer Agents. *Angew. Chemie - Int. Ed.* **2014**, *53*, 2422–2427.
<https://doi.org/10.1002/anie.201308666>.
- (101) Bedford, R. B.; Hall, M. A.; Hodges, G. R.; Huwe, M.; Wilkinson, M. C. Simple Mixed Fe-Zn Catalysts for the Suzuki Couplings of Tetraarylborates with Benzyl Halides and 2-Halopyridines. *Chem. Commun.* **2009**, *42*, 6430–6432.
<https://doi.org/10.1039/b915945b>.
- (102) Agata, R.; Kawamura, S.; Isozaki, K.; Nakamura, M. Iron-Catalyzed Alkyl-Alkyl Negishi Coupling of Organoaluminum Reagents. *Chem. Lett.* **2018**, *48*, 238–241.
<https://doi.org/10.1246/cl.180954>.
- (103) Xi, Z.; Zhou, Y.; Chen, W. Efficient Negishi Coupling Reactions of Aryl Chlorides Catalyzed by Binuclear and Mononuclear Nickel-N-Heterocyclic Carbene Complexes. *J. Org. Chem.* **2008**, *73*, 8497–8501.
<https://doi.org/10.1021/jo8018686>.
- (104) Gerber, R.; Frech, C. M. Negishi Cross-Coupling Reactions Catalyzed by an Aminophosphine-Based Nickel System: A Reliable and General Applicable

- Reaction Protocol for the High-Yielding Synthesis of Biaryls. *Chem. - A Eur. J.* **2011**, *17*, 11893–11904. <https://doi.org/10.1002/chem.201101037>.
- (105) Xie, L. G.; Wang, Z. X. Nickel-Catalyzed Cross-Coupling of Aryltrimethylammonium Iodides with Organozinc Reagents. *Angew. Chemie - Int. Ed.* **2011**, *50*, 4901–4904. <https://doi.org/10.1002/anie.201100683>.
- (106) Zhang, X. Q.; Wang, Z. X. Cross-Coupling of Aryltrimethylammonium Iodides with Arylzinc Reagents Catalyzed by Amido Pincer Nickel Complexes. *J. Org. Chem.* **2012**, *77*, 3658–3663. <https://doi.org/10.1021/jo300209d>.
- (107) Nakamura, M.; Ito, S.; Matsuo, K.; Nakamura, E. Iron-Catalyzed Chemoselective Cross-Coupling of Primary and Secondary Alkyl Halides with Arylzinc Reagents. *Synlett* **2005**, *11*, 1794–1798. <https://doi.org/10.1055/s-2005-871541>.
- (108) Bedford, R. B.; Huwe, M.; Wilkinson, M. C. Iron-Catalysed Negishi Coupling of Benzyl Halides and Phosphates. *Chem. Commun.* **2009**, *5*, 600–602. <https://doi.org/10.1039/b818961g>.
- (109) Hatakeyama, T.; Nakagawa, N.; Nakamura, M. Iron-Catalyzed Negishi Coupling toward an Effective Olefin Synthesis. *Org. Lett.* **2009**, *11*, 4496–4499. <https://doi.org/10.1021/ol901555r>.
- (110) Ito, S.; Fujiwara, Y. I.; Nakamura, E.; Nakamura, M. Iron-Catalyzed Cross-Coupling of Alkyl Sulfonates with Arylzinc Reagents. *Org. Lett.* **2009**, *11*, 4306–4309. <https://doi.org/10.1021/ol901610a>.
- (111) Tamura, M.; Kochi, J. Coupling of Grignard Reagents with Organic Halides. *Synth.* **1971**, *1971*, 303–305. <https://doi.org/10.1055/s-1971-35043>.
- (112) Adams, C. J.; Bedford, R. B.; Carter, E.; Gower, N. J.; Haddow, M. F.; Harvey, J.

- N.; Huwe, M.; Cartes, M. Á.; Mansell, S. M.; Mendoza, C.; et al. Iron(I) in Negishi Cross-Coupling Reactions. *J. Am. Chem. Soc.* **2012**, *134*, 10333–10336. <https://doi.org/10.1021/ja303250t>.
- (113) Messinis, A. M.; Luckham, S. L. J.; Wells, P. P.; Gianolio, D.; Gibson, E. K.; O'Brien, H. M.; Sparkes, H. A.; Davis, S. A.; Callison, J.; Elorriaga, D.; et al. The Highly Surprising Behaviour of Diphosphine Ligands in Iron-Catalysed Negishi Cross-Coupling. *Nat. Catal.* **2019**, *2*, 123–133. <https://doi.org/10.1038/s41929-018-0197-z>.
- (114) Smith, S. W.; Fu, G. C. Nickel-Catalyzed Asymmetric Cross-Couplings of Racemic Propargylic Halides with Arylzinc Reagents. *J. Am. Chem. Soc.* **2008**, *130*, 12645–12647. <https://doi.org/10.1021/ja805165y>.
- (115) Choi, J.; Fu, G. C. Catalytic Asymmetric Synthesis of Secondary Nitriles via Stereoconvergent Negishi Arylations and Alkenylations of Racemic α -Bromonitriles. *J. Am. Chem. Soc.* **2012**, *134*, 9102–9105. <https://doi.org/10.1021/ja303442q>.
- (116) Do, H. Q.; Chandrashekar, E. R. R.; Fu, G. C. Nickel/Bis(Oxazoline)-Catalyzed Asymmetric Negishi Arylations of Racemic Secondary Benzylic Electrophiles to Generate Enantioenriched 1,1-Diarylalkanes. *J. Am. Chem. Soc.* **2013**, *135*, 16288–16291. <https://doi.org/10.1021/ja408561b>.
- (117) Liang, Y.; Fu, G. C. Catalytic Asymmetric Synthesis of Tertiary Alkyl Fluorides: Negishi Cross-Couplings of Racemic α,α -Dihaloketones. *J. Am. Chem. Soc.* **2014**, *136*, 5520–5524. <https://doi.org/10.1021/ja501815p>.
- (118) Liang, Y.; Fu, G. C. Stereoconvergent Negishi Arylations of Racemic Secondary

- Alkyl Electrophiles: Differentiating between a CF₃ and an Alkyl Group. *J. Am. Chem. Soc.* **2015**, *137*, 9523–9526. <https://doi.org/10.1021/jacs.5b04725>.
- (119) Terao, J.; Todo, H.; Watanabe, H.; Ikumi, A.; Kambe, N. Nickel-Catalyzed Cross-Coupling Reaction of Alkyl Halides with Organozinc and Grignard Reagents with 1,3,8,10-Tetraenes as Additives. *Angew. Chemie - Int. Ed.* **2004**, *43*, 6180–6182. <https://doi.org/10.1002/anie.200460246>.
- (120) Jensen, A. E.; Knochel, P. Nickel-Catalyzed Cross-Coupling between Functionalized Primary or Secondary Alkylzinc Halides and Primary Alkyl Halides. *J. Org. Chem.* **2002**, *67*, 79–85. <https://doi.org/10.1021/jo0105787>.
- (121) Smith, S. W.; Fu, G. C. Nickel-Catalyzed Negishi Cross-Couplings of Secondary Nucleophiles with Secondary Propargylic Electrophiles at Room Temperature. *Angew. Chemie - Int. Ed.* **2008**, *47*, 9334–9336. <https://doi.org/10.1002/anie.200802784>.
- (122) Mu, X.; Shibata, Y.; Makida, Y.; Fu, G. C. Control of Vicinal Stereocenters through Nickel-Catalyzed Alkyl–Alkyl Cross-Coupling. *Angew. Chemie - Int. Ed.* **2017**, *56*, 5821–5824. <https://doi.org/10.1002/anie.201702402>.
- (123) Cordier, C. J.; Lundgren, R. J.; Fu, G. C. Enantioconvergent Cross-Couplings of Racemic Alkylmetal Reagents with Unactivated Secondary Alkyl Electrophiles: Catalytic Asymmetric Negishi α -Alkylations of N-Boc-Pyrrolidine. *J. Am. Chem. Soc.* **2013**, *135*, 10946–10949. <https://doi.org/10.1021/ja4054114>.
- (124) Huo, H.; Gorsline, B. J.; Fu, G. C. Catalyst-Controlled Doubly Enantioconvergent Coupling of Racemic Alkyl Nucleophiles and Electrophiles. *Science* **2020**, *367*, 559–564. <https://doi.org/10.1126/science.aaz3855>.

- (125) Bedford, R. B.; Nakamura, M.; Gower, N. J.; Haddow, M. F.; Hall, M. A.; Huwe, M.; Hashimoto, T.; Okopie, R. A. Iron-Catalysed Suzuki Coupling? A Cautionary Tale. *Tetrahedron Lett.* **2009**, *50*, 6110–6111. <https://doi.org/10.1016/j.tetlet.2009.08.022>.
- (126) Miyaura, N.; Suzuki, A. Stereoselective Synthesis of Arylated (E)-Alkenes by the Reaction of Alk-1-Enylboranes with Aryl Halides in the Presence of Palladium Catalyst. *J. Chem. Soc. Chem. Commun.* **1979**, *19*, 866–867. <https://doi.org/10.1039/C39790000866>.
- (127) O'Brien, H. M.; Manzotti, M.; Abrams, R. D.; Elorriaga, D.; Sparkes, H. A.; Davis, S. A.; Bedford, R. B. Iron-Catalysed Substrate-Directed Suzuki Biaryl Cross-Coupling. *Nat. Catal.* **2018**, *1*, 429–437. <https://doi.org/10.1038/s41929-018-0081-x>.
- (128) Hatakeyama, T.; Hashimoto, T.; Kathriarachchi, K. K. A. D. S.; Zenmyo, T.; Seike, H.; Nakamura, M. Iron-Catalyzed Alkyl-Alkyl Suzuki-Miyaura Coupling. *Angew. Chemie - Int. Ed.* **2012**, *51*, 8834–8837. <https://doi.org/10.1002/anie.201202797>.
- (129) Blakey, S. B.; MacMillan, D. W. C. The First Suzuki Cross-Couplings of Aryltrimethylammonium Salts. *J. Am. Chem. Soc.* **2003**, *125*, 6046–6047. <https://doi.org/10.1021/ja034908b>.
- (130) Tobisu, M.; Xu, T.; Shimasaki, T.; Chatani, N. Nickel-Catalyzed Suzuki-Miyaura Reaction of Aryl Fluorides. *J. Am. Chem. Soc.* **2011**, *133*, 19505–19511. <https://doi.org/10.1021/ja207759e>.
- (131) Quasdorf, K. W.; Antoft-Finch, A.; Liu, P.; Silberstein, A. L.; Komaromi, A.; Blackburn, T.; Ramgren, S. D.; Houk, K. N.; Snieckus, V.; Garg, N. K. Suzuki-

- Miyaura Cross-Coupling of Aryl Carbamates and Sulfamates: Experimental and Computational Studies. *J. Am. Chem. Soc.* **2011**, *133*, 6352–6363. <https://doi.org/10.1021/ja200398c>.
- (132) Tobisu, M.; Shimasaki, T.; Chatani, N. Nickel-Catalyzed Cross-Coupling of Aryl Methyl Ethers with Aryl Boronic Esters. *Angew. Chemie - Int. Ed.* **2008**, *47*, 4866–4869. <https://doi.org/10.1002/anie.200801447>.
- (133) Leowanawat, P.; Zhang, N.; Percec, V. Nickel Catalyzed Cross-Coupling of Aryl C-O Based Electrophiles with Aryl Neopentylglycolboronates. *J. Org. Chem.* **2012**, *77*, 1018–1025. <https://doi.org/10.1021/jo2022982>.
- (134) Nakamura, M.; Hatakeyama, T.; Hashimoto, T.; Kondo, Y.; Fujiwara, Y.; Seike, H.; Takaya, H.; Tamada, Y.; Ono, T. Iron-Catalyzed Suzuki-Miyaura Coupling of Alkyl Halides. *J. Am. Chem. Soc.* **2010**, *132*, 10674–10676. <https://doi.org/10.1021/ja103973a>.
- (135) Zhou, J.; Fu, G. C. Suzuki Cross-Couplings of Unactivated Secondary Alkyl Bromides and Iodides. *J. Am. Chem. Soc.* **2004**, *126*, 1340–1341. <https://doi.org/10.1021/ja039889k>.
- (136) Zultanski, S. L.; Fu, G. C. Nickel-Catalyzed Carbon-Carbon Bond-Forming Reactions of Unactivated Tertiary Alkyl Halides: Suzuki Arylations. *J. Am. Chem. Soc.* **2013**, *135*, 624–627. <https://doi.org/10.1021/ja311669p>.
- (137) Wilsily, A.; Tramutola, F.; Owston, N. A.; Fu, G. C. New Directing Groups for Metal-Catalyzed Asymmetric Carbon-Carbon Bond-Forming Processes: Stereoconvergent Alkyl-Alkyl Suzuki Cross-Couplings of Unactivated Electrophiles. *J. Am. Chem. Soc.* **2012**, *134*, 5794–5797.

<https://doi.org/10.1021/ja301612y>.

- (138) Lu, Z.; Wilsily, A.; Fu, G. C. Stereoconvergent Amine-Directed Alkyl-Alkyl Suzuki Reactions of Unactivated Secondary Alkyl Chlorides. *J. Am. Chem. Soc.* **2011**, *133*, 8154–8157. <https://doi.org/10.1021/ja203560q>.
- (139) Owston, N. A.; Fu, G. C. Asymmetric Alkyl-Alkyl Cross-Couplings of Unactivated Secondary Alkyl Electrophiles: Stereoconvergent Suzuki Reactions of Racemic Acylated Halohydrins. *J. Am. Chem. Soc.* **2010**, *132*, 11908–11909. <https://doi.org/10.1021/ja105924f>.
- (140) Zultanski, S. L.; Fu, G. C. Catalytic Asymmetric γ -Alkylation of Carbonyl Compounds via Stereoconvergent Suzuki Cross-Couplings. *J. Am. Chem. Soc.* **2011**, *133*, 15362–15364. <https://doi.org/10.1021/ja2079515>.

Chapter 2. Iron-Catalyzed Suzuki-Miyaura Crossed -Coupling Reactions Between Alkyl Halides and Unactivated Aryl Boronic Esters

Note: Part of chapter 2 appears in *Org. Lett.* **2018**, *20* (17), 5233–5237.

2.1 Introduction

Transition-metal catalyzed cross-coupling reactions between organohalides and organometallic reagents are robust methodologies for the efficient construction of carbon-carbon and carbon-heteroatom bonds in organic synthesis.¹ Industry and academia rely on cross-coupling reactions because of their efficiency, scalability, and functional-group tolerance, resulting in the development of extensive libraries of compounds now available to synthetic chemists.² An attractive cross-coupling variant is the Suzuki-Miyaura cross-coupling reaction, which employs nucleophilic organoboron reagents and organohalide electrophiles.³ The Suzuki-Miyaura reaction is particularly appealing because organoboron reagents are relatively nontoxic, easily synthesized, and air stable, allowing for easy handling compared to other more air and water sensitive organometallic reagents employed in other cross-coupling reactions.

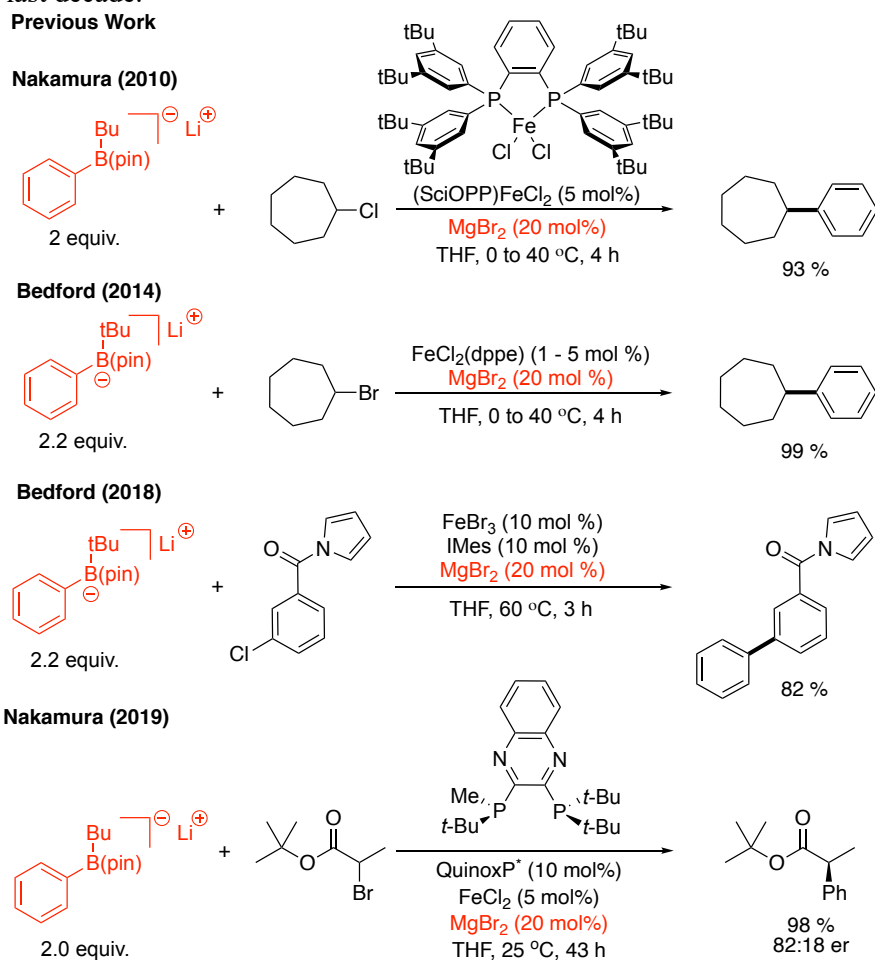
Despite the successful implementation of Suzuki-Miyaura cross-coupling reactions in industry for the synthesis of complex drug molecules,⁴ predominately employed palladium-based catalysts suffer from high cost and toxicity and requiring extensive purification from the final active pharmaceutical ingredient.⁵ Furthermore, palladium-based catalysts can exhibit undesirable reactivity due to rapid β -hydride elimination reactions, forming stable palladium-olefin complexes.⁶ As a result, the Suzuki-Miyaura reaction has been primarily used for substrates containing C(sp²)-hybridized centers for the construction of flat molecules with biaryl moieties. Tremendous advances in ligand design⁷ and pre-catalyst development⁸ over the past 20 years has greatly increased the reactivity of palladium-based complexes, leading to the development of challenging cross-coupling reactions using sterically encumbered substrates⁹ as well as primary alkyl electrophiles.¹⁰

However, these examples are typically limited to primary alkyl halides due to palladium proceeding through an S_N2 oxidative addition.⁷

To address the economic and synthetic limitations that plague palladium-based catalysts, recent efforts have been devoted to using non-noble first row transition metals, particularly with the use of nickel,¹¹ iron¹² and cobalt-based catalysts (Chapter 1).¹³ Nickel has recently emerged as an effective catalyst for the use of alkyl electrophiles with aryl and alkyl organoboron nucleophiles. Seminal work from the Fu group has greatly advanced the use of nickel-based catalysts for Suzuki-Miyaura couplings of alkyl halides, especially for enantioselective variants and $C(sp^3)$ - $C(sp^3)$ bond forming reactions.⁶ Similarly, iron-based catalysts have enjoyed a recent renaissance in popularity since their original discovery by Kochi in the 1970s as competent metals for cross-coupling reactions for the incorporation of $C(sp^3)$ -hybridized centers.¹⁴ Furstner,^{15,16} Nakamura,¹⁷ Bedford,¹⁸ Hu,¹⁹ and others have pioneered the use of iron-based catalysts for a variety of cross-coupling reactions as presented in Chapter 1.²⁰ The utilization of iron-based catalysts would be economically and environmentally beneficial since iron is highly abundant in the earth's crust and less toxic compared to palladium and nickel salts.⁵ Moreover, iron-based catalysts often demonstrate unique reactivity, providing fast reaction kinetics and access to reaction pathways that utilize one and/or two-electron redox processes. The distinguishing features of iron-based catalysts have led to the development of cross-coupling of $C(sp^2)$ and $C(sp^3)$ containing organohalides with alkyl,¹ aryl,¹² vinyl,^{21,22} or alkynyl²³ organometallic reagents. Despite significant advances of iron-mediated cross-coupling reactions using Grignard reagents (i.e. Kumada-type) and organozinc reagents (i.e. Negishi-type), there has been a dearth of iron-based catalysts used for Suzuki-Miyaura cross-coupling reactions. The few known

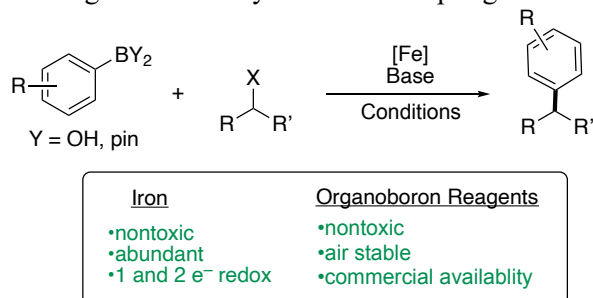
examples of Suzuki-Miyaura reactions rely on highly activated borate species generated by the addition of alkyl lithium reagents to boronic esters and require the use of additives (MgBr_2) to achieve high yields (Scheme 2.1).^{24,25} The requirement for highly activated boronic esters has limited its industrial application, which inspired us to investigate the underlying reasons for these demanding conditions. The need for activated borates and magnesium bromides additives are surprising considering the efficiency of iron-based catalyst in Kumada cross-couplings (Chapter 1). In addition, the development of a Suzuki-Miyaura reaction catalyzed by an iron-based catalyst would be a worthwhile endeavor and highly beneficial for the pharmaceutical industry because of the synergistic environmental

Scheme 2.1. Previously developed iron-catalyzed Suzuki-Miyaura cross-coupling reactions over the last decade.



and reactivity advantages associated with boron nucleophiles and iron cross-coupling (Scheme 2.2).

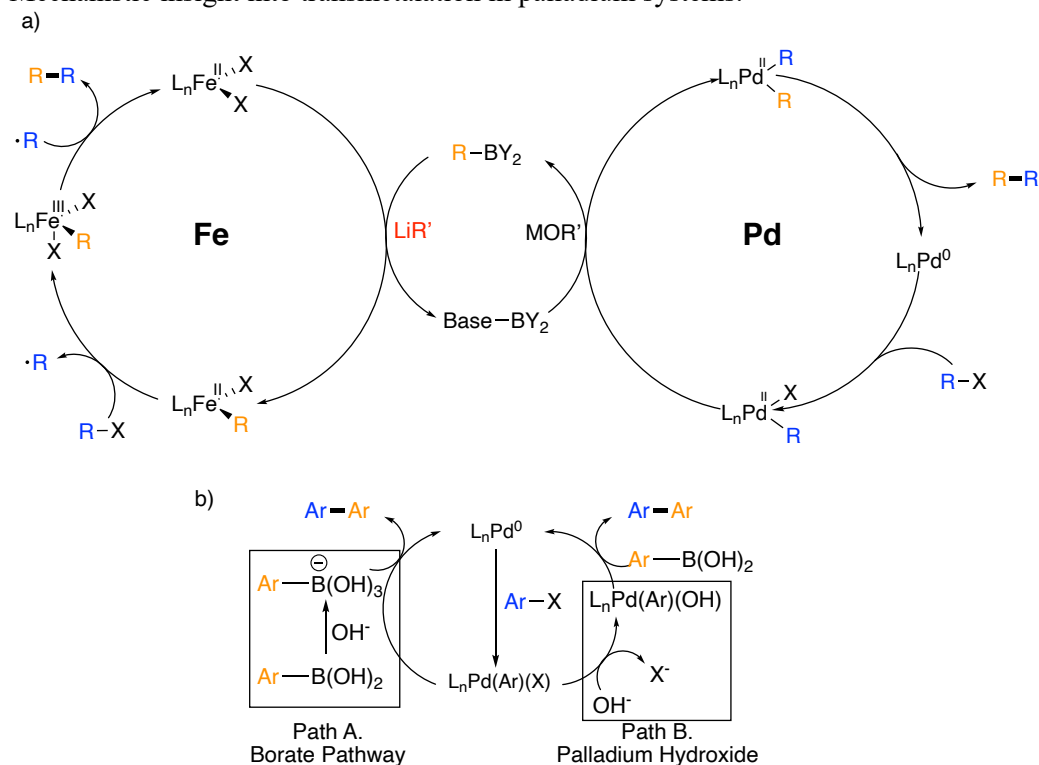
Scheme 2.2. Benefits of using a Suzuki-Miyaura cross-coupling reaction and iron-based catalyst.



2.2 Overcoming Aggregation

Considering the fast iron-catalyzed Kumada cross-couplings and the comparatively sluggish Suzuki-Miyaura cross-coupling reactions (requiring highly activated borates) we hypothesized that the key step in an iron-catalyzed Suzuki-Miyaura cross-coupling reaction is the transmetalation event (Scheme 2.3a). Extensive studies of the transmetalation event in palladium-catalyzed systems have led to the proposal of multiple viable pathways by the groups of Soderquist and Lloyd-Jones (Scheme 2.3b).²⁶⁻²⁸ Recently, significant insight has been obtained for key intermediates involved in the transmetalation step of palladium-catalyzed Suzuki-Miyaura couplings. Hartwig and coworkers identified a palladium hydroxide species as the catalytically competent and kinetically relevant transmetalation partner, rather than a slower pathway involving a palladium halide complex and borate species that results from base activation of the boronic acid (Scheme 2.4).²⁹ The disparity in reactivity between these two pathways was significant, with rates constants that were over four orders of magnitude greater for the palladium hydroxide compared to the borate. Consistent with palladium hydroxides being involved in boron-to-palladium transmetalation reactions, Denmark and coworkers were able to use rapid injection NMR

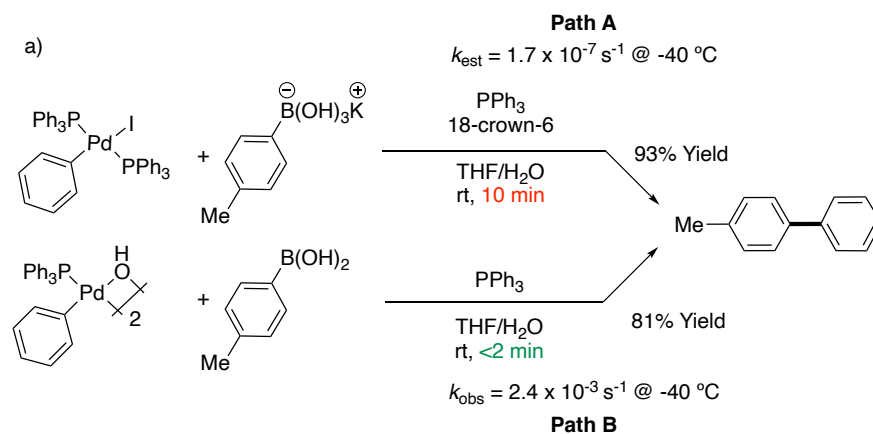
Scheme 2.3. a) Mechanistic comparison between iron and palladium-based catalysts. b) Mechanistic insight into transmetalation in palladium systems.



spectroscopy to characterize a transient intermediate containing an essential Pd-O-B linkage, which brings the palladium species in close proximity with the boronic acid prior to transmetalation (Scheme 2.5).³⁰ Using this same approach, the Denmark group was also able to identify similar pretransmetalation species when using arylboronic esters under palladium catalysis, which revealed that boronic esters can transmetalate without prior hydrolysis.³¹

While none of these previous mechanistic studies definitively rule out a transmetalation pathway that involves a borate intermediate, the studies implicate the importance of palladium hydroxides in catalytic cross-coupling reactions. Unlike palladium hydroxides and alkoxides which can exist as mononuclear complexes in solution or as monomer-dimer equilibrium mixtures, iron alkoxides and especially hydroxides are

Scheme 2.4 Reactivity studies implicating a palladium hydroxide over a borate pathway.



prone to irreversible aggregation.³² Furthermore, based on our experience and the experience of other groups,³² the base additives ($M_x(\text{CO}_3)_y$, MOR, etc.) typically used in palladium-catalyzed cross-coupling reactions led to stable iron aggregates, which we hypothesized would be detrimental to Suzuki-Miyaura cross-couplings.

Another hypothesis for the slow transmetalation reactions in iron catalyzed Suzuki-Miyaura cross-coupling reactions is unfavorable thermodynamics for transmetalation from boron to iron. Due to iron (EN = 1.8) being less electronegative than boron (EN = 2.0), exchange of the electronegative halogen ligand from iron to boron may be a thermodynamically uphill transformation. To investigate this possibility, Dr. Michael Crockett in our lab developed a computational model using density functional theory

Scheme 2.5. Characterization of a pretransmetalation intermediate with a Pd-O-B linkage.

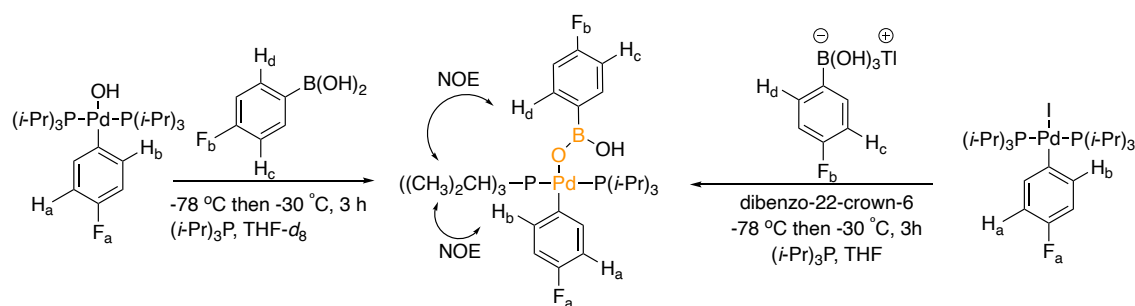
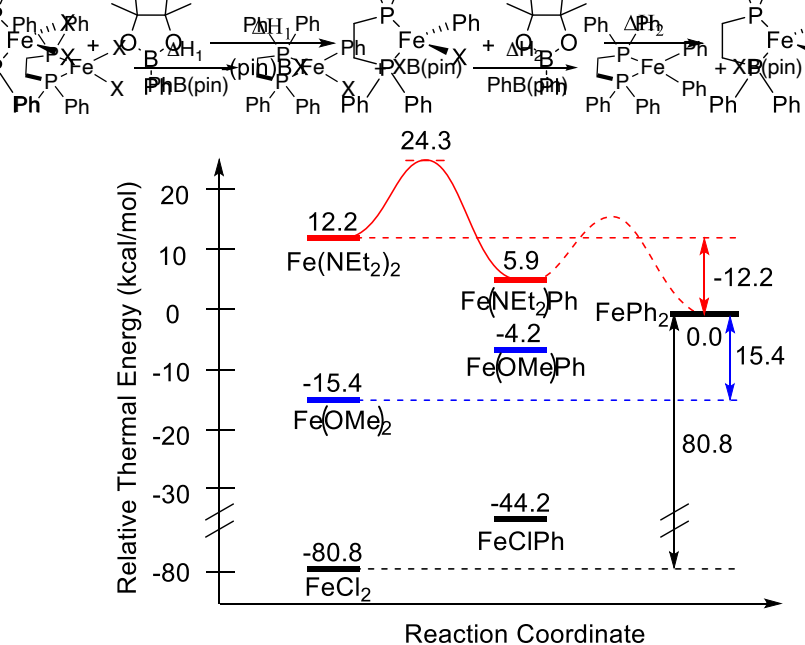


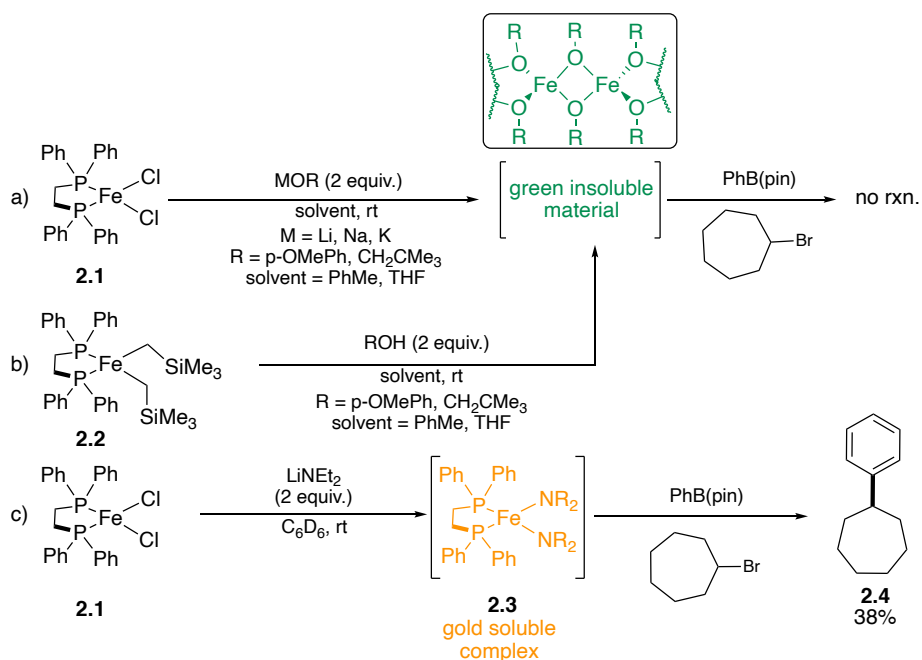
Figure 2.1 DFT (B3LYP/6-31G*) computed thermodynamic energies for transmetalation from boron to iron using PhB(pin) and (dppe)FeX₂ complexes.



(DFT) to probe the transmetalation reaction between phenylboronic pinacol ester (PhB(pin)) and bis(1,2-diphenylphosphino)ethane (dppe)FeX₂ complexes (Figure 2.1).^{33,34} Various (dppe)FeX₂ complexes bearing different anionic ligands (X⁻, OR⁻, NR₂⁻) were evaluated because of their potential involvement as intermediates in iron cross-coupling reactions as seen by other groups, which was discussed in Chapter 1.^{25,35} The results from Dr. Crockett's computations showed transmetalation reactions from PhB(pin) to (dppe)FeCl₂ and (dppe)FePhCl were thermodynamically unfavorable (black trace, Figure 2.1), which has also been reported for similar calculations carried out using palladium-based complexes.³⁶ In contrast, transmetalation reactions from (dppe)Fe(OMe)₂ were significantly less uphill than those from the halides ($\Delta H = 80$ vs. 15 kcal/mol), and thermodynamically and kinetically favorable at room temperature with (dppe)Fe(NEt₂)₂ ($\Delta H = -12.2$ kcal/mol, $\Delta H^\ddagger = 12.1$) (red trace, Figure 2.1).

Given the promising results that were obtained from the computational studies, Dr. Michael Crockett attempted to synthesize discrete $(dppe)Fe(OR)_2$ and $(dppe)Fe(NR_2)_2$ complexes through salt-metathesis and protonolysis routes³² in order to test their stoichiometric reactivity for cross-coupling (Scheme 2.6a-c).³³ Regardless of the identity of the metal alkoxide or alcohol, green insoluble solids were formed that were inactive for cross-coupling when exposed to PhB(pin) and cycloheptyl bromide. To our satisfaction, a

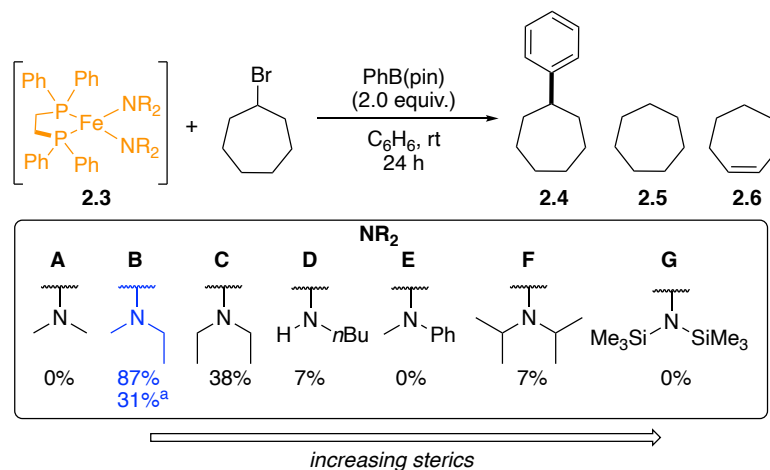
Scheme 2.6. Stoichiometric reactions to synthesize iron alkoxides via a) salt metathesis route or b) protonolysis route. c) Stoichiometric reactions showing the synthesis of an iron amide and its competency for cross-coupling.



golden homogeneous solution resulted when Dr. Michael Crockett reacted $(dppe)FeCl_2$ (2.1) with lithium diethylamide. This solution produced cross-coupled product 2.4 in 38% yield when PhB(pin) and cycloheptyl bromide were added to the reaction mixture.

Various *in-situ* derived iron amides were evaluated in the stoichiometric cross-coupling reaction between PhB(pin) and bromocycloheptane (Scheme 2.7).^{33,34} This screen revealed an optimal size for the lithium amide reagent that was necessary to achieve high

Scheme 2.7. Screening of various (dppe)Fe(NR₂)₂ complexes, derived from different sized lithium amides, in stoichiometric reactions between PhB(pin) and bromocycloheptane.



^a10 mol% (dppe)Fe(NR₂)₂ used.

yields of the cross-coupled product **2.4**. Sterically encumbered lithium amides such as lithium diisopropylamide (LDA) or lithium bis(trimethylsilyl)amide (LiHMDS) led to poor or 0% yield of product **2.4** respectively. On the other hand, sterically small lithium amides such as lithium dimethylamide or lithium butylamide led to no product at all. A significant increase in yield was observed when lithium ethylmethylamide was used as the base, forming the desired cross-coupled product **2.4** in 87% yield, with the only byproducts being cycloheptane (**2.5**) and cycloheptene (**2.6**). The iron complex **2.3B** could be used in catalytic quantities at 10 mol% when using lithium ethylmethyl amide to yield desired product **2.4**, albeit in low yields. Nevertheless, the reaction exhibited two turnovers, which suggested that a catalytic iron-mediated Suzuki-Miyaura cross-coupling protocol could be developed with the use of lithium amide bases to disfavor aggregation and promote transmetalation.

2.3 Reaction Optimization

To optimize the catalytic reaction, a variety of phosphine and nitrogenous ligands were screened for the coupling reaction between PhB(pin) and cycloheptyl bromide using lithium ethylmethylamide as the optimal base (Table 2.1). Phosphine ligand frameworks were promising candidates as ancillary ligands since bisphosphines are known to stabilize iron(II) centers in Kumada, Negishi and Suzuki-Miyaura C(sp²)-C(sp³) cross-coupling

Table 2.1. Effect of monodentate and bidentate phosphorus ligands on an iron-catalyzed Suzuki-Miyaura cross-coupling reaction between PhB(pin) and bromocycloheptane.

Entry	Ligand	X (%)	2.4(%)	2.5(%)	2.6(%)	
1	No ligand	0	25	15	48	
2	PPh ₃	20	25	23	28	
3	PCy ₃	20	29	20	36	
4		20	28	18	38	
5		n = 2, R = Ph	10	31	20	28
6		n = 3, R = Ph	10	35	22	27
7		n = 4, R = Ph	10	36	20	28
8		n = 2, R = Me	10	31	41	6
9		10	31	28	20	
10		10	32	24	29	
11		10	28	25	35	
12		R = H	10	37	23	27
13		R = <i>t</i> -Bu	10	43	28	12

reactions between aryl nucleophiles and alkyl electrophiles.^{18,25} With the help of Dr. Michael Crockett, an extensive investigation of monodentate and bidentate phosphine ligands was undertaken with various electronic and steric constraints (Table 2.1). As a baseline reaction, iron dichloride was evaluated as a catalyst, which provided 25% of **2.4** with significant amounts of alkene product **2.6** (Table 2.1, entry 1). Monodentate phosphines typically gave yields slightly lower than dppb (36%) regardless of their structure (entries 2-4). Similarly, the chelate size of bidentate phosphines and more electron-rich phosphines did not lead to any improvements (entries 5-8). Other phosphines including dppf (entry 9), (*rac*)-BINAP (entry 10), and Xantphos (entry 11) also did not improve yields relative to dppb. Finally, the sterically restricted dppbz ligand (entry 12) was comparable to dppb but the related, more sterically encumbered SciOPP (entry 13) ligand afforded the desired product in the highest yield of any of the bisphosphines studied (43%). This bisphosphine was the same ligand that the Nakamura group had found to be optimal for Kumada and Suzuki-Miyaura cross-coupling reactions between aryl nucleophiles and alkyl halides.^{17,25} As the Neidig group has elegantly shown occurring in Nakamura's systems using (SciOPP)FeCl₂,³⁵ we hypothesize that the steric bulk of SciOPP is beneficial for catalysis by favoring monomeric and unsaturated iron centers as well to sequester off-cycle species.

We next investigated commonly used bidentate and tridentate ligands based on nitrogenous heterocycles, such as pyridine and oxazoline (Table 2.2). Whereas bipyridine ligands and pyridine bis(oxazoline) ligands (pyBox) resulted in similar yields of **2.4** (entries 1-2), exploration of C₂-symmetric bis(oxazoline) ligands (Box) led to little improvement relative to the bisphosphine ligands (entries 3-6). These ligands have shown

great utility for many transition-metal catalyzed transformations, especially for cross-coupling reactions catalyzed by first row transition metals such as nickel and copper.³⁷ Additionally, bis(oxazoline) ligands are easily sterically and electronically tuned through modification of substituents on either the oxazoline ring or the methylene backbone. While

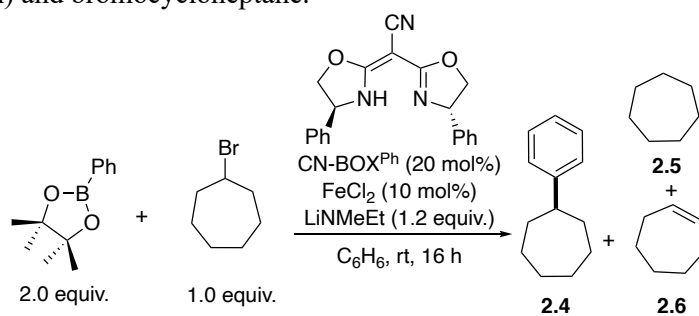
Table 2.2. Effect of bidentate and tridentate nitrogenous ligands on an iron-catalyzed Suzuki-Miyaura cross-coupling reaction between PhB(pin) and bromocycloheptane.

Entry	Ligand	X(%)	2.4(%)	2.5(%)	2.6(%)
1		10	30	20	26
2		10	34	27	13
3		10	36	14	16
4		10	25	16	26
5		10	17	13	8
6		10	27	16	35
7		10	58	14	10
8		20	72	6	6

phenyl-Box ligands with a methylene bridge show a similar yield to dppb (entry 3), isopropylidene linkers led to reduced yields of cross-coupled products (entry 5). However, when using a *tert*-butyl-Box ligand, no difference in yield was seen when for ligands containing methylene (entry 4) or isopropylidene linkers (entry 6). Continuing the screen, we found the most efficient bis(oxazoline) in this class was the commercially available cyanobis(oxazoline), ligand which gave yields of **2.4** that were superior to dpbz and SciOPP (entries 7-8). Using the cyanobis(oxazoline) (CN-Box^{Ph}) ligand, we found enhanced yields were achieved when an additional equivalent of ligand was used, leading to lower amounts of side products in **2.5** and **2.6**. We hypothesized this ligand performed better than other bis(oxazoline) ligands because of its increased acidity,³⁸ which could lead to ligand deprotonation under the basic reaction conditions.

With optimal ligand in hand, we next explored the role of the solvent, focusing on using greener alternatives to benzene (Table 2.3). Various classes of green solvents were screened, such as methyl *tert*-butyl ether (MTBE), *tert*-amyl alcohol, and 2-methyl-THF

Table 2.3. Solvent evaluation for iron-catalyzed Suzuki-Miyaura cross-coupling reaction between PhB(pin) and bromocycloheptane.



Entry	Solvent	2.4 (%)	2.5 (%)	2.6 (%)
1	Benzene	76	7	6
2	2-methyl-THF	2	5	0
3	MTBE	24	8	6
4	<i>t</i> -Amyl Alcohol	0	0	0
5	Toluene	45	N/A	N/A
6	NMP	0	0	0

but yields were significantly reduced relative to benzene (entries 2-4). Toluene was the only solvent that provided comparable yields to benzene, which indicate the importance of aromatic solvents for promoting effective cross-coupling (entry 5). The beneficial effects of aromatic solvents may be due to stabilization of low valent iron species or carbon-centered radicals.³⁵ In addition, *N*-methylpyrrolidine (NMP), which is an effective solvent in many iron-catalyzed Kumada cross-couplings, was tested, but it was highly detrimental to cross-coupling (entry 6). Furthermore, an array of boron-derived transmetalating reagents were examined (Table 2.4), and PhB(pin) was found to be the most competent cross-coupling partner. Stark differences in reactivity were seen for phenylboronic neopentyl esters, which were incompatible with the iron-catalyzed cross-coupling reaction

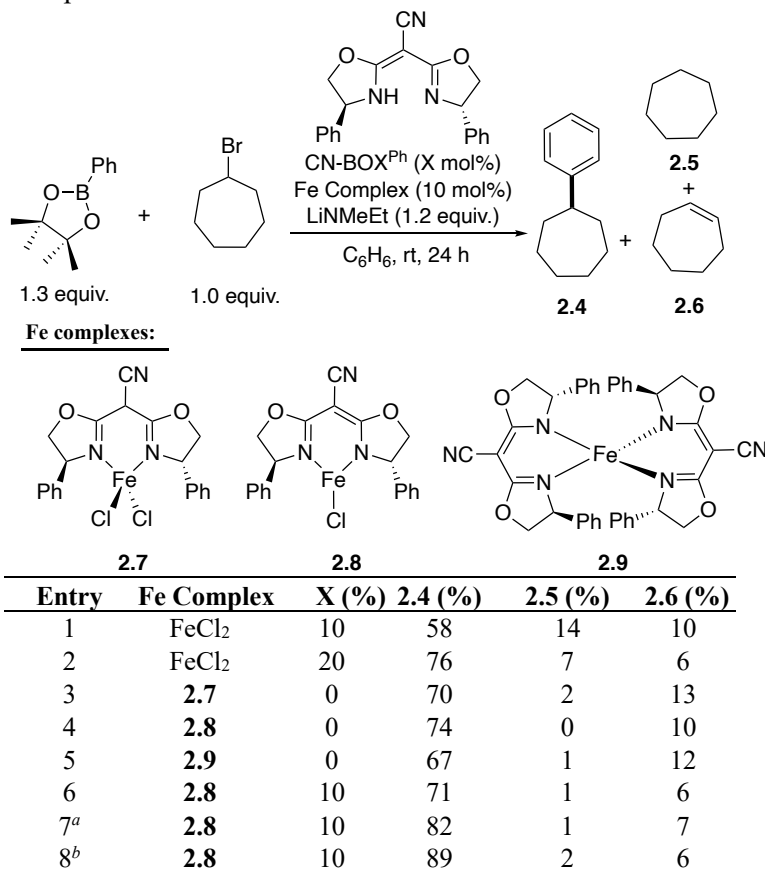
Table 2.4. Effect of transmetalating reagent on cross-coupling reaction between boron nucleophiles and bromocycloheptane.

entry	PhBX _n	2.4 (%)	2.5 (%)	2.6 (%)
1		76	7	6
2		5	0	2
3		0	0	0
4		0	0	0
5		0	24	2
6		0	0	0

reported here despite being one of the best transmetalating reagents for palladium-catalyzed cross-coupling reactions.³¹ We hypothesize that the phenylboronic neopentyl esters are inefficient coupling partners due to the reagents readily reacting with lithium ethylmethanamide to make particularly stable borate species.^{33,34} In the analogous palladium-catalyzed reactions, phenylboronic neopentyl esters are hypothesized to be superior because of faster rates of hydrolysis to the boronic acid.³¹

Table 2.5 provides an abbreviated set of the final optimization process. We hypothesized that reactions using *in situ* formed catalysts would result in a diverse speciation of iron complexes that might be detrimental to the yields of the reaction. We

Table 2.5. Dependency of the iron-catalyzed Suzuki-Miyaura cross-coupling reaction on the identity of the iron precursor.



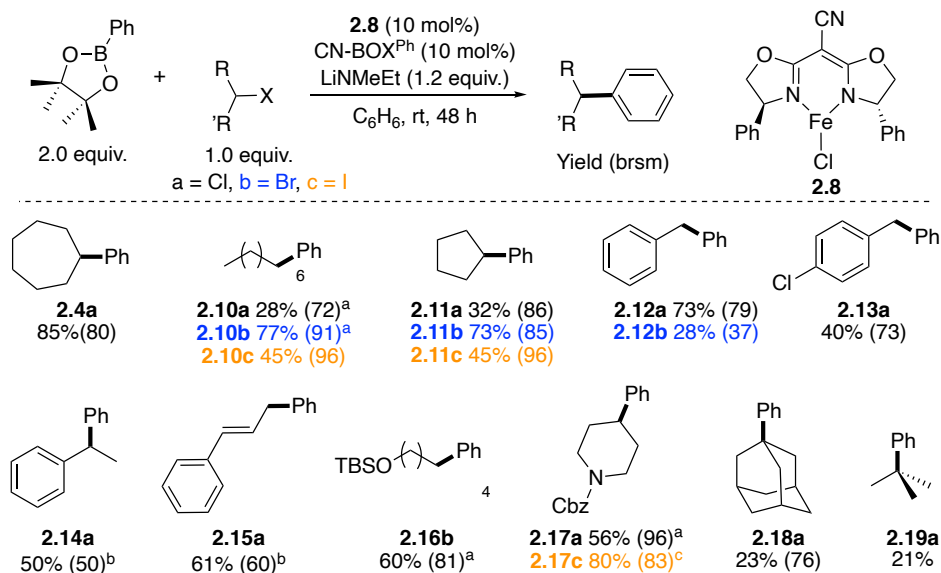
^a48h. ^b**2.8** (10 mol%) and LiNMeEt (0.6 equiv.) added after 6 h.

also suspected the protonation state of the ligand was important due to the acidity of the cyanobis(oxazoline) ligand. To test our hypotheses, Dr. Michael Crockett and I synthesized and tested iron complexes with a neutral cyano-Box ligand (**2.7**), a deprotonated cyanobis(oxazoline) ligand (**2.8**) and a homoleptic complex containing two deprotonated cyanobis(oxazoline) ligands (**2.9**). This last complex was synthesized in response to our observation that two equivalents of the cyanobis(oxazoline) ligand relative to iron led to better performance than one equivalent of ligand (entries 1 vs. 2). All three complexes were found to be catalytically active and provided product yields comparable to each other. These results suggest that the three precatalysts can be converted to a catalytically active species during the reaction (entries 3-5). Complex **2.8**, containing one deprotonated cyanobis(oxazoline) ligand was found to be particularly effective producing 74% of product **2.4** and completely shutting down the formation of the cycloheptane byproduct **2.5** after 24 hours. Adding an additional 10% of the ligand to a reaction catalyzed by complex **2.8** led to reduced cycloheptene (**2.6**) formation, despite slightly lower yields (71% vs 74%) (entry 6). The lower yields in the reaction were attributed to slower reaction rates in the presence of exogenous ligand. Supporting this notion, a reaction carried out for 48 hours led to nearly full conversion of cycloheptyl bromide and 82% yield of the desired product (entry 7). An alternative procedure was also developed to increase the yield of the cross-coupled product, which may be necessary for more challenging substrates: after reaction for 6 hours under reaction conditions from entry 6, an additional 10 mol% of **2.8** and 0.6 equivalents of lithium ethylmethanamide were added to the reaction. This procedure resulted in full conversion of the cycloheptyl bromide substrate and 89% yield of the cross-coupled product **3** (entry 8).

2.4 Substrate Scope Evaluation and Pharmaceutical Target

The generality of the reaction with respect to the alkyl halide coupling partner was then explored (Figure 2.2). We found primary and secondary unactivated alkyl bromides were well tolerated under the reaction conditions though primary alkyl halides required heating to achieve high yields (**2.10**, **2.11**). Under nearly all reaction conditions, unactivated alkyl bromides were superior substrates to alkyl iodides which in turn were superior to alkyl chlorides (**2.10**, **2.11**). The reverse trend was seen with activated alkyl halides, where chlorides were now superior to bromides (**2.12a**, **2.14b**). The change in chemoselectivity could be rationalized by the propensity of the benzylic radical to form, leading to homodimer formation. An additional reason for the observed chemoselectivity are the low yields based on recovered starting material (brsm) for the alkyl bromides that contain weaker C-X bonds. The reaction could also tolerate some functional groups

Figure 2.2. Alkyl halide substrate scope of an iron-catalyzed Suzuki-Miyaura cross-coupling.

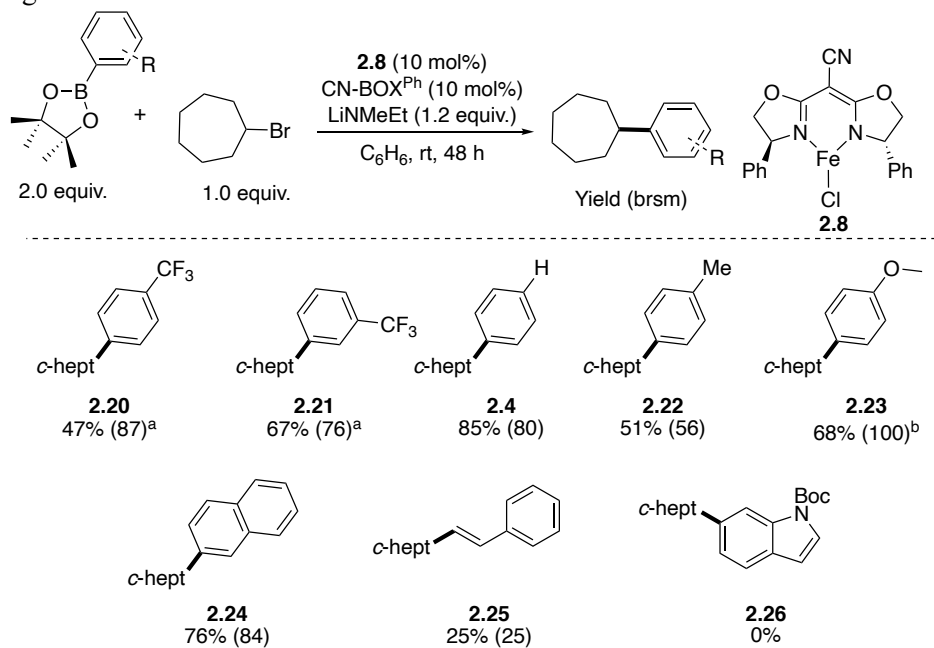


All reactions carried out at 0.5 mmol scale in alkyl halide. ^aReaction run at 50 °C. ^b0.1 mmol of **2.8** and 0.6 mmol of LiNMeEt added after 24 h. ^cSolvent was toluene.

including aryl chlorides (**2.13a**), silyl-protected alcohols (**2.16b**) and Cbz-protected amines (**2.17a**). However, alkyl halides containing acidic protons, such as ketones, esters, amides and nitriles were not tolerated under these reaction conditions. These substrate scope limitations are presumably due to the highly basic nature of the lithium amide base. Additionally, some tertiary alkyl halides worked for cross-coupling, such as adamantyl (**2.18a**) and *tert*-butyl chloride (**2.19a**), albeit in low yields (23%, 21%) and yields brsm.

The generality of the reaction was also surveyed with respect to the arylboronic ester, which was carried out by Alexander Wong (Figure 2.3). The reaction was efficient for a series of para-substituted arylboronic esters with electron withdrawing (**2.20**, **2.21**), neutral (**2.11**) and electron donating substituents (**2.22-2.24**). However, reactions with electron-deficient boronic esters required heating to achieve appreciable yields. We attribute the requirement for higher reaction temperatures to the greater Lewis acidity of

Figure 2.3. Arylboronic ester substrate scope of an iron-catalyzed Suzuki-Miyaura cross-coupling.

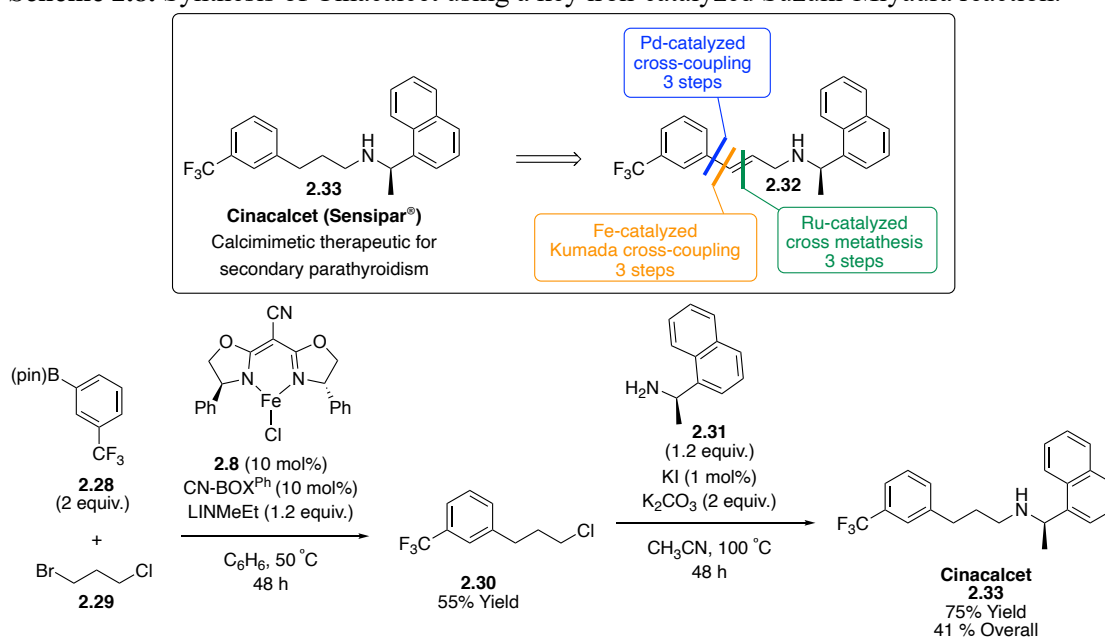


All reactions carried out at 0.5 mmol scale in alkyl halide. ^aReaction run at 50 °C. ^b0.1 mmol of **2.8** and 0.6 mmol of LiNMeEt added after 24 h.

the electron-deficient arylboronic esters and the stability of the borate species that may form. Heating helps to perturb the equilibrium between borate and neutral arylboronic ester toward the latter species, which is required for catalysis (*vide infra*). The reaction was inefficient with alkenyl boronic esters, leading to low yields and formation of many unidentified side-products (**2.25**). Due to the abundance of heterocycles in medically relevant molecules, heteroaromatic boronic esters were also evaluated. Unfortunately, these class of substrates (**2.26**) were not tolerated under the reaction conditions.

We next wanted to demonstrate the utility of our cross-coupling method through the synthesis of a pharmaceutically relevant molecule. Among those available, Cinacalcet (**2.33**), an Amgen derived drug used to treat secondary parathyroidism, stood out as an attractive candidate since most methods rely on noble metal catalysis (Scheme 2.8).^{39–41} One notable feature of the methods utilizing noble metal catalysts is that they either proceed through the reduction of an amide⁴² or reductive amination,³⁹ while a substitution

Scheme 2.8. Synthesis of Cinacalcet using a key iron-catalyzed Suzuki-Miyaura reaction.



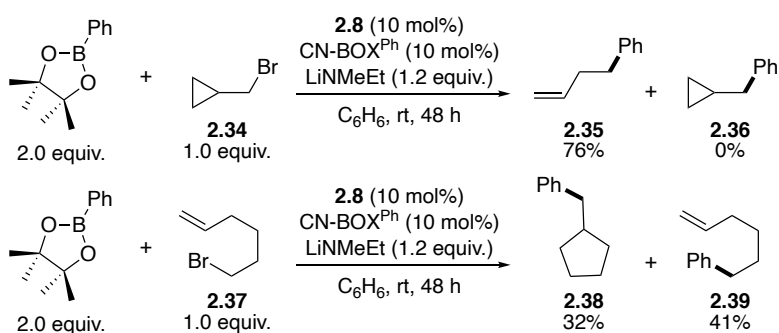
approach has not yet been demonstrated. Additionally, we found these previous methods all require three steps, including a hydrogenation of a penultimate alkene intermediate (**2.32**). To circumvent the hydrogenation reaction, which often time utilizes palladium on carbon, we hypothesized that with our iron cross-coupling reaction, Cinacalcet could be accessed in two steps from commodity chemicals (**2.28**, **2.29**). Using our iron cross-coupling reaction, we took advantage of the chemoselectivity of our catalyst for unactivated alkyl bromides over chlorides to deliver intermediate **2.30** in 55% yield. This alkyl chloride intermediate **2.30** was then used to monoalkylate chiral amine **2.31** under S_N2 reaction conditions to deliver Cinacalcet (**2.33**) in 75% yield with a 41% overall yield. This route currently represents the shortest reported synthesis of Cinacalcet (**2.33**) in 2 steps from commercially available starting materials and without the use of noble metal catalysts. Additionally, this method only requires heating up to 100 °C, while the other reported iron-based system used to synthesize Cinacalcet requires cooling to -70 °C.³⁹ Despite the environmental benefits of the previous system³⁹ using an iron-based catalyst, the necessity for cooling would be an expensive feature for reaction scale up for the pharmaceutical industry.

2.5 Mechanistic Experiments and Considerations

Our mechanistic understanding of this iron-catalyzed Suzuki-Miyaura cross-coupling reaction promoted by lithium amides has been guided by the iron(II)/(III) mechanism put forth by the Nakamura and Neidig groups.^{25,35} As discussed in Chapter 1, these iron-catalyzed cross-coupling reactions use a highly activated arylborate species to promote transmetalation and involve carbon-centered radical intermediates. To probe whether this reaction was proceeding through a similar radical-based mechanism, we

carried out catalytic reactions using radical clock substrates **2.34** and **2.37** (Scheme 2.9). Using cyclopropylmethyl bromide **2.34**, we saw exclusive ring-opened product (**2.35**) and with 6-bromohexene **2.37** we observed a near 1:1 mixture of cyclized:uncyclized (**2.38**, **2.39**) products. These results are consistent with Nakamura's system which proceeds through a carbon-centered radical intermediate.²⁷ However, a metal-mediated two-electron process seen with some palladium systems cannot be ruled out.⁴³

Scheme 2.9. Radical clock substrates as probes for carbon-centered radical intermediates.



To gain more insight into the mechanism, we noted the major differences between our system and the Nakamura system. The critical need for the specific reactants, cyanobis(oxazoline) ligand, lithium amide base and an unactivated arylboronic ester, to obtain effective cross-coupling provided us with handles for learning more about the mechanism. We first gained some insight into the beneficial effects on yield from additional cyanobis(oxazoline) ligand through time course studies (Figures 2.4, 2.5, 2.6). From these studies, we observed that reactions carried out with an excess of ligand proceeded at slower reaction rates for formation of **2.4** but overall higher yields of **2.4** (85% vs. X%). The slower reactivity seen with reactions containing extra ligand was verified by monitoring initial reaction rates (Figure 2.6). These findings were presumably due to longer catalyst lifetimes. With the addition of a second equivalent of cyanobis(oxazoline) ligand

Figure 2.4. Time course of a catalytic reaction with extra ligand.

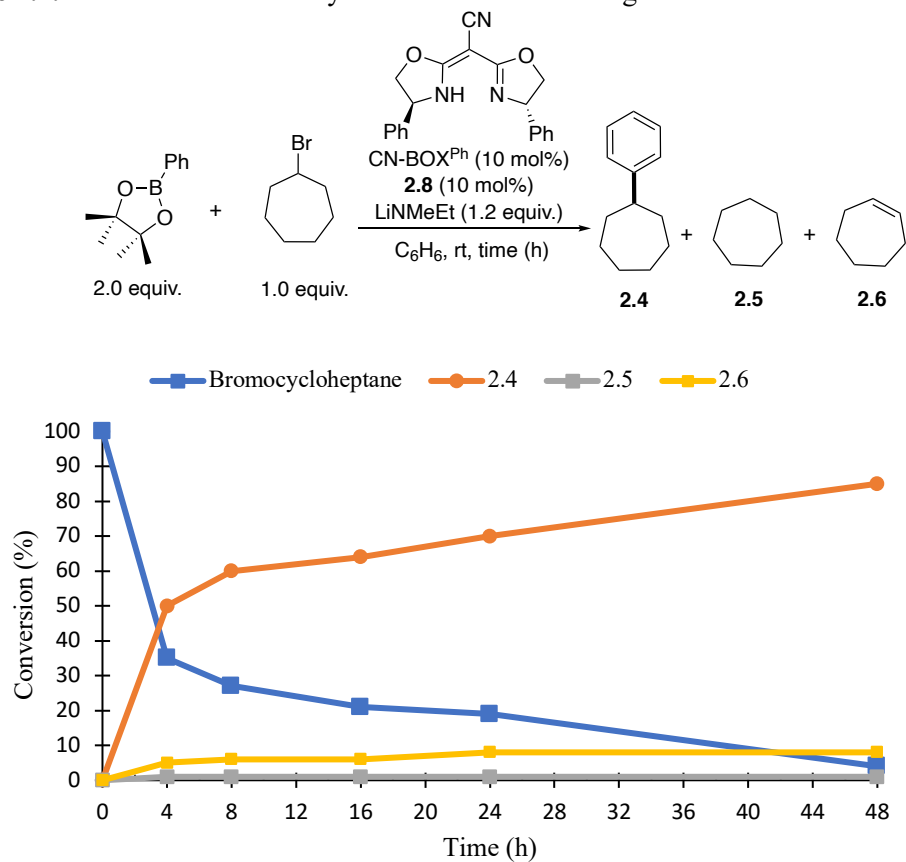
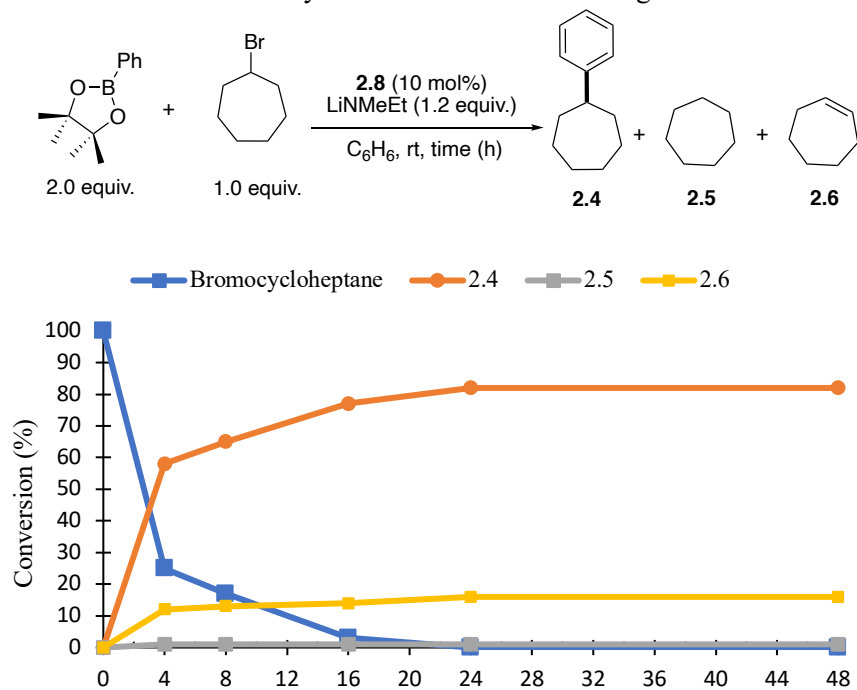
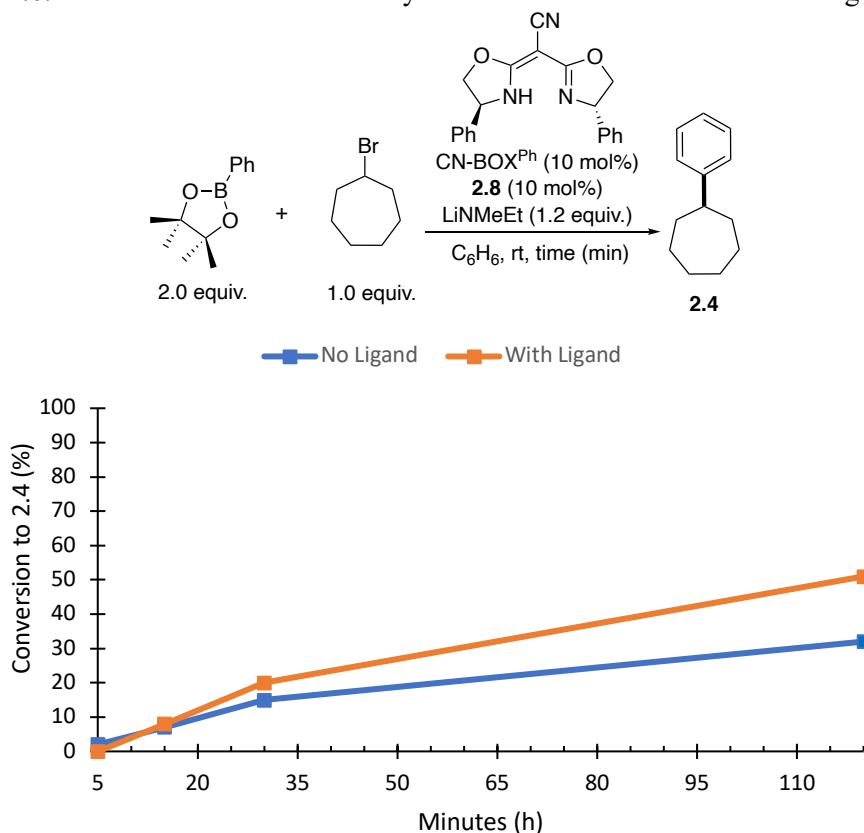


Figure 2.5. Time course of a catalytic reaction without extra ligand.



relative to **2.8**, a species capable of forming would be the homoleptic iron complex **2.9**. W6

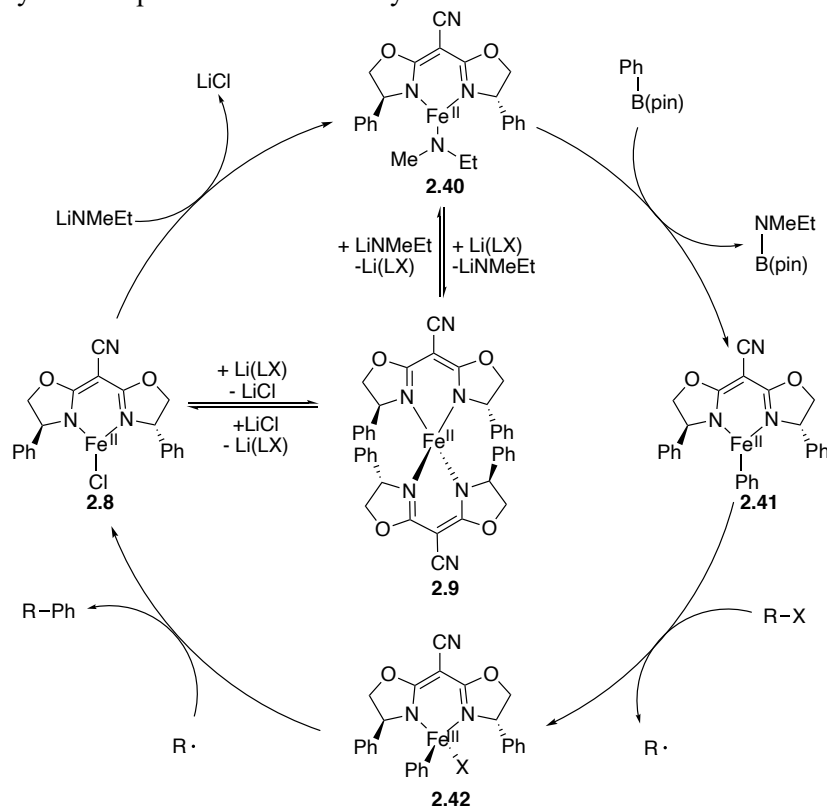
Figure 2.6. Initial rate kinetics for a catalytic reaction with and without extra ligand.



hypothesize this homoleptic species could provide a resting state for the iron complex to prevent unwanted off-cycle pathways, such as aggregation and byproduct formation. With these findings, a working mechanistic hypothesis analogous to Nakamura's could account for our observations (Scheme 2.10).²⁵ In this mechanism, homoleptic complex **2.9** is not on the catalytic cycle, which explains the slower reaction rates under conditions where **2.9** is formed. This mechanistic hypothesis also explains why cyanobis(oxazoline) ligands are superior to the methylene or isopropylidene bis(oxazoline) ligands. The equilibration of **2.8** to **2.9** or **2.40** to **2.9** is facilitated by a ligand that can be deprotonated by the lithium amide base but that does not undergo irreversible formation of **2.9**.

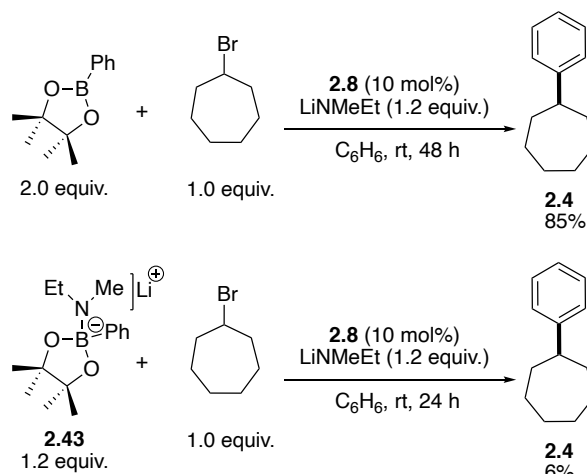
In addition to the role of the cyanobis(oxazoline) ligand, we believe the lithium amide base serves two critical roles in the mechanism proposed in Scheme 2.10. The first

Scheme 2.10. Working mechanistic hypothesis for an iron catalyzed Suzuki-Miyaura reaction between arylboronic pinacol esters and alkyl halides.



role the amide base serves is to deprotonate the cyanobis(oxazoline) ligand to favor formation of iron complex **2.8** or homoleptic complex **2.9**. We hypothesize the anionic nature of the cyano-Box ligand helps to strengthen the metal-ligand interaction as well as the ligand providing steric bulk proximal to the iron center. Both these factors contribute to the success of the coupling reaction by disfavoring undesirable aggregation. The second role of the lithium amide is to convert the iron halide **2.8** into a putative iron amide species **2.40** via salt metathesis (Scheme 2.10). The iron amide **2.40** serves as the key iron intermediate for transmetalation (*vide infra*). This supposition is largely based on computational studies, which show that boron-to-iron transmetalation is made thermodynamically downhill and kinetically fast from an iron amide intermediate (*vide*

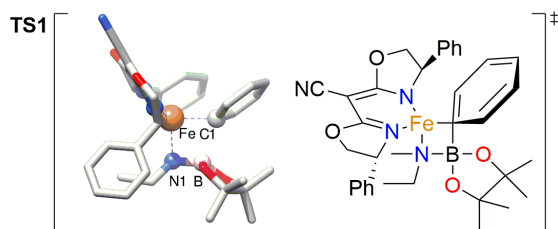
Scheme 2.12. Comparison of cross-coupling reactivity proceeding through a putative iron amide species or a borate pathway.



infra). Dr. Michael Crockett has repeated these calculations with the cyanobis(oxazoline) iron complexes and found that the thermodynamics are much the same as with (dppe)Fe(NEt₂)₂, but the transition-state barriers are lower for the cyanobis(oxazoline) iron amide complex **2.40** (12.1 vs. 7.3 kcal/mol for ΔH^\ddagger) (Scheme 2.11).³³

Another possible mechanism for transmetalation involves a borate pathway rather than through iron amide **2.40**. It is certainly true that PhB(pin) reacts immediately with lithium ethylmethylamide to make a borate species (**2.43**), which we have observed by ¹¹B NMR spectroscopy. However, it is noteworthy that when we purposely add this borate species in the cross-coupling reaction, we observe greatly diminished yields compared to when the lithium amide and boronic ester are added to the reaction separately (Scheme

Scheme 2.11. DFT (B3LYP/631G*) calculations for the transition state obtained for transmetalation reaction between iron amide **2.40** and PhB(pin).



2.12). When a reaction using the borate is heated to 50 °C, yields do increase (68%) but reaction rates are slow compared to reactions when they are added separately.

2.6 Conclusion:

In summary, an iron-catalyzed Suzuki-Miyaura cross-coupling reaction between alkyl halides and unactivated aryl boronic esters was developed. The major challenge associated with developing iron-catalyzed Suzuki-Miyaura reactions using alkoxide bases stems from formation of undesired aggregation. Through computational studies and stoichiometric reactions, it was found that lithium amides are effective base additives to promote transmetalation and prevent aggregation events. Additionally, the use of a monoanionic cyanobis(oxazoline) ligand was found to be essential for cross-coupling by disfavoring aggregation and extending the catalyst lifetime. The cross-coupling reaction worked efficiently with unactivated and activated primary and secondary alkyl halides, a variety of electronically disparate arylboronic pinacol esters, and demonstrated moderate functional group tolerance. The synthesis of Amgen's pharmaceutical Cinacalcet was accomplished in two steps from commercially available starting materials using the iron catalyzed cross-coupling reaction. This method represents the shortest reported synthesis of Cinacalcet and does not involve the use of a noble metal. Radical clock experiments and reactivity studies are supportive of a radical-based mechanism proceeding through an iron(II)/(III) cycle.

2.7 Experimental:

General Considerations. Unless stated otherwise, all reactions were carried out in oven-dried glassware in a nitrogen-filled glovebox or using standard Schlenk-line techniques.⁴⁴ Solvents including dichloromethane, pentane, toluene, diethyl ether, and tetrahydrofuran were purified by passage through two activated alumina columns under a blanket of argon⁴⁵ and then degassed by brief exposure to vacuum. Phenylboronic acid, 2-naphthaleneboronic acid, 4-methoxyphenylboronic acid, *p*-tolylboronic acid, 4-trifluoromethylphenylboronic acid, 3-trifluoromethylphenylboronic acid pinacol ester were bought from Oakwood Chemicals and dried over P₂O₅ followed by passage through an alumina plug in the glovebox before use. All prepared boronic pinacol esters were used after passage through alumina under a nitrogen atmosphere. Methylethyl amine was purchased from TCI America; diisopropylamine and lithium dimethylamide were purchased from Alfa Aesar, butylamine and diethylamine were purchased from Sigma-Aldrich and (R)-(+)-1-(1-Naphthyl)ethylamine was purchased from Oakwood Chemicals. All amines that were liquids at room temperature were dried over calcium hydride for at least 24 hours before being vacuum-distilled. 2,3-dimethyl-2,3-butanediol and 2,2-dimethylpropane-1,3-diol were purchased from Alfa and used without further purification. Anhydrous iron (II) chloride was purchased from Sigma Aldrich and used without further purification. All bisphosphines were purchased from Sigma-Aldrich, Fisher Scientific, TCI America, Oakwood, or Strem Chemicals and dried over P₂O₅ before use in the glovebox. All bis(oxazoline) ligands including (4*S*)-(+)-Phenyl- α -[(4*S*)-phenyloxazolidin-2-ylidene]-2-oxazoline-2-acetonitrile were purchased from Sigma-Aldrich and dried over P₂O₅ before use in the glovebox. Purchased alkyl halides were dried over calcium hydride for at least

24 hours before being vacuum-distilled, while all solids were dried over P_2O_5 before use in the glovebox. All alkyl halides were purchased from Sigma-Aldrich, Oakwood Chemicals and Fisher Scientific.

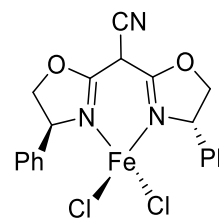
1H , ^{11}B , $\{^1H\}^{13}C$, and ^{19}F nuclear magnetic resonance (NMR) spectra were recorded at ambient temperature on Varian VNMRs operating at 400 MHz, 500 MHz, or 600 MHz for 1H NMR at 160 MHz for ^{11}B NMR, 125 MHz for $\{^1H\}^{13}C$ or 470 MHz for ^{19}F NMR. All $\{^1H\}^{13}C$ NMR was collected while broad-band decoupling was applied to the 1H region. The residual protio solvent impurity was used as an internal reference for 1H NMR spectra and $\{^1H\}^{13}C$ NMR spectra. Boron trifluoride diethyl etherate was used as an external standard ($BF_3 \cdot O(C_2H_5)_2$: 0.0 ppm) for ^{11}B NMR and ^{19}F NMR ($BF_3 \cdot O(C_2H_5)_2$: -153.0 ppm). The line listing for NMR spectra of diamagnetic compounds are reported as follows: chemical shift (multiplicity, coupling constant, integration) while paramagnetic compounds are reported as chemical shift (peak width at half height, number of protons). Solvent suppressed spectra were collected for paramagnetic compounds in THF using the PRESAT macro on the VNMR software. Infrared (IR) spectra were recorded on a Bruker Alpha attenuated total reflectance infrared spectrometer. High-resolution mass spectra were obtained at the Boston College Mass Spectrometry Facility on a JEOL AccuTOF DART instrument.

Computational Procedures. All computations were carried out using Density Functional Theory (DFT) methodology employing the hybrid B3LYP functional (composed of Becke's 1988 exchange functional and Lee, Yang, and Parr's correlation functional) in conjunction with the 6-31G* basis set.⁴⁶ All calculations with phosphine ligands were carried out in a tetrahydrofuran (THF) solvent simulated by Tomasi's Polarizable

Continuum Model (PCM).⁴⁷ Stationary-point characterization of all optimized geometries were carried out by means of frequency calculations utilizing the same level of theory as was used in the geometry optimizations. Gibbs free energies and enthalpies (computed at 298 K and 1 atm) and zero-point corrected energies were calculated using the computed normal mode frequencies (not scaled). All calculations were carried out using Gaussian 09 program All iron complexes were calculated in the quintet state. In all cases for minima, the intermediate (triplet) and low (singlet) spin states were higher in energy between 15 and 40 kcal/mol.

Synthesis of (2,2-bis((S)-4-phenyl-4,5-dihydrooxazol-2-yl)aceto

nitrile)FeCl₂, (CNBox^{Ph})FeCl₂ (2.7). To a 20 mL scintillation vial equipped with a stir-bar was added iron dichloride (0.3 g, 0.9 mmol) and THF (10 mL). After stirring for one hour, 2,2-bis((S)-4-phenyl-



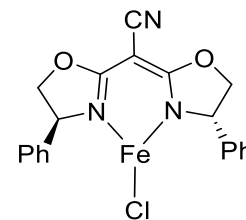
4,5-dihydrooxazol-2-yl)acetonitrile (0.115 g, 0.9 mmol) was added. The solution became clear and slightly yellow almost immediately. After stirring for 12 hours the solvent was removed *en vacuo* and the oil was triturated with pentane. This yielded an off-white solid (0.285 g, 69%). ¹H NMR (500 MHz, THF) δ -30 (*w*_{1/2} = 307 Hz, 4H), -4.2 (*w*_{1/2} = 59 Hz, 2H), -3.8 (*w*_{1/2} = 33 Hz, 4H), -1.1 (*w*_{1/2} = 21 Hz, 2H), 10.8 (*w*_{1/2} = 76 Hz, 2H) , 56.8 (*w*_{1/2} = 512 Hz, 1H) ppm. IR: 2201, 1595, 1533, 1493, 1452, 1067, 697 cm⁻¹.

Synthesis of (2,2-bis((S)-4-phenyl-4,5-dihydrooxazol-2-yl)acetonitrile)FeCl, (CNBox^{Ph})FeCl (2.8). To a 20 mL scintillation vial equipped

with a stir-bar was added iron dichloride (0.1 g, 0.3 mmol) and THF (10 mL). After stirring for one hour, Li-2,2-bis((S)-4-phenyl-4,5-

dihydrooxazol-2-yl)acetonitrile (0.380 g, 0.3 mmol) was added. The solution became clear and yellow-brown almost immediately. After stirring for 12 hours the solvent was removed *en vacuo* and the oil triturated with pentane. This yielded an off-white solid (0.42 g, 90%).

¹H NMR (500 MHz, THF) δ -30 ($w_{1/2}$ = 307 Hz, 4H), -4.2 ($w_{1/2}$ = 59 Hz, 2H), -3.8 ($w_{1/2}$ = 33 Hz, 4H), -1.1 ($w_{1/2}$ = 21 Hz, 2H), 10.8 ($w_{1/2}$ = 76 Hz, 2H), 56.8 ($w_{1/2}$ = 512 Hz, 1H) ppm. IR: 2203, 1606, 1533, 1440, 1067, 694 cm⁻¹. Elemental analysis for C₂₀H₁₆ClFeN₃O₂•(LiCl)₂(THF)_{2.3} calc'd: C, 52.21%; H, 5.17%; N 6.23%. Found: C, 52.21%, H, 5.13%, N 6.62%.



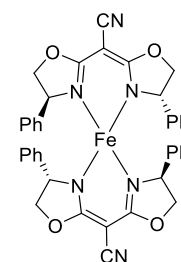
Synthesis of (2,2-bis((S)-4-phenyl-4,5-dihydrooxazol-2-yl)acetonitrile)₂Fe, (CNBox^{Ph})₂FeCl (2.9): To a 20 mL scintillation vial equipped

with a stir-bar was added iron dichloride (0.032 g, 0.25 mmol) and THF (10 mL). After stirring for one hour Li-2,2-bis((S)-4-phenyl-4,5-dihydrooxazol-2-

yl)acetonitrile (0.170 g, 0.5 mmol) was added. The solution became clear and

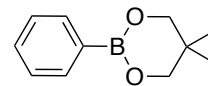
brown almost immediately. After stirring for 12 hours the solvent was removed *en vacuo*

to yield a light tan solid (0.110 g, 63%). ¹H NMR (500 MHz, THF) broad resonances, δ -27.3 ($w_{1/2}$ = 406 Hz, 2H), -6.0 ($w_{1/2}$ = 86 Hz, 4H), -0.4 ($w_{1/2}$ = 49 Hz, 2H), 7.3 ($w_{1/2}$ = 31 Hz, 1H), 18.8 ($w_{1/2}$ = 150 Hz, 2H), 78.4 ($w_{1/2}$ = 604 Hz, 1H) ppm. IR: 2204, 1595, 1510, 1425, 1068, 697 cm⁻¹.



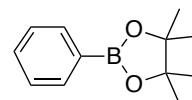
General procedure for the synthesis of boronic esters All boronic esters were prepared according to a procedure adapted from previous syntheses.⁴⁸

Synthesis of 5,5-Dimethyl-2-phenyl-1,3,2-dioxaborinane. On the Schlenk line under a nitrogen atmosphere, phenyl-boronic acid (1.00 g, 8.20 mmol) and



anhydrous pentane (22 mL) were added to an oven-dried two-neck flask containing a stir bar. The flask was brought to 0 °C and neopentanol glycol (0.94 g, 9.02 mmol) was added neat and stirred at room temperature for 24 hours. Sodium sulfate was added to the solution and then filtered with diethyl ether. The solvent was removed under reduced pressure to give a crude white solid that was filtered through a plug of silica eluting with dichloromethane to yield the product that was analytically pure by ¹H NMR spectroscopy (1.40 g, 90% yield). ¹H NMR (500 MHz, CDCl₃) δ 1.03 (s, 6H), 3.77 (s, 4H), 7.37-7.33 (m, 2H), 7.40-7.45 (m, 1H), 7.78-7.82 (d, 2H) ppm. ¹¹B NMR (128 MHz, CDCl₃) δ 26.9 ppm. ¹H-NMR matched previously reported values.⁴⁹

Synthesis of 4,4,5,5-Tetramethyl-2-phenyl-1,3,2-dioxaborolane. On the Schlenk line under a nitrogen atmosphere, phenyl-boronic acid (5.00 g, 41.0



mmol) and anhydrous pentane (110 mL) were added to an oven-dried two-neck flask containing a stir bar. The flask was brought to 0 °C and pinacol (5.08 g, 43 mmol) was added neat and stirred at room temperature for 24 hours. Sodium sulfate was added to the solution and then filtered with diethyl ether. The solvent was removed under reduced pressure to give a crude white solid that was filtered through a plug of silica eluting with dichloromethane to yield the product that was analytically pure by ¹H NMR spectroscopy (7.50 g, 90% yield). ¹H NMR (500 MHz, CDCl₃) δ 1.35 (s, 6H), 7.35-7.39 (m, 2H), 7.43-

7.48 (m, 1H), 7.79-7.83 (m, 2H) ppm. ^{11}B NMR (128 MHz, CDCl_3) δ 31.0 ppm. ^1H -NMR matched previously reported values.⁵⁰

General procedure for iron-catalyzed Suzuki-Miyaura cross-coupling, Procedure

A: In a nitrogen-filled glovebox complex **2.8** (21 mg, 0.05 mmol), 2,2-bis((S)-4-phenyl-4,5-dihydrooxazol-2-yl)acetonitrile ligand (16.5 mg, 0.05 mmol) and lithium-ethylmethyl amide (38.5 mg, 0.6 mmol) were added to a 7 mL vial containing a stir bar. Benzene (5 mL) was added to the stirring vial followed immediately by a 1 mL benzene solution of phenylboronic acid pinacol ester (204 mg, 1.0 mmol) and alkyl halide (0.5 mmol). The reaction was stirred vigorously and after 15 minutes, a precipitate formed. After 48 hours of stirring, the reaction was brought out of the glovebox and quenched with a saturated aqueous solution of ammonium chloride (10 mL). The aqueous phase was washed with dichloromethane (3 x 40 mL) and the combined organic phases were dried over sodium sulfate and filtered. Trimethoxybenzene (42 mg, 0.25 mmol) was added as an internal standard before evaporating the solvent. A spectroscopic yield was determined by ^1H NMR spectroscopy before the crude product was purified by silica column chromatography.

General procedure for iron-catalyzed Suzuki-Miyaura cross-coupling, Procedure

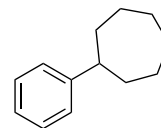
B: In a nitrogen filled glovebox, complex **2.8** (21 mg, 0.05 mmol), 2,2-bis((S)-4-phenyl-4,5-dihydrooxazol-2-yl)acetonitrile ligand (16.5 mg, 0.05 mmol) and lithium-ethylmethyl amide (38.5 mg, 0.6 mmol) were added to a 7 mL vial containing a stir bar. Benzene (5 mL) was added to the stirring vial followed immediately by a 1 mL benzene solution of phenylboronic acid pinacol ester (204 mg, 1.0 mmol) and alkyl halide (0.5 mmol). The reaction was sealed with a teflon cap and electrical tape. It was then removed from the glovebox and stirred vigorously at 50 °C. A precipitate forms on the vial wall after 10

minutes of stirring. After 48 hours, the reaction was quenched with a saturated aqueous solution of ammonium chloride (10 mL) and the aqueous phase was washed with dichloromethane (3 x 40 mL). The combined organic phases were dried over sodium sulfate and filtered. Trimethoxybenzene (42 mg, 0.25 mmol) was added as an internal standard before evaporating the solvent. A spectroscopic yield was determined by ¹H NMR spectroscopy before the crude product was purified by silica column chromatography.

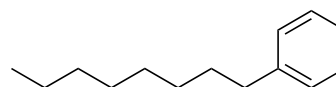
General procedure for iron-catalyzed Suzuki-Miyaura cross-coupling, Procedure C: In a nitrogen filled glovebox, complex **2.8** (21 mg, 0.05 mmol), 2,2-bis((S)-4-phenyl-4,5-dihydrooxazol-2-yl)acetonitrile ligand (16.5 mg, 0.05 mmol) and lithium-ethylmethyl amide phenylboronic acid pinacol ester borate (161 mg, 0.6 mmol) were added to a 7 mL vial with a stir bar. Benzene (5 mL) was added to the stirring vial followed immediately by a 1 mL benzene solution of phenylboronic acid pinacol ester (82 mg, 0.4 mmol) and alkyl halide (0.5 mmol). The reaction was stirred vigorously at room temperature. After 15 minutes, a precipitate formed. After stirring 24 hours, an additional aliquot of complex **2.8** (10.5 mg, 0.025 mmol) and lithium ethylmethylamide (19.25 mg, 0.3 mmol) were added to the reaction mixture. The reaction was sealed and stirred for another 24 hours. After this time, the reaction was brought out of the glovebox and quenched with a saturated aqueous solution of ammonium chloride (10 mL) and the aqueous phase was washed with dichloromethane (3 x 40 mL). The combined organic phases were dried over sodium sulfate and filtered. Trimethoxybenzene (42 mg, 0.25 mmol) was added as an internal standard before evaporating the solvent. A spectroscopic NMR yield was taken before the crude was purified by silica column chromatography to afford pure product. Specific column conditions are provided below for each substrate.

Substrate Scope:

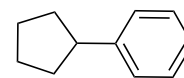
Phenylcycloheptane (2.4). Phenylcycloheptane was synthesized from bromocycloheptane by Procedure A and purified by silica gel flash column chromatography, eluting with 100% hexanes to afford product as a colorless oil (85% spectroscopic yield / 85% brsm, 80% isolated yield). ¹H-NMR matched previously reported values.²⁴ $R_f = 0.60$ (100% hexane) ¹H NMR (500 MHz, CDCl₃): δ 1.46 – 1.78 (m, 8H), 1.80 (ddd, $J = 13.4, 6.6, 3.4$ Hz, 2H), 1.92 (ddt, $J = 13.5, 6.6, 3.3$ Hz, 2H), 2.66 (tt, $J = 10.7, 3.7$ Hz, 1H), 7.08 – 7.23 (m, 2H), 7.23 – 7.33 (m, 2H) ppm.



Phenyloctane (2.10). Phenyloctane was synthesized from octylbromide by Procedure B and purified by silica gel flash column chromatography, eluting with 100% hexanes to afford product as a colorless oil (85% spectroscopic yield / 91% brsm, 77% isolated yield). ¹H-NMR matched previously reported values.²⁴ $R_f = 0.60$ (100% hexane) ¹H NMR (500MHz, CDCl₃) δ 0.86 – 0.91 (m, 3H), 1.25 – 1.33 (m, 10H), 1.59 – 1.64 (m, 2H), 2.60 (t, $J = 7.8$ Hz, 2H), 7.18 (d, $J = 7.6$ Hz, 3H), 7.27 (t, $J = 7.4$ Hz, 2H) ppm. Phenyloctane was also synthesized from octyl chloride by Procedure B (28% spectroscopic yield / 72% brsm, 28% isolated yield) and octyl iodide by Procedure A (47% spectroscopic yield, / 91% brsm, 45% isolated yield).

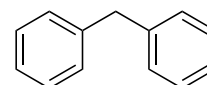


Phenylcyclopentane (2.11). Phenylcyclopentane was synthesized from bromocyclopentane by Procedure A and purified by silica gel flash column chromatography, eluting with 100% Hexanes to afford product as a colorless oil (80% spectroscopic yield / 85% brsm, 73% isolated yield). ¹H-NMR matched previously reported values.²⁴ $R_f = 0.60$ (100% hexane) ¹H NMR (500MHz, CDCl₃) δ 1.53

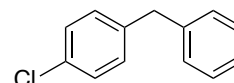


– 1.74 (m, 4H), 1.75 – 1.87 (m, 2H), 1.99 – 2.14 (m, 2H), 2.99 (tt, $J = 9.5, 7.4$ Hz, 1H), 7.09 – 7.39 (m, 5H) ppm. Phenylcyclopentane was also synthesized from chlorocyclopentane by Procedure A (32% spectroscopic yield / 86% brsm, 32% isolated yield) and iodocyclopentane by Procedure A (45% spectroscopic yield, / 96% brsm, 45% isolated yield).

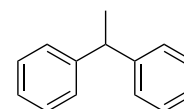
Diphenylmethane (2.12). Diphenylmethane was synthesized from benzyl chloride by Procedure A and purified by silica gel flash column chromatography, eluting with 100% hexanes to afford product as a colorless oil (79% spectroscopic yield / 79% brsm, 73% isolated yield). $^1\text{H-NMR}$ matched previously reported values.²⁴ $R_f = 0.50$ (100% hexane) $^1\text{H NMR}$ (500MHz, CDCl_3) δ 4.01 (s, 2H), 7.20 (s, 2H), 7.19 – 7.28 (m, 6H), 7.27 – 7.36 (m, 4H) ppm. Diphenylmethane was also synthesized from benzyl bromide (28% spectroscopic yield / 37% brsm).



1-benzyl-4-chlorobenzene (2.13). 1-benzyl-4-chlorobenzene was synthesized from 4-Chlorobenzyl chloride by Procedure A and purified by silica gel flash column chromatography, eluting with 100% Hexanes to afford product as a colorless oil (54% spectroscopic yield / 73% brsm, 40% isolated yield). $^1\text{H-NMR}$ matched previously reported values.⁵¹ $R_f = 0.50$ (100% hexane) $^1\text{H NMR}$ (500MHz, CDCl_3) δ 3.95 (s, 2H), 7.17 – 7.39 (m, 9H) ppm.

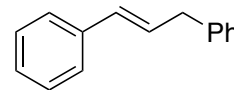


1,1-diphenylethane (2.14). 1,1-diphenylethane was synthesized from 1-chloroethylbenzene by Procedure C and purified by silica gel flash column chromatography, eluting with 100% Hexanes to afford product as a colorless oil (50% spectroscopic yield / 50% brsm, product isolated as a mixture with biphenyl). $^1\text{H-NMR}$ matched previously reported values.⁵¹ $R_f = 0.50$ (100% hexane) $^1\text{H NMR}$ (500MHz,

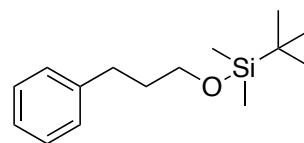


CDCl₃) δ 1.66 (d, $J = 7.2$ Hz, 3H), 4.17 (q, $J = 7.3$ Hz, 1H), 7.19 (t, $J = 7.2$ Hz, 2H), 7.22 – 7.25 (m, 4H), 7.29 (t, $J = 7.6$ Hz, 4H) ppm.

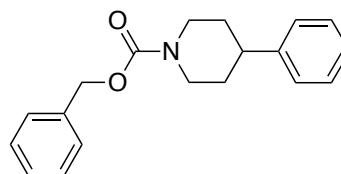
1,3-diphenylpropene **(2.15)**. 1,3-diphenylpropene was synthesized from 3-chloropropenylbenzene by Procedure A and purified by silica gel flash column chromatography, eluting with 100% Hexanes to afford product as a colorless oil (61% spectroscopic yield / 61% brsm, 60% isolated yield). ¹H-NMR matched previously reported values.²⁴ $R_f = 0.20$ (100% hexane) ¹H NMR (500MHz, CDCl₃) δ 3.56 (d, $J = 6.7$ Hz, 2H), 6.36 (dt, $J = 15.8, 6.9$ Hz, 1H), 6.46 (d, $J = 15.8$ Hz, 1H), 7.15 – 7.39 (m, 10H) ppm.



3-Phenylpropoxy-tert-butyldimethylsilane **(2.16)**. 3-Phenylpropoxy-tert-butyldimethylsilane was synthesized from 3-bromopropoxy-tert-butyldimethylsilane by Procedure B and purified by silica gel flash column chromatography, eluting with 100% Hexanes to afford product as a colorless oil (65% spectroscopic yield / 81% brsm, 60% isolated yield). ¹H-NMR matched previously reported values.⁵² $R_f = 0.15$ (100% pentane) ¹H NMR (500MHz, CDCl₃) δ 0.5 (s, 6H), 0.91 (s, 9H), 1.79 – 1.89 (m, 2H), 2.64 – 2.71 (m, 2H), 3.64 (t, $J = 6.3$ Hz, 2H), 3.64 (t, $J = 5.7$ Hz, 2H), 7.14 – 7.22 (m, 3H), 7.27 (m, 2H) ppm.

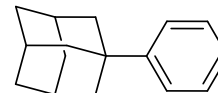


4-phenylpiperidine-1-carboxylic acid benzyl ester **(2.17)**. 4-phenylpiperidine-1-carboxylic acid benzyl ester was synthesized from 4-bromopiperidine-1-carboxylic acid benzyl ester by Procedure B and purified by silica gel flash column chromatography, eluting with 1:5 EtOAc/Hexanes to afford product as a colorless oil (70% spectroscopic yield / 96% brsm, 56% isolated yield). ¹H-NMR matched previously reported values.⁵³ R_f

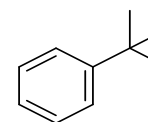


= 0.20 (1:5 EtOAc/hexane) ^1H NMR (500MHz, CDCl_3) δ 1.56 – 1.72 (m, 2H), 1.85 (d, J = 12.7 Hz, 2H), 2.67 (tt, J = 12.2, 3.6 Hz, 1H), 2.89 (t, J = 12.9 Hz, 2H), 4.32 (s, 2H), 5.16 (s, 2H), 7.17 – 7.25 (m, 3H), 7.26 – 7.42 (m, 7H) ppm.

Adamantylbenzene (**2.18**). Adamantylbenzene was synthesized from chloroadamantane by Procedure A, using phenylboronic acid pinacol ester. The yield of this compound was determined by GC because it is formed as a mixture with biadamantyl which coelutes with from silica gel (23% GC yield). The identity of the peak was confirmed through an authentic sample as well as GCMS.

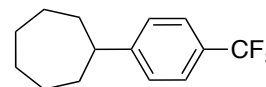


tert-butylbenzene (**2.19**). *Tert*-butylbenzene was synthesized from 2-chloro-2-methylpropane by Procedure A, using phenylboronic acid pinacol ester. The yield of this compound was determined by GC

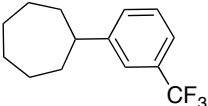


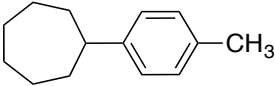
(21% GC yield). The identity of the peak was confirmed through an authentic sample as well as GCMS.

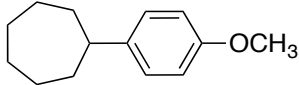
(4-trifluoromethyl)phenyl)cycloheptane (**2.21**). (4-trifluoromethyl)phenyl)cycloheptane was synthesized from

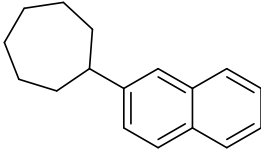


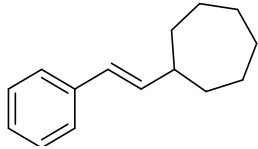
bromocycloheptane by Procedure B, using (4-trifluoromethyl)phenyl boronic acid pinacol ester in place of phenylboronic acid pinacol ester. Product was purified by silica gel flash column chromatography, eluting with 100% hexanes to afford purified product as a white crystalline solid (47% spectroscopic yield / 87% brsm, 47% isolated yield). ^1H -NMR matched previously reported values.²⁴ R_f = 0.50 (100% hexane), ^1H NMR (500 MHz, CDCl_3) δ 1.64 (m, 8H), 1.82 (s, 2H), 1.94 – 1.86 (m, 2H), 2.72 (tt, 1H), 7.52 (d, J = 8.0 Hz, 2H) ppm.

(3-trifluoromethyl)phenyl)cycloheptane (**2.22**) (3-trifluoromethyl) phenyl)cycloheptane was synthesized from  bromocycloheptane by Procedure B, using (3-trifluoromethyl)phenyl) boronic acid pinacol ester in place of phenylboronic acid pinacol ester. Product was purified by silica gel flash column chromatography, eluting with 100% hexanes to afford purified product as a white crystalline solid (67% spectroscopic yield / 76% brsm, 67% isolated yield). $R_f = 0.80$ (100% hexane), ^1H NMR (500 MHz, CDCl_3) δ 1.75 – 1.62, 1.82 (s, 2H), 1.90 (d, $J = 15.6$ Hz, 2H), 2.74 (m, 1H), 7.48 (t, $J = 7.7$ Hz, 2H), 7.70 (d, $J = 7.9$ Hz, 1H), 7.97 (d, $J = 7.5$ Hz, 1H) ppm. $\{^1\text{H}\}^{13}\text{C}$ NMR (125 MHz, CDCl_3) δ 27.1 (s), 27.8 (s), 36.7 (s), 46.9 (s), 122.4 (q, $J = 3.9$ Hz), 123.4 (q, $J = 3.8$ Hz), 124.3 (q, $J = 270.6$ Hz), 128.6 (s), 130.1 (q, $J = 1.4$ Hz), 130.5 (q, $J = 31.4$ Hz), 150.7 (s) ppm. ^{19}F NMR (470 MHz, CDCl_3) δ -62.1 (s) ppm. IR: 2922, 1446, 1327, 1158, 1121, 1073, 796, 702, 664 cm^{-1} . HRMS (ESI) m/z $[\text{M}]^+$ calcd. For $\text{C}_{14}\text{H}_{17}\text{F}_3$ 242.12769; found 242.12858.

p-tolylcycloheptane (**2.23**). *p*-tolylcycloheptane was synthesized from bromocycloheptane by Procedure B using *p*- tolylboronic acid pinacol ester in place of phenylboronic acid pinacol ester. Product was purified by silica gel flash column chromatography, eluting with 30% EtOAc in Hexane to afford purified product as a colorless oil (51% spectroscopic yield / 56% brsm, 51% isolated yield). ^1H -NMR matched previously reported values.⁵⁴ $R_f = 0.70$ (100% hexane) ^1H NMR (400 MHz, CDCl_3) $\delta = 1.67$ - 1.55 (m, 8H), 1.82 - 1.73 (2H), 1.93 - 1.84 (m, 2H), 2.31 (s, 3H), 2.66-2.58 (m, 1H), 7.08 (s, 4H) ppm.

(4-methoxyphenyl)cycloheptane (**2.24**). (4-methoxyphenyl)cyclo heptane was synthesized from bromocycloheptane by Procedure C using (4-) boronic acid pinacol ester in place of phenylboronic acid pinacol ester. Product was purified by silica gel flash column chromatography, eluting with 30% EtOAc in Hexane to afford purified product as a colorless oil (68% spectroscopic yield / 100% brsm, 68% isolated yield). ¹H-NMR matched previously reported values.²⁴ R_f = 0.60 (10% EtOAc in hexane) ¹H NMR (500 MHz, CDCl₃) δ = 1.65-1.49 (m, 6H), 1.72-1.65 (m, 2H), 1.82-1.73 (m, 2H), 1.93-1.83 (m, 2H), 2.66-2.57 (m, 1H), 3.78 (s, 3H), 6.83-6.81 (m, 2H), 7.12-7.10 (m, 2H) ppm.

2-cycloheptylnaphthalene (**2.25**). 2-cycloheptylnaphthalene was synthesized from bromocycloheptane by Procedure A, using naphthalene-2-boronic acid pinacol ester in place of phenylboronic acid pinacol ester. Product was purified by silica gel flash column chromatography, eluting with 100% Hexanes to afford purified product as a white crystalline (84% spectroscopic yield / 84% brsm, 76% isolated yield). ¹H-NMR matched previously reported values.⁵⁵³ R_f = 0.45 (100% hexane) ¹H NMR (500 MHz, CDCl₃) δ = 1.85-1.58 (m, 10H), 2.01-1.98, (m, 2H), 2.86-2.81 (m, 1H), 7.44-7.45 (m, 3H), 7.61 (s, 1H), 7.79-7.75(m, 3H) ppm.

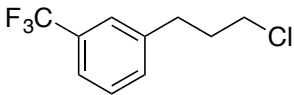
(E)-styrenylcycloheptane (**2.26**). (E)-styrenylcycloheptane was synthesized from bromocycloheptane by Procedure A using (E)-styrenyl boronic acid pinacol ester in place of phenylboronic acid pinacol ester. Product was purified by silica gel flash column chromatography, eluting with pure Hexane to afford purified product as a colorless oil (27% spectroscopic yield / 25% brsm, 25% isolated yield). ¹H-NMR matched previously reported values.⁵⁶ R_f

= 0.80 (100% hexane), ^1H NMR (600 MHz, CDCl_3) δ 1.39-1.47 (m, 2H), 1.47-1.58 (m, 4H), 1.59-1.67 (m, 2H), 1.67-1.75 (m, 2H), 1.79-1.86 (m, 2H), 2.33 (ddq, $J = 13.1, 8.6, 4.1$ Hz, 1H), 6.22 (dd, $J = 15.9, 7.6$ Hz, 1H), 6.32 (d, $J = 15.9$ Hz, 1H), 7.18 (t, $J = 7.2$ Hz, 1H), 7.28 (t, $J = 7.6$ Hz, 2H), 7.34 (d, $J = 7.6$ Hz, 2H).

Cross-coupling reaction between PhB(pin) and cyclopropylmethylbromide. In a nitrogen-filled glovebox complex **2.8** (21 mg, 0.05 mmol), 2,2-bis((S)-4-phenyl-4,5-dihydrooxazol-2-yl)acetonitrile ligand (16.5 mg, 0.05 mmol) and lithium-ethylmethyl amide (38.5 mg, 0.6 mmol) were added to a 7 mL vial containing a stir bar. Benzene (5 mL) was added to the stirring vial followed immediately by a 1 mL benzene solution of phenylboronic acid pinacol ester (204 mg, 1.0 mmol) and cyclopropylmethylbromide (67 mg, 48 μL , 0.5 mmol). The reaction was stirred vigorously and after 15 minutes, a precipitate formed. After 48 hours of stirring, the reaction was brought out of the glovebox and quenched with a saturated aqueous solution of ammonium chloride (10 mL). The aqueous phase was washed with dichloromethane (3 x 40 mL) and the combined organic phases were dried over sodium sulfate and filtered. Trimethoxybenzene (42 mg, 0.25 mmol) was added as an internal standard before evaporating the solvent. A spectroscopic yield was determined by ^1H NMR spectroscopy before the crude product was further purified. This product was purified by silica gel flash column chromatography, eluting with 100% hexanes to afford purified product as a colorless oil (76% spectroscopic yield / 76% brsm, 55% isolated yield).²⁴ $R_f = 0.80$ (100% hexane), ^1H NMR (500 MHz, CDCl_3) δ 2.36 (q, $J = 7.3$ Hz, 2H), 2.69 (t, $J = 8.2$ Hz, 2H), 4.99 (dd, $J = 13.7, 26$ Hz, 2H), 5.84 (m, 1H), 7.17 (m, 2H), 7.25 (m, 2H), 7.44 (m, 1H) ppm.

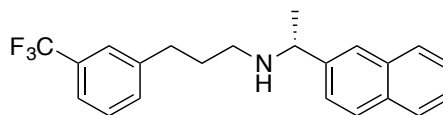
Cross-coupling reaction between PhB(pin) and 6-bromohex-1-ene. In a nitrogen-filled glovebox complex **2.8** (21 mg, 0.05 mmol), 2,2-bis((S)-4-phenyl-4,5-dihydrooxazol-2-yl)acetonitrile ligand (16.5 mg, 0.05 mmol) and lithium-ethylmethyl amide (38.5 mg, 0.6 mmol) were added to a 7 mL vial containing a stir bar. Benzene (5 mL) was added to the stirring vial followed immediately by a 1 mL benzene solution of phenylboronic acid pinacol ester (204 mg, 1.0 mmol) and 6-bromohex-1-ene (81 mg, 67 μ L, 0.5 mmol). The reaction was stirred vigorously and after 15 minutes, a precipitate formed. After 48 hours of stirring, the reaction was brought out of the glovebox and quenched with a saturated aqueous solution of ammonium chloride (10 mL). The aqueous phase was washed with dichloromethane (3 x 40 mL) and the combined organic phases were dried over sodium sulfate and filtered. Trimethoxybenzene (42 mg, 0.25 mmol) was added as an internal standard before evaporating the solvent. This reaction produced a mixture of the cyclized and uncyclized products. To verify the ratio the mixture was also analyzed by gas chromatography as well as the relative integration of the alkene peaks to the overlapping benzylic peaks by NMR. The ratio is between 1.25:1 (GC) and 1.56:1 (NMR) for cyclized to uncyclized products. Hex-5-enylbenzene⁵⁷ R_f = 0.60 (100% hexane). ¹H NMR (500 MHz, CDCl₃) δ 1.45 (m, 2H), 1.65 (m, 2H), 2.10 (m, 2H), 2.62 (t, J = 7.5 Hz, 2H), 5.00 (dd, J = 13.7, 26 Hz, 2H), 5.81 (ddt, J = 16.9, 10.1, 6.7 Hz, 1H), 7.18 (m, 3H), 7.26 (m, 2H) ppm. Cyclopentylmethylbenzene⁵⁸ R_f = 0.60 (100% hexane). ¹H NMR (500 MHz, CDCl₃) δ 1.21 (m, 2H), 1.53 (m, 2H), 1.65 (m, 2H) 1.71 (m, 2H) 2.10 (m, 1H) 2.6 (d, J = 7.5 Hz, 2H), 7.18 (m, 3H), 7.26 (m, 2H) ppm.

Cross-coupling reaction between Phenyl boronic acid neopentyl glycol ester and cycloheptyl bromide. In a nitrogen-filled glovebox complex **2.8** (21 mg, 0.05 mmol), 2,2-bis((S)-4-phenyl-4,5-dihydrooxazol-2-yl)acetonitrile ligand (16.5 mg, 0.05 mmol) and lithium-ethylmethyl amide (38.5 mg, 0.6 mmol) were added to a 7 mL vial containing a stir bar. Benzene (5 mL) was added to the stirring vial followed immediately by a 1 mL benzene solution of phenylboronic acid neopentyl glycol ester (190 mg, 1.0 mmol), tetradecane (25 mg, 32 μ L, 0.125 mmol) and bromocycloheptane (88 mg, 68 μ L, 0.5 mmol). The reaction was stirred vigorously and after 5 minutes, a precipitate formed. After 48 hours of stirring, the reaction was brought out of the glovebox and quenched with a drop of water, dried with sodium sulfate, and filtered through celite. The mixture was then analyzed by GC using an achiral column with tetradecane as the internal standard. Phenylcycloheptane was formed in 5% yield.

Synthesis of 1-(3-chloropropyl)-3-(trifluoromethyl)benzene (2.31). In a nitrogen filled glovebox, complex **2.8** (84 mg, 0.20 mmol), cyano-  phenyl-bisoxazoline ligand (66 mg, 0.20 mmol) and lithium-ethylmethyl amide (156 mg, 2.40 mmol) were added to a 20 mL vial containing a stir bar. Benzene (15 mL) was added to the stirring vial followed immediately by a 5 mL benzene solution of *m*-trifluoromethylboronic acid pinacol ester (1.09 g, 4.00 mmol) and 1-bromo-3-chloropropane (197 μ L, 314 mg, 2.00 mmol). The vial was sealed using electrical tape before being brought outside the glovebox. The reaction was stirred vigorously at 50 °C. A precipitate formed on the vial wall after 10 minutes of stirring. After 48 hours, the reaction was quenched with a saturated aqueous solution of ammonium chloride (10 mL)

and the aqueous phase was washed with dichloromethane (3 x 40 mL). The combined organic phases were dried over sodium sulfate and filtered. Trimethoxybenzene (42 mg, 0.25 mmol) was added as an internal standard before evaporating the solvent. A spectroscopic yield of 60% was determined by ^1H NMR spectroscopy before the crude product was purified by silica gel flash column chromatography, eluting with hexanes to afford the product ($R_f = 0.50$), which was then further isolated from the bisarylated product (although it doesn't affect the subsequent reaction) through distillation ($R_f = 0.50$). The product was obtained as a colorless oil (244.9 mg, 55%). IR (neat): 2958, 2866, 2360, 1449, 1325, 1161, 1095, 1072, 900, 799, 701, 658 cm^{-1} ; ^1H NMR (400 MHz, CDCl_3): δ 2.04 – 2.14 (m, 2H), 2.85 (t, $J = 7.5$ Hz, 2H), 3.53 (t, $J = 6.3$ Hz, 2H), 7.37 – 7.49 (m, 4H); $\{^1\text{H}\}^{13}\text{C}$ NMR (125 MHz, CDCl_3): δ 32.55, 33.71, 43.88, 123.08 (q, $^3J = 3.9$ Hz), 124.10 (q, $^1J = 272.43$ Hz), 125.17 (q, $^3J = 3.9$ Hz), 128.9, 130.81 (q, $^2J = 32.41$ Hz), 131.93, 141.59. ^{19}F NMR (470 MHz, CDCl_3): δ -62.56 ppm. HRMS (ESI) m/z $[\text{M}]^+$ calcd. For $\text{C}_{10}\text{H}_{10}\text{F}_3\text{Cl}$ 222.64; found 222.04.

Synthesis of Cinacalcet (2.33). To a 20 mL Schlenk tube was added alkyl chloride (240 mg, 1.08 mmol),



present as a mixture of **36** and bisarylated product, potassium iodide (40 mg, 0.24 mmol) and potassium carbonate (331 mg, 2.40 mmol). On a Schlenk line, the Schlenk tube was evacuated and backfilled with nitrogen and then (*R*)-(+)-1-(1-naphthyl)ethan-1-amine (**2.32**, 231 μL , 246 mg, 1.44 mmol) was added by syringe after addition of anhydrous acetonitrile (4 mL). The flask was sealed and then heated to 100 $^\circ\text{C}$ for 48 hours. At this time, the reaction was cooled, the insoluble material was filtered, and the solvent evaporated to yield a brown oil. The crude product was dissolved in dichloromethane (20 mL), washed with

5% aqueous hydrochloric acid (25 mL), saturated sodium bicarbonate solution (25 mL), and deionized water (25 mL). The combined organic phases were dried over sodium sulfate, filtered, and the solvent was removed under reduced pressure. The product was isolated as a pure colorless oil (270 mg, 70%). $^1\text{H-NMR}$ matched previously reported values.⁵⁹ $R_f = 0.30$ (1:1 EtOAc/hexane), $^1\text{H NMR}$ (400 MHz, CDCl_3): δ 1.36 (bs, 1H), 1.49 (d, $J = 6.6$ Hz, 3H), 1.84 (tt, $J = 7.4$ Hz, 2H), 2.55 – 2.79 (m, 4H), 4.62 (q, $J = 6.6$ Hz, 1H), 7.28 – 7.38 (m, 2H), 7.39 – 7.55 (m, 5H), 7.61 – 7.67 (m, 1H), 7.75 (d, $J = 8.1$ Hz, 1H), 7.88 (dd, $J = 7.6, 1.7$ Hz, 1H), 8.17 – 8.22 (m, 1H). $^{13}\text{C NMR}$ (500 MHz, CDCl_3) δ 23.56, 31.83, 33.37, 47.23, 53.73, 122.58 (q, $^3J = 4.3$ Hz), 122.62, 122.88, 124.24 (q, $^1J = 274.33$ Hz), 124.99 (q, $^3J = 3.7$ Hz), 125.27, 125.64, 125.72, 127.15, 128.6, 128.94, 130.52 (q, $^2J = 31.9$ Hz), 131.3, 131.72, 133.95, 141.17, 143.04. HRMS (ESI) m/z $[\text{M}]^+$ calcd. For $\text{C}_{22}\text{H}_{22}\text{F}_3\text{N}$ 357.41; found 357.18. α_{589}^{24} ($c = 1.0, \text{CHCl}_3$) = +21.8°

Figure S2.1: Plots of the Mulliken charge distribution obtained from DFT (B3LYP/631G*) calculations for the transition state obtained for transmetalation reaction between $(\text{dppe})\text{Fe}(\text{NEt}_2)_2$ and $\text{PhB}(\text{pin})$. Mulliken charge distribution for $\text{PhB}(\text{pin})$ is also shown for reference.

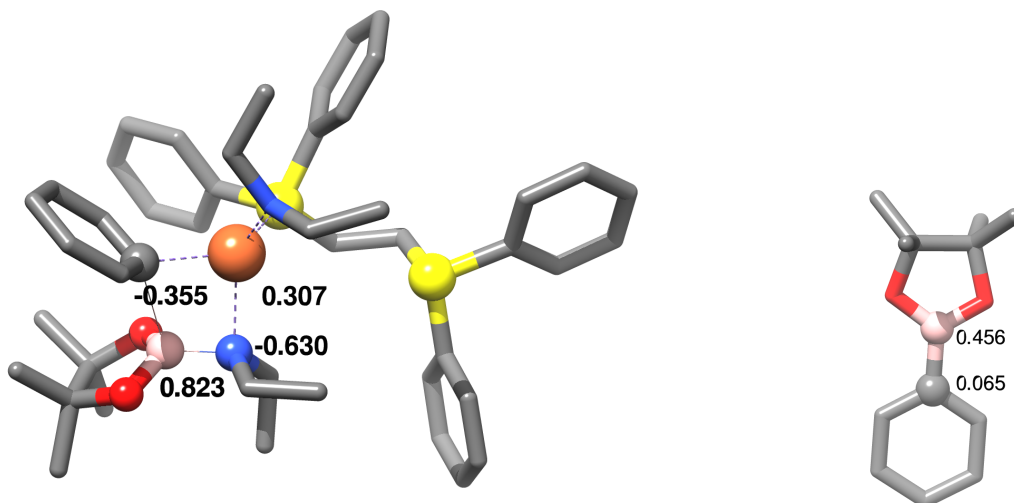
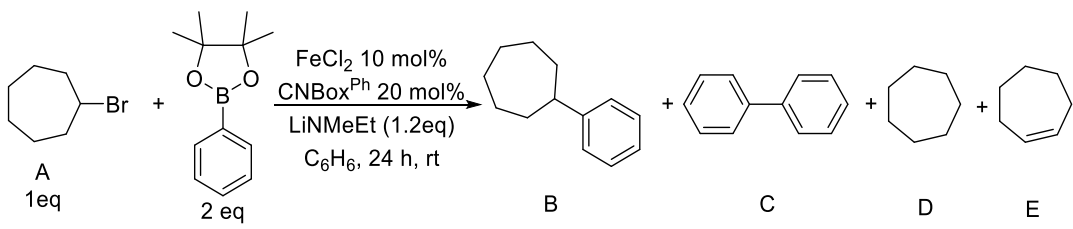


Table S2.1: Control reactions for the iron-catalyzed Suzuki-Miyaura cross-coupling reaction between PhB(pin) and cycloheptyl bromide



Omissions	A	B	C	D	E
no FeCl ₂	100	0	0	0	0
no LiNMeEt	90	0	0	2	0
no CNBox ^{Ph}	0	29	6	11	40
no PhB(pin)	42	0	0	32	1
no cycloheptylbromide	0	0	5	0	0

Figure S2.2: ¹¹B NMR (128MHz) in THF of reaction between lithium ethylmethylamide and PhB(pin). Broad resonance centered at -3 ppm is from the borosilicate glass NMR tube. ¹¹B shift of PhB(pin) is 31 ppm

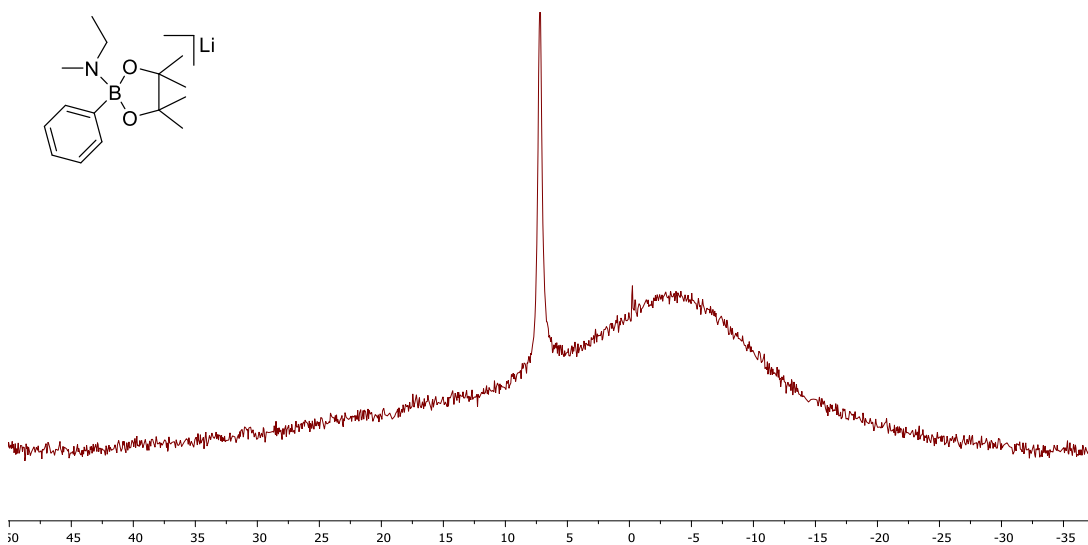
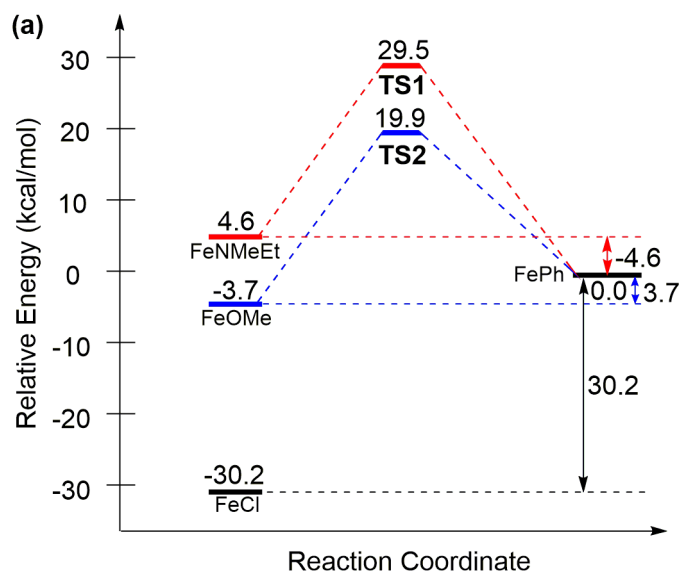
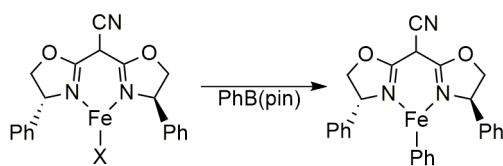


Figure S2.3: DFT (B3LYP/6-31G*) computed energies for transmetalation from boron to iron in reactions between PhB(pin) and CNBox^{Ph}FeX (X = anionic ligand)



2.8 References:

- (1) Jana, R.; Pathak, T. P.; Sigman, M. S. Advances in Transition Metal (Pd,Ni,Fe)-Catalyzed Cross-Coupling Reactions Using Alkyl-Organometallics as Reaction Partners. *Chem. Rev.* **2011**, *111*, 1417–1492. <https://doi.org/10.1021/cr100327p>.
- (2) Brown, D. G.; Boström, J. Analysis of Past and Present Synthetic Methodologies on Medicinal Chemistry: Where Have All the New Reactions Gone? *J. Med. Chem.* **2016**, *59*, 4443–4458. <https://doi.org/10.1021/acs.jmedchem.5b01409>.
- (3) Suzuki, A.; Miyaura, N.; Yamada, K. First Suzuki. *Tetrahedron Lett.* **1979**, *36*, 3437–3440. [https://doi.org/10.1016/S0040-4039\(01\)95429-2](https://doi.org/10.1016/S0040-4039(01)95429-2).
- (4) Link, J. O.; Taylor, J. G.; Xu, L.; Mitchell, M.; Guo, H.; Liu, H.; Kato, D.; Kirschberg, T.; Sun, J.; Squires, N.; et al. Discovery of Ledipasvir (GS-5885): A Potent, Once-Daily Oral NS5A Inhibitor for the Treatment of Hepatitis C Virus Infection. *J. Med. Chem.* **2014**, *57*, 2033–2046. <https://doi.org/10.1021/jm401499g>.
- (5) Egorova, K. S.; Ananikov, V. P. Toxicity of Metal Compounds: Knowledge and Myths. *Organometallics* **2017**, *36*, 4071–4090. <https://doi.org/10.1021/acs.organomet.7b00605>.
- (6) Choi, J.; Fu, G. C. Transition Metal-Catalyzed Alkyl-Alkyl Bond Formation: Another Dimension in Cross-Coupling Chemistry. *Science* **2017**, *356*, 559–564. <https://doi.org/10.1126/science.aaf7230>.
- (7) Martin, R.; Buchwald, S. L. Palladium-Catalyzed Suzuki-Miyaura Cross-Coupling Reactions Employing Dialkylbiaryl Phosphine Ligands. *Acc. Chem. Res.* **2008**, *41*, 1461–1473. <https://doi.org/10.1021/ar800036s>.
- (8) Hazari, N.; Melvin, P. R.; Beromi, M. M. Well-Defined Nickel and Palladium

- Precatalysts for Cross-Coupling. *Nat. Rev. Chem.* **2017**, *1*, 1–17.
<https://doi.org/10.1038/s41570-017-0025>.
- (9) Bhayana, B.; Fors, B. P.; Buchwald, S. L. A Versatile Catalyst System for Suzuki-Miyaura Cross-Coupling Reactions of C(Sp²)-Tosylates and Mesylates. *Org. Lett.* **2009**, *11*, 3954–3957. <https://doi.org/10.1021/ol9015892>.
- (10) Netherton, M. R.; Dai, C.; Neuschütz, K.; Fu, G. C. Room-Temperature Alkyl-Alkyl Suzuki Cross-Coupling of Alkyl Bromides That Possess β Hydrogens [1]. *J. Am. Chem. Soc.* **2001**, *123*, 10099–10100. <https://doi.org/10.1021/ja011306o>.
- (11) Richmond, E.; Moran, J. Recent Advances in Nickel Catalysis Enabled by Stoichiometric Metallic Reducing Agents. *Synthesis* **2017**, *50*, 499–513. <https://doi.org/10.1055/s-0036-1591853>.
- (12) Kyne, S. H.; Lefèvre, G.; Ollivier, C.; Petit, M.; Ramis Cladera, V. A.; Fensterbank, L. Iron and Cobalt Catalysis: New Perspectives in Synthetic Radical Chemistry. *Chem. Soc. Rev.* **2020**, *49*, 8501–8542. <https://doi.org/10.1039/d0cs00969e>.
- (13) Cahiez, G.; Moyeux, A. Cobalt-Catalyzed Cross-Coupling Reactions. *Chem. Rev.* **2010**, *110*, 1435–1462. <https://doi.org/10.1021/cr9000786>.
- (14) Tamura, M.; Kochi, J. Vinylation of Grignard Reagents. Catalysis by Iron. *J. Am. Chem. Soc.* **1971**, *93*, 1487–1489. <https://doi.org/10.1021/ja00735a030>.
- (15) Fürstner, A.; Leitner, A. Iron-Catalyzed Cross-Coupling Reactions of Alkyl-Grignard Reagents with Aryl Chlorides, Tosylates, and Triflates. *Angew. Chemie - Int. Ed.* **2002**, *41*, 609–612. [https://doi.org/10.1002/1521-3773\(20020215\)41:4<609::AID-ANIE609>3.0.CO;2-M](https://doi.org/10.1002/1521-3773(20020215)41:4<609::AID-ANIE609>3.0.CO;2-M).
- (16) Martin, R.; Fürstner, A. Cross-Coupling of Alkyl Halides with Aryl Grignard

- Reagents Catalyzed by a Low-Valent Iron Complex. *Angew. Chemie - Int. Ed.* **2004**, *43*, 3955–3957. <https://doi.org/10.1002/anie.200460504>.
- (17) Hatakeyama, T.; Fujiwara, Y. I.; Okada, Y.; Itoh, T.; Hashimoto, T.; Kawamura, S.; Ogata, K.; Takaya, H.; Nakamura, M. Kumada-Tamao-Corriu Coupling of Alkyl Halides Catalyzed by an Iron-Bisphosphine Complex. *Chem. Lett.* **2011**, *40*, 1030–1032. <https://doi.org/10.1246/cl.2011.1030>.
- (18) Bedford, R. B.; Carter, E.; Cogswell, P. M.; Gower, N. J.; Haddow, M. F.; Harvey, J. N.; Murphy, D. M.; Neeve, E. C.; Nunn, J. Simplifying Iron-Phosphine Catalysts for Cross-Coupling Reactions. *Angew. Chemie - Int. Ed.* **2013**, *52*, 1285–1288. <https://doi.org/10.1002/anie.201207868>.
- (19) Bauer, G.; Wodrich, M. D.; Scopelliti, R.; Hu, X. Iron Pincer Complexes as Catalysts and Intermediates in Alkyl-Aryl Kumada Coupling Reactions. *Organometallics* **2015**, *34*, 289–298. <https://doi.org/10.1021/om501122p>.
- (20) Mako, T. L.; Byers, J. A. Recent Advances in Iron-Catalysed Cross Coupling Reactions and Their Mechanistic Underpinning. *Inorg. Chem. Front.* **2016**, *3*, 766–790. <https://doi.org/10.1039/c5qi00295h>.
- (21) Ilies, L.; Asako, S.; Nakamura, E. Iron-Catalyzed Stereospecific Activation of Olefinic C–H Bonds with Grignard Reagent for Synthesis of Substituted Olefins. *J. Am. Chem. Soc.* **2011**, *133*, 7672–7675. <https://doi.org/10.1021/ja2017202>.
- (22) Hashimoto, T.; Hatakeyama, T.; Nakamura, M. Stereospecific Cross-Coupling between Alkenylboronates and Alkyl Halides Catalyzed by Iron-Bisphosphine Complexes. *J. Org. Chem.* **2012**, *77*, 1168–1173. <https://doi.org/10.1021/jo202151f>.
- (23) Hatakeyama, T.; Okada, Y.; Yoshimoto, Y.; Nakamura, M. Tuning

- Chemoselectivity in Iron-Catalyzed Sonogashira-Type Reactions Using a Bisphosphine Ligand with Peripheral Steric Bulk: Selective Alkynylation of Nonactivated Alkyl Halides. *Angew. Chemie - Int. Ed.* **2011**, *50*, 10973–10976. <https://doi.org/10.1002/anie.201104125>.
- (24) Bedford, R. B.; Brenner, P. B.; Carter, E.; Carvell, T. W.; Cogswell, P. M.; Gallagher, T.; Harvey, J. N.; Murphy, D. M.; Neeve, E. C.; Nunn, J.; et al. Expedient Iron-Catalyzed Coupling of Alkyl, Benzyl and Allyl Halides with Arylboronic Esters. *Chem. - A Eur. J.* **2014**, *20*, 7935–7938. <https://doi.org/10.1002/chem.201402174>.
- (25) Nakamura, M.; Hatakeyama, T.; Hashimoto, T.; Kondo, Y.; Fujiwara, Y.; Seike, H.; Takaya, H.; Tamada, Y.; Ono, T. Iron-Catalyzed Suzuki-Miyaura Coupling of Alkyl Halides. *J. Am. Chem. Soc.* **2010**, *132*, 10674–10676. <https://doi.org/10.1021/ja103973a>.
- (26) Butters, M.; Harvey, J. N.; Jover, J.; Lennox, A. J. J.; Lloyd-Jones, G. C.; Murray, P. M. Aryl Trifluoroborates in Suzuki-Miyaura Coupling: The Roles of Endogenous Aryl Boronic Acid and Fluoride. *Angew. Chemie - Int. Ed.* **2010**, *49*, 5156–5160. <https://doi.org/10.1002/anie.201001522>.
- (27) Lennox, A. J. J.; Lloyd-Jones, G. C. Transmetalation in the Suzuki-Miyaura Coupling: The Fork in the Trail. *Angew. Chemie - Int. Ed.* **2013**, *52*, 7362–7370. <https://doi.org/10.1002/anie.201301737>.
- (28) Matos, K.; Soderquist, J. A. Alkylboranes in the Suzuki-Miyaura Coupling: Stereochemical and Mechanistic Studies. *J. Org. Chem.* **1998**, *63*, 461–470. <https://doi.org/10.1021/jo971681s>.

- (29) Carrow, B. P.; Hartwig, J. F. Distinguishing between Pathways for Transmetalation in Suzuki-Miyaura Reactions. *J. Am. Chem. Soc.* **2011**, *133*, 2116–2119. <https://doi.org/10.1021/ja1108326>.
- (30) Thomas, A. A.; Wang, H.; Zahrt, A. F.; Denmark, S. E. Structural, Kinetic, and Computational Characterization of the Elusive Arylpalladium(II)Boronate Complexes in the Suzuki-Miyaura Reaction. *J. Am. Chem. Soc.* **2017**, *139*, 3805–3821. <https://doi.org/10.1021/jacs.6b13384>.
- (31) Thomas, A. A.; Zahrt, A. F.; Delaney, C. P.; Denmark, S. E. Elucidating the Role of the Boronic Esters in the Suzuki-Miyaura Reaction: Structural, Kinetic, and Computational Investigations. *J. Am. Chem. Soc.* **2018**, *140*, 4401–4416. <https://doi.org/10.1021/jacs.8b00400>.
- (32) Biernesser, A. B.; Li, B.; Byers, J. A. Redox-Controlled Polymerization of Lactide Catalyzed by Bis(Imino)Pyridine Iron Bis(Alkoxide) Complexes. *J. Am. Chem. Soc.* **2013**, *135*, 16553–16560. <https://doi.org/10.1021/ja407920d>.
- (33) Crockett, M. P. The Development of Iron Catalysts for Suzuki-Miyaura Cross-Coupling and the Reactivity Discovered Along the Way, Boston College Chemistry, 2020.
- (34) Crockett, M. P.; Tyrol, C. C.; Wong, A. S.; Li, B.; Byers, J. A. Iron-Catalyzed Suzuki-Miyaura Cross-Coupling Reactions between Alkyl Halides and Unactivated Arylboronic Esters. *Org. Lett.* **2018**, *20*, 5233–5237. <https://doi.org/10.1021/acs.orglett.8b02184>.
- (35) Daifuku, S. L.; Kneebone, J. L.; Snyder, B. E. R.; Neidig, M. L. Iron(II) Active Species in Iron-Bisphosphine Catalyzed Kumada and Suzuki-Miyaura Cross-

- Couplings of Phenyl Nucleophiles and Secondary Alkyl Halide. *J. Am. Chem. Soc.* **2015**, *137*, 11432–11444. <https://doi.org/10.1021/jacs.5b06648>.
- (36) Audran, G.; Brémond, P.; Marque, S. R. A.; Siri, D.; Santelli, M. Calculated Linear Free Energy Relationships in the Course of the Suzuki-Miyaura Coupling Reaction. *Tetrahedron* **2014**, *70*, 2272–2279. <https://doi.org/10.1016/j.tet.2014.02.011>.
- (37) Connon, R.; Roche, B.; Rokade, B. V.; Guiry, P. J. Further Developments and Applications of Oxazoline-Containing Ligands in Asymmetric Catalysis. *Chem. Rev.* **2021**, *11*, 6373–6521. <https://doi.org/10.1021/acs.chemrev.0c00844>.
- (38) Dong, Y.; Lund, C. J.; Porter, G. J.; Clarke, R. M.; Zheng, S. L.; Cundari, T. R.; Betley, T. A. Enantioselective C-H Amination Catalyzed by Nickel Iminyl Complexes Supported by Anionic Bisoxazoline (BOX) Ligands. *J. Am. Chem. Soc.* **2021**, *143*, 817–829. <https://doi.org/10.1021/jacs.0c09839>.
- (39) Tewari, N.; Maheshwari, N.; Medhane, R.; Nizar, H.; Prasad, M. A Novel Method for the Large Scale Synthesis of Cinacalcet Hydrochloride Using Iron Catalyzed C-C Coupling. *Org. Process Res. Dev.* **2012**, *16*, 1566–1568. <https://doi.org/10.1021/op300164y>.
- (40) Barniol-Xicotá, M.; Leiva, R.; Escolano, C.; Vázquez, S. Syntheses of Cinacalcet: An Enantiopure Active Pharmaceutical Ingredient (API). *Synth.* **2016**, *48*, 783–803. <https://doi.org/10.1055/s-0035-1561506>.
- (41) Van Wagenen, B. C., Moe, S. T., Balandrin, M. F., DelMar, E. G., Nemeth, E. F. U.S. Patent PCT/US1995/013704, 2001.
- (42) Thiel, O., Bernard, C., Larsen, R., Martinelli, M. J., Raza, M. T. PCT Int. Appl. WO2009002427, 2009.

- (43) Kambe, N.; Iwasaki, T.; Terao, J. Pd-Catalyzed Cross-Coupling Reactions of Alkyl Halides. *Chem. Soc. Rev.* **2011**, *40*, 4937–4947. <https://doi.org/10.1039/c1cs15129k>.
- (44) Burger, B. J.; Bercaw, J. E. Vacuum Line Techniques for Handling Air-Sensitive Organometallic Compounds. In *Experimental Organometallic Chemistry*; Wayda, A. L., Darensbourg, M. Y., Eds.; *American Chemical Society*, **1987**; 79–115. <https://doi.org/10.1021/bk-1987-0357.ch004>.
- (45) Pangborn, A. B.; Giardello, M. A.; Grubbs, R. H.; Rosen, R. K.; Timmers, F. J. Safe and Convenient Procedure for Solvent Purification. *Organometallics* **1996**, *15*, 1518–1520. <https://doi.org/10.1021/om9503712>.
- (46) Rassolov, V. A.; Pople, J. A.; Ratner, M. A.; Windus, T. L. 6-31G* Basis Set for Atoms K through Zn. *J. Chem. Phys.* **1998**, *109*, 1223–1229. <https://doi.org/10.1063/1.476673>.
- (47) Miertuš, S.; Scrocco, E.; Tomasi, J. Electrostatic Interaction of a Solute with a Continuum. A Direct Utilizaion of AB Initio Molecular Potentials for the Prevision of Solvent Effects. *Chem. Phys.* **1981**, *55*, 117–129. [https://doi.org/10.1016/0301-0104\(81\)85090-2](https://doi.org/10.1016/0301-0104(81)85090-2).
- (48) Potter, B.; Edelstein, E. K.; Morken, J. P. Modular, Catalytic Enantioselective Construction of Quaternary Carbon Stereocenters by Sequential Cross-Coupling Reactions. *Org. Lett.* **2016**, *18*, 3286–3289. <https://doi.org/10.1021/acs.orglett.6b01580>.
- (49) Delaney, C. P.; Kassel, V. M.; Denmark, S. E. Potassium Trimethylsilanolate Enables Rapid, Homogeneous Suzuki-Miyaura Cross-Coupling of Boronic Esters.

- ACS Catal.* **2019**, *10*, 73–80. <https://doi.org/10.1021/acscatal.9b04353>.
- (50) Iwamoto, T.; Okuzono, C.; Adak, L.; Jin, M.; Nakamura, M. Iron-Catalysed Enantioselective Suzuki-Miyaura Coupling of Racemic Alkyl Bromides. *Chem. Commun.* **2019**, *55*, 1128–1131. <https://doi.org/10.1039/c8cc09523j>.
- (51) Vasilopoulos, A.; Zultanski, S. L.; Stahl, S. S. Feedstocks to Pharmacophores: Cu-Catalyzed Oxidative Arylation of Inexpensive Alkylarenes Enabling Direct Access to Diarylalkanes. *J. Am. Chem. Soc.* **2017**, *139*, 7705–7708. <https://doi.org/10.1021/jacs.7b03387>.
- (52) Ichikawa, T.; Netsu, M.; Mizuno, M.; Mizusaki, T.; Takagi, Y.; Sawama, Y.; Monguchi, Y.; Sajiki, H. Development of a Unique Heterogeneous Palladium Catalyst for the Suzuki–Miyaura Reaction Using (Hetero)Aryl Chlorides and Chemoselective Hydrogenation. *Adv. Synth. Catal.* **2017**, *359*, 2269–2279. <https://doi.org/10.1002/adsc.201700156>.
- (53) Huihui, K. M. M.; Caputo, J. A.; Melchor, Z.; Olivares, A. M.; Spiewak, A. M.; Johnson, K. A.; DiBenedetto, T. A.; Kim, S.; Ackerman, L. K. G.; Weix, D. J. Decarboxylative Cross-Electrophile Coupling of N-Hydroxyphthalimide Esters with Aryl Iodides. *J. Am. Chem. Soc.* **2016**, *138*, 5016–5019. <https://doi.org/10.1021/jacs.6b01533>.
- (54) Xia, C. L.; Xie, C. F.; Wu, Y. F.; Sun, H. M.; Shen, Q.; Zhang, Y. Efficient Cross-Coupling of Aryl Grignard Reagents with Alkyl Halides by Recyclable Ionic Iron(III) Complexes Bearing a Bis(Phenol)-Functionalized Benzimidazolium Cation. *Org. Biomol. Chem.* **2013**, *11*, 8135–8144. <https://doi.org/10.1039/c3ob41376d>.

- (55) Tobisu, M.; Takahira, T.; Chatani, N. Nickel-Catalyzed Cross-Coupling of Anisoles with Alkyl Grignard Reagents via C-O Bond Cleavage. *Org. Lett.* **2015**, *17*, 4352–4355. <https://doi.org/10.1021/acs.orglett.5b02200>.
- (56) Yang, F.; Fu, S. Y.; Chu, W.; Li, C.; Tong, D. G. Monodisperse Amorphous CuB₂₃ Alloy Short Nanotubes: Novel Efficient Catalysts for Heck Coupling of Inactivated Alkyl Halides and Alkenes. *RSC Adv.* **2014**, *4*, 45838–45843. <https://doi.org/10.1039/c4ra08517e>.
- (57) Graham, T. J. A.; Poole, T. H.; Reese, C. N.; Goess, B. C. Regioselective Semihydrogenation of Dienes. *J. Org. Chem.* **2011**, *76*, 4132–4138. <https://doi.org/10.1021/jo200262r>.
- (58) Yus, M.; Ortiz, R. Tandem Intramolecular Carbolithiation-Lithium/Zinc Transmetalation and Applications to Carbon-Carbon Bond-Forming Reactions. *European J. Org. Chem.* **2004**, *18*, 3833–3841. <https://doi.org/10.1002/ejoc.200400349>.
- (59) Guérin, C.; Bellosta, V.; Guillamot, G.; Cossy, J. Mild Nonpimerizing N - Alkylation of Amines by Alcohols without Transition Metals. *Org. Lett.* **2011**, *13*, 3534–3537. <https://doi.org/10.1021/ol201351a>.

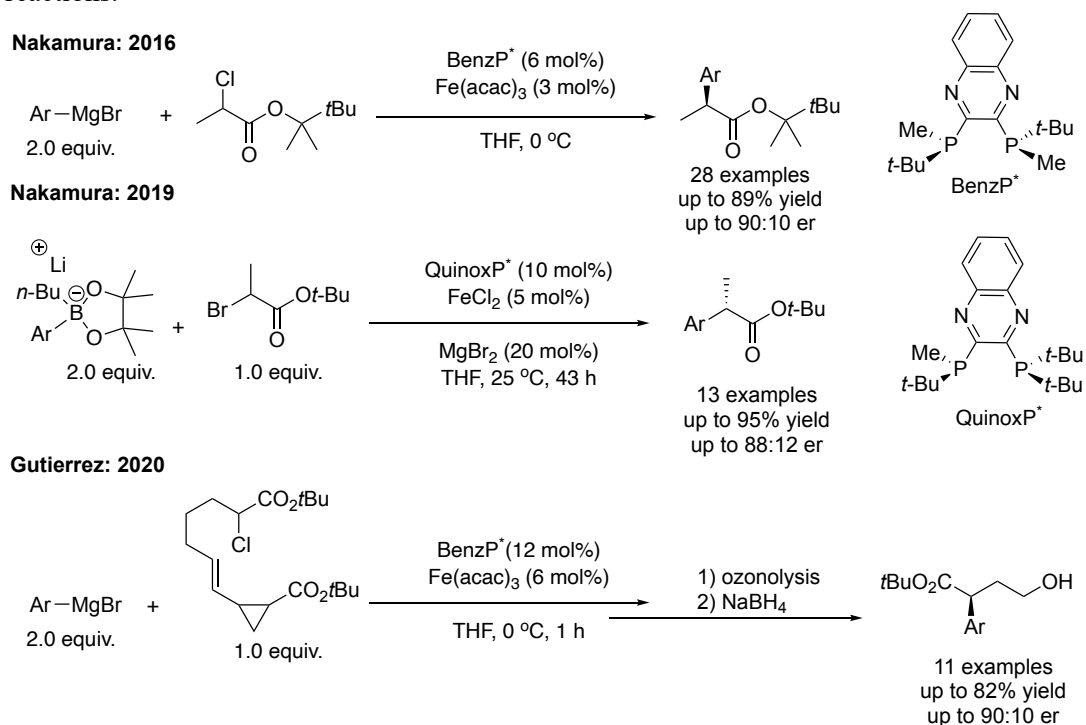
Chapter 3. Enantioconvergent Suzuki–Miyaura Cross-Coupling to Afford Enantioenriched 1,1-Diarylalkanes Using an Iron-Based Catalyst

Note: Part of chapter 3 appears in *Chem. Commun.* **2020**, 56 (93), 14661–14664.

3.1 Introduction

At the turn of the 21st century, a renaissance occurred in the field of iron cross-coupling.¹⁻³ Despite the advances in the field as discussed in Chapter 1, enantioselective cross-coupling reactions that utilize iron-based catalysts are exceedingly rare and have been greatly overshadowed by the tremendous achievements in enantioconvergent systems employing nickel-based catalysts.⁴ In fact, only three enantioselective cross coupling reactions that utilize iron-based catalysts have been reported (Chapter 1).⁵⁻⁷ Two of these systems came from the Nakamura group who demonstrated that chiral bisphosphine iron complexes catalyze the enantioselective C(sp²)-C(sp³) Kumada and Suzuki-Miyaura coupling reactions, providing enantiomeric ratios (ee) up to 90:10 (Scheme 3.1). The Gutierrez group later built upon these systems using the same chiral bisphosphine iron complex to mediate a tandem radical cyclization and enantioselective C(sp²)-C(sp³)

Scheme 3.1. State-of-the art enantioselective iron-catalyzed C(sp²)-C(sp³) cross-coupling reactions.



Kumada cross-coupling with selectivities up to 90:10 er. However, all of these reactions use α -haloesters as electrophiles and none of them use unactivated boronic esters as nucleophiles. Due to the scarcity of these systems, the development of new enantioselective iron-catalyzed cross-coupling reactions to afford new classes of substrates would be highly desirable.

3.2 Approach Toward the Synthesis of Chiral 1,1-Diarylalkanes

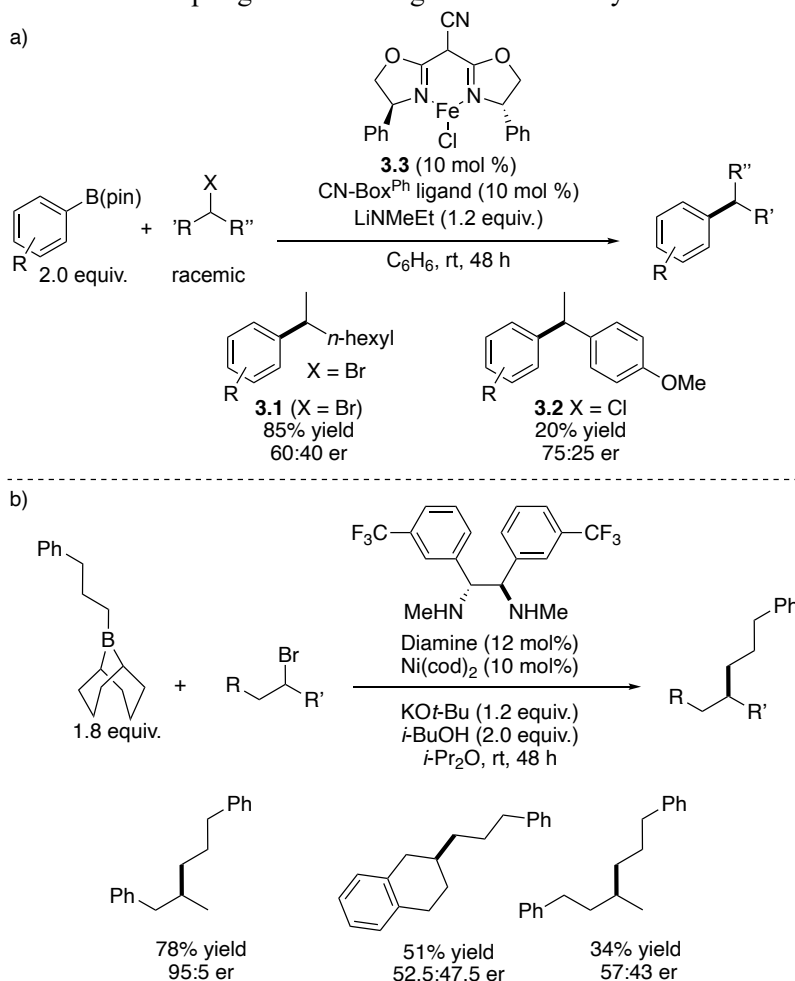
In Chapter 2, an iron-based complex supported by a chiral cyanobis(oxazoline) ligand was developed for Suzuki-Miyaura cross coupling reactions between alkyl halides and unactivated aryl boronic esters.⁸ Given that the method utilized a chiral catalyst and tolerated secondary alkyl halides, we hypothesized that it would be suitable for the stereoselective cross-coupling of secondary alkyl electrophiles and arylboronic ester nucleophiles to afford enantioenriched cross-coupled products.

Preliminary reactions were carried out between 2-bromooctane and Ph-B(pin), which led to high yields of cross-coupled product (85% yield). However, stereochemical analysis by supercritical fluid chromatography (SFC) revealed only a slight enantioinduction with a 60:40 er (Scheme 3.2a). Though the enantioselectivities were low, these results were significant because of the current challenges with developing enantioselective cross-coupling reactions using unactivated alkyl halides. In fact, there is only one such system by the Fu group using a nickel-based system using homobenzylic bromides (Scheme 3.2b).⁹ Furthermore in the same system, they screened other secondary unactivated alkyl halides which provided similar low selectivities to what we found. If instead we carried out the cross-coupling reactions with activated alkyl halides such as 1-(1-chloroethyl)-4-methoxybenzene, we could obtain higher selectivities (75:25 er) at the

expense of yield (Scheme 3.2a). Product **3.2** was especially interesting because it contained the 1,1,-diarylalkane unit which is a common motif in pharmaceutically relevant molecules.

Blockbuster pharmaceuticals such as Zolofit[®], Detrol[®], SGLT2 inhibitors and Lysodren[®] all contain the chiral 1,1-diaryl alkane motif which provides them with a range of therapeutic properties (Figure 3.1a).¹⁰ Despite the fact that one enantiomer of these drugs is often the more potent,¹¹ the drugs are either sold as racemates, mixtures of diastereomers, or are obtained in enantioenriched form as a result of a late stage resolution.¹² These tactics

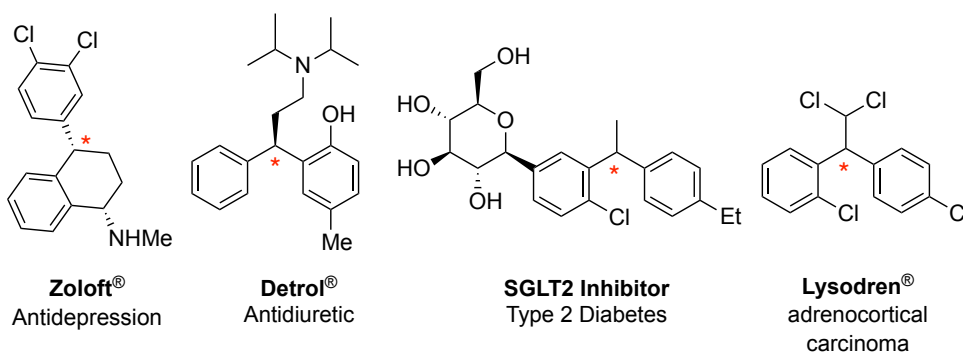
Scheme 3.2. a) Exploratory enantioselective reactions between arylboronic esters and alkyl halides catalyzed by an iron-based catalyst. b) State-of-the art nickel-based system for enantioselective cross-coupling reaction using unactivated alkyl halides.



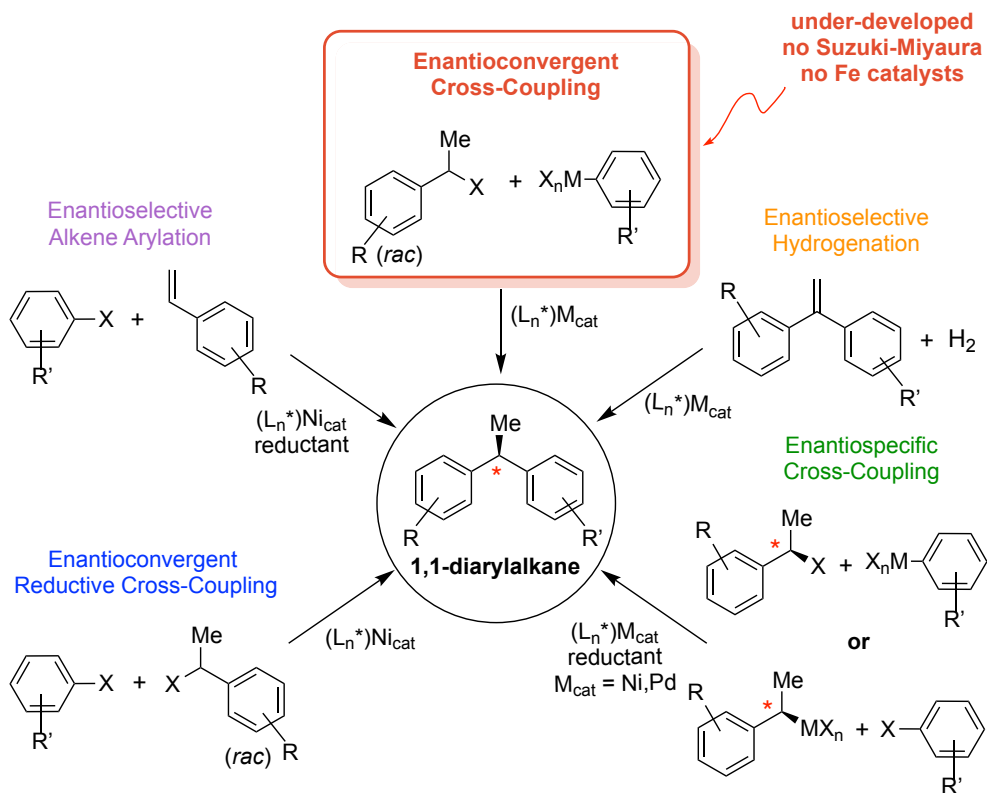
are a likely symptom of synthetic limitations that have prevented access to enantiomerically enriched 1,1-diaryl alkanes. Consequently, the enantioselective synthesis of the 1,1-diarylalkane subunit has become a popular contemporary topic for synthetic organic chemists.¹³ Current approaches toward such motifs include asymmetric hydrogenation of 1,1-diarylalkenes,^{14,15} nucleophilic and radical additions to alkenes,¹⁶⁻¹⁸

Figure 3.1. a) Commonly used pharmaceutical drugs containing the 1,1-diarylalkane motif. b) Stereoselective methods to synthesize enantioenriched 1,1-diarylalkanes.

a) some pharmaceuticals containing 1,1-diarylalkanes:



b) stereoselective methods for 1,1-diarylalkane synthesis:

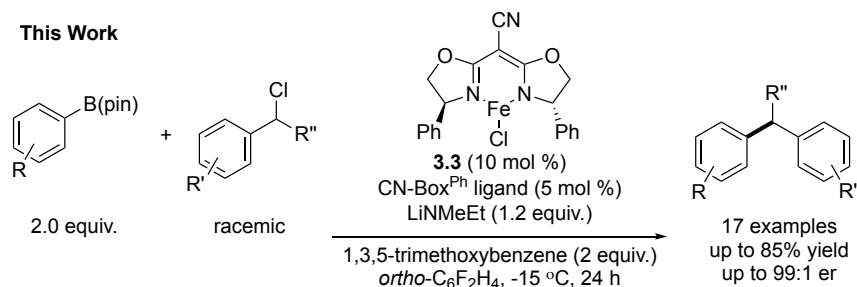


and stereospecific^{19–21} as well as stereoconvergent^{22,23} cross coupling reactions (Figure 3.1b). Though these methods provide access to the chiral 1,1-diarylalkane motif, each of these approaches is presented with one or more limitation. Asymmetric hydrogenation often relies on expensive noble metals with sophisticated ligand frameworks and furthermore requires the catalyst to discriminate between sterically and electronically similar substituents. Limitations with respect to the other methods are that enantioselective alkene functionalization rely on the use of stoichiometric reductants or noble metal co-catalysts, enantiospecific cross-coupling relies on the non-trivial synthesis and purification of enantiomerically enriched substrates, and enantioselective reductive cross-coupling utilizes a large excess of reductant and additives. Finally, enantioconvergent cross-coupling has only been demonstrated once. However, this Negishi system developed by the Fu group suffers from the use of air-sensitive organozinc reagents and requires large amounts of stoichiometric additives.²³

A method that is surprisingly absent from this list is a stereoconvergent Suzuki-Miyaura cross coupling reaction between benzylic halides and aryl boronic esters. Such a reaction would closely mimic the ubiquitous Suzuki-Miyaura cross coupling reactions that have become a mainstay in the pharmaceutical industry for the construction of C–C bonds between two C(sp²)-hybridized substrates.²⁴ In this chapter, a Suzuki-Miyaura cross-coupling reaction between benzylic chlorides and unactivated arylboronic-pinacol esters is described that fills this gap in synthetic methodology (Scheme 3.3).²⁵ The method represents only the second example of an enantioconvergent cross-coupling reaction used to access enantioenriched 1,1-diarylalkanes,²³ and the first example that employs an iron-based catalyst. Additionally, we expand the nascent scope of enantioselective iron-based

cross-coupling reactions and demonstrate their value in chemical synthesis with the synthesis of enantioenriched 1,1-diarylalkanes.

Scheme 3.3. Development of an enantioselective Suzuki-Miyaura reaction between arylboronic esters and benzylic halides catalyzed by an iron-based catalyst.



3.3 Optimization of an Enantioselective Suzuki-Miyaura Reaction Using an Iron-Based Catalyst

Exploratory reactions were carried out between (1-chloroethyl)benzene (**3.4**) and 2-naphthylboronic pinacol ester (**3.5**) under our previously reported conditions⁸ using cyano(bisoxazoline) iron(II) chloride complex **3.3** as the catalyst precursor. 2-naphthylboronic pinacol ester **3.5** was used in place of 4-methoxyphenylboronic pinacol ester used previously (Scheme 3.2a) due to higher yields. Analysis of the reaction mixture showed the formation of 1,1-diarylalkane product **3.6** in 64% yield and with an enantiomeric ratio (er) of 74:26 (Table 3.1, entry 1). A competitive side product was compound **3.7**, which results from the homodimerization of the benzylic halide starting material **3.4**. In all cases, the homodimer was formed as a 1:1 mixture of the meso and racemic diastereomers as determined by ¹H-NMR spectroscopy and chiral HPLC analysis. To increase yields of **3.6**, an evaluation of solvents was carried out with the reaction in benzene as a baseline (entry 1). As we have observed in Chapter 1, the use of ethereal solvents was detrimental (entry 2, 0% yield) while the other aromatic solvents performed similarly to benzene (entries 3-6).⁸ We presume ethereal solvents are detrimental to

Table 3.1. Evaluation of solvents for the Suzuki-Miyaura coupling between 2-naphthylboronic ester and 1-chloroethylbenzene catalyzed by an iron-based complex.

Entry	Solvent	Yield 3.6 ^a (%)	er 3.6 ^b (<i>S</i> : <i>R</i>)	Yield 3.7 ^a (%)
1	Benzene	64	74:26	10
2	MTBE	13	N/A	10
3	Trifluorotoluene	55	76:24	12
4	Fluorobenzene	49	81:19	8
5	Anisole	61	74:26	9
6	1,2-Difluorobenzene	66	76:24	11

^aYields of products determined through the use of ¹H-NMR spectroscopy analysis using 1,3,5-trimethoxybenzene as an internal standard ^bEnantiomeric ratios were determined by HPLC analysis and absolute configuration by comparison to literature optical rotations or literature HPLC retention times.

catalysis due to their coordinating ability, leading to off-cycle iron species. Fluorinated aromatic solvents (entries 3,4,6) performed well (44-66% yield) and even led to higher selectivities when fluorobenzene was used (entry 4). 1,2-difluorobenzene led to similar yields and selectivity to benzene so was used for further optimization because of its lower freezing point (f.p. -34 °C).

To obtain higher yields of **3.6**, we tested commonly used additives that have been shown to suppress homo-dimerization in similar nickel-catalyzed reductive cross-couplings.²⁵ When sodium iodide was used as an additive, lower yields of **3.6** and higher amounts of homodimer **3.7** was obtained (Table 3.2, entry 2). The reaction benefited from the use of an electron-rich aromatic additive 1,3,5-trimethoxybenzene (1,3,5-TMB), leading to higher yields of **3.6**. This 1,3,5-TMB effect was also seen in a different cross-

Table 3.2. Evaluation of additives for the Suzuki-Miyaura coupling between 2-naphthylboronic ester and 1-chloroethylbenzene catalyzed by an iron-based complex.

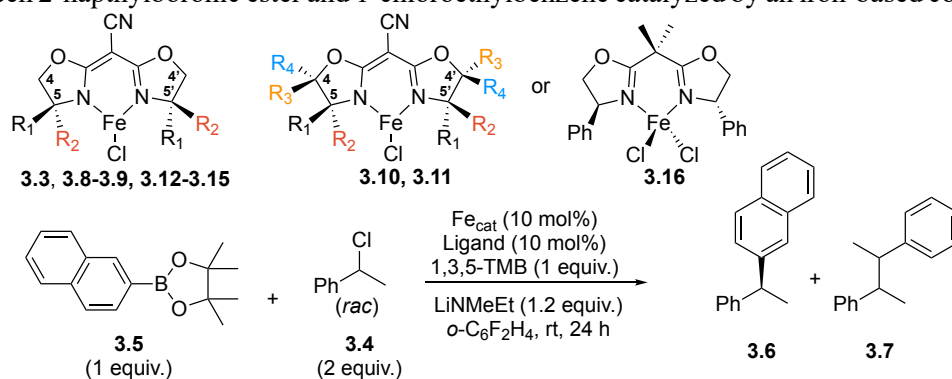
Entry	Additive	Yield 3.6 ^a (%)	er 3.6 ^b (S:R)	Yield 3.7 ^a (%)
1	None	66	76:24	11
2 ^c	NaI	45	76:24	20
3	1,3,5-TMB	73	79:21	9
4	1,2,4-TMB	Trace	N/A	90

^aYields of products determined through the use of ¹H-NMR spectroscopy analysis using 1,3,5-trimethoxybenzene as an internal standard ^bEnantiomeric ratios were determined by HPLC analysis and absolute configuration by comparison to literature optical rotations or literature HPLC retention times.

coupling reaction between **3.5** and 4-methoxyphenylboronic pinacol ester, leading to significantly higher yields of cross-coupled product (25% w/o 1,3,5-TMB vs. 42%). To gain more insight into the beneficial effects of the 1,3,5-TMB additive, 1,2,4-TMB was also used as a stoichiometric additive. However, this reaction led to near quantitative yields of homodimer **3.7** and none of the desired product.

With these optimal reaction conditions, iron complexes containing a variety of aromatic and aliphatic substituted cyanobis(oxazoline) ligands were evaluated (Table 3.3). For this ligand screen, we found using the preformed iron complex **3.3** was necessary to obtain **3.6** in high yield, although identical enantioselectivity was observed for a reaction generating **3.3** *in situ* (entry 1). Increasing the steric bulk of the aryl group installed on C4 and C4' of the ligand led to low conversion of **3.4** and lower yields and enantioselectivities of **3.6** (entries 3-4) relative to **3.3**. In the case of iron complex **3.9**, homodimer **3.7** was the major product, which was presumably due to the increased steric encumbrance of mesityl

Table 3.3. Evaluation of cyanobis(oxazoline) ligands for the Suzuki-Miyaura coupling between 2-naphthylboronic ester and 1-chloroethylbenzene catalyzed by an iron-based complex.



Entry	Fe _{cat}	R ₁	R ₂	R ₃	R ₄	X	3.6 (%) ^[a]	er of 3.6 ^[b]	3.7 (%) ^[a]
1 ^{c,d,e}	FeCl ₂	Ph	H	H	H	CN	19	74:26	19
2	3.3	Ph	H	H	H	CN	73	79:21	9
3	3.8	H	3,5- <i>t</i> BuPh	H	H	CN	36	32:68	9
4	3.9	Mes	H	H	H	CN	15	65:35	27
5	3.10	H	Ph	H	Ph	CN	71	26:74	5
6	3.11	Ph	H	Ph	Ph	CN	64	65:35	13
7	3.12	Bn	H	H	H	CN	8	61:39	33
8	3.13	<i>t</i> Bu	H	H	H	CN	0	N/A	0
9	3.14	<i>i</i> Pr	H	H	H	CN	16	73:27	20
10	3.15	Ph	H	H	H	H	57	76:24	18
11	3.16	Ph	N/A	N/A	N/A	N/A	0	N/A	45

^aYields of products determined through the use of ¹H-NMR spectroscopy analysis using 1,3,5-trimethoxybenzene as an internal standard ^bEnantiomeric ratios were determined by HPLC analysis and absolute configuration by comparison to literature optical rotations or literature HPLC retention times. ^cC₆H₆ was used as the solvent. ^dNo 1,3,5-TMB additive. ^e20 mol% ligand was added.

substitution (entry 4). Adding various phenyl substitution to C₄, C_{4'}, C₅, and C_{5'} positions of the ligand resulted in similar or decreased yields and enantioselectivities compared reactions catalysed by **3.3** (entries 5-6). Replacing aromatic substituents with aliphatic substituents on C₄ and C_{4'} of the oxazoline ring was detrimental to the cross-coupling reaction and led to low conversion of alkyl chloride **3.4** (entries 7-9). Reactions with

aliphatic substituted cyanobis(oxazoline) ligands also led to low enantioselectivities of **3.6**, likely due to the competing background reaction with iron dichloride. We found that removal of the cyano functionality installed in the backbone of the bis(oxazoline) ligand had little effect on enantioselectivity (entry 10). However, yield was affected when using this more electron rich ligand **3.15**, which led to lower amounts of **3.6** and higher amounts of **3.5**. This outcome could be attributed to the more electron-rich iron complex **3.15** which led to higher amounts of benzylic radical due to more facile halogen abstraction. Although bis(oxazoline) ligands with geminal di-substitution installed on the bridging carbon exhibit enhanced enantioselectivity in many stereoselective reactions,²⁷ only **3.7** was obtained when such a ligand was used here (entry 11). This result is consistent with findings discussed in Chapter 2, which required a monoanionic ligand to prevent catalyst death likely through metal aggregates.⁸

Since ligand modifications did not improve yield or selectivity, iron complex **3.3** was used for the final optimization because the ligand in **3.3** is commercially available and relatively easy to synthesize. In Chapter 2, we found that an extra equivalent of ligand was generally needed to obtain high yields of the cross-coupled product at the expense of slower reaction rates.⁸ We hypothesized that the extra ligand formed an off cycle homoleptic complex containing two cyanobis(oxazoline) ligands, which extended catalyst lifetime by preventing catalyst aggregation. Since benzylic halides have weak carbon-halogen bonds that are more susceptible to homolysis, we hypothesized that using extra ligand was detrimental for this class of electrophiles, leading to increased production of **3.7**. Consistent with this hypothesis, when a reaction was carried out without extra ligand, higher yields of **3.6** was observed with concomitant decreased yields of **3.7** (Table 3.4, entry 2). Control

Table 3.4. Evaluation of cyanobis(oxazoline) ligands for the Suzuki-Miyaura coupling between 2-naphthylboronic ester and 1-chloroethylbenzene catalyzed by an iron-based complex.

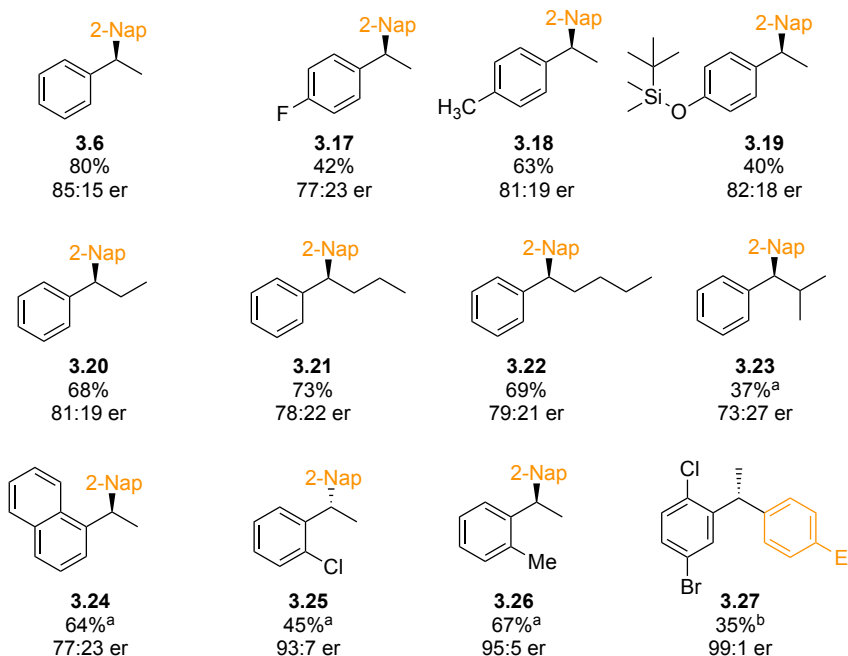
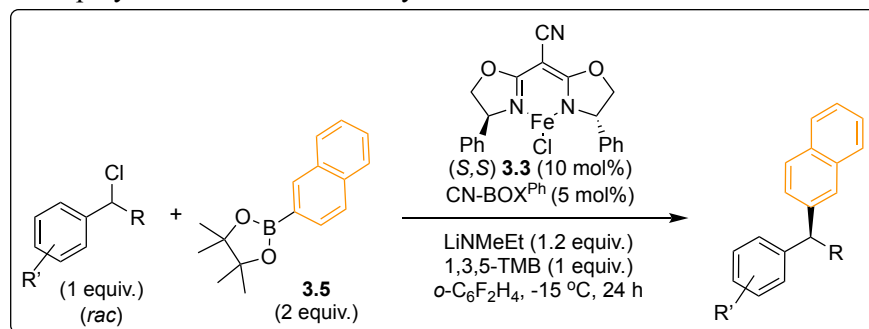
Entry	X (mol%)	T (°C)	Yield 3.6 ^a (%)	er 3.6 ^b (<i>S</i> : <i>R</i>)	Yield 3.7 ^a (%)
1	10	rt	73	79:21	9
2	0	rt	90	77:23	5
3 ^c	0	rt	68	75:25	9
4	10	-15	90	80:20	0
5	5	-15	90	85:15	0
6	10	-25	57	78:22	0

^aYields of products determined through the use of ¹H-NMR spectroscopy analysis using 1,3,5-trimethoxybenzene as an internal standard ^bEnantiomeric ratios were determined by HPLC analysis and absolute configuration by comparison to literature optical rotations or literature HPLC retention times. ^cNo 1,3,5-TMB added.

experiments confirmed once again that 1,3,5-TMB led to higher yields (entry 1 vs. entry 3). The beneficial effect on yield was noticeably more pronounced without added ligand (entry 1 vs. entry 2). To improve enantioselectivity of **3.6** and suppress formation of **3.7**, reactions were performed at lower temperatures at the expense of reactivity. Reactions carried out at -15 °C led to high yields of **3.6** with improved enantioselectivity (e.r. = 85:15), particularly with 5% ligand to maximize selectivity (entries 4,5). However reactions carried out below -15 °C led to low conversions of **3.4** and low selectivity of **3.6** most likely due to the competing background reaction (entry 6). Notable from these reactions at lower temperatures was the complete suppression of **3.7** formation.

3.4 Substrate Scope

Table 3.5. Alkyl halide substrate scope for an iron-catalyzed Suzuki-Miyaura reaction between 2-naphthylboronic ester and benzylic halides.



Yields of product are isolated yields and enantiomeric ratios were determined through the use of HPLC analysis.
^a15 mol% **3.3**, no extra ligand, 1,3,5-TMB (2 equiv.) and LiNMe₂ used. ^b40 mol% **3.3**, no extra ligand, 1,3,5-TMB (2 equiv.) and -10 °C.

With optimized conditions in hand, the scope of the benzylic halide coupling partner was evaluated (Table 3.5). Para-substituted benzylic halides containing electron withdrawing (**3.17**) and electron donating (**3.18**, **3.19**) functional groups led to lower yields than **3.6**, but only modestly affected enantioselectivity. Unfortunately the instability of the 4-methoxyphenyl substituted benzylic halide precluded its use for cross-coupling. With a series of electronically disparate benzylic halides, a Hammett analysis was attempted but

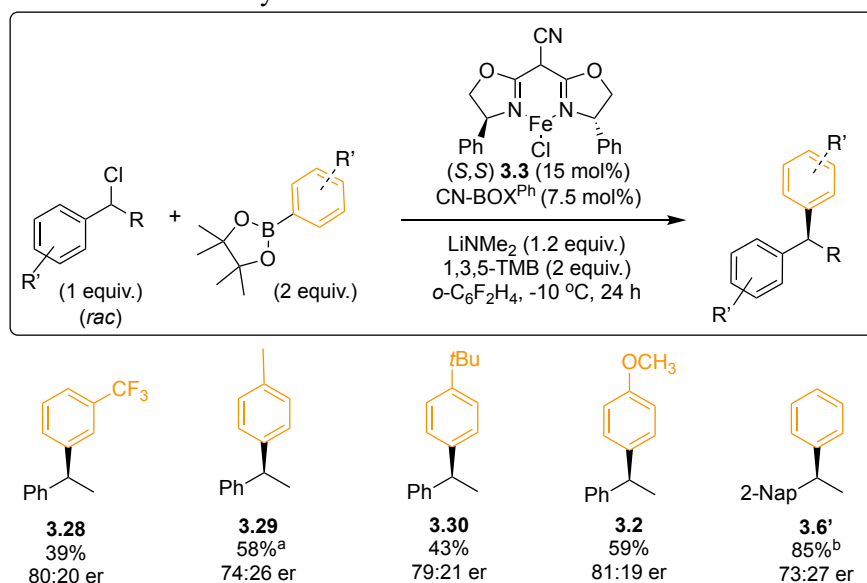
no correlation was seen between surverying selectivity. Increasing the chain length of the alkyl substituent from ethyl to *n*-butyl (**3.20-3.22**) led to similar yields (68-69% vs. 80%), but lower enantioselectivities to **3.6**. We hypothesized that increasing steric bulk at either the alkyl or aryl site of the benzyl halide would help to achieve higher enantioinduction. To test this hypothesis, we first evaluated a substrate with branching adjacent to the alkyl halide (entry **3.23**). A reduced yield and enantioselectivity (37%, 73:27 er) was observed, even when using higher catalyst loadings. Considerable amounts of benzylic homodimer formed, which suggests either radical recombination or radical rebound is disfavored.

When steric bulk was provided by the aryl group, high enantioselectivities (er \geq 93:7) were obtained particularly for benzylic halides containing ortho-substituted aryl groups (**3.25-3.27**). This high enantioinduction was not seen with the 1-naphthyl substituted product **3.24**, which we presume was due to the tied-back nature of the naphthyl ring. These substrates are important because ortho-substituted 1,1-diarylethanes are common motifs in many pharmaceuticals (Figure 3.1a), and are challenging to obtain in high enantiopurity using previous methods.^{22,23,28} To compensate for the lower reactivity of these sterically demanding substrates, higher loadings of **3.3** and 1,3,5-TMB were required. Additionally, using lithium dimethylamide instead of lithium ethylmethylamide was beneficial to obtain appreciable yields of **3.26**. In addition to being a common motif in pharmaceuticals, product **3.25** is a versatile synthetic intermediate because it can be used further as the electrophile in cross coupling reactions, converted into a nucleophile for cross-coupling reactions through Miyaura borylation, or be converted to an aromatic without ortho-substitution through protodechlorination.¹⁶

To demonstrate the synthetic utility of the method, we synthesized an intermediate of an SGLT2 inhibitor used to treat type II diabetes (Figure 3.1a).²⁹ Using 40 mol% of **3.3**, product **3.27** was formed in modest yield (35%) but with excellent enantioselectivity (99:1 er). Elaboration of this intermediate to the SGLT2 inhibitor has previously been reported through glycosylation of the aryl bromide,¹⁸ which remains unreacted in the cross coupling reaction. In addition to aryl bromides, the reaction demonstrated moderate functional group tolerance with silyl-protected alcohols (**3.19**), aryl chlorides (**3.25**) and ethers (**3.2**) all being well tolerated.

With respect to the scope of the boronic ester coupling partner, arylboronic pinacol ester coupling partners derived from PhB(pin) were less reactive than naphthylboronic pinacol ester **3.5** (Table 3.6). Consequently, reactions involving these nucleophiles required higher temperatures (-10 °C) and higher catalyst loadings (15 mol%) to obtain useful yields of cross-coupled product. The higher reactivity of extended π -conjugated

Table 3.6. Alkyl halide substrate scope for an iron-catalyzed Suzuki-Miyaura reaction between 2-naphthylboronic ester and benzylic halides.



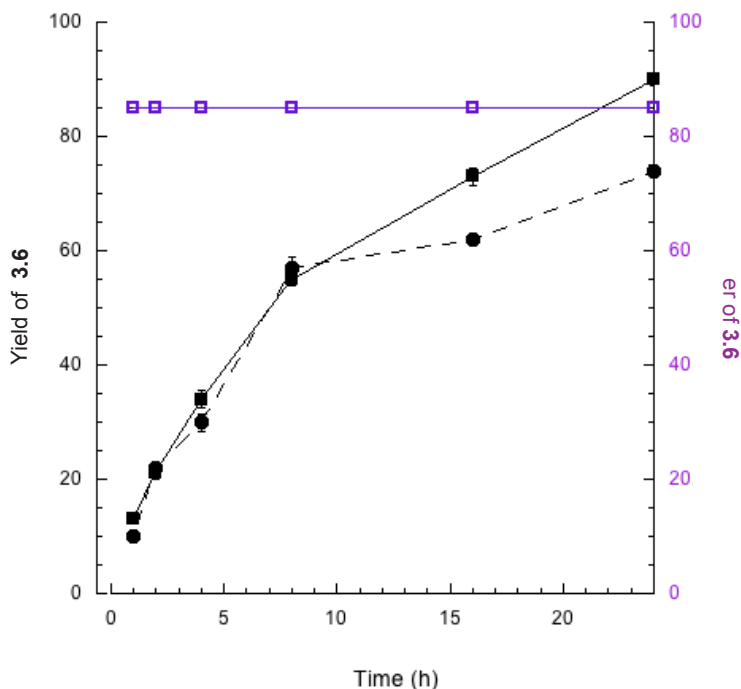
Yields of product are isolated yields and enantiomeric ratios were determined by through the use of HPLC analysis.
^aLiNMeEt used. ^bStandard reaction conditions shown in Figure 3.2 were used.

coupling partners has been observed before, and it has been attributed to metal-arene binding facilitating key steps in the catalytic cycle.³⁰ A similar effect is likely here as supported by the high yields of **3.31**. Despite moving to less reactive arylboronic pinacol esters, only a small erosion in enantioselectivity was observed (**3.28-3.30**, **3.2**, **3.6'**) compared to the benzyl halide scope. As was found with varying the naphthyl halides, varying the electronic nature of the boronic ester had minimal effect on enantioselectivity and no trend was seen in terms of yield or selectivity.

3.5 Mechanistic Insights:

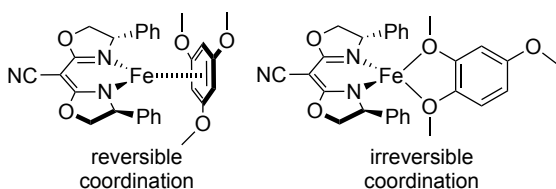
A puzzling feature of the reaction was the benefit of using 1,3,5-TMB as an additive. Analyzing the reaction over time in the presence and absence of 1,3,5-TMB provided some insight into the role of 1,3,5-TMB (Figure 3.4). These experiments revealed that addition

Figure 3.4. Effects on yield (closed symbols) and er (open symbols) of **3.6** for the coupling reaction between 1-chloroethylbenzene and 2-naphthylboronic pinacol ester catalyzed by **3.3** in the absence (circles) and presence (squares) of 1,3,5-TMB at -15 °C



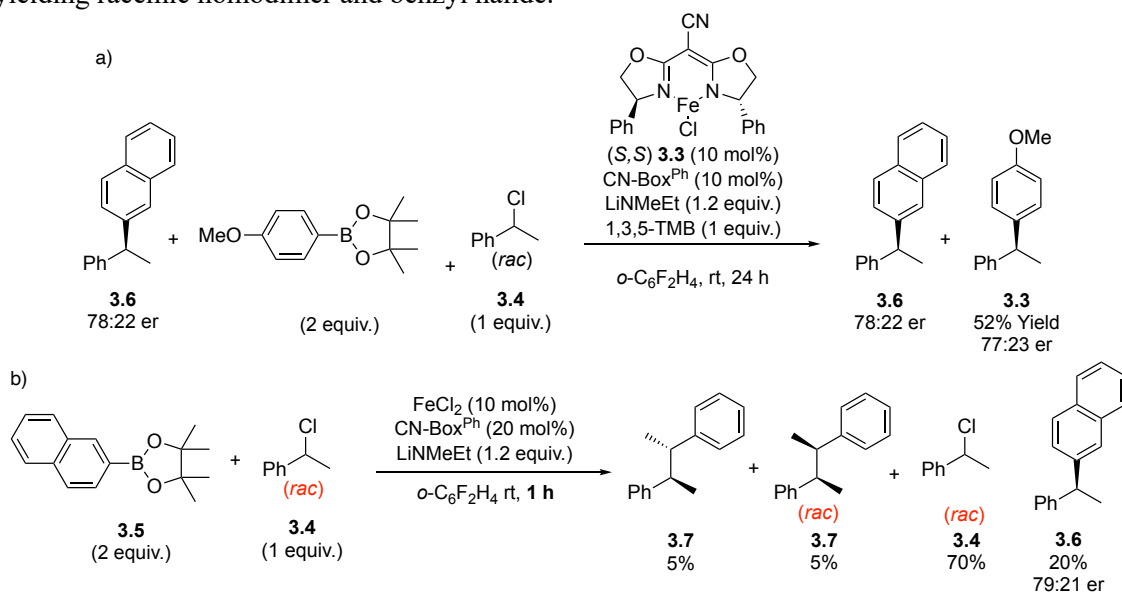
of 1,3,5-TMB had no effect on the initial rate of the reaction nor did it impact the selectivity of the reaction. The major difference was observed at long reaction times where higher yields were obtained in the presence of 1,3,5-TMB. This result suggested that the primary role for 1,3,5-TMB is to extend catalyst lifetime, perhaps by preventing unwanted catalyst aggregation by stabilization of low valent intermediates. It is possible that the additive could be acting as a labile ligand for stabilizing low-valent iron species, which has been reported previously.³¹ This effect would account for the different effects on yield between the trimethoxybenzene isomers (Table 3.2). We hypothesize the 1,3,5-TMB additive benefits from reversible η^6 binding, the 1,2,4-TMB additive can coordinate κ^2 , leading to irreversible binding to iron as shown in Scheme 3.4.

Scheme 3.4. Comparison of potential binding modes of 1,3,5-TMB and 1,2,4-TMB.



Several observations provided additional information about the mechanism for stereoinduction in the cross-coupling reaction.^{32,33} Importantly, the enantioselectivity of the reaction remained constant throughout the reaction (Figure 3.4, Scheme 3.5a). Additionally, when stereoenriched **3.6** was introduced at the onset of a different cross-coupling reaction, no loss in its enantiopurity occurred over the course of the reaction (Scheme 3.5). Both results demonstrate that the basic reaction conditions employed do not lead to product epimerization, even at room temperature. In addition, racemic alkyl halide was recovered from a reaction taken to partial completion, and the homodimerization product **3.7** was obtained as a near statistical mixture of all three possible stereoisomers

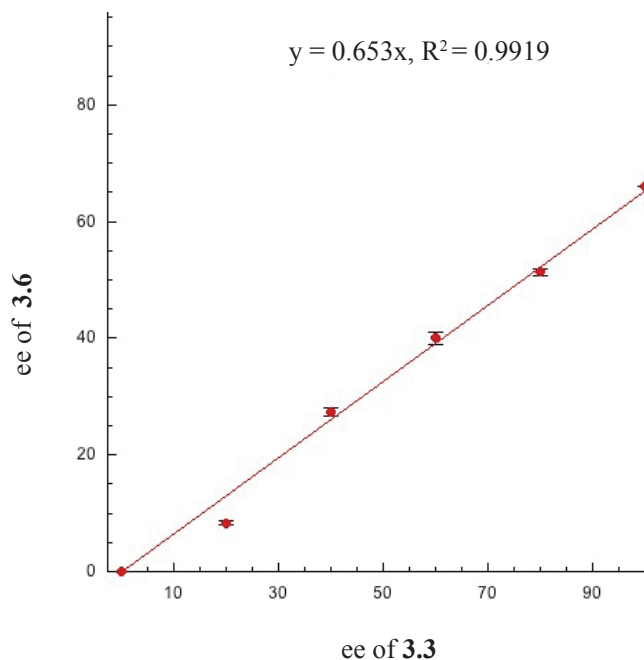
Scheme 3.5. a) Subjection of enantiomerically enriched **3.6** to a cross-coupling reaction between 1-chloroethylbenzene and 4-methoxyphenyl boronic pinacol ester catalyzed by **3.3**. b) Reaction taken to partial conversion between 1-chloroethylbenzene and 2-naphthylboronic pinacol ester yielding racemic homodimer and benzyl halide.



(*S,S*:*R,R*:*R,S* ~ 1:1:2) (Scheme 3.5b). These findings are most consistent with a stereoconvergent cross-coupling reaction mechanism that likely proceeds through a free radical intermediate formed without kinetic resolution of the alkyl halide. The mechanism for stereoconvergence is likely through an unselective halogen atom abstraction step.^{5,6,34}

To gain information about the nuclearity of the catalyst during the selectivity determining step,³⁵ stereoselectivity was evaluated as the catalyst stereopurity was altered. These reactions revealed a linear relationship between product and catalyst enantiopurity (Figure 3.5), which suggested that the stereoselectivity-determining step in the cross-coupling reaction likely occurs at a metal center containing one cyanobis(oxazoline) ligand. Interestingly, reaction of 2-(1-chloroethyl)naphthalene with PhB(pin) produced **3.6** with a similar yield but lower enantioselectivity (73:27 e.r.) as obtained for the complementary reaction between **3.5** and **3.4**, which also led to **3.6** but with higher

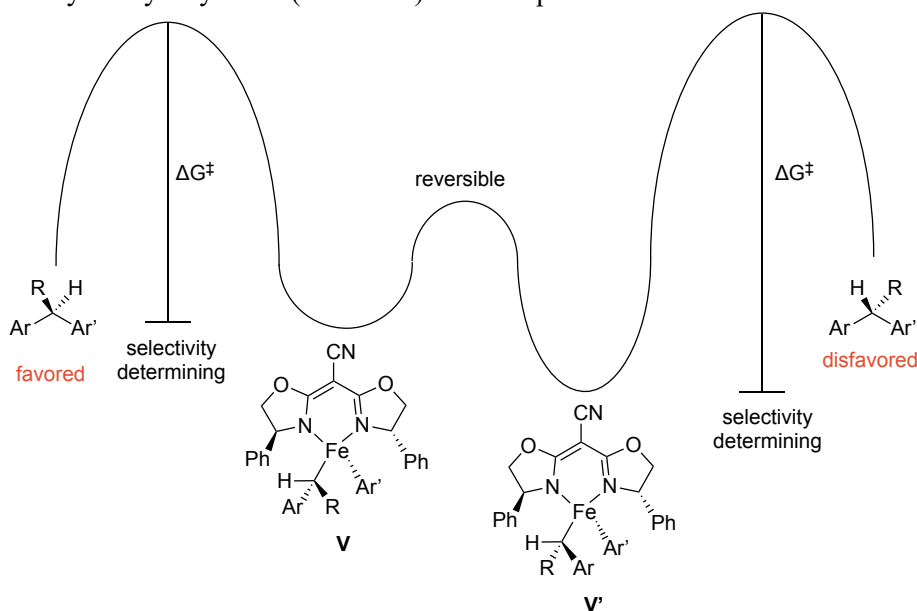
Figure 3.5. Non-linear effect experiment between enantiopurity of **3.3** and **3.6**.



enantioselectivity (85:15 e.r.). This observation implicates the presence of the electrophile and nucleophile in the selectivity-determining step. These results also indicate the importance in the identity of the putative iron aryl species, which can engage in carbon-carbon bond formation with the carbon-centered radical.

A plausible catalytic cycle that is consistent with all of the facts uncovered in these mechanistic experiments is shown in Scheme 3.6. Precatalyst **I** engages in salt metathesis with the lithium amide to form iron(II) amide **II**. This intermediate competitively undergoes transmetalation with the aryl boronic ester to form iron(II) aryl **IV** and unselective halogen abstraction to form iron(III) amide-halide **III** and a carbon-centered radical. The carbon-centered radical escapes the solvent cage and reversibly recombines with **IV** to form iron(III) aryl-alkyl species **V**.³⁶ We believe the carbon-centered radical escapes the solvent cage because of the formation of bibenzyl product **3.7**. Complex **V** is poised for reductive elimination to form the formally iron(I) complex **VII** and the cross-

Figure 3.6. Curtin-Hammett scenario for a C(sp²)-C(sp³) Suzuki-Miyaura cross-coupling reaction catalyzed by a cyanobis(oxazoline) iron complex.



cannot definitively verify our hypothesis of a Curtin-Hammett scenario, but what is clear from our mechanistic experiments is that the enantiodetermining step occurs from a single metal center. We favor the mechanism shown in Scheme 3.6 as opposed to other possible mechanisms that utilize one metal complex such as those discussed in Chapter 2 throughout the catalytic cycle for several reasons. One possibility is that radical recombination occurs after halogen atom abstraction from iron(II) aryl species **IV**. In such a mechanism, an iron(IV) intermediate would be formed, which is unlikely under the reducing reaction conditions. A radical rebound mechanism to form the C–C bond avoids forming an iron(IV) intermediate, but this step would be the selectivity determining step of the reaction if this mechanism were operative. We disfavor a radical rebound step as the selectivity determining step because it is very similar to the microscopic reverse of halogen abstraction, which is an unselective event (see Scheme 3.5). Additionally, a radical rebound process would have the C–C bond formation event farther away from the chiral ligand,

which would lead to lower selectivities than a radical recombination pathway. For these reasons, we favor a bimetallic mechanism that resembles similar mechanisms previously proposed for other cross coupling reactions catalyzed by iron-based^{32,33,38,39} and nickel-based^{34,36} catalysts.

3.6 Conclusion:

In conclusion, the first enantioselective Suzuki-Miyaura reaction used to synthesize enantioenriched 1,1-diarylalkanes was developed. The method relies on a reactive iron-based catalyst that proceeds through a stereoconvergent cross-coupling mechanism between racemic benzylic halides and unactivated aryl boronic esters. The anionic cyano(bisoxazoline) ligand and 1,3,5-TMB additive employed were important to extend catalyst lifetime resulting in high yields of the cross coupled products. In addition to being the first catalyst reported for this transformation, the iron-based catalyst demonstrates reactivity that expands the substrate scope compared to existing nickel-based catalysts that have previously been developed for similar cross-coupling reactions.^{22,40} Notable were the high selectivities observed for cross-coupling reactions involving challenging ortho-substituted diarylalkane substrates, which are difficult to access using existing methods. This advantage was illustrated by the highly selective synthesis of an intermediate to an SGLT2 inhibitor. More importantly, this method expands the classes of electrophiles that can engage in enantioselective iron cross-coupling reactions. Future work will be directed at identifying important catalyst features that will enable the development of more stereoselective cross-couplings catalyzed by iron-based complexes. From this ligand development, a broader array of cross-coupling partners and substrate classes can be accessed.

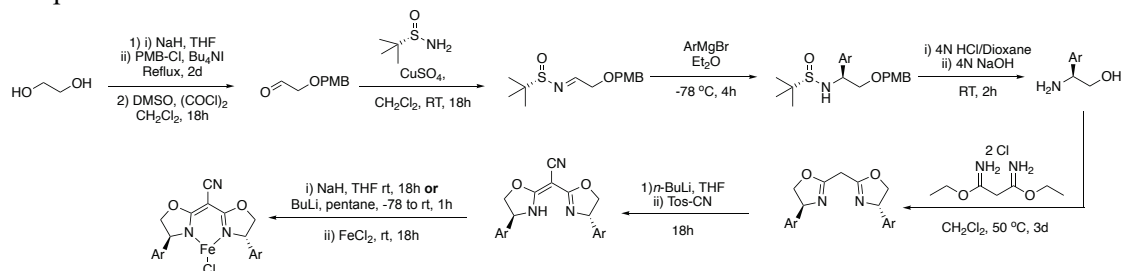
3.7 Experimental:

General Considerations. Unless stated otherwise, all reactions were carried out in oven-dried glassware in a nitrogen-filled glovebox or using standard Schlenk-line techniques.⁴¹ Solvents including dichloromethane, pentane, toluene, diethyl ether, and tetrahydrofuran were purified by passage through two activated alumina columns under a blanket of argon and then degassed by brief exposure to vacuum.⁴² Phenylboronic acid, 2-naphthaleneboronic acid, 4-methoxyphenylboronic acid, *p*-*t*Bu-phenylboronic acid, *p*-tolylboronic acid and 4,4,5,5-tetramethyl-2-(3-(trifluoromethyl)phenyl)-1,3,2-dioxaborolane were bought from Oakwood Chemicals and dried over P₂O₅ followed by passage through an alumina plug in the glovebox before use. All prepared boronic pinacol esters were used after passage through alumina under a nitrogen atmosphere. Methyl ethyl amine was purchased from TCI America. Lithium dimethylamide and 2,3-dimethyl-2,3-butanediol were purchased from Alfa and used without further purification. Anhydrous iron (II) chloride was purchased from Sigma Aldrich and used without further purification. Bis(oxazoline) ligand (4*S*)-(+)-Phenyl- α -[(4*S*)-phenyloxazolidin-2-ylidene]-2-oxazoline-2-acetonitrile was purchased from Sigma-Aldrich and dried over P₂O₅ before use in the glovebox. All alkyl halides were purchased from Sigma-Aldrich, Oakwood Chemicals and Fisher Scientific. Liquid alkyl halides were dried over calcium hydride for at least 24 hours before being vacuum-distilled, while all solids were dried over P₂O₅ before use in the glovebox. ¹H, ¹¹B and {¹H}¹³C, nuclear magnetic resonance (NMR) spectra were recorded at ambient temperature on Varian VNMRs operating at 400 MHz, 500 MHz, or 600 MHz for ¹H NMR, at 160 MHz for ¹¹B NMR and 125 MHz for {¹H}¹³C. All {¹H}¹³C NMR was

collected while broad-band decoupling was applied to the ^1H region. The residual protio solvent impurity was used as an internal reference for ^1H NMR spectra and $\{^1\text{H}\}^{13}\text{C}$ NMR spectra. Boron trifluoride diethyl etherate was used as an external standard ($\text{BF}_3 \cdot \text{O}(\text{C}_2\text{H}_5)_2$; 0.0 ppm) for ^{11}B NMR. The line listing for NMR spectra of diamagnetic compounds are reported as follows: chemical shift (multiplicity, coupling constant, integration) while paramagnetic compounds are reported as chemical shift (peak width at half height, number of protons). Solvent suppressed spectra were collected for paramagnetic compounds in protio THF using the PRESAT macro on the VNMR software. Infrared (IR) spectra were recorded on a Bruker Alpha attenuated total reflectance infrared spectrometer. High-resolution mass spectra were obtained at the Boston College Mass Spectrometry Facility on a JEOL AccuTOF DART instrument. Enantiomeric ratios were determined by HPLC analysis (high-performance liquid chromatography) with an Agilent 1200 series instrument with Chiral Technologies Chiralcel OD-H (4.6 x 250 mm), Chiral Technologies Chiralcel OJ-H (4.6 x 250 mm) or Chiral Technologies Chiralcel IC (4.6 x 250 mm) columns eluting with HPLC grade hexanes and isopropyl alcohol. Racemic samples were prepared using a 1:1 mixture of the (*R*),(*R*)-CN-BOX^{Ph}FeCl and (*S*),(*S*)-CN-BOX^{Ph}FeCl complexes which led to some discrepancies in obtaining purely racemic HPLC traces. Optical rotations were measured on a Rudolph Research Analytical Autopol IV Polarimeter.

Synthetic Procedures:

Figure S3.1. Synthesis of cyano-bis(oxazoline) ligands and cyano-bisoxazoline iron chloride complexes.

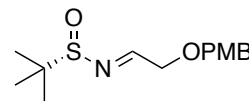


Synthesis of cyano-bis(oxazoline) ligands.

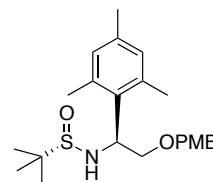
Synthesis of 2-(4-methoxybenzyloxy)ethanol. To an oven-dried 500 mL, two-neck flask with reflux condenser and stir bar under a N₂ atmosphere was added anhydrous tetrahydrofuran (100 mL). Sodium hydride (3.92 g, 98.0 mmol, 60% in mineral oil.) was added followed by dropwise addition of ethylene glycol (9.01 mL, 161.1 mmol) at which point the reaction effervesced. After 30 minutes, 4-methoxybenzyl chloride (7.24 mL, 53.6 mmol) and tetrabutylammonium iodide (1.96 g, 53.6 mmol) were added. The reaction was brought to reflux and allowed to stir for 18 hours. The reaction was quenched with saturated NH₄Cl (aq) (65 mL). The collected aqueous layers were extracted with ethyl acetate (50 mL x 3) and the combined organic layers were dried over Na₂SO₄, filtered, and concentrated *in vacuo*. The crude mixture was purified by silica gel column chromatography (1:1 EtOAc/Hex) to yield a yellow oil (6.94 g, 71%) (R_f = 0.3, 1:1 EtOAc/Hex); ¹H NMR (500MHz, CDCl₃) δ 3.56-3.59 (m, 2H), 3.73-3.76 (m, 2H), 3.81 (s, 3H), 4.50 (s, 2H), 6.87-6.89 (d, *J* = 8.7 Hz, 2H), 7.25-7.29 (d, *J* = 8.4 Hz, 2H) ppm. Spectral data are in accordance with the literature.⁴³

Synthesis of 2-4(4-methoxybenzyloxy)acetaldehyde. To an oven-dried 1 L, three-neck flask with stir bar under a N₂ atmosphere was added anhydrous dichloromethane (350 mL) and oxalyl chloride (5.95 mL, 68.4 mmol). The flask was brought to -78°C in a dry ice acetone bath and DMSO (9.39 mL, 132.0 mmol) was added dropwise. The reaction was allowed to stir for 30 minutes before dropwise addition of PMB-protected alcohol solution in CH₂Cl₂ (9.82 g, 53.9 mmol). After three hours at -78°C was added triethylamine (36.1 mL, 259 mmol). The reaction was allowed to slowly warm to room temperature and was allowed to stir overnight. The reaction was quenched with deionized H₂O (240 mL). The collected aqueous layers were extracted with dichloromethane (3 x 400 mL) and washed with 400 mL 1M HCl and 400 mL saturated NaHCO₃ (aq). The combined organic layers were dried over Na₂SO₄, filtered, and concentrated *in vacuo*. The crude mixture was purified by silica gel column chromatography (1:3 EtOAc/Hex) to yield a clear oil (12.78 g, 85%) R_f = 0.40 (1:1 EtOAc/Hex); ¹H NMR (500MHz, CDCl₃) δ 3.81 (s, 3H), 4.07 (s, 2H), 6.88-6.91 (d, *J* = 8.6 Hz, 2H), 7.27-7.31 (d, *J* = 8.6 Hz, 2H), 9.70 (t, *J* = 0.9 Hz, 1H) ppm. Spectral data are in accordance with the literature.⁴³

Synthesis of (S,E)-N-(2-(4-methoxybenzyloxy)ethylidene)-2-methylpropane-2-sulfonamide, To an oven-dried 100 mL two-neck flask with stir bar



under a N₂ atmosphere was added anhydrous dichloromethane (55 mL), (S)-2-methylpropane-2-sulfonamide (3.26 g, 26.9 mmol), aldehyde (4.4 g, 24.4 mmol) and anhydrous copper sulfate (5.25 g, 32.9 mmol). The reaction immediately turned light green and was allowed to stir overnight. The reaction was filtered through a plug of celite and washed with excess dichloromethane. The solvent was removed *in vacuo* and crude mixture purified by silica gel



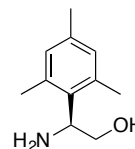
column chromatography (35% EtOAc/Hex) to yield a light-yellow oil (5.83 g, 84%). $R_f = 0.45$ (35% EtOAc/Hex); $^1\text{H NMR}$ (500MHz, CDCl_3) δ 8.12 (t, $J = 3.18$ Hz, 1 H), 7.27-7.30 (d, $J = 8.6$ Hz, 2H), 6.88-6.91 (d, $J = 8.6$ Hz, 2H), 4.57 (s, 2H), 4.37 (dd, $J = 3.51, 1.49$ Hz, 2H), 3.81 (s, 3H), 1.22 (s, 9H) ppm. Spectral data are in accordance with the literature.⁴⁴

Synthesis of (*S*)-*N*-(*S*)-mesityl-2-(4-methoxybenzyloxy)ethyl)-2-methylpropane-2-sulfonamine. To an oven-dried 50 mL, two-neck flask with reflux condenser and stir bar under a N_2 atmosphere was added anhydrous diethyl ether (36 mL), magnesium (1.22 g, 50.2 mmol) and mesityl bromide (5.67 mL, 37.6 mmol). The flask was brought to reflux at 90°C and allowed to stir for 3 hours at which point a brown-orange solution formed. To a new oven-dried 250 mL, two-neck flask with reflux condenser and stir bar under a N_2 atmosphere was added anhydrous toluene (21 mL) and (*S,E*)-*N*-(2-(4-methoxybenzyloxy)ethylidene)-2-methylpropane-2-sulfonamide (3.18 g, 12.5 mmol). The flask was brought to -78°C in a dry ice acetone bath before dropwise addition of the Grignard solution. After complete addition, the solution was allowed to stir at -78°C for 2 hours. The reaction was quenched with saturated NH_4Cl (aq) and the collected aqueous layers were extracted with ethyl acetate (3 x 30 mL). The combined organic layers were dried over Na_2SO_4 , filtered, and concentrated *in vacuo*. The viscous oil was filtered through a plug of celite, eluting with hexanes to remove the protodemetalated Grignard reagents and then filtered with 40% EtOAc:Hex to collect sulfonamine as a yellow oil. $R_f = 0.1$ (40:60 EtOAc/Hex); $^1\text{H NMR}$ (500MHz, CDCl_3) δ 1.19 (s, 9H), 2.23 (s, 6H), 2.28 (s, 3H), 3.51 (dd, $J = 10.0, 5.0$ Hz, 1H), 3.81 (s, 3H), 3.95 (t, $J = 10.3$ Hz, 1H), 4.46 (d, $J = 11.6$ Hz, 1H), 4.56 (AB_q , $J = 11.6$ Hz, 2H), 5.12 (ddd, $J = 10.5, 4.1, 1.2$ Hz, 1H), 6.81 (s, 2H),

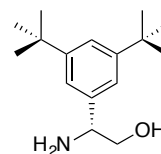
6.87 (d, 2H, J = 8.4 Hz), 7.26 (d, 2H, J = 8.8 Hz) ppm. Spectral data are in accordance with the literature.⁴⁵

General procedure for synthesis of amino alcohols: To an oven-dried 250 mL, two-neck flask with stir bar under a N₂ atmosphere was added anhydrous methanol (50 mL) and sulfonamide (9.26 mmol, 1 equiv.). 4M HCl in dioxane (43.52 mL, 174 mmol) was added dropwise and the reaction was allowed to stir for 1 hour with tracking by TLC analysis (10% MeOH:CH₂Cl₂). The reaction mixture was concentrated *in vacuo*. The crude oil was passed through a silica gel plug, eluting with 50% EtOAc/Hex to eliminate sulfur impurities, followed by 10% MeOH: CH₂Cl₂ to elute product. The product was concentrated *in vacuo*. The crude amine (9.26 mmol, 1 equiv.) was dissolved in anhydrous methanol (19.31 mL) and 10% Pd/C (2.26 g, 2.1 mmol) and 4M HCl in dioxane (20 mL, 80 mmol) were added. The N₂ atmosphere was replaced with a H₂ balloon and the reaction was allowed to stir for 24 hours. Upon completion, the reaction was filtered through a plug of celite with EtOAc and solvent was removed *in vacuo*. The concentrate was dissolved in 80 mL of EtOAc and added to 80 mL of 4M NaOH and allowed to stir for 20 minutes. The collected aqueous layers were extracted with (3 x 30 mL) ethyl acetate. The combined organic layers were dried over Na₂SO₄, filtered, and concentrated *in vacuo* to yield a white or yellow solid which could be further purified if necessary by silica gel column chromatography (10% MeOH:CH₂Cl₂).

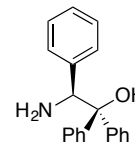
(S)-2-amino-2-mesitylethanol was synthesized according to the general procedure using (S)-N-(S)-mesityl-2(4-methoxybenzyloxy)ethyl)-2-methylpropane-2-sulfinamine (3.46 g, 9.26 mmol) which afforded a white, crystalline solid (1.2 g, 75%). $R_f = 0.1$ (10% MeOH/CH₂Cl₂); ¹H NMR (500MHz, CDCl₃) δ 2.24 (s, 3H), 2.40 (s, 6H), 3.62 (dd, $J = 10.7, 5.2$ Hz, 1H), 3.82 (t, $J = 12$ Hz, 1H), 4.47 (dd, $J = 10.0, 5.2$ Hz, 1H), 6.83 (s, 2H) ppm. Spectral data are in accordance with the literature.⁴⁵



(S)-2-amino-2-3,5-di-tert-butylphenylethanol was synthesized according to the general procedure using (S)-N-(S)-3,5-di-tert-butylphenyl-2(4-methoxybenzyloxy)ethyl)-2-methylpropane-2-sulfinamine (2.83 g, 5.97 mmol) which afforded a white, crystalline solid (1.21 g, 81%). $R_f = 0.1$ (10% MeOH/CH₂Cl₂); ¹H NMR (500MHz, CDCl₃) δ 7.35 (t, $J = 2.0$ Hz 1H), 7.16 (d, $J = 1.9$ Hz, 2H), 4.03 (dd, $J = 8.4, 4.4$ Hz, 1H), 3.75 (dd, $J = 10.6, 4.5$ Hz, 1H), 3.56 (dd, $J = 10.7, 8.4$ Hz, 1H), 1.58 (s, 2H), 1.33 (s, 18H) ppm. Spectral data are in accordance with the literature.⁴⁶



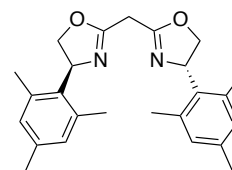
(S)-2-amino-2-1,1,2-triphenylethanol. To an oven-dried 250 mL, two-neck flask with reflux condenser and stir bar under a N₂ atmosphere was added bromo(phenyl)magnesium (3 M, 16.53 mL) in diethyl ether (90 mL). The flask was cooled to 0 °C before batchwise addition of (S)-2-phenylglycine methyl ester hydrochloride (2 g, 9.92 mmol) over 10 minutes. The reaction was brought to reflux and allowed to stir for 24 hours. The reaction was cooled to room temperature and quenched



with deionized H₂O (30 mL). The collected aqueous layers were extracted with ethyl acetate (3 x 30 mL). The combined organic layers were dried over Na₂SO₄, filtered, and concentrated *in vacuo* to yield a pure yellow-white solid which was recrystallized from hot methanol (1.52 g, 5.25 mmol, 52.96% yield). R_f = 0.1 (10% MeOH/CH₂Cl₂); ¹H NMR (500 MHz, CDCl₃) δ 1.59 (bs, 2H), 4.65 (s, 1H), 5.00 (s, 1H), 6.95 – 7.06 (m, 3H), 7.07 – 7.16 (m, 7H), 7.27 (t, *J* = 7.5 Hz, 1H), 7.40 (t, *J* = 7.4 Hz, 2H), 7.74 (d, *J* = 7.2 Hz, 2H) ppm. Spectral data are in accordance with the literature.⁴⁷

General procedure for synthesis of bisoxazolines: To an oven-dried 50 mL, two-neck flask with stir bar under a N₂ atmosphere was added anhydrous CH₂Cl₂ (4 mL) and diethyl malonimidate dihydrochloride (1.19 mmol) and the flask was cooled to 0 °C. Amino alcohol (2.38 mmol) was added and the reaction was allowed to stir at room temperature for 3 days. After this time the reaction was quenched with ice water (30 mL). The collected aqueous layers were extracted with CH₂Cl₂ (3 x 30 mL). The combined organic layers were dried over Na₂SO₄, filtered, and concentrated *in vacuo* to yield a crude yellow oil which was further purified by silica gel column chromatography (1-10% MeOH/CH₂Cl₂). Product was collected as a yellow/orange oil.

2,2-Methylene-[(4*S*)-mesityl-2-oxazoline] was synthesized according to the general procedure using malonimidate dihydrochloride (275 mg, 1.19 mmol) and (*R*)-2-amino-2-

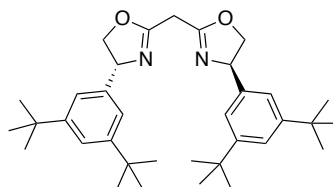


(mesitylphenyl)ethanol (427 mg, 2.38 mmol) to afford a yellow/orange oil (200 mg, 43%). R_f = 0.5 (10% MeOH/CH₂Cl₂); ¹H NMR (500 MHz, CDCl₃) δ 2.24 (s, 3H), 2.29 (s, 6H),

3.49 (s, 2H), 4.17 (dd, $J = 9.4, 1.39$ Hz, 2H), 4.63 (dd, $J = 9.89, 3.18$ Hz, 2H), 5.66 (t, $J = 10.9$, 2H), 6.82 (s, 4H) ppm. HRMS (ESI) m/z $[M]^+$ calcd. for $C_{25}H_{30}N_2O_2$ 390.57; found 390.24.

2,2-methylene-[(4R)-3,5-t-Butylphenyl-2-oxazoline] was

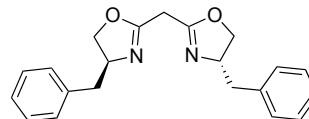
synthesized according to the general procedure using malonimidate dihydrochloride (557 mg, 2.41 mmol) and (*R*)-



2-amino-2-(3,5-di-tertbutylphenyl)ethanol (1.21 g, 4.85 mmol) to afford a yellow/orange oil (840 mg, 82%). $R_f = 0.5$ (10% MeOH/ CH_2Cl_2) 1H NMR (500MHz, $CDCl_3$) δ 7.33 (s, 2H), 7.11 (d, $J = 3.6$ Hz, 4H), 5.21 (t, $J = 8.9$ Hz, 2H), 4.67 (dd, $J = 9.8, 3.8$ Hz, 2H), 4.25 (dd, $J = 8.0, 4.6$ Hz, 2H), 3.61 (s, 2H), 1.29 (s, 36H) ppm. Spectral data are in accordance with the literature.⁴⁶

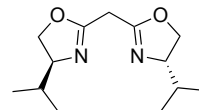
2,2-Methylene-[(4S)-benzyl-2-oxazoline] was synthesized

according to the general procedure using malonimidate dihydrochloride (8.44 g, 36.5 mmol) and (*R*)-2-amino-2-



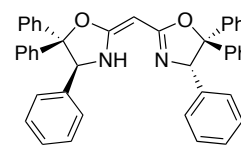
(benzyl)ethanol (11.03 g, 73.0 mmol) to afford an off-white solid (10.0 g, 81%). $R_f = 0.4$ (10% MeOH/ CH_2Cl_2); 1H NMR (500MHz, $CDCl_3$) δ 2.68 (dd, $J = 13.9, 8.6$ Hz, 2H), 3.12 (dd, $J = 13.8, 5.4$ Hz, 2H), 3.32 (t, $J = 1.1$ Hz, 2H), 4.02 (dd, $J = 8.5, 7.2$ Hz, 2H), 4.24 (dd, $J = 9.4, 8.5$ Hz, 2H), 4.40 – 4.49 (m, 2H), 7.20 – 7.24 (m, 6H), 7.30 (tt, $J = 7.1, 1.0$ Hz, 4H) ppm. Spectral data are in accordance with the literature.⁴⁸

2,2'-Methylene-[(4*S*)-isopropyl-2-oxazoline] was synthesized according to the general procedure using malonimidate dihydrochloride (1.25 g, 5.4



mmol) and (*R*)-2-amino-2-(isopropyl)ethanol (1.12 g, 10.8 mmol) to afford an off-white solid (865 mg, 83%). R_f = 0.35 (10% MeOH/CH₂Cl₂); ¹H NMR (500MHz, CDCl₃) δ 0.87 (d, J = 6.8 Hz, 6H), 0.94 (d, J = 6.8 Hz, 6H), 1.75 (dp, J = 14.1, 7.4, 7.0 Hz, 2H), 3.33 (d, J = 2.3 Hz, 2H), 3.33 (s, 2H), 3.89 – 4.02 (m, 2H), 4.26 (dd, J = 9.6, 8.3 Hz, 2H) ppm. Spectral data are in accordance with the literature.⁴⁹

2,2'-Methylenebis[(4*S*)-4,5,5-triphenyl-2-oxazoline] was synthesized according to the general procedure using malonimidate



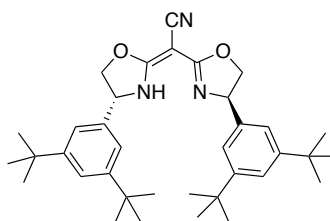
dihydrochloride (599 mg, 2.59 mmol) and (*R*)-2-amino-2-(isopropyl)ethanol (1.5 g, 5.18 mmol) to afford a yellow solid (891 mg, 59%). R_f = 0.25 (10% MeOH/CH₂Cl₂); ¹H NMR (500MHz, CDCl₃) δ 3.91 (s, 2H), 6.05 (s, 2H), 7.04–6.88 (m, 16H), 7.12–7.10 (m, 4H), 7.34 (t, J = 6.95 Hz, 2H), 7.40 (dd, J = 7.25, 6.95 Hz, 4H), 7.68 (d, J = 7.25 Hz, 4H). Spectral data are in accordance with the literature.⁵⁰

General procedure for synthesis of cyanobis(oxazolines): To an oven-dried 25 mL, two-neck flask with stir bar under a N₂ atmosphere was added anhydrous tetrahydrofuran (4 mL) and bisoxazoline (0.46 mmol). The flask was cooled to -78 °C and *n*BuLi in Hexanes (2.6 M, 0.18 mL, 0.46 mmol) was added dropwise to the flask followed by TMEDA (0.067 mL, 0.46 mmol). The reaction was allowed to stir at -78 °C down for 1 hour before dropwise addition of a tosyl cyanide (80 mg, 0.46 mmol) solution in THF (1 mL). After stirring at room temperature overnight the reaction was quenched with saturated NH₄Cl

(aq) (20 mL) and the reaction was stirred for an additional 5 minutes before separating the layers. The collected aqueous layers were extracted with Et₂O (3 x 30 mL) and CH₂Cl₂ (2 x 20 mL). The combined organic layers were dried over Na₂SO₄, filtered, and concentrated *in vacuo* to yield a crude yellow solid which was purified by neutral alumina column chromatography (20% EtOAc/Hex) to yield a white solid.

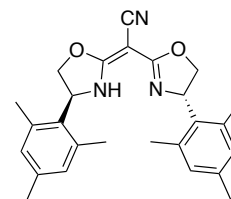
Bis-[(4R)-(3,5-tert-butylphenyl)-4,5-dihydro-oxazol-2-yl]-

acetonitrile (3.8a) was synthesized according to the general procedure using 2,2-methylene-[(4S)-3,5-di-tertbutylphenyl-2-oxazoline] (535 mg, 1.01 mmol) and tosyl cyanide (192 mg, 1.01 mmol) to afford a white solid (230 mg, 41%). *R*_f = 0.2 (1:4 EtOAc:Hexanes), [α_D²⁴] = -31.2° (c = 1.20, CHCl₃), ¹H NMR (500 MHz, CDCl₃) δ 7.37 (s, 2H), 7.06 (s, 4H), 5.13 (s, 2H), 4.84 (s, 2H), 4.35 (s, 2H), 1.28 (s, 36H). ¹³C NMR (125 MHz, CDCl₃) 31.6, 35.1, 65.6, 76.4, 121.1, 123, 129.9, 139.3, 151.8, 167.9; HRMS (ESI) *m/z* [M]⁺ calcd. For C₃₆H₄₉N₃O₂ 555.3898; found 555.3898. Spectral data are in accordance with the literature.⁵¹



Bis-[(4S)-(mesityl)-4,5-dihydro-oxazol-2-yl]-acetonitrile (3.9a) was

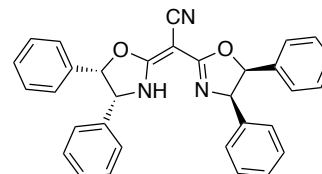
synthesized according to the general procedure using 2,2-methylene-[(4S)-mesityl-2-oxazoline] (1.5 g, 4.90 mmol) and tosyl cyanide (887 mg, 4.90 mmol) to afford a white solid (1.62 g, 49%). *R*_f = 0.24 (20% EtOAc/Hex), [α_D²⁴] = 227.9° (c = 5.0, CHCl₃), ¹H NMR (500MHz, CDCl₃) δ 2.24 (s, 3H), 2.27 (s, 6H), 4.34 (t,



$J = 8.6\text{Hz}$, 2H), 4.80 (t, $J = 10\text{Hz}$, 2H), 5.62 (t, $J = 9.68\text{ Hz}$, 2H), 6.84 (s, 4H); ^{13}C NMR (125MHz, CDCl_3) δ 20.3, 20.7, 60, 73.2, 130.6, 131.7, 136.8, 137.8, 167.1; IR (neat) 2921, 2206, 1643, 1587, 1458, 1053; HRMS (ESI) m/z $[\text{M}]^+$ calcd. For $\text{C}_{26}\text{H}_{29}\text{N}_3\text{O}_2$ 415.1806; found 415.1816.

2,2-Methylene-[(4*R*,5*S*)-diphenyl-2-oxazoline]Bis-[(4*R*,5*S*)-(diphenyl)-4,5-dihydro-oxazol-2-yl]-acetonitrile. (3.10a) was synthesized according

to the general procedure using 2,2-methylene-[(4*R*,5*S*)-(diphenyl-2-oxazoline] (1.0 g, 2.2 mmol) and tosyl cyanide

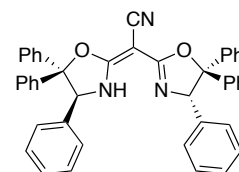


(399 mg, 2.2 mmol) to afford a white solid (600 mg, 57%). $R_f = 0.40$ (10% MeOH/ CH_2Cl_2)

, $[\alpha]_D^{24} = -80.43^\circ$ ($c = 2.2$, CHCl_3), ^1H NMR (500MHz, CDCl_3) δ 5.49 (d, $J = 9\text{ Hz}$, 2H), 6.08 (d, $J = 9\text{ Hz}$, 2H), 6.89-6.86 (m, 4H), 7.00-6.95 (m, 4H), (m, 12H). ^{13}C NMR (125 MHz, CDCl_3) 50.5, 69.1, 88.6, 126.5, 127.5, 128.0, 128.1, 128.2, 128.22, 134.5, 136.7, 168.3; HRMS (ESI) m/z $[\text{M}]^+$ calcd. For $\text{C}_{32}\text{H}_{25}\text{N}_3\text{O}_2$ 483.2016; found 483.2020. Spectral data are in accordance with the literature.⁵¹

Bis-[(4*S*)-4,5,5-triphenyl-4,5-dihydro-oxazol-2-yl]-acetonitrile

(3.11a) was synthesized according to the general procedure using 2,2-Methylene-[(4*S*)-4,4,5-triphenyl-2-oxazoline] (891 mg, 1.46 mmol)

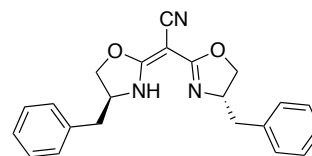


and tosyl cyanide (264 mg, 1.46 mmol) to afford a white solid (603 mg, 65%). $R_f = 0.20$ (20% EtOAc/Hex), $[\alpha]_D^{24} = -111.1^\circ$ ($c = 0.70$, CHCl_3), ^1H NMR (600 MHz, CDCl_3 - d) δ 5.86 (s, 2H), 6.95 (dd, $J = 6.6, 2.8\text{ Hz}$, 4H), 6.99 (s, 10H), 7.07 (dd, $J = 5.1, 2.0\text{ Hz}$, 6H), 7.39 (t, $J = 7.4\text{ Hz}$, 2H), 7.47 (t, $J = 7.6\text{ Hz}$, 4H), 7.74 (d, $J = 7.7\text{ Hz}$, 4H). ^{13}C NMR (125

MHz, CDCl₃) δ 76.46, 82.96, 97.98, 110.01, 128.90, 129.13, 129.77, 130.09, 130.59, 130.65, 130.74, 131.08, 131.33, 140.19, 141.52, 145.68, 168.84.; IR (neat) 3207, 2207, 1642, 1575, 1347, 1069, 693; HRMS (ESI) m/z [M]⁺ calcd. For C₄₄H₃₄N₃O₂ molecular weight: 635.2628; found 635.2646.

Bis-[(4S)-benzyl-4,5-dihydro-oxazol-2-yl]-acetonitrile (3.12a)

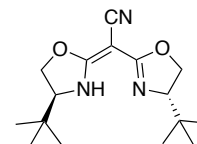
was synthesized according to the general procedure using 2,2-methylene-[(4S)- benzyl -2-oxazoline] (1.0 g, 3.0 mmol) and



tosyl cyanide (542 mg, 3.0 mmol) to afford a white solid (350 mg, 32%). $R_f=0.35$ (10% MeOH/CH₂Cl₂), $[\alpha_D^{24}] = 21.99^\circ$ (c = 0.30, CHCl₃), ¹H NMR (500MHz, CDCl₃) δ 2.75 (dd, $J = 13.7, 7.5$ Hz, 2H), 2.96 (dd, $J = 13.7, 6.4$ Hz, 2H), 4.20 (dd, $J = 8.5, 6.3$ Hz, 2H), 4.36 (p, $J = 6.9$ Hz, 2H), 4.42 – 4.48 (m, 2H), 7.16 (d, $J = 7.4$ Hz, 4H), 7.22 – 7.33 (m, 6H). ¹³C NMR (124 MHz, CDCl₃) 41.8, 46.7, 62.3, 73.3, 127.2, 129, 129.2, 137, 167.2; HRMS (ESI) m/z [M]⁺ calcd. For C₂₂H₂₁N₃O₂ 359.1716; found 359.1707. Spectral data are in accordance with the literature.⁵¹

Bis-[(4S)-(tert-butyl)-4,5-dihydro-oxazol-2-yl]-acetonitrile (3.13a)

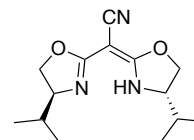
was synthesized according to the general procedure using 2,2-methylene-[(4S)- tertbutyl -2-oxazoline] (400 mg, 1.5 mmol) and tosyl



cyanide (272 mg, 1.5 mmol) to afford a white solid (350 mg, 80%). $\alpha_D^{24} = 62.5^\circ$ (c 0.6, CHCl₃), $R_f=0.30$ (10% MeOH/CH₂Cl₂); ¹H NMR (500MHz, CDCl₃) δ 0.89 (s, 18H), 3.87 (dd, $J = 9.3, 6.8$ Hz, 2H), 4.27 (dd, $J = 8.9, 6.8$ Hz, 2H), 4.41 (t, $J = 9.1$ Hz, 2H). ¹³C NMR

(125 MHz, CDCl₃) 25.3, 33.7, 53.5, 70.0, 70.2, 167.1. Spectral data are in accordance with the literature.⁵¹

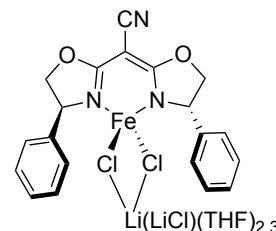
Bis-[(4*S*)-(isopropyl)-4,5-dihydro-oxazol-2-yl]-acetonitrile (3.14a)



was synthesized according to the general procedure using 2,2-methylene-[(4*S*)-isopropyl-2-oxazoline] (500 mg, 2.1 mmol) and tosyl cyanide (380 mg, 2.1 mmol) to afford a white solid (400 mg, 72%). $R_f=0.35$ (10% MeOH/CH₂Cl₂), $[\alpha_D^{24}] = 15.07^\circ$ ($c = 2.60$, CHCl₃), IR 2951, 2867, 2208, 1637, 1579, 1469, 1377, 1265, 1070 (neat). ¹H NMR (500MHz, CDCl₃) δ 0.90 (d, $J = 6.7$ Hz, 6H), 0.97 (d, $J = 6.7$ Hz, 6H), 1.73 (dq, $J = 13.4, 6.7$ Hz, 1H), 3.87 (dt, $J = 8.9, 7.1$ Hz, 2H), 4.16 (dd, $J = 8.7, 7.1$ Hz, 2H), 4.48 (t, $J = 8.8$ 3Hz, 2H). ¹³C NMR (125 MHz, CDCl₃) 18.5, 18.7, 33.0, 67.1, 72.1, 117.2, 167.2; HRMS (ESI) m/z [M]⁺ calcd. For C₁₄H₂₁N₃O₂ 263.1707; found 263.1707.

Synthesis of (2,2-bis((*S*)-4-phenyl-4,5-dihydrooxazol-2-yl)acetonitrile) Iron

Chloride (3.3). To an oven-dried 25 mL, two-neck flask with stir bar under a N₂ atmosphere was added 2,2-bis((*S*)-4-phenyl-4,5-dihydrooxazol-2-yl)acetonitrile (0.81 g, 2.5 mmol).



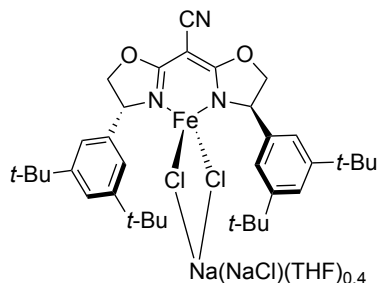
Tetrahydrofuran (5 mL) was added followed by dropwise addition of *n*-butyl-lithium (2.1 M, 1.19 mL, 2.5 mmol) at -78 °C. This mixture was stirred for 1 hour before being pumped down to a white/yellow solid. The solid was brought into the glovebox and washed thoroughly with pentane. To a 20 mL scintillation vial equipped with a stir-bar was added iron dichloride (0.31 g, 2.5 mmol) and THF (5 mL). After stirring for one hour, the lithium salt was added as a THF solution and allowed to stir for 24 hours. The solvent was removed *in vacuo* and pentane was added to precipitate the complex as a white solid. This yielded

an off-white solid (0.95 g, 81%). $[\alpha_D^{24}] -322^\circ$ (c = 0.50, THF), $^1\text{H NMR}$ (500 MHz, THF) δ -26.95 ($w_{1/2}$ = 307 Hz, 4H), -3.87 ($w_{1/2}$ = 110 Hz, 3H), -3.51 ($w_{1/2}$ = 83 Hz, 3H), -0.60 ($w_{1/2}$ = 59 Hz, 2H), 11.12 ($w_{1/2}$ = 76 Hz, 2H), 57.58 ($w_{1/2}$ = 512 Hz, 1H). IR: 2203, 1606, 1533, 1440, 1067, 694 cm^{-1} . Elemental analysis for $\text{C}_{20}\text{H}_{16}\text{ClFeN}_3\text{O}_2 \cdot (\text{LiCl})_2(\text{THF})_{2.3}$ calc'd: C, 52.21%; H, 5.17%; N 6.23%. Found: C, 52.21%, H, 5.13%, N 6.62%.

General procedure for synthesis of cyanobis(oxazoline) iron chloride complexes: To a 20 mL scintillation vial with stir bar under a N_2 atmosphere was added cyanobis(oxazoline) (0.81 g, 2.5 mmol) and sodium hydride (60 mg, 2.5 mmol). The reaction was allowed to stir overnight. In the glovebox, to a new 20 mL scintillation vial equipped with a stir-bar was added iron dichloride (0.31 g, 2.5 mmol) and THF (5 mL). After stirring for one hour, the sodium salt was added as a THF solution and allowed to stir for 24 hours. The solvent was removed *in vacuo* and pentane was added to precipitate the complex as a white solid. This yielded an off-white solid (0.95 g, 81%). $^1\text{H-NMR}$ spectrums were taken in a 10 mM LiCl THF solution to help solubilize the complexes. Elemental analysis of the following iron complexes revealed samples with C, H, and N ratios that match what would be expected for the desired complexes containing variable amounts of NaCl and THF. This difficulty has been observed previously in the purification of similar complexes.⁵² The elemental analysis of complex **11** could not be accurately determined.

(2,2-bis((R)-4-(3,5-tertbutylphenyl)-4,5-dihydrooxazol-2-yl)acetonitrile) Iron Chloride

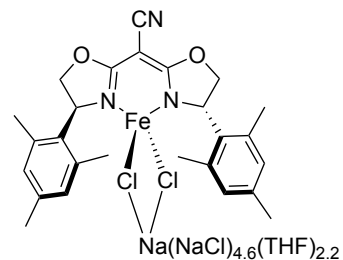
(3.8) was synthesized according to the general procedure using 2,2-bis((S)-4-(3,5-tertbutylphenyl)-4,5-dihydrooxazol-2-yl)acetonitrile (166 mg, 0.3 mmol), sodium hydride (7.2 mg, 0.3 mmol) and FeCl₂ (100 mg, 0.3 mmol) to afford an



off-white solid (632 mg, 98%). [α_D^{24}] = -26° (c = 0.50, THF), IR: 2959, 2205, 1607, 1429, 1362, 1248, 2075, 873, 712 cm⁻¹. ¹H NMR (600 MHz, THF) δ -27.46 ($w_{1/2}$ = 382 Hz, 2H), -12.93 ($w_{1/2}$ = 300 Hz, 3H), -5.31 ($w_{1/2}$ = 44 Hz, 1H), -0.70 ($w_{1/2}$ = 41 Hz, 36 H), 7.40 ($w_{1/2}$ = 76 Hz, 3H), 12.02 ($w_{1/2}$ = 100 Hz, 1H), 35.81 ($w_{1/2}$ = 524 Hz, 1H). (Compound contained minor species). Elemental analysis for C₃₆H₄₈ClFeN₃O₂•(NaCl)₂(THF)_{0.4} calc'd: C, 57.03%; H, 6.51%; N, 5.31%. Found C, 57.20%; H, 6.48%; N, 5.31%.

(2,2-bis((S)-4-(mesityl)-4,5-dihydrooxazol-2-yl)acetonitrile) Iron Chloride (3.9) was

synthesized according to the general procedure using 2,2-bis((S)-4-(isopropyl)-4,5-dihydrooxazol-2-yl)acetonitrile (566 mg, 1.36 mmol), sodium hydride (36 mg, 1.5 mmol) and FeCl₂ (38.0 mg, 0.68 mmol) to afford an off-white solid (200 mg, 29%). [α_D^{24}] = 66°

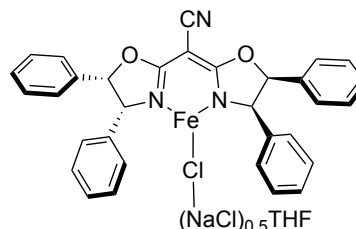


(c = 0.50, THF), IR: 2361, 2202, 1616, 1539, 1427. ¹H NMR (600 MHz, THF) δ -20.80 ($w_{1/2}$ = 262 Hz, 6H), -16.12 ($w_{1/2}$ = 102 Hz, 1H), -12.44 ($w_{1/2}$ = 100 Hz, 2H), -10.02 ($w_{1/2}$ = 73 Hz, 2H), -8.06 ($w_{1/2}$ = 100 Hz, 6H), -5.79 ($w_{1/2}$ = 48 Hz, 7H), -3.81 ($w_{1/2}$ = 48 Hz, 2H), 11.57 ($w_{1/2}$ = 86 Hz, 2H), 62.14 ($w_{1/2}$ = 531 Hz, 1H). Elemental analysis for

$C_{26}H_{28}ClFeN_3O_2 \cdot (NaCl)_{5.6}(THF)_{2.2}$ calc'd: C, 42.23%; H, 4.64%; N, 4.25%. Found C, 42.23%; H, 4.81%; N, 4.31%.

(2,2-bis((R)-4-(-(4R,5S)-diphenyl)-4,5-dihydrooxazol-2-yl)acetonitrile) Iron Chloride

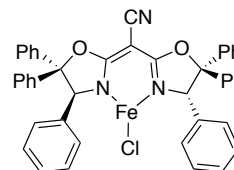
(3.10) was synthesized according to the general procedure using 2,2-bis((S)-4-((4R,5S)-diphenyl)-4,5-dihydrooxazol-2-yl)acetonitrile (250 mg, 0.52 mmol), sodium hydride (13.7



mg, 0.57 mmol) and iron dichloride (65.5 mg, 0.52 mmol) to afford an off-white solid (252 mg, 85%). $[\alpha_D^{24}] = -80^\circ$ (c = 0.50, THF), IR: 2205, 1622, 1545, 1429, 1054, 758, 695, 604, 528 cm^{-1} . 1H NMR (600 MHz, THF) δ -25.14 ($w_{1/2} = 451$ Hz, 4H), -8.42 ($w_{1/2} = 139$ Hz, 2H), -2.69 ($w_{1/2} = 112$ Hz, 4H), -0.14 ($w_{1/2} = 85$ Hz, 1H), , 6.18 ($w_{1/2} = 85$ Hz, 3H), 8.11 ($w_{1/2} = 122$ Hz, 4H), 8.39 ($w_{1/2} = 81$ Hz, 5H), 53.99 ($w_{1/2} = 663$ Hz, 1H). Elemental analysis for $C_{32}H_{24}ClFeN_3O_2 \cdot (NaCl)_{0.5}THF$ calc'd: C, 64.04%; H, 4.78%; N, 6.22%. Found: C, 63.49%, H, 4.28%, N, 6.50%.

(2,2-bis((S)-4-(-(4S,5S,5R)-diphenyl)-4,5-dihydrooxazol-2-yl)acetonitrile) Iron

Chloride (3.11) was synthesized according to the general procedure using 2,2-bis((S)-4-((4R,5S,5R)-triphenyl)-4,5-dihydrooxazol-2-yl)acetonitrile (530 mg, 0.84 mmol), sodium hydride (20 mg, 0.84

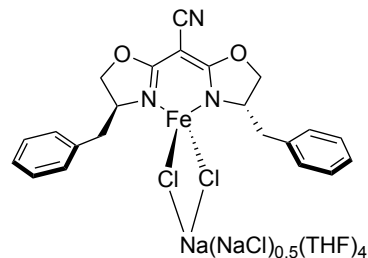


mmol) and iron dichloride (47 mg, 0.84 mmol) to afford an off-white solid (400 mg, 65%). $[\alpha_D^{24}] = -112^\circ$ (c = 0.50, THF). IR: 2196, 1612, 1529, 1428. 1H NMR (600 MHz, THF) δ -23.75 ($w_{1/2} = 840$ Hz, 4H), -3.79 ($w_{1/2} = 208$ Hz, 6H), -1.21 ($w_{1/2} = 127$ Hz, 2H), 5.03 ($w_{1/2}$

= 141 Hz, 4H), 8.17 ($w_{1/2}$ = 130 Hz, 4H), 9.19 ($w_{1/2}$ = 173 Hz, 6H), 9.65 ($w_{1/2}$ = 230 Hz, 6H), 51.63 ($w_{1/2}$ = 742 Hz, 1H). Elemental analysis for $C_{44}H_{32}ClFeN_3O_2$ calc'd: C, 72.79%; H, 4.44; N, 5.79%. Found: C, 73.68%, H, 4.96%, N, 4.86%.

(2,2-bis((S)-4-(benzyl)-4,5-dihydrooxazol-2-yl)acetonitrile)Iron Chloride (3.12) was

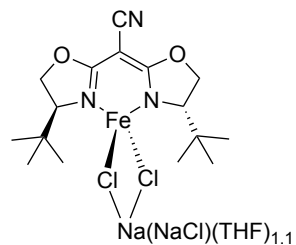
synthesized according to the general procedure using 2,2-bis((S)-4-(benzyl)-4,5-dihydrooxazol-2-yl)acetonitrile (350 mg, 0.97 mmol), sodium hydride (25.7 mg, 1.07 mmol) and iron dichloride (123 mg, 0.97 mmol) to afford



an off-white solid (350 mg, 79%). $[\alpha_D^{24}] = 6^\circ$ ($c = 0.50$, THF), IR: 2361, 2207, 1623, 1538, 1433, 1030, 701, 505 cm^{-1} . 1H NMR (600 MHz, THF) δ -62.82 ($w_{1/2}$ = 656 Hz, 2H), -42.45 ($w_{1/2}$ = 484 Hz, 2H), -5.04 ($w_{1/2}$ = 163 Hz, 5H), -4.77 ($w_{1/2}$ = 112 Hz, 3H), 37.21 ($w_{1/2}$ = 560 Hz, 2H). (One peak was unable to be integrated due to overlapping with THF resonances) Elemental analysis for $C_{22}H_{20}ClFeN_3O_2 \cdot (NaCl)_{1.5}(THF)_4$ calc'd: C, 55.27%; H, 6.35%; N, 5.09%. Found: C, 55.54%; H, 6.85%; N, 4.02%.

(2,2-bis((S)-4-(tertbutyl)-4,5-dihydrooxazol-2-yl)acetonitrile) Iron Chloride (3.13) was

synthesized according to the general procedure using 2,2-bis((S)-4-(tertbutyl)-4,5-dihydrooxazol-2-yl)acetonitrile (200 mg, 0.69 mmol), sodium hydride (18.2 mg, 0.76 mmol) and iron dichloride

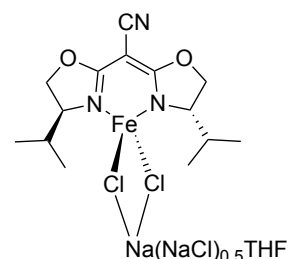


(0.1 g, 0.3 mmol) to afford an off-white solid (260 mg, 99%). IR: 2200, 1602, 1536, 1440, 1068, 744 cm^{-1} . Elemental analysis for $C_{16}H_{24}ClFeN_3O_2 \cdot (NaCl)_2(THF)_{1.1}$ calc'd: C, 42.43%; H, 5.73%; N, 7.26%. Found: C, 42.38%; H, 5.40%; N, 8.04%. 1H -NMR

spectroscopy could not be used on this complex due to its insolubility in THF and other organic solvents.

(2,2-bis((S)-4-(isopropyl)-4,5-dihydrooxazol-2-yl)acetonitrile)

Iron Chloride (3.14) was synthesized according to the general procedure using 2,2-bis((S)-4-(isopropyl)-4,5-dihydrooxazol-2-yl)acetonitrile (134 mg, 0.54 mmol), sodium hydride (12.5 mg,



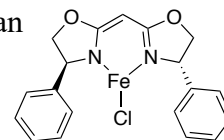
0.54 mmol) and FeCl₂ (30.2 mg, 0.54 mmol) to afford an off-white solid (110 mg, 57%).

$[\alpha_D^{24}] = 66^\circ$ (c = 0.50, THF), IR: 2201, 1619. ¹H NMR (600 MHz, THF) δ -68.44 ($w_{1/2} = 728$ Hz, 1H), -23.41 ($w_{1/2} = 241$ Hz, 6H), -18.15 ($w_{1/2} = 114$ Hz, 6H), -7.90 ($w_{1/2} = 88$ Hz, 2H), -3.21 ($w_{1/2} = 24$ Hz, 1H), 4.54 ($w_{1/2} = 29$ Hz, 1H), 37.41 ($w_{1/2} = 560$ Hz, 1H).

Elemental analysis for C₁₄H₂₀ClFeN₃O₂·(NaCl)_{1.5}THF calc'd: C, 42.11; H, 5.50; N, 8.18.

Found: C, 41.31%, H, 5.03%, N, 8.78%.

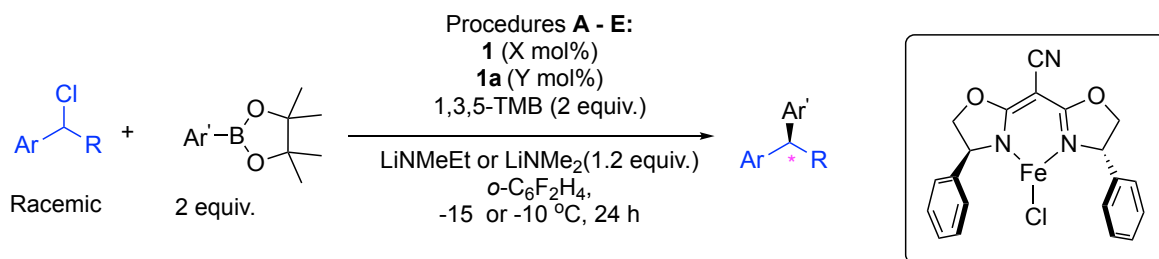
2,2'-methylene-[(4S)-phenyl-2-oxazoline] Iron Chloride (3.15). To an oven-dried 25 mL, two-neck flask with stir bar under a N₂ atmosphere was added 2,2'-methylene-[(4S)-phenyl-2-oxazoline] (224 mg, 0.73 mmol).



Tetrahydrofuran (3 mL) was added followed by dropwise addition of *n*-butyl-lithium (2.1 M, 0.35 mL, 0.731 mmol) at -78°C. This mixture was stirred for 1 hour before being pumped down to a white/yellow solid. The solid was brought into the glovebox and washed thoroughly with pentane. To a 20 mL scintillation vial equipped with a stir-bar was added iron dichloride (40.8 mg, 0.731 mmol) and THF (5 mL). After stirring for one hour, the lithium salt was added as a THF solution and allowed to stir for 24 hours. The solvent was

removed *in vacuo* and pentane was added to precipitate the complex as a yellow solid (290 mg, 99%). $[\alpha_D^{24}] = 250^\circ$ ($c = 0.50$, THF). IR: 2960, 1596, 1452, 1266, 1027, 758, 698. ^1H NMR (600 MHz, THF) -15.76 ($w_{1/2} = 442$ Hz, 4H), -0.79 ($w_{1/2} = 139$ Hz, 3H), 25.02 ($w_{1/2} = 276$ Hz, 2H), 28.39 ($w_{1/2} = 185$ Hz, 2H), 30.94 ($w_{1/2} = 345$ Hz, 2H), 40.14 ($w_{1/2} = 360$ Hz, 2H), 115.54 – 117.92 ($w_{1/2} = 560$ Hz, 1H). Elemental analysis for $\text{C}_{19}\text{H}_{17}\text{ClFeN}_2\text{O}_2$ calc'd: C, 57.53%; H, 4.32%; N, 7.06%. Found: C, 56.60%; H, 6.47%; N, 8.26%.

General procedure for enantioselective iron complex-catalyzed Suzuki-Miyaura cross-coupling between benzylic chlorides and arylboronic pinacol esters



Standard Reaction Conditions (Conditions A): To a 10 mL one-neck flask with stir bar under a N_2 atmosphere was added **3.3** (10.54 mg, 25.0 μmol), **3.3a** (3.91 mg, 12.5 μmol), 1,3,5-trimethoxybenzene (42.0 mg, 0.25 mmol) and lithium methylethylamide (19.0 mg, 0.30 mmol). A vacuum adapter fitted with a teflon stopcock was assembled to the flask and the flask brought outside of the glovebox, secured to the Schlenk line, and cooled to -15 °C. To the flask was added a 1,2-difluorobenzene solution (3 mL) of arylboronic acid pinacol ester (0.50 mmol) and alkyl halide (0.25 mmol). The reaction was allowed to stir vigorously for 24 hours at -15 °C. Typically, the reaction turns a pale brown color and stays heterogenous throughout the course of the reaction with solid depositing on the sides

of the flask. After 24 hours, the reaction was quenched with saturated NH_4Cl (aq) (10 mL) and the collected aqueous layers were extracted with dichloromethane (3 x 40 mL). The combined organic layers were dried over Na_2SO_4 , filtered, and concentrated *in vacuo*. An NMR yield was determined from the crude reaction mixture using the added 1,3,5-trimethoxybenzene reagent as the internal standard. The benzylic proton resonances were used as diagnostic peaks for determining the NMR yield. The crude mixture was purified by silica gel column chromatography (Hexanes).

Reaction with lithium dimethylamide and no added exogenous ligand (Conditions B):

To a 10 mL one-neck flask with stir bar under a N_2 atmosphere was added **3.3** (15.8 mg, 37.5 μmol), 1,3,5-trimethoxybenzene (84.1 mg, 0.50 mmol) and lithium-dimethyl amide (15.4 mg, 0.30 mmol). A vacuum adapter fitted with a teflon stopcock was assembled to the flask and the flask brought outside of the glovebox, secured to the Schlenk line, and cooled to $-15\text{ }^\circ\text{C}$. To the flask was added a 1,2-difluorobenzene solution (3 mL) of arylboronic acid pinacol ester (0.50 mmol) and alkyl halide (0.25 mmol). The reaction was allowed to stir vigorously for 24 hours at $-15\text{ }^\circ\text{C}$. Typically, the reaction turns a pale brown color and stays heterogenous throughout the course of the reaction with solid depositing on the sides of the flask. After 24 hours, the reaction was quenched with saturated NH_4Cl (aq) (10 mL) and the collected aqueous layers were extracted with dichloromethane (3 x 40 mL). The combined organic layers were dried over Na_2SO_4 , filtered, and concentrated *in vacuo*. An NMR yield was determined from the crude reaction mixture using the added 1,3,5-trimethoxybenzene reagent as the internal standard. The benzylic proton resonances were used as diagnostic peaks for determining the NMR yield. The crude mixture was purified by silica gel column chromatography (Hexanes).

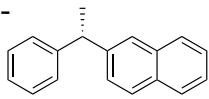
Reaction run at -10° C with lithium dimethylamide (Conditions C): To a 10 mL one-neck flask with stir bar under a N₂ atmosphere was added **3.3** (15.8 mg, 37.5 μmol), **3.3a** (6.21 mg, 18.75 μmol), 1,3,5-trimethoxybenzene (84.1 mg, 0.50 mmol) and lithium-dimethyl amide (15.4 mg, 0.30 mmol). A vacuum adapter fitted with a teflon stopcock was assembled to the flask and the flask brought outside of the glovebox, secured to the Schlenk line, and cooled to -10 °C. To the flask was added a 1,2-difluorobenzene solution (3 mL) of arylboronic acid pinacol ester (0.50 mmol) and alkyl halide (0.25 mmol). The reaction was allowed to stir vigorously for 24 hours at -10 °C. Typically, the reaction turns a pale brown color and stays heterogenous throughout the course of the reaction with solid depositing on the sides of the flask. After 24 hours, the reaction was quenched with saturated NH₄Cl (aq) (10 mL) and the collected aqueous layers were extracted with dichloromethane (3 x 40 mL). The combined organic layers were dried over Na₂SO₄, filtered, and concentrated *in vacuo*. An NMR yield was determined from the crude reaction mixture using the added 1,3,5-trimethoxybenzene reagent as the internal standard. The benzylic proton resonances were used as diagnostic peaks for determining the NMR yield. The crude mixture was purified by silica gel column chromatography (Hexanes).

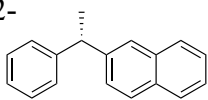
Reaction run at -10° C with lithium methylethylamide (Conditions D): To a 10 mL one-neck flask with stir bar under a N₂ atmosphere was added **3.3** (15.8 mg, 37.5 μmol), **3.3a** (6.21 mg, 18.75 μmol), 1,3,5-trimethoxybenzene (84.1 mg, 0.50 mmol) and lithium-dimethyl amide (15.4 mg, 0.30 mmol). A vacuum adapter fitted with a teflon stopcock was assembled to the flask and the flask brought outside of the glovebox, secured to the Schlenk line, and cooled to -10 °C. To the flask was added a 1,2-difluorobenzene solution (3 mL) of arylboronic acid pinacol ester (0.50 mmol) and alkyl halide (0.25 mmol). The reaction

was allowed to stir vigorously for 24 hours at -10 °C. Typically, the reaction turns a pale brown color and stays heterogenous throughout the course of the reaction with solid depositing on the sides of the flask. After 24 hours, the reaction was quenched with saturated NH₄Cl (aq) (10 mL) and the collected aqueous layers were extracted with dichloromethane (3 x 40 mL). The combined organic layers were dried over Na₂SO₄, filtered, and concentrated *in vacuo*. An NMR yield was determined from the crude reaction mixture using the added 1,3,5-trimethoxybenzene reagent as the internal standard. The benzylic proton resonances were used as diagnostic peaks for determining the NMR yield. The crude mixture was purified by silica gel column chromatography (Hexanes).

Reaction run at -10° C, 40% catalyst loading, lithium dimethylethylamide and no added exogenous ligand (Conditions E): To a 10 mL one-neck flask with stir bar under a N₂ atmosphere was added **3.3** (42.57 mg, 0.10 mmol), 1,3,5-trimethoxybenzene (84.1 mg, 0.50 mmol) and lithium methylethylamide (19.0 mg, 0.30 mmol). A vacuum adapter fitted with a teflon stopcock was assembled to the flask and the flask brought outside of the glovebox, secured to the Schlenk line, and cooled to -10 °C. To the flask was added a 1,2-difluorobenzene solution (3 mL) of arylboronic acid pinacol ester (0.50 mmol) and alkyl halide (0.25 mmol). The reaction was allowed to stir vigorously for 24 hours at -10 °C. Typically, the reaction turns a pale brown color and stays heterogenous throughout the course of the reaction with solid depositing on the sides of the flask. After 24 hours, the reaction was quenched with saturated NH₄Cl (aq) (10 mL) and the collected aqueous layers were extracted with dichloromethane (3 x 40 mL). The combined organic layers were dried over Na₂SO₄, filtered, and concentrated *in vacuo*. An NMR yield was determined from the

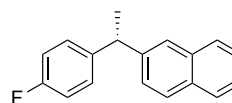
crude reaction mixture using the added 1,3,5-trimethoxybenzene reagent as the internal standard. The benzylic proton resonances were used as diagnostic peaks for determining the NMR yield. The crude mixture was purified by silica gel column chromatography (Hexanes).

(S)-1-(1-Phenylethyl)naphthalene (3.6) was synthesized from 1-chloroethylbenzene and 2-naphthylboronic pinacol ester according to 
General Procedure A. Product was purified by silica gel flash column chromatography, eluting with hexanes to afford purified product as a colorless oil (91% spectroscopic yield, 80% isolated yield), $R_f = 0.60$ (5% Et₂O in Hexanes, (85:15 er)) $[\alpha_D^{24}] = 20.2^\circ$ (c = 1.00, CHCl₃), Chiral Column HPLC (OD-H) 1 mL/ min, 100% Hexanes (85:15 er)) ¹H NMR (400 MHz, CDCl₃) δ 1.77 (d, $J = 7.2$ Hz, 3H), 4.35 (q, $J = 7.2$ Hz, 1H), 7.22 (td, $J = 6.8, 1.9$ Hz, 1H), 7.26 – 7.36 (m, 5H), 7.42 – 7.52 (m, 2H), 7.73 (s, 1H), 7.77 (d, $J = 8.5$ Hz, 1H), 7.82 (dd, $J = 7.9, 5.9$ Hz, 2H) ppm; ¹³C NMR (125MHz, CDCl₃) δ 21.0, 40.1, 125.6, 126.1, 126.3, 127.1, 127.8, 128.0, 128.2, 128.6, 132.3, 133.7, 144.0, 146.4 ppm; HRMS (ESI) m/z [M]⁺ calcd. for C₁₈H₁₆ molecular Weight: 232.13; found 231.12. Spectral data are in accordance with the literature.²⁰ Absolute configuration assigned by reference to literature retention times of chiral column HPLC and sign of optical rotation.²⁰

(S)-1-(1-Phenylethyl)naphthalene (3.6) was synthesized from 2-chloronaphthylbenzene and phenylboronic pinacol ester according to 
General Procedure A. Product was purified by silica gel flash column chromatography, eluting with hexanes to afford purified product as a colorless oil (90% spectroscopic yield,

85% isolated yield), $R_f = 0.60$ (5% Et₂O in Hexanes, (85:15 er)) $[\alpha_D^{24}] = 20.2^\circ$ (c = 1.00, CHCl₃), Chiral Column HPLC (OD-H) 1 mL/ min, 100% Hexanes (73:27 er)) ¹H NMR (400 MHz, CDCl₃) δ 1.77 (d, $J = 7.2$ Hz, 3H), 4.35 (q, $J = 7.2$ Hz, 1H), 7.22 (td, $J = 6.8, 1.9$ Hz, 1H), 7.26 – 7.36 (m, 5H), 7.42 – 7.52 (m, 2H), 7.73 (s, 1H), 7.77 (d, $J = 8.5$ Hz, 1H), 7.82 (dd, $J = 7.9, 5.9$ Hz, 2H) ppm; ¹³C NMR (125MHz, CDCl₃) δ 21.0, 40.1, 125.6, 126.1, 126.3, 127.1, 127.8, 128.0, 128.2, 128.6, 132.3, 133.7, 144.0, 146.4 ppm; HRMS (ESI) m/z [M]⁺ calcd. for C₁₈H₁₆ molecular weight: 232.1169; found 232.1168. Spectral data are in accordance with the literature.²⁰ Absolute configuration assigned by reference to literature retention times of chiral column HPLC and sign of optical rotation.²⁰

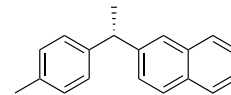
(S)-2-(1-(4-fluorophenyl)ethyl)naphthalene (3.17) was



synthesized from 1-(1-chloroethyl)-4-fluoro-benzene and 2-naphthylboronic pinacol ester according to General Procedure A. Product was purified by silica gel flash column chromatography, eluting with hexanes to afford purified product as a white solid (54% spectroscopic yield, 42% isolated yield). $R_f = 0.60$ (5% Et₂O in Hexanes), $[\alpha_D^{24}] = 12.8^\circ$ (c = 2.8, CHCl₃), Chiral Column HPLC (OD-H) 1 mL/ min, 100% Hexanes (77:23 er)) ¹H NMR (400 MHz, CDCl₃) δ 1.71 (d, $J = 7.2$ Hz, 3H), 4.30 (q, $J = 7.2$ Hz, 1H), 6.97 (t, $J = 8.7$ Hz, 2H), 7.21 (dd, $J = 8.7, 5.6$ Hz, 2H), 7.26 (s, 1H), 7.39 – 7.50 (m, 2H), 7.67 (s, 1H), 7.74 (d, $J = 8.5$ Hz, 1H), 7.79 (d, $J = 7.9$ Hz, 2H) ppm. ¹³C NMR (125MHz, CDCl₃) δ 21.90, 44.10, 125.27, 125.45, 126.01, 126.62, 127.56, 127.69, 128.03, 129.09 (d, $J = 8.0$ Hz), 132.10, 133.48, 141.87 (d, $J = 3.2$ Hz), 143.53, 161.28 (d, $J = 244.0$ Hz). ppm; HRMS (ESI) m/z [M]⁺ calcd. for C₁₈H₁₅F molecular weight: 250.1067; found 250.1074. Spectral data are in accordance with the literature.²⁰ Absolute configuration

assigned by reference to literature retention times of chiral column HPLC and sign of optical rotation.²⁰

(S)-2-(1-(p-tolyl)ethyl)naphthalene (3.18) was synthesized from 1-(1-chloroethyl)-4-methylbenzene and 2-naphthylboronic pinacol ester according to



General Procedure A. Product was purified by silica gel flash column chromatography, eluting with hexanes to afford purified product as a colorless oil (78% spectroscopic yield,

63 % isolated yield). $R_f = 0.60$ (5% Et₂O in Hexanes), $[\alpha_D^{24}] = 13.2^\circ$ (c = 3.4, CHCl₃),

Chiral Column HPLC (OD-H) 1 mL/ min, 100% Hexanes (82:18 er) ¹H NMR (400 MHz,

CDCl₃) δ 1.76 (d, $J = 7.2$ Hz, 3H), 2.35 (s, 3H), 4.32 (q, $J = 7.2$ Hz, 1H), 7.11–7.22 (m,

4H), 7.34 (dd, $J = 8.5, 1.8$ Hz, 1H), 7.43–7.52 (m, 2H), 7.72–7.76 (m, 1H), 7.78 (d, $J = 8.5$

Hz, 1H), 7.80–7.85 (m, 2H) ppm; ¹³C NMR (125MHz, CDCl₃) δ 21.0, 21.8, 44.4, 125.3,

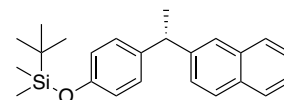
125.3, 125.9, 126.8, 127.5, 127.6, 127.7, 127.9, 129.1, 132.1, 133.5, 135.6, 143.3, 144.0

ppm; HRMS (ESI) m/z [M]⁺ calcd. for C₁₈H₁₅F molecular weight: 246.1239; found

246.1325. Spectral data are in accordance with the literature.²⁰ Absolute configuration

assigned by reference to literature retention times of chiral column HPLC and sign of optical rotation.²⁰

(+)-2-(1-(4-tert-butyltrimethylsilyloxy)ethyl)naphthalene (3.19) was synthesized from 1-(4-tert-Butyltrimethylsilyloxy)phenylchloride and 2-



naphthylboronic pinacol ester according to General Procedure A..

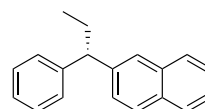
Product was purified by silica gel flash column chromatography, eluting with hexanes to afford purified product as a colorless oil (45% spectroscopic yield, 40% isolated yield). $R_f = 0.35$

(Hexanes) $[\alpha_D^{24}] = 10.8^\circ$ (c = 3.2, CHCl₃), Chiral Column HPLC (OD-H) 1 mL/ min, 100%

Hexanes (82:18 er), ¹H NMR (400 MHz, CDCl₃) δ 0.20 (s, 6H), 0.99 (s, 10H), 1.71 (d, J

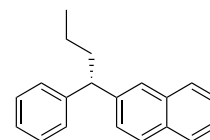
= 7.2 Hz, 3H), 4.27 (q, $J = 7.2$ Hz, 1H), 6.77 (d, $J = 8.4$ Hz, 2H), 7.12 (d, $J = 8.4$ Hz, 2H), 7.31 (dd, $J = 8.5, 1.8$ Hz, 1H), 7.40 – 7.49 (m, 2H), 7.67 (s, 1H), 7.75 (d, $J = 8.5$ Hz, 1H), 7.80 (d, $J = 8.0$ Hz, 2H) ppm. ^{13}C NMR (125 MHz, CDCl_3) δ 1.74, 20.84, 24.64, 28.36, 46.74, 122.45, 127.91, 127.94, 128.54, 129.50, 130.20, 130.35, 130.51, 131.26, 134.70, 136.18, 141.48, 146.95, 156.47 ppm. IR (neat); 2955, 2923, 2872, 2859, 1458, 1378. HRMS (ESI) m/z $[\text{M}]^+$ calcd. For $\text{C}_{24}\text{H}_{30}\text{OSi}$ molecular weight: 362.2129; found 362.2139.

(S)-2-(1-phenylpropyl)naphthalene (3.20) was synthesized from 1-



chloropropylbenzene and 2-naphthylboronic pinacol ester according to General Procedure A. Product was purified by silica gel flash column chromatography, eluting with hexanes to afford purified product as a colorless oil (84% spectroscopic yield, 68% isolated yield). $R_f = 0.60$ (5% Et_2O in Hexanes), $[\alpha_D^{24}] = 6.7^\circ$ ($c = 3.56$, CHCl_3), Chiral Column HPLC (OD-H) 1 mL/ min, 100% Hexanes (81:19 er) ^1H NMR (400 MHz, CDCl_3) δ 0.98 (t, $J = 7.3$ Hz, 3H), 2.14 – 2.28 (m, 2H), 3.99 (t, $J = 7.7$ Hz, 1H), 7.20 (qq, $J = 5.0, 2.3$ Hz, 1H), 7.28 – 7.34 (m, 4H), 7.37 (dd, $J = 8.5, 1.8$ Hz, 1H), 7.46 (dddd, $J = 21.2, 8.0, 6.8, 1.4$ Hz, 2H), 7.73 – 7.78 (m, 2H), 7.81 (ddd, $J = 13.8, 8.1, 1.3$ Hz, 2H) ppm. ^{13}C NMR (125MHz, CDCl_3) δ 12.8, 28.5, 53.3, 125.3, 125.9, 125.9, 126.1, 126.8, 127.5, 127.7, 128.0, 128.2, 128.4, 132.1, 142.6, 145.0 ppm. HRMS (ESI) m/z $[\text{M}]^+$ calcd. for $\text{C}_{19}\text{H}_{18}$ molecular weight: 246.1329; found 246.1325. Spectral data are in accordance with the literature.²⁰ Absolute configuration assigned by reference to literature retention times of chiral column HPLC and sign of optical rotation.²⁰

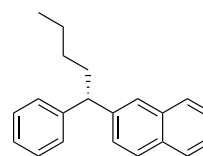
(S)-2-(1-phenylbutyl)naphthalene (3.21) was synthesized from 1-



chlorobutylbenzene and 2-naphthylboronic pinacol ester according to General Procedure A. Product was purified by silica gel flash column

chromatography, eluting with hexanes to afford purified product as a colorless oil (77% spectroscopic yield, 73% isolated yield). $R_f = 0.60$ (5% Et₂O in Hexanes), $[\alpha_D^{24}] = 5.2^\circ$ ($c = 3.41$, CHCl₃), Chiral Column HPLC (OD-H) 1 mL/ min, 100% Hexanes (79:21 er), ¹H NMR (600 MHz, CDCl₃) δ 0.97 (t, $J = 7.4$ Hz, 3H), 1.35 (h, $J = 7.5$ Hz, 2H), 2.09 – 2.22 (m, 2H), 4.10 (t, $J = 7.8$ Hz, 1H), 7.16 – 7.22 (m, 1H), 7.26 – 7.34 (m, 4H), 7.36 (dd, $J = 8.5, 1.8$ Hz, 1H), 7.44 (dddd, $J = 21.7, 8.1, 6.8, 1.4$ Hz, 2H), 7.72 – 7.77 (m, 2H), 7.80 (ddd, $J = 14.2, 8.4, 1.4$ Hz, 2H) ppm. ¹³C NMR (125 MHz, CDCl₃) 16.78, 23.86, 40.35, 53.75, 127.96, 128.52, 128.54, 128.73, 129.49, 130.21, 130.35, 130.66, 131.04, 134.78, 136.20, 145.41, 147.84. IR (neat); 3055, 3024, 2954, 2925, 2869, 1451, 722 ppm. HRMS (ESI) m/z [M]⁺ calcd. for C₂₀H₂₀ molecular weight: 260.1481; found 260.1574. Absolute configuration assigned by analogy to sign of optical rotation for **3.20**.²⁰

(S)-2-(1-phenylpentyl)naphthalene (3.22) was synthesized from 1-chloropentylbenzene and 2-naphthylboronic pinacol ester according to General Procedure A. Product was purified by silica gel flash column

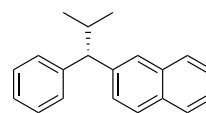


chromatography, eluting with hexanes to afford purified product as a colorless oil (91% spectroscopic yield, 69% isolated yield). $R_f = 0.60$ (5% Et₂O in Hexanes), $[\alpha_D^{24}] = 7.4^\circ$ ($c = 4.6$, CHCl₃), Chiral Column HPLC (OD-H) 1 mL/ min, 100% Hexanes (78:22 er), ¹H NMR (600 MHz, CDCl₃) δ 0.92 (t, $J = 7.2$ Hz, 3H), 1.35 – 1.46 (m, 2H), 2.12 – 2.25 (m, 2H), 4.09 (t, $J = 7.8$ Hz, 1H), 7.21 (tt, $J = 6.4, 2.1$ Hz, 1H), 7.28 – 7.35 (m, 4H), 7.38 (dd, $J = 8.4, 1.8$ Hz, 1H), 7.42 – 7.50 (m, 2H), 7.73 – 7.79 (m, 2H), 7.82 (dd, $J = 15.1, 8.0$ Hz, 2H) ppm. ¹³C NMR (125 MHz, CDCl₃) δ 16.72, 25.44, 32.97, 37.92, 42.44, 54.08, 127.98, 128.55, 128.56, 128.74, 129.50, 130.24, 130.39, 130.67, 131.07, 134.81, 136.23, 145.47, 147.91 ppm. IR (neat); 3055, 3024, 2954, 2927, 2857, 1506, 698. HRMS (ESI) m/z [M]⁺

calcd. for C₂₁H₂₂ molecular weight: 274.1642; found 274.1639. Absolute configuration assigned by analogy to sign of optical rotation for **3.20**.²⁰

(-)-2-(2-methyl-1-phenylpropyl)naphthalene (3.23) was synthesized

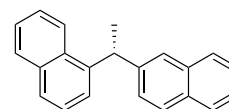
from 1-chloroisobutylbenzene and 2-naphthylboronic pinacol ester



according to General Procedure A. Product was purified by silica gel flash column chromatography, eluting with hexanes to afford purified product as a colorless oil (39% spectroscopic yield, 37% isolated yield). R_f = 0.60 (5% Et₂O in Hexanes), [α_D²⁴] = -2.9° (c = 1.3, CHCl₃), Chiral Column HPLC (1B) 0.8 mL/ min, 100% Hexanes (73:273 er). ¹H NMR (400 MHz, CDCl₃) δ 0.92 (ddd, J = 10.1, 6.5, 1.2 Hz, 6H), 2.62 (tt, J = 12.8, 6.6 Hz, 1H), 3.59 (d, J = 10.8 Hz, 1H), 7.10 – 7.17 (m, 1H), 7.23 – 7.29 (m, 1H), 7.33 – 7.36 (m, 2H), 7.39 (ddt, J = 8.1, 6.9, 1.4 Hz, 1H), 7.41 – 7.46 (m, 2H), 7.72 – 7.81 (m, 4H) ppm. ¹³C NMR (125 MHz, CDCl₃) δ 5.87, 24.50, 24.57, 34.28, 63.56, 127.84, 128.45, 128.63, 128.92, 129.20, 130.14, 130.27, 130.66, 130.74, 131.03, 136.22, 145.06, 147.34 ppm. IR (neat); 3055, 3023, 2953, 2923, 2853, 1494, 699. HRMS (ESI) m/z [M]⁺ calcd. for C₂₀H₂₀ molecular weight: 260.1557; found 260.1603.

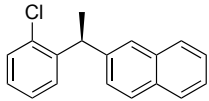
(-)-1-(1-(naphthalen-2-yl)ethyl)naphthalene (3.24) was synthesized

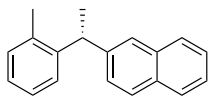
from 1-(1-chloroethyl)naphthalene and 2-naphthylboronic pinacol



ester according to General Procedure B. Product was purified by silica gel flash column chromatography, eluting with hexanes to afford purified product as a colorless oil (64 % spectroscopic yield, 64% isolated yield). R_f = 0.55 (5% Et₂O in Hexanes), [α_D²⁴] = -20.63° (c = 1.25, CHCl₃), Chiral Column HPLC (1C) 0.8 mL/ min, 100% Hexanes (77:23 er) ¹H NMR (400 MHz, CDCl₃) δ 1.86 (d, J = 7.1 Hz, 3H), 5.09 (q, J = 7.1 Hz, 1H), 7.34 (dd, J = 8.5, 1.9 Hz, 1H), 7.38 – 7.49 (m, 6H), 7.68 – 7.82 (m, 5H), 7.87 (dd, J = 6.4, 3.4 Hz, 1H),

8.08 – 8.13 (m, 1H) ppm; ^{13}C NMR (125 MHz, CDCl_3) δ 22.40, 40.68, 123.93, 124.59, 125.30, 125.33, 125.45, 125.50, 125.87, 125.91, 126.80, 127.05, 127.54, 127.70, 128.01, 128.78, 131.74, 132.07, 133.56, 134.00, 141.47, 144.13 ppm. HRMS (ESI) m/z $[\text{M}]^+$ calcd. for $\text{C}_{22}\text{H}_{18}$ molecular weight: 282.1391; found 282.1403. Spectral data are in accordance with the literature.⁵³

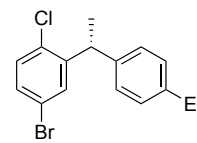
(-)-2-(1-(*o*-chloro)ethyl)naphthalene (3.25) was synthesized from 1-chloro-2-(1-chloroethyl) benzene and 2-naphthylboronic pinacol ester  according to General Procedure B. Product was purified by silica gel flash column chromatography, eluting with hexanes to afford purified product as a colorless oil (54% spectroscopic yield, 45% isolated yield). $R_f = 0.60$ (5% Et_2O in Hexanes) $[\alpha_D^{24}] = -51.4^\circ$ ($c = 2.5$, CHCl_3), Chiral Column HPLC (OD-H) 1 mL/ min, 100% Hexanes (93:7 er), ^1H NMR (400 MHz, CDCl_3) δ 1.71 (d, $J = 7.2$ Hz, 3H), 4.82 (q, $J = 7.2$ Hz, 1H), 7.09 – 7.27 (m, 3H), 7.31 (dd, $J = 8.5, 1.8$ Hz, 1H), 7.37 (dd, $J = 7.7, 1.4$ Hz, 1H), 7.44 (tt, $J = 8.5, 6.0$ Hz, 2H), 7.69 (s, 1H), 7.74 (d, $J = 8.5$ Hz, 1H), 7.76 – 7.82 (m, 2H) ppm. ^{13}C NMR (125 MHz, CDCl_3) δ 21.9, 41.1, 125.3, 125.4, 126.1, 126.1, 126.7, 126.9, 127.5, 127.7, 127.9, 130.4, 132.0, 133.5, 136.1, 143.7, 143.8 ppm. HRMS (ESI) m/z $[\text{M}]^+$ calcd. for $\text{C}_{18}\text{H}_{15}\text{Cl}$ molecular weight: 266.0849; found 266.0857. Spectral data are in accordance with the literature.¹⁶ Absolute configuration assigned by reference to literature retention times of chiral column HPLC and sign of optical rotation.¹⁶

(-)-2-(1-(*o*-tolyl)ethyl)naphthalene (3.26) was synthesized from 1-chloro-2-(1-methylethyl)benzene and 2-naphthylboronic pinacol ester 

according to General Procedure B. Product was purified by silica gel flash column chromatography, eluting with hexanes to afford purified product as a colorless oil (70 % spectroscopic yield, 67% isolated yield). $R_f = 0.60$ (5% Et₂O in Hexanes), $[\alpha_D^{24}] = -11.6^\circ$ ($c = 1.93$, CHCl₃), Chiral Column HPLC (OD-H) 1 mL/ min, 100% Hexanes (95:5 er) ¹H NMR (400 MHz, CDCl₃) δ 1.72 (d, $J = 7.2$ Hz, 3H), 2.30 (s, 3H), 4.50 (q, $J = 7.2$ Hz, 1H), 7.17 (d, $J = 4.5$ Hz, 2H), 7.23 (dt, $J = 8.0, 4.3$ Hz, 1H), 7.26 – 7.34 (m, 2H), 7.40 – 7.49 (m, 2H), 7.62 (s, 1H), 7.74 (d, $J = 8.5$ Hz, 1H), 7.79 (t, $J = 9.1$ Hz, 2H) ppm. ¹³C NMR (125 MHz, CDCl₃) δ 19.93, 22.08, 41.25, 125.42, 125.57, 126.01, 126.21, 126.31, 127.03, 127.06, 127.68, 127.82, 128.04, 130.59, 132.14, 133.65, 136.30, 143.83, 143.95 ppm. HRMS (ESI) m/z [M]⁺ calcd. for C₁₉H₁₈ molecular weight: 246.1399; found 246.1403. Spectral data are in accordance with the literature.⁵³

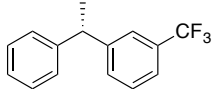
(+)-4-bromo-1-chloro-2-(1-(4-ethylphenyl)ethyl)benzene (3.27) was

synthesized from 4-bromo-1-chloro-2-(1-chloroethyl)benzene and 2-naphthylboronic pinacol ester according to General Procedure E.



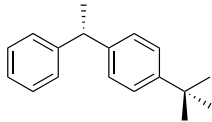
Product was purified by silica gel flash column chromatography, eluting with hexanes to afford purified product as a colorless oil (45% spectroscopic yield, 35% isolated yield). A minor impurity seen in alkyl region of ¹³C was inseparable by silica gel column chromatography. $R_f = 0.50$ (Hexanes) $[\alpha_D^{24}] = 29.3^\circ$ ($c = 1.8$, CHCl₃), Chiral Column HPLC (OD-H) 0.8 mL/ min, 100% Hexanes (99:1 er). ¹H NMR (400 MHz, CDCl₃) δ 1.24 (t, $J = 7.6$ Hz, 3H), 1.59 (d, $J = 7.2$ Hz, 3H), 2.63 (q, $J = 7.6$ Hz, 2H), 4.57 (q, $J = 7.2$ Hz, 1H), 7.14 (s, 4H), 7.21-7.27 (m, 1H), 7.25 (d, $J = 2.3$ Hz, 1H), 7.35 (d, $J = 2.3$ Hz, 1H) ppm. ¹³C NMR (125 MHz, CDCl₃) 15.4, 21.1, 28.4, 40.6, 120.6, 127.5, 127.9, 130.3, 130.9, 131.5,

141.2, 142.3, 146.1, 152.4 ppm. IR (neat); 2955, 2922, 2872, 2859, 1457, 1378. HRMS (ESI) m/z $[M]^+$ calcd. for $C_{16}H_{16}BrCl$ molecular weight: 322.0042; found 322.0040.

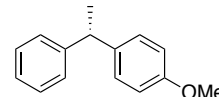
(R)-1-(1-phenylethyl)-3-(trifluoromethyl)benzene. (3.28) was  synthesized from 1-chloroethylbenzene and *m*-trifluoromethylphenylboronic pinacol ester according to General Procedure C. Product was purified by silica gel flash column chromatography, eluting with 5% Et₂O in hexanes to afford purified product as a colorless oil (44% spectroscopic yield, 39% isolated yield). The dimer of the alkyl halide was a minor impurity which was inseparable by silica gel column chromatography. $R_f = 0.43$ (5% Et₂O in Hexanes), $[\alpha_D^{24}] = 0.52^\circ$ ($c = 0.77$, CHCl₃), Chiral Column HPLC (OJ-H 1 mL/min, 100% Hexanes (80:20 er)) ¹H NMR (500 MHz, CDCl₃) δ 1.69 (dd, $J = 7.2, 2.3$ Hz, 3H), 4.23 (q, $J = 7.2$ Hz, 1H), 7.24 (ddt, $J = 7.7, 5.9, 2.6$ Hz, 3H), 7.33 (td, $J = 7.9, 2.3$ Hz, 2H), 7.43 – 7.38 (m, 2H), 7.50 – 7.45 (m, 1H) 7.52 (s, 1H) ppm. ¹³C NMR (125MHz, CDCl₃) δ 21.7, 44.6, 123.0 (q, $J = 3.8$ Hz), 124.2 (q, $J = 3.8$ Hz), 124.7, 126.4, 127.5, 128.6, 128.8, 130.5 (q, $J = 32$ Hz), 131.1, 145.3, 147.3 ppm. HRMS (ESI) m/z $[M]^+$ calcd. for $C_{15}H_{13}F_3$ molecular weight: 250.0890; found 250.0886. Spectral data are in accordance with the literature.⁵⁴ Absolute configuration assigned by reference to literature retention times of chiral column HPLC and sign of optical rotation.⁵⁵

(S)-1-methyl-4-(1-phenylethyl)benzene (3.29) was synthesized from 1-chloroethylbenzene and *p*-tolylboronic pinacol ester according to General Procedure D. Product was purified by silica gel flash column chromatography, eluting with 10% Et₂O in hexanes to afford purified product as a colorless oil (67% spectroscopic yield,

58% isolated yield). $R_f = 0.4$ (5% Et₂O in Hexanes), $[\alpha_D^{24}] = -1.3^\circ$ ($c = 0.15$, CHCl₃), Chiral Column HPLC (OD-H 1 mL/ min, 100% Hexanes (74:26 er)) ¹H NMR (500 MHz, CDCl₃) δ 1.62 (d, $J = 7.2$ Hz, 3H), 2.31 (s, 3H), 4.12 (q, $J = 7.2$ Hz, 1H), 7.07 – 7.13 (m, 4H), 7.17 (t, $J = 7.1$ Hz, 1H), 7.20 – 7.23 (m, 2H), 7.26-7.29 (m, 2H) ppm. ¹³C NMR (125MHz, CDCl₃) δ 20.98, 21.95, 44.40, 125.94, 127.49, 127.58, 128.34, 129.06, 135.48, 143.42, 146.62 ppm. Spectral data are in accordance with the literature.³⁶ Absolute configuration assigned by reference to literature retention times of chiral column HPLC and sign of optical rotation.³⁶

(S)-1-tertbutyl-4-(1-phenylethyl)benzene (3.30) was synthesized from 1-chloroethylbenzene and *p*-tert-butylphenylboronic pinacol ester  according to General Procedure C. Product was purified by silica gel flash column chromatography, eluting with 10% Et₂O in hexanes to afford purified product as a colorless oil (47% spectroscopic yield, 43% isolated yield). $R_f = 0.5$ (5% Et₂O in Hexanes), $[\alpha_D^{24}] = 1.28^\circ$ ($c = 0.312$, CHCl₃), Chiral Column HPLC (OJ-H, 1 mL/ min, 100% Hexanes (79:21 er)) ¹H NMR (500 MHz, CDCl₃) δ 1.30 (s, 9H), 1.64 (d, $J = 7.2$ Hz, 3H), 4.13 (q, $J = 7.3$ Hz, 1H), 7.15 – 7.20 (m, 3H), 7.23 – 7.36 (m, 6H), 7.44 – 7.57 (AB_q, $J = 31$ Hz) ppm. ¹³C NMR (125MHz, CDCl₃) δ 22.06, 31.55, 34.50, 44.50, 125.36, 126.10, 127.32, 127.78, 128.47, 143.39, 146.77 ppm. HRMS (ESI) m/z [M]⁺ calcd. for C₁₅H₂₂ molecular weight: 238.1644; found 238.1638. Spectral data are in accordance with the literature.³⁶ Absolute configuration assigned by reference to literature retention times of chiral column HPLC and sign of optical rotation.³⁶

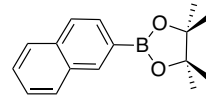
(S)-1-methoxy-4-(1-phenylethyl)benzene (3.2) was synthesized from 1-chloroethylbenzene and *p*-methoxyphenylboronic pinacol ester



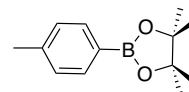
according to General Procedure C. Product was purified by silica gel flash column chromatography, eluting with 10% Et₂O in hexanes to afford purified product as a colorless oil (67% spectroscopic yield, 59% isolated yield). $R_f = 0.43$ (10% Et₂O in Hexanes), $[\alpha_D^{24}] = 4.49^\circ$ (c = 0.8, CHCl₃), Chiral Column HPLC (OJ-H) 1 mL/ min, 99:1 Hexanes:IPA (81:19 er) ¹H NMR (400 MHz, CDCl₃) δ 1.63 (d, $J = 7.2$ Hz, 3H), 3.79 (s, 3H), 4.12 (q, $J = 7.2$ Hz, 1H), 6.84 (d, $J = 9.0$ Hz, 2H), 7.15 ($J = 8.7$ Hz, 2H), 7.18 – 7.24 (m, 3H), 7.25 – 7.30 (m, 3H) ppm; ¹³C NMR (125MHz, CDCl₃) δ 22.27, 44.15, 55.46, 113.93, 126.13, 127.74, 128.53, 128.72, 138.77, 146.98, 158.04 ppm. HRMS (ESI) m/z [M]⁺ calcd. for C₁₅H₁₆O molecular weight: 212.1271; found 212.1274. Spectral data are in accordance with the literature.¹⁴ Absolute configuration assigned by reference to literature retention times of chiral column HPLC and sign of optical rotation.¹⁴

General procedure for the preparation of arylboronic pinacol esters. All boronic esters were prepared according to a procedure adapted from previous syntheses.⁵⁶ To an oven-dried 250 mL two-neck flask containing a stir bar under a nitrogen atmosphere was added arylboronic acid (30 mmol) and anhydrous pentane (110 mL). The flask was brought to 0 °C and pinacol (31 mmol) was added to the reaction. The reaction was stirred at room temperature for 24 hours. Na₂SO₄ was added to the solution and then filtered, washed with diethyl ether, and concentrated *in vacuo* to yield a crude white solid. The white solid was dissolved in dichloromethane and passed through a plug of silica gel eluting with excess dichloromethane to afford product that was analytically pure by ¹H NMR spectroscopy.

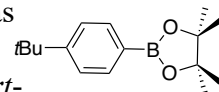
4,4,5,5-tetramethyl-2-(naphthalen-2-yl)-1,3,2-dioxaborolane (3.5) was synthesized according to the general procedure using naphthalen-2-ylboronic acid (10 g, 58.14 mmol) and pinacol (6.87 g, 58.14 mmol) to afford a crystalline white solid (12 g, 81%). ¹H NMR (400 MHz, CDCl₃) δ 1.39 (s, 12 H), 7.48 (m, 2 H), 7.81–7.84 (m, 3H), 7.85–7.89 (m, 1H), 8.37 (s, 1H) ppm. ¹¹B NMR (160 MHz, CDCl₃) δ 30.30 ppm. Spectral data are in accordance with the literature.⁵



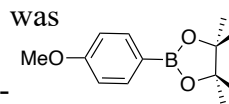
4,4,5,5-tetramethyl-2-(*p*-tolyl)-1,3,2-dioxaborolane was synthesized according to the general procedure using *p*-tolylboronic acid (1.00 g, 7.36 mmol) and pinacol (912 mg, 7.36 mmol) to afford a crystalline white solid (1.55 g, 96%). ¹H NMR (400 MHz, CDCl₃) δ 1.33 (s, 12H), 2.36 (s, 3H), 7.18 (d, *J* = 7.8 Hz, 2H), 7.70 (d, *J* = 7.9 Hz, 2H) ppm. ¹¹B NMR (160 MHz, CDCl₃) δ 32.44 ppm. Spectral data are in accordance with the literature.⁵



2-(4-(*tert*-butyl)phenyl)-4,4,5,5-tetramethyl-1,3,2-dioxaborolane was synthesized according to the general procedure using (4-(*tert*-butyl)phenyl)boronic acid (2.00 g, 11.23 mmol) and pinacol (1.33 g, 11.23 mmol) to afford a crystalline white solid (2.80 g, 96%). ¹H NMR (400 MHz, Chloroform-*d*) δ 1.32 (s, 9H), 1.33 (s, 12H), 7.41 (d, *J* = 8.4 Hz, 2H), 7.76 (d, *J* = 8.3 Hz, 2H) ppm. ¹¹B NMR (160 MHz, CDCl₃) δ 25.60 ppm. Spectral data are in accordance with the literature.⁵⁷



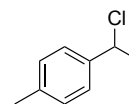
2-(4-methoxyphenyl)-4,4,5,5-tetramethyl-1,3,2-dioxaborolane was



synthesized according to the general procedure using (4-methoxyphenyl)boronic acid (3.25 g, 21.39 mmol) and pinacol (6.87 g, 58.14 mmol) to afford a crystalline white solid (4.50 g, 89%). ^1H NMR (500 MHz, Chloroform-*d*) δ 1.33 (s, 12H), 3.83 (s, 3H), 6.89 (d, $J = 8.8$ Hz, 2H), 7.75 (d, $J = 8.7$ Hz, 2H) ppm. ^{11}B NMR (160 MHz, CDCl_3) δ 30.68 ppm. Spectral data are in accordance with the literature.⁵⁷

General procedure for the preparation of benzylic chlorides: All benzylic chlorides were prepared according to a procedure adapted from previous syntheses.²² To an oven-dried 100 mL two-neck flask containing a stir bar under a nitrogen atmosphere was added benzylic alcohol (10 mmol) and anhydrous CH_2Cl_2 (20 mL). The flask was equipped with an outlet connected to a beaker of NaHCO_3 (aq) to quench HCl gases. The flask was brought to 0 °C and thionyl chloride (10 mmol) was added dropwise. The reaction was allowed to stir at room temperature for 1-18 hours and monitored by TLC. The reaction was concentrated *in vacuo* to yield a crude oil which was either purified by Kugelrohr distillation or passed through a plug of silica gel eluting with hexanes. Product was afforded that was analytically pure by ^1H NMR spectroscopy.

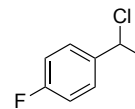
1-(1-chloroethyl)-4-methyl-benzene was synthesized according to the general procedure using 1-(*p*-tolyl)ethanol (1.5 mL, 10.9 mL) to afford



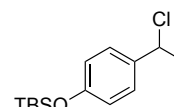
purified product as a colorless oil (1.0 g, 59%). $R_f = 0.9$ (20% EtOAc/Hex). ^1H NMR (600 MHz, Chloroform-*d*) δ 1.49 (d, $J = 6.4$ Hz, 4H), 2.35 (s, 3H), 4.87 (qd, $J = 6.6, 2.3$ Hz,

1H), 7.17 (d, $J = 7.8$ Hz, 2H), 7.27 (d, $J = 8.0$ Hz, 2H) ppm. Spectral data are in accordance with the literature.⁵⁸

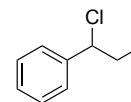
1-(1-chloroethyl)-4-fluoro-benzene was synthesized according to the general procedure using 1-(*p*-fluoro)ethanol (1.5 mL, 11.9 mmol) to afford purified product as a colorless oil (1.5 g, 77%). $R_f = 0.9$ (20% EtOAc/Hex). $^1\text{H NMR}$ (400 MHz, Chloroform-*d*) δ 1.47 (d, $J = 6.4$ Hz, 3H), 4.88 (qd, $J = 6.4, 3.2$ Hz, 1H), 7.02 (t, $J = 8.7$ Hz, 2H), 7.29 – 7.38 (m, 2H) ppm. Spectral data are in accordance with the literature.⁵⁸



***tert*-butyl(4-(1-chloroethyl)phenoxy)dimethylsilane** was synthesized according to the general procedure using 1-(4-((*tert*-butyldimethylsilyl)oxy)phenyl)ethan-1-ol (1.15 mL, 17.6 mmol) to afford purified product as a colorless oil (4.0 g, 84%). ($R_f = 0.9$, Hexanes). $^1\text{H NMR}$ (600 MHz, CDCl_3) δ 0.20 (s, 6H), 0.95 – 1.01 (m, 9H), 1.83 (d, $J = 6.8$ Hz, 3H), 5.08 (q, $J = 6.8$ Hz, 1H), 6.80 (d, $J = 8.7$ Hz, 2H), 7.28 (d, $J = 8.5$ Hz, 2H) ppm. $^{13}\text{C NMR}$ (101 MHz, CDCl_3) δ -4.31, 18.28, 25.77, 26.57, 58.87, 120.12, 127.83, 135.72, 155.71 ppm.; IR (neat): 2956, 2929, 2858, 1607, 1512, 1268. HRMS (ESI) m/z $[\text{M}]^+$ calcd. For $\text{C}_{14}\text{H}_{23}\text{OSiCl}$ molecular weight: 270.1276; found 270.1280.



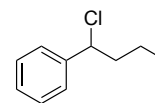
1-chloroethylbenzene was synthesized according to the general procedure using 1-phenylpropan-1-ol (1.15 mL, 17.6 mmol) to afford purified product as a colorless oil (4.0 g, 84%). $R_f = 0.9$ (20% EtOAc/Hex). $^1\text{H NMR}$ (600 MHz, CDCl_3) δ



1.00 (t, $J = 7.3$ Hz, 3H), 2.03 – 2.20 (m, 2H), 4.79 (dd, $J = 8.0, 6.4$ Hz, 1H), 7.28 – 7.32 (m, 1H), 7.33 – 7.41 (m, 4H) ppm. Spectral data are in accordance with the literature.⁵⁸

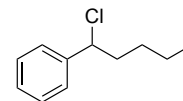
1-chlorobutylbenzene was synthesized according to the general procedure

using 1-phenylbutan-1-ol (1.50 mL, 9.79 mmol) to afford purified product



as a colorless oil (1.33 g, 80%). $R_f = 0.9$ (20% EtOAc/Hex). $^1\text{H NMR}$ (600 MHz, CDCl_3) δ 0.93 (t, $J = 7.4$ Hz, 3H), 1.26 – 1.35 (m, 1H), 1.43 (ddd, $J = 13.1, 10.3, 5.6$ Hz, 1H), 1.68 (ddt, $J = 13.5, 9.9, 5.8$ Hz, 1H), 1.74 – 1.84 (m, 2H), 4.68 (ddd, $J = 8.5, 6.0, 3.0$ Hz, 1H), 7.24 – 7.30 (m, 1H), 7.32 – 7.36 (m, 3H) ppm. Spectral data are in accordance with the literature.⁵⁹

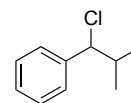
1-chloropentylbenzene was synthesized according to the general procedure using 1-phenylpentan-1-ol (1.50 mL, 8.77 mmol) to afford



purified product as a colorless oil (1.34 g, 83%). $R_f = 0.9$ (20% EtOAc/Hex) $^1\text{H NMR}$ (400 MHz, CDCl_3) δ 0.89 (t, $J = 7.1$ Hz, 3H), 1.20 – 1.53 (m, 4H), 1.96 – 2.21 (m, 2H), 4.84 (dd, $J = 8.1, 6.5$ Hz, 1H), 7.24 – 7.46 (m, 5H) ppm. Spectral data are in accordance with the literature.⁵⁹

(1-chloro-2-methylpropyl)benzene was synthesized according to the general

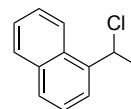
procedure using 2-methyl-1-phenylpropan-1-ol (1.50 mL, 10.0 mmol) to



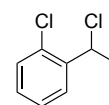
afford purified product as a colorless oil (1.31 g, 77%). $R_f = 0.9$ (20% EtOAc/Hex). $^1\text{H NMR}$ (600 MHz, CDCl_3) δ 0.79 (d, $J = 6.8$ Hz, 3H), 1.00 (d, $J = 6.6$ Hz, 3H), 4.36 (dd, J

= 6.9, 3.0 Hz, 1H), 7.24 – 7.36 (m, 5H) ppm. Spectral data are in accordance with the literature.⁶⁰

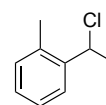
1-(1-chloroethyl)naphthalene was synthesized according to the general procedure using 1-phenylpentan-1-ol (1.50 mL, 8.77 mmol) to afford purified product as a colorless oil (1.34 g, 83%). $R_f = 0.9$ (20% EtOAc/Hex). $^1\text{H NMR}$ (600 MHz, CDCl_3) δ 2.06 (dd, $J = 6.9, 0.9$ Hz, 3H), 5.90 (q, $J = 6.8$ Hz, 1H), 7.45 – 7.54 (m, 2H), 7.55 – 7.61 (m, 1H), 7.71 (d, $J = 7.2$ Hz, 1H), 7.82 (d, $J = 8.2$ Hz, 1H), 7.88 (d, $J = 8.1$ Hz, 1H), 8.19 (d, $J = 8.5$ Hz, 1H) ppm. Spectral data are in accordance with the literature.⁵⁹



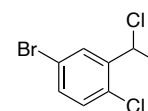
1-chloro-2-(1-chloroethyl)benzene was synthesized according to the general procedure using 1-(2-chlorophenyl)ethan-1-ol (1.50 g, 9.58 mmol) to afford purified product as a colorless oil (1.34 g, 79%). $R_f = 0.9$ (20% EtOAc/Hex). $^1\text{H NMR}$ (400 MHz, CDCl_3) δ 1.82 (d, $J = 6.8$ Hz, 3H), 5.58 (q, $J = 6.8$ Hz, 1H), 7.18 – 7.27 (m, 1H), 7.28 – 7.38 (m, 2H), 7.64 (dd, $J = 7.8, 1.7$ Hz, 1H) ppm. Spectral data are in accordance with the literature.⁵⁹



1-(1-chloroethyl)-2-methylbenzene To a 100 mL 1-(*o*-tolyl)ethan-1-ol (2.00 mL, 14.69 mmol) to afford purified product as a colorless oil (2.00 g, 88%). $R_f = 0.9$ (20% EtOAc/Hex). $^1\text{H NMR}$ (500 MHz, CDCl_3) δ 1.87 (d, $J = 6.9$ Hz, 3H), 2.42 (s, 3H), 5.35 (q, $J = 6.8$ Hz, 1H), 7.13 – 7.28 (m, 4H), 7.53 (dd, $J = 7.6, 1.5$ Hz, 1H) ppm. Spectral data are in accordance with the literature.⁵⁸

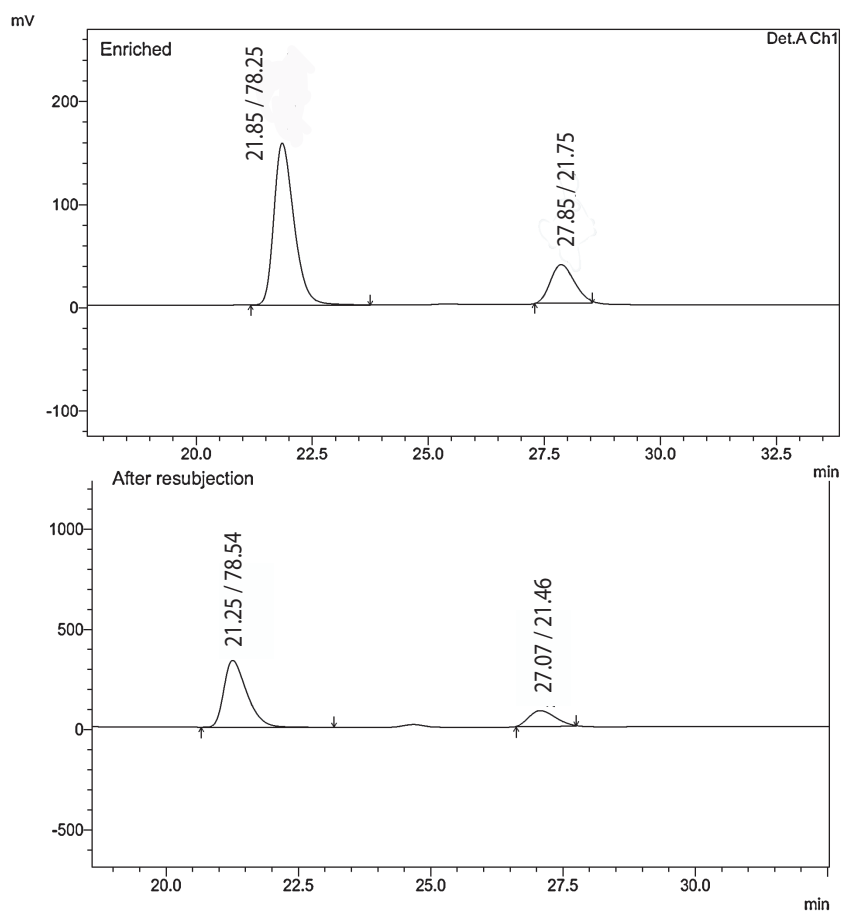
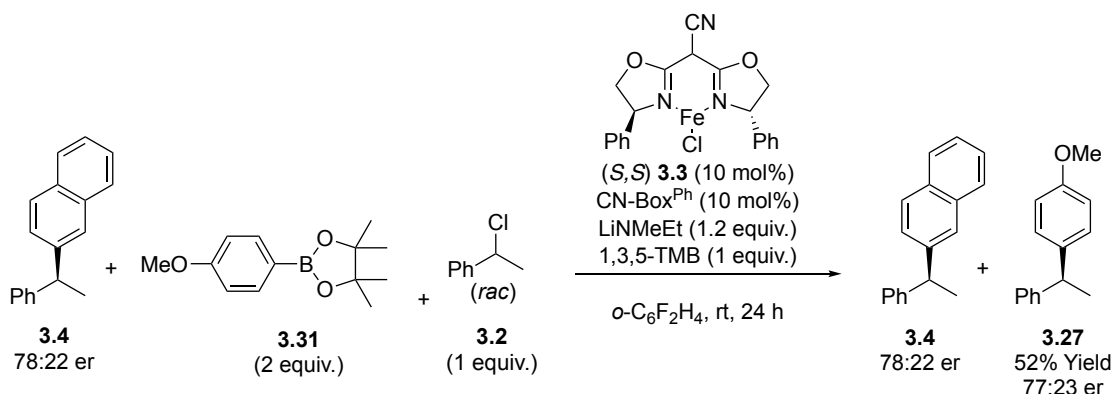


4-bromo-1-chloro-2-(1-chloroethyl)benzene To a two-neck flask with stir bar under a N_2 atmosphere was added 1-(5-bromo-2-chlorophenyl)ethan-1-



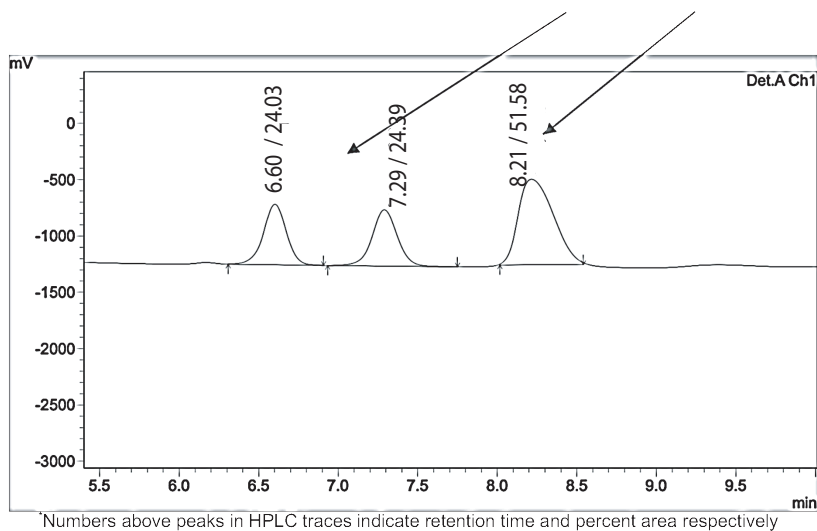
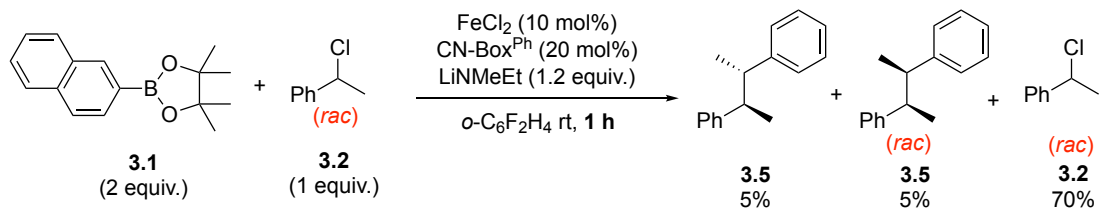
ol(1.55 g, 6.58 mmol) and anhydrous CH₂Cl₂(25 mL). PCl₅ (1.37 g, 6.58 mmol) was added to the flask at 0° C. The reaction was slowly warmed to room temperature and allowed to stir for 2 hours. The reaction was quenched with deionized H₂O (10 mL) and the collected aqueous layers were extracted with dichloromethane (3 x 40 mL). The combined organic layers were washed with NaHCO₃ (aq) (20 mL), dried over Na₂SO₄, filtered, and concentrated *in vacuo*. The concentrate was passed through a plug of silica gel and washed with excess hexanes to afford purified product as a colorless oil (2.00 g, 88%). (R_f = 0.9, Hexanes); ¹H NMR (400 MHz, CDCl₃) δ 1.80 (d, *J* = 7.0, 3H), 5.42 – 5.51 (q, 1H), 7.23 (t, *J* = 7.2 Hz, 1H), 7.35 (d, *J* = 8.6, 1H), 7.76 (s, 1H) ppm.¹³C NMR (101 MHz, Chloroform-*d*) δ 25.51, 53.69, 121.00, 130.96, 130.99, 132.26, 141.97, 223.78 ppm; IR (neat):2926, 2852, 1465, 1389, 1263, 1070. HRMS (ESI) *m/z* [M]⁺ calcd. For C₈H₆Cl₂Br molecular weight: 251.9113; found 251.9103.

Scheme S3.1: Subjection of enantiomerically enriched diarylalkane product to a cross-coupling reaction between 1-chloroethylbenzene and 4-methoxyphenyl boronic pinacol ester



*Numbers above peaks in HPLC traces indicate retention time and percent area respectively

Scheme S3.2: Analysis of the enantiopurity of dimer product 3.7 after catalysis.



3.8 References:

- (1) Fürstner, A.; Leitner, A.; Méndez, M.; Krause, H. Iron-Catalyzed Cross-Coupling Reactions. *J. Am. Chem. Soc.* **2002**, *124*, 13856–13863. <https://doi.org/10.1021/ja027190t>.
- (2) Mako, T. L.; Byers, J. A. Recent Advances in Iron-Catalysed Cross Coupling Reactions and Their Mechanistic Underpinning. *Inorg. Chem. Front.* **2016**, *3*, 766–790. <https://doi.org/10.1039/c5qi00295h>.
- (3) Egorova, K. S.; Ananikov, V. P. Toxicity of Metal Compounds: Knowledge and Myths. *Organometallics* **2017**, *36*, 4071–4090. <https://doi.org/10.1021/acs.organomet.7b00605>.
- (4) Fu, G. C. Transition-Metal Catalysis of Nucleophilic Substitution Reactions: A Radical Alternative to S_N1 and S_N2 Processes. *ACS Cent. Sci.* **2017**, *3*, 692–700. <https://doi.org/10.1021/acscentsci.7b00212>.
- (5) Iwamoto, T.; Okuzono, C.; Adak, L.; Jin, M.; Nakamura, M. Iron-Catalysed Enantioselective Suzuki-Miyaura Coupling of Racemic Alkyl Bromides. *Chem. Commun.* **2019**, *55*, 1128–1131. <https://doi.org/10.1039/c8cc09523j>.
- (6) Jin, M.; Adak, L.; Nakamura, M. Iron-Catalyzed Enantioselective Cross-Coupling Reactions of α -Chloroesters with Aryl Grignard Reagents. *J. Am. Chem. Soc.* **2015**, *137*, 7128–7134. <https://doi.org/10.1021/jacs.5b02277>.
- (7) Liu, L.; Lee, W.; Yuan, M.; Acha, C.; Geherty, M. B.; Williams, B.; Gutierrez, O. Intra- and Intermolecular Fe-Catalyzed Dicarbofunctionalization of Vinyl Cyclopropanes. *Chem. Sci.* **2020**, *11*, 3146–3151.

<https://doi.org/10.1039/D0SC00467G>.

- (8) Crockett, M. P.; Tyrol, C. C.; Wong, A. S.; Li, B.; Byers, J. A. Iron-Catalyzed Suzuki-Miyaura Cross-Coupling Reactions between Alkyl Halides and Unactivated Arylboronic Esters. *Org. Lett.* **2018**, *20*, 5233–5237. <https://doi.org/10.1021/acs.orglett.8b02184>.
- (9) Saito, B.; Fu, G. C. Enantioselective Alkyl-Alkyl Suzuki Cross-Couplings of Unactivated Homobenzylic Halides. *J. Am. Chem. Soc.* **2008**, *130*, 6694–6695. <https://doi.org/10.1021/ja8013677>.
- (10) Ameen, D.; Snape, T. J. Chiral 1,1-Diaryl Compounds as Important Pharmacophores. *Med. Chem. Comm.* **2013**, *4*, 893–907. <https://doi.org/10.1039/c3md00088e>.
- (11) Devalia, J. L.; Hanotte, F.; Baltes, E.; De Vos, C. A Randomized, Double-Blind, Crossover Comparison among Cetirizine, Levocetirizine, and Ucb 28557 on Histamine-Induced Cutaneous Responses in Healthy Adult Volunteers. *Allergy Eur. J. Allergy Clin. Immunol.* **2001**, *56*, 50–57. <https://doi.org/10.1034/j.1398-9995.2001.00726.x>.
- (12) Nguyen, L. A.; He, H.; Pham-Huy, C. Chiral Drugs: An Overview. *Int. J. Biomed. Sci.* **2006**, *2*, 85–100.
- (13) Jia, T.; Cao, P.; Liao, J. Enantioselective Synthesis of Gem -Diarylethenes by Transition Metal-Catalyzed Asymmetric Arylations (TMCAAr). *Chem. Sci.* **2018**, *9*, 546–559. <https://doi.org/10.1039/c7sc03404k>.
- (14) Chen, J.; Chen, C.; Ji, C.; Lu, Z. Cobalt-Catalyzed Asymmetric Hydrogenation of 1,1-Diarylethenes. *Org. Lett.* **2016**, *18*, 1594–1597.

<https://doi.org/10.1021/acs.orglett.6b00453>.

- (15) Mazuela, J.; Verendel, J. J.; Coll, M.; Schöffner, B.; Börner, A.; Andersson, P. G.; Pàmies, O.; Diéguez, M. Iridium Phosphite-Oxazoline Catalysts for the Highly Enantioselective Hydrogenation of Terminal Alkenes. *J. Am. Chem. Soc.* **2009**, *131*, 12344–12353. <https://doi.org/10.1021/ja904152r>.
- (16) Anthony, D.; Lin, Q.; Baudet, J.; Diao, T. Nickel-Catalyzed Asymmetric Reductive Diarylation of Vinylarenes. *Angew. Chemie - Int. Ed.* **2019**, *58*, 3198–3202. <https://doi.org/10.1002/anie.201900228>.
- (17) Logan, K. M.; Brown, M. K. Catalytic Enantioselective Arylboration of Alkenylarenes. *Angew. Chemie - Int. Ed.* **2017**, *56*, 851–855. <https://doi.org/10.1002/anie.201609844>.
- (18) Wu, L.; Wang, F.; Wan, X.; Wang, D.; Chen, P.; Liu, G. Asymmetric Cu-Catalyzed Intermolecular Trifluoromethylarylation of Styrenes: Enantioselective Arylation of Benzylic Radicals. *J. Am. Chem. Soc.* **2017**, *139*, 2904–2907. <https://doi.org/10.1021/jacs.6b13299>.
- (19) R., Y. I. M. J. A. G. C. O. A. M. C. E. M. N. S. J. E. Stereospecific Nickel-Catalyzed Cross-Coupling Reactions of Alkyl Grignard Reagents and Identification of Selective Anti-Breast-Cancer Agents. *Angew. Chem. Int. Ed.* **2014**, *53*, 2422–2427. <https://doi.org/https://doi.org/10.1002/anie.201308666>.
- (20) Zhou, Q.; Srinivas, H. D.; Dasgupta, S.; Watson, M. P. Nickel-Catalyzed Cross-Couplings of Benzylic Pivalates with Arylboroxines: Stereospecific Formation of Diarylalkanes and Triarylmethanes. *J. Am. Chem. Soc.* **2013**, *135*, 3307–3310. <https://doi.org/10.1021/ja312087x>.

- (21) Glasspoole, B. W.; Oderinde, M. S.; Moore, B. D.; Antoft-Finch, A.; Crudden, C. M. Highly Chemoselective and Enantiospecific Suzuki-Miyaura Cross-Couplings of Benzylic Organoboronic Esters. *Synth.* **2013**, *45*, 1759–1763. <https://doi.org/10.1055/s-0033-1338875>.
- (22) Poremba, K. E.; Kadunce, N. T.; Suzuki, N.; Cherney, A. H.; Reisman, S. E. Nickel-Catalyzed Asymmetric Reductive Cross-Coupling to Access 1,1-Diarylalkanes. *J. Am. Chem. Soc.* **2017**, *139*, 5684–5687. <https://doi.org/10.1021/jacs.7b01705>.
- (23) Do, H. Q.; Chandrashekar, E. R. R.; Fu, G. C. Nickel/Bis(Oxazoline)-Catalyzed Asymmetric Negishi Arylations of Racemic Secondary Benzylic Electrophiles to Generate Enantioenriched 1,1-Diarylalkanes. *J. Am. Chem. Soc.* **2013**, *135*, 16288–16291. <https://doi.org/10.1021/ja408561b>.
- (24) Suzuki, A.; Miyaura, N.; Yamada, K. A New Stereospecific Cross-Coupling by the Palladium Catalyzed Reaction of 1-Alkenylboranes with 1-Alkenyl or 1-Alkynyl Halides. *Tetrahedron Lett.* **1979**, *36*, 3437–3440. [https://doi.org/10.1016/S0040-4039\(01\)95429-2](https://doi.org/10.1016/S0040-4039(01)95429-2).
- (25) Tyrol, C. C.; Yone, N. S.; Gallin, C. F.; Byers, J. A. Iron-Catalysed Enantioconvergent Suzuki-Miyaura Cross-Coupling to Afford Enantioenriched 1,1-Diarylalkanes. *Chem. Commun.* **2020**, *56*, 14661–14664. <https://doi.org/10.1039/d0cc05003b>.
- (26) Cherney, A. H.; Reisman, S. E. Nickel-Catalyzed Asymmetric Reductive Cross-Coupling between Vinyl and Benzyl Electrophiles. *J. Am. Chem. Soc.* **2014**, *136*, 14365–14368. <https://doi.org/10.1021/ja508067c>.
- (27) Poremba, K. E.; Kadunce, N. T.; Suzuki, N.; Cherney, A. H.; Reisman, S. E. Nickel-

- Catalyzed Asymmetric Reductive Cross-Coupling To Access 1,1-Diarylalkanes. *J. Am. Chem. Soc.* **2017**, *139*, 5684–5687. <https://doi.org/10.1021/jacs.7b01705>.
- (28) DeLano, T. J.; Reisman, S. E. Enantioselective Electroreductive Coupling of Alkenyl and Benzyl Halides via Nickel Catalysis. *ACS Catal.* **2019**, *9*, 6751–6754. <https://doi.org/10.1021/acscatal.9b01785>.
- (29) Changying, L Yiliang, L Weiren, X Yuli, W Guilong, Z Yongheng, S Lida, T Meixang, Z. Preparation Method of a Class of Phenyl C-Glucoside Derivative Intermediates. CN104860793 (A), 2014.
- (30) Tollefson, E. J.; Hanna, L. E.; Jarvo, E. R. Stereospecific Nickel-Catalyzed Cross-Coupling Reactions of Benzylic Ethers and Esters. *Acc. Chem. Res.* **2015**, *48*, 2344–2353. <https://doi.org/10.1021/acs.accounts.5b00223>.
- (31) Daifuku, S. L.; Kneebone, J. L.; Snyder, B. E. R.; Neidig, M. L. Iron(II) Active Species in Iron-Bisphosphine Catalyzed Kumada and Suzuki-Miyaura Cross-Couplings of Phenyl Nucleophiles and Secondary Alkyl Halides. *J. Am. Chem. Soc.* **2015**, *137*, 11432–11444. <https://doi.org/10.1021/jacs.5b06648>.
- (32) Sharma, A. K.; Sameera, W. M. C.; Jin, M.; Adak, L.; Okuzono, C.; Iwamoto, T.; Kato, M.; Nakamura, M.; Morokuma, K. DFT and AFIR Study on the Mechanism and the Origin of Enantioselectivity in Iron-Catalyzed Cross-Coupling Reactions. *J. Am. Chem. Soc.* **2017**, *139*, 16117–16125. <https://doi.org/10.1021/jacs.7b05917>.
- (33) Lee, W.; Zhou, J.; Gutierrez, O. Mechanism of Nakamura's Bisphosphine-Iron-Catalyzed Asymmetric C(Sp²)-C(Sp³) Cross-Coupling Reaction: The Role of Spin in Controlling Arylation Pathways. *J. Am. Chem. Soc.* **2017**, *139*, 16126–16133. <https://doi.org/10.1021/jacs.7b06377>.

- (34) Yin, H.; Fu, G. C. Mechanistic Investigation of Enantioconvergent Kumada Reactions of Racemic α -Bromoketones Catalyzed by a Nickel/Bis(Oxazoline) Complex. *J. Am. Chem. Soc.* **2019**, *141*, 15433–15440. <https://doi.org/10.1021/jacs.9b08185>.
- (35) Puchot, C.; Agami, C.; Samuel, O.; Dunach, E.; Zhao, S.; Kagan, H. B. Nonlinear Effects in Asymmetric Synthesis. Examples in Asymmetric Oxidations and Aldolization Reactions. *J. Am. Chem. Soc.* **1986**, *108*, 2353–2357. <https://doi.org/10.1021/ja00269a036>.
- (36) Gutierrez, O.; Tellis, J. C.; Primer, D. N.; Molander, G. A.; Kozlowski, M. C. Nickel-Catalyzed Cross-Coupling of Photoredox-Generated Radicals: Uncovering a General Manifold for Stereoconvergence in Nickel-Catalyzed Cross-Couplings. *J. Am. Chem. Soc.* **2015**, *137*, 4896–4899. <https://doi.org/10.1021/ja513079r>.
- (37) Smith, J. M.; Sadique, A. R.; Cundari, T. R.; Rodgers, K. R.; Lukat-Rodgers, G.; Lachicotte, R. J.; Flaschenriem, C. J.; Vela, J.; Holland, P. L. Studies of Low-Coordinate Iron Dinitrogen Complexes. *J. Am. Chem. Soc.* **2006**, *128*, 756–769. <https://doi.org/10.1021/ja052707x>.
- (38) Bauer, G.; Wodrich, M. D.; Scopelliti, R.; Hu, X. Iron Pincer Complexes as Catalysts and Intermediates in Alkyl-Aryl Kumada Coupling Reactions. *Organometallics* **2015**, *34*, 289–298. <https://doi.org/10.1021/om501122p>.
- (39) Crockett, M. P.; Wong, A. S.; Li, B.; Byers, J. A. Rational Design of an Iron-Based Catalyst for Suzuki–Miyaura Cross-Couplings Involving Heteroaromatic Boronic Esters and Tertiary Alkyl Electrophiles. *Angew. Chemie Int. Ed.* **2020**, *59*, 5392–5397. <https://doi.org/10.1002/anie.201914315>.

- (40) Lou, S.; Fu, G. C. Nickel/Bis(Oxazoline)-Catalyzed Asymmetric Kumada Reactions of Alkyl Electrophiles: Cross-Couplings of Racemic α -Bromoketones. *J. Am. Chem. Soc.* **2010**, *132*, 1264–1266. <https://doi.org/10.1021/ja909689t>.
- (41) Burger, B. J.; Bercaw, J. E. Vacuum Line Techniques for Handling Air-Sensitive Organometallic Compounds. In *Experimental Organometallic Chemistry*; Wayda, A. L., Darensbourg, M. Y., Eds.; American Chemical Society, 1987; pp 79–115. <https://doi.org/10.1021/bk-1987-0357.ch004>.
- (42) Pangborn, A. B.; Giardello, M. A.; Grubbs, R. H.; Rosen, R. K.; Timmers, F. J. Safe and Convenient Procedure for Solvent Purification. *Organometallics* **1996**, *15*, 1518–1520. <https://doi.org/10.1021/om9503712>.
- (43) Kurosawa, F.; Nakano, T.; Soeta, T.; Endo, K.; Ukaji, Y. (Z)-Selective Enol Triflation of α -Alkoxyacetaldehydes: Application to Synthesis of (Z)-Allylic Alcohols via Cross-Coupling Reaction and [1,2]-Wittig Rearrangement. *J. Org. Chem.* **2015**, *80*, 5696–5703. <https://doi.org/10.1021/acs.joc.5b00647>.
- (44) Eno, M. S.; Lu, A.; Morken, J. P. Nickel-Catalyzed Asymmetric Kumada Cross-Coupling of Symmetric Cyclic Sulfates. *J. Am. Chem. Soc.* **2016**, *138*, 7824–7827. <https://doi.org/10.1021/jacs.6b03384>.
- (45) Crimmins, M. T.; Shamszad, M. Highly Selective Acetate Aldol Additions Using Mesityl-Substituted Chiral Auxiliaries. *Org. Lett.* **2007**, *9*, 149–152. <https://doi.org/10.1021/ol062688b>.
- (46) Zuo, Z.; Cong, H.; Li, W.; Choi, J.; Fu, G. C.; MacMillan, D. W. C. Enantioselective Decarboxylative Arylation of α -Amino Acids via the Merger of Photoredox and Nickel Catalysis. *J. Am. Chem. Soc.* **2016**, *138*, 1832–1835.

<https://doi.org/10.1021/jacs.5b13211>.

- (47) Kristensen, T. E.; Vestli, K.; Hansen, F. K.; Hansen, T. New Phenylglycine-Derived Primary Amine Organocatalysts for the Preparation of Optically Active Warfarin. *European J. Org. Chem.* **2009**, *30*, 5185–5191. <https://doi.org/10.1002/ejoc.200900664>.
- (48) Liu, F.; Zhong, J.; Zhou, Y.; Gao, Z.; Walsh, P. J.; Wang, X.; Ma, S.; Hou, S.; Liu, S.; Wang, M.; et al. Cobalt-Catalyzed Enantioselective Negishi Cross-Coupling of Racemic α -Bromo Esters with Arylzincs. *Chemistry - A European Journal*. **2018**, *24*, 2059–2064. <https://doi.org/10.1002/chem.201705463>.
- (49) Marinova, M.; Torres-Werlé, M.; Taupier, G.; Maise-François, A.; Achard, T.; Boeglin, A.; Dorkenoo, K. D. H.; Bellemin-Laponnaz, S. Chiral Self-Sorting Process with Ditopic Ligands: Alternate or Block Metallopolymer Assembly as a Function of the Metal Ion. *ACS Omega* **2019**, *4*, 2676–2683. <https://doi.org/10.1021/acsomega.8b03484>.
- (50) Tsutsumi, K.; Itagaki, K.; Nomura, K. Synthesis and Structural Analysis of Palladium(II) Complexes Containing Neutral or Anionic C₂-Symmetric Bis(Oxazoline) Ligands: Effects of Substituents in the 5-Position. *ACS Omega* **2017**, *2*, 3886–3900. <https://doi.org/10.1021/acsomega.7b00457>.
- (51) Nolin, K. A.; Ahn, R. W.; Kobayashi, Y.; Kennedy-Smith, J. J.; Toste, F. D. Enantioselective Reduction of Ketones and Imines Catalyzed by (CN-Box)Re^V - Oxo Complexes. *Chem. - A Eur. J.* **2010**, *16*, 9555–9562. <https://doi.org/10.1002/chem.201001164>.
- (52) Eckert, N. A.; Smith, J. M.; Lachicotte, R. J.; Holland, P. L. Low-Coordinate Iron(II)

- Amido Complexes of β -Diketiminates: Synthesis, Structure, and Reactivity. *Inorg. Chem.* **2004**, *43*, 3306–3321. <https://doi.org/10.1021/ic035483x>.
- (53) Shen, X.; Liu, P.; Liu, Y.; Liu, Y.; Dai, B. One-Pot Reductive Coupling Reactions of Acetyl Naphthalene Derivatives, Tosylhydrazide, with Arylboronic Acids. *Tetrahedron* **2017**, *73*, 785–793. <https://doi.org/10.1016/j.tet.2016.12.068>.
- (54) Semba, K.; Ariyama, K.; Zheng, H.; Kameyama, R.; Sakaki, S.; Nakao, Y. Reductive Cross-Coupling of Conjugated Arylalkenes and Aryl Bromides with Hydrosilanes by Cooperative Palladium/Copper Catalysis. *Angew. Chemie - Int. Ed.* **2016**, *55*, 6275–6279. <https://doi.org/10.1002/anie.201511975>.
- (55) Cheng, X.; Lu, H.; Lu, Z. Enantioselective Benzylic C–H Arylation via Photoredox and Nickel Dual Catalysis. *Nat. Commun.* **2019**, *10*, 1–7. <https://doi.org/10.1038/s41467-019-11392-6>.
- (56) Potter, B.; Edelstein, E. K.; Morken, J. P. Modular, Catalytic Enantioselective Construction of Quaternary Carbon Stereocenters by Sequential Cross-Coupling Reactions. *Org. Lett.* **2016**, *18*, 3286–3289. <https://doi.org/10.1021/acs.orglett.6b01580>.
- (57) Yamamoto, T.; Morita, T.; Takagi, J.; Yamakawa, T. NiCl₂(PMe₃)₂-Catalyzed Borylation of Aryl Chlorides. *Org. Lett.* **2011**, *13*, 5766–5769. <https://doi.org/10.1021/ol202267t>.
- (58) Liang, S.; Hammond, G. B.; Xu, B. Metal-Free Regioselective Hydrochlorination of Unactivated Alkenes via a Combined Acid Catalytic System. *Green Chem.* **2018**, *20*, 680–684. <https://doi.org/10.1039/c7gc03665e>.
- (59) Savela, R.; Wärnå, J.; Murzin, D. Y.; Leino, R. Iron Catalyzed Halogenation of

Benzylic Aldehydes and Ketones. *Catal. Sci. Technol.* **2015**, *5*, 2406–2417.
<https://doi.org/10.1039/c5cy00067j>.

- (60) Stach, T.; Dräger, J.; Huy, P. H. Nucleophilic Substitutions of Alcohols in High Levels of Catalytic Efficiency. *Org. Lett.* **2018**, *20*, 2980–2983.
<https://doi.org/10.1021/acs.orglett.8b01023>.

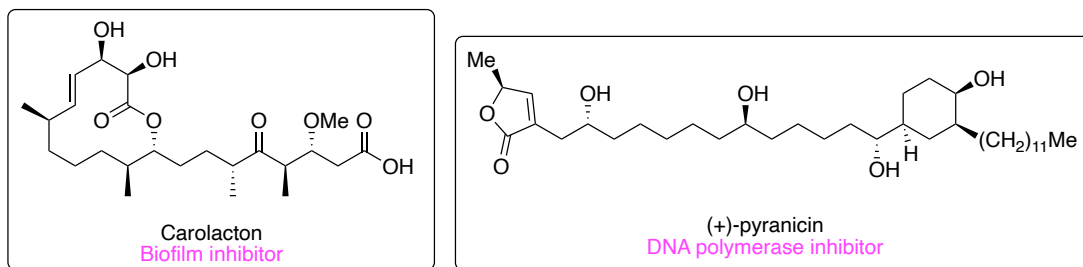
**Chapter 4. Iron-Catalyzed Suzuki-Miyaura
Cross-Coupling Reaction Between
Unactivated Alkyl Halides and Alkyl Boranes**

4.1 Introduction

Suzuki-Miyaura cross-coupling reactions have proven to be reliable and efficacious methods toward generating carbon-carbon bonds.¹ In response to the attractiveness of these methods, we have developed efficient iron-catalyzed Suzuki-Miyaura C(sp²)-C(sp³) cross-coupling reactions^{2,3} including an enantioselective variant⁴. However, expanding our methodology toward more challenging C(sp³)-C(sp³) couplings had not been accomplished. These C(sp³)-C(sp³) couplings remain elusive,⁵ where most of the reported carbon-carbon bond formations between organic electrophiles and boron nucleophiles are limited to C(sp²)-C(sp²) and C(sp²)-C(sp³) couplings. In fact, only 1% of all Suzuki-Miyaura reactions reported to date are C(sp³)-C(sp³) couplings.³ Due to these methodological gaps, there has been an over-representation of linear and disc-shaped drugs within the medicinal chemistry space, while spherical morphologies remain heavily underexplored.⁶ Incorporation of more architectural complexity to small-molecule drug candidates has been shown to be highly beneficial in drug discovery,⁷ as sp³-hybridized carbons are ubiquitous in many important bioactive natural products (Figure 4.1).⁸

With a growing interest in “escaping flat land” and increasing incorporation of C(sp³)-hybridization, unproductive pathways such as β-hydride elimination must be

Figure 4.1. Representative examples of highly saturated natural product.

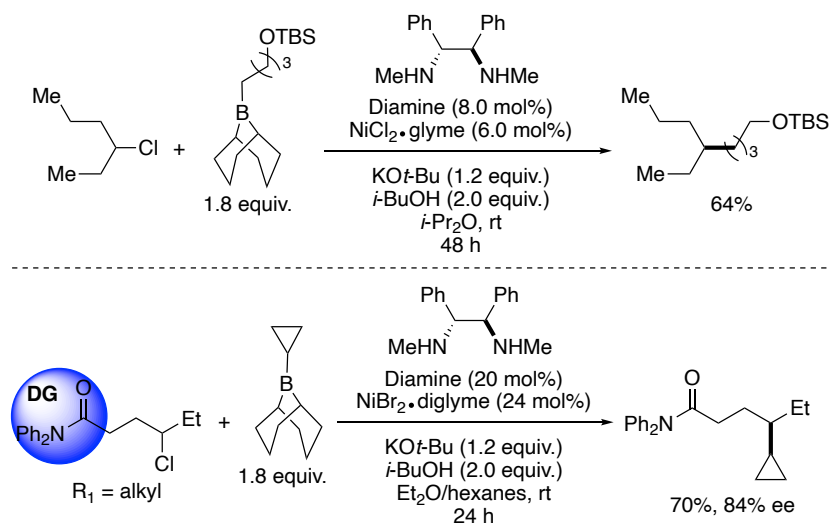


prevented. Despite the success of palladium-based catalysts for the construction of biaryl moieties, these group 10 metal catalysts are historically plagued by facile β -hydride elimination events.⁵ For this reason, palladium-based catalysts are uncommonly used for C(sp³)-C(sp³) cross-coupling reactions. The known examples require electron-rich and sterically hindered phosphine ligands to react efficiently with primary alkyl electrophiles^{9,10} and some secondary electrophiles.¹¹

To overcome the undesirable reactivity, first-row transition metals such as nickel and iron have been explored. Unlike palladium, first-row transition metals have unique electronic properties by being able to access to 1 and 2 electron pathways and multiple spin states.⁵ These properties make them well suited to engage in reactions with alkyl electrophiles because of the propensity of carbon-halogen bonds to undergo metal-induced homolysis.^{12,13} Of these metals, there are more examples where nickel is used as a catalyst, with an impressive collection of nickel-based C(sp³)-C(sp³) Suzuki-Miyaura systems being developed over the past two decades by the Fu group.⁵ These systems showcase the ability of nickel-based catalysts to couple primary and secondary alkyl halides with primary alkylborane reagents,^{10,14,15} as well as the development of highly selective enantioconvergent variants by taking advantage of directing groups (Scheme 4.1).¹⁶⁻²⁰

Though considerable work has been accomplished with nickel-based catalysts for C(sp³)-C(sp³) Suzuki-Miyaura cross-couplings, limitations continue to hinder the generality of these methods. In particular there exists only one example utilizing a secondary alkylborane nucleophile,¹⁹ limited examples of electrophiles that contain heteroaromatic functionality,^{20,21} no examples utilizing a methyl containing boron nucleophile or electrophile, and no examples utilizing boronic ester nucleophiles.

Scheme 4.1. Examples of nickel-catalyzed C(sp³)-C(sp³) couplings including an enantioselective variant

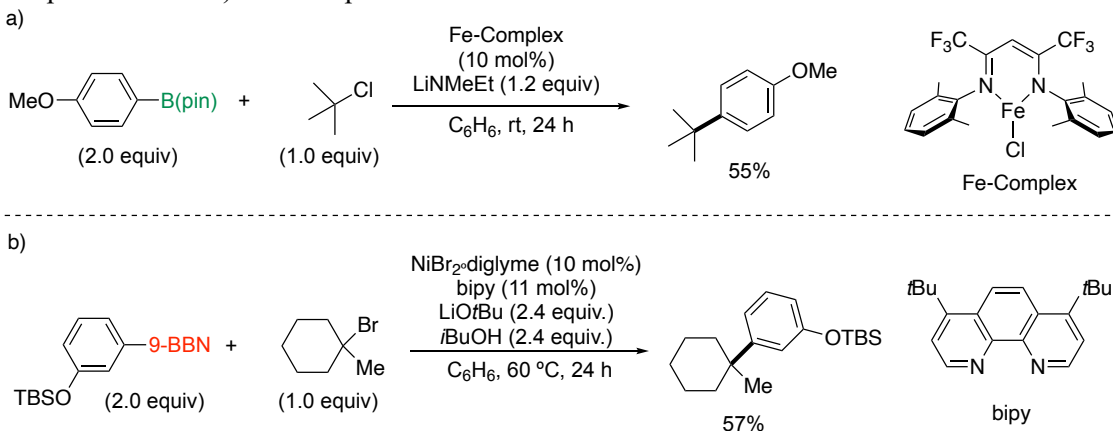


Regarding these reactivity limitations, iron-based catalysts would provide an attractive alternative to nickel and palladium-based catalysts. Iron benefits from having non-toxic properties²² and high abundance in the earth's crust,²³ as well as engaging in efficient reactivity with alkyl electrophiles,^{24,25} displaying rapid reaction rates²⁶ and having a relatively lower propensity for undergoing β -hydride elimination compared to palladium and nickel.²⁷ The propensity of iron-based complexes to favor β -hydride elimination less than nickel complexes can be explained by a thermodynamic argument. Iron, being an earlier transition metal than the group 10 metals, engages in less efficient back-bonding with olefins. Additionally, iron is usually high spin with five or more d electrons and possess no unoccupied d-orbitals, which are required for β -hydride elimination.²⁸

The combination of these unique qualities make iron an ideal candidate for these challenging C(sp³)-C(sp³) cross-coupling reactions and have led to the discovery of new reactivity inaccessible with nickel-based catalysts within our own lab. We have found that highly reactive β -diketiminate iron catalysts were able to couple unactivated arylboronic

pinacol esters with tertiary alkyl halides.³ This iron-based system demonstrated a wide nucleophile scope, using meta and para-substituted arylboronic esters with electron donating and withdrawing groups. When a nickel bipyridyl complex was used for an analogous reaction, the system demonstrated complementary reactivity to iron by demonstrating a wider electrophile scope. However this nickel-based system required more reactive and air sensitive aryl-9-borabicyclo[3.3.1]nonane (9-BBN) reagents (Scheme 4.2).^{3,29} Despite being a C(sp³)-C(sp²) coupling reaction, the comparison between the iron and nickel-based systems distinctly highlights the higher reactivity of iron-based catalysts relative to nickel for this challenging tertiary arylation coupling reaction.

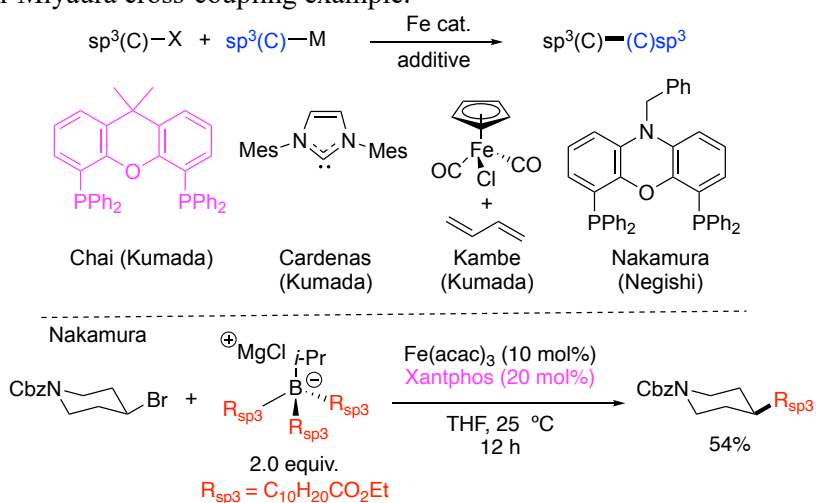
Scheme 4.2. Comparison of Suzuki-Miyaura tertiary arylation reactions using a a) nickel-complex²⁹ and an b) iron complex.³



Only within the past decade have iron-based catalysts been used for constructing C(sp³)-C(sp³) bonds,³⁰⁻³⁴ with only one reported Suzuki-Miyaura coupling. (Scheme 4.3) Though the one reported iron-catalyzed Suzuki-Miyaura reaction demonstrates the feasibility of iron-based catalysts for challenging C(sp³)-C(sp³) cross-couplings, much improvement can still be achieved. In this one iron-based system, electrophiles are limited to primary alkyl bromides, with the only secondary examples being in six-membered rings, while the trialkylborane nucleophile requires Grignard activation and can only

transmetalate primary alkyl fragments. To improve upon this system, we hoped to access wider range of secondary alkyl halides including alkyl chlorides, utilize secondary alkyl-9-BBN reagents, and provide novel methylating reactions. To achieve this goal, a combination of mechanistic investigation and rational ligand design was required. This chapter aims to show these efforts that led toward the development of a Suzuki-Miyaura C(sp³)-C(sp³) cross-coupling reactions using an iron-based catalyst, further expanding the synthetic toolbox available to iron cross-coupling reactions.

Scheme 4.3. Examples of state-of-the art iron-catalyzed C(sp³)-C(sp³) couplings including a single Suzuki-Miyaura cross-coupling example.

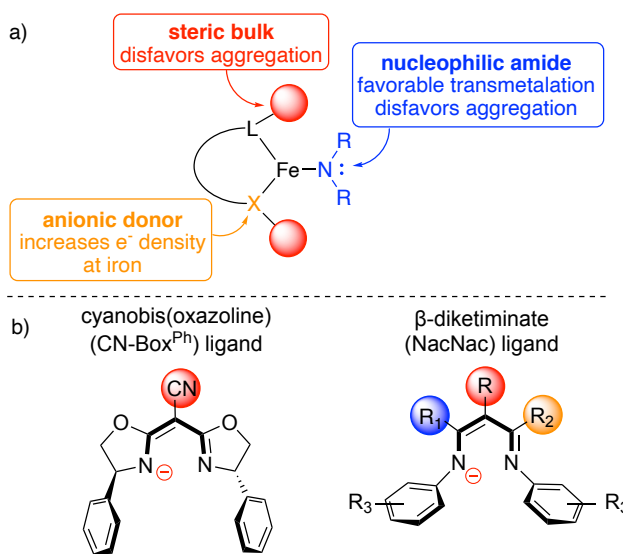


4.2 Mechanistically Guided Ligand Design

To develop an iron-based catalyst capable of mediating a C(sp³)-C(sp³) cross coupling reaction, insight into our working mechanistic hypothesis from our previous catalytic systems provided some key ligand features essential for efficient catalysis.²⁻⁴ In our proposed mechanism (Figure 4.2), iron halide (**I**) undergoes salt-metathesis with the lithium amide to produce an iron-amide intermediate (**II**). Species **II** can engage in transmetalation with the boron nucleophile to yield an iron aryl intermediate (**III**) or halogen abstraction to form a carbon-centered radical and an iron (III) (**VI**). Intermediate

A ligand class that met these mechanistically driven design principles were β -diketiminate or NacNac ligands which have been extensively used by the Holland group to stabilize low coordinate iron species.^{35,36} NacNac ligands provide stronger sigma-donation³⁵ than the less basic cyanobis(oxazoline) ligands used in chapters 2 and 3, provide greater steric and electronic tunability and are less synthetically intensive to prepare (Figure 4.3b). In our laboratory, we have demonstrated the benefits of using β -diketiminate ligands for iron, where challenging heteroaromatic boronic ester and tertiary alkyl halide coupling partners can be accessed.³ Due to the high reactivity and modularity of iron

Figure 4.3. Rational and mechanistically guided ligand design principles



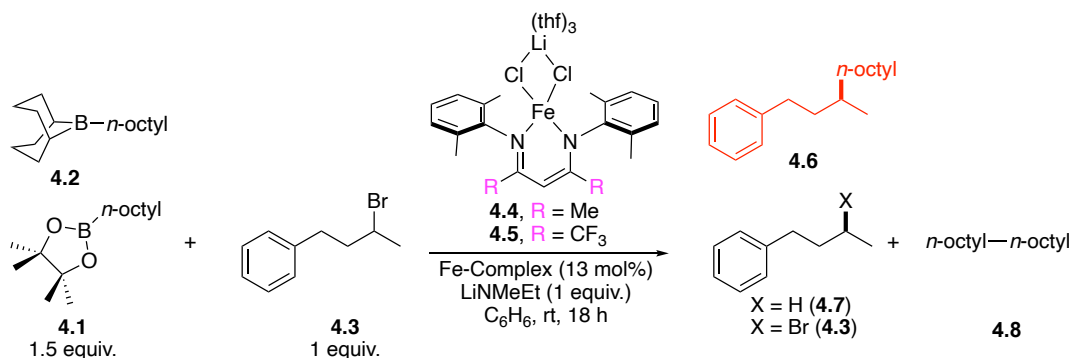
complexes containing the NacNac ligand, this ligand class would be a highly desirable framework for developing iron catalysts capable of achieving $C(sp^3)$ - $C(sp^3)$ Suzuki-Miyaura cross coupling reactions.

Initial Discovery and Optimization of Reaction Parameters

Preliminary investigation into the development of an iron-catalyzed C(sp³)-C(sp³) Suzuki-Miyaura cross-coupling reaction began with the coupling between *n*-octylboronic pinacol ester (**4.1**) and 3-bromobutylbenzene (**4.3**) with lithium methylethylamide (LiNMeEt) as the amide base. As discussed in Section 4.1, a β-diketimate ligand framework was advantageous for probing reactivity and was used for the initial discovery process and reaction optimization. In particular, iron(II) halide complexes **4.4** and **4.5**, containing either a methyl or trifluoromethyl ligand backbone, with 2,6-dimethylaryl imine arms were used for reaction optimization. These two complexes were chosen because of their high catalytic performance in a similar C(sp²)-C(sp³) cross-coupling reaction.³ The disparate electronic properties of these two complexes led to profound effects on catalytic reactivity, particularly with the efficiency of iron complex **4.5** using tertiary alkyl halides (Scheme 4.2a).

When this Suzuki-Miyaura cross-coupling reaction was performed in benzene with either iron complex **4.4** or **4.5**, cross-coupled product **4.6** was not detected by GC-FID analysis (Table 4.1, entries 1-2). The lack of product **4.6** and high mass recovery of starting material **4.3** was consistent with inefficient transmetalation due to either unsuitable steric and/or electronic parameters of the alkylboronic ester. To test this hypothesis, lithium dimethylamide (LiNMe₂) was used as a sterically less-encumbering base possessing similar electronics to lithium methylethylamide (entry 3). With a smaller base to engage in the 4-centered transition-state required prior to transmetalation, we were pleased to see formation of product **4.6** using fluorinated iron complex **4.5** (Figure 4.4). Despite low yields, this result represents the first reported example of a C(sp³)-C(sp³) Suzuki-Miyaura reaction using an unactivated alkylboronic ester as a coupling partner. Use of larger lithium

Table 4.1. Reaction discovery and initial optimization of reaction parameters for the Suzuki-Miyaura cross-coupling between *n*-octyl-B(pin)/*n*-octyl-9-BBN and 3-bromobutylbenzene.

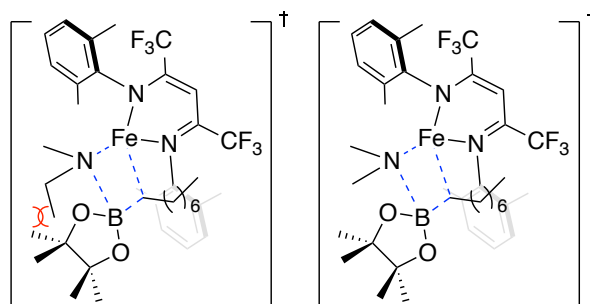


Entry	Fe-Complex	Deviation from Conditions	4.6 (%) ^[a]	4.7 (%) ^[a]	4.3 (%) ^[a]	4.8 (%) ^[a]	
1	4.4	None	0	trace	98	0	
2	4.5	None	0	trace	98	0	
3	4.5	LiNMe ₂ instead of LiNMeEt	15	75	5	3 58	∅1
4	4.4	4.2 instead of 4.1	4	3	88	5	
5	4.5	<i>n</i> - 4.2 instead of 4.1	20	5	70	5	
6	4.5	4.2 instead of 4.1 / LiNMe ₂ instead of LiNMeEt	75	3	21	1	

^[a] Yields determined by through the use of GC-FID analysis using tetradecane as an internal standard.

amide bases than methylethyl amide led to little to no conversion of electrophile **4.3**. In addition to sterics, electronic parameters were evaluated by using 9-BBN alkylboranes as a more reactive boron nucleophile source to favor transmetalation. Low to moderate yields of cross-coupled product **4.6** were seen using both iron complexes **4.4** and **4.5** respectively, when using lithium methylethylamide as the base additive (entries 4,5). Use of the smaller lithium dimethylamide with fluorinated catalyst **4.5** led to a dramatic increase in yield of product **4.6** in excellent yield and yield based on recovered starting material (brsm) (entry 6). It is important to note that trace amounts of alkane or alkene product were formed,

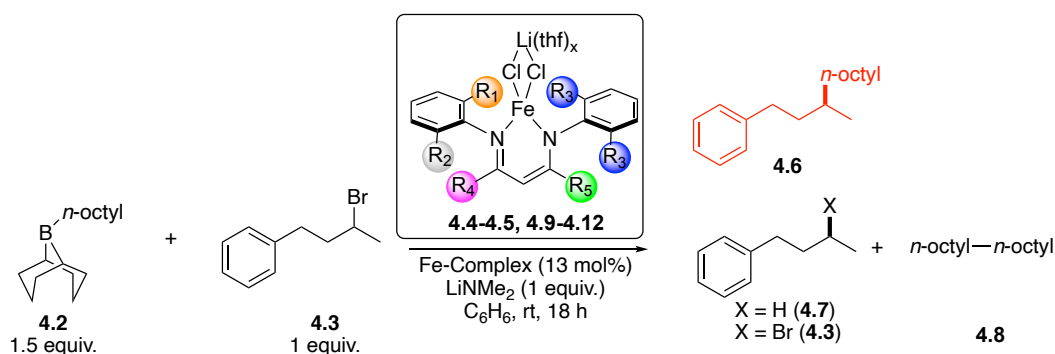
Figure 4.4. Hypothesized steric encumbrance during the 4-centered transition state of transmetalation using various sized amides.



which is indicative of the suppression of β -hydride elimination. Undesired β -hydride elimination events commonly plagues this class of $C(sp^3)$ - $C(sp^3)$ cross-coupling reactions.

Next, an evaluation of iron(II) β -diketiminate complexes was performed. It is important to note that discrete, preformed iron chloride complexes were used for this study since *in-situ* catalyst generation from mixing $FeCl_2$ and ligand led to reduced yields of **4.6** (Table 4.2, entry 1). Additionally, we found that the supporting β -diketiminate ligand framework was essential for selective cross-coupling as $FeCl_2$ was inefficient at catalysis, leading to alkene byproducts as the major mass balance (Table 4.2, entry 2). The reaction was found to be exceptionally sensitive to the electronics of the ligand. The replacement of methyl for trifluoromethyl into the ligand backbone provided a nearly 2-fold increase in yield of cross-coupled product **4.6**, demonstrating the importance of electron-deficiency in promoting one or more of the elementary steps of the catalytic cycle (Table 2, entries 3-4). In addition to electronics, the reaction was also sensitive to the steric bulk proximal to the iron-center provided by the aryl imine groups. The optimal steric profile was 2,6-dimethyl substitution while bulky 2,6-diisopropyl substitution led to low reaction efficiency and selectivity, presumably due to slow transmetalation rates (**4.9**, entry 5). To further probe the effects of modulating steric and electronic parameters of the β -diketiminate ligand,

Table 4.2. Survey of iron(II) β -diketiminate precatalysts for the Suzuki-Miyaura cross-coupling between *n*-octyl-9-BBN and 3-bromobutylbenzene.



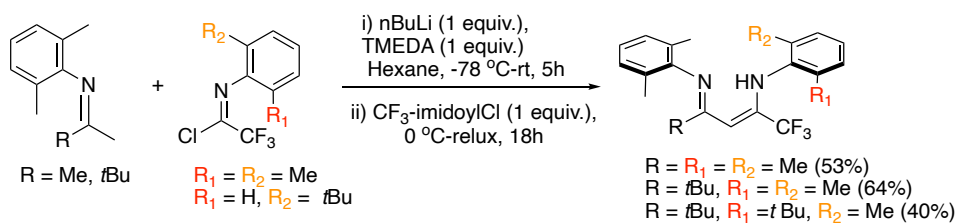
Entry	Fe-Complex	R ₁	R ₂	R ₃	R ₄	R ₅	4.6 (%) ^[a]	4.7 (%) ^[a]	4.3 (%) ^[a]	4.8 (%) ^[a]
1	4.5 ^[b]	Me	Me	Me	CF ₃	CF ₃	49	5	25	1
2	FeCl ₂	-	-	-	-	-	4	8	25	6
3	4.4	Me	Me	Me	Me	Me	47	8	17	6
4	4.5	Me	Me	Me	CF ₃	CF ₃	75	3	21	1
5	4.9	<i>i</i> Pr	<i>i</i> Pr	<i>i</i> Pr	CF ₃	CF ₃	6	8	0	8
6	4.10	Me	Me	Me	CF ₃	Me	76	10	14	6
7	4.11	Me	Me	Me	CF ₃	<i>t</i> Bu	82	4	14	3
8	4.12	<i>t</i> Bu	H	Me	CF ₃	<i>t</i> Bu	68	9	21	6
9	4.11 ^[c]	Me	Me	Me	CF ₃	<i>t</i> Bu	96	4	0	5

^[a] Yields determined through the use of GC-FID analysis using tetradecane as an internal standard.

^[b] 4.4 generated *in-situ* by reaction of free ligand with FeCl₂ ^[c] 2 equivalents of alkylborane 4.8 and 1.2 equivalents of LiNMe₂ used.

backbone modifications were made to afford C_s and a C₁ symmetric ligands. These dissymmetric ligands, containing one trifluoromethyl and one alkyl group in the backbone,

Scheme 4.4. Synthesis of C_s and C₁ symmetric β -diketiminate ligands.



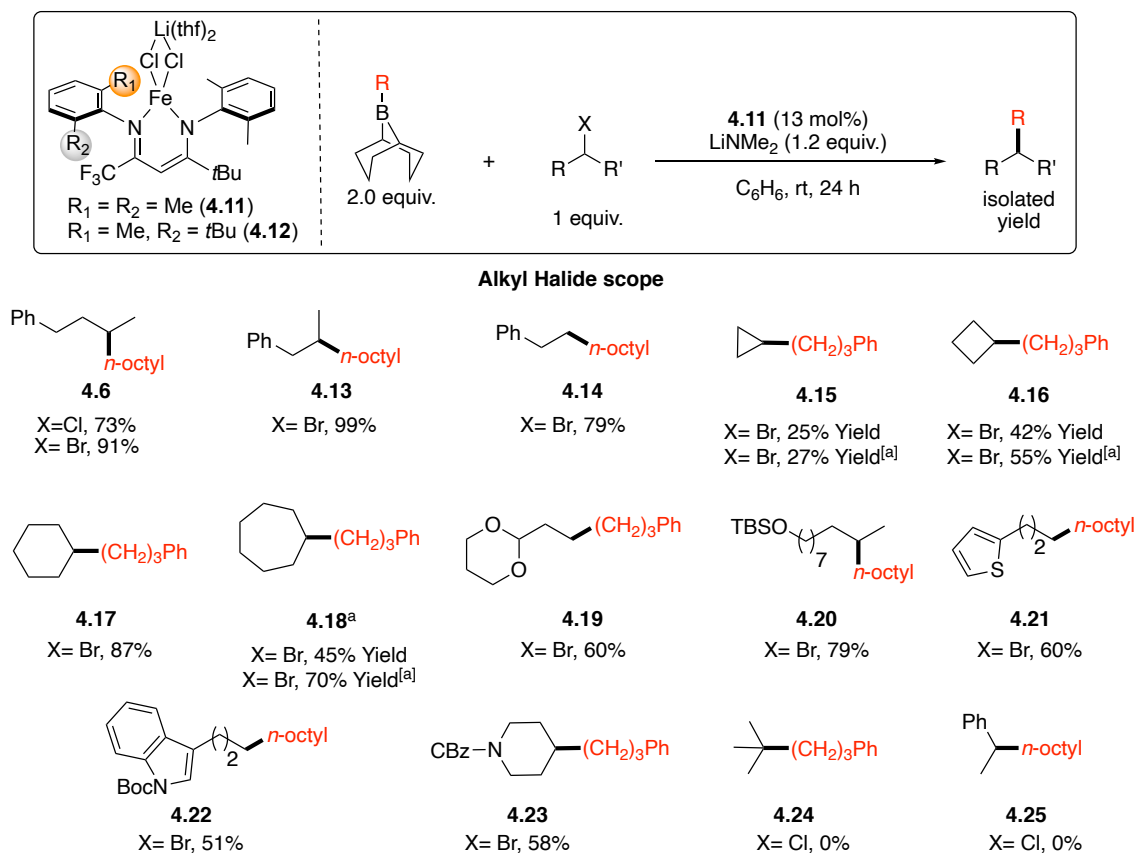
were made in moderate to good yields (40-64%) through an alkylation route, coupling an aryl imine to a trifluoromethyl imidoyl chloride (Scheme 4.4). From surveying these ligands, we found that substituting a methyl for a *tert*-butyl group in the ligand backbone was most beneficial for cross-coupling. This trend is especially true while maintaining 2,6-dimethyl substitution on the aryl imine arms (entries 6-8). Overall, iron complex **4.11** proved to be the optimal iron complex for cross-coupling, providing nearly quantitative yield of **4.5** after increasing equivalents of alkylborane and lithium amide base (Table 4.2, entry 9).

4.3 Substrate Scope Evaluation

The generality of the cross-coupling reaction for the alkyl halide coupling partner was evaluated next (Table 4.3). The reaction was general for a variety of unactivated primary and secondary acyclic alkyl halides providing good to excellent yields of cross-coupled product (e.g., **4.6**, **4.13-4.14**). Noteworthy is the use of an alkyl chloride as a competent coupling partner, which represents the first reported example involving an iron-based catalyst (e.g., **4.6**). Unlike acyclic alkyl halides, cyclic alkyl halides afforded cross-coupled products in significantly lower yields, with the exception of bromocyclohexane (e.g., **4.15-4.17**). Higher yields with four (**4.16**) and seven-membered cycloalkyl bromides could be obtained using sterically less encumbered C_1 -symmetric iron complex **4.12**. At this time, we do not have a good hypothesis to explain the differences between cyclic and acyclic alkyl halides, besides a possible effect on ring strain. Small, cyclic alkyl halide, cyclopropyl bromide, still produced comparatively low yields of cross-coupled product **4.15**, even when **4.12** was used as the catalyst. The reaction conditions were tolerant to a variety of functional groups despite some limitations with respect to functional group

compatibility, particularly with electrophiles containing acidic protons. These functional groups included acetals (**4.19**), silyl-protected alcohols (**4.20**), thiophenes (**4.21**), *N*-Boc-protected indoles (**4.22**) and Cbz-protected piperidines (**4.23**), which represent some functionalities we have not yet been able to access in our previous catalytic systems.^{2,3} Noteworthy from this list were the efficiency of heteroaromatic-containing alkyl halides since few of these substrates have been reported in analogous reactions catalyzed by nickel-based catalysts.^{20,21} In addition to successfully-targeted substrate classes, it is also important to note those that were unsuccessful. These substrate classes included tertiary

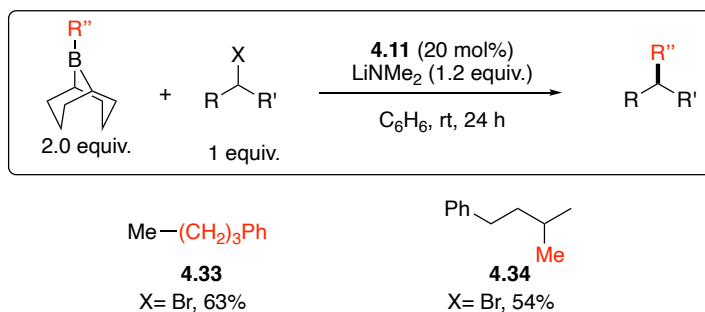
Table 4.3. Alkyl halide scope of an iron-catalyzed alkyl-alkyl Suzuki-Miyaura cross-coupling evaluating both alkyl halide and borane coupling partners.



(66%) of cross-coupled product **4.29**. Unfortunately, bulkier cyclic boranes and acyclic secondary boranes led to no observable product formation (**4.30-4.31**).

Given the generality that the reaction demonstrated for a variety of alkyl halide and alkylborane substrates, we decided to see if the cross-coupling reaction would be compatible for installing methyl groups into small molecules. Such a capability would be particularly important in the area of medicinal chemistry due to the “magic methyl” effect known to elicit favorable medicinal properties.³⁹ Cross-coupling reactions would be a convenient way to install methyl groups into biologically active small-molecules at sp^3 -hybridized sites, but there are minimal examples in the literature with most being C-H activation reactions catalyzed by palladium and nickel-based complexes.^{40,41} Methylation reactions were carried out using our established reaction conditions and iron catalyst **4.11**, leading to formation of cross-coupled product **4.33** in 63% yield when methyl iodide was used as the methylating source (Scheme 4.5). Likewise, when Me-9-BBN was used as the methylating reagent, **4.34** could be obtained in 54% yield. To the best of our knowledge, these coupling-partners have not previously been reported in analogous iron or nickel-catalyzed $C(sp^3)$ - $C(sp^3)$ Suzuki-Miyaura reactions. The results with methyl iodide were particularly intriguing because, unlike palladium-based catalysts that often undergo

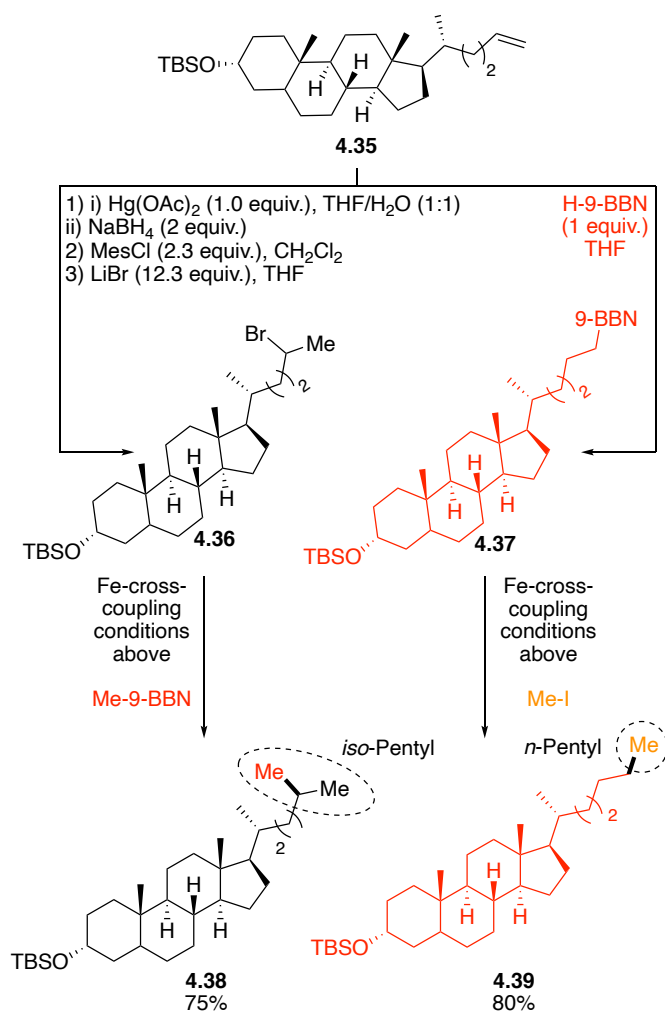
Scheme 4.5. Complementary methylation reactions.



oxidative addition through an S_N2 mechanism,⁴² the mechanism for the oxidative addition of alkyl halides using iron-based catalysts often occur through single-electron pathways.¹² Such mechanisms would lead to an unstable methyl radical intermediate that would be significantly more difficult to form compared to radical intermediates derived from primary, secondary, or tertiary alkyl halides.

Regardless to the mechanisms that are operative, the two methylation reactions provide complementary means for installing methyl groups in complex small molecules.

Scheme 4.6. Lithocholic acid derivatization leading to isomeric products.



To showcase this fact, we decided to functionalize steroids derived from lithocholic acid, since steroid functionalization has been an active area of research.⁴³ (Scheme 4.6). Using a sequence of standard transformations, lithocholic acid derivative **4.35** could be converted into alkyl halide **4.36** or alkylborane **4.37**, which could serve as the electrophile and nucleophile in cross-coupling reactions, respectively. Methylation of **4.36** using Me-9-BBN led to **4.38** in 75% yield. Similarly, methylation of **4.37** using methyl iodide led to 80% of **4.39**. The two products **4.38** and **4.39** are isomeric and constitute the formal addition of a methyl group in two different positions to lithocholic acid derivative **4.35**. Access to these isomers is only made possible because the cross-coupling reaction is compatible with nucleophilic and electrophilic methylating sources.

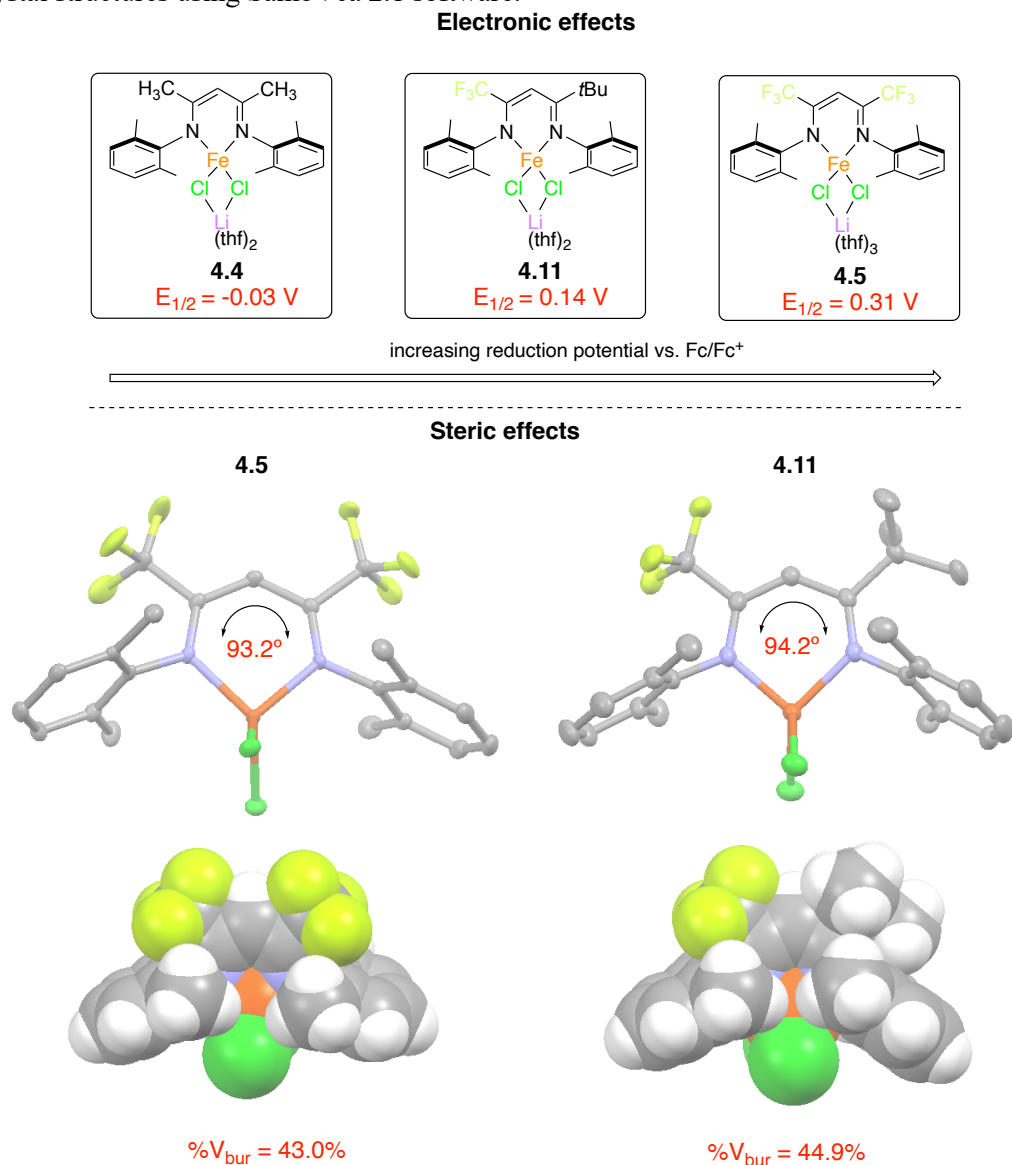
4.4 Elucidation of Mechanistic Features and the Catalytic Cycle

Having established this newly developed C(sp³)-C(sp³) cross-coupling methodology, more experiments were needed to provide insight into the mechanism of the reaction and how it compared to our previously developed alkyl-aryl coupling reaction.³ One mechanistic aspect that we wanted to understand was the sensitivity of the reaction to the identity of the ligand.

When considering the distinguishing features of the ligand in iron complex **4.11**, notable are the beneficial effects of the CF₃ and *t*-Bu groups in obtaining high yields. To help rationalize these favored substitutions, the reduction potentials of iron complexes **4.4**, **4.5** and **4.11** were measured. Iron complex **4.11** was found to have a higher reduction potential relative to methyl substituted **4.4** (0.14 V vs. -0.03 V relative to Fc/Fc⁺), but lower when compared to bis-trifluoromethyl substituted iron complex **4.5** (0.14 V vs 0.31 V relative to Fc/Fc⁺). The incorporation of CF₃ and *t*-Bu groups into the ligand backbone

leads to an optimal reduction potential in-between the two catalysts (Figure 4.5). Although sterics and electronics of complex **4.11** were changed simultaneously, we attribute the beneficial effects of the CF₃ group to increasing the electron deficiency of the iron center. The electron deficiency of **4.11** may help facilitate reductive elimination as well as to affect

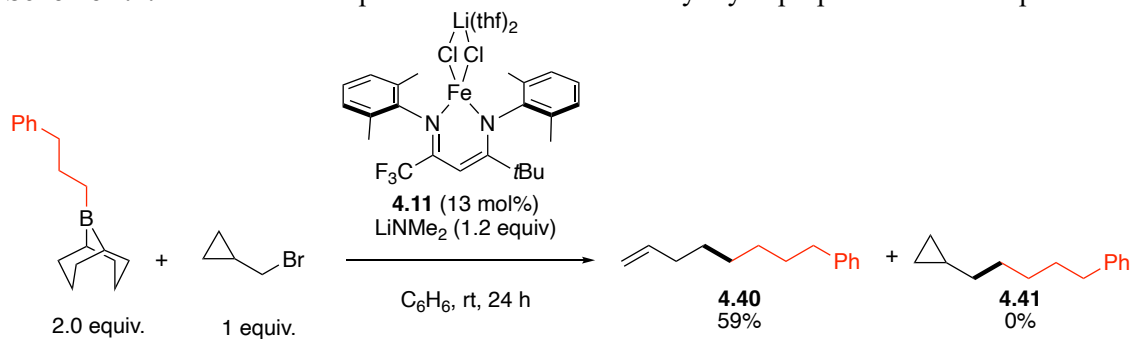
Figure 4.5: Comparison of ligand effects on the electronic and steric properties of iron complexes **4.4**, **4.5** and **4.11**. Hydrogen atoms, lithium chloride and tetrahydrofuran were omitted in the crystal structures for clarity. Lithium chloride and tetrahydrofuran were omitted in the space-filling models. The percent buried volume was determined from the crystal structures using SambVca 2.1 software.



the relative rates of transmetalation and halogen abstraction. We have also attributed the beneficial effects of the *tert*-butyl group when comparing the crystal structures of iron chloride complexes **4.5** and **4.11**, by the increased ligand bite-angle from 93.2° to 94.2°. A consequence of this larger bite angle is contraction of the aryl imine substituents, which serves to decrease the cone angle of the β -diketiminato ligand and increase the buried volume of the iron center.⁴⁴ This effect has previously been noted and has a profound influence on the reactivity of β -diketiminato iron complexes in dinitrogen reduction reactions.³⁵ Figure 4.5 contains a space filling diagram of the crystal structures of **4.5** and **4.11**, which helps visualize the impact that the *tert*-butyl substituents installed in the ligand backbone have on the coordination environment of the complex. While it is difficult to say is how the steric environment of **4.11** benefits the cross-coupling reactions, one possibility is that the larger buried volume (44.9% for **4.11** vs. 43.0% for **4.5**) helps protect the iron center from aggregation or off-cycle pathways. We hypothesize the steric protection of **4.11** provided by the larger bite angle of the ligand leads to a longer-lived catalyst. Overall, the beneficial features of iron complex **4.11** is clearly due to a proper balance between sterics and electronics. The optimal steric and electronic properties of **4.11** is likely important to multiple steps in the catalytic cycle and/or prevents catalyst aggregation and decomposition.

In addition to understanding the ligand effects, we aimed to probe whether these reactions proceed through a radical-based mechanism. To serve this goal, radical clock experiments were performed using 1-bromomethylcyclopropane. Exclusive ring-opened product (**4.40**) was generated, even when attempted at higher catalyst loadings, which is supportive of a radical-based mechanism where you can estimate the lifetime of the radical.

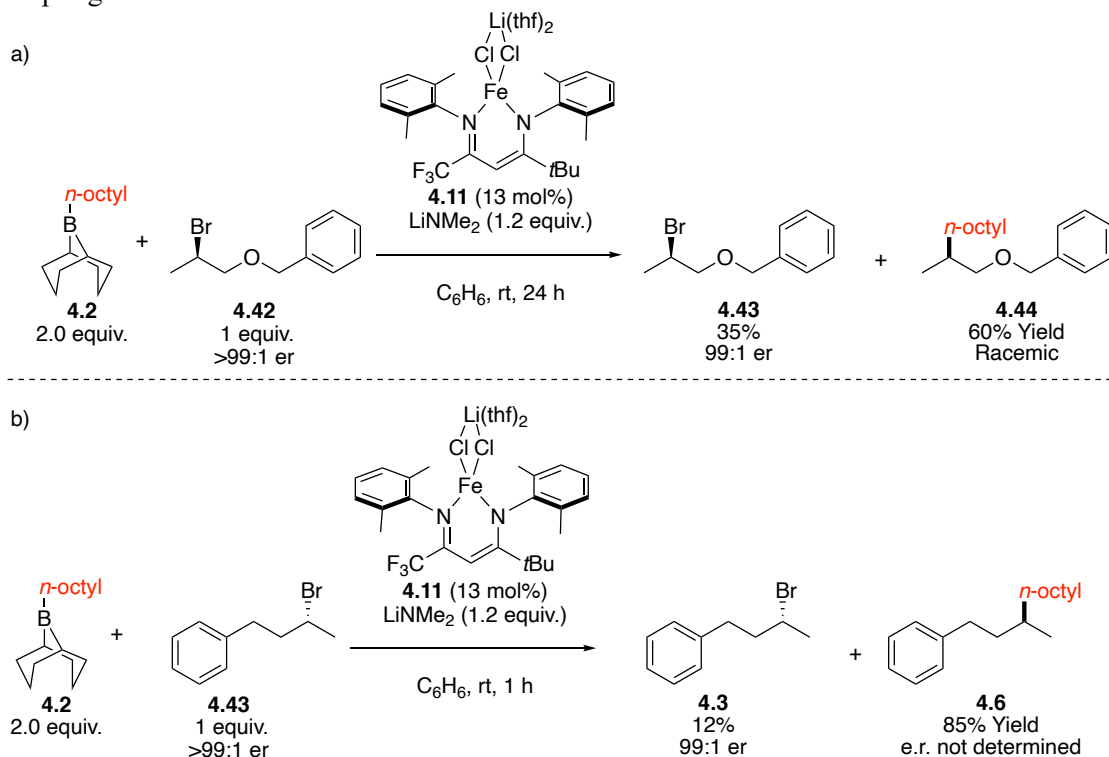
Scheme 4.7: Radical clock experiment with 1-bromomethyl-cyclopropane as a radical probe.



However, these results cannot rule out a metal-mediated ring-opening mechanism (Scheme 4.7).⁴⁵ Further evidence for a radical mechanism came from probing the stereochemical outcome of an enantiomerically-enriched alkyl bromide after catalysis. When subjecting alkyl bromide **4.42** to cross-coupling conditions, racemic cross-coupled product was seen (**4.44**, Scheme 4.8a). These results suggest a stereoconvergent process consistent with a carbon-centered radical intermediate.⁴⁶ These results also suggest the lifetime of the radical is longer than 10^8 s^{-1} , which is the rate of alkyl radical inversion.⁴⁷ Furthermore, the starting material collected after catalysis (**4.43**) remained enantiomerically-enriched, suggesting that halogen-abstraction is an irreversible process, leading to an alkyl radical readily capable of epimerizing. Enantiopure electrophile **4.43** was also seen using a unfunctionalized substrate in (*R*)-3-bromobutylbenzene under identical reaction conditions which we used to rule out potential metal coordination to **4.42** which could serve as a directing group (Scheme 4.8b). However, we were unsuccessful in assessing the stereopurity of the cross-coupled product due to challenges with separating enantiomers using HPLC analysis.

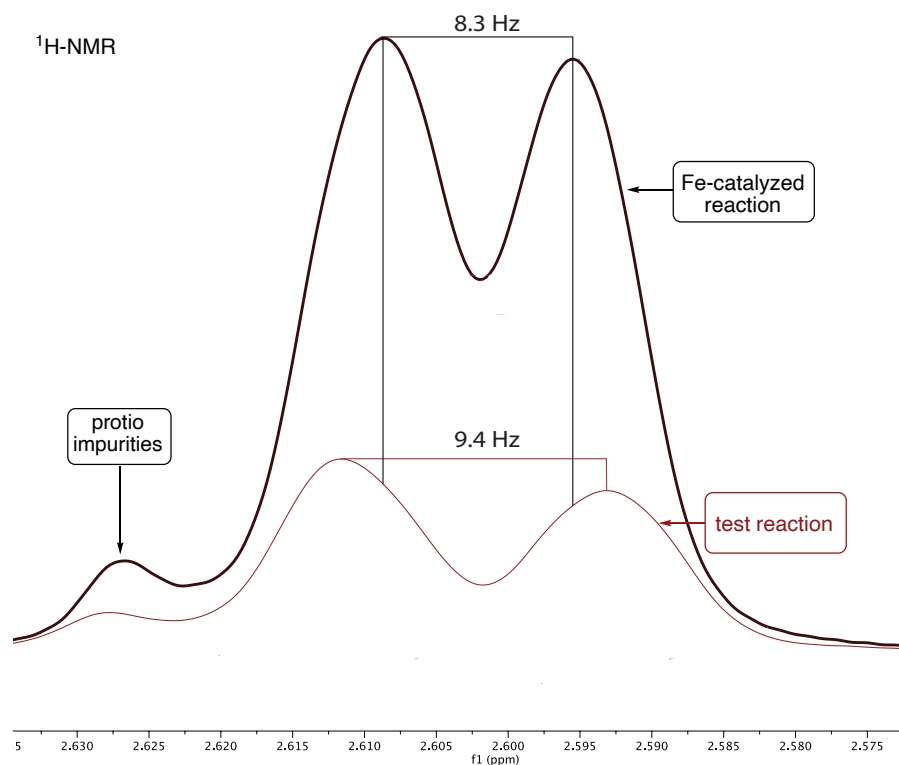
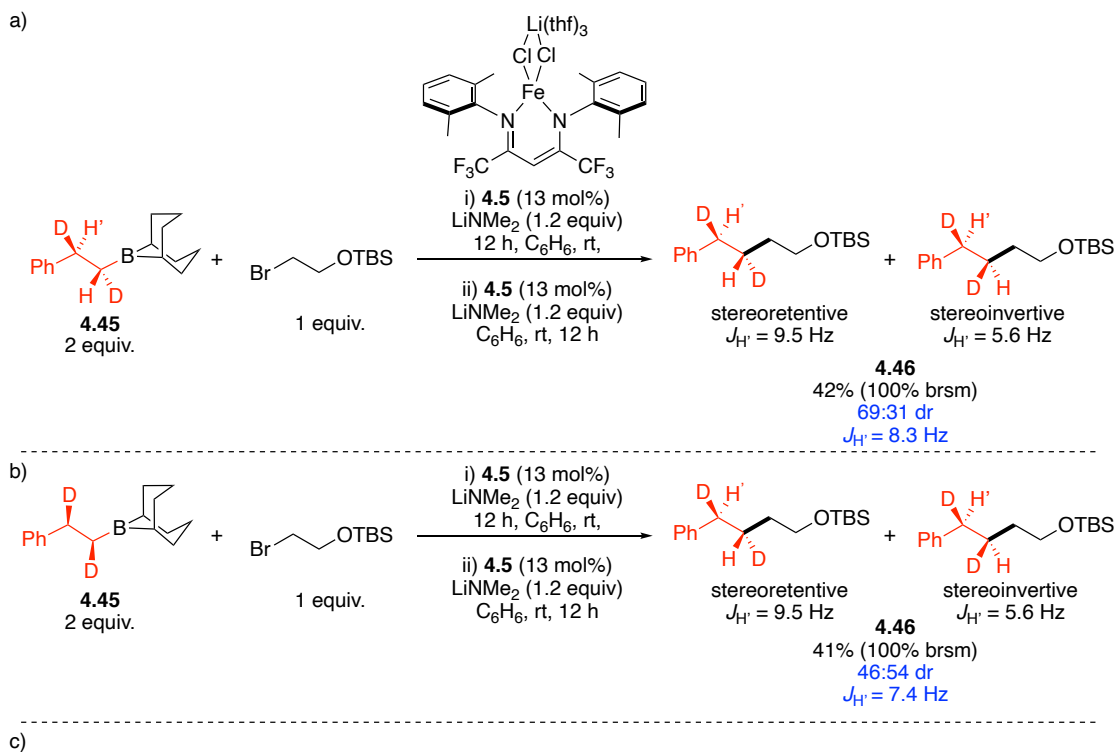
In addition to probing the stereochemical outcome of enantiopure electrophile, the stereochemical outcome of the alkyl borane was also investigated. This goal was

Scheme 4.8: a) Stereochemical outcome of an enantiomerically enriched alkyl halide after cross-coupling. b) Stereochemical outcome of an enantiomerically enriched alkyl halide after cross-coupling.



accomplished by using the deuterium-labeled, diastereomerically pure alkylborane (**4.45**) recently used by Jarvo⁴⁸ and invented by Whitesides.⁴⁹ Jarvo and coworkers discovered that with the use of diastereomerically-enriched **4.45**, they could determine whether transmetalation proceeded with retention or inversion through ¹H-NMR analysis of the cross-coupled product. More specifically, the two diastereomeric products could be distinguished by the value of their benzylic proton coupling constant where the anti-product has a *J*-value of 9.5 Hz and the syn-product has a *J*-value of 5.6 Hz. Using this protocol, we carried out an iron cross-coupling reaction between anti-alkylborane **4.45** and 2-(bromoethoxy)trimethylsilane to afford cross-coupled product **4.46**. Stereochemical analysis of product **4.46** by ¹H-NMR spectroscopy was indicative of a mixture of

Scheme 4.9: a,b) Stereochemical outcome of transmetalation using a diastereomerically pure deuterated alkylborane. b) ¹H-NMR stereochemical analysis of product **4.46** from test reaction (red trace) and iron-catalyzed reaction (black trace).

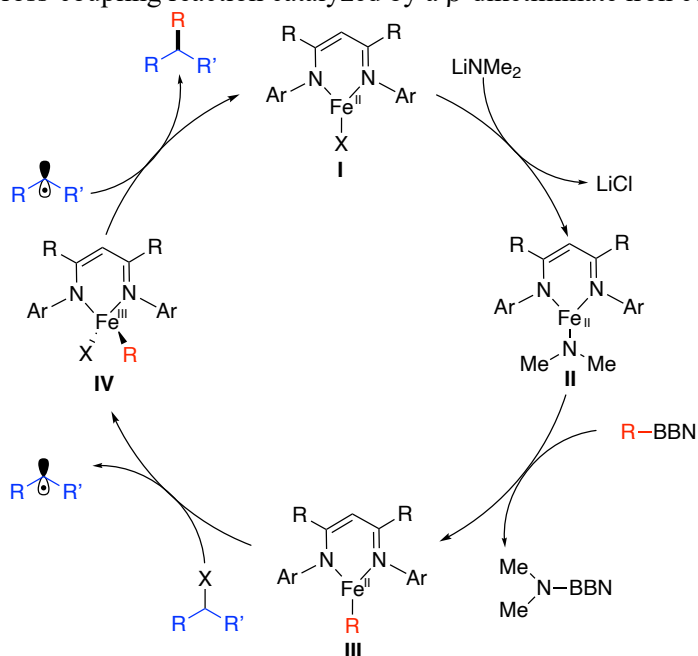


diastereomers since the coupling constant we observed was in-between the J -value

investigation. To validate these unexpected results, a control reaction was carried out, performing the same nickel-catalyzed reaction as the Jarvo group. As expected, when the anti-diastereomer of the alkylborane was used, the literature reported 9.5 Hz *J*-value was seen as shown in Scheme 4.9, which validated our experimental findings. These unanticipated experimental results are mechanistically intriguing and suggestive of a doubly stereoconvergent mechanism. These preliminary results hold promise for future development of novel stereoselective cross-coupling reactions using racemic alkyl halides and racemic alkylborane coupling partners. These types of doubly stereoconvergent cross-coupling reactions are rare and only seen with nickel-catalyzed Negishi systems.⁵¹ Additional diastereomerically pure alkylborane probes are currently being synthesized in our laboratory to verify our results with alkylborane **4.45**.

With a clearer picture of the mechanistic cycle from these mechanistic experiments, we propose monometallic and bimetallic mechanisms. The unified monometallic mechanism shown in Scheme 4.10 is one viable possibility. In a monometallic Fe(II/III) mechanism similar to our previous C(sp³)-C(sp²) Suzuki-Miyaura system (Scheme 4.11).³ Iron halide **I** undergoes salt metathesis with the lithium amide to form **II**, which then is active for transmetalation with the alkyl borane to form complex **III**. Complex **III** can then engage in an irreversible halogen-abstraction event forming a carbon-centered radical and **IV**, which can then proceed through a radical rebound to form the carbon-carbon bond and regenerate **I**. In terms of the epimerization of the alkyl fragment originating from the alkyl borane, it is unclear whether that occurs from complex **III** or **IV**. At this time, we currently disfavor a radical recombination from **IV** since a high valent Fe(IV) would form which is unlikely under the reducing reaction conditions.

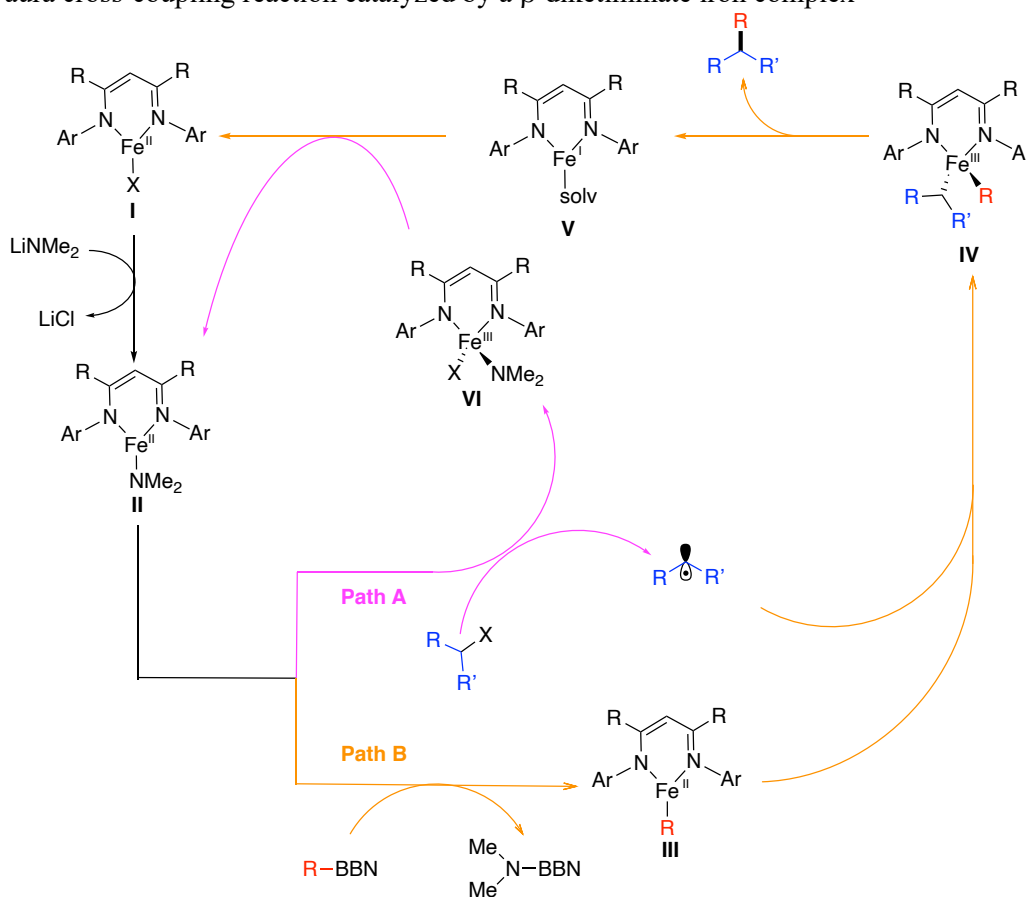
Scheme 4.11: Proposed monometallic Fe(II/III) mechanistic cycle for a C(sp³)-C(sp³) Suzuki-Miyaura cross-coupling reaction catalyzed by a β -diketiminato iron complex



Despite the monometallic Fe(II/III) cycle we proposed being consistent with the experimental and mechanistic data collected, we cannot rule out a bimetallic mechanism whereby iron amide complex **II** can serve as the halogen-abstracter and transmetalation agent (Scheme 4.12). In this mechanism as described in chapter 3, iron halide (**I**) undergoes salt metathesis with the lithium amide to form iron amide (**II**) which can either undergo transmetalation with the alkylborane to form **III** in Path B (orange) or halogen abstraction to form **VI** and a carbon radical in Path A (pink). Our group has recently discovered this bimetallic mechanism to be operative for iron-catalyzed C(sp³)-C(sp²) Suzuki-Miyaura cross-coupling using a cyanobis(oxazoline)⁴ (see chapter 3) and β -diketiminato ligand.³ This conclusion was drawn from the results of stoichiometric reactions done by Dr. Michael Crockett, probing the reactivity of an iron phenyl (**4.47**) and diethylamide complex (**4.48**) which could be isolated as dimeric red-orange and black solids respectively.⁵² It is

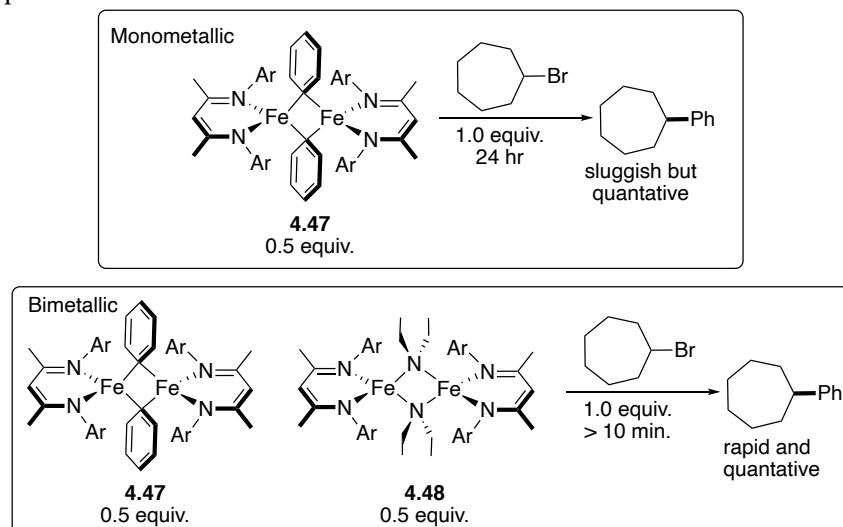
important to note that the iron amide was monomeric in solution as determined by diffusion ordered spectroscopy (DOSY), despite being dimeric in the solid state.³ The results showed that the rates of phenylcycloheptane production with the iron phenyl complex were quantitative but sluggish, requiring over 24 hours for completion, but quantitative within minutes using a 1:1 mixture of iron-amido to iron phenyl (Scheme 4.13).

Scheme 4.12: Proposed bimetallic Fe(II/III) mechanistic cycle for a C(sp³)-C(sp³) Suzuki-Miyaura cross-coupling reaction catalyzed by a β -diketiminato iron complex



To probe whether the C(sp³)-C(sp³) Suzuki-Miyaura cross-coupling reaction was proceeding through a similar bimetallic mechanism, inspiration was drawn from the prior stoichiometric reactions. We first attempted to synthesize discrete iron intermediates along the catalytic cycle to probe their reactivity. Similar reaction conditions developed by our

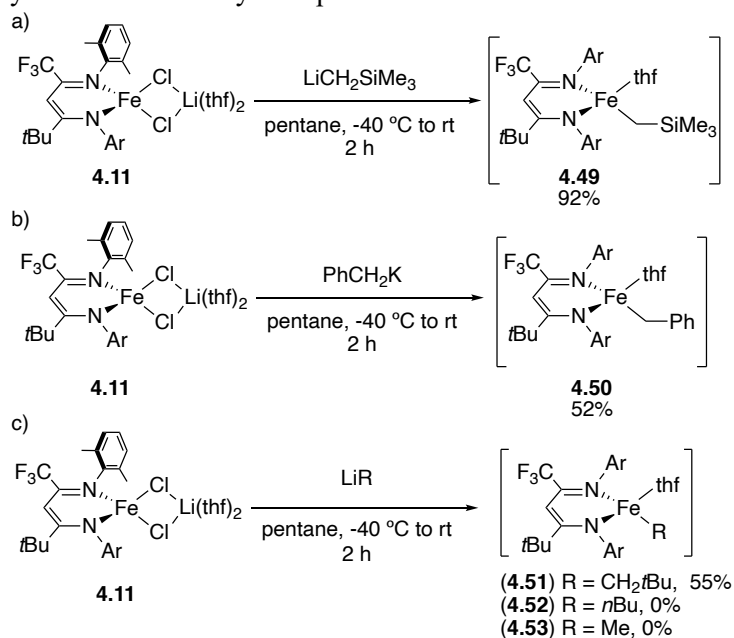
Scheme 4.13: Stoichiometric reactions from a C(sp³)-C(sp²) Suzuki-Miyaura cross-coupling reaction supportive of a bimetallic mechanism



group and others using organometallic reagents as alkylating agents to afford iron alkyls,^{3,53,54} were used to synthesize iron alkyl complexes from the corresponding iron chloride **4.11** (Scheme 4.14). It was found that only iron alkyl complexes without β -hydrogens (CH_2TMS , CH_2Ph , CH_2tBu) could be successfully synthesized and were isolated as red/black solids after recrystallization in cold hexane (**4.49-4.451**). For this reason, synthesis of an iron butyl complex was unsuccessful using butyl lithium as an alkyl source, presumably due to decomposition from rapid β -hydride elimination (**4.52**).⁵⁵ Additionally, syntheses of an iron methyl complex were attempted using methyl lithium and methyl magnesium bromide as methylating sources, but both approaches led to facile catalyst decomposition. Although the methyl ligand possesses no β -hydrogens, its small size most likely provides inadequate steric encumbrance to confer kinetic stability to the iron complex.

To synthesize the corresponding iron amido complexes, protonolysis of iron alkyl complex **4.49** with diethylamine and methylethylamine was achieved to afford iron amides

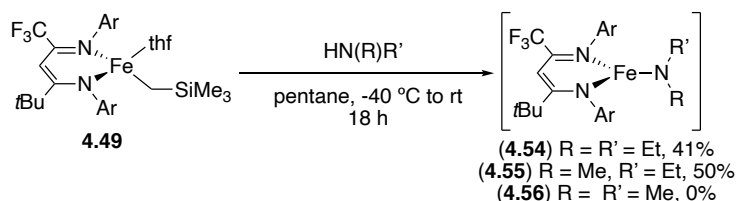
Scheme 4.14: Synthesis of iron alkyl complexes



4.54 and **4.55** respectively as dark purple solids (Scheme 4.15). Unfortunately, the synthesis of the iron amido complex from dimethylamine led to irreproducible results, which we hypothesize is due to the small steric size of the dimethylamido leading to complex decomposition or irreversible aggregation (**4.56**).

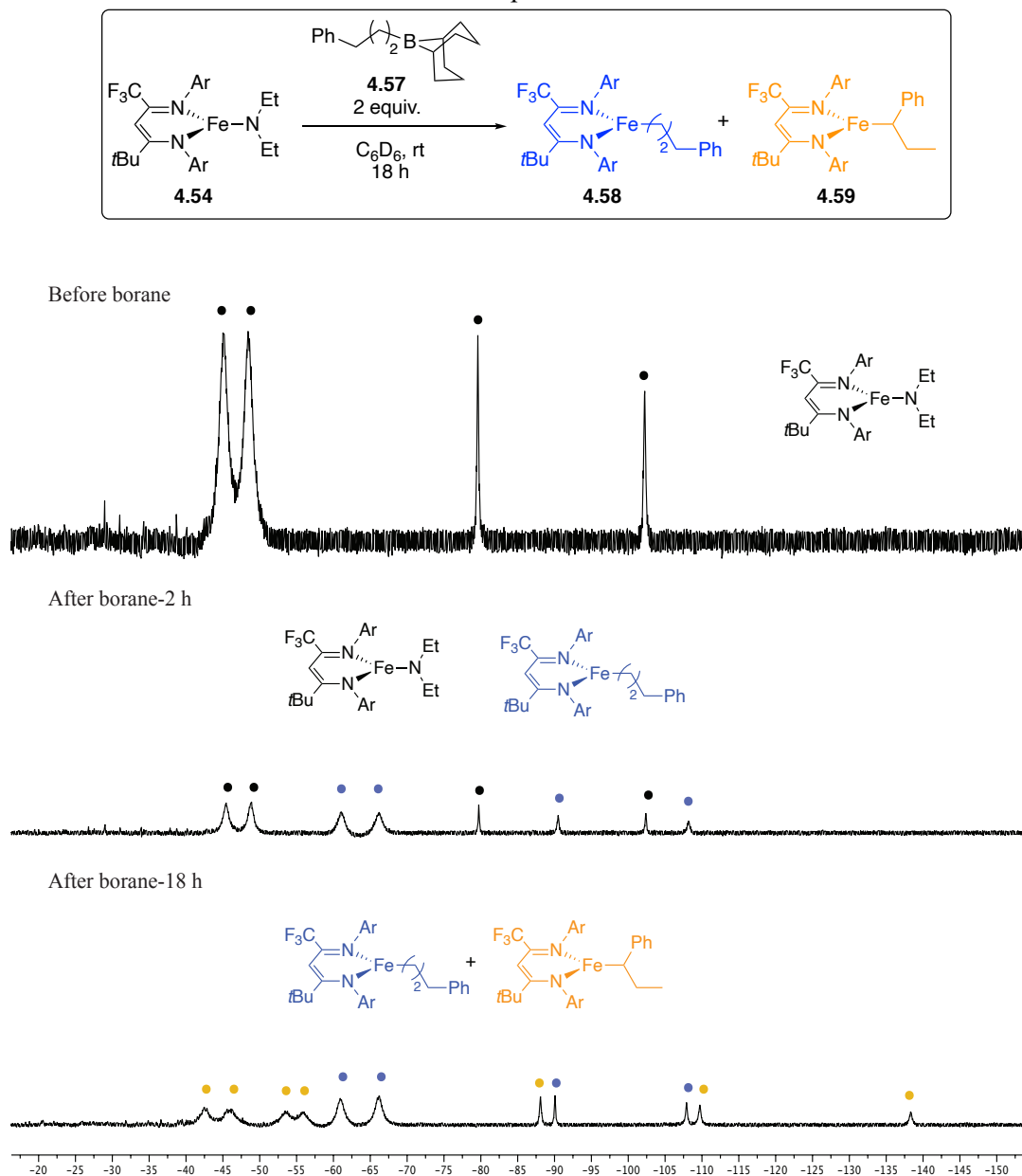
Despite these synthetic limitations, interesting reactivity was seen with iron amide complex **4.54** when subjected to a primary alkylborane containing β -hydrogens (Scheme 4.16). Iron complex **4.54** underwent sluggish transmetalation with alkylborane **4.57** to form evidence that suggested the formation of the putative primary iron alkyl complex **4.58**. These results were consistent with the inefficient catalytic reactions and so required excess

Scheme 4.15: Synthesis of iron amido complexes.



alkylborane and overnight to go to completion. After complete transmetalation, two distinct iron alkyl complexes were evident by $^1\text{H-NMR}$ spectroscopy as seen in Figure 4.16 (black and blue labeled peaks). The appearance of two chemically distinct aryl methyl peaks at -43 ppm and -55 ppm, formed from a newly created stereogenic center, is indicative of isomerization to the thermodynamically more stable benzylic iron complex **4.59** formed

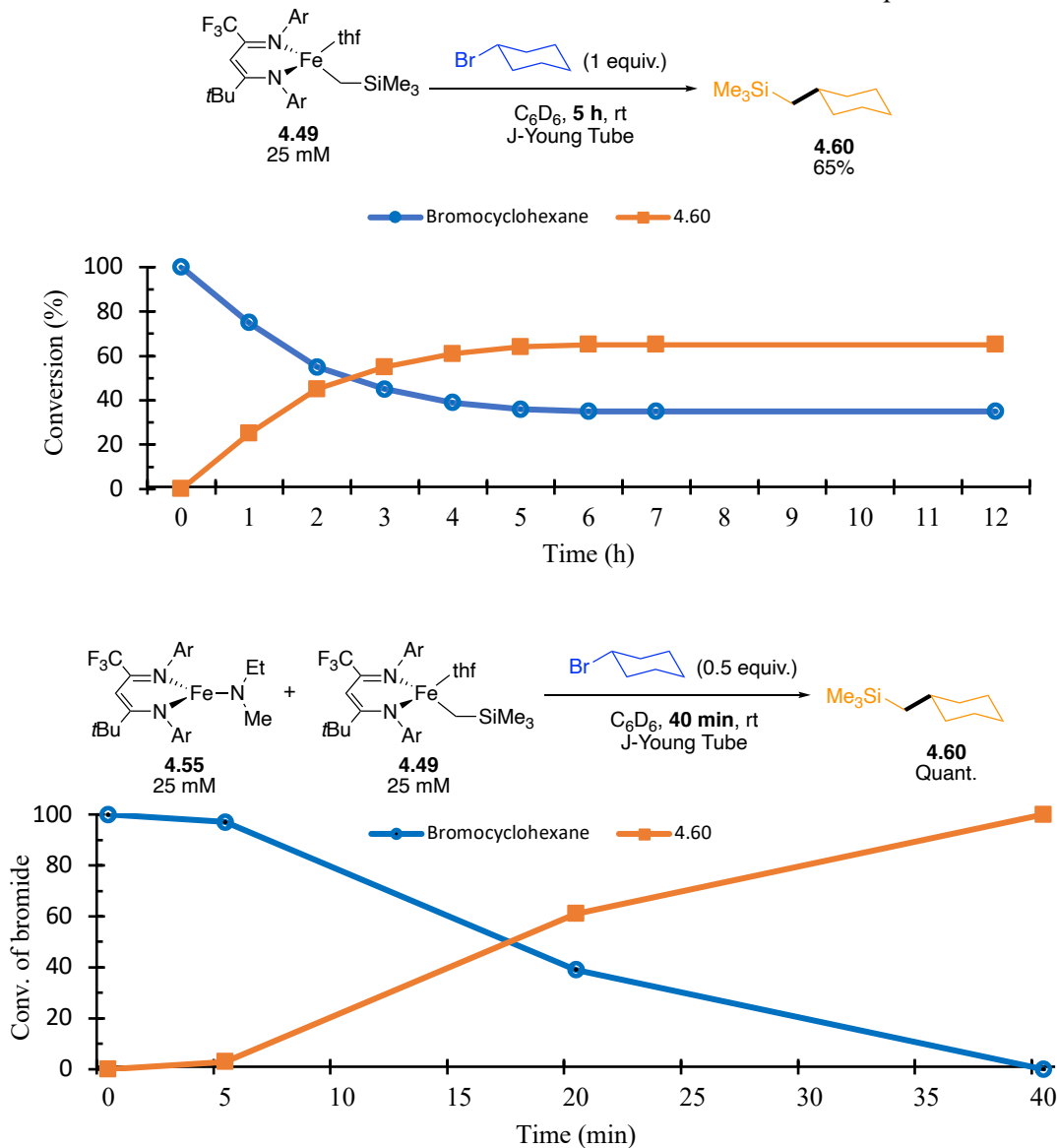
Scheme 4.16: *In situ* observation of iron alkyl complexes with β -hydrogens through a transmetalation route as seen in the $^1\text{H-NMR}$ spectrum.



from chain-walking. This behavior has been reported before by the Holland group with similar β -diketiminate iron alkyl complexes.⁵³ Perhaps more interesting from these findings are that iron alkyl complexes containing β -hydrogens can be synthesized from this transmetalation route, however attempts at isolation have proven unsuccessful so far. It is interesting to note that no isomerized product was seen in the catalytic reactions using alkylborane **4.57**. This outcome suggests cross-coupling is faster than isomerization or that isomerization is reversible and cross-coupling is far slower from **4.59** than from **4.58**.

Having successfully synthesized discrete iron alkyl and iron amido complexes, stoichiometric reactions were carried out to help distinguish between a monometallic or a bimetallic mechanism. From cursory reactions, it was found that iron neopentyl complex **4.51** and iron diethylamide complex **4.54** displayed sluggish stoichiometric reaction kinetics when reacted with alkyl halide and alkylborane respectively (4.18a). Consequently, species **4.51** and **4.54** were not used for further studies. When iron alkyl complex **4.49** was subjected to 1 equivalent of bromocyclohexane in deuterated benzene, the reaction was sluggish, requiring over 5 hours to reach 65% yield of cross-coupled product **4.61** (Scheme 4.17, Scheme 4.18b). However, if a 1:1 mixture of iron alkyl complex **4.49** to iron amido complex **4.55** was reacted with half an equivalent of bromocyclohexane, product **4.61** was produced in nearly quantitative yield within 40 minutes (Scheme 4.17, Scheme 4.18b). These results suggest both mechanisms are catalytically competent but show only the bimetallic mechanism providing kinetically relevant reactivity. Unfortunately, we could not compare the rates of the catalytic reaction

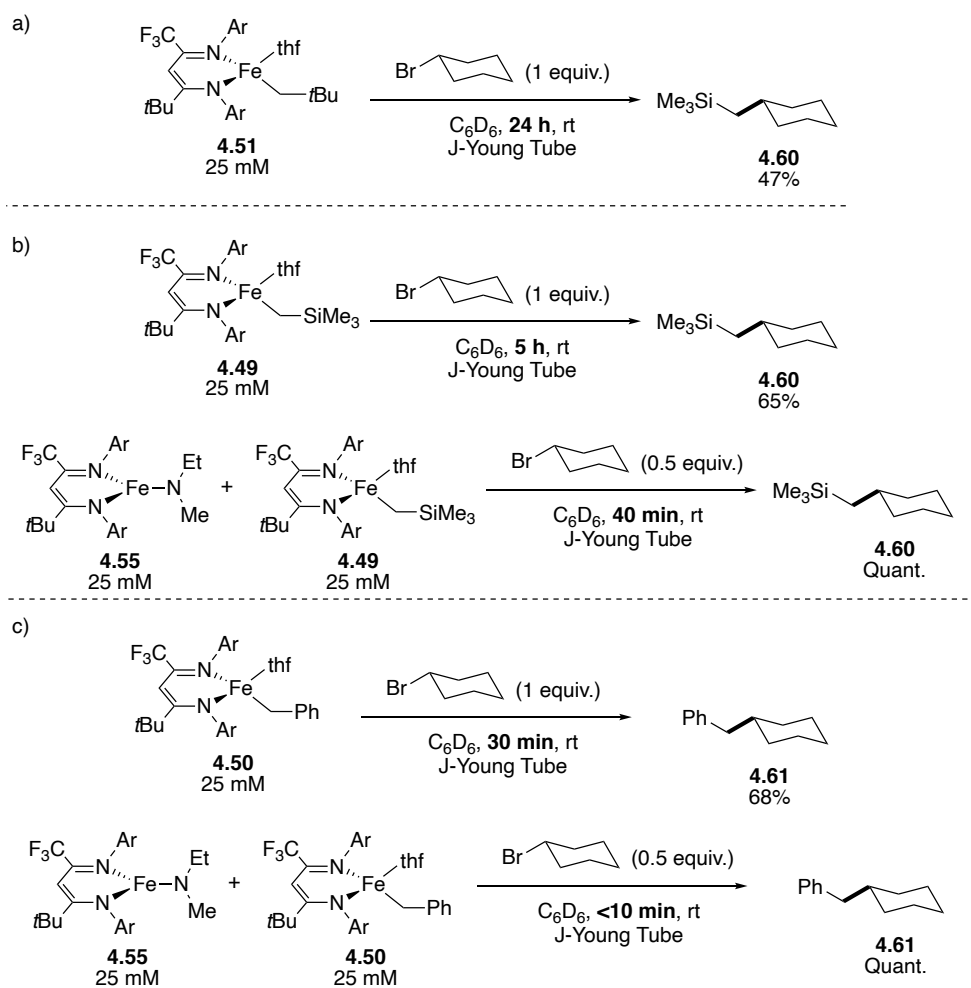
Scheme 4.17: Time course studies of **4.49** with and without iron amido complex **4.55**.



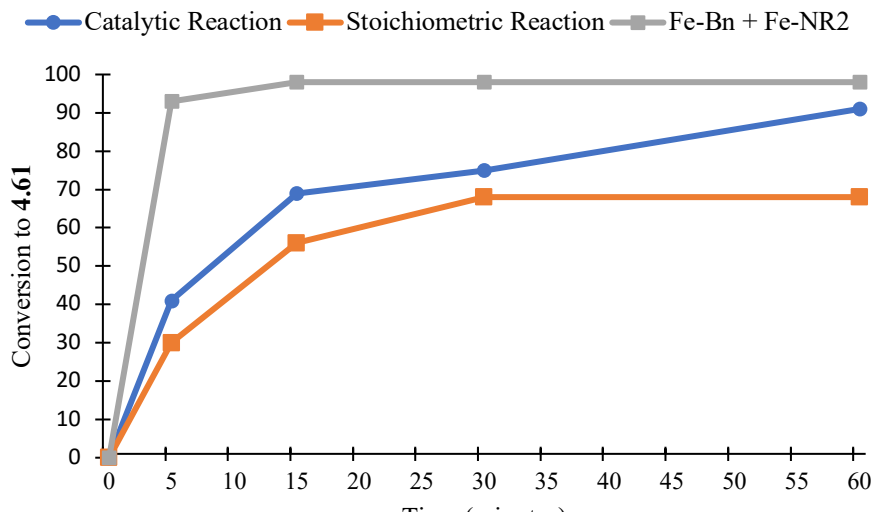
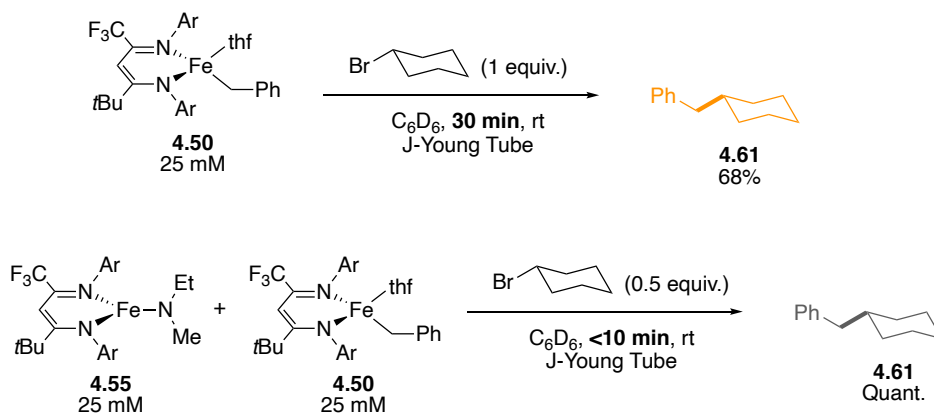
using these two substrates due to the incompatibility of the TMS group and lithium amide. Since the bulky trimethylsilyl group may be slowing down reaction kinetics at a significant rate, less bulky iron benzyl complex **4.50** was used for an identical study. The reaction of iron complex **4.50** with one equivalent of bromocyclohexane yielded benzylcyclohexane (**4.61**) in 68% yield within 30 minutes (Scheme 4.18c, Scheme 4.19). Similar to the

previous reaction, if a 1:1 mixture of iron alkyl complex **4.50** to iron amido complex **4.55** was reacted with half an equivalent of bromocyclohexane, product **4.61** was produced within minutes in quantitative yield (Scheme 4.18c, Scheme 4.19). The results from these stoichiometric reactions provide compelling evidence supportive of a bimetallic mechanism rather than a monometallic mechanism. When comparing the monometallic and bimetallic reaction rates to the catalytic reaction (Scheme 4.19), it is apparent that both reactions are catalytically competent, but only the bimetallic reaction is kinetically relevant. Support for the bimetallic mechanism can also be seen by analyzing the initial

Scheme 4.18: Stoichiometric reactions with iron amido complex **4.55** and a) iron alkyl complex **4.49** and b) iron alkyl complex **4.50**.



Scheme 4.19: Stoichiometric reaction time course studies of **4.50** with (grey trace) and without (orange trace) iron amido complex **4.55**. The catalytic reaction (blue trace) with 13 mol% **4.11** and Bn-9-BBN also shown in graph for comparison of reaction rates.

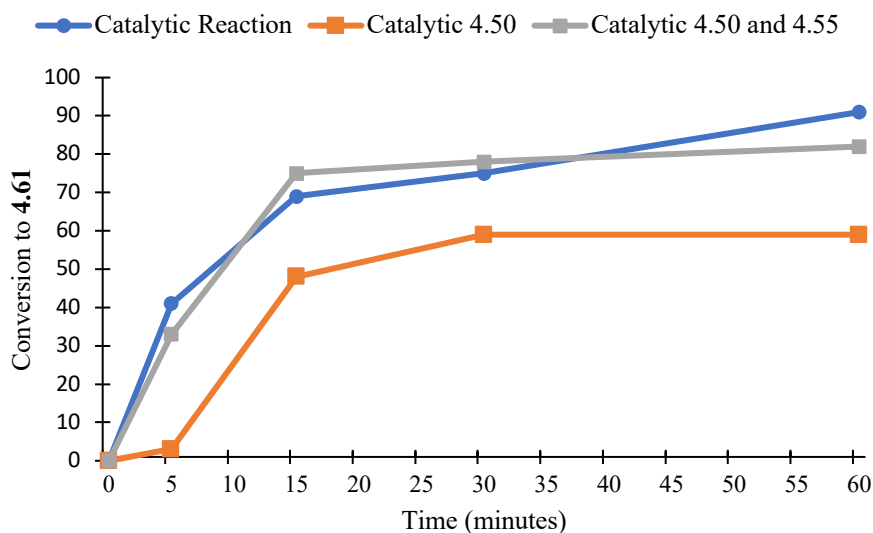
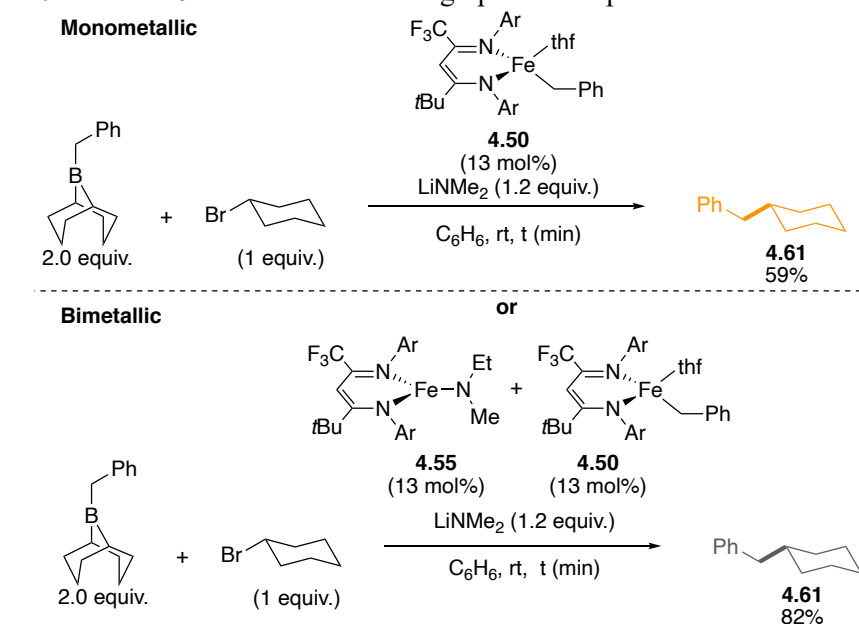


rate kinetics of catalytic reactions using **4.50** and **4.55** at catalytic loadings (Scheme 4.20).

When using catalytic quantities of a 1:1 mixture of **4.50** and **4.55**, the reaction had identical reaction rates as the catalytic reaction using complex **4.11**. However, reactions run with catalytic amounts of **4.50** led to slower reaction rates compared to the catalytic reaction catalyzed by **4.11**, which is also consistent with a bimetallic mechanism. Interestingly, these results also demonstrate the catalytic competency of iron alkyls to carry out cross-coupling at kinetically relevant rates which was not seen with the iron phenyl,⁵² suggestive

of the greater sigma-donation provided by the alkyl ligands to the iron center. A consequence of a bimetallic mechanism is independent catalyst optimization where catalysts could be finely tuned to carry out either halogen abstraction or transmetalation. A bulky catalyst capable of only carrying out halogen abstraction could generate a carbon-centered radical, which could then be intercepted by an iron alkyl species (**II**) formed from

Scheme 4.20: Initial rate kinetics of catalytic reactions using **4.50** with (grey trace) and without (orange trace) iron amido complex **4.55**. The catalytic reaction (blue trace) with 13 mol% **4.11** and Bn-9-BBN also shown in graph for comparison of reaction rates.



transmetalation (see Scheme 4.11). This type of approach would be highly advantageous for developing enantioselective reactions from an operational and economic standpoint, as only one catalyst would have to be chiral.

Conclusion

In conclusion, we have demonstrated the first iron-catalyzed Suzuki-Miyaura system to achieve good to excellent yields of C(sp³)-C(sp³) couplings with a wide array of secondary alkyl halides, particularly with alkyl chlorides, heteroaromatic-containing alkyl halides, methylating agents, and secondary alkyl boranes. In particular we present the first example using cyclobutyl-9-BBN as a coupling partner which holds promise for future development to access a pool of previously unreactive secondary nucleophile coupling partners. We have also demonstrated the use of electrophilic and nucleophilic methylating reagents for Suzuki-Miyaura C(sp³)-C(sp³) cross-coupling reactions. These reactions using an electrophilic methylating reagent remain unprecedented using first-row transition metals and are convenient methods for installing methyl groups in cross-coupling reactions. Guided by mechanistically driven ligand design, the use of a β -diketiminato ligand with one CF₃ and one *t*-Bu group in the backbone was found to provide high yields of cross-coupled product. With this iron complex, the reaction displays improved substrate scope and functional group tolerance. We attribute this feature to the high reactivity of iron catalysts and of the borane reagents, which buffer the reaction. Mechanistic experiments are supportive of a radical mechanism with an irreversible halogen abstraction event as well as stereoablative transmetalation. Additionally, stoichiometric reactions with discrete iron alkyl and iron amido complexes provide compelling evidence for a bimetallic rather than monometallic mechanism. This mechanistic manifold would be highly beneficial for

both independent catalyst optimization and the development of challenging enantioselective C(sp³)-C(sp³) cross-coupling reactions. In the future, improved mechanistic understanding of these processes is intended, which is expected to lead to new reaction development including doubly stereoconvergent C(sp³)-C(sp³) cross-coupling reactions, use of a wider class of secondary alkylboranes and use of unactivated alkylboronic esters as coupling partners.

4.5 Experimental

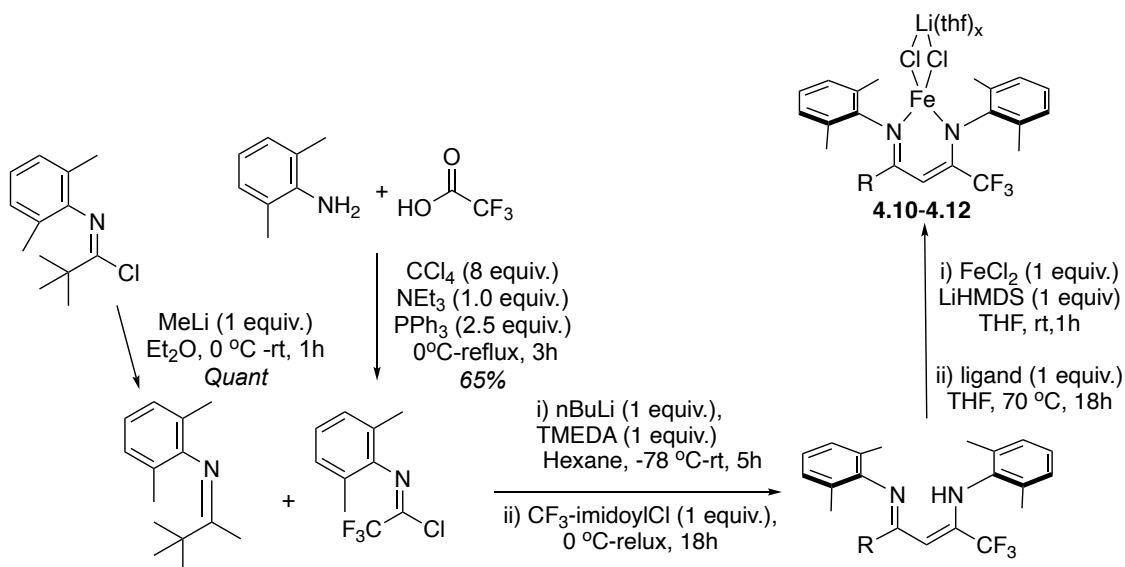
General Considerations. Unless stated otherwise, all reactions were carried out in oven-dried glassware in a nitrogen-filled glovebox or using standard Schlenk-line techniques.⁵⁶ Solvents including dichloromethane, pentane, toluene, diethyl ether, and tetrahydrofuran were purified by passage through two activated alumina columns under a blanket of argon and then degassed by brief exposure to vacuum.⁵⁷ Lithium dimethylamide was purchased from Alfa Aesar and brought into the glovebox immediately. Purchased alkyl halides were dried over calcium hydride for at least 24 hours before being vacuum-distilled, while all solids were dried over P₂O₅ before use in the glovebox. All alkyl halides were purchased from Sigma-Aldrich, Oakwood Chemicals and Fisher Scientific. ¹H, ¹¹B, ¹H}¹³C, and ¹⁹F nuclear magnetic resonance (NMR) spectra were recorded at ambient temperature on Varian VNMRs operating at 400 MHz, 500 MHz, or 600 MHz for ¹H NMR at 160 MHz for ¹¹B NMR, 125 MHz for ¹H}¹³C or 470 MHz for ¹H}¹⁹F NMR. All ¹H}¹³C NMR was collected while broad-band decoupling was applied to the ¹H region. The residual protio solvent impurity was used as an internal reference for ¹H NMR spectra and ¹H}¹³C NMR spectra. Boron trifluoride diethyl etherate was used as an external standard (BF₃·O(C₂H₅)₂: 0.0 ppm) for ¹¹B NMR and ¹H}¹⁹F NMR (BF₃·O(C₂H₅)₂: -153.0 ppm). The line listing for NMR spectra of diamagnetic compounds are reported as follows: chemical shift (multiplicity, coupling constant, integration) while paramagnetic compounds are reported as chemical shift (peak width at half height, number of protons). Solvent suppressed spectra were collected for paramagnetic compounds in THF using the PRESAT macro on the VNMR software. Infrared (IR) spectra were recorded on a Bruker Alpha attenuated total reflectance infrared spectrometer. High-resolution mass spectra

were obtained at the Boston College Mass Spectrometry Facility on a JEOL AccuTOF DART instrument. Single crystal X-ray Intensity data were measured on a Bruker Kappa Apex Duo diffractometer using a high brightness I μ S copper source with multi-layer mirrors. The low temperature device used was an Oxford 700 series Cryostream system with temperature range of 80-400 K. An Olympus SZ1145 stereo zoom microscope was used to view and mount crystals. The crystal structure was solved using ShellX. Cyclic voltammetry was conducted using a CHIInstrument electrochemical analyzer and a 3-electrode configuration, where a glassy carbon rod was used as the working electrode and Pt electrodes used as the counter electrode and reference electrode. 1M N(n-Bu) $_4$ PF $_6$ in THF was used as the electrolyte for cyclic voltammetry measurements.

Synthetic Procedures:

General Preparation of Ligands and Iron Complexes:

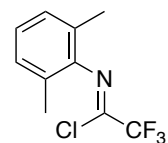
Scheme S1. Synthesis of Ligands and Iron Complexes



General Procedure for Synthesis of Imidoyl Chlorides:

Imidoyl chlorides were synthesized according to a literature procedure.⁵⁸ A two-necked round bottom flask under N₂ equipped with a reflux condenser and a magnetic stir bar was charged with PPh₃ (17.02 g, 2.5 equiv.). CCl₄ (10.42 mL, 4.15 equiv) and anhydrous NEt₃ (3.62 mL, 1.0 equiv) were added and the mixture cooled to 0 °C. Trifluoroacetic acid (2 mL, 1.0 equiv) was added dropwise and the mixture stirred at 0 °C for 10 min. The aniline (3.21 mL, 1.0 equiv) was added dropwise followed by addition of CCl₄ (10.42 mL, 4.15 equiv) and the mixture stirred at 0 °C for 10 min. The cooling bath was replaced with an oil bath and the mixture refluxed for 3 hours. The resulting paste was allowed to cool down to room temperature and residual CCl₄ was removed under reduced pressure at room temperature. The solid was triturated with hexane and the suspension stirred vigorously for 10 min, then filtered over a pad of celite and the solid washed thoroughly with hexane. The solvent was removed under reduced pressure and the crude product purified by Kugelrohr distillation to afford a colorless oil (4.01 g, 65%).

(Z)-N-(2,6-dimethylphenyl)-2,2,2-trifluoroacetimidoyl chloride was prepared according to the general procedure (4 g, 65% Yield). ¹H NMR (500MHz, CDCl₃) δ 2.06 (s, 6H), 7.04 – 7.10 (m, 3H). ¹⁹F NMR (470 MHz, CDCl₃) δ -71.2 ppm. Spectral data match that of literature.⁵⁸



(Z)-N-(2-(*tert*-butyl)phenyl)-2,2,2-trifluoroacetimidoyl chloride was

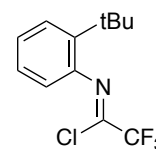
prepared according to the general procedure (6g, 84%). IR (neat) 2961,

1697, 1483, 1219, 1192. ¹H NMR (500MHz, CDCl₃) δ 1.33 (s, 9H), 6.79

– 6.85 (m, 1H), 7.22 – 7.26 (m, 2H), 7.44 – 7.48 (m, 1H). ¹³C NMR (125MHz, CDCl₃)

29.87, 35.27, 115.94, 118.14, 119.89, 126.63, 126.97, 127.36, 141.86, 142.41. ¹⁹F NMR

(470 MHz, CDCl₃) δ -71.8 ppm.



(Z)-N-(2,6-dimethylphenyl)-3,3-dimethylbutan-2-imine. A two-

necked round bottom flask under N₂ with an addition funnel and magnetic stir bar was charged with imidoyl chloride (7g, 31.3 mmol) and dry

diethyl ether (35 mL). The flask was brought to 0°C and MeLi (1.6M, 21.51 mL, 34.4

mmol) was added dropwise. The reaction was allowed to warm to room temperature and

allowed to stir for 1 hour. The reaction was carefully quenched with saturated ammonium

chloride solution and the aqueous phase was washed with diethyl ether (3 x 20 mL). The

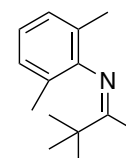
combined organic phases were dried over sodium sulfate and filtered. The solvent was

removed under reduced pressure and the crude product purified by Kugelrohr distillation

to afford a colorless oil (6.36 g, 100%). ¹H NMR (500MHz, CDCl₃) δ 1.28 (s, 9H), 1.62

(s, 3H), 1.96 (s, 6H), 6.84 (t, *J* = 7.5 Hz, 1H), 6.96 – 7.01 (m, 2H). Spectral data match that

of literature.⁵⁹



General Procedure for the Synthesis of β-diketiminate Ligands:

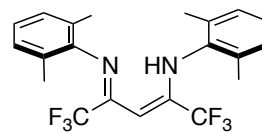
Ligands were synthesized according to a literature procedure.⁵⁹ A two-necked round

bottom flask under N₂ equipped with a reflux condenser and a magnetic stir bar was

charged with dry hexane (10 mL), imine (1.16g, 1 equiv.) and TMEDA (853 uL, 1 equiv.) The reaction was brought to -78°C before dropwise addition of BuLi (2.05 M, 2.77 mL, 1 equiv.). The reaction was allowed to warm to room temperature and stirred for 5 hours. A hexane solution (5 mL) of imidoyl chloride (1.5 g, 1 equiv.) was added dropwise and the reaction refluxed overnight. The reaction was carefully quenched with saturated ammonium chloride solution and the aqueous phase was washed with hexane (3 x 20 mL). The combined organic phases were dried over sodium sulfate and filtered. The solvent was removed under reduced pressure. The yellow oil was dissolved in minimal hexane and a large excess of methanol was added to the flask. Solvent was partially evaporated and product was collected on a frit as a fine yellow powder (1.01 g, 40%).

Synthesis of 1,1,1,5,5,5-hexafluoro-2,4-bis[(2,6-dimethylphenyl)imino]pentane (4.5a)

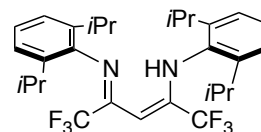
Synthesized according to an alternate literature procedure⁶⁰ using 2,6-dimethylaniline (10.28 g, 84.84 mmol) and 1,1,1,5,5,5-



hexafluoro-2,4-pentanedione (1.88 mL, 14.14 mmol) and afforded the product as a yellow crystalline solid (2.6 g, 44% yield). ¹H NMR (500 MHz, CDCl₃) δ 2.16 (s, 12H), 5.89 (s, 1H), 7.08 – 7.00 (m, 6H), 11.87 (s, 1H). ¹⁹F NMR (470 MHz, CDCl₃) δ -67.7 ppm. NMR spectra are in agreement with literature precedence.⁶⁰

Synthesis of 1,1,1,5,5,5-hexafluoro-2,4-bis[(2,6-diisopropylphenyl)imino]pentane (4.9a).

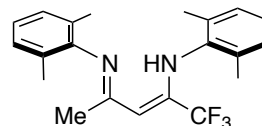
Synthesized according to an alternate literature procedure⁶⁰ using 2,6-diisopropylaniline (15.04 g, 84.84 mmol)



and 1,1,1,5,5,5-hexafluoro-2,4-pentanedione (1.88 mL, 14.14 mmol) and afforded the

product as a yellow crystalline solid (4.0 g, 53% yield). ^1H NMR (500 MHz, CDCl_3) δ 1.11 (d, $J = 6.9$ Hz, 12H), 1.23 (d, $J = 6.8$ Hz, 12H), 5.81 (s, 1H), 7.13 (d, $J = 7.0$ Hz, 4H), 7.20 (dd, $J = 8.6, 6.7$ Hz, 2H), 11.21 (s, 1H). ^{19}F NMR (470 MHz, CDCl_3) δ -65.5 ppm. NMR spectrum is in agreement with literature precedence.⁶⁰

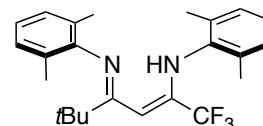
1,1,1-trifluoro-2,4-bis-[(2,6-dimethylphenyl)imino]pentane (4.10a) was synthesized according to the general procedure using *N*-phenylpropan-2-imine (*Z*)-*N*-(2,6-dimethylphenyl)-2-imine (0.5 g, 3.1 mmol)



and (*Z*)-*N*-(2-(*tert*-butyl)phenyl)-2,2,2-trifluoroacetimidoyl chloride (730 mg, 3.1 mmol) to yield a yellow solid (0.60 g, 53%). IR (neat) 2920, 1615, 1546, 1503, 1269, 1138, 1084; ^1H NMR (500MHz, CDCl_3) δ 1.82 (s, 3H), 2.17 (d, $J = 7.3$ Hz, 12H), 5.38 (s, 1H), 6.95 (dd, $J = 8.3, 6.6$ Hz, 1H), 7.00 – 7.12 (m, 5H), 12.16 (s, 1H). ^{13}C NMR (125MHz, CDCl_3) δ 18.37, 18.41, 89.49 (q, $J = 4.3$ Hz), 119.42 (q, $J = 285.5$ Hz), 124.34, 127.54, 128.24, 130.75, 132.83, 140.88, 143.65, 149.99 (q, $J = 27.7$ Hz), 162.88. ^{19}F NMR (470 MHz, CDCl_3) δ -67.6 ppm; HRMS (ESI) m/z $[\text{M}]^+$ calcd. for $\text{C}_{21}\text{H}_{23}\text{F}_3\text{N}_2$ 361.1889; found 360.1186.

1,1,1-trifluoro-5,5,5-trimethyl-2,4-bis[(2,6-dimethylphenyl)imino]pentane (4.11a)

was synthesized according to the general procedure using (*Z*)-*N*-(2,6-dimethylphenyl)-3,3-dimethylbutan-2-imine (1.9 g, 9.3

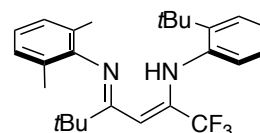


mmol) and (*Z*)-*N*-(2,6-dimethylphenyl)-2,2,2-trifluoroacetimidoyl chloride (2 g, 8.5 mmol) to yield a yellow solid (2.2 g, 64%). IR (neat) 2955, 1636, 1566, 1499, 1465, 1300, 1175, 1132; ^1H NMR (500MHz, CDCl_3) 1.13 (s, 9H), 2.17 (d, $J = 11.9$ Hz, 12H), 5.64 (s, 1H),

6.90 (t, $J = 7.5$ Hz, 1H), 6.96 – 7.06 (m, 5H), 12.15 (s, 1H). ^{13}C NMR (125MHz, CDCl_3) 18.49, 19.03, 29.66, 41.50, 90.12, 120.43 (q, $J = 279$ Hz), 123.44, 125.84, 127.67, 127.71, 128.52, 134.70, 140.08, 145.93, 146.37 (q, $J = 28.2$ Hz), 172.93. ^{19}F NMR (470 MHz, CDCl_3) δ -66.9 ppm; HRMS (ESI) m/z $[\text{M}]^+$ calcd. for $\text{C}_{24}\text{H}_{29}\text{F}_3\text{N}_2$ 402.2356; found 402.2346.

1,1,1-trifluoro-5,5,5-trimethyl-2-[(2,6-dimethylphenylimino)]-4-[(2-

tertbutylphenylimino)]pentane (4.12a) was synthesized



according to the general procedure using (*Z*)-*N*-(2,6-

dimethylphenyl)-3,3-dimethylbutan-2-imine (1.2 g, 5.7 mmol) and (*Z*)-*N*-(2-(*tert*-

butyl)phenyl)-2,2,2-trifluoroacetimidoyl chloride (1.5 g, 5.7 mmol) to yield a yellow solid

(1.0 g, 40%). IR (neat) 2959, 1608, 1558, 1478, 1345, 1173, 1112; ^1H NMR (500MHz,

CDCl_3) δ 1.12 (s, 9H), 1.29 (s, 9H), 2.10 (s, 6H), 5.72 (s, 1H), 6.83 – 6.90 (m, 2H), 6.94

(d, $J = 7.5$ Hz, 2H), 7.06 (t, $J = 7.2$ Hz, 1H), 7.11 (d, $J = 7.7$ Hz, 1H), 7.33 (dd, $J = 8.0, 1.6$

Hz, 1H), 12.37 (s, 1H). ^{13}C NMR (125MHz, CDCl_3) δ 18.96, 28.46, 29.69, 29.81, 30.54,

35.31, 40.95, 93.54, 118.62, 119.46, 122.28, 123.95, 124.95, 125.37, 125.90, 126.28,

126.56, 127.70, 127.89, 128.45, 129.52, 142.26, 142.60, 144.66, 145.67 (d, $J = 27.3$ Hz),

172.44. ^{19}F NMR (470 MHz, CDCl_3) δ -61.1 ppm; HRMS (ESI) m/z $[\text{M}]^+$ calcd. for

$\text{C}_{26}\text{H}_{33}\text{F}_3\text{N}_2$ 430.2664; found 430.2669.

Synthesis of **2,4-bis[(2,6-methylphenyl)imino]pentane iron chloride complex (4.4)**. To

an oven-dried round-bottom flask equipped with stirbar was added

2,4-bis[(2,6-dimethylphenyl)imino]pentane (3.0 g, 9.8 mmol) and

pentane (40 mL, 0.244 M). On the Schlenk line, the mixture was

cooled to -78 °C and degassed by placing the solution under

vacuum for at least 5 minutes. A solution of butyl lithium in hexanes (22.5 mL, 2.3 M, 9.8

mmol) was added dropwise while stirring. In most cases, a white precipitate formed

rapidly. The reaction mixture was warmed to room temperature while stirring before the

solvent was removed under vacuum. The sealed reaction vessel was transferred into a

glovebox, where the solid was collected on a frit and washed with cold pentane (5 mL at -

40 °C). The solid was dried and weighed to determine stoichiometry for the next step. No

characterization of the lithium salts of the ligand were carried out. The collected

deprotonated ligand (9.8 mmol) was then dissolved in THF (10 mL) in a 20 mL scintillation

vial. This solution was added dropwise to a slurry of iron dichloride (9.8 mmol) in THF

(10 mL) prepared in a separate scintillation vial equipped with stir bar. This mixture was

allowed to stir overnight. The resulting solution was cooled and passed through celite

which was washed with additional THF (~10 mL), then concentrated under vacuum. The

resulting semi-solid was then washed with pentane, dried, and collected to afford a yellow

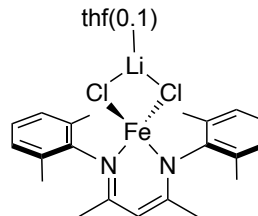
crystalline solid (3.3 g, 58% yield). ¹H NMR (400 MHz, THF) δ -68.7 (*w*_{1/2} = 180 Hz, 6H),

-52 (*w*_{1/2} = 100 Hz, 2H), -39.7 (*w*_{1/2} = 264 Hz, 1H), 6.1 (*w*_{1/2} = 254 Hz, 12H), 16.1 (*w*_{1/2} =

82 Hz, 4H) ppm. IR: 2916, 1519, 1373, 1038, 760 cm⁻¹. Elemental analysis for

C₂₁H₂₅ClFeN₂•(LiCl)(C₄H₈O)_{0.1} calc'd C 66.09% H 6.69% N 37.20% Found C 55.71% H

5.69% N 6.06%. NMR spectrum is in agreement with literature precedence.³ Elemental



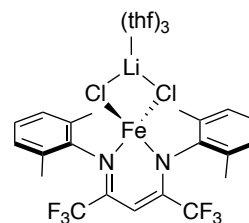
analysis of the following iron complexes revealed samples with C, H, and N ratios that match what would be expected for the desired complexes containing variable amounts of LiCl and THF. This difficulty has been observed previously in the purification of similar complexes.³⁶

General Procedure for the Synthesis of fluorinated β -diketiminate Iron Chloride Complexes:

In the glovebox, to an oven-dried 40 mL vial with stir bar was added FeCl₂ (432 mg, 1 equiv.) to THF (30 mL) followed by LiHMDS (570 mg, 1 equiv.). The reaction was allowed to stir for 1 hour before addition of the ligand (1.37 g, 1 equiv.) as a solid. The reaction was then heated to 70 °C for 18 hours. The solution was filtered through a pad of celite and solvent removed under reduced pressure to yield a colored solid which was recrystallized in pentane at -30 °C. Elemental analysis of the following iron complexes revealed samples with C, H, and N ratios that match what would be expected for the desired complexes containing variable amounts of LiCl and THF. This difficulty has been observed previously in the purification of similar complexes.³⁶

1,1,1,5,5,5-hexafluoro-2,4-bis[(2,6-dimethylphenyl)imino]pentane iron chloride

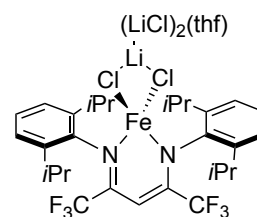
complex (4.5) was synthesized according to the general procedure using 1,1,1,5,5,5-hexafluoro-2,4-bis[(2,6-dimethylphenyl)imino]pentane (1.50 g, 3.62 mmol) LiHMDS (606 mg, 3.62 mmol) and FeCl₂ (459 mg, 3.62 mmol) to yield a purple-red powder (1 g, 40%). IR: 1564, 1173, 1136, 769 cm⁻¹. ¹H NMR (500 MHz, THF)



δ -76.7 ($w_{1/2}$ = 445 Hz, 1H), -53.9 ($w_{1/2}$ = 89 Hz, 2H), 15.5 ($w_{1/2}$ = 356 Hz, 12H), 18.7 ($w_{1/2}$ = 760 Hz, 4H). ^{19}F NMR (470 MHz, THF) δ -205.9 ppm. IR: 1564,1173,1136,769 cm^{-1} . Elemental analysis for $\text{C}_{21}\text{H}_{19}\text{ClF}_6\text{FeN}_2 \cdot (\text{LiCl})(\text{C}_4\text{H}_8\text{O})_{2.08}$ calc'd C 50.52% H 5.15% N 4.02% Found C 49.27% H 5.03% N 3.88%. NMR spectrum is in agreement with literature precedence.³

1,1,1,5,5,5-hexafluoro-2,4-bis[(2,6-diisopropylphenyl)imino]pentane iron chloride complex (4.9) was synthesized according to the general

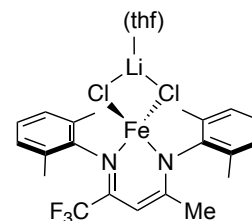
procedure using 1,1,1,5,5,5-hexafluoro-2,4-bis[(2,6-diisopropylphenyl)imino]pentane (2.00 g, 3.80 mmol) LiHMDS



(636 mg, 3.80 mmol) and FeCl_2 (481 mg, 3.80 mmol) to yield a purple-red powder (1.5 g, 49%). IR (neat) 2959, 1439, 1290, 1218, 1170, 1122. ^1H NMR (500 MHz, THF) δ -75.24 ($w_{1/2}$ = 333 Hz, 1H), -42.33 ($w_{1/2}$ = 70 Hz, 3H), -21.21 ($w_{1/2}$ = 951 Hz, 3H), -10.77 ($w_{1/2}$ = 179 Hz, 16 H), 1.24 ($w_{1/2}$ = 77 Hz, 6H), 16.50 ($w_{1/2}$ = 63 Hz, 6H). ^{19}F NMR (470 MHz, THF) δ -191.7 ppm. IR: 2959, 1440, 1290, 1171, 1122, 1039, 774 cm^{-1} . Elemental analysis for $\text{C}_{29}\text{H}_{35}\text{ClFeF}_6 \text{N}_2 \cdot (\text{LiCl})_2(\text{THF})$ calc'd: C, 51.22%; H, 5.60%; N 3.62%. Found: C, 51.01%, H, 5.94%, N 3.09%.

1,1,1-trifluoro-2,4-bis-[(2,6-dimethylphenyl)imino]pentane iron chloride complex

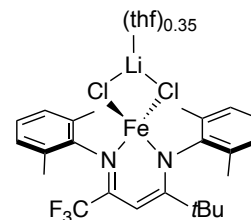
(4.10) was synthesized according to the general procedure using 1,1,5,5,5-hexafluoro-2,4-bis[(2,6-dimethylphenyl)imino]pentane (410 mg, 1.14 mmol) LiHMDS (190 mg, 1.14 mmol) and FeCl_2 (144 mg, 1.14 mmol) to yield a bright orange solid (650 mg,



90%). ^1H NMR (500 MHz, THF) δ -92.2 ($w_{1/2}$ = 197.6 Hz, 3H), -57.3 ($w_{1/2}$ = 87.0 Hz, 1H), -50.1 ($w_{1/2}$ = 495.4 Hz, 1H), -49.0 ($w_{1/2}$ = 86.9 Hz, 1H), 7.8 ($w_{1/2}$ = 310.0 Hz, 6H), 11.0 ($w_{1/2}$ = 312.0 Hz, 6H), 15.9 ($w_{1/2}$ = 75.2, 2H), 17.3 ($w_{1/2}$ = 75.2 Hz, 2H). ^{19}F NMR (470 MHz, THF) δ -120.2 ppm. IR: 2977, 1533, 1427, 1296, 1223, 1168, 1132, 1044, 768 cm^{-1} . Elemental analysis for $\text{C}_{21}\text{H}_{22}\text{ClFeF}_3\text{N}_2 \cdot (\text{LiCl})(\text{THF})$ calc'd: C, 53.13%; H, 5.14%; N 5.00%. Found: C, 52.14%, H, 5.71%, N 3.99%. Elemental analysis of the following iron complexes revealed samples with C, H, and N ratios that match what would be expected for the desired complexes containing variable amounts of LiCl and THF. This difficulty has been observed previously in the purification of similar complexes.³⁶

1,1,1-trifluoro-5,5,5-trimethyl-2,4-bis[(2,6-dimethylphenyl)imino]pentane iron

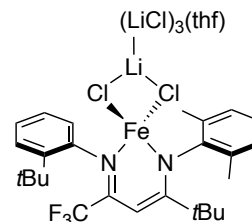
chloride complex (4.11) was synthesized according to the general procedure using 1,1,1-trifluoro-5,5,5-trimethyl-2,4-bis[(2,6-dimethylphenyl)imino]pentane (1.37 g, 3.41 mmol), LiHMDS (570 mg, 3.41 mmol) and FeCl_2 (432 mg, 3.41 mmol)



to yield an orange-yellow powder (1.5 g, 64%). IR (neat) 2959, 1441.1293, 1169, 1129. ^1H NMR (500 MHz, THF) δ -71.2 ($w_{1/2}$ = 112.9, 1H), -57.2 ($w_{1/2}$ = 86.5 Hz, 1H), -53.8 ($w_{1/2}$ = 525.1 Hz, 1H), 9.83 ($w_{1/2}$ = 120.8 Hz, 9H), 13.6 ($w_{1/2}$ = 331.6 Hz, 6Hf), 19.0 ($w_{1/2}$ = 70.9 Hz, 2H), 22.0 ($w_{1/2}$ = 366.13, 8H). ^{19}F NMR (470 MHz, THF) δ -152.2 ppm; IR: 2978, 1557, 1428, 1294, 1167, 1134, 1042, 768 cm^{-1} . Elemental analysis for $\text{C}_{24}\text{H}_{28}\text{F}_3\text{N}_2 \cdot (\text{LiCl})(\text{THF})_{0.35}$ calc'd: C, 54.45%; H, 5.55%; N 4.99%. Found: C, 54.45%, H, 6.06%, N, 4.18%.

1,1,1-trifluoro-5,5,5-trimethyl-2-[(2,6-dimethylphenylimino)]-4-[(2-tertbutylphenylimino)]pentane iron chloride complex (4.12)

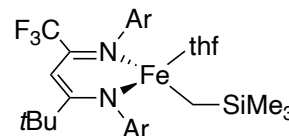
was synthesized according to the general procedure using 1,1,1-trifluoro-5,5,5-trimethyl-2-[(2,6-dimethylphenylimino)]-4-[(2-tertbutylphenylimino)]pentane (500 mg, 1.16 mmol), LiHMDS



(570 mg, 1.16 mmol) and FeCl₂ (147 mg, 1.16 mmol) to yield a orange-yellow powder (800 mg, 97%). IR (neat) 2955, 1549, 1422, 1299, 1226, 1166, 1133. ¹H NMR (500 MHz, THF) δ -70.0 (*w*_{1/2} = 78.2 Hz, 1H), -55.4 (*w*_{1/2} = 66.2 Hz, 1H), -5.2 (*w*_{1/2} = 359.6 Hz, 9H), -0.53 (*w*_{1/2} = 18.6 Hz, 4H), 8.1 (*w*_{1/2} = 254.6 Hz, 2H), 10.2 (*w*_{1/2} = 95.8 Hz, 9H), 18.4 (*w*_{1/2} = 39.1, 1H), 20.5 (*w*_{1/2} = 51.0 Hz, 1H), 21.3 (*w*_{1/2} = 57.7, 1H), 21.6 (*w*_{1/2} = 45.7 Hz, 1H), 27.1 (*w*_{1/2} = 345.2 Hz, 2H). ¹⁹F NMR (470 MHz, THF) δ -120.2 ppm; IR: 2977, 1533, 1427, 1296, 1168, 1132, 1044, 768 cm⁻¹. Elemental analysis for C₂₆H₃₂ClFeN₂F₃•(LiCl)₃(THF) calc'd: C, 50.04%; H, 5.60%; N 3.89%. Found: C, 50.65%, H, 5.95%, N 3.60%.

1,1,1-trifluoro-5,5,5-trimethyl-2,4-bis[(2,6-dimethylphenyl)imino]pentane CH₂TMS tetrahydrofuran adduct (4.49). In the glovebox, to a 7 mL scintillation vial equipped with

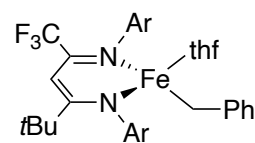
magnetic stir bar was added 1,1,1-trifluoro-5,5,5-trimethyl-2,4-bis[(2,6-dimethylphenyl)imino]pentane iron chloride complex



(4.11) (477 mg, 0.850 mmol) and pentane (4 mL). This mixture was allowed to cool to -40 °C in the freezer. A solution of LiCH₂TMS (80 mg, 1.0 equiv) in pentane (1 mL) was added to the stirring reaction mixture. The reaction vessel was sealed and the reaction turned dark red immediately. The reaction was allowed to stir for 2 hour, at which point the precipitate

was filtered off through celite and the filtrate concentrated in vacuo. The residue was dissolved in minimal hexane and transferred to a vial to recrystallize in the freezer overnight. The mother liquor was decanted to afford the product as a red/black solid (480 mg, 91% yield). ^1H NMR (500 MHz, C_6D_6) δ 39.52 ($w_{1/2}$ = 442 Hz, 9H), 26.86 ($w_{1/2}$ = 168 Hz, 9H), -7.45 ($w_{1/2}$ = 88 Hz, 2H), -51.55 ($w_{1/2}$ = 639 Hz, 6H), -57.39 ($w_{1/2}$ = 626 Hz, 6H), -83.50 ($w_{1/2}$ = 128 Hz, 1H), -98.56 ($w_{1/2}$ = 1533 Hz, 1H). ^{19}F NMR (470 MHz, THF) δ -18-89 ppm; IR: 2949, 1558, 1428, 1296, 1138, 1090 cm^{-1} . Elemental analysis for $\text{C}_{32}\text{H}_{47}\text{N}_2\text{FeSiOF}_3$ calc'd C 62.33% H 7.68% N 4.54% Found C 55.73% H 6.38% N 4.69%. Elemental analysis of the following iron complexes revealed samples with C, H, and N ratios that match what would be expected for the desired complexes containing variable amounts of LiCl and THF. This difficulty has been observed previously in the purification of similar complexes.³⁶

1,1,1-trifluoro-5,5,5-trimethyl-2,4-bis[(2,6-dimethylphenyl)imino]pentane iron benzyl tetrahydrofuran adduct (4.50). In the glovebox, to a 7 mL scintillation vial equipped with magnetic stir bar was added 1,1,1-trifluoro-5,5,5-trimethyl-2,4-bis[(2,6-dimethylphenyl)imino]pentane

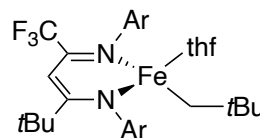


iron chloride complex (**4.11**) (105 mg, 0.155 mmol) and pentane (2 mL). This mixture was allowed to cool to -40 $^{\circ}\text{C}$ in the freezer. A solution of benzyl potassium (KBn) (26 mg, 1.3 equiv) in pentane (1 mL) was added to the stirring reaction mixture. The reaction vessel was sealed and the reaction turned dark red immediately. The reaction was allowed to stir for 1 hour, at which point the precipitate was filtered off through celite and the filtrate concentrated in vacuo. The residue was dissolved in minimal hexane and transferred to a

vial to recrystallize in the freezer overnight. The mother liquor was decanted to afford the product as a black solid (50 mg, 52% yield). ^1H NMR (500 MHz, C_6D_6) δ 33.99 ($w_{1/2} = 91$ Hz, 2H), 16.39 ($w_{1/2} = 170$ Hz, 9H), 13.75 ($w_{1/2} = 95$ Hz, 2H), 6.69 ($w_{1/2} = 92$ Hz, 2H), -16.70 ($w_{1/2} = 798$ Hz, 6H), -19.56 ($w_{1/2} = 1047$ Hz, 1H), -48.31 ($w_{1/2} = 176$ Hz, 1H), -69.81 ($w_{1/2} = 406$ Hz, 1H), -86.62 ($w_{1/2} = 228$ Hz, 1H), -87.61 ($w_{1/2} = 206$ Hz, 1H). ^{19}F NMR (470 MHz, THF) δ -92.9 ppm; IR: 2957, 1554, 1426, 1292, 1132, 1091 cm^{-1} . Elemental analysis for $\text{C}_{35}\text{H}_{43}\text{N}_2\text{FeOF}_3$ calc'd C 67.74% H 6.98% N 4.51% Found C 57.42% H 5.90% 74.16%. Elemental analysis of the following iron complexes revealed samples with C, H, and N ratios that match what would be expected for the desired complexes containing variable amounts of LiCl and THF. This difficulty has been observed previously in the purification of similar complexes.³⁶

1,1,1-trifluoro-5,5,5-trimethyl-2,4-bis[(2,6-dimethylphenyl)imino]pentane neopentyl tetrahydrofuran adduct (4.51). In the glovebox, to a 7 mL scintillation vial equipped with

magnetic stir bar was added 1,1,1-trifluoro-5,5,5-trimethyl-2,4-bis[(2,6-dimethylphenyl)imino]pentane iron chloride

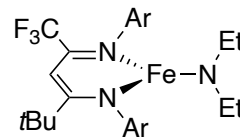


complex (**4.11**) (100 mg, 0.147 mmol) and pentane (2 mL). This mixture was allowed to cool to -40 $^{\circ}\text{C}$ in the freezer. A solution of LiCH_2tBu (11.49 mg, 1.0 equiv) in pentane (1 mL) was added to the stirring reaction mixture. The reaction vessel was sealed and the reaction turned dark red immediately. The reaction was allowed to stir for 1 hour, at which point the precipitate was filtered off through celite and the filtrate concentrated in vacuo. The residue was dissolved in minimal pentane and transferred to a vial to recrystallize in the freezer overnight. The iron complex would not recrystallize so was isolated as a viscous

dark red oil/solid (40 mg, 51% yield). ^1H NMR (500 MHz, C_6D_6) δ 105.09 ($w_{1/2} = 974$ Hz, 9H), 29.84 ($w_{1/2} = 170$ Hz, 9H), 3.74 ($w_{1/2} = 170$ Hz, 2H), -1.09 ($w_{1/2} = 90$ Hz, 2H), -12.71 ($w_{1/2} = 67$ Hz, 2H), -66.43 ($w_{1/2} = 651$ Hz, 6H), -73.10 ($w_{1/2} = 588$ Hz, 6H), -90.75 ($w_{1/2} = 105$ Hz, 2H), -106.94 ($w_{1/2} = 139$ Hz, 1H). ^{19}F NMR (470 MHz, THF) δ -5.48 ppm; IR: 2957, 1554, 1426, 1292, 1132, 1091 cm^{-1} . Elemental analysis was not obtained due to troubles transferring the viscous oil to an ampoule for flame sealing.

1,1,1-trifluoro-5,5,5-trimethyl-2,4-bis[(2,6-dimethylphenyl)imino]pentane iron *N,N*-diethylamide (4.54). In the glovebox, to a 20 mL scintillation vial

equipped with magnetic stir bar was added 1,1,1-trifluoro-5,5,5-trimethyl-2,4-bis[(2,6-dimethylphenyl)imino]pentane CH_2TMS

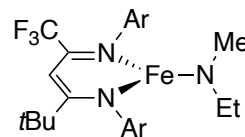


tetrahydrofuran adduct (**4.46**) (111 mg, 0.180 mmol) and pentane (2 mL). To this mixture was added diethylamine (18.6 μL , 1.0 equiv). The resulting mixture was allowed to stir overnight, turning from dark red to purple. The pentane was removed in vacuo and the residue dissolved in minimal hexane and transferred to a vial to recrystallize in the freezer overnight to afford the product as a dark purple solid (40 mg, 41% yield). ^1H NMR (500 MHz, C_6D_6) δ 51.16 ($w_{1/2} = 968$ Hz, 6H), 45.55 ($w_{1/2} = 805$ Hz, 1H), 23.92 ($w_{1/2} = 278$ Hz, 9H), 5.33 ($w_{1/2} = 219$ Hz, 2H), -1.20 ($w_{1/2} = 201$ Hz, 2H), -40.38 ($w_{1/2} = 687$ Hz, 6H), -43.80 ($w_{1/2} = 653$ Hz, 6H), -76.67 ($w_{1/2} = 224$ Hz, 1H), -98.44 ($w_{1/2} = 291$ Hz, 1H), -87.61 ($w_{1/2} = 206$ Hz, 1H). ^{19}F NMR (470 MHz, THF) δ -106.75 ppm; IR: 2957, 1554, 1426, 1292, 1132, 1091 cm^{-1} . Elemental analysis for $\text{C}_{28}\text{H}_{38}\text{N}_3\text{FeF}_3$ calc'd C 63.52% H 7.23% N 7.94% Found C 60.33% H 6.85% N 7.00%. Elemental analysis of the following iron complexes revealed samples with C, H, and N ratios that match what would be

expected for the desired complexes containing variable amounts of LiCl and THF. This difficulty has been observed previously in the purification of similar complexes.³⁶

1,1,1-trifluoro-5,5,5-trimethyl-2,4-bis[(2,6-dimethylphenyl)imino]pentane iron *N,N*-methylethylamide (4.55). In the glovebox, to a 20 mL

scintillation vial equipped with magnetic stir bar was added 1,1,1-



trifluoro-5,5,5-trimethyl-2,4-bis[(2,6-dimethylphenyl)imino]pentane

CH₂TMS

tetrahydrofuran adduct (**4.46**) (135 mg, 0.219 mmol) and pentane (2 mL). To this mixture was added methylethylamine (18.8 μ L, 1.0 equiv). The resulting mixture was allowed to stir overnight, turning from dark red to purple. The pentane was removed in vacuo and the residue dissolved in minimal hexane and transferred to a vial to recrystallize in the freezer overnight to afford the product as a dark purple solid (60 mg, 53% yield). ¹H NMR (500 MHz, C₆D₆) δ 51.27 ($w_{1/2}$ = 1106 Hz, 3H), 21.49 ($w_{1/2}$ = 248 Hz, 9H), -33.16 ($w_{1/2}$ = 1009 Hz, 6H), -37.73 ($w_{1/2}$ = 1036 Hz, 6H), -74.94 ($w_{1/2}$ = 273 Hz, 1H), -96.49 ($w_{1/2}$ = 483 Hz, 1H). ¹⁹F NMR (470 MHz, THF) δ -116.33 ppm; IR: 2957, 1554, 1426, 1292, 1132, 1091 cm⁻¹. Elemental analysis for C₂₇H₃₆N₃FeF₃ calc'd C 62.92% H 7.04% N 8.15% Found C 57.62% H 6.50% 6.56%. Elemental analysis of the following iron complexes revealed samples with C, H, and N ratios that match what would be expected for the desired complexes containing variable amounts of LiCl and THF. This difficulty has been observed previously in the purification of similar complexes.³⁶

Synthesis of Steroid Precursors:

(5R)-5-((3R,8R,9S,10S,13R,14S,17R)-3-((tert-butyldimethylsilyl)oxy)-10,13-

dimethylhexadecahydro-1H-cyclopenta[a]phenanthren-17-yl)hexan-2-ol (4.37). To a

2 neck 50-mL round-bottom flask with stir bar under

N₂ charged with mercuric acetate (1.30 g, 4.08

mmol) in THF (10 mL) and deionized water (10

mL) was added a THF solution of (6mL) (1'',1''-dimethylethyl)dimethyl{[(3 α)-20-(1'-

buten-4'-yl)pregnan-3-yl]oxy}silane (2e) and 20-(1'-buten-4'-yl)pregnane⁶¹ (1.93 g, 4.08

mmol) dropwise at room temperature. The slurry turned from clear to orange upon

addition and the reaction was allowed to for 3 hours for the yellow color to dissipate. The

reaction mixture was alkalinized with sodium hydroxide (3 M, 4.08 mL) followed by an

aqueous solution of sodium borohydride (0.5 M, 16.30 mL). After 1 hour the reaction

mixture was saturated with NaCl, the organic layer separated, and the aqueous layer was

further extracted with EtOAc (4 x 60ml). The combined organic extracts were then washed

with water (3 x 25 ml) and the solution dried over anhydrous Na₂SO₄. After evaporation

of the solvents under vacuum, the crude foam was passed through a plug of silica gel first

washing with pure hexanes followed by a wash with 30% EtOAc/Hex wash into another

flask to obtain purified alcohol as a white solid (1.31 g, 65.5%). IR (neat) 3346, 2856, 1738,

1462, 1251, 1078, 834, 773; ¹H NMR (500 MHz, CDCl₃) δ 0.04 (s, 6H), 0.62 (s, 3H),

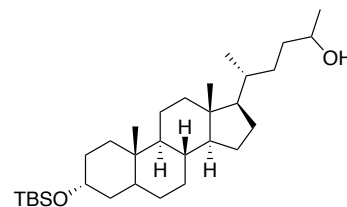
0.80 – 0.95 (m, 16H), 0.96 – 1.58 (m, 26H), 1.68 – 1.87 (m, 4H), 1.93 (d, *J* = 12.3 Hz, 1H),

3.57 (tt, *J* = 10.5, 4.7 Hz, 1H), 3.72 (dp, *J* = 12.3, 6.2 Hz, 1H). ¹³C NMR (125 MHz, CDCl₃)

δ -3.97, 12.17, 18.49, 18.82, 20.58, 23.55, 24.38, 25.71, 26.57, 27.47, 28.48, 31.19, 31.93,

32.08, 34.75, 35.75, 35.82, 35.93, 36.04, 37.09, 40.32, 40.38, 42.47, 42.84, 56.26, 56.58,

68.74, 69.00, 73.00. HRMS (ESI) *m/z* [M]⁺ calcd. for C₃₁H₅₈O₂Si 490.4259.; found



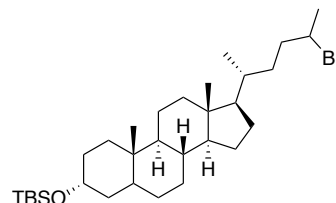
490.4279.

(((3*R*,8*R*,9*S*,10*S*,13*R*,14*S*,17*R*)-17-((2*R*)-5-bromohexan-2-yl)-10,13-dimethylhexadecahydro-1*H*-cyclopenta[*a*]phenanthren-3-yl)oxy)(*tert*-

butyl)dimethylsilane (4.36). To a 2 neck 100-mL

round-bottom flask with stir bar under N₂ charged

with rac-(5*R*)-5-[rac-(3*R*,5*R*,8*R*,9*S*,10*S*,13*R*,14*S*,17*R*)-



3-[*tert*-butyl(dimethyl)silyl]oxy-10,13-dimethyl-2,3,4,5,6,7,8,9,11,12,14,15,16,17-

tetradecahydro-1*H*-cyclopenta[*a*]phenanthren-17-yl]hexan-2-ol (0.75 g, 1.53

mmol) in dichloromethane (50 mL) was added methanesulfonyl chloride (402.55 mg,

3.51 mmol, 272.54 μ L) at 0 °C. The reaction was allowed to stir for 1 hour at 0 °C while

monitoring by TLC (20% EtOAc/Hex). The reaction was quenched with H₂O and extracted

with EtOAc (3 x 30 mL). The organic layers were collected, dried with sodium sulfate and

solvent evaporated to yield a off white powder which was used without further purification

(846 mg, 97.5%). IR (neat) 2926, 2855, 1448, 1250, 1079, 835; ¹H NMR (600MHz, CDCl₃)

δ 0.06 (s, 6H), 0.63 (s, 3H), 0.80 – 0.97 (m, 17H), 0.97 – 1.61 (m, 20H), 1.71 (dd, *J* = 6.7,

5.2 Hz, 3H), 1.72 – 1.89 (m, 4H), 1.94 (d, *J* = 12.4 Hz, 1H), 3.58 (tt, *J* = 10.5, 4.6 Hz, 1H),

4.10 (t, *J* = 6.5 Hz, 1H). ¹³C NMR (125 MHz, CDCl₃) δ -4.44, 12.17, 18.49, 18.77, 18.94,

20.96, 23.55, 24.37, 26.14, 26.41, 26.57, 26.84, 27.46, 28.43, 31.19, 34.03, 34.11, 34.75,

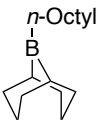
35.28, 35.66, 35.75, 36.03, 37.09, 37.79, 38.10, 40.30, 40.37, 42.46, 42.85, 52.72, 52.82,

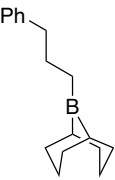
56.15, 56.18, 56.57, 72.99. HRMS (ESI) *m/z* [M]⁺ calcd. for C₃₁H₅₅OSiBr 550.3246; found

550.3278.

General Preparation of Alkyl 9-BBN Reagents:

To a 20 mL vial equipped with stir bar under an N₂ atmosphere was added distilled alkene (7.8 mmol, 1.04 equiv.) to a 1M THF solution of 9-borabicyclo[3.3.1]nonane (7.5 mmol, 1.00 equiv.) dropwise at room temperature. The reaction was allowed to stir for 2-3 hours at room temperature after which conversion was determined by ¹¹B-NMR. After complete conversion the solvent was evaporated *in vacuo*. The clear viscous oil was weighed and diluted with benzene to reach a 0.5 M stock solution which was stored at -20 °C.

***B*-octyl-9-borabicyclo(3,3,1)nonane**⁶² was synthesized according to the general preparation using 1-octene (0.98 mL, 6.24 mmol, 1.04 equiv.) and  9-borabicyclo[3.3.1]nonane (12.00 mL, 6.00 mmol, 1.00 equiv.) to afford the borane as a colorless oil (1.40 g, 100% yield). Benzene was added to make a 0.5 M solution which was stored at -20 °C. ¹¹B NMR (160 MHz, C₆H₆) δ 88.0. NMR spectrum is in agreement with literature precedence.⁶²

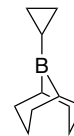
***B*-(3-phenylpropyl)-9-borabicyclo[3.3.1]nonane**⁶² was synthesized according to the general preparation using allylbenzene (1.03 mL, 7.80 mmol, 1.04 equiv.) and 9-borabicyclo[3.3.1]nonane (15.00 mL, 7.50 mmol,  1.00 equiv.) to afford the borane as a colorless oil (1.78 g, 99% yield). Benzene was added to make a 0.5 M solution which was stored at -20 °C. ¹¹B NMR (160 MHz, C₆H₆) δ 89.7. NMR spectrum is in agreement with literature precedence.⁶²

B-cyclopropanyl-9-borabicyclo(3,3,1)nonane.⁶³ To an oven-dried 100 mL Schlenk flask

with stir bar under N₂ was added 9-methoxy-9-borabicyclo[3.3.1]nonane

in hexane (1 M, 5.13 mL, 0.95 equiv.) The hexane was removed *in*

vacuo and diethyl ether (20 mL) was added to redissolve the borinic acid.



The solution was cooled to -78 °C and bromo(cyclopropyl)magnesium (0.45 M, 12 mL, 1

equiv.) was added dropwise. The reaction was allowed to warm to room temperature and

stirred for 30 minutes. The solvent was removed *in vacuo* to yield a white solid which was

resuspended in hexane (25 mL). The reaction was allowed to stir overnight during which

time magnesium salts precipitated. The Schlenk flask was brought into the glovebox and

the magnesium salts were filtered and washed with excess pentane (20 mL). The filtrate

was concentrated to yield a colorless oil (630 mg, 3.89 mmol 72% yield). Benzene was

added to make a 0.5 M solution which was stored at -20 °C. ¹¹B NMR (160 MHz, C₆H₆) δ

81.36. NMR spectrum is in agreement with literature precedence.⁶³

B-cyclobutanyl-9-borabicyclo(3,3,1)nonane. To an oven-dried 100 mL

Schlenk flask with stir bar under N₂ was added 9-methoxy-9-

borabicyclo[3.3.1]nonane in hexane (1 M, 5.54 mL, 1.00 equiv.) The hexane

was removed *in vacuo* and diethyl ether (20 mL) was added to redissolve the borinic acid.

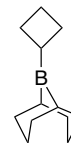
The solution was cooled to -78 °C and bromo(cyclopropyl)magnesium (0.41 M, 13.5 mL,

1 equiv.) was added dropwise. The reaction was allowed to warm to room temperature and

stirred for 30 minutes. The solvent was removed *in vacuo* to yield a white solid which was

resuspended in hexane (25 mL). The reaction was allowed to stir overnight during which

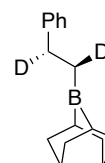
time magnesium salts precipitated. The Schlenk flask was brought into the glovebox and



the magnesium salts were filtered and washed with excess pentane (20 mL). The filtrate was concentrated to yield a colorless oil (400 mg, 2.27 mmol 41% yield). Benzene was added to make a 0.5 M solution which was stored at -20 °C. ¹¹B NMR (160 MHz, C₆H₆) δ 83.32.

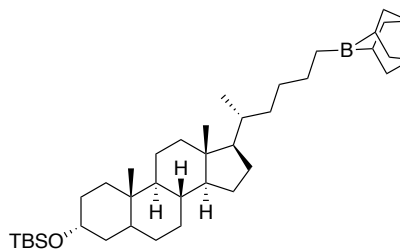
Synthesis of [(*E*)-1,2-dideuteriovinyl]benzene.⁴⁸ In the glovebox to an oven-dried 2-neck 25 mL flask with 180° joint with Teflon stopcock and stirbar was added chloro(deuterio)zirconium;cyclopentane (1.68 g, 6.50 mmol, 1 equiv.) in diethyl ether (8 mL). The heterogeneous white solution was brought out of the glovebox and 2-deuterioethynylbenzene (737 mg, 7.15 mmol, 1.1 equiv.) in toluene (1 mL) was added to the vial dropwise, and allowed to stir under N₂ atmosphere. The heterogenous solution was allowed to stir for 3 hours at which point the solution became a dark orange solution. The toluene was evaporated into a secondary trap on the Schlenk line and the dark orange goo was dissolved in diethyl ether (4 mL) and water (157.99 mg, 8.77 mmol, 1.35 equiv.) was added at a rate of 100 uL/hr dropwise at 0 °C. White/orange solid formed and the solution was filtered through a frit and the yellow filtrate was collected and solvent evaporated under partial vacuum on the rotary evaporator so only the diethyl ether was removed. The yellow oil was distilled under vacuum at room temperature using a Kugelrohr to afford a colorless liquid which brought into the glovebox. Spectral data match that of literature.⁶⁴

anti-*B*-(2-phenylethyl-1,2-*d*₂)-9-borabicyclo[3.3.1]nonane⁴⁸ was synthesized according to the general preparation using [(*E*)-1,2-dideuteriovinyl]benzene (60 mg, 0.565 mmol, 1.10 equiv.) and 9-borabicyclo[3.3.1]nonane (1.03 mL, 0.514 mmol, 1.00 equiv.) to afford the borane as a colorless oil (117 mg, 68% yield). Benzene



was added to make a 0.5 M solution which was stored at -20 °C. ^{11}B NMR (160 MHz, C_6H_6) δ 88.52.

(((3*R*,8*R*,9*S*,10*S*,13*R*,14*S*,17*R*)-17-((2*R*)-6-(9-borabicyclo[3.3.1]nonan-9-yl)hexan-2-yl)-10,13-dimethylhexadecahydro-1*H*-cyclopenta[*a*]phenanthren-3-yl)oxy)(*tert*-



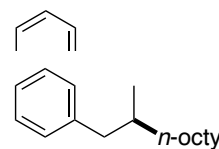
butyl)dimethylsilane was synthesized according to the general preparation using *tert*-butyl(((3*R*,8*R*,9*S*,10*S*,13*R*,14*S*,17*R*)-17-((*R*)-hex-5-en-2-yl)-10,13-dimethylhexadecahydro-1*H*-cyclopenta[*a*]phenanthren-3-yl)oxy)dimethylsilane (322 mg, 0.681 mmol, 1.10 equiv.) and 9-borabicyclo[3.3.1]nonane (1.36 mL, 0.681 mmol, 1.00 equiv.) to afford the borane as a colorless oil (405mg, 99% yield). Benzene was added to make a 0.5 M solution which was stored at -20 °C. ^{11}B NMR (160 MHz, C_6H_6) δ 87.99.

General Procedure for Iron-Catalyzed alkyl-alkyl Suzuki-Miyaura Cross Coupling:

To a 7 mL vial equipped with stir bar under an N_2 atmosphere was added iron complex (32.5 μmol , 0.13 equiv. or 50.0 μmol , 0.20 equiv.) and lithium dimethylamide (0.30 mmol, 1.2 equiv.). To this vial was added a 0.5 M stock solution of alkylborane in benzene (0.50 mmol, 2 equiv.) followed by a 1 mL benzene solution of alkyl halide (0.25 mmol, 1 equiv.) in benzene (1.00 mL). Additional benzene (5.00 mL) was added to the reaction vial at which point the reaction turned dark purple-red. The reaction was allowed to stir for 24 hours at room temperature. The reaction was quenched with a drop of water and filtered through a plug of silica gel, eluting with additional hexanes and ethyl acetate. 1,3,5-

trimethoxybenzene (21 mg, 0.125 mmol) was added as an internal standard before evaporating the solvent *in vacuo*. An NMR yield was determined by analyzing the ^1H NMR spectrum of the crude reaction mixture using 1,3,5-trimethoxybenzene as an internal standard. The product was then purified by either silica gel or neutral alumina flash column chromatography eluting with mixtures of hexane and ethyl acetate.

(3-methylundecyl)benzene (4.6) was synthesized according to the general procedure using 3-bromobutylbenzene (53.0 mg, 0.25 mmol), *n*-octyl-9-BBN (0.50 M, 1.00 mL, 0.50 mmol) and Complex

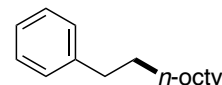


7 (22.1 mg, 32.5 μmol) to afford product as a colorless oil (55.5 mg, 96% NMR yield, 91% isolated) as well as using 3-chlorobutylbenzene (42 mg, 0.25 mmol) and Complex 7 (22.1 mg, 32.5 μmol) to afford product as a colorless oil (45 mg, 91% NMR Yield, 73% isolated). $R_f = 0.8$ (Hexanes, silica gel). ^1H NMR (600MHz, CDCl_3) δ 0.88 (t, $J = 6.8$ Hz, 3H), 0.92 (d, $J = 6.3$ Hz, 3H), 1.20 – 1.09 (m, 1H), 1.37 – 1.19 (m, 13H), 1.50 – 1.38 (m, 2H), 1.69 – 1.56 (m, 1H), 2.64 (m, 1H), 2.56 (m, 1H), 7.22 – 7.11 (m, 3H), 7.30 – 7.22 (m, 2H). Spectral data match that of literature.⁶⁵

(2-methyldecyl)benzene (4.13) was synthesized according to the general procedure using 2-bromopropylbenzene (30.0 mg, 0.15 mmol), *n*-octyl-9-BBN (0.50 M, 1.00 mL, 0.50 mmol) and Complex 7 (13.3 mg, 19.6 μmol) to afford product as a colorless oil (34 mg, 99% NMR yield, 97% isolated). $R_f = 0.8$ (Hexanes, silica gel). ^1H NMR (500 MHz, CDCl_3) δ 0.87 (d, $J = 6.6$ Hz, 3H), 0.92 (t, $J = 6.9$ Hz, 3H), 1.28 (m, 14H), 1.74 (dq, $J = 14.0, 6.7$

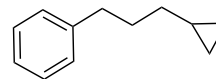
Hz, 1H), 2.38 (dd, $J = 13.2, 8.1$ Hz, 1H), 2.67 (dd, $J = 13.5, 6.0$ Hz, 1H), 7.20 (m, 3H), 7.29 (m, 2H). Spectral data match that of literature.⁶⁶

Decylbenzene (4.14) was synthesized according to the general procedure using 2-bromoethylbenzene (46.0 mg, 0.25 mmol), *n*-



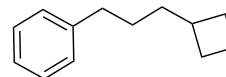
octyl-9-BBN (0.50 M, 1.00 mL, 0.50 mmol) and Complex **7** (22.1 mg, 32.5 μ mol) to afford product as a colorless oil (32 mg, 81% NMR yield, 79% isolated). $R_f = 0.8$ (Hexanes, silica gel). ¹H NMR (400MHz, CDCl₃) δ 0.88 (t, $J = 6.9$ Hz, 3H), 1.26–1.30 (m, 14H), 1.56–1.63 (m, 2H), 2.60 (t, $J = 7.5$ Hz, 2H), 7.14–7.19 (m, 3H), 7.25–7.30 (m, 2H). Spectral data match that of literature.⁶⁷

(3-cyclopropylpropyl)benzene (4.15) was synthesized according to the general procedure using cyclopropylbromide (30.2 mg, 0.25



mmol), 3-phenylpropyl-9-BBN (0.50 M, 1.00 mL, 0.50 mmol) and Complex **7** (22.1 mg, 32.5 μ mol) to afford product as a colorless oil (10 mg, 34% NMR yield, 25% isolated). $R_f = 0.8$ (Hexanes, silica gel). ¹H NMR (600 MHz, Chloroform-*d*) δ -0.02 – 0.01 (m, 2H), 0.35 – 0.44 (m, 2H), 0.68 (ddt, $J = 10.3, 7.6, 3.8$ Hz, 1H), 1.24 (dd, $J = 14.9, 7.1$ Hz, 2H), 1.68 – 1.76 (m, 2H), 2.63 (t, $J = 7.7$ Hz, 2H), 7.17 (m, 3H), 7.24 – 7.29 (m, 2H). Spectral data match that of literature.⁶⁸

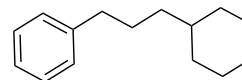
(3-cyclobutylpropyl)benzene (4.16) was synthesized according to the general procedure using cyclobutylbromide (33.8 mg, 0.25



mmol), 3-phenylpropyl-9-BBN (0.50 M, 1.00 mL, 0.50 mmol) and Complex **8** (23.0 mg, 32.5 μ mol) to afford product as a colorless oil (24 mg, 60% NMR yield, 55% isolated). R_f

= 0.8 (Hexanes, silica gel). $^1\text{H NMR}$ (500 MHz, Chloroform-*d*) δ 1.42 (m, 2H), 1.48 – 1.63 (m, 4H), 1.81 (m, 2H), 2.02 (dtd, $J = 11.5, 8.0, 2.9$ Hz, 2H), 2.28 (hept, $J = 7.8$ Hz, 1H), 2.58 (t, $J = 7.7$ Hz, 2H), 7.14 – 7.20 (m, 3H), 7.24 – 7.31 (m, 2H). Spectral data match that of literature.⁶⁸

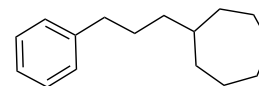
(3-Cyclohexylpropyl)benzene (4.17) was synthesized



according to the general procedure using bromocyclohexane

(26.7 mg, 0.25 mmol), 3-phenylpropyl-9-BBN (0.50 M, 1.00 mL, 0.50 mmol) and Complex **7** (22.1 mg, 32.5 μmol) to afford product as a colorless oil (44 mg, 96% NMR yield, 87% isolated) $R_f = 0.8$ (Hexanes, silica gel). $^1\text{H NMR}$ (600 MHz, Chloroform-*d*) δ 0.81 – 0.93 (m, 2H), 1.09 – 1.27 (m, 6H), 1.57 – 1.74 (m, 7H), 2.58 (t, $J = 7.8$ Hz, 2H), 7.17 (d, $J = 7.5$ Hz, 3H), 7.24 – 7.30 (m, 2H). $R_f = 0.75$ (Hexanes). Spectral data match that of literature.⁶⁹

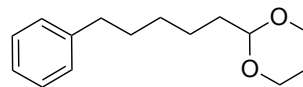
(3-cycloheptylpropyl)benzene (4.18) was synthesized



according to the general procedure using bromocycloheptane

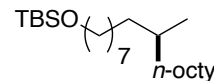
(44.2 mg, 0.25 mmol), 3-phenylpropyl-9-BBN (0.50 M, 1.00 mL, 0.50 mmol) and Complex **8** (23.0 mg, 32.5 μmol) to afford product as a colorless oil (38 mg, 79% NMR yield, 70% isolated) $R_f = 0.8$ (Hexanes, silica gel). $^1\text{H NMR}$ (500 MHz, Chloroform-*d*) δ 1.18 (dtd, $J = 13.5, 9.6, 2.7$ Hz, 2H), 1.25 – 1.36 (m, 2H), 1.36 – 1.72 (m, 5H), 1.54 – 1.75 (m, 8H), 2.57 – 2.64 (m, 2H), 7.17 – 7.22 (m, 3H), 7.26 – 7.33 (m, 2H). Spectral data match that of literature.¹⁵

2-(5-Phenylpentyl)-1,3-dioxane (4.19) was synthesized according to the general procedure using 2-(2-bromoethyl)-



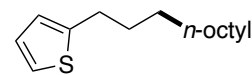
1,3-dioxane (48.8 mg, 0.25 mmol), 3-phenylpropyl-9-BBN (0.50 M, 1.00 mL, 0.50 mmol) and Complex **7** (22.1 mg, 32.5 μ mol) to afford product as a colorless oil (59 mg, 63% NMR yield, 60% isolated, silica gel). $R_f = 0.05$ (95:5 hexane : ethyl acetate). ^1H NMR (400MHz, CDCl_3) δ 1.29 – 1.39 (m, 3H), 1.39 – 1.47 (m, 2H), 1.56 – 1.67 (m, 4H), 2.08 (qt, $J = 12.6, 5.0$ Hz, 1H), 2.58 – 2.63 (m, 2H), 3.75 (ddt, $J = 12.3, 10.4, 2.4$ Hz, 2H), 4.10 (ddt, $J = 10.4, 5.0, 1.4$ Hz, 2H), 4.50 (t, $J = 5.2$ Hz, 1H), 7.17 (dt, $J = 6.0, 1.6$ Hz, 3H), 7.24 – 7.30 (m, 2H). Spectral data match that of literature.³¹

tert-butyl dimethyl((9-methylheptadecyl)oxy)silane (4.20) was synthesized according to the general procedure using 9-



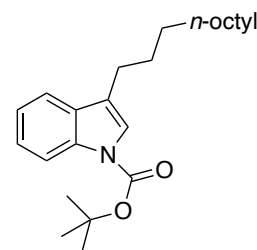
bromodecoxy-tert-butyl-dimethyl-silane (88.0 mg, 0.25 mmol) *n*-octyl-9-BBN (0.50 M, 1.00 mL, 0.50 mmol) and Complex **7** (22.1 mg, 32.5 μ mol) to afford product as a colorless oil (70 mg, 79% NMR yield, 79% isolated, silica gel). IR (neat) 2924, 2854, 1463, 1255, 1098; ^1H NMR (500MHz, CDCl_3) δ 0.06 (s, 6H), 0.85 (d, $J = 6.6$ Hz, 3H), 0.91 (s, 9H), 1.21-1.39 (m, 24H), 1.47 – 1.58 (m, 2H), 3.61 (t, $J = 6.6$ Hz, 2H); ^{13}C NMR (125MHz, CDCl_3) δ -5.10, 10.36, 14.27, 18.54, 19.88, 22.86, 25.99, 26.15, 27.24, 27.26, 29.54, 29.63, 29.86, 30.13, 30.21, 32.10, 32.92, 33.07, 37.27, 63.51. HRMS (ESI) m/z $[\text{M}]^+$ calcd. for $\text{C}_{24}\text{H}_{52}\text{OSi}$ 384.3860; found 384.3860.

2-undecylthiophene (4.21) was synthesized according to the general procedure using 2-(3-bromopropyl)thiophene (51.0 mg,



0.25 mmol), *n*-octyl-9-BBN ((0.50 M, 1.00 mL, 0.50 mmol) and Complex **7** (22.1 mg, 32.5 μ mol) to afford product as a colorless oil (36 mg, 68% NMR yield, 60% isolated). $R_f = 0.6$ (Hexane, silica gel). ^1H NMR (500MHz, CDCl_3) δ 0.88 (t, $J = 6.81$ Hz, 3H), 1.41-1.18 (m, 16H), 1.74-1.61 (m, 2H), 2.81 (t, $J = 7.64$ Hz, 2H), 6.76 (dd, $J = 3.14, 1.12$ Hz, 1H), 6.89 (dd, $J = 5.16, 3.35$ Hz, 1H), 7.08 (dd, $J = 5.11, 1.20$ Hz, 1H). Spectral data match that of literature.⁷⁰

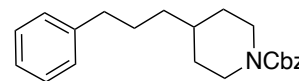
***tert*-butyl 3-undecyl-1*H*-indole-1-carboxylate (4.22)** was synthesized according to the general procedure using *tert*-butyl 3-(3-bromopropyl)-1*H*-



indole-1-carboxylate (85.1 mg, 0.25 mmol), *n*-octyl-9-BBN (0.50 M, 1.00 mL, 0.50 mmol) and Complex **7** (22.1 mg, 32.5 μ mol) to afford product as a colorless oil (48 mg, 55% NMR

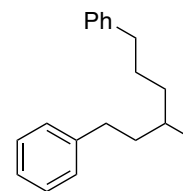
yield, 51% isolated) $R_f = 0.35$ (95:5 hexane : ethyl acetate in neutral alumina). ^1H NMR (500MHz, CDCl_3) δ 1.43 (ddt, $J = 16.6, 14.1, 5.8$ Hz, 4H), 1.67 (s, 13H), 2.58 - 2.64 (m, 2H), 2.64 - 2.71 (m, 2H), 7.14 - 7.36 (m, 8H), 7.49 - 7.54 (m, 1H), 8.12 (s, 1H). ^{13}C NMR (125 MHz, CDCl_3) δ 14.11, 22.69, 24.91, 28.24, 29.26, 29.34, 29.50, 29.60, 29.61, 29.63, 29.68, 31.91, 83.19, 115.20, 119.04, 121.53, 122.18, 124.11, 130.89, 135.54, 149.91. IR (neat) 2923, 2853, 1731, 1453, 1369, 1156, 744; HRMS (ESI) m/z $[\text{M}]^+$ calcd. for $\text{C}_{24}\text{H}_{37}\text{NO}_2$ 371.2904; found 371.2897.

Benzyl 4-(3-phenylpropyl)piperidine-1-carboxylate (4.23)



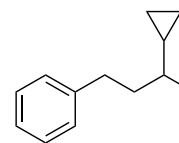
was synthesized according to the general procedure using benzyl 4-bromopiperidine-1-carboxylate (74.5 mg, 0.25 mmol), 3-phenylpropyl-9-BBN (0.50 M, 1.00 mL, 0.50 mmol) and Complex 7 (22.1 mg, 32.5 μ mol) to afford product as a colorless oil (49 mg, 60% NMR yield, 58% isolated, silica gel) $R_f = 0.15$ (9:1 hexane : ethyl acetate, silica gel). ^1H NMR (400MHz, CDCl_3) δ 1.06 – 1.16 (m, 2H), 1.28 (dd, $J = 15.6, 6.9$ Hz, 2H), 1.41 (tdt, $J = 10.5, 6.8, 3.7$ Hz, 1H), 1.57 – 1.70 (m, 4H), 2.59 (t, $J = 7.7$ Hz, 2H), 2.74 (s, 2H), 4.15 (s, 2H), 5.12 (s, 2H), 7.13 – 7.22 (m, 3H), 7.24 – 7.32 (m, 3H), 7.33-7.39 (m, 4H). Spectral data match that of literature.⁶⁹

(3-methylhexane-1,6-diyl)dibenzene (4.26) was synthesized



according to the general procedure using 3-bromobutylbenzene (53.0 mg, 0.25 mmol), 3-phenylpropyl-9-BBN (0.50 M, 1.00 mL, 0.50 mmol) and Complex 7 (22.1 mg, 32.5 μ mol) to afford product as a colorless oil $R_f = 0.8$ (Hexanes). (38 mg, 63% NMR yield, 60% isolated, silica gel). ^1H NMR (500MHz, CDCl_3) δ 0.94 (d, $J = 6.4$ Hz, 3H), 1.17 – 1.33 (m, 1H), 1.34 – 1.73 (m, 6H), 2.58 (m, 4H), 7.14 – 7.24 (m, 6H), 7.24 – 7.32 (m, 4H). Spectral data match that of literature.²⁰

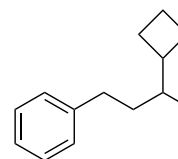
(3-cyclopropylbutyl)benzene (4.28) was synthesized according to



the general procedure using 3-bromobutylbenzene (53.0 mg, 0.25 mmol), cyclopropyl-9-BBN (0.50 M, 1.00 mL, 0.50 mmol) and Complex 7 (33.9 mg, 50.0 μ mol) to afford product as a colorless oil (32.3 mg, 78% NMR yield, 74% isolated) $R_f = 0.8$ (Hexanes, silica gel). ^1H NMR (500MHz, CDCl_3) δ 0.01 (dq,

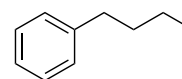
$J = 9.4, 4.7$ Hz, 1H), 0.10 (dq, $J = 9.2, 4.7$ Hz, 1H), 0.33 – 0.49 (m, 2H), 0.53 (m, 1H), 0.73 (m, 1H), 1.02 (d, $J = 6.7$ Hz, 3H), 1.55 – 1.66 (m, 1H), 1.78 (m, 1H), 2.68 (t, $J = 8.2$ Hz, 2H), 7.18 (m, 3H), 7.28 (m, 2H). Spectral data match that of literature.⁶⁸

(3-cyclobutylbutyl)benzene (4.29) was synthesized according to the general procedure using 3-bromobutylbenzene (53.0 mg, 0.25 mmol), cyclobutyl-9-BBN (0.50 M, 1.00 mL, 0.50 mmol) and



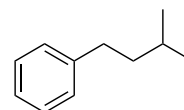
Complex 7 (33.9 mg, 50.0 μ mol) to afford product as a colorless oil (32.3 mg, 78% NMR yield, 74% isolated) $R_f = 0.8$ (Hexanes, silica gel). IR (neat) 2956, 2925, 2854, 1454, 697; ^1H NMR (500MHz, CDCl_3) δ 0.83, (t, $J = 6.6$ Hz, 3H), 1.24 – 1.32 (m, 1H), 1.38 (ddtd, $J = 15.5, 9.1, 6.5, 3.8$ Hz, 1H), 1.58 – 1.74 (m, 4H), 1.78 – 1.87 (m, 1H), 1.94 – 2.11 (m, 3H), 2.51 (ddd, $J = 13.6, 10.5, 6.3$ Hz, 1H), 2.69 (ddd, $J = 13.7, 10.8, 5.1$ Hz, 1H), 7.15 – 7.22 (m, 3H), 7.26 – 7.32 (m, 2H). ^{13}C NMR (125 MHz, CDCl_3) δ 16.16, 17.68, 27.00, 27.36, 33.52, 36.02, 39.51, 42.57, 128.24, 128.31, 143.24. HRMS (ESI) m/z $[\text{M}]^+$ calcd. for $\text{C}_{14}\text{H}_{20}$ 188.1636.; found 188.1638.

Butylbenzene (4.33) was synthesized according to the general procedure using methyl iodide (35.5 mg, 0.25 mmol), 3-



phenylpropyl-9-BBN (0.50 M, 1.00 mL, 0.50 mmol) and Complex 7 (22.1 mg, 32.5 μ mol) to afford product as a colorless oil (21 mg, 69% NMR yield, 63% isolated) $R_f = 0.8$ (Hexanes, silica gel). ^1H NMR (600MHz, CDCl_3) δ 0.92 (t, $J = 7.4$ Hz, 3H), 1.35 (h, $J = 7.4$ Hz, 2H), 1.59 (p, $J = 7.4$ Hz, 2H), 2.60 (t, $J = 7.8$ Hz, 2H), 7.17 (dd, $J = 7.9, 2.1$ Hz, 3H), 7.25 – 7.29 (m, 2H). Spectral data match that of literature.⁷¹

Isopentylbenzene (4.34) was synthesized according to the general procedure using 3-bromobutylbenzene (53.0 mg, 0.25 mmol), Me-9-



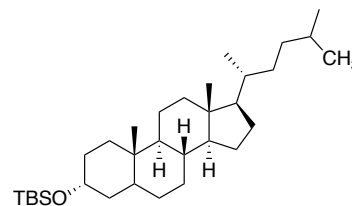
BBN (0.50 M, 1.00 mL, 0.50 mmol) and Complex **7** (33.9 mg, 50 μ mol) to afford product as a colorless oil (37 mg, 61% NMR yield, 54% isolated) $R_f = 0.8$ (Hexanes, silica gel). ^1H NMR (500MHz, CDCl_3) δ 0.94 (d, $J = 6.5$ Hz, 6H), 1.47 – 1.55 (m, 2H), 1.60 (dq, $J = 13.2, 6.7$ Hz, 1H), 2.58 – 2.64 (m, 2H), 7.13 – 7.21 (m, 3H), 7.27 (t, $J = 7.6$ Hz, 2H). Spectral data match that of literature.⁷²

tert-butyl(((3R,8R,9S,10S,13R,14S,17R)-10,13-dimethyl-17-((R)-5-methylhexan-2-yl)hexadecahydro-1H-cyclopenta[a]phenanthren-3-yl)oxy)dimethylsilane (4.38) was

synthesized according to the general procedure using tert-

butyl-dimethyl-[[rac-(3R,5R,8R,9S,10S,13R,14S,17R)-

10,13-dimethyl-17-[rac-(1R)-4-bromo-1-methyl-pentyl]-



2,3,4,5,6,7,8,9,11,12,14,15,16, 17-tetradecahydro-1H-cyclopenta[a]phenanthren-3-

yl]oxy]silane (69.2 mg, 0.125 mmol), methyl-9-BBN (0.50 M, 0.50 mL, 0.50 mmol) and

Complex **7** (33.9 mg, 50.0 μ mol) to afford product as a colorless oil (49 mg, 81% NMR

yield, 80% isolated) $R_f = 0.63$ (Hexanes, silica gel). IR (neat) 2926, 2855, 1462, 1251,

1080, 834; ^1H NMR (600MHz, CDCl_3) δ 0.06 (s, 6H), 0.63 (s, 3H), 0.81 – 0.93 (m, 24H),

0.95 – 1.48 (m, 19H), 1.50 – 1.58 (m, 2H), 1.72 – 1.87 (m, 4H), 1.95 (dt, $J = 12.5, 3.3$ Hz,

1H), 3.58 (tt, $J = 11.0, 4.6$ Hz, 1H). ^{13}C NMR (125 MHz, CDCl_3) δ -4.43, 12.16, 18.50,

18.85, 20.99, 22.54, 23.27, 23.57, 24.41, 26.14, 26.60, 27.50, 28.46, 28.55, 31.20, 33.72,

34.76, 35.49, 35.76, 36.05, 36.09, 37.11, 40.34, 40.41, 42.49, 42.83, 56.41, 57.62, 73.02.

.HRMS (ESI) m/z $[\text{M}]^+$ calcd. for $\text{C}_{32}\text{H}_{60}\text{OSi}$ 488.4333; found 488.4330.

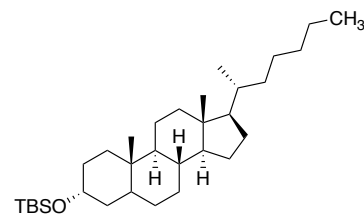
***tert*-butyl(((3*R*,8*R*,9*S*,10*S*,13*R*,14*S*,17*R*)-17-((*R*)-heptan-2-yl)-10,13-**

dimethylhexadecahydro-1*H*-cyclopenta[*a*]phenanthren-3-yl)oxy)dimethylsilane

(4.39) was synthesized according to the general

procedure using iodomethane (15.5 μ L, 0.25 mmol),

(((3*R*,8*R*,9*S*,10*S*,13*R*,14*S*,17*R*)-17-((2*R*)-6-(9-



borabicyclo[3.3.1]nonan-9-yl)hexan-2-yl)-10,13-dimethylhexadecahydro-1*H*-

cyclopenta[*a*]phenanthren-3-yl)oxy)(*tert*-butyl)dimethylsilane (0.50 M, 1.00 mL, 0.50

mmol) and Complex **7** (33.9 mg, 50.0 μ mol) to afford product as a colorless oil (92 mg,

77% NMR yield, 75.3% isolated) R_f = 0.63 (Hexanes, silica gel). IR (neat) 2927, 2856,

1462, 1250, 1095, 835; ^1H NMR (600 MHz, CDCl_3) δ 0.05 (s, 6H), 0.62 (s, 3H), 0.85 –

0.92 (m, 18H), 0.93 – 1.45 (m, 24H), 1.49 – 1.57 (m, 2H), 1.78 (m, 4H), 1.94 (dt, J = 12.7,

3.3 Hz, 1H), 3.57 (tt, J = 10.5, 4.6 Hz, 1H). ^{13}C NMR (125 MHz, CDCl_3) δ -4.44, 12.17,

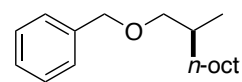
14.30, 18.48, 18.82, 21.00, 22.92, 23.57, 24.42, 25.97, 26.14, 26.61, 27.50, 28.49, 31.21,

31.76, 32.57, 34.76, 35.77, 35.96, 36.06, 36.07, 37.11, 40.36, 40.42, 42.50, 42.84, 56.51,

56.62, 73.02. HRMS (ESI) m/z [M] $^+$ calcd. for $\text{C}_{32}\text{H}_{60}\text{OSi}$ 488.4323; found 488.4330.

2-[(Methyldecyloxy)methyl]benzene (4.44) was synthesized

according to the general procedure using [(2*R*)-2-



bromopropoxy]methylbenzene (57.0 mg, 0.25 mmol), *n*-octyl-9-BBN (0.50 M, 1.00 mL,

0.50 mmol) and Complex **7** (22.1 mg, 32.5 μ mol) to afford product as a colorless oil with

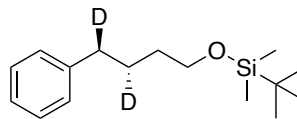
trace ligand (40 mg, 60% NMR yield, 60% isolated) R_f = 0.3 (Hexanes, silica gel). ^1H

NMR (600MHz, CDCl_3) δ 0.88 (t, J = 7.0 Hz, 3H), 0.92 (d, J = 6.7 Hz, 3H), 1.20 – 1.34

(m, 13H), 1.37 – 1.45 (m, 1H), 1.71 – 1.80 (m, 1H), 3.23 (dd, J = 9.1, 6.8 Hz, 1H), 3.32

(dd, $J = 9.0, 5.9$ Hz, 1H), 4.50 (d, $J = 3.2$ Hz, 2H), 7.24 – 7.30 (m, 1H), 7.33 (d, $J = 4.4$ Hz, 4H). Spectral data match that of literature.⁷³

***anti*-3,4-Dideuterio-4-phenylbutoxy(tert-butyl)dimethylsilane (4.45)** was synthesized according to the general procedure using 2-bromoethoxy-
tert-butyl-dimethyl-silane (59.8 mg, 0.25 mmol), *anti*-1,2-



dideuterio-2-phenyl-ethyl-9-BBN (0.50 M, 1.00 mL, 0.50 mmol) and Complex **3** (22.5 mg, 32.5 μ mol). After 12 hours, additional lithium dimethyl amide (15.3 mg, 0.30 mmol) and Complex **3** (22.5 mg, 32.5 μ mol) were added and the reaction was allowed to stir for an additional 12 hours before isolating product as a pale yellow oil (20 mg, 42% NMR yield, 30% isolated) $R_f = 0.1$ (Hexanes, silica gel). ¹H NMR (600MHz, CDCl₃) δ 0.03 (s, 5H), 0.88 (s, 9H), 1.55 (t, $J = 6.8$ Hz, 2H), 1.60 – 1.66 (m, 1H), 2.59 (d, $J = 8.2$ Hz, 1H), 3.62 (t, $J = 6.5$ Hz, 2H), 7.17 (d, $J = 7.4$ Hz, 3H), 7.24 – 7.29 (m, 2H). Spectral data match that of literature.⁴⁸

Figure S3.1. Topographic steric map of iron complex **4.11** showing buried volume percentages as determined by the program SambVca.

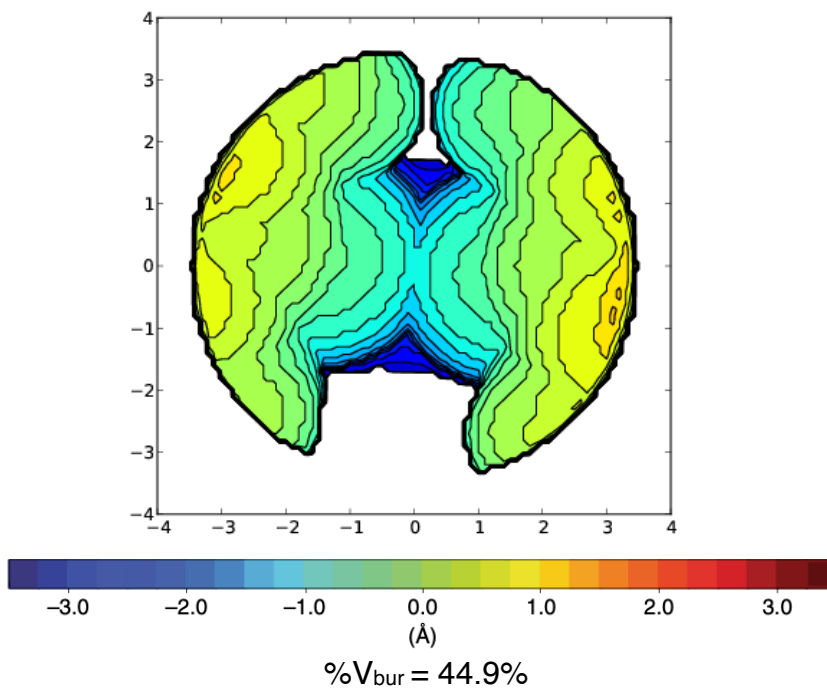


Figure S3.2. Topographic steric map of iron complex **4.5** showing buried volume percentages as determined by the program SambVca.

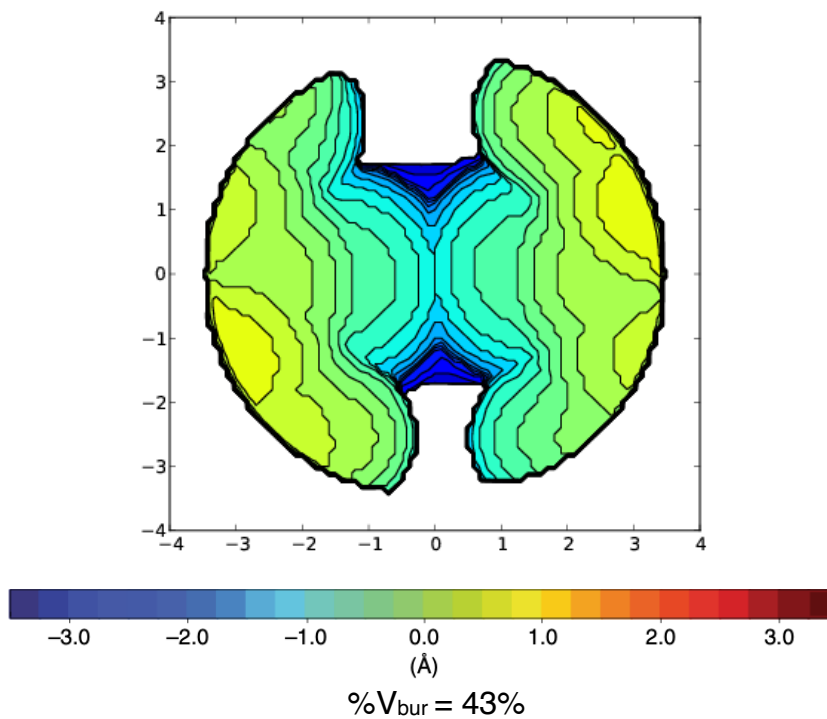


Figure S3.3. Cyclic voltammogram for complex **4.4** carried out at a scan rate of 0.1V/s using 1M N(n-Bu)₄PF₆ in THF as the electrolyte.

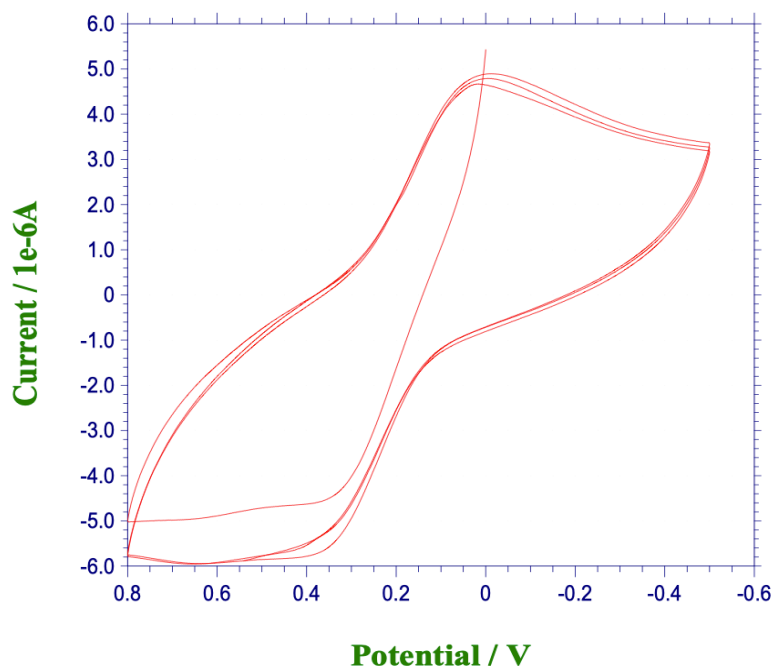


Figure S3.4. Cyclic voltammogram for complex **4.11** carried out at a scan rate of 0.1V/s using 1M N(n-Bu)₄PF₆ in THF as the electrolyte.

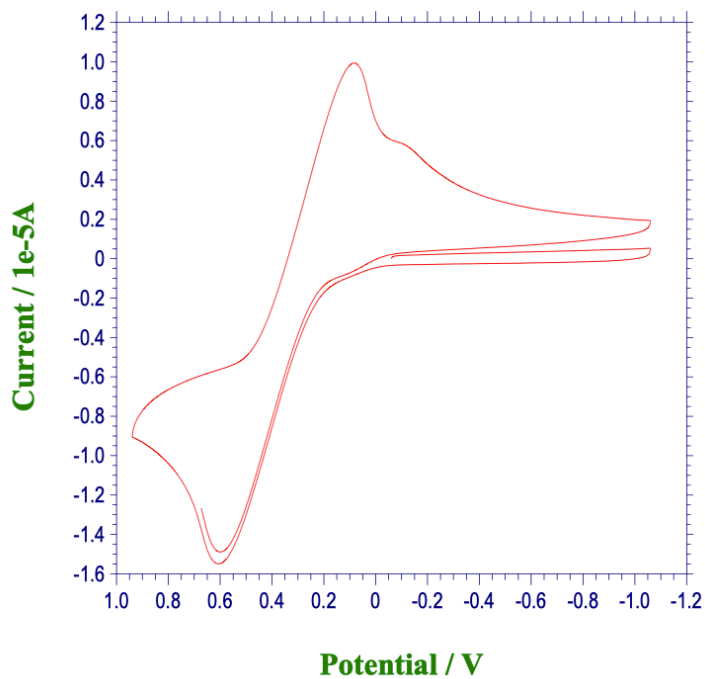
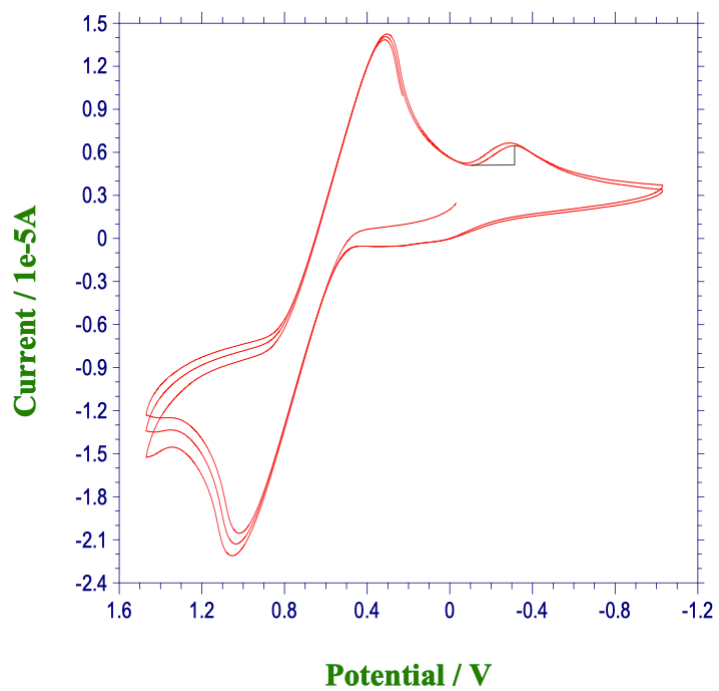


Figure S3.5. Cyclic voltammogram for complex **4.5** carried out at a scan rate of 0.1V/s using 1M N(n-Bu)₄PF₆ in THF as the electrolyte.



4.6 References

- (1) Jana, R.; Pathak, T. P.; Sigman, M. S. Advances in Transition Metal (Pd,Ni,Fe)-Catalyzed Cross-Coupling Reactions Using Alkyl-Organometallics as Reaction Partners. *Chem. Rev.* **2011**, *111*, 1417–1492. <https://doi.org/10.1021/cr100327p>.
- (2) Crockett, M. P.; Tyrol, C. C.; Wong, A. S.; Li, B.; Byers, J. A. Iron-Catalyzed Suzuki-Miyaura Cross-Coupling Reactions between Alkyl Halides and Unactivated Arylboronic Esters. *Org. Lett.* **2018**, *20*, 5233–5237. <https://doi.org/10.1021/acs.orglett.8b02184>.
- (3) Crockett, M. P.; Wong, A. S.; Li, B.; Byers, J. A. Rational Design of an Iron-Based Catalyst for Suzuki–Miyaura Cross-Couplings Involving Heteroaromatic Boronic Esters and Tertiary Alkyl Electrophiles. *Angew. Chemie Int. Ed.* **2020**, *59*, 5392–5397. <https://doi.org/10.1002/anie.201914315>.
- (4) Tyrol, C. C.; Yone, N. S.; Gallin, C. F.; Byers, J. A. Iron-Catalysed Enantioconvergent Suzuki-Miyaura Cross-Coupling to Afford Enantioenriched 1,1-Diarylalkanes. *Chem. Commun.* **2020**, *56*, 14661–14664. <https://doi.org/10.1039/d0cc05003b>.
- (5) Choi, J.; Fu, G. C. Transition Metal-Catalyzed Alkyl-Alkyl Bond Formation: Another Dimension in Cross-Coupling Chemistry. *Science* **2017**, *356*, 559–564. <https://doi.org/10.1126/science.aaf7230>.
- (6) Brown, D. G.; Boström, J. Analysis of Past and Present Synthetic Methodologies on Medicinal Chemistry: Where Have All the New Reactions Gone? *J. Med. Chem.* **2016**, *59*, 4443–4458. <https://doi.org/10.1021/acs.jmedchem.5b01409>.
- (7) Lovering, F.; Bikker, J.; Humblet, C. Escape from Flatland: Increasing Saturation

- as an Approach to Improving Clinical Success. *J. Med. Chem.* **2009**, *52*, 6752–6756.
<https://doi.org/10.1021/jm901241e>.
- (8) Tabassum, S.; Zahoor, A. F.; Ahmad, S.; Noreen, R.; Khan, S. G.; Ahmad, H. *Cross-Coupling Reactions towards the Synthesis of Natural Products*; Springer International Publishing, 2021. <https://doi.org/10.1007/s11030-021-10195-6>.
- (9) Netherton, M. R.; Dai, C.; Neuschütz, K.; Fu, G. C. Room-Temperature Alkyl-Alkyl Suzuki Cross-Coupling of Alkyl Bromides That Possess β Hydrogens. *J. Am. Chem. Soc.* **2001**, *123*, 10099–10100. <https://doi.org/10.1021/ja011306o>.
- (10) Lou, S., Fu, G. C. Palladium-Catalyzed Alkyl-Alkyl Suzuki Cross-Couplings of Primary Alkyl Bromides At Room Temperature. *Org. Synth.* **2010**, *87*, 299. <https://doi.org/10.15227/orgsyn.087.0299>.
- (11) López-Pérez, A.; Adrio, J.; Carretero, J. C. Palladium-Catalyzed Cross-Coupling Reaction of Secondary Benzylic Bromides with Grignard Reagents. *Org. Lett.* **2009**, *11*, 5514–5517. <https://doi.org/10.1021/ol902335c>.
- (12) Mako, T. L.; Byers, J. A. Recent Advances in Iron-Catalysed Cross Coupling Reactions and Their Mechanistic Underpinning. *Inorg. Chem. Front.* **2016**, *3*, 766–790. <https://doi.org/10.1039/c5qi00295h>.
- (13) Diccianni, J. B.; Diao, T. Mechanisms of Nickel-Catalyzed Cross-Coupling Reactions. *Trends in Chem.* **2019**, *1*, 830–844.
- (14) Liang, Y.; Fu, G. C. Nickel-Catalyzed Alkyl-Alkyl Cross-Couplings of Fluorinated Secondary Electrophiles: A General Approach to the Synthesis of Compounds Having a Perfluoroalkyl Substituent. *Angew. Chemie - Int. Ed.* **2015**, *54*, 9047–9051. <https://doi.org/10.1002/anie.201503297>.

- (15) Saito, B.; Fu, G. C. Alkyl-Alkyl Suzuki Cross-Couplings of Unactivated Secondary Alkyl Halides at Room Temperature. *J. Am. Chem. Soc.* **2007**, *129*, 9602–9603. <https://doi.org/10.1021/ja074008l>.
- (16) Jiang, X.; Gandelman, M. Enantioselective Suzuki Cross-Couplings of Unactivated 1-Fluoro-1-Haloalkanes: Synthesis of Chiral β -, γ -, δ -, and ϵ -Fluoroalkanes. *J. Am. Chem. Soc.* **2015**, *137*, 2542–2547. <https://doi.org/10.1021/jacs.5b00473>.
- (17) Lu, Z.; Wilsily, A.; Fu, G. C. Stereoconvergent Amine-Directed Alkyl-Alkyl Suzuki Reactions of Unactivated Secondary Alkyl Chlorides. *J. Am. Chem. Soc.* **2011**, *133*, 8154–8157. <https://doi.org/10.1021/ja203560q>.
- (18) Wilsily, A.; Tramutola, F.; Owston, N. A.; Fu, G. C. New Directing Groups for Metal-Catalyzed Asymmetric Carbon-Carbon Bond-Forming Processes: Stereoconvergent Alkyl-Alkyl Suzuki Cross-Couplings of Unactivated Electrophiles. *J. Am. Chem. Soc.* **2012**, *134*, 5794–5797. <https://doi.org/10.1021/ja301612y>.
- (19) Zultanski, S. L.; Fu, G. C. Catalytic Asymmetric γ -Alkylation of Carbonyl Compounds via Stereoconvergent Suzuki Cross-Couplings. *J. Am. Chem. Soc.* **2011**, *133*, 15362–15364. <https://doi.org/10.1021/ja2079515>.
- (20) Saito, B.; Fu, G. C. Enantioselective Alkyl-Alkyl Suzuki Cross-Couplings of Unactivated Homobenzylic Halides. *J. Am. Chem. Soc.* **2008**, *130*, 6694–6695. <https://doi.org/10.1021/ja8013677>.
- (21) Di Franco, T.; Boutin, N.; Hu, X. Suzuki-Miyaura Cross-Coupling Reactions of Unactivated Alkyl Halides Catalyzed by a Nickel Pincer Complex. *Synth.* **2013**, *45*, 2949–2958. <https://doi.org/10.1055/s-0033-1338544>.

- (22) Egorova, K. S.; Ananikov, V. P. Toxicity of Metal Compounds: Knowledge and Myths. *Organometallics* **2017**, *36*, 4071–4090. <https://doi.org/10.1021/acs.organomet.7b00605>.
- (23) Hunt, A. J.; Matharu, A. S.; King, A. H.; Clark, J. H. The Importance of Elemental Sustainability and Critical Element Recovery. *Green Chem.* **2015**, *17*, 1949–1950. <https://doi.org/10.1039/c5gc90019k>.
- (24) Nakamura, M.; Hatakeyama, T.; Hashimoto, T.; Kondo, Y.; Fujiwara, Y.; Seike, H.; Takaya, H.; Tamada, Y.; Ono, T. Iron-Catalyzed Suzuki-Miyaura Coupling of Alkyl Halides. *J. Am. Chem. Soc.* **2010**, *132*, 10674–10676. <https://doi.org/10.1021/ja103973a>.
- (25) Bedford, R. B.; Brenner, P. B.; Carter, E.; Carvell, T. W.; Cogswell, P. M.; Gallagher, T.; Harvey, J. N.; Murphy, D. M.; Neeve, E. C.; Nunn, J.; et al. Expedient Iron-Catalyzed Coupling of Alkyl, Benzyl and Allyl Halides with Arylboronic Esters. *Chem. - A Eur. J.* **2014**, *20*, 7935–7938. <https://doi.org/10.1002/chem.201402174>.
- (26) Furstner, A.; Leitner, A.; Mndez, M.; Krause, H. Iron-Catalyzed Cross-Coupling Reactions Iron-Catalyzed Cross-Coupling Reactions. *Tetrahedron* **2002**, *124*, 13856–13863. <https://doi.org/10.1021/ja027190t>.
- (27) Wang, X.; Wang, S.; Xue, W.; Gong, H. Nickel-Catalyzed Reductive Coupling of Aryl Bromides with Tertiary Alkyl Halides. *J. Am. Chem. Soc.* **2015**, *137*, 11562–11565. <https://doi.org/10.1021/jacs.5b06255>.
- (28) Bellows, S. M.; Cundari, T. R.; Holland, P. L. Spin Crossover during β -Hydride Elimination in High-Spin Iron(II)- and Cobalt(II)-Alkyl Complexes.

- Organometallics* **2013**, *32*, 4741–4751. <https://doi.org/10.1021/om400325x>.
- (29) Zultanski, S. L.; Fu, G. C. Nickel-Catalyzed Carbon-Carbon Bond-Forming Reactions of Unactivated Tertiary Alkyl Halides: Suzuki Arylations. *J. Am. Chem. Soc.* **2013**, *135*, 624–627. <https://doi.org/10.1021/ja311669p>.
- (30) Dongol, K. G.; Koh, H.; Sau, M.; Chai, C. L. L. Iron-Catalysed Sp³-Sp³ Cross-Coupling Reactions of Unactivated Alkyl Halides with Alkyl Grignard Reagents. *Adv. Synth. Catal.* **2007**, *349*, 1015–1018. <https://doi.org/10.1002/adsc.200600383>.
- (31) Guisán-Ceinos, M.; Tato, F.; Buñuel, E.; Calle, P.; Cárdenas, D. J. Fe-Catalysed Kumada-Type Alkyl-Alkyl Cross-Coupling. Evidence for the Intermediacy of Fe(I) Complexes. *Chem. Sci.* **2013**, *4*, 1098–1104. <https://doi.org/10.1039/c2sc21754f>.
- (32) Iwasaki, T.; Shimizu, R.; Imanishi, R.; Kuniyasu, H.; Kambe, N. Cross-Coupling Reaction of Alkyl Halides with Alkyl Grignard Reagents Catalyzed by Cp-Iron Complexes in the Presence of 1,3-Butadiene. *Chem. Lett.* **2018**, *47*, 763–766. <https://doi.org/10.1246/cl.180201>.
- (33) Agata, R.; Kawamura, S.; Isozaki, K.; Nakamura, M. Iron-Catalyzed Alkyl-Alkyl Negishi Coupling of Organoaluminum Reagents. *Chem. Lett.* **2018**, *48*, 238–241. <https://doi.org/10.1246/cl.180954>.
- (34) Hatakeyama, T.; Hashimoto, T.; Kathriarachchi, K. K. A. D. S.; Zenmyo, T.; Seike, H.; Nakamura, M. Iron-Catalyzed Alkyl-Alkyl Suzuki-Miyaura Coupling. *Angew. Chemie - Int. Ed.* **2012**, *51*, 8834–8837. <https://doi.org/10.1002/anie.201202797>.
- (35) Chen, C.; Bellows, S. M.; Holland, P. L. Tuning Steric and Electronic Effects in Transition-Metal β -Diketiminato Complexes. *Dalt. Trans.* **2015**, *44*, 16654–16670. <https://doi.org/10.1039/c5dt02215k>.

- (36) Eckert, N. A.; Smith, J. M.; Lachicotte, R. J.; Holland, P. L. Low-Coordinate Iron(II) Amido Complexes of β -Diketiminates: Synthesis, Structure, and Reactivity. *Inorg. Chem.* **2004**, *43*, 3306–3321. <https://doi.org/10.1021/ic035483x>.
- (37) Cordier, C. J.; Lundgren, R. J.; Fu, G. C. Enantioconvergent Cross-Couplings of Racemic Alkylmetal Reagents with Unactivated Secondary Alkyl Electrophiles: Catalytic Asymmetric Negishi α -Alkylations of N-Boc-Pyrrolidine. *J. Am. Chem. Soc.* **2013**, *135*, 10946–10949. <https://doi.org/10.1021/ja4054114>.
- (38) Mu, X.; Shibata, Y.; Makida, Y.; Fu, G. C. Control of Vicinal Stereocenters through Nickel-Catalyzed Alkyl–Alkyl Cross-Coupling. *Angew. Chemie - Int. Ed.* **2017**, *56*, 5821–5824. <https://doi.org/10.1002/anie.201702402>.
- (39) Schönherr, H.; Cernak, T. Profound Methyl Effects in Drug Discovery and a Call for New C-H Methylation Reactions. *Angew. Chemie - Int. Ed.* **2013**, *52*, 12256–12267. <https://doi.org/10.1002/anie.201303207>.
- (40) Gee, A.; Windhorst, A. Pd-Mediated Rapid Cross-Couplings Using [^{11}C] Methyl Iodide : Groundbreaking Labeling. *Labelled Compounds and Radiopharmaceuticals* **2015**, *58*, 73-85. <https://doi.org/10.1002/jlcr.3253>.
- (41) Vasilopoulos, A.; Krska, S. W.; Stahl, S. S. C(Sp³) – H Methylation Enabled by Peroxide Photosensitization and Ni-Mediated Radical Coupling. **2021**, *403*, 398–403.
- (42) Miyaura, N.; Suzuki, A. Palladium-Catalyzed Cross-Coupling Reactions of Organoboron Compounds. *Chem. Rev.* **1995**, *95*, 2457–2483. <https://doi.org/10.1021/cr00039a007>.
- (43) Fernández-cabezón, L.; Galán, B.; García, J. L. New Insights on Steroid

- Biotechnology. *Front. Microbiol.* **2018**, *9*, 1-15.
<https://doi.org/10.3389/fmicb.2018.00958>.
- (44) Falivene, L.; Cao, Z.; Petta, A.; Serra, L.; Poater, A.; Oliva, R.; Scarano, V.; Cavallo, L. Towards the Online Computer-Aided Design of Catalytic Pockets. *Nat. Chem.* **2019**, *11*, 872–879. <https://doi.org/10.1038/s41557-019-0319-5>.
- (45) Breitenfeld, J.; Ruiz, J.; Wodrich, M. D.; Hu, X. Bimetallic Oxidative Addition Involving Radical Intermediates in Nickel-Catalyzed Alkyl-Alkyl Kumada Coupling Reactions. *J. Am. Chem. Soc.* **2013**, *135*, 12004–12012. <https://doi.org/10.1021/ja4051923>.
- (46) Kyne, S. H.; Lefèvre, G.; Ollivier, C.; Petit, M.; Ramis Cladera, V. A.; Fensterbank, L. Iron and Cobalt Catalysis: New Perspectives in Synthetic Radical Chemistry. *Chem. Soc. Rev.* **2020**, *49*, 8501–8542. <https://doi.org/10.1039/d0cs00969e>.
- (47) Griller, D.; Ingold1, K. U.; Krusic2, P. J.; Fischer, H. On the Configuration of the Tert-Butyl Radical. *J. Am. Chem. Soc.* **1978**, *100*, 6750–6752. <https://doi.org/10.1021/ja00489a035>.
- (48) Taylor, B. L. H.; Jarvo, E. R. Stereochemistry of Transmetalation of Alkylboranes in Nickel-Catalyzed Alkyl-Alkyl Cross-Coupling Reactions. *J. Org. Chem.* **2011**, *76*, 7573–7576. <https://doi.org/10.1021/jo201263r>.
- (49) Bock, P. L.; Boschetto, D. J.; Rasmussen, J. R.; Demers, J. P.; Whitesides, G. M. Stereochemistry of Reactions at Carbon-Transition Metal σ Bonds. $(\text{CH}_3)_3\text{CCHDCHDFe}(\text{CO})_2\text{C}_5\text{H}_5$. *J. Am. Chem. Soc.* **1974**, *96*, 2814–2825. <https://doi.org/10.1021/ja00816a025>.
- (50) Schrock, R. R.; Seidel, S. W.; Mösch-Zanetti, N. C.; Shih, K. Y.; O'Donoghue, M.

- B.; Davis, W. M.; Reiff, W. M. Synthesis and Decomposition of Alkyl Complexes of Molybdenum(IV) That Contain a $[(\text{Me}_3\text{SiNCH}_2\text{CH}_2)_3\text{N}]_3^-$ Ligand. Direct Detection of α -Elimination Processes That Are More than Six Orders of Magnitude Faster than β -Elimination Processes. *J. Am. Chem. Soc.* **1997**, *119*, 11876–11893. <https://doi.org/10.1021/ja970697x>.
- (51) Huo, H.; Gorsline, B. J.; Fu, G. C. Catalyst-Controlled Doubly Enantioconvergent Coupling of Racemic Alkyl Nucleophiles and Electrophiles. *Science*, **2020**, *367*, 559-564. <https://doi.org/10.1126/science.aaz3855>.
- (52) Crockett, M. P. The Development of Iron Catalysts for Suzuki-Miyaura Cross-Coupling and the Reactivity Discovered Along the Way, Boston College Chemistry, 2020.
- (53) Vela, J.; Vaddadi, S.; Cundari, T. R.; Smith, J. M.; Gregory, E. A.; Lachicotte, R. J.; Flaschenriem, C. J.; Holland, P. L. Reversible Beta-Hydrogen Elimination of Three-Coordinate Iron(II) Alkyl Complexes: Mechanistic and Thermodynamic Studies. *Organometallics* **2004**, *23*, 5226–5239. <https://doi.org/10.1021/om049415+>.
- (54) Przyojski, J. A.; Veggeberg, K. P.; Arman, H. D.; Tonzetich, Z. J. Mechanistic Studies of Catalytic Carbon-Carbon Cross-Coupling by Well-Defined Iron NHC Complexes. *ACS Catal.* **2015**, *5*, 5938–5946. <https://doi.org/10.1021/acscatal.5b01445>.
- (55) Trovitch, R. J.; Lobkovsky, E.; Chirik, P. J. Bis(Imino)Pyridine Iron Alkyls Containing β -Hydrogens: Synthesis, Evaluation of Kinetic Stability, and Decomposition Pathways Involving Chelate Participation. *J. Am. Chem. Soc.* **2008**,

130, 11631–11640. <https://doi.org/10.1021/ja803296f>.

- (56) Burger, B. J.; Bercaw, J. E. Vacuum Line Techniques for Handling Air-Sensitive Organometallic Compounds. In *Experimental Organometallic Chemistry*; Wayda, A. L., Darensbourg, M. Y., Eds.; American Chemical Society, 1987; pp 79–115. <https://doi.org/10.1021/bk-1987-0357.ch004>.
- (57) Pangborn, A. B.; Giardello, M. A.; Grubbs, R. H.; Rosen, R. K.; Timmers, F. J. Safe and Convenient Procedure for Solvent Purification. *Organometallics* **1996**, *15*, 1518–1520. <https://doi.org/10.1021/om9503712>.
- (58) Pedroni, J.; Cramer, N. 2-(Trifluoromethyl)Indoles via Pd(0)-Catalyzed C(Sp³)-H Functionalization of Trifluoroacetimidoyl Chlorides. *Org. Lett.* **2016**, *18*, 1932–1935. <https://doi.org/10.1021/acs.orglett.6b00795>.
- (59) Badiei, Y. M.; Dinescu, A.; Dai, X.; Palomino, R. M.; Heinemann, F. W.; Cundari, T. R.; Warren, T. H. Copper-Nitrene Complexes in Catalytic C-H Amination. *Angew. Chemie - Int. Ed.* **2008**, *47*, 9961–9964. <https://doi.org/10.1002/anie.200804304>.
- (60) Kundu, S.; Greene, C.; Williams, K. D.; Salvador, T. K.; Bertke, J. A.; Cundari, T. R.; Warren, T. H. Three-Coordinate Copper(II) Aryls: Key Intermediates in C-O Bond Formation. *J. Am. Chem. Soc.* **2017**, *139*, 9112–9115. <https://doi.org/10.1021/jacs.7b04046>.
- (61) Eignerová, B.; Drac, M. Perfluoroalkylation through Cross-Metathesis between Alkenes and (Perfluoroalkyl)Propenes. *Eur. J. Org. Chem.* **2008**, *2008*, 4493–4499. <https://doi.org/10.1002/ejoc.200800230>.
- (62) Yang, C. T.; Zhang, Z. Q.; Liu, Y. C.; Liu, L. Copper-Catalyzed Cross-Coupling

- Reaction of Organoboron Compounds with Primary Alkyl Halides and Pseudohalides. *Angew. Chemie - Int. Ed.* **2011**, *50*, 3904–3907. <https://doi.org/10.1002/anie.201008007>.
- (63) Fang, G. Y.; Wallner, O. A.; Di Blasio, N.; Ginesta, X.; Harvey, J. N.; Aggarwal, V. K. Asymmetric Sulfur Ylide Reactions with Boranes: Scope and Limitations, Mechanism and Understanding. *J. Am. Chem. Soc.* **2007**, *129*, 14632–14639. <https://doi.org/10.1021/ja074110i>.
- (64) Smith, P. J.; Crowe, D. A. J.; Westaway, K. C. Using Secondary Alpha Deuterium Kinetic Isotope Effects to Determine the Stereochemistry of an E2 Reaction; the Stereochemistry of the E2 Reaction of 1-Chloro-2-Phenylethane with Potassium *Tert*-Butoxide in *Tert*-Butyl Alcohol. *Can. J. Chem.* **2001**, *79*, 1145–1152. <https://doi.org/10.1139/cjc-79-7-1145>.
- (65) Lu, X.; Xiao, B.; Zhang, Z.; Gong, T.; Su, W.; Yi, J.; Fu, Y.; Liu, L. Practical Carbon-Carbon Bond Formation from Olefins through Nickel-Catalyzed Reductive Olefin Hydrocarbonation. *Nat. Commun.* **2016**, *7*, 1–8. <https://doi.org/10.1038/ncomms11129>.
- (66) Ren, P.; Vechorkin, O.; Von Allmen, K.; Scopelliti, R.; Hu, X. A Structure-Activity Study of Ni-Catalyzed Alkyl-Alkyl Kumada Coupling. Improved Catalysts for Coupling of Secondary Alkyl Halides. *J. Am. Chem. Soc.* **2011**, *133*, 7084–7095. <https://doi.org/10.1021/ja200270k>.
- (67) Hashimoto, T.; Maruyama, T.; Yamaguchi, T.; Matsubara, Y.; Yamaguchi, Y. Cross-Coupling Reactions of Alkyl Halides with Aryl Grignard Reagents Using a Tetrachloroferrate with an Innocent Counteranion. *Adv. Synth. Catal.* **2019**, *361*,

4232–4236. <https://doi.org/10.1002/adsc.201900568>.

- (68) Liu, J. H.; Yang, C. T.; Lu, X. Y.; Zhang, Z. Q.; Xu, L.; Cui, M.; Lu, X.; Xiao, B.; Fu, Y.; Liu, L. Copper-Catalyzed Reductive Cross-Coupling of Nonactivated Alkyl Tosylates and Mesylates with Alkyl and Aryl Bromides. *Chem. - A Eur. J.* **2014**, *20*, 15334–15338. <https://doi.org/10.1002/chem.201405223>.
- (69) Lu, Z.; Fu, G. C. Alkyl-Alkyl Suzuki Cross-Coupling of Unactivated Secondary Alkyl Chlorides. *Angew. Chemie - Int. Ed.* **2010**, *49*, 6676–6678. <https://doi.org/10.1002/anie.201003272>.
- (70) Yu, F.; Wang, T.; Zhou, H.; Li, Y.; Zhang, X.; Bao, H. Iron(III)-Catalyzed Ortho-Preferred Radical Nucleophilic Alkylation of Electron-Deficient Arenes. *Org. Lett.* **2017**, *19*, 6538–6541. <https://doi.org/10.1021/acs.orglett.7b03244>.
- (71) Eckert, P.; Organ, M. G. The Role of LiBr and ZnBr₂ on the Cross-Coupling of Aryl Bromides with Bu₂Zn or BuZnBr. *Chem. - A Eur. J.* **2019**, *25*, 15751–15754. <https://doi.org/10.1002/chem.201903931>.
- (72) Le Bailly, B. A. F. L.; Greenhalgh, M. D.; Thomas, S. P. Iron-Catalysed, Hydride-Mediated Reductive Cross-Coupling of Vinyl Halides and Grignard Reagents. *Chem. Commun.* **2012**, *48*, 1580–1582. <https://doi.org/10.1039/c1cc14622j>.
- (73) Bekish, A. V.; Prokhorevich, K. N.; Kulinkovich, O. G. Transformation of Esters into 2-Substituted Allyl Halides via Tertiary Cyclopropanols: Application in the Stereoselective Synthesis of (2S,3S,7S)-3,7-Dimethyl-2-Pentadecyl Acetate, the Sex Pheromone of the Pine Sawfly Neodiprion Sertifer. *European J. Org. Chem.* **2006**, *22*, 5069–5075. <https://doi.org/10.1002/ejoc.200600481>.

Appendix A. Spectral Data.

Appendix A.1 Spectral Data for Chapter 2

Figure 1 – ^1H NMR(500 MHz) spectrum of 2.7.

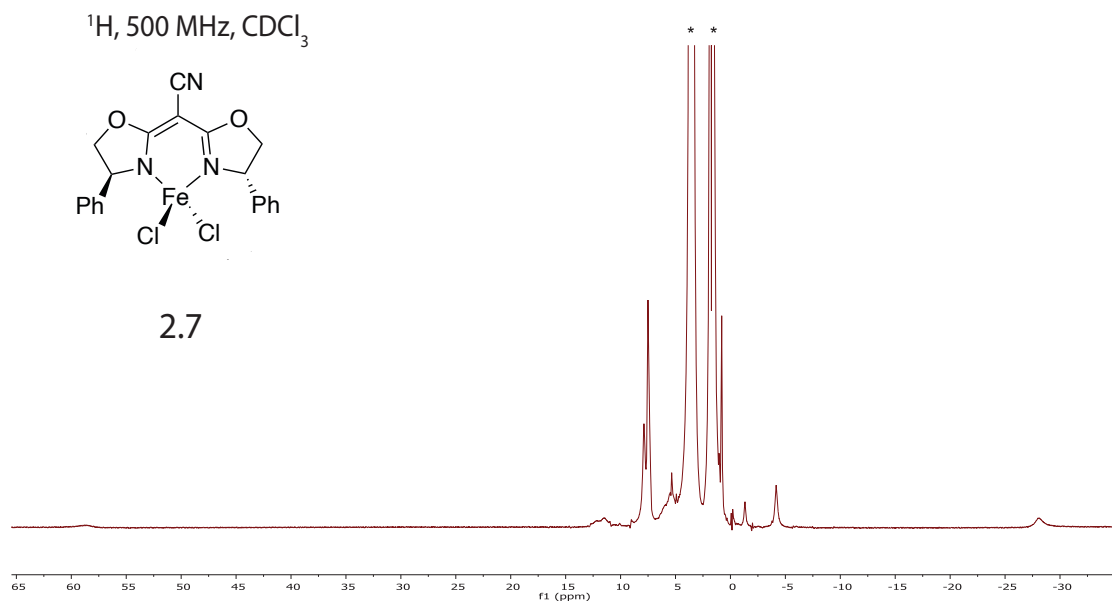


Figure 2– ^1H NMR(500 MHz) spectrum of 2.8.

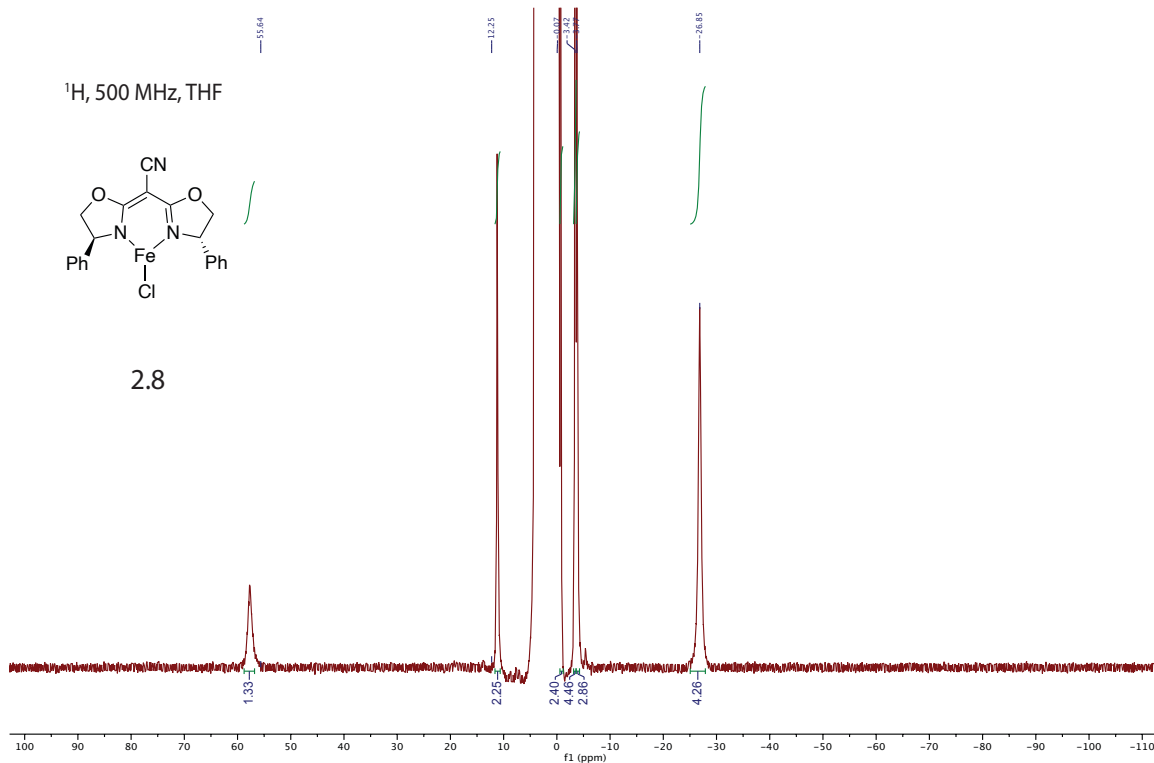


Figure 3 – ^1H NMR(400 MHz) spectrum of 2.9.

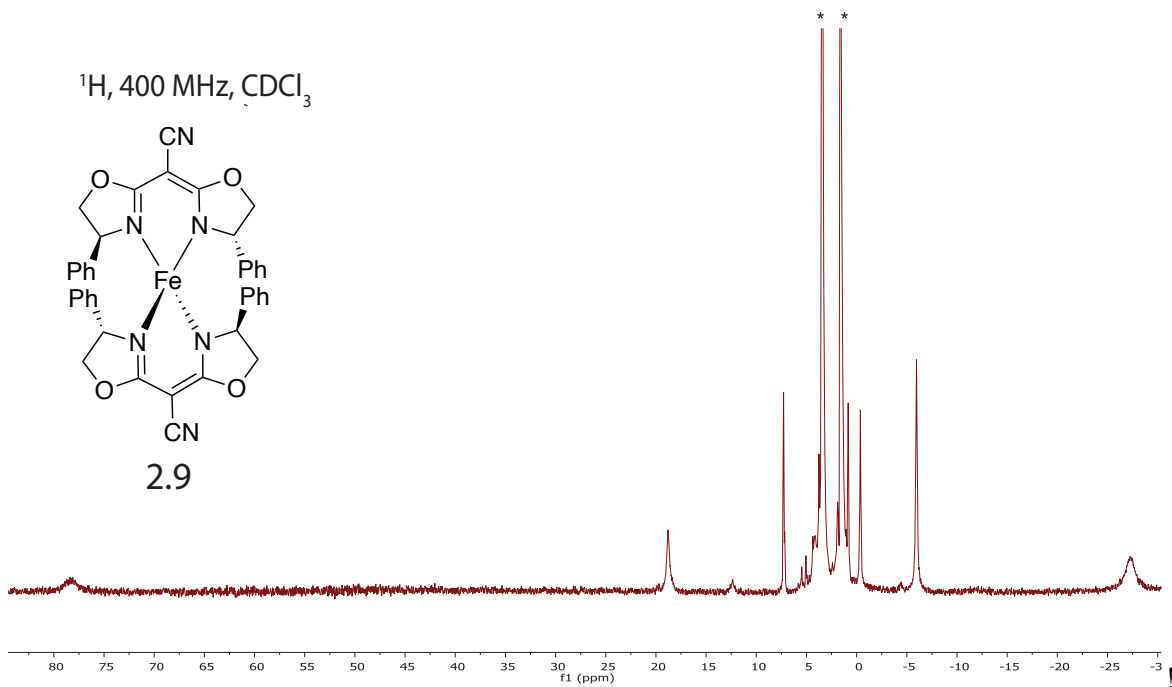


Figure 4 – ^1H NMR(500 MHz) of 2.21.

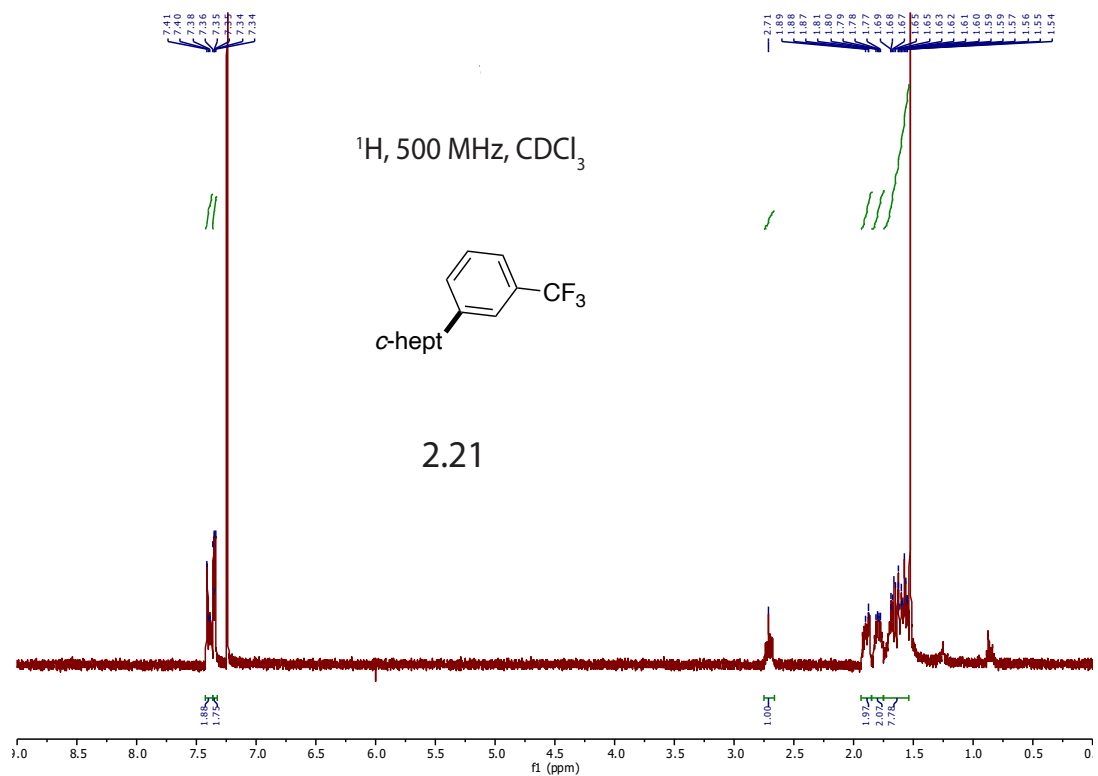


Figure 5 – $\{^1\text{H}\}^{13}\text{C}$ NMR(125 MHz) spectrum of of **2.21**.

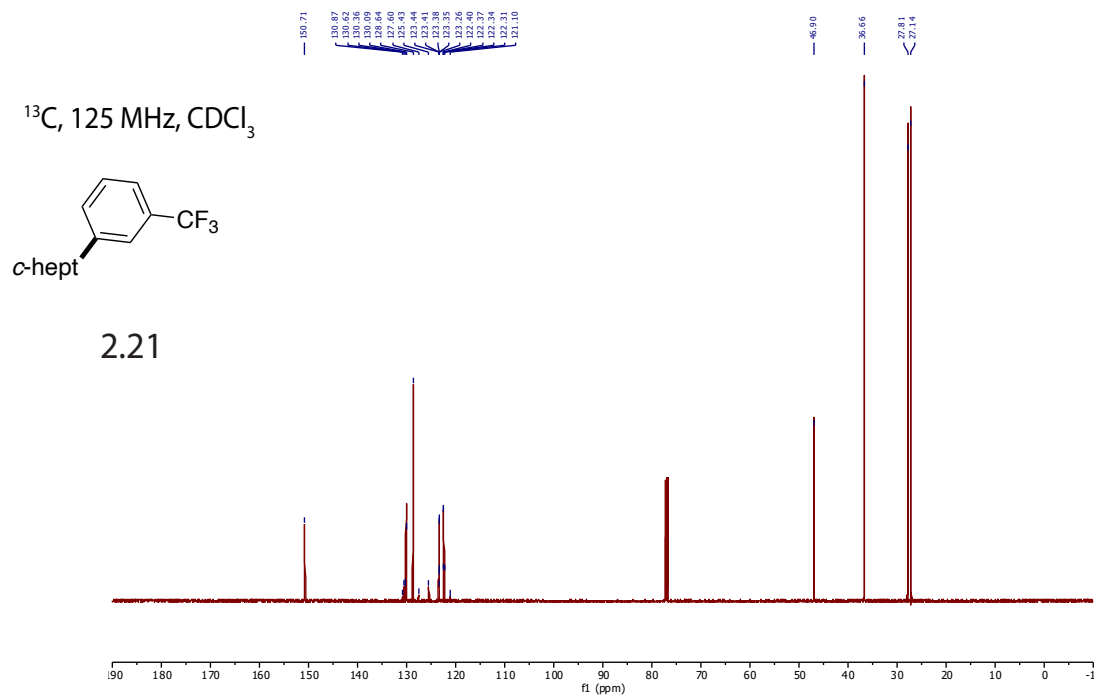


Figure 6 – ^{19}F NMR(470MHz) spectrum of **2.21**.

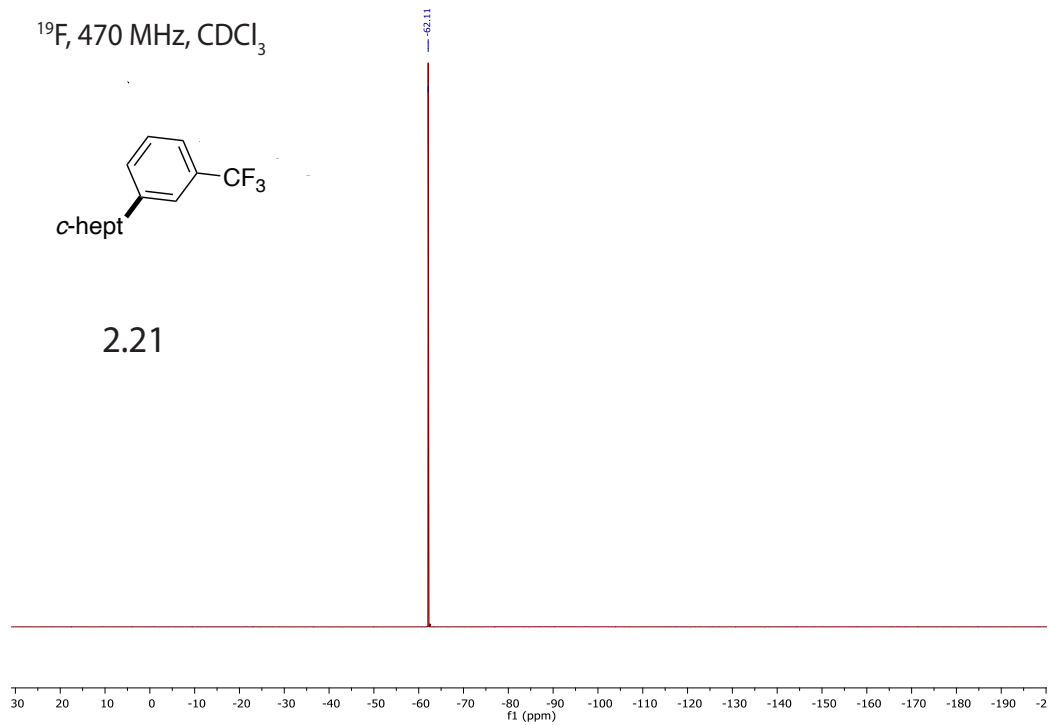


Figure 7 – ^1H NMR(500 MHz) spectrum of 2.30.

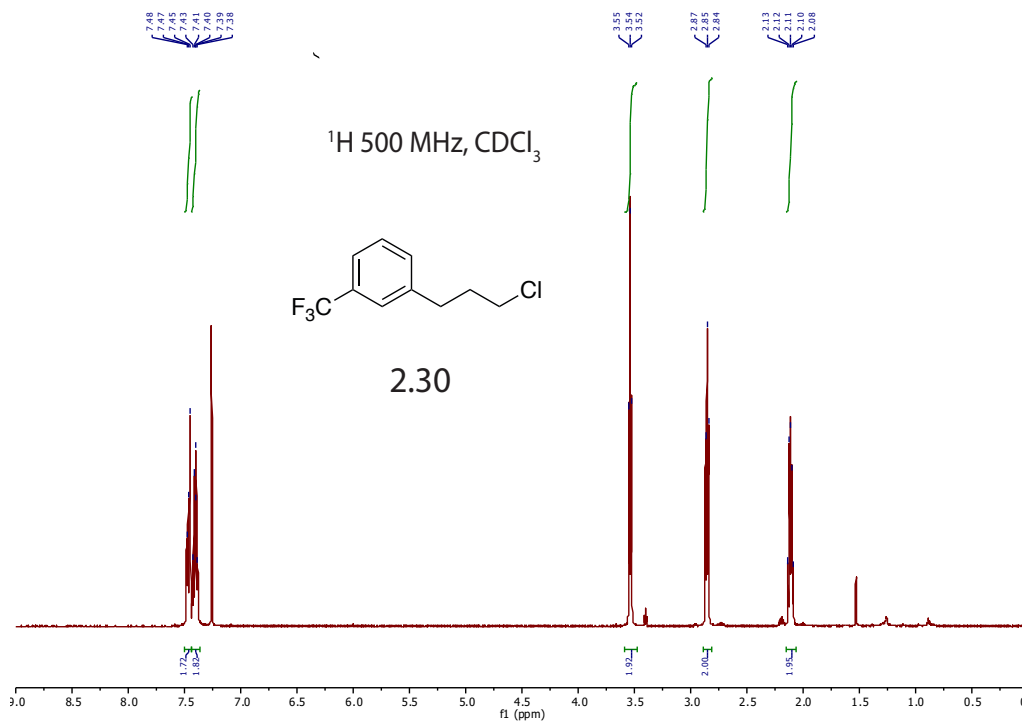


Figure 8 – ^{13}C NMR(125 MHz) spectrum of spectrum of 2.30.

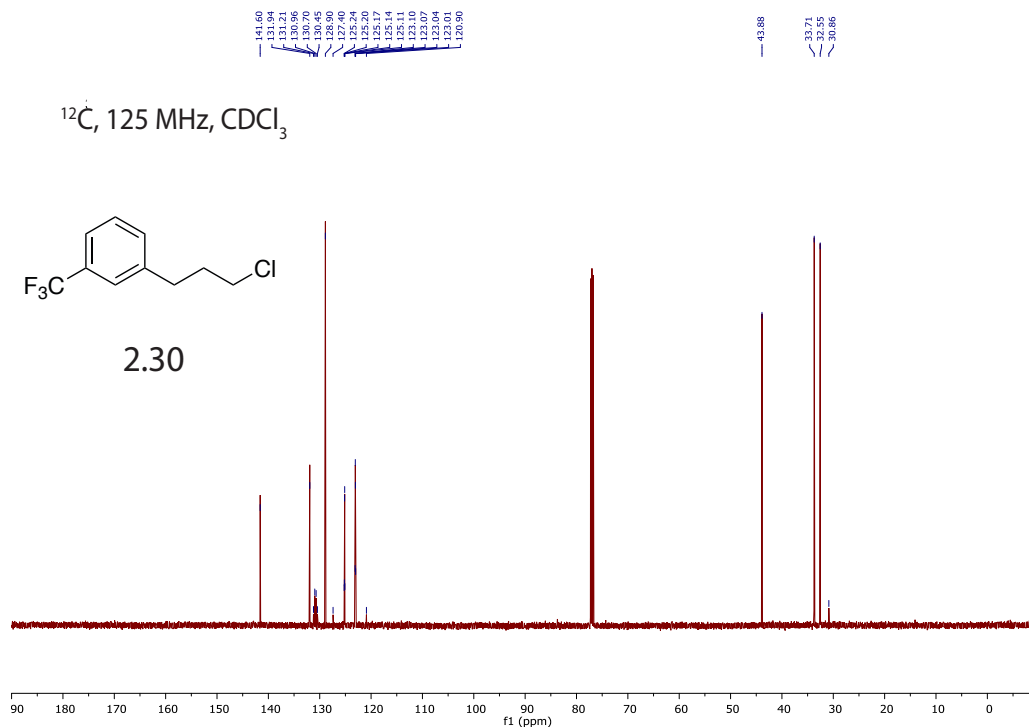
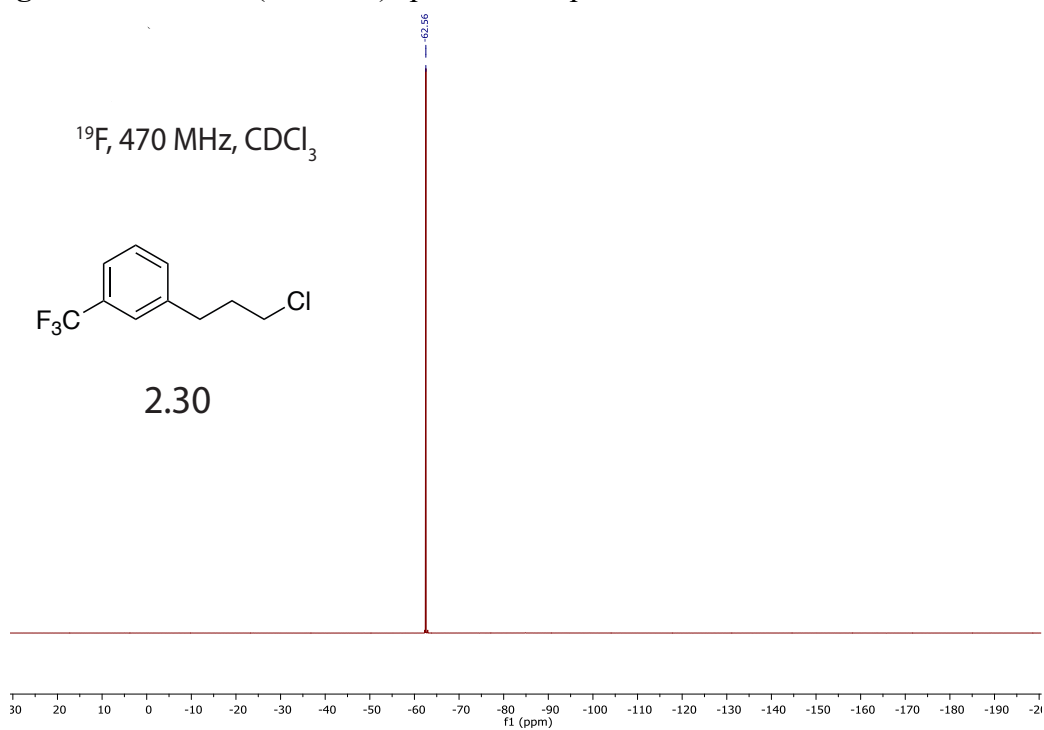


Figure 9 – ^{19}F NMR(470MHz) spectrum of spectrum of **2.30**.



Appendix A.2 Spectral Data for Chapter 3

Figure 10 – ^1H NMR(500 MHz) spectrum of *tert*-butyl(4-(1-chloroethyl)phenoxy)dimethylsilane.

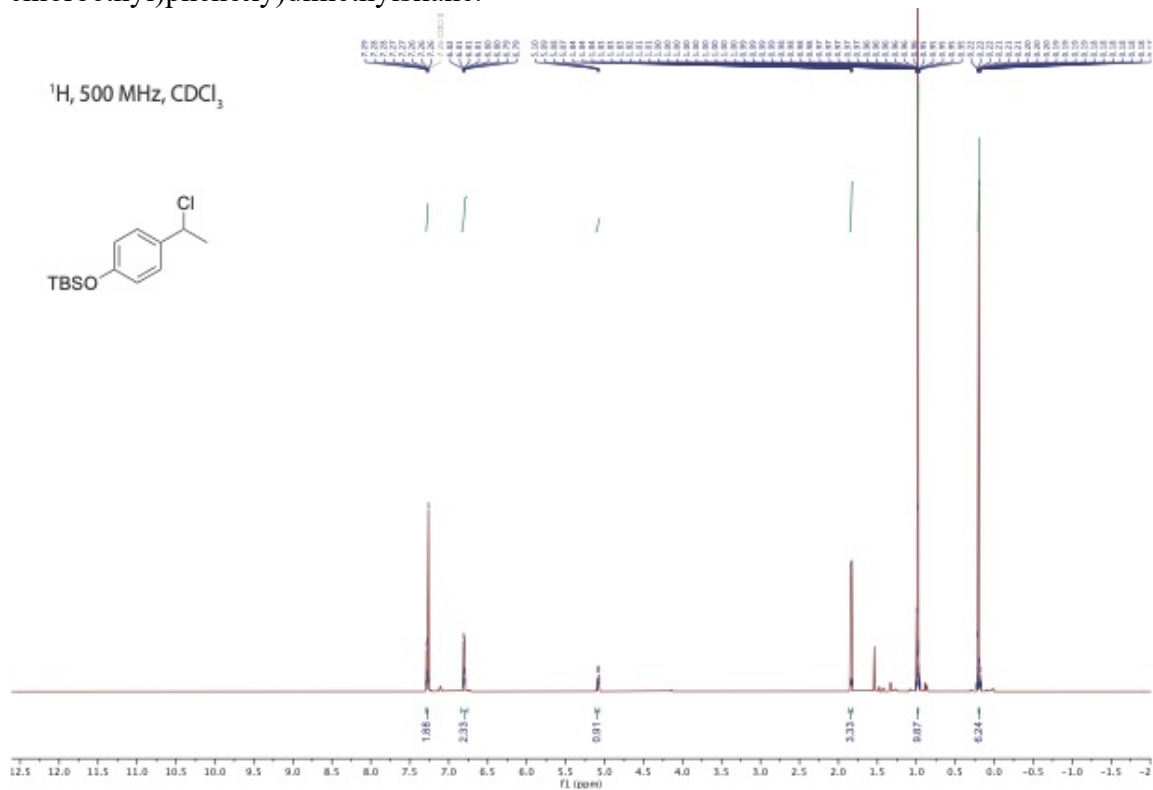


Figure 11 – ^{13}C NMR(125 MHz) spectrum of *tert*-butyl(4-(1-chloroethyl)phenoxy)dimethylsilane.

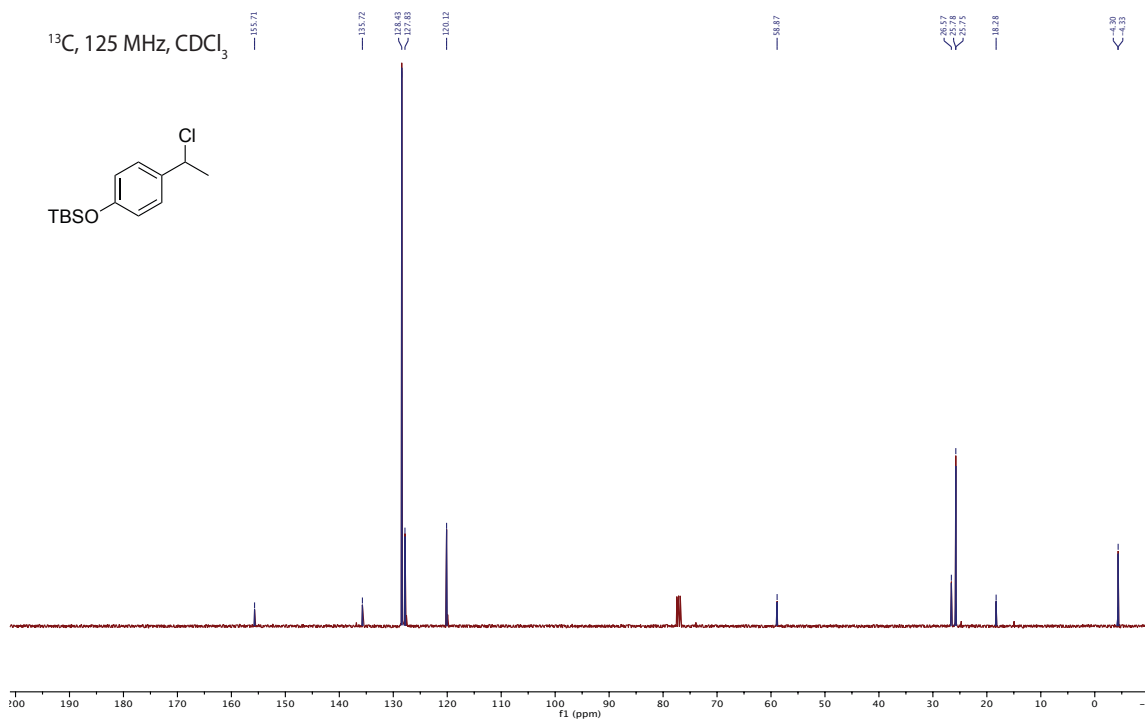


Figure 12 – ^1H NMR(500 MHz) spectrum of 4-bromo-1-chloro-2-(1-chloroethyl)benzene

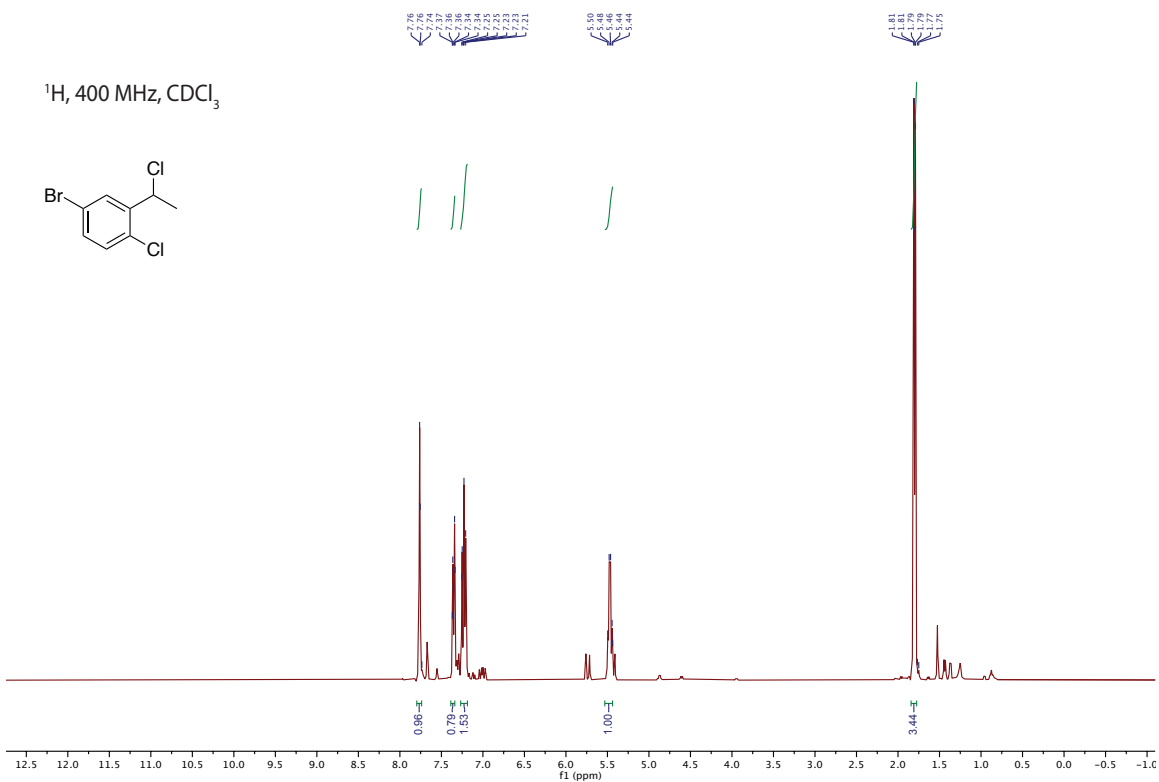


Figure 13 – ^{13}C NMR(125 MHz) spectrum of 4-bromo-1-chloro-2-(1-chloroethyl)benzene

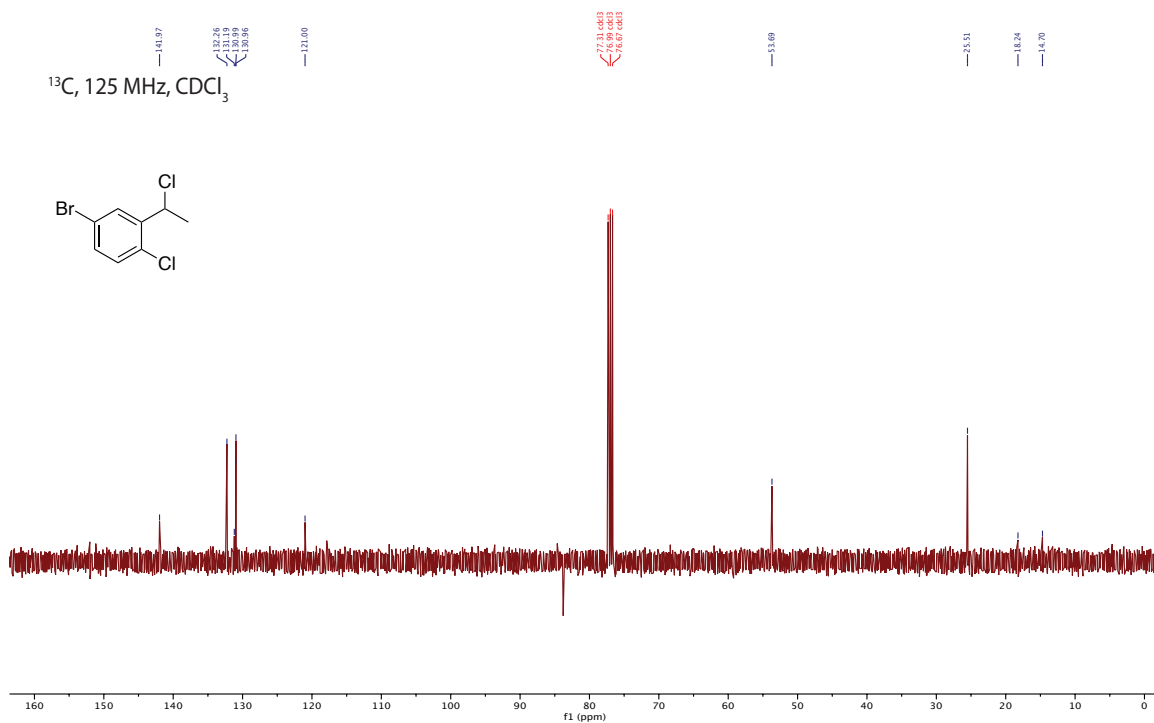


Figure 14 – ^1H NMR(500 MHz) spectrum of 2,2-Methylene-[(4S)-mesityl-2-oxazoline].

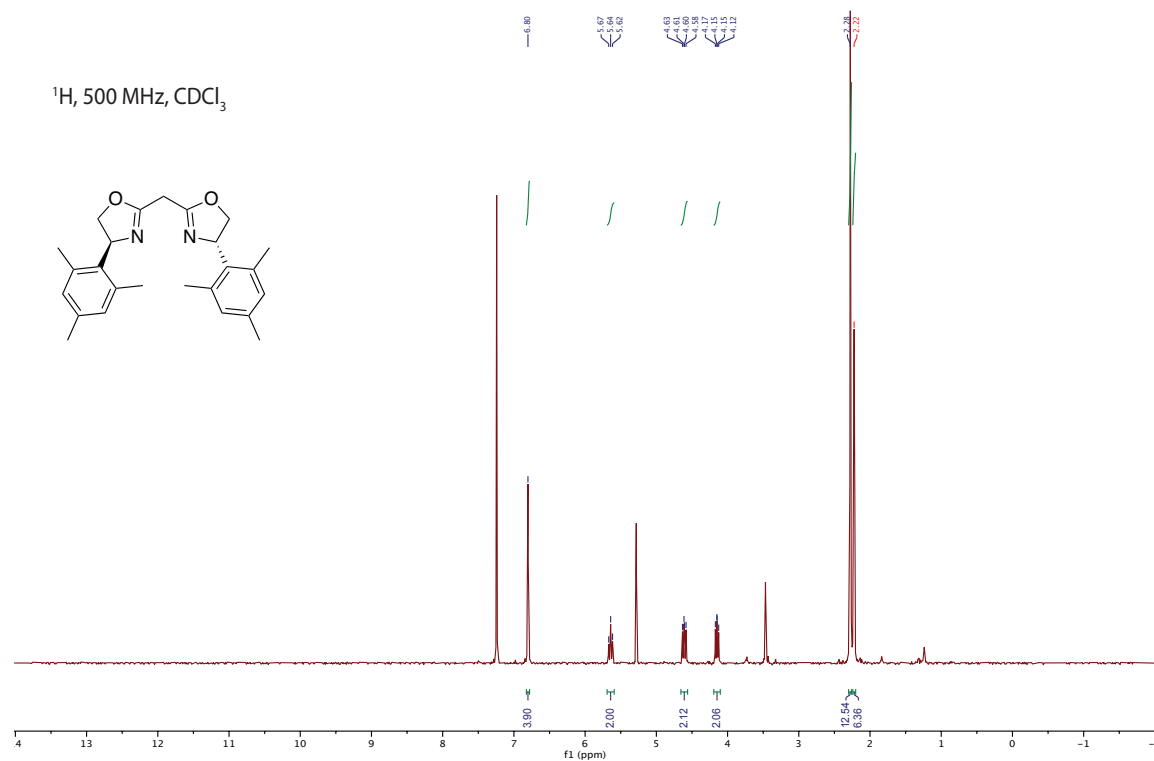


Figure 15 – ¹H NMR(500 MHz) spectrum of 3.9a.

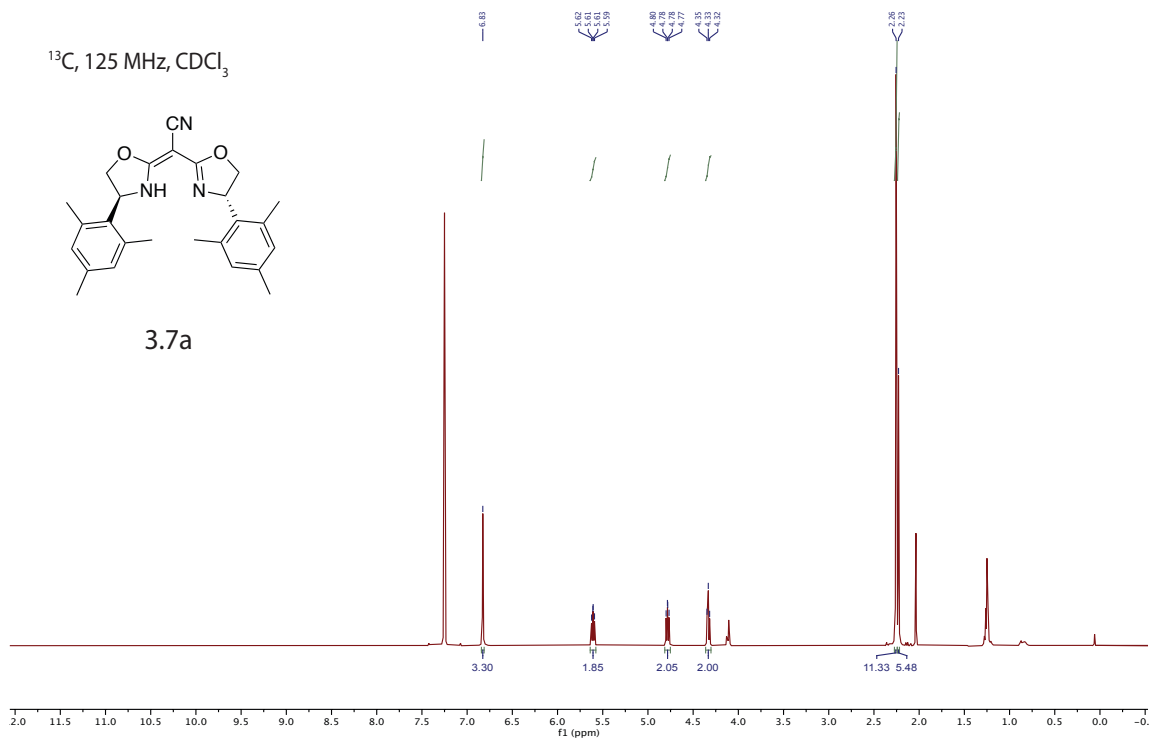


Figure 16 – ¹³C NMR(125 MHz) spectrum of 3.9a.

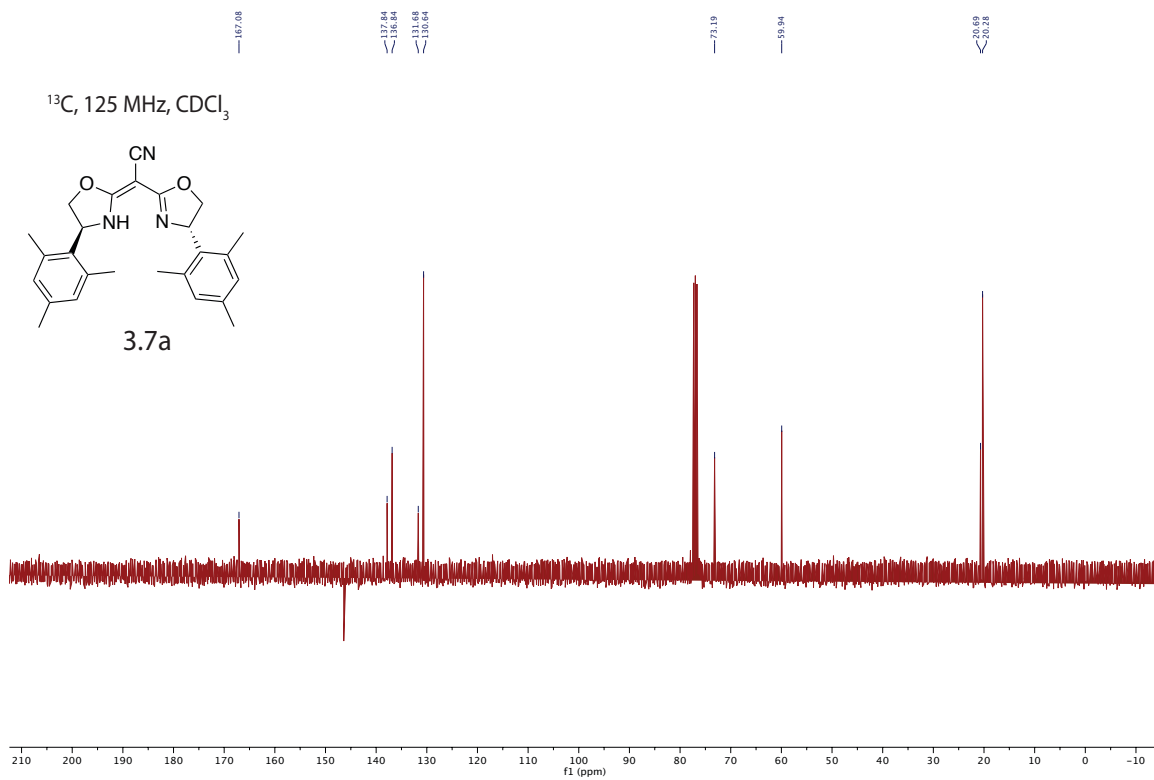


Figure 17 – ^1H NMR(500 MHz) spectrum of **3.10a**.

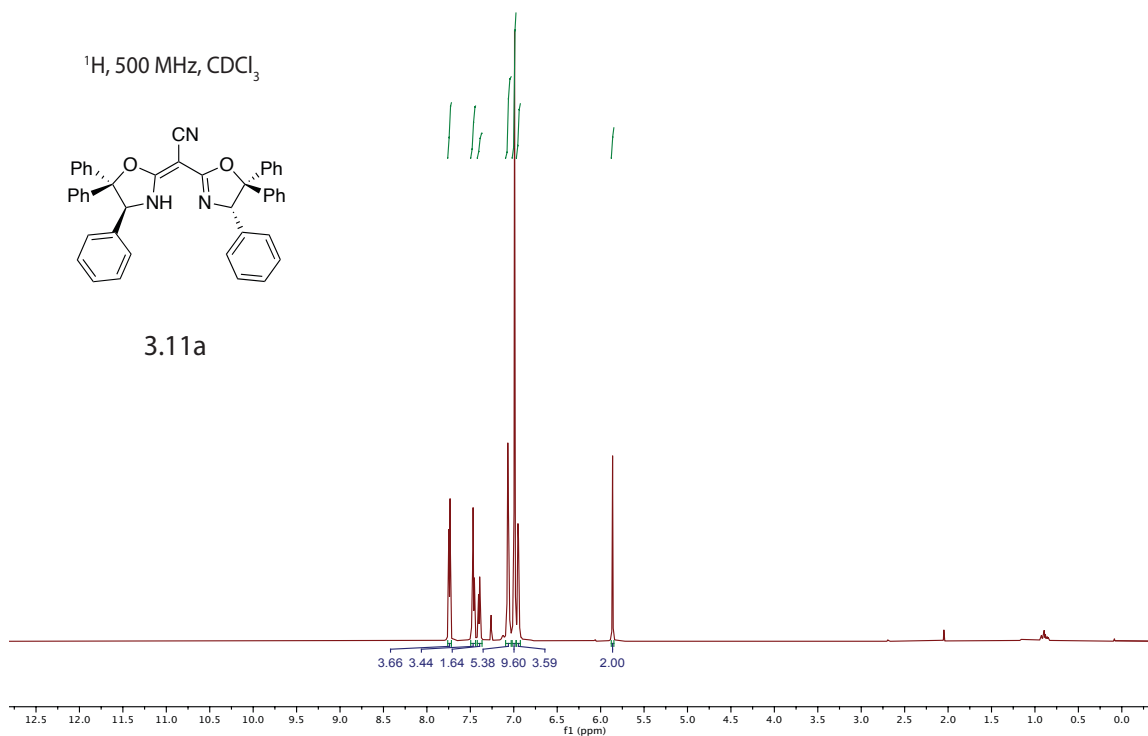


Figure 18 – ^1H NMR(500 MHz) spectrum of **3.3**.

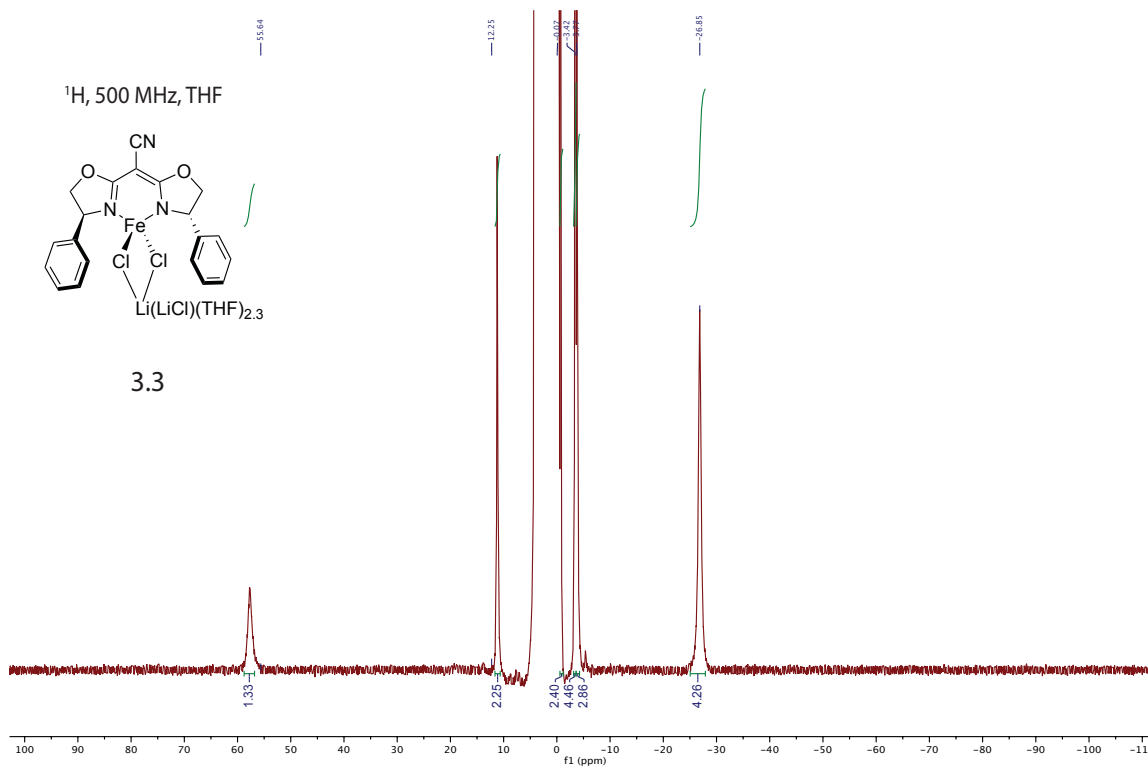


Figure 19 – ^1H NMR(500 MHz) spectrum of 3.8.

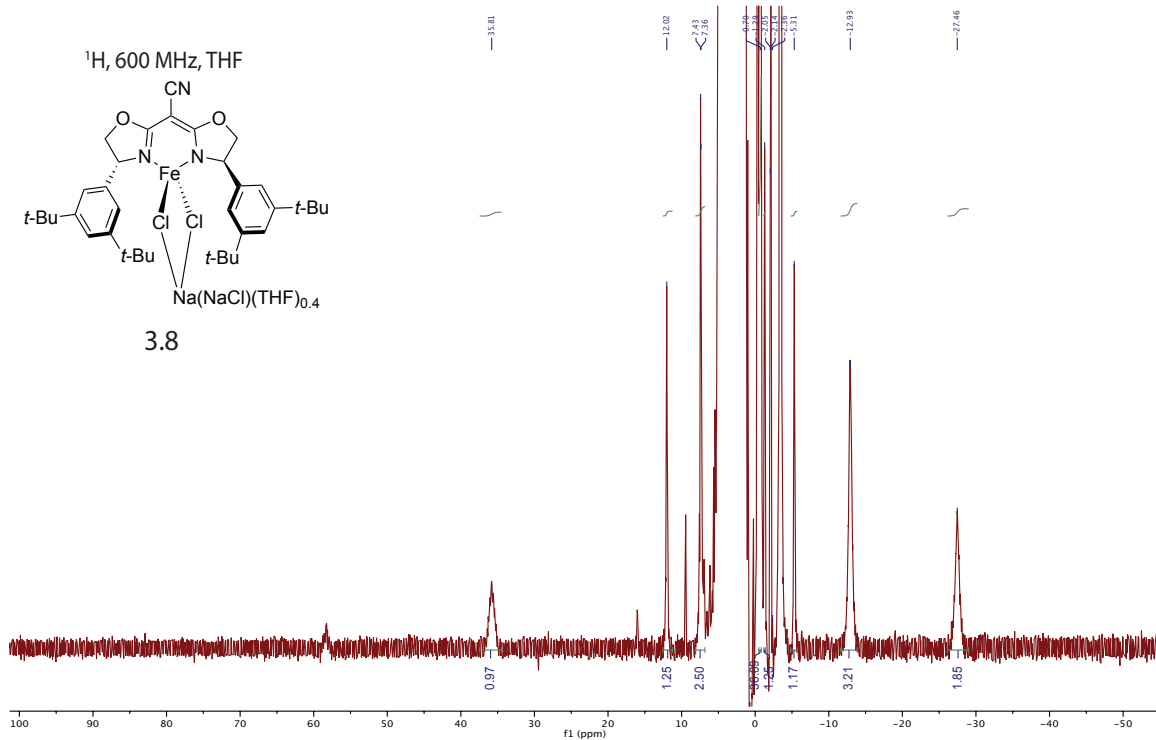


Figure 20 – ^1H NMR(500 MHz) spectrum of 3.9.

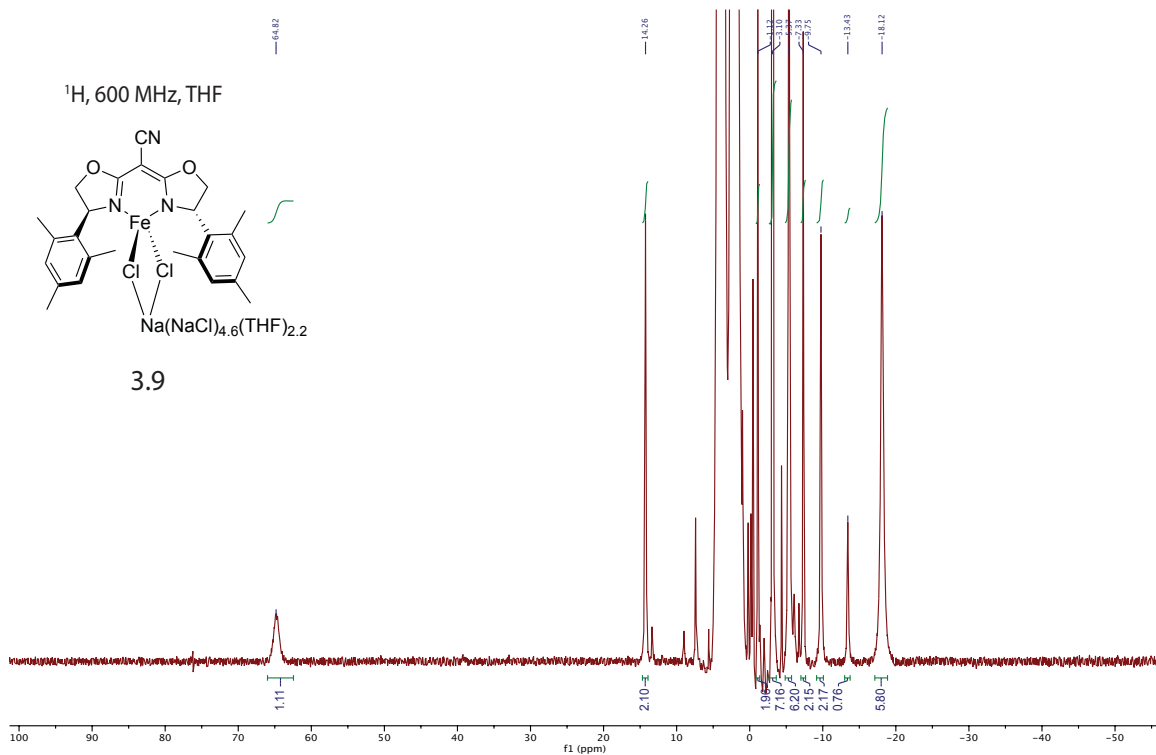


Figure 21 – ¹H NMR(500 MHz) spectrum of 3.10.

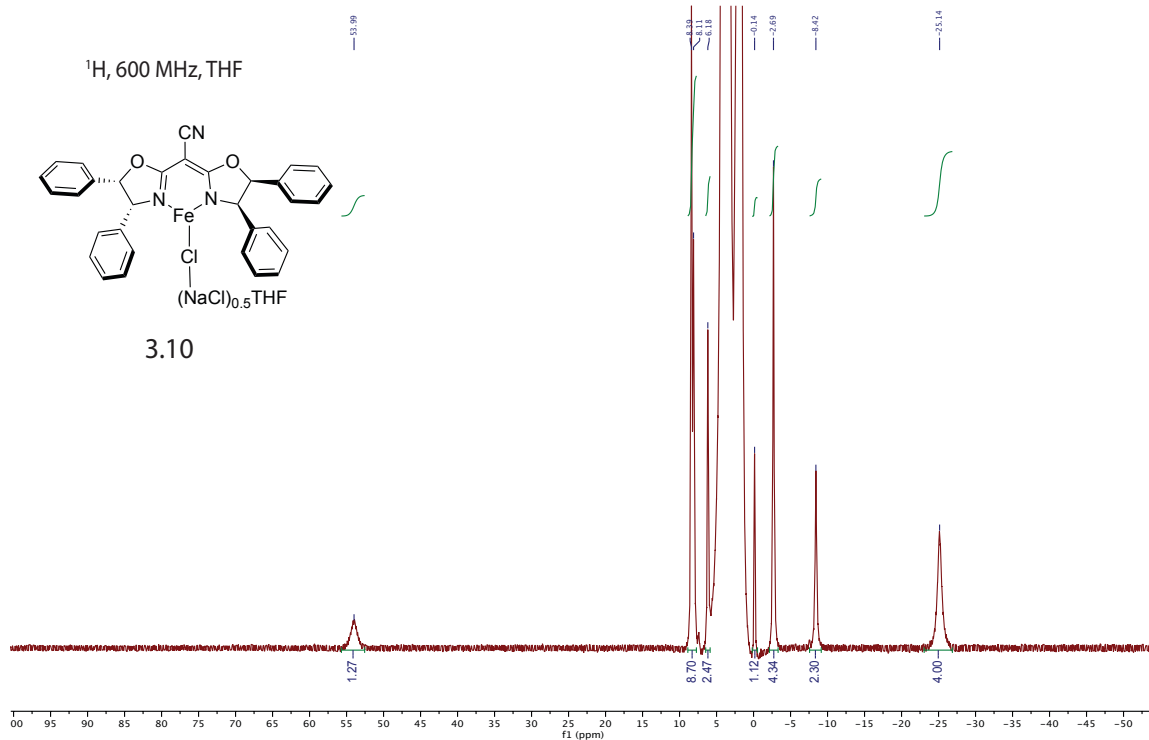


Figure 22 – ¹H NMR(500 MHz) spectrum of 3.11.

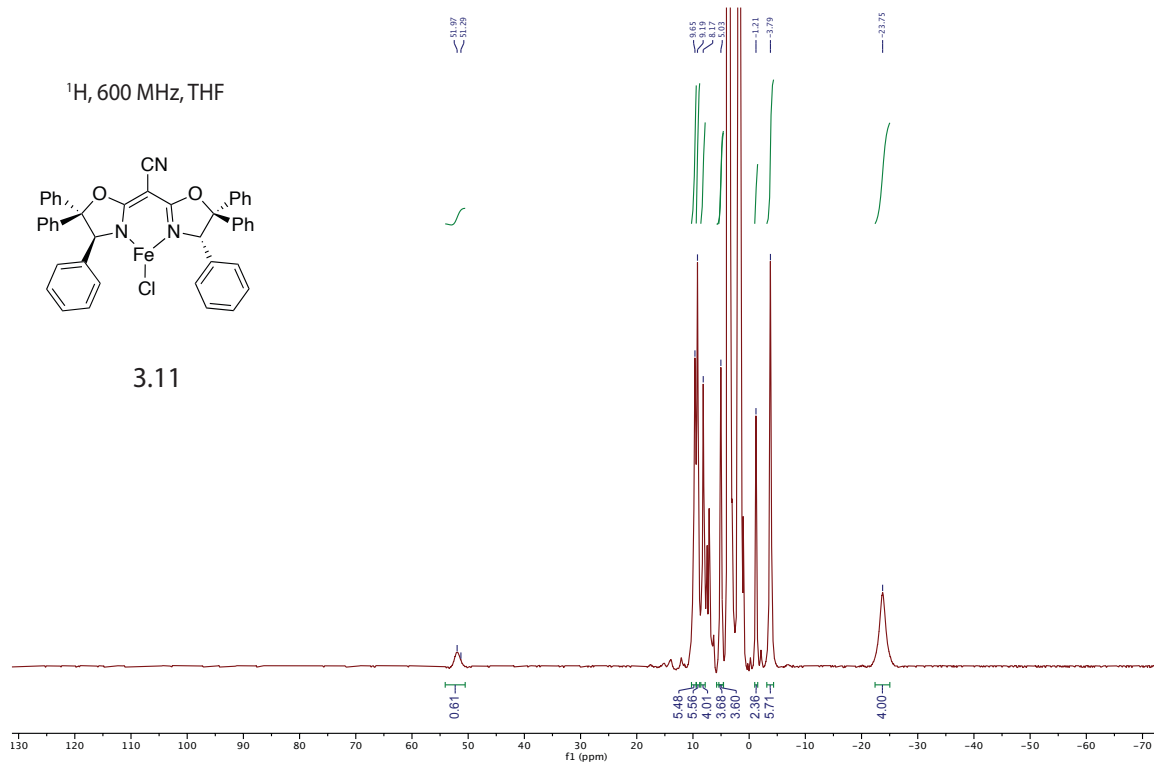


Figure 23 – ^1H NMR(500 MHz) spectrum of 3.12.

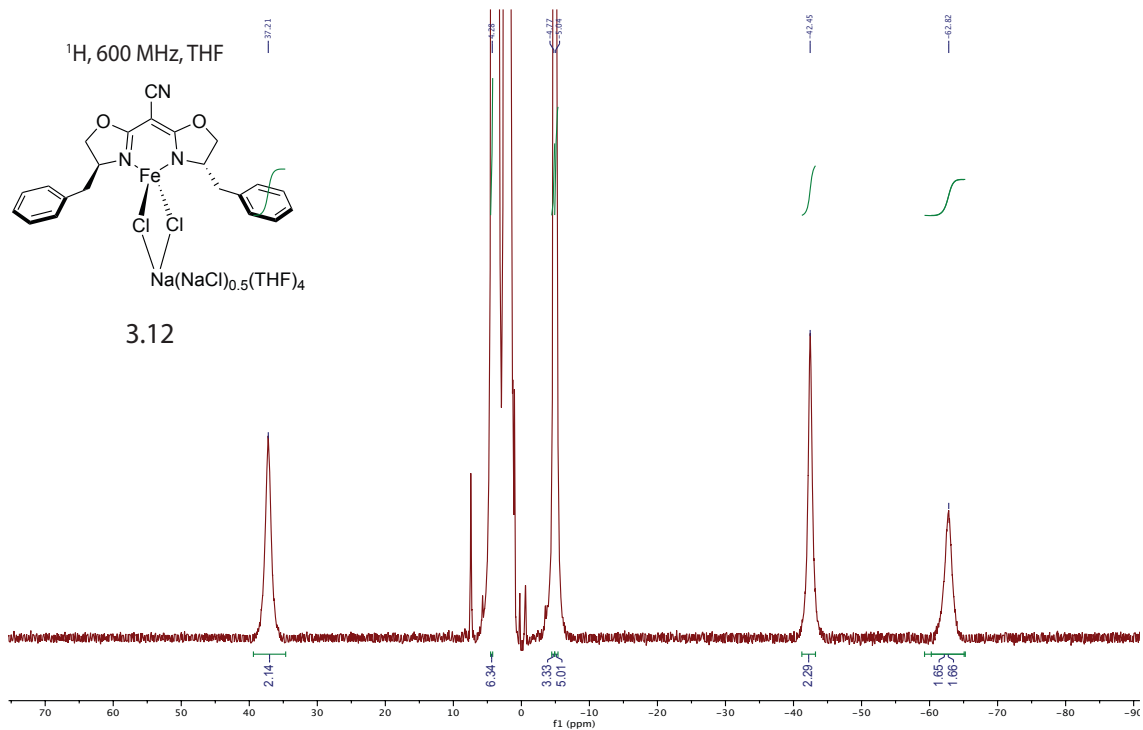


Figure 24 – ^1H NMR(500 MHz) spectrum of 3.14.

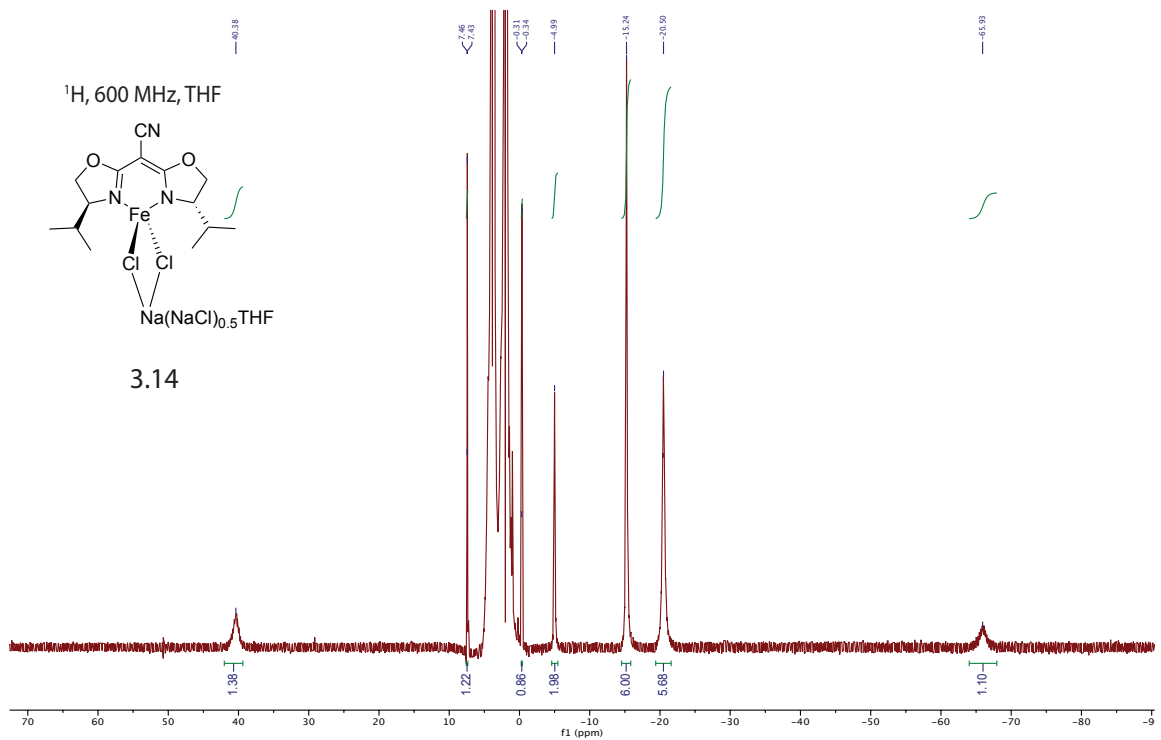


Figure 25 – ¹H NMR(500 MHz) spectrum of 3.15.

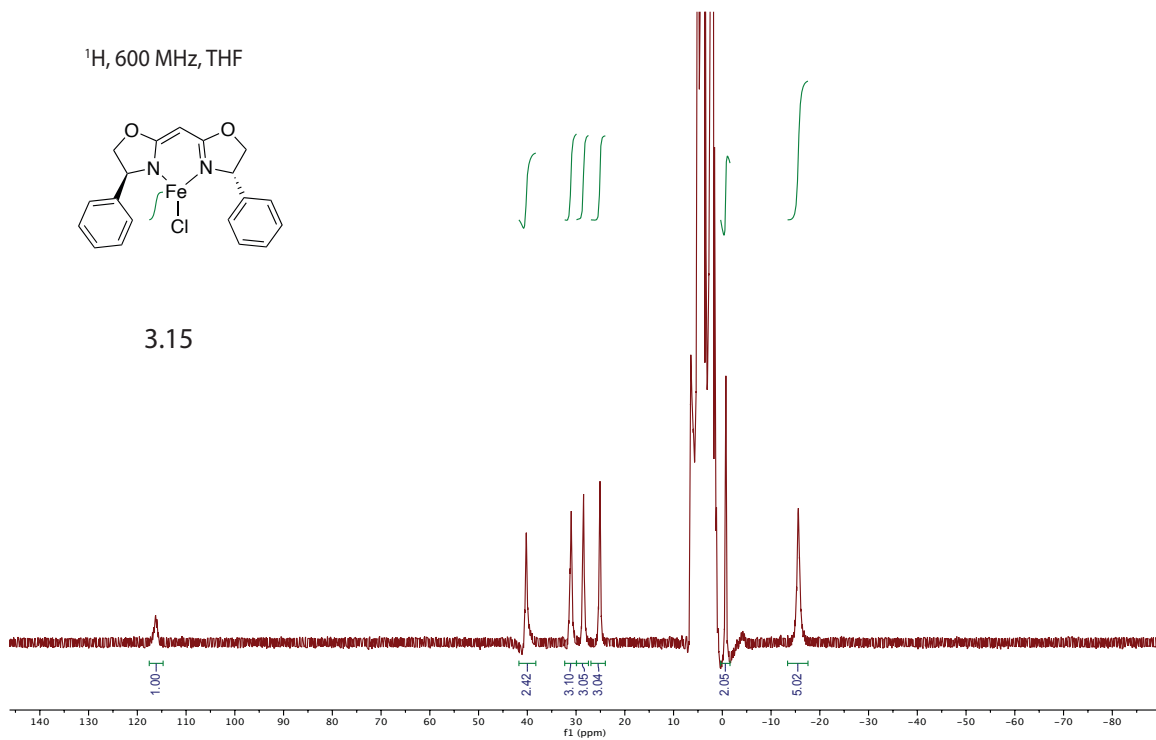


Figure 26 – ¹H NMR(500 MHz) spectrum of 3.19.

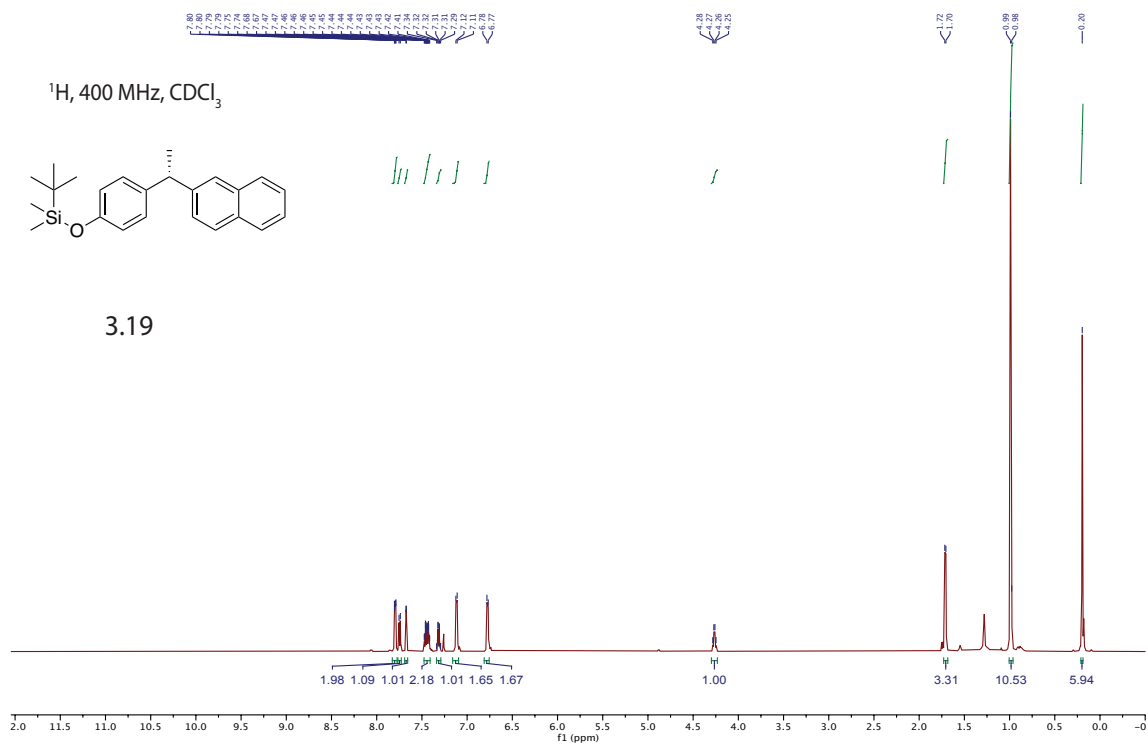


Figure 29 – ^{13}C NMR(125 MHz) spectrum of 3.21.

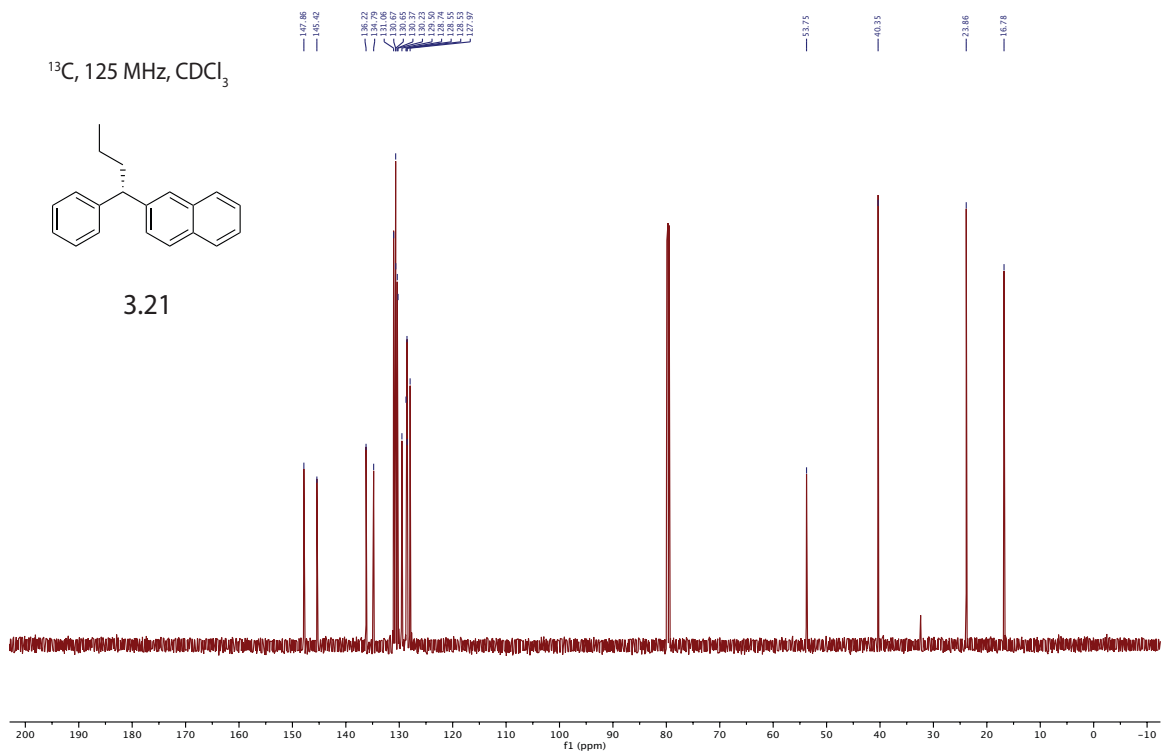


Figure 30 – ^1H NMR(500 MHz) spectrum of 3.22.

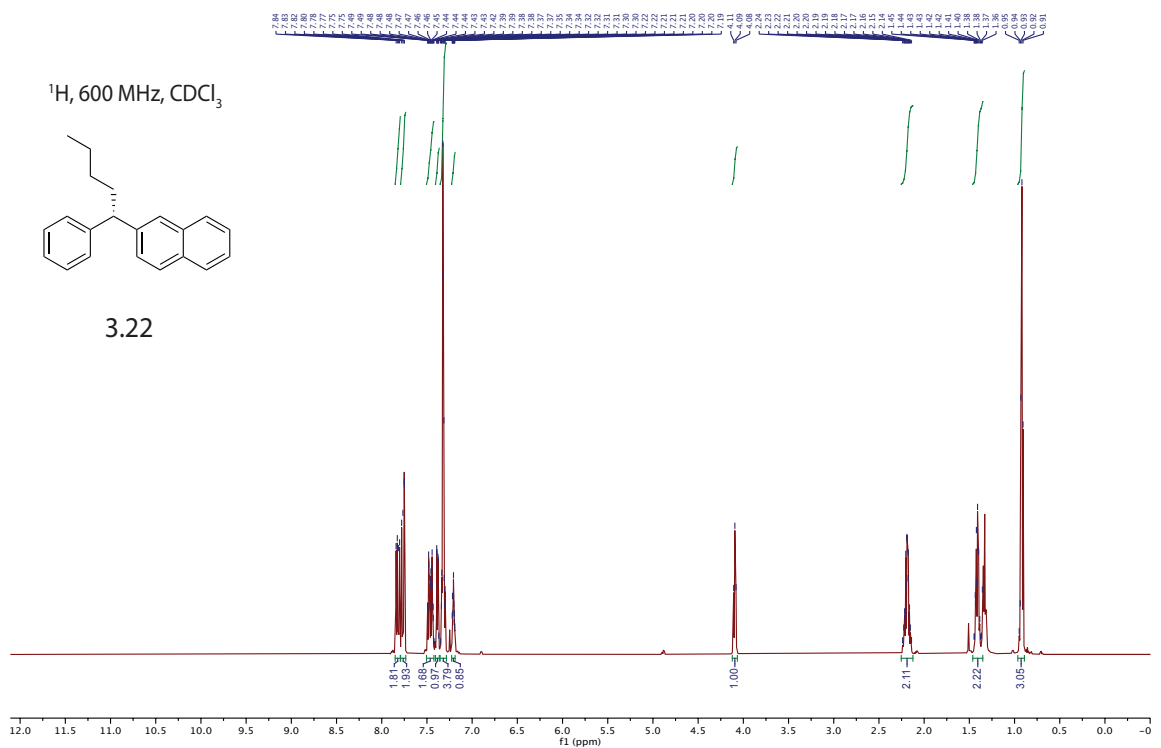


Figure 31 – ^{13}C NMR(125 MHz) spectrum of 3.22.

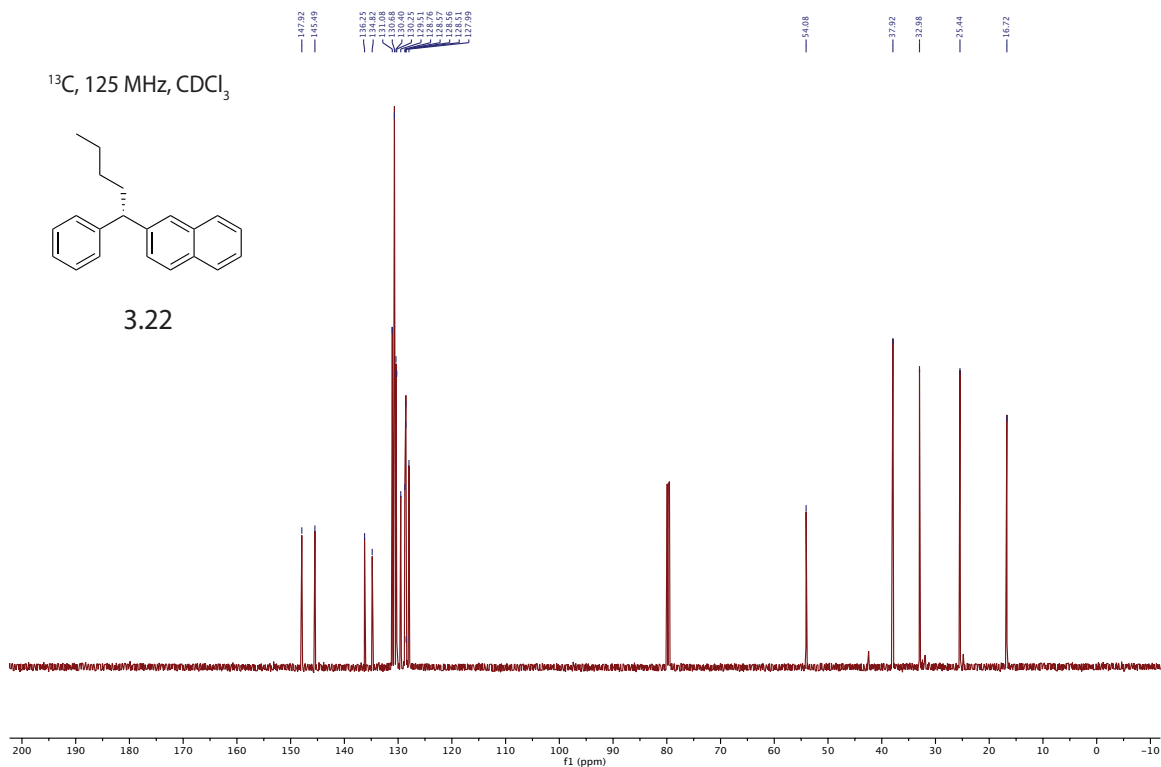


Figure 32 – ^1H NMR(500 MHz) spectrum of 3.23.

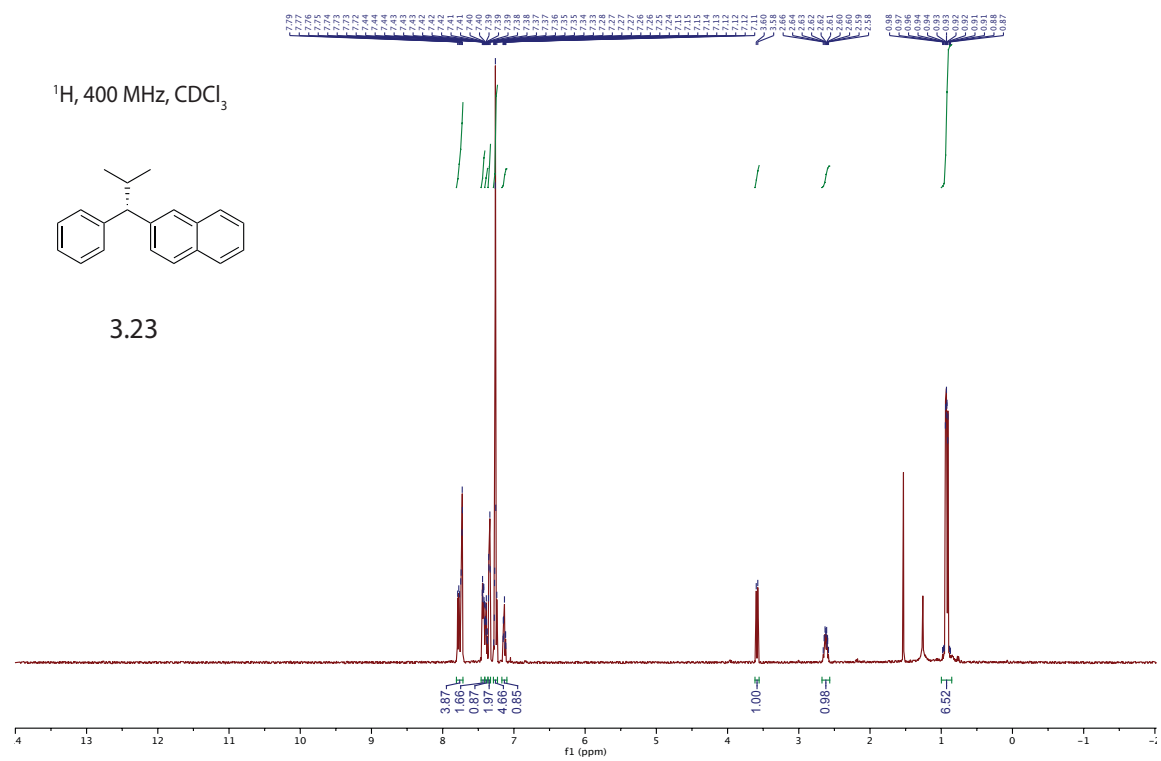


Figure 33 – ^{13}C NMR(125 MHz) spectrum of 3.23.

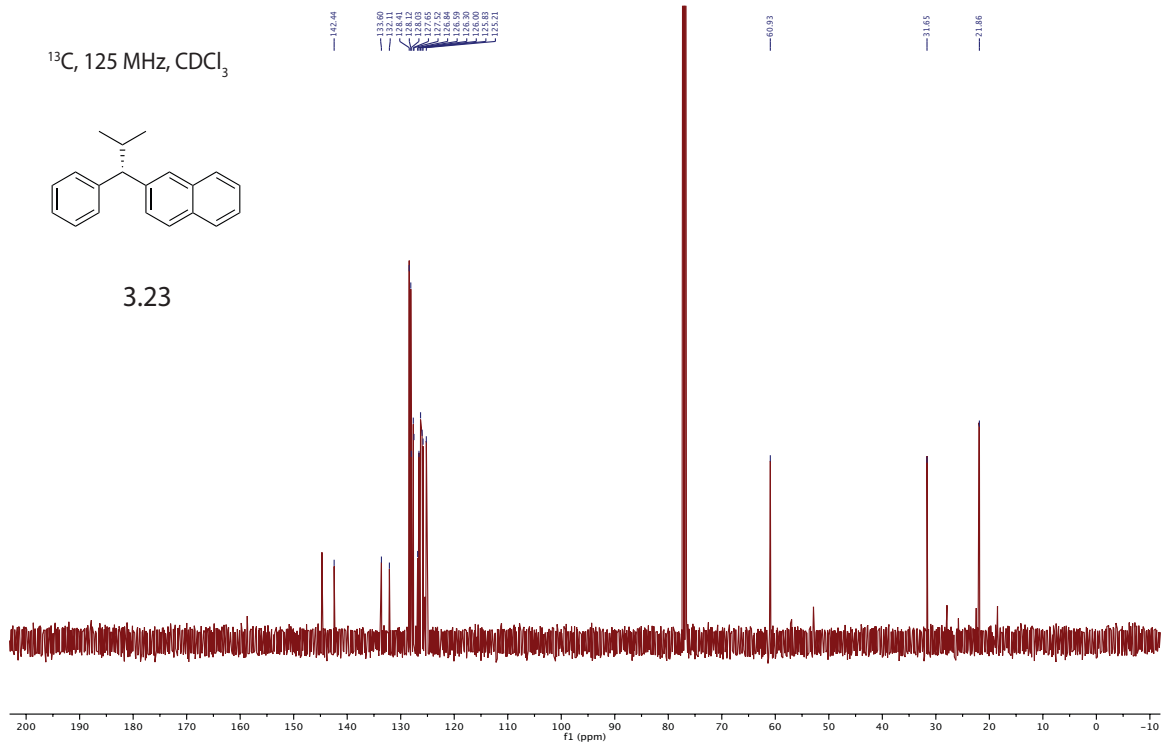


Figure 34 – ^1H NMR(500 MHz) spectrum of 3.24.

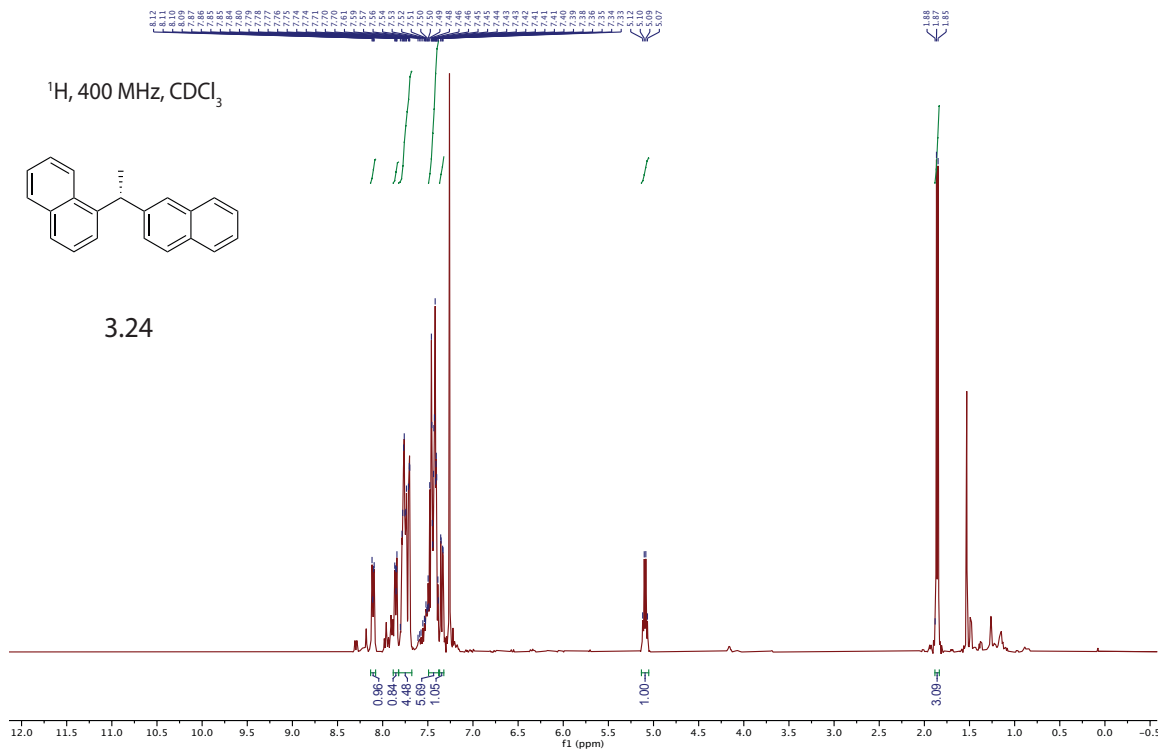
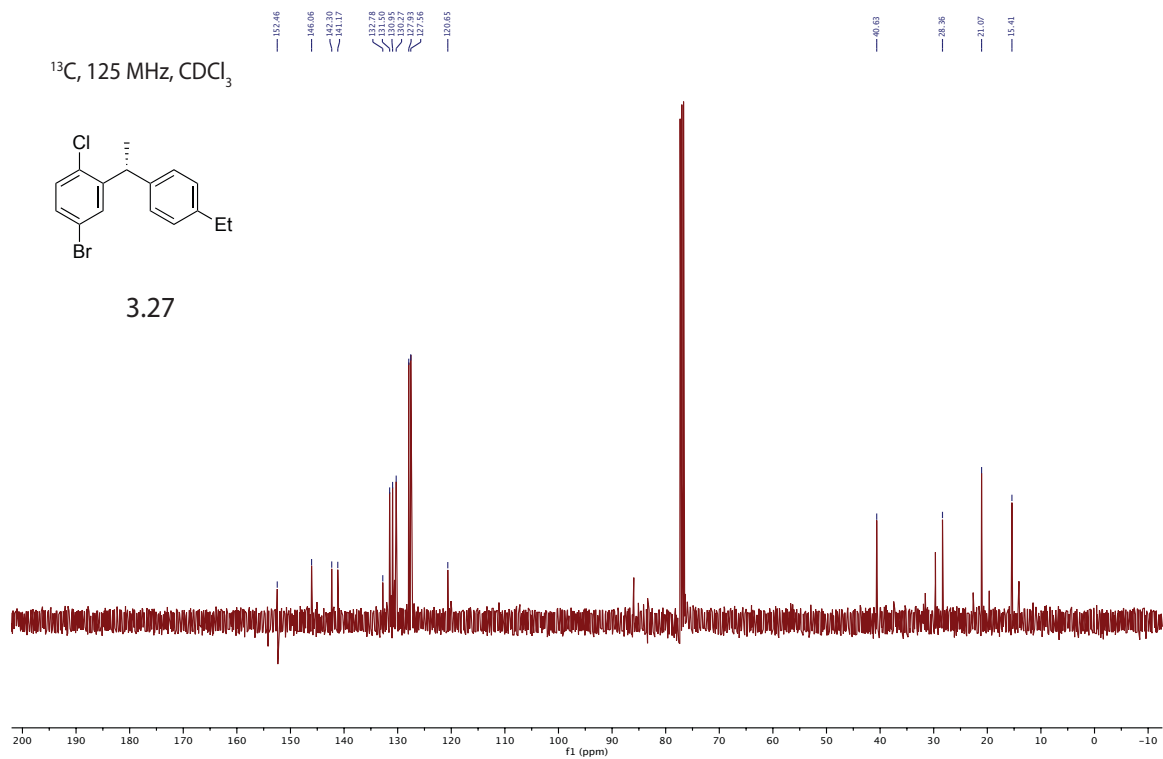


Figure 37 – ^{13}C NMR(125 MHz) spectrum of **3.27**.



Appendix A.3 Spectral Data for Chapter 4

Figure 38 – ^1H NMR(500 MHz) spectrum of (*Z*)-*N*-(2,6-dimethylphenyl)-2,2,2-trifluoroacetimidoyl chloride)

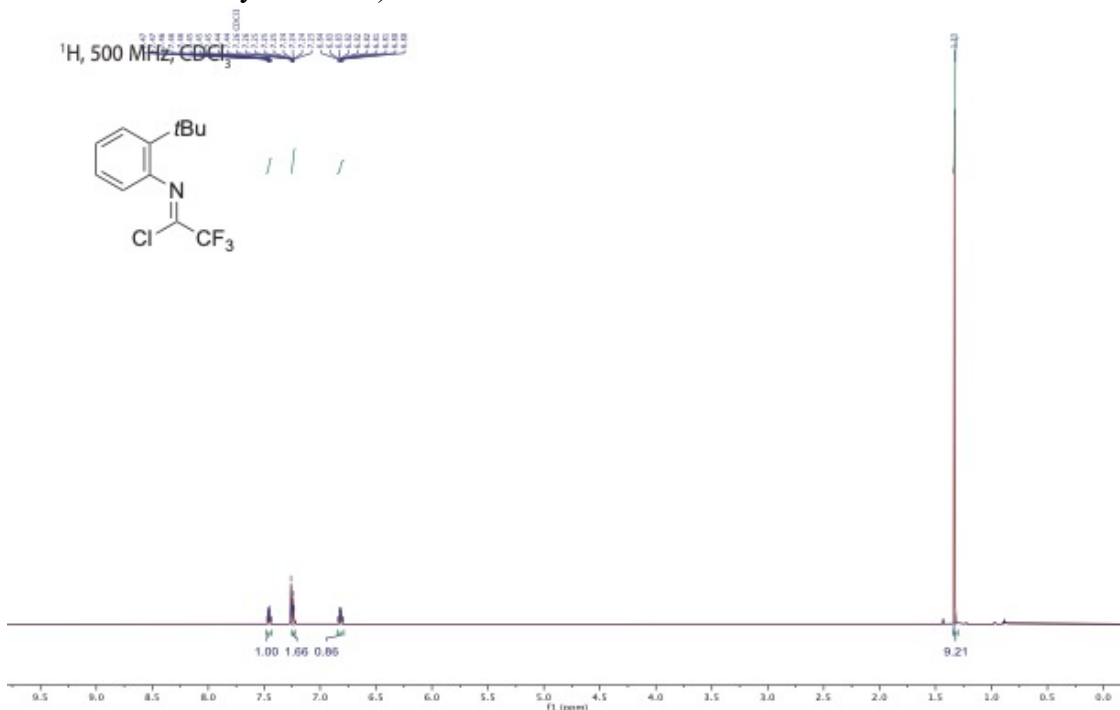


Figure 39 – ^{13}C NMR(125 MHz) spectrum of (*Z*)-*N*-(2,6-dimethylphenyl)-2,2,2-trifluoroacetimidoyl chloride)

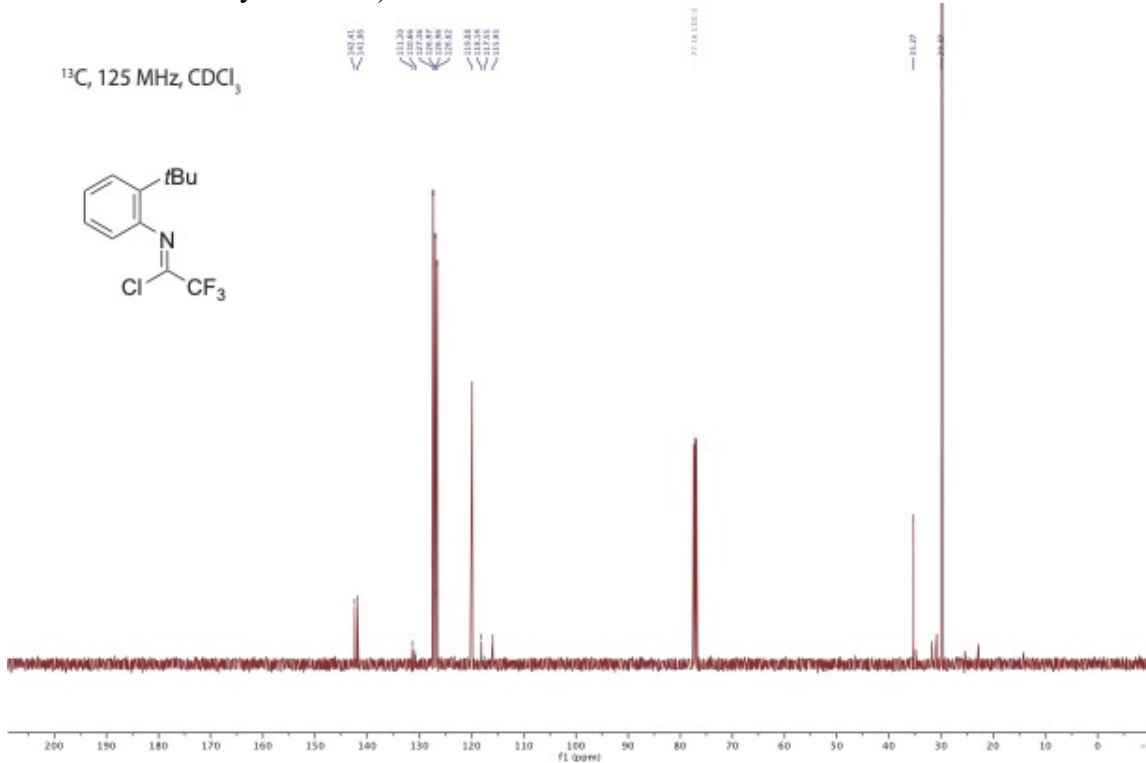


Figure 40 – ^{19}F NMR(470MHz) spectrum of of (*Z*)-*N*-(2,6-dimethylphenyl)-2,2,2-trifluoroacetimidoyl chloride)

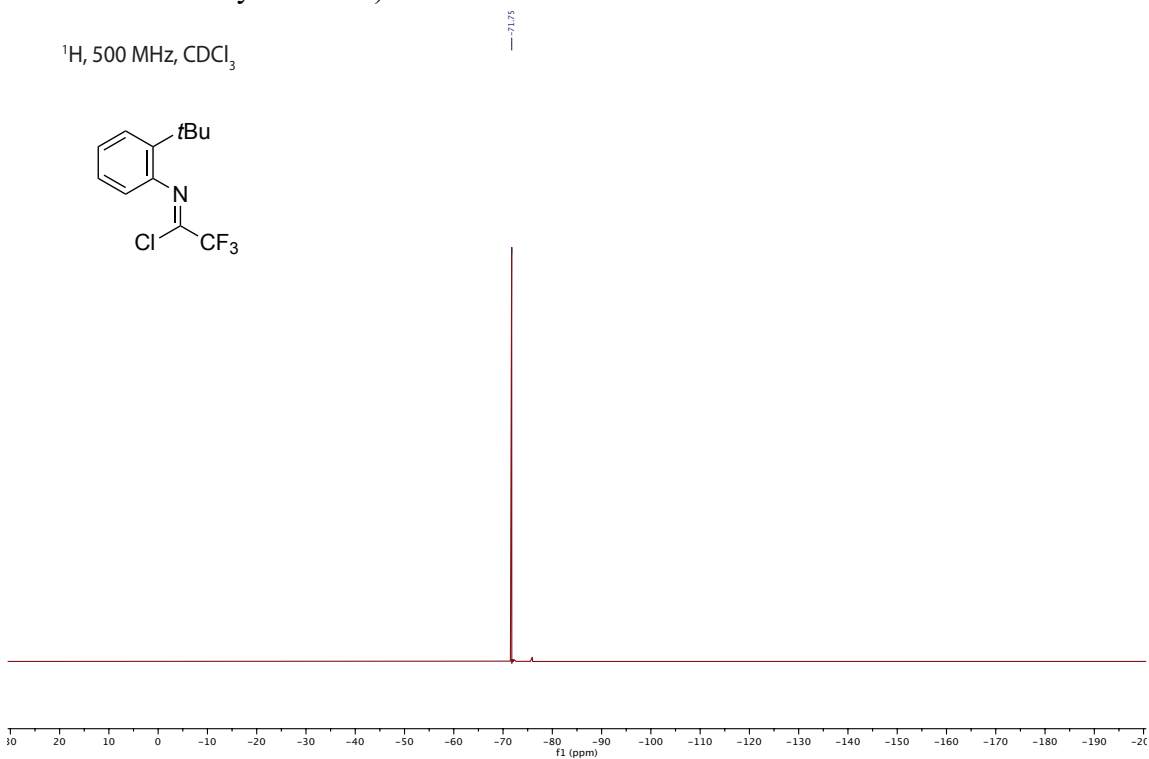


Figure 41 – ^1H NMR(500 MHz) spectrum spectrum of **4.10a**.

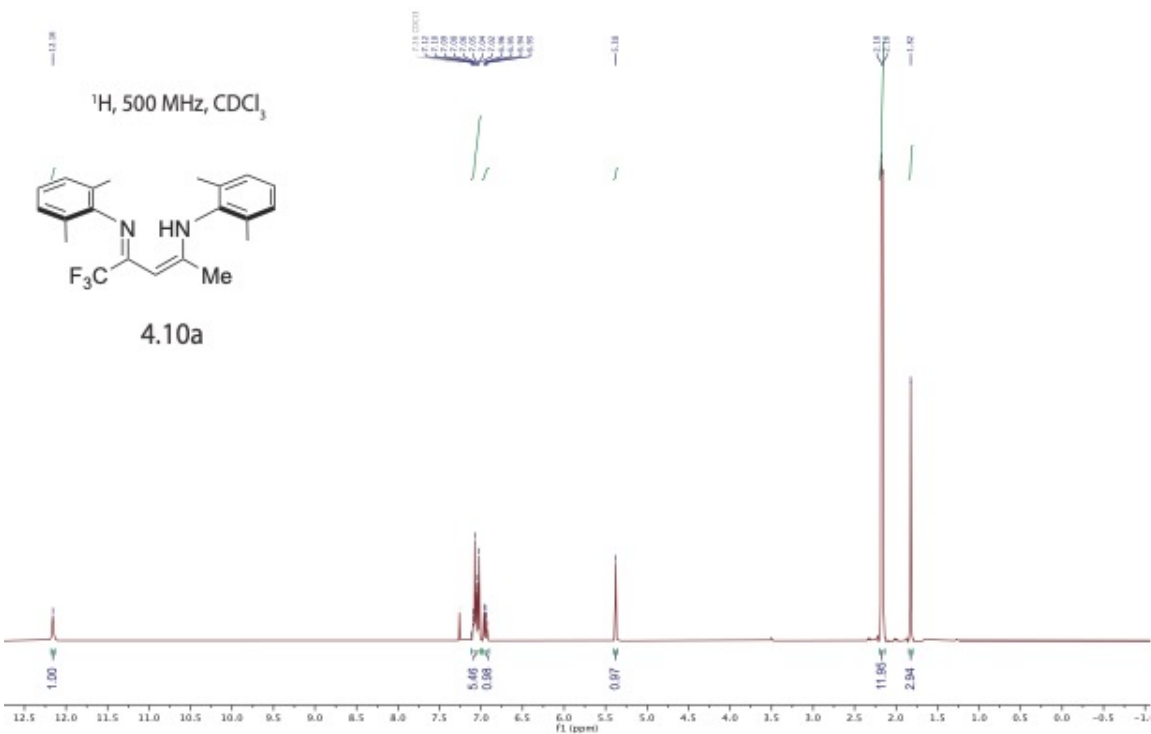


Figure 44 – ^1H NMR(500 MHz) spectrum of **4.11a**.

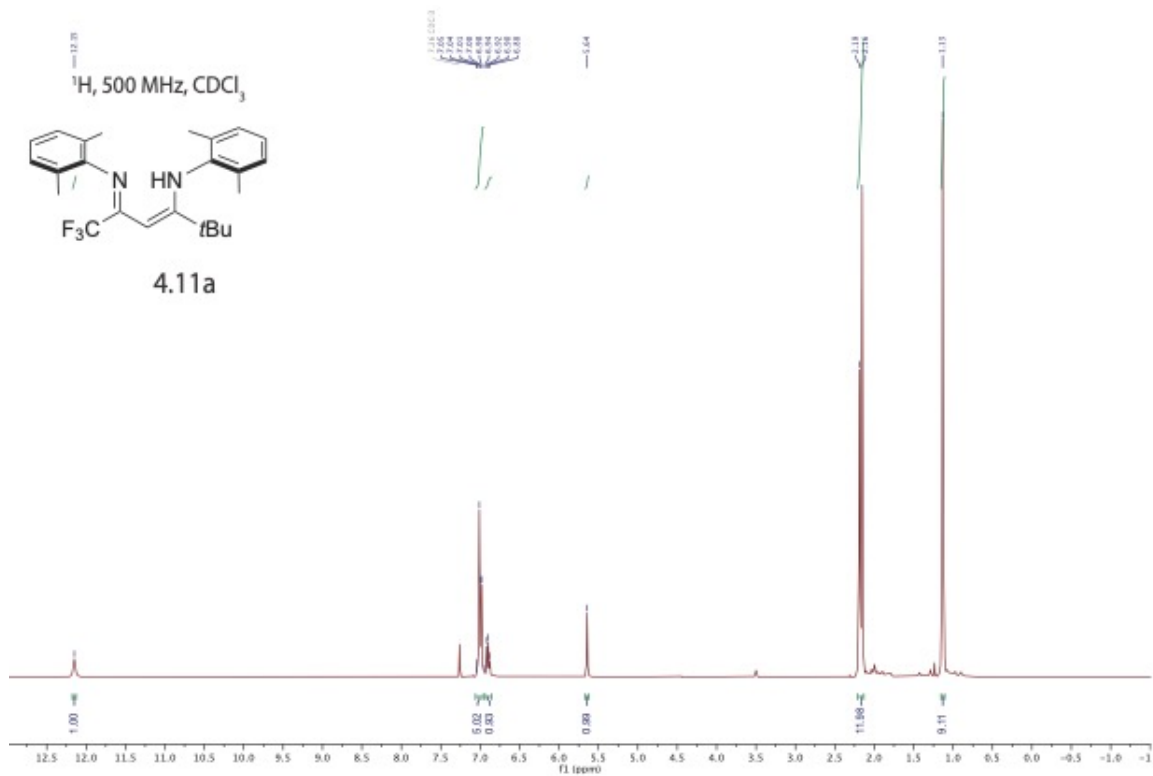


Figure 45 – ^{13}C NMR(125 MHz) spectrum of **4.11a**.

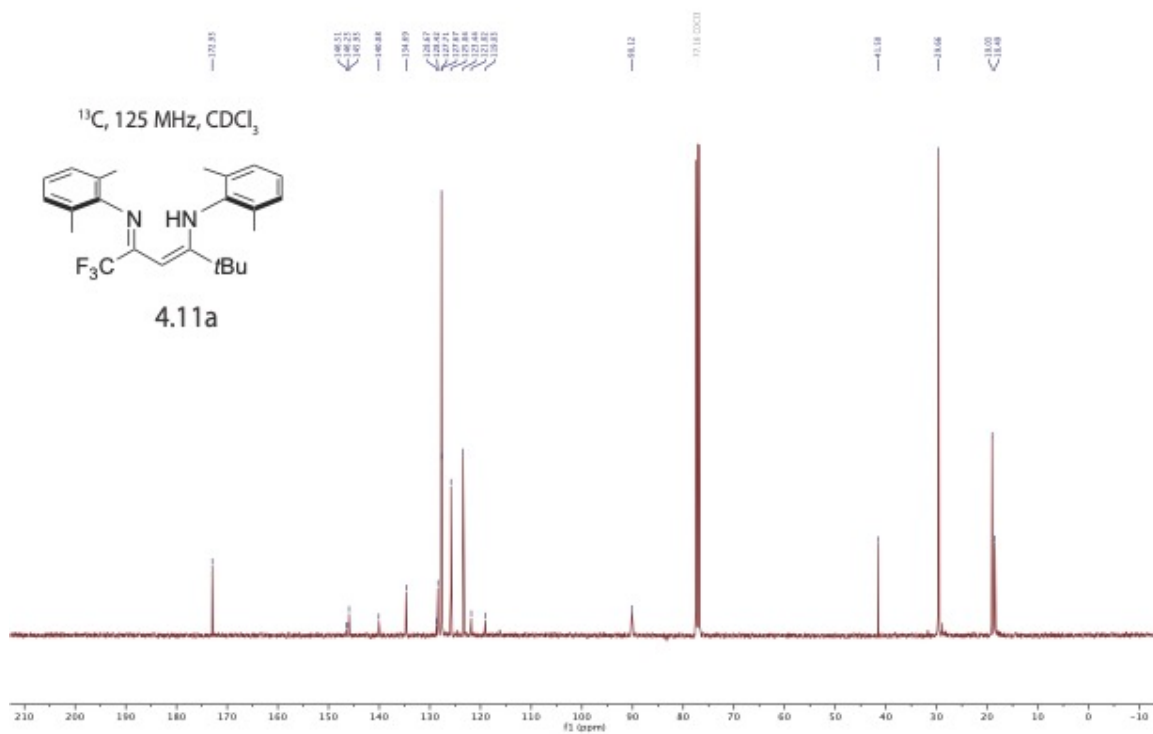


Figure 46 – ^{19}F NMR(470MHz) spectrum of 4.11a.

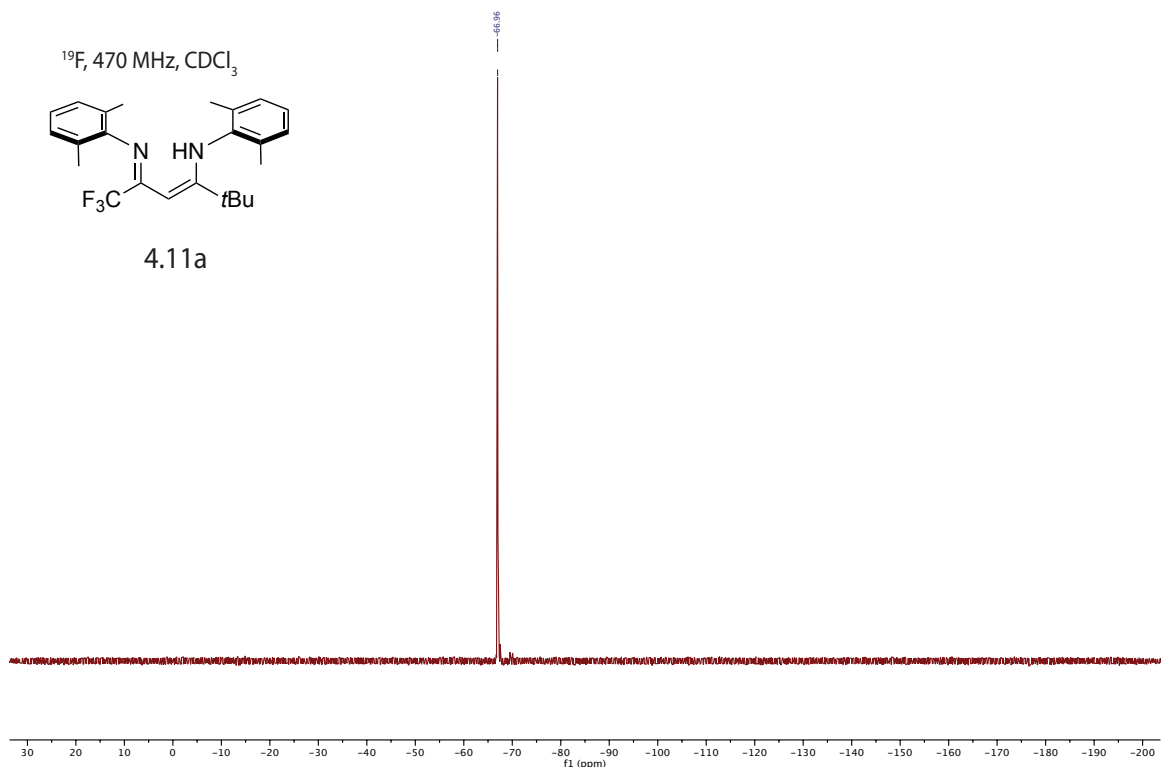


Figure 47 – ^1H NMR(500 MHz) spectrum of 4.12a.

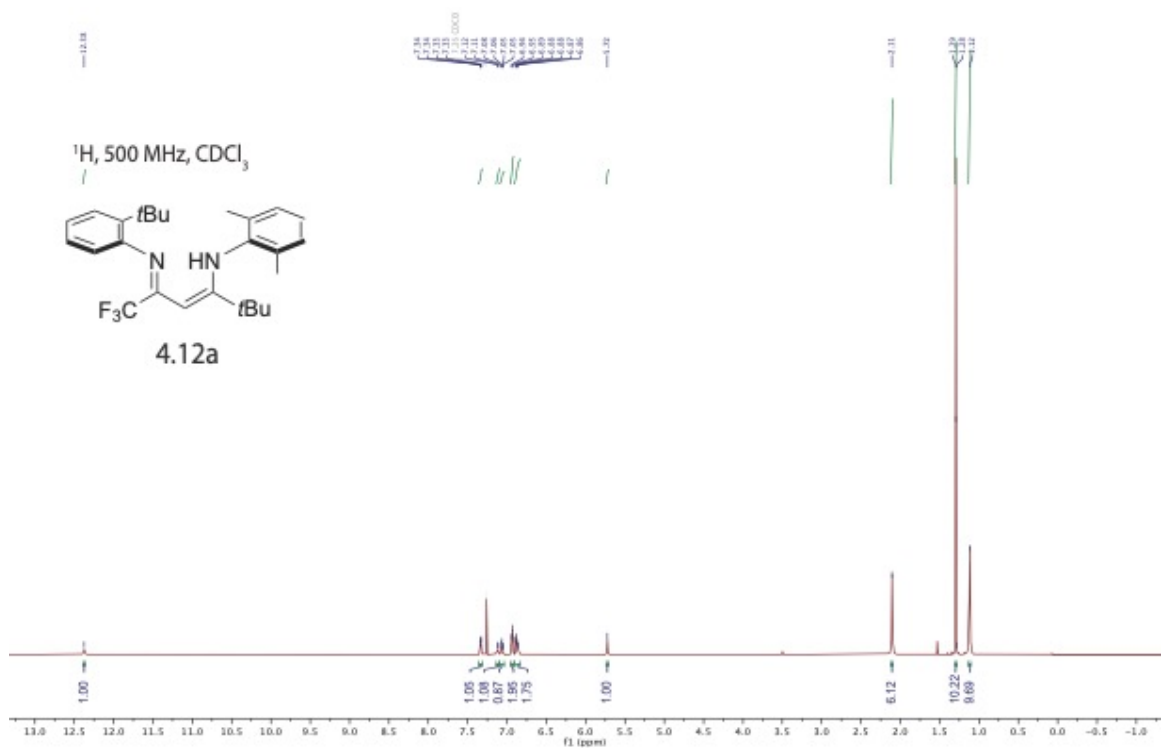


Figure 48 – ^{13}C NMR(125 MHz) spectrum of 4.12a.

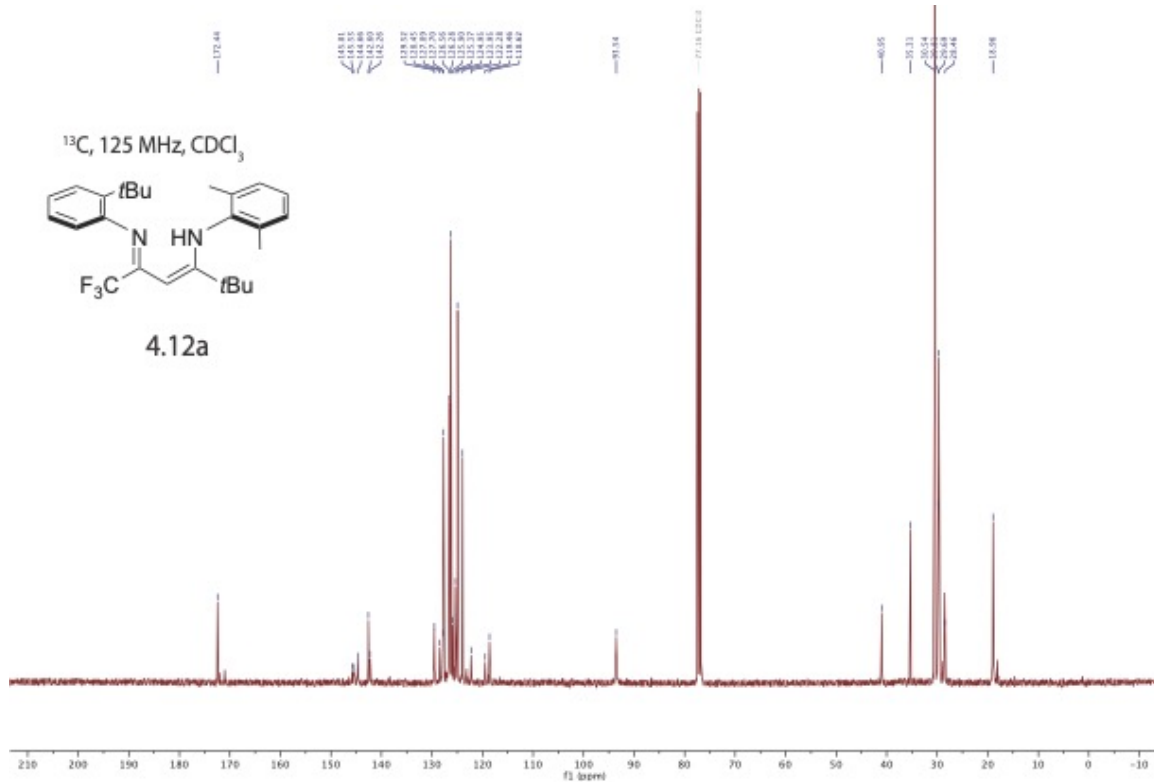


Figure 49 – ^{19}F NMR(470MHz) spectrum of 4.12a.

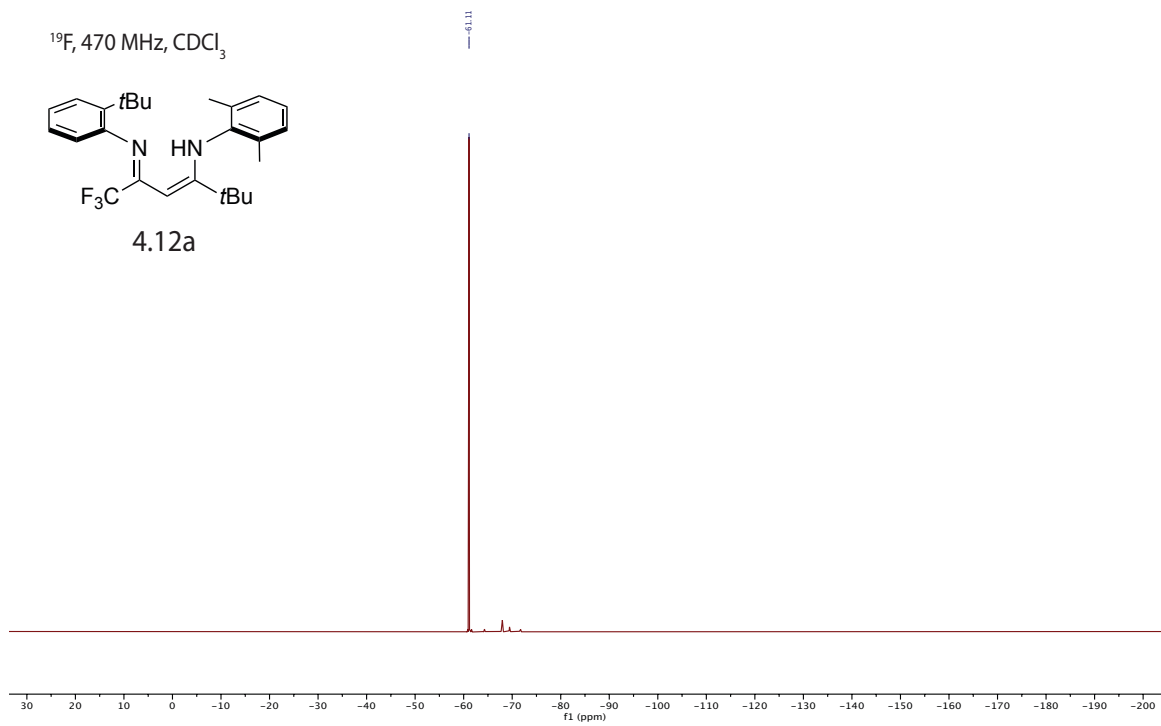


Figure 50 – ^1H NMR(500 MHz) spectrum 4.9.

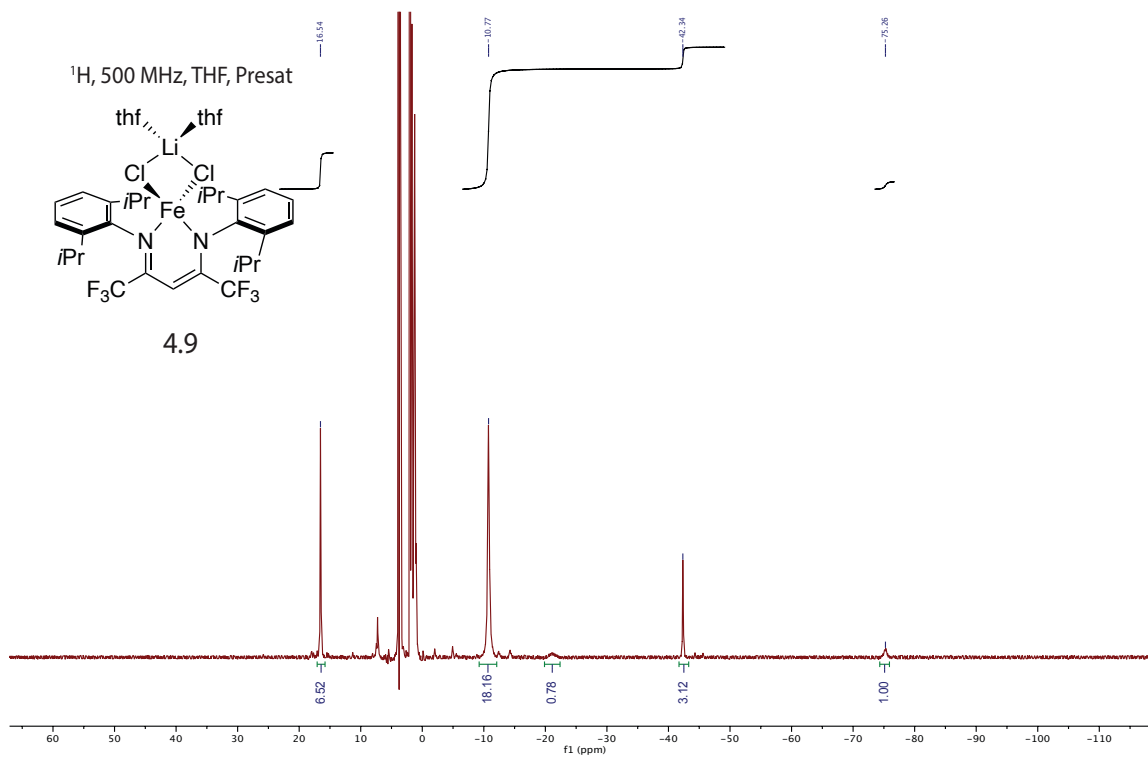


Figure 51 – ^{19}F NMR(470MHz) spectrum of 4.9.

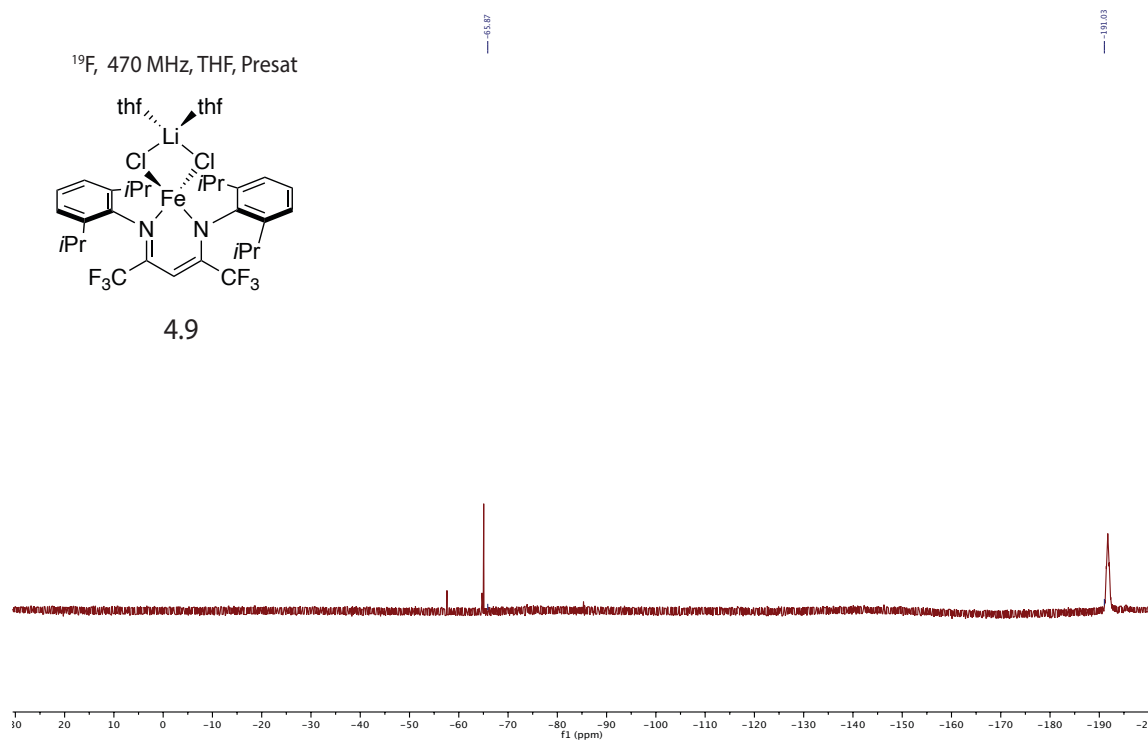


Figure 52 – ^1H NMR(500 MHz) spectrum of 4.10.

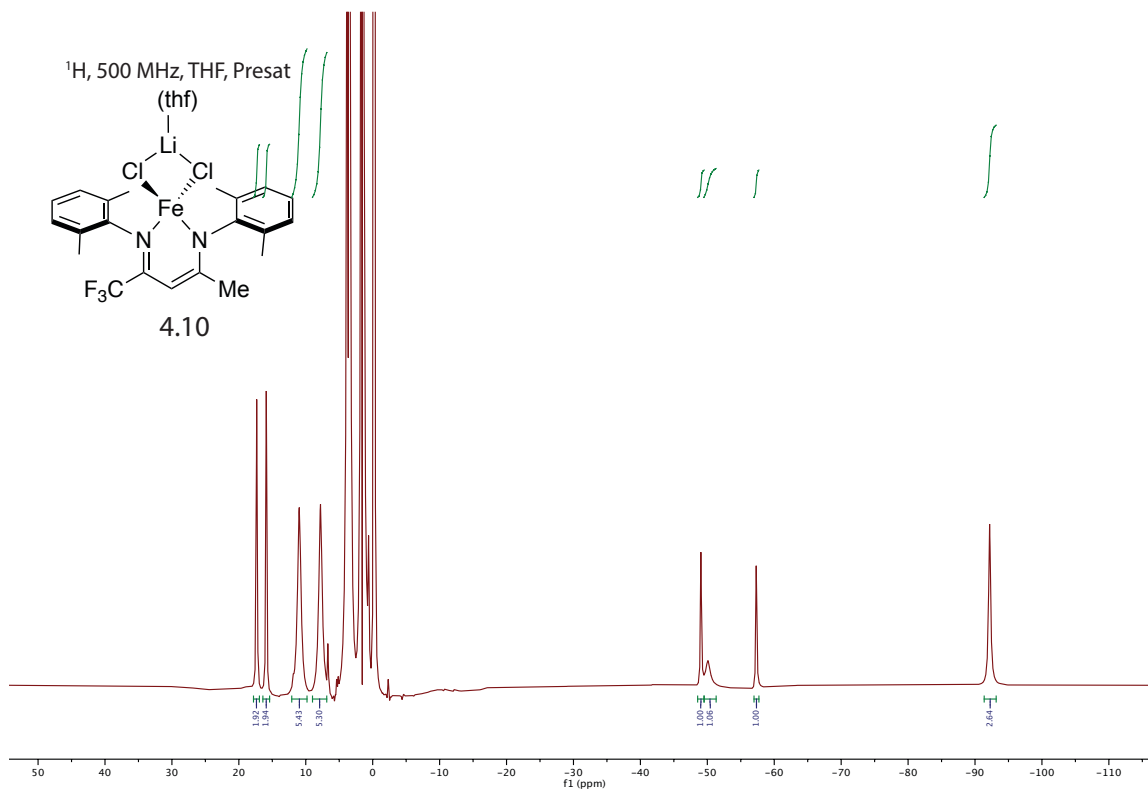


Figure 53 – ^{19}F NMR(470MHz) spectrum of 4.10.

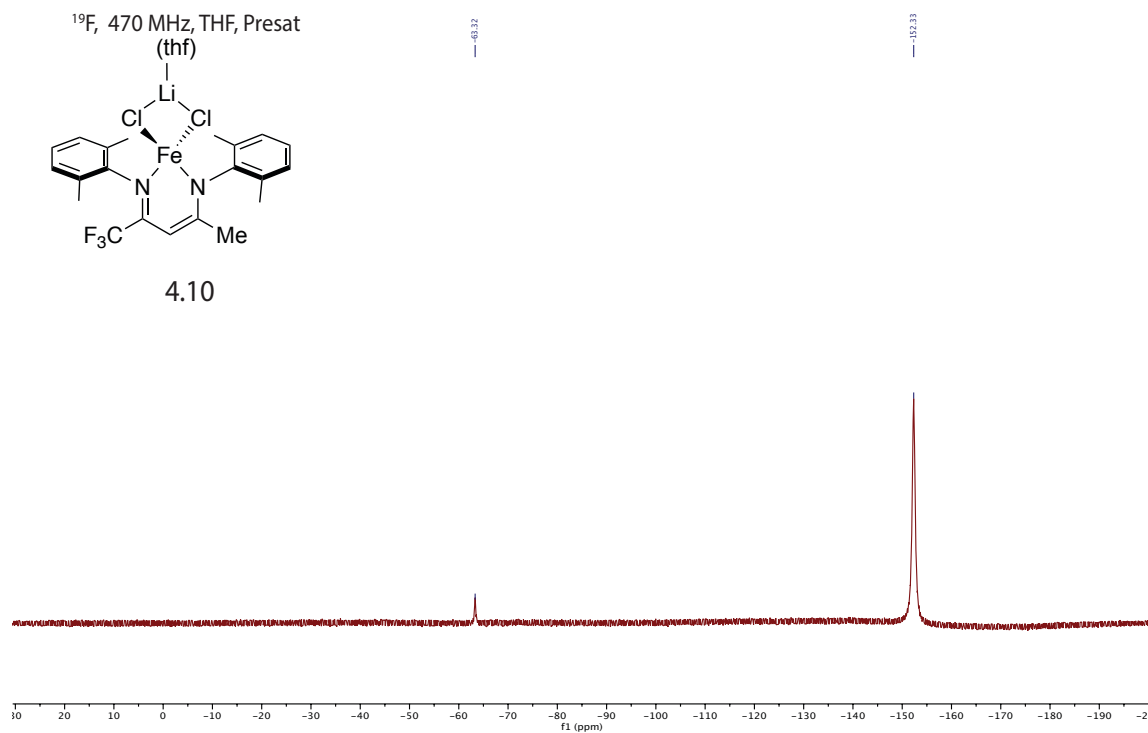


Figure 54 – ¹H NMR(500 MHz) spectrum of 4.11.

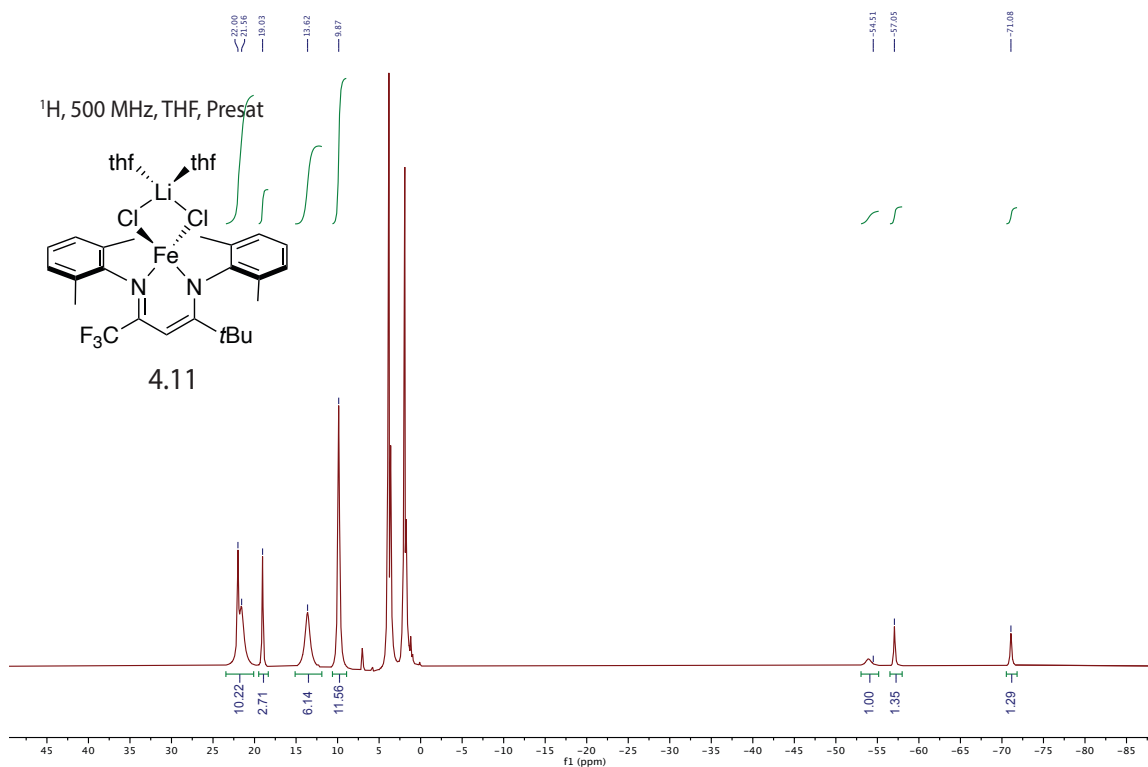


Figure 55 – ¹⁹F NMR(470MHz) spectrum 4.11.

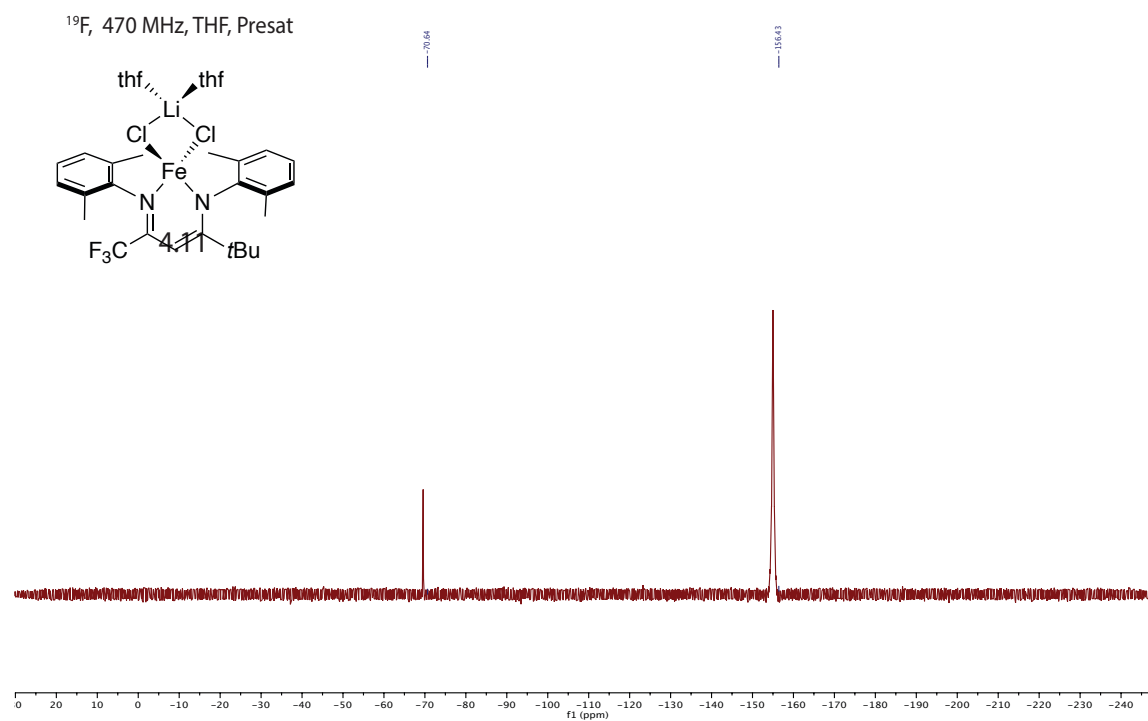


Figure 56 – ^1H NMR(500 MHz) spectrum 4.12.

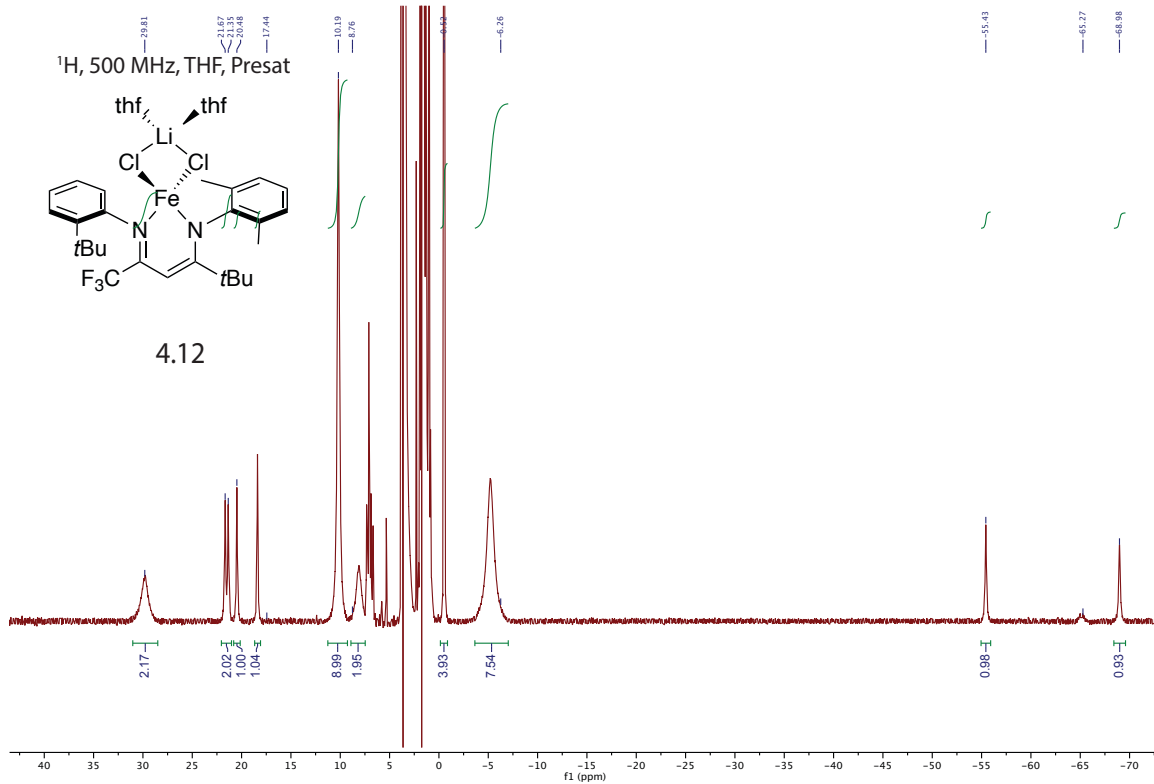


Figure 57 – ^{19}F NMR(470MHz) spectrum 4.12.

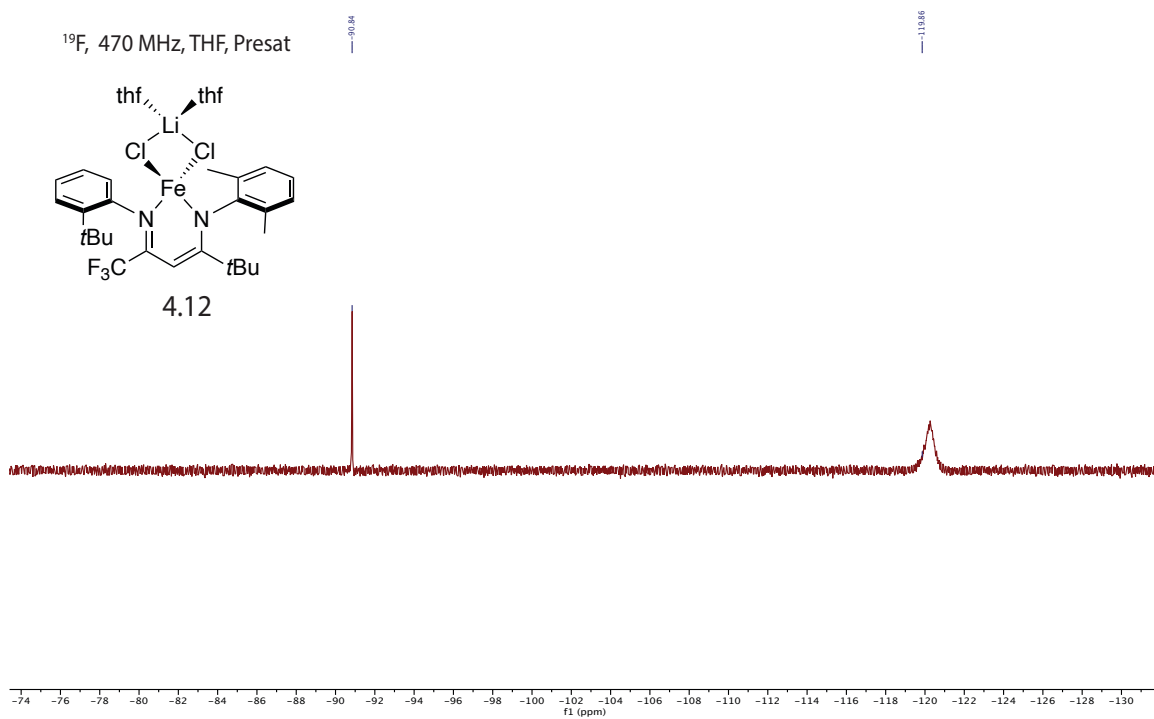


Figure 58 – ^1H NMR(500 MHz) spectrum 4.49.

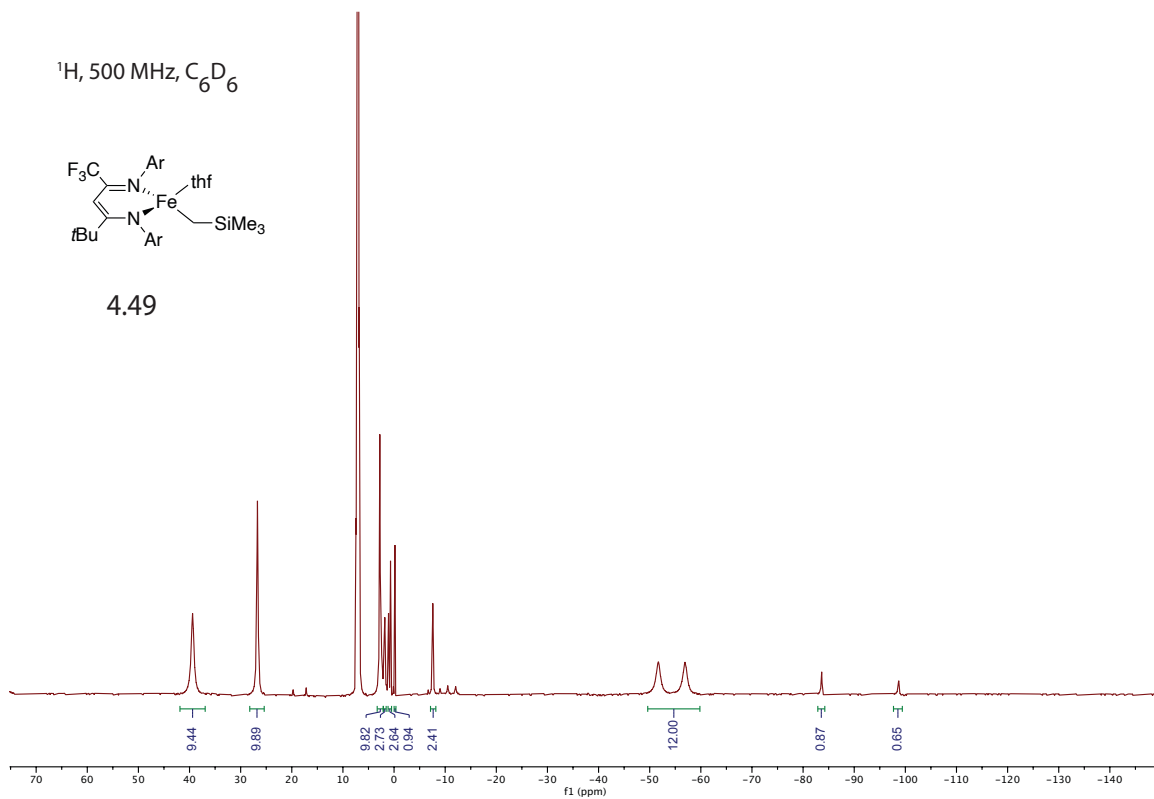


Figure 59 – ^{19}F NMR(470MHz) spectrum 4.49.

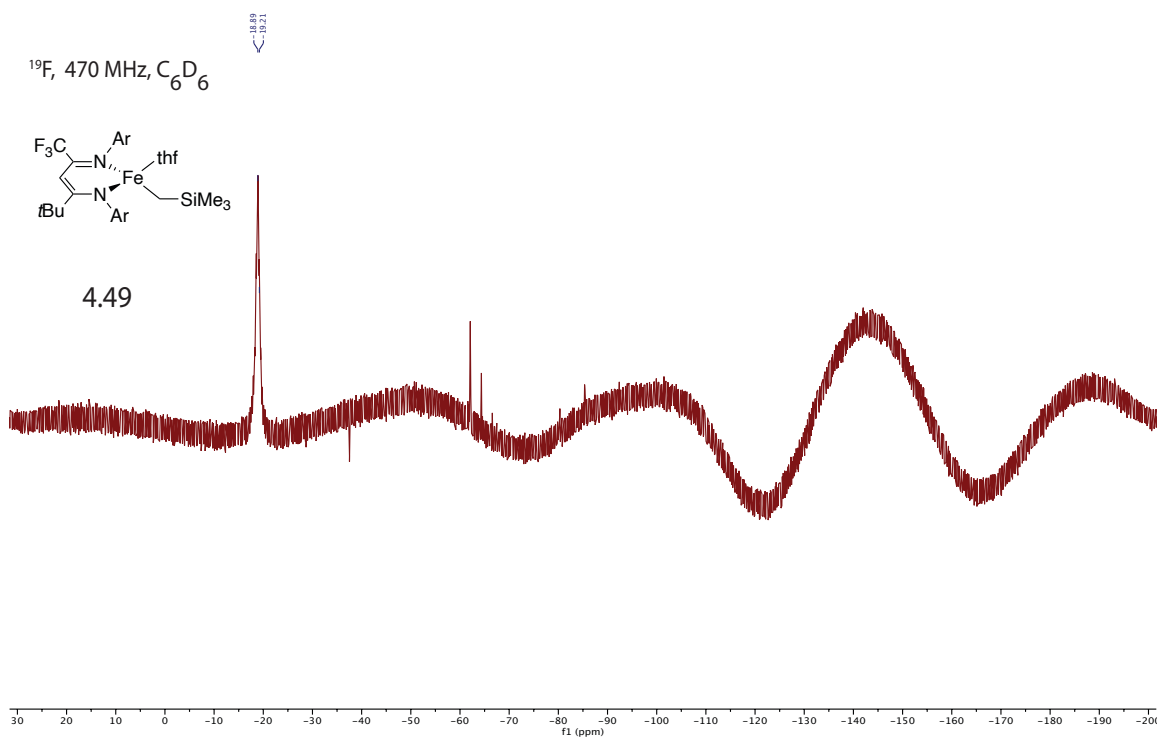


Figure 60 – ^1H NMR(500 MHz) spectrum of 4.51.

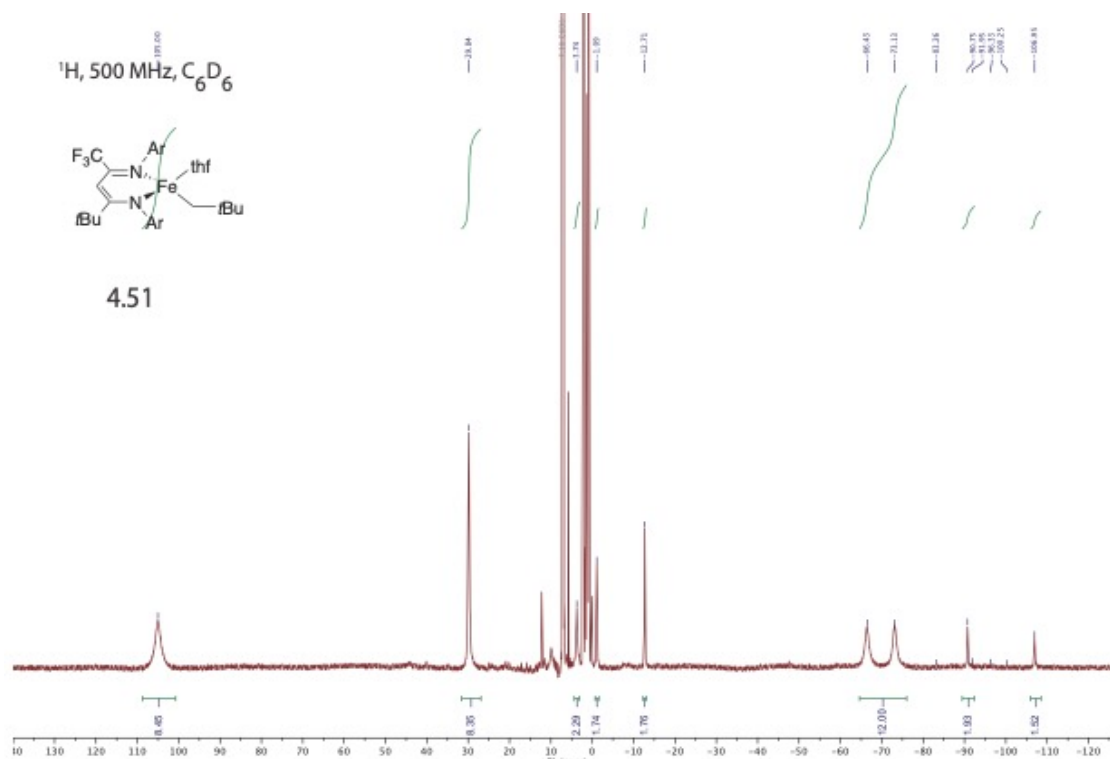


Figure 61 – ^1H NMR(500 MHz) spectrum of 4.52.

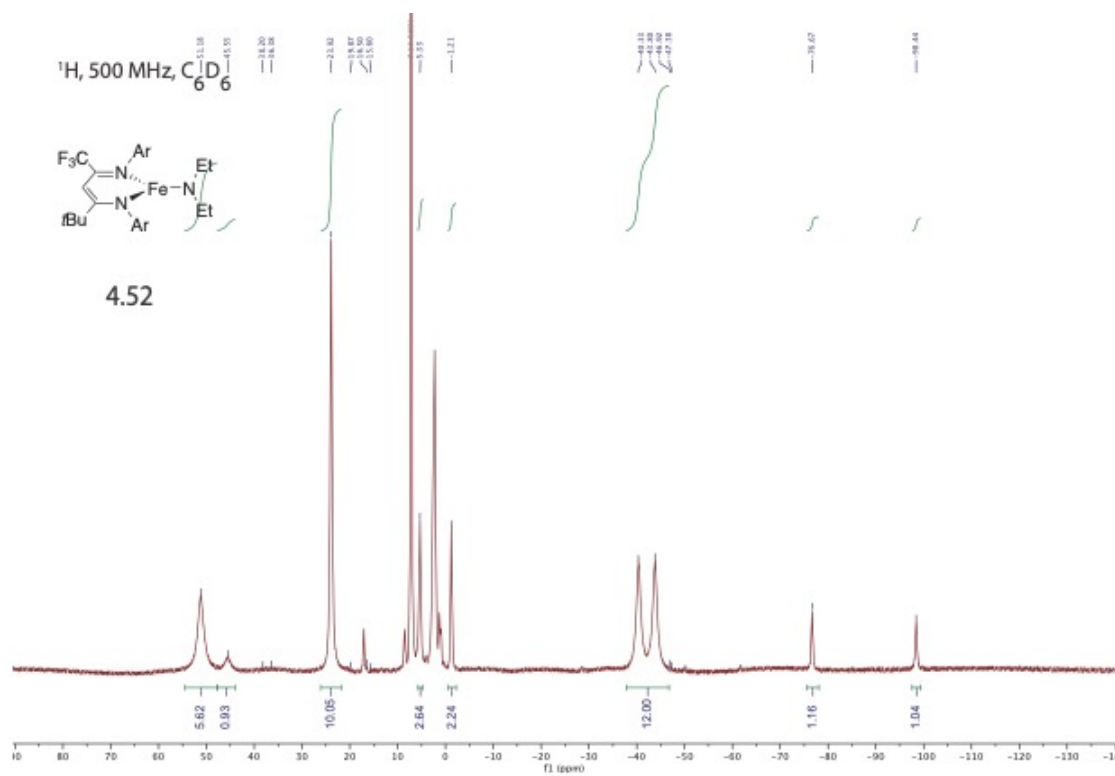


Figure 62 – ^{19}F NMR(470MHz) spectrum of 4.52.

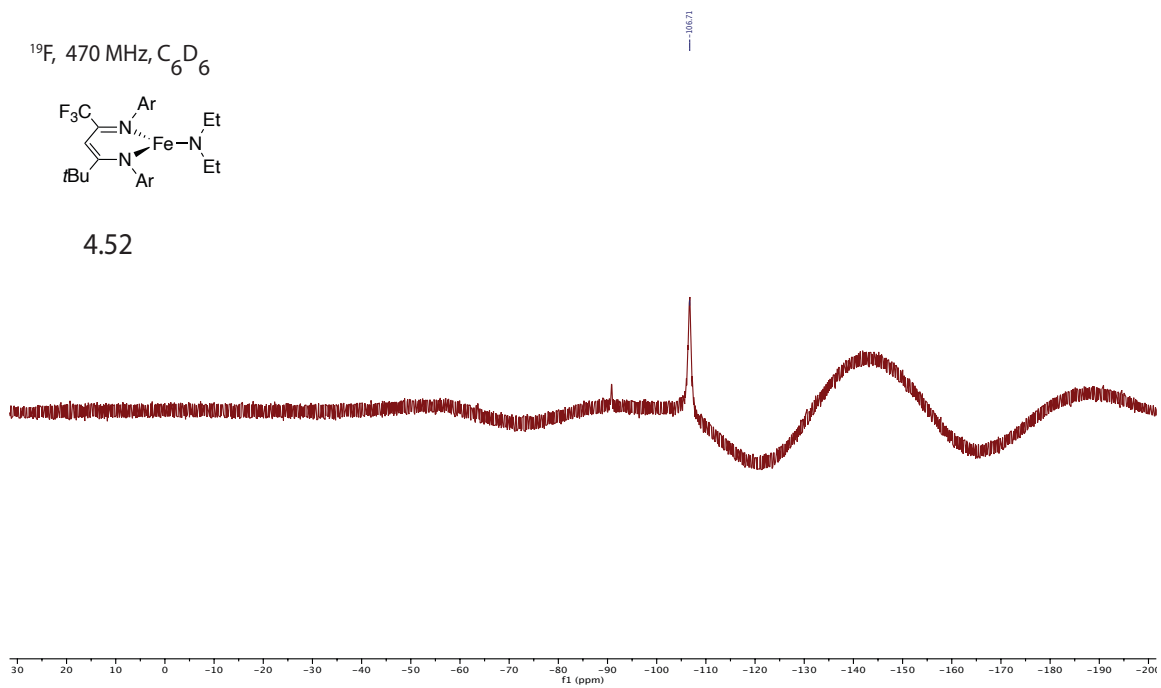


Figure 63 – ^1H NMR(500 MHz) spectrum of 4.53.

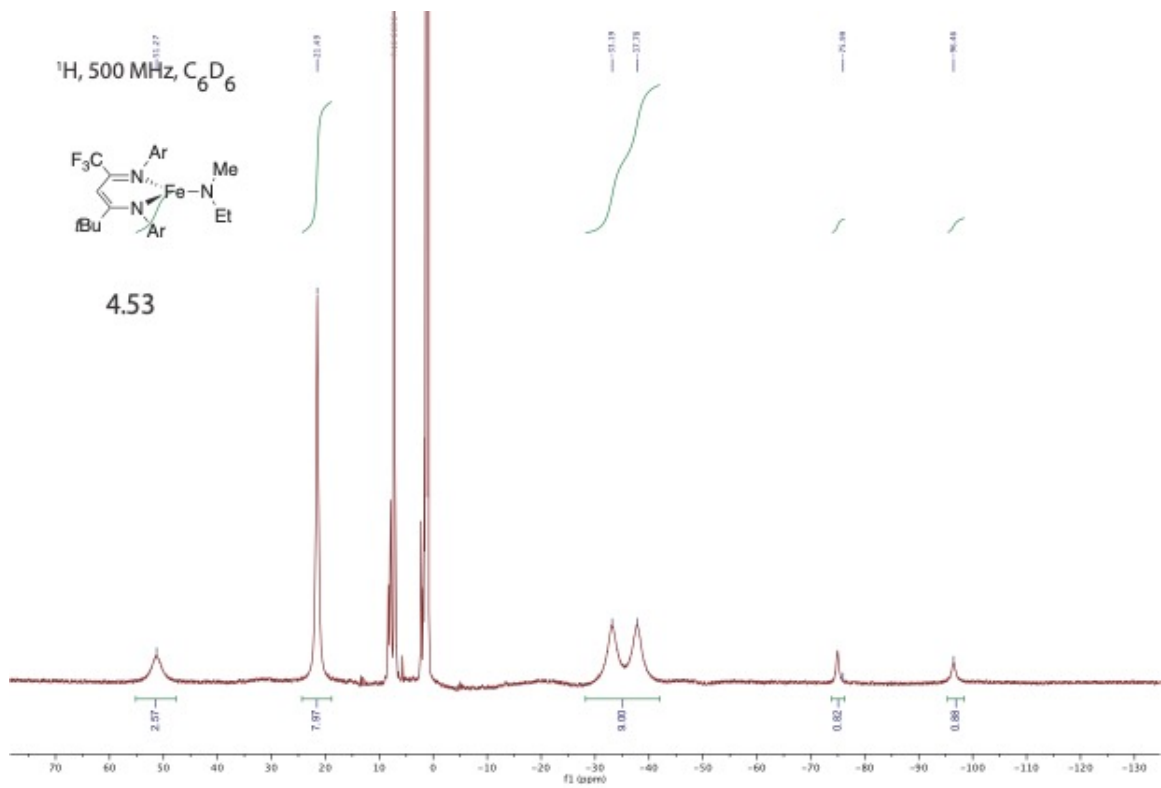


Figure 64 – ^{19}F NMR(470MHz) spectrum of 4.53.

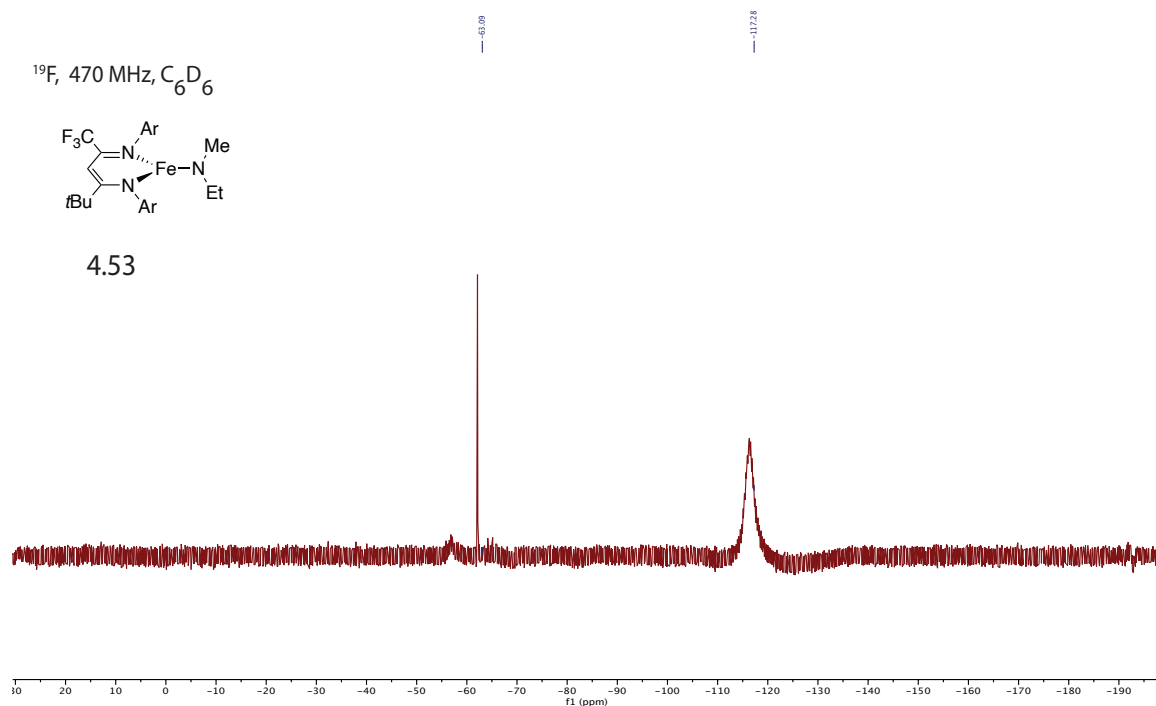


Figure 65 – ^1H NMR(500 MHz) spectrum of 4.22.

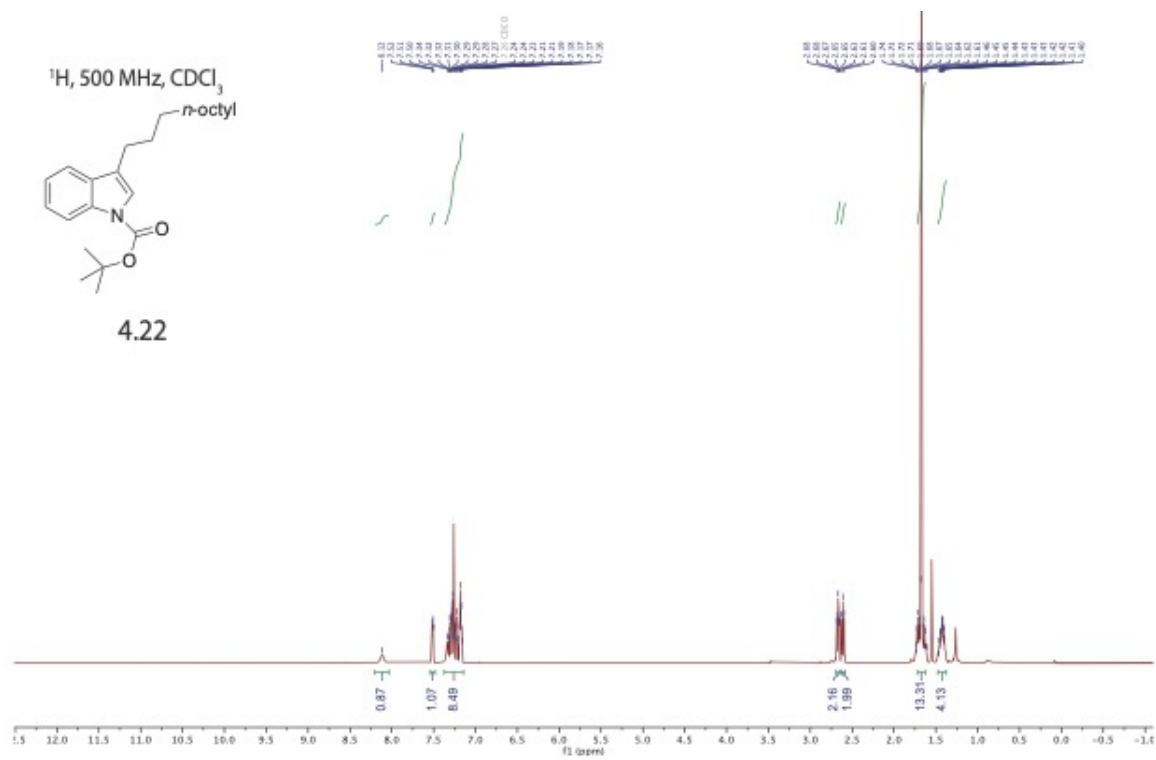


Figure 66 – ^{13}C NMR(125 MHz) spectrum of 4.22.

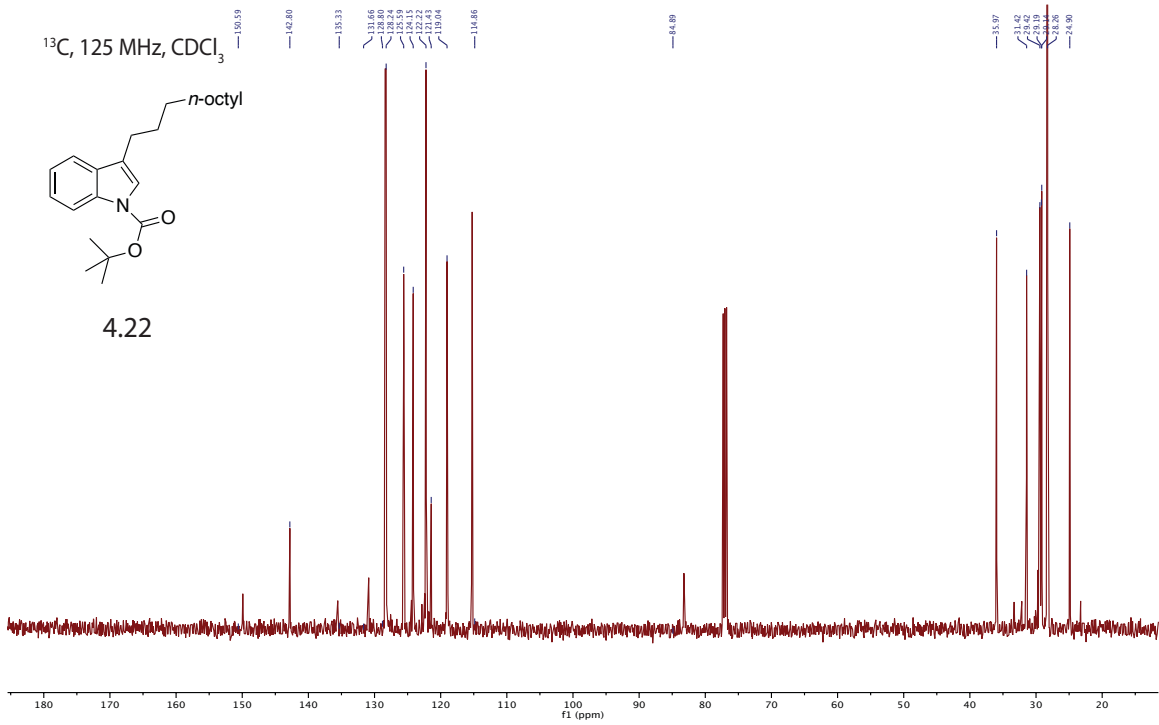


Figure 67 – ¹H NMR(500 MHz) spectrum of 4.29.

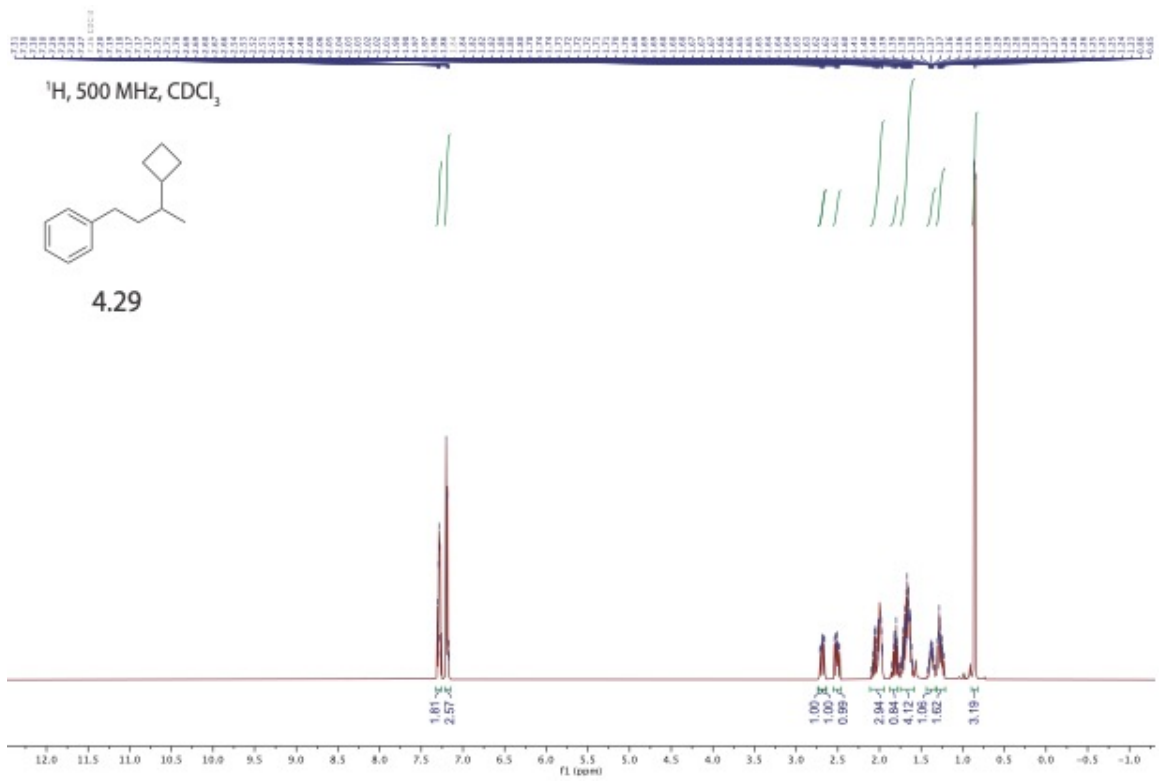


Figure 72 – ^{13}C NMR(125 MHz) spectrum of 4.37.

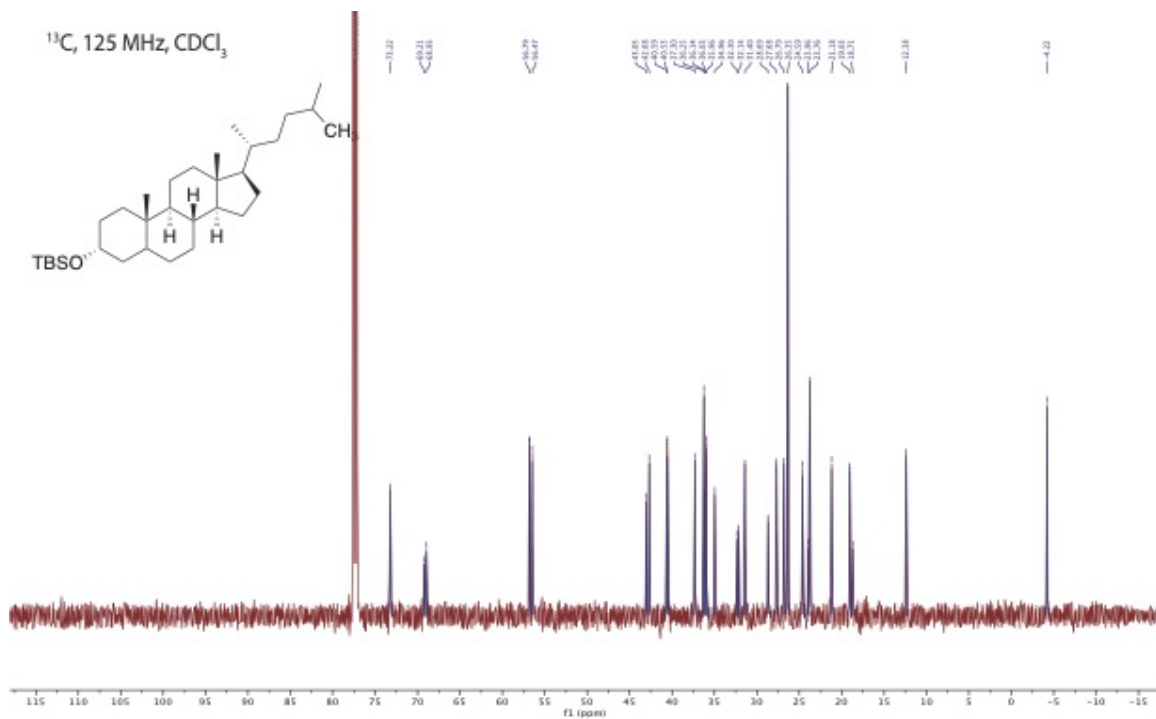


Figure 73 – ^1H NMR(500 MHz) spectrum of 4.38.

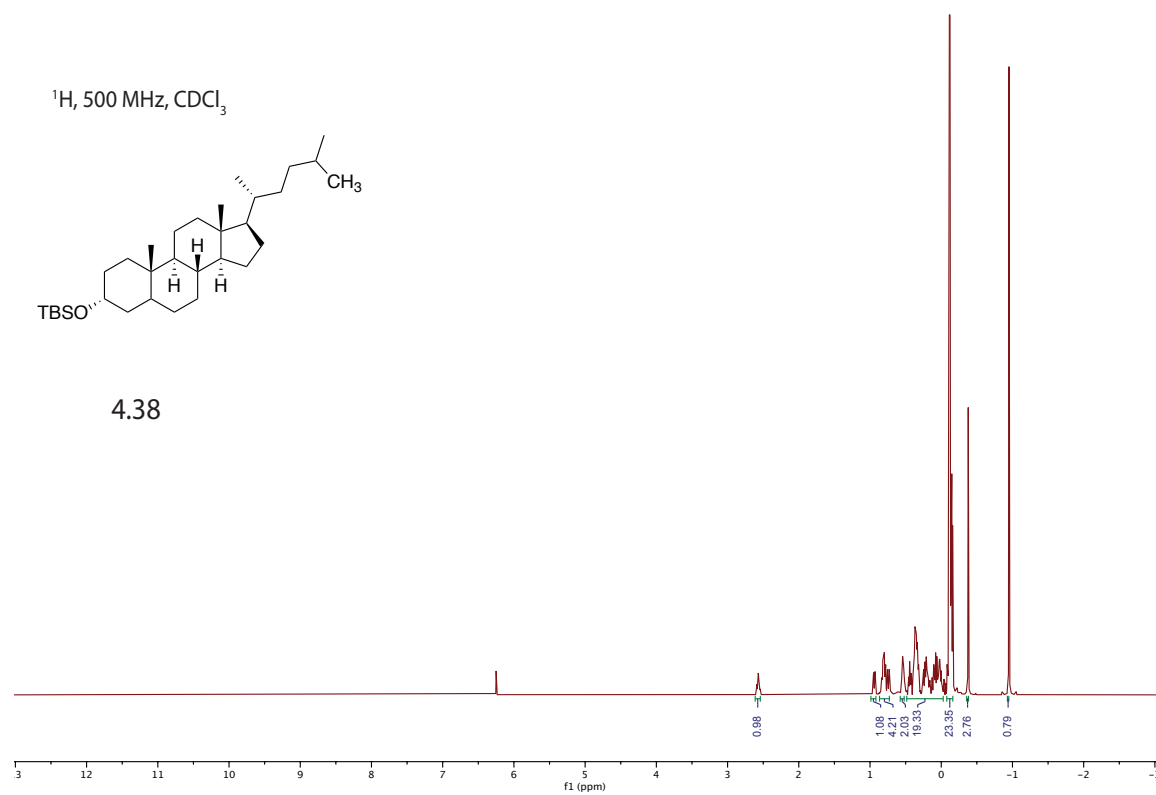
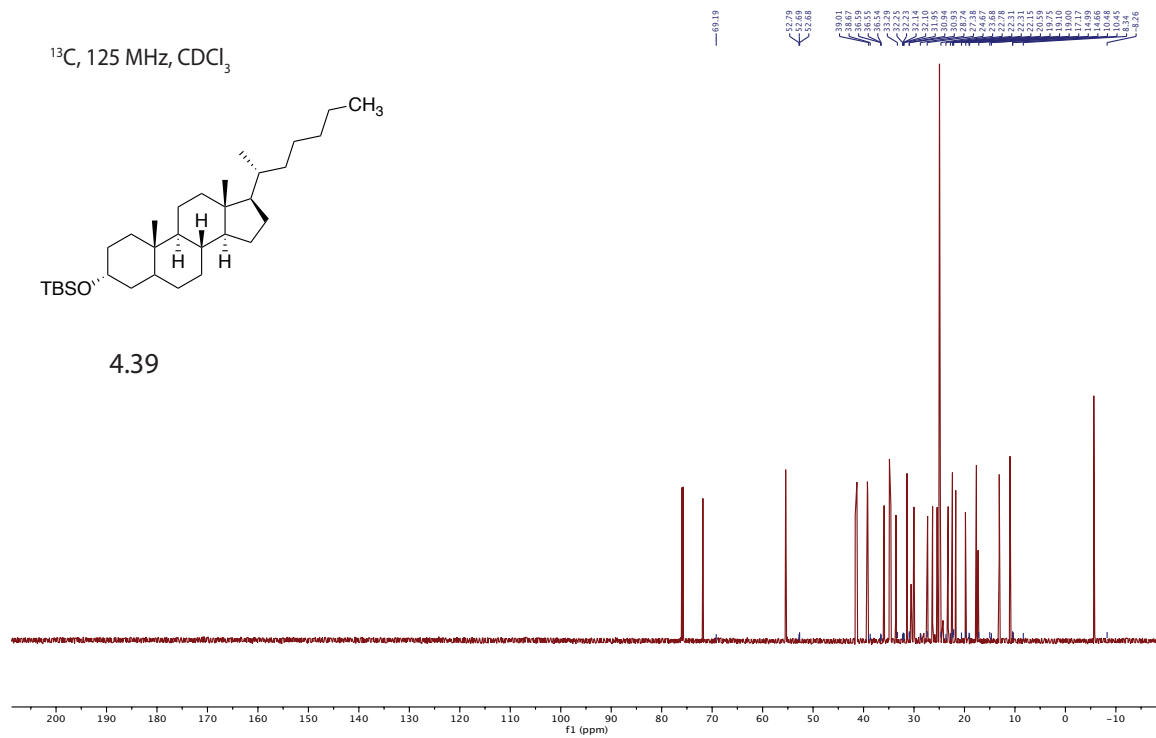


Figure 76 – ^{13}C NMR(125 MHz) spectrum of 4.39.



Appendix B. X-Ray Crystallographic Data

Appendix B.1 X-Ray Crystallography Data from Chapter 1

Appendix B.1.1 Crystallographic Data for 2.8

Figure 80: G: X-ray crystal structure of 2.8 with thermal ellipsoids represented at the 50% probability level.

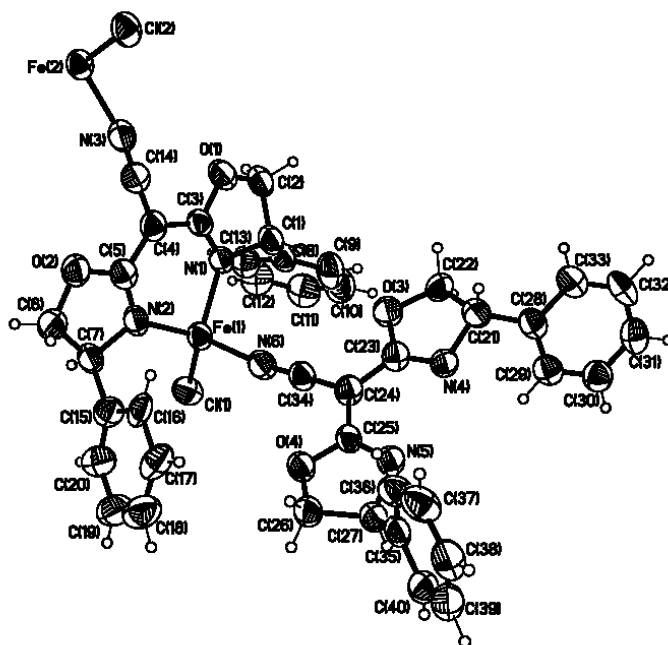


Table 1: Crystal data and structure refinement for 2.8.

Identification code	C20H16ClFeN3O2(C7H8)	
Empirical formula	C27 H24 Cl Fe N3 O2	
Formula weight	513.79	
Temperature	100(2) K	
Wavelength	1.54178 Å	
Crystal system	Triclinic	
Space group	P1	
Unit cell dimensions	a = 8.3005(6) Å	a = 102.056(3)°.
	b = 12.6220(9) Å	b = 108.314(3)°.
	c = 12.6491(8) Å	g = 91.449(3)°.
Volume	1224.45(15) Å ³	
Z	2	

Density (calculated)	1.394 Mg/m ³
Absorption coefficient	6.176 mm ⁻¹
F(000)	532
Crystal size	0.360 x 0.180 x 0.160 mm ³
Theta range for data collection	3.598 to 66.735°.
Index ranges	-9<=h<=9, -14<=k<=15, -12<=l<=15
Reflections collected	4332
Independent reflections	4332 [R(int) = 0.0468]
Completeness to theta = 66.735°	99.9 %
Absorption correction	Semi-empirical from equivalents
Max. and min. transmission	0.7528 and 0.4070
Refinement method	Full-matrix least-squares on F ²
Data / restraints / parameters	4332 / 718 / 743
Goodness-of-fit on F ²	1.051
Final R indices [I>2sigma(I)]	R1 = 0.0820, wR2 = 0.2184
R indices (all data)	R1 = 0.0835, wR2 = 0.2204
Absolute structure parameter	0.128(8)
Extinction coefficient	n/a
Largest diff. peak and hole	1.310 and -0.479 e.Å ⁻³

Table 2: Bond lengths [Å] and angles [°] for complex **2.8**.

Fe(1)-N(2)	1.999(8)
Fe(1)-N(1)	2.027(7)
Fe(1)-N(6)	2.043(9)
Fe(1)-Cl(1)	2.231(3)
Fe(2)-N(4)#1	2.018(7)
Fe(2)-N(5)#1	2.020(8)
Fe(2)-N(3)	2.066(9)
Fe(2)-Cl(2)	2.236(3)
O(3)-C(23)	1.347(12)
O(3)-C(22)	1.438(13)
O(4)-C(25)	1.330(11)
O(4)-C(26)	1.456(11)

N(1)-C(3)	1.266(13)
N(1)-C(1)	1.500(12)
N(2)-C(5)	1.296(14)
N(2)-C(7)	1.487(12)
N(3)-C(14)	1.161(14)
N(4)-C(23)	1.283(12)
N(4)-C(21)	1.490(12)
N(5)-C(25)	1.303(12)
N(5)-C(27)	1.476(12)
N(6)-C(34)	1.198(14)
O(1)-C(3)	1.346(12)
O(1)-C(2)	1.455(15)
O(2)-C(5)	1.349(12)
O(2)-C(6)	1.438(15)
C(1)-C(8)	1.466(18)
C(1)-C(2)	1.544(17)
C(1)-H(1)	1.0000
C(2)-H(2A)	0.9900
C(2)-H(2B)	0.9900
C(3)-C(4)	1.439(14)
C(4)-C(14)	1.402(15)
C(4)-C(5)	1.403(14)
C(6)-C(7)	1.535(18)
C(6)-H(6A)	0.9900
C(6)-H(6B)	0.9900
C(7)-C(15)	1.503(15)
C(7)-H(7)	1.0000
C(8)-C(9)	1.370(18)
C(8)-C(13)	1.396(18)
C(9)-C(10)	1.39(2)
C(9)-H(9)	0.9500
C(10)-C(11)	1.35(2)
C(10)-H(10)	0.9500
C(11)-C(12)	1.38(2)
C(11)-H(11)	0.9500

C(12)-C(13)	1.37(2)
C(12)-H(12)	0.9500
C(13)-H(13)	0.9500
C(15)-C(20)	1.37(2)
C(15)-C(16)	1.41(2)
C(16)-C(17)	1.42(2)
C(16)-H(16)	0.9500
C(17)-C(18)	1.38(3)
C(17)-H(17)	0.9500
C(18)-C(19)	1.36(4)
C(18)-H(18)	0.9500
C(19)-C(20)	1.38(3)
C(19)-H(19)	0.9500
C(20)-H(20)	0.9500
C(21)-C(28)	1.505(15)
C(21)-C(22)	1.520(15)
C(21)-H(21)	1.0000
C(22)-H(22A)	0.9900
C(22)-H(22B)	0.9900
C(23)-C(24)	1.431(13)
C(24)-C(34)	1.383(13)
C(24)-C(25)	1.411(13)
C(26)-C(27)	1.553(13)
C(26)-H(26A)	0.9900
C(26)-H(26B)	0.9900
C(27)-C(35)	1.495(14)
C(27)-H(27)	1.0000
C(28)-C(29)	1.363(16)
C(28)-C(33)	1.412(15)
C(29)-C(30)	1.381(16)
C(29)-H(29)	0.9500
C(30)-C(31)	1.373(17)
C(30)-H(30)	0.9500
C(31)-C(32)	1.375(19)
C(31)-H(31)	0.9500

C(32)-C(33)	1.384(17)
C(32)-H(32)	0.9500
C(33)-H(33)	0.9500
C(35)-C(36)	1.379(17)
C(35)-C(40)	1.400(15)
C(36)-C(37)	1.376(17)
C(36)-H(36)	0.9500
C(37)-C(38)	1.36(2)
C(37)-H(37)	0.9500
C(38)-C(39)	1.40(2)
C(38)-H(38)	0.9500
C(39)-C(40)	1.359(17)
C(39)-H(39)	0.9500
C(40)-H(40)	0.9500
C(1S)-C(2S)	1.31(3)
C(1S)-C(6S)	1.44(4)
C(1S)-C(7S)	1.55(4)
C(2S)-C(3S)	1.35(4)
C(2S)-H(2S)	0.9500
C(3S)-C(4S)	1.35(3)
C(3S)-H(3S)	0.9500
C(4S)-C(5S)	1.55(4)
C(4S)-H(4S)	0.9500
C(5S)-C(6S)	1.27(5)
C(5S)-H(5S)	0.9500
C(6S)-H(6S)	0.9500
C(7S)-H(7S1)	0.9800
C(7S)-H(7S2)	0.9800
C(7S)-H(7S3)	0.9800
C(8S)-C(9S)	1.26(3)
C(8S)-C(13S)	1.27(4)
C(8S)-C(14S)	1.55(5)
C(9S)-C(10S)	1.48(4)
C(9S)-H(9S)	0.9500
C(10S)-C(11S)	1.39(3)

C(10S)-H(10S)	0.9500
C(11S)-C(12S)	1.34(5)
C(11S)-H(11S)	0.9500
C(12S)-C(13S)	1.46(5)
C(12S)-H(12S)	0.9500
C(13S)-H(13S)	0.9500
C(14S)-H(14A)	0.9800
C(14S)-H(14B)	0.9800
C(14S)-H(14C)	0.9800
N(2)-Fe(1)-N(1)	91.1(3)
N(2)-Fe(1)-N(6)	111.5(4)
N(1)-Fe(1)-N(6)	96.9(3)
N(2)-Fe(1)-Cl(1)	116.2(3)
N(1)-Fe(1)-Cl(1)	132.7(2)
N(6)-Fe(1)-Cl(1)	106.5(3)
N(4)#1-Fe(2)-N(5)#1	92.1(3)
N(4)#1-Fe(2)-N(3)	114.1(4)
N(5)#1-Fe(2)-N(3)	94.1(3)
N(4)#1-Fe(2)-Cl(2)	115.7(2)
N(5)#1-Fe(2)-Cl(2)	131.0(2)
N(3)-Fe(2)-Cl(2)	108.0(3)
C(23)-O(3)-C(22)	106.0(7)
C(25)-O(4)-C(26)	105.9(7)
C(3)-N(1)-C(1)	108.5(8)
C(3)-N(1)-Fe(1)	125.8(6)
C(1)-N(1)-Fe(1)	124.7(6)
C(5)-N(2)-C(7)	108.2(8)
C(5)-N(2)-Fe(1)	125.5(7)
C(7)-N(2)-Fe(1)	126.1(7)
C(14)-N(3)-Fe(2)	167.8(8)
C(23)-N(4)-C(21)	108.2(8)
C(23)-N(4)-Fe(2)#2	124.6(6)
C(21)-N(4)-Fe(2)#2	126.3(6)
C(25)-N(5)-C(27)	108.4(7)

C(25)-N(5)-Fe(2)#2	124.9(6)
C(27)-N(5)-Fe(2)#2	126.5(6)
C(34)-N(6)-Fe(1)	172.1(8)
C(3)-O(1)-C(2)	105.1(8)
C(5)-O(2)-C(6)	106.7(9)
C(8)-C(1)-N(1)	117.4(9)
C(8)-C(1)-C(2)	113.5(10)
N(1)-C(1)-C(2)	99.4(8)
C(8)-C(1)-H(1)	108.7
N(1)-C(1)-H(1)	108.7
C(2)-C(1)-H(1)	108.7
O(1)-C(2)-C(1)	104.0(8)
O(1)-C(2)-H(2A)	111.0
C(1)-C(2)-H(2A)	111.0
O(1)-C(2)-H(2B)	111.0
C(1)-C(2)-H(2B)	111.0
H(2A)-C(2)-H(2B)	109.0
N(1)-C(3)-O(1)	116.8(8)
N(1)-C(3)-C(4)	127.1(8)
O(1)-C(3)-C(4)	116.1(9)
C(14)-C(4)-C(5)	120.6(8)
C(14)-C(4)-C(3)	117.1(8)
C(5)-C(4)-C(3)	122.2(9)
N(2)-C(5)-O(2)	116.5(9)
N(2)-C(5)-C(4)	127.8(9)
O(2)-C(5)-C(4)	115.7(9)
O(2)-C(6)-C(7)	105.8(8)
O(2)-C(6)-H(6A)	110.6
C(7)-C(6)-H(6A)	110.6
O(2)-C(6)-H(6B)	110.6
C(7)-C(6)-H(6B)	110.6
H(6A)-C(6)-H(6B)	108.7
N(2)-C(7)-C(15)	112.9(8)
N(2)-C(7)-C(6)	102.1(9)
C(15)-C(7)-C(6)	114.4(9)

N(2)-C(7)-H(7)	109.1
C(15)-C(7)-H(7)	109.1
C(6)-C(7)-H(7)	109.1
C(9)-C(8)-C(13)	117.4(12)
C(9)-C(8)-C(1)	121.1(12)
C(13)-C(8)-C(1)	121.4(10)
C(8)-C(9)-C(10)	121.5(14)
C(8)-C(9)-H(9)	119.3
C(10)-C(9)-H(9)	119.3
C(11)-C(10)-C(9)	120.4(13)
C(11)-C(10)-H(10)	119.8
C(9)-C(10)-H(10)	119.8
C(10)-C(11)-C(12)	119.4(14)
C(10)-C(11)-H(11)	120.3
C(12)-C(11)-H(11)	120.3
C(13)-C(12)-C(11)	120.3(14)
C(13)-C(12)-H(12)	119.9
C(11)-C(12)-H(12)	119.9
C(12)-C(13)-C(8)	121.0(12)
C(12)-C(13)-H(13)	119.5
C(8)-C(13)-H(13)	119.5
N(3)-C(14)-C(4)	177.9(10)
C(20)-C(15)-C(16)	118.2(14)
C(20)-C(15)-C(7)	125.8(14)
C(16)-C(15)-C(7)	116.0(12)
C(15)-C(16)-C(17)	118.1(17)
C(15)-C(16)-H(16)	121.0
C(17)-C(16)-H(16)	121.0
C(18)-C(17)-C(16)	122(2)
C(18)-C(17)-H(17)	119.0
C(16)-C(17)-H(17)	119.0
C(19)-C(18)-C(17)	118.5(17)
C(19)-C(18)-H(18)	120.7
C(17)-C(18)-H(18)	120.7
C(18)-C(19)-C(20)	120(2)

C(18)-C(19)-H(19)	119.8
C(20)-C(19)-H(19)	119.8
C(15)-C(20)-C(19)	122(2)
C(15)-C(20)-H(20)	118.8
C(19)-C(20)-H(20)	118.8
N(4)-C(21)-C(28)	114.9(9)
N(4)-C(21)-C(22)	100.9(8)
C(28)-C(21)-C(22)	114.2(9)
N(4)-C(21)-H(21)	108.8
C(28)-C(21)-H(21)	108.8
C(22)-C(21)-H(21)	108.8
O(3)-C(22)-C(21)	105.4(8)
O(3)-C(22)-H(22A)	110.7
C(21)-C(22)-H(22A)	110.7
O(3)-C(22)-H(22B)	110.7
C(21)-C(22)-H(22B)	110.7
H(22A)-C(22)-H(22B)	108.8
N(4)-C(23)-O(3)	116.0(8)
N(4)-C(23)-C(24)	128.2(9)
O(3)-C(23)-C(24)	115.8(8)
C(34)-C(24)-C(25)	118.9(8)
C(34)-C(24)-C(23)	118.4(8)
C(25)-C(24)-C(23)	122.8(8)
N(5)-C(25)-O(4)	116.2(8)
N(5)-C(25)-C(24)	127.3(8)
O(4)-C(25)-C(24)	116.4(8)
O(4)-C(26)-C(27)	103.8(7)
O(4)-C(26)-H(26A)	111.0
C(27)-C(26)-H(26A)	111.0
O(4)-C(26)-H(26B)	111.0
C(27)-C(26)-H(26B)	111.0
H(26A)-C(26)-H(26B)	109.0
N(5)-C(27)-C(35)	112.7(8)
N(5)-C(27)-C(26)	100.4(7)
C(35)-C(27)-C(26)	116.2(8)

N(5)-C(27)-H(27)	109.0
C(35)-C(27)-H(27)	109.0
C(26)-C(27)-H(27)	109.0
C(29)-C(28)-C(33)	117.1(10)
C(29)-C(28)-C(21)	124.0(9)
C(33)-C(28)-C(21)	118.9(10)
C(28)-C(29)-C(30)	122.4(10)
C(28)-C(29)-H(29)	118.8
C(30)-C(29)-H(29)	118.8
C(31)-C(30)-C(29)	120.0(11)
C(31)-C(30)-H(30)	120.0
C(29)-C(30)-H(30)	120.0
C(30)-C(31)-C(32)	119.5(10)
C(30)-C(31)-H(31)	120.2
C(32)-C(31)-H(31)	120.2
C(31)-C(32)-C(33)	120.3(9)
C(31)-C(32)-H(32)	119.9
C(33)-C(32)-H(32)	119.9
C(32)-C(33)-C(28)	120.7(11)
C(32)-C(33)-H(33)	119.6
C(28)-C(33)-H(33)	119.6
N(6)-C(34)-C(24)	178.5(10)
C(36)-C(35)-C(40)	119.0(10)
C(36)-C(35)-C(27)	121.3(9)
C(40)-C(35)-C(27)	119.8(10)
C(37)-C(36)-C(35)	121.2(11)
C(37)-C(36)-H(36)	119.4
C(35)-C(36)-H(36)	119.4
C(38)-C(37)-C(36)	120.3(13)
C(38)-C(37)-H(37)	119.8
C(36)-C(37)-H(37)	119.8
C(37)-C(38)-C(39)	118.6(11)
C(37)-C(38)-H(38)	120.7
C(39)-C(38)-H(38)	120.7
C(40)-C(39)-C(38)	121.6(11)

C(40)-C(39)-H(39)	119.2
C(38)-C(39)-H(39)	119.2
C(39)-C(40)-C(35)	119.2(12)
C(39)-C(40)-H(40)	120.4
C(35)-C(40)-H(40)	120.4
C(2S)-C(1S)-C(6S)	114(3)
C(2S)-C(1S)-C(7S)	125(4)
C(6S)-C(1S)-C(7S)	116(4)
C(1S)-C(2S)-C(3S)	125(3)
C(1S)-C(2S)-H(2S)	117.7
C(3S)-C(2S)-H(2S)	117.7
C(2S)-C(3S)-C(4S)	123(3)
C(2S)-C(3S)-H(3S)	118.5
C(4S)-C(3S)-H(3S)	118.5
C(3S)-C(4S)-C(5S)	110(3)
C(3S)-C(4S)-H(4S)	124.9
C(5S)-C(4S)-H(4S)	124.9
C(6S)-C(5S)-C(4S)	120(3)
C(6S)-C(5S)-H(5S)	120.1
C(4S)-C(5S)-H(5S)	120.1
C(5S)-C(6S)-C(1S)	123(3)
C(5S)-C(6S)-H(6S)	118.6
C(1S)-C(6S)-H(6S)	118.6
C(1S)-C(7S)-H(7S1)	109.5
C(1S)-C(7S)-H(7S2)	109.5
H(7S1)-C(7S)-H(7S2)	109.5
C(1S)-C(7S)-H(7S3)	109.5
H(7S1)-C(7S)-H(7S3)	109.5
H(7S2)-C(7S)-H(7S3)	109.5
C(9S)-C(8S)-C(13S)	127(3)
C(9S)-C(8S)-C(14S)	111(3)
C(13S)-C(8S)-C(14S)	122(3)
C(8S)-C(9S)-C(10S)	115(2)
C(8S)-C(9S)-H(9S)	122.3
C(10S)-C(9S)-H(9S)	122.3

C(11S)-C(10S)-C(9S)	121(3)
C(11S)-C(10S)-H(10S)	119.5
C(9S)-C(10S)-H(10S)	119.5
C(12S)-C(11S)-C(10S)	117(3)
C(12S)-C(11S)-H(11S)	121.3
C(10S)-C(11S)-H(11S)	121.3
C(11S)-C(12S)-C(13S)	119(2)
C(11S)-C(12S)-H(12S)	120.6
C(13S)-C(12S)-H(12S)	120.6
C(8S)-C(13S)-C(12S)	119(3)
C(8S)-C(13S)-H(13S)	120.3
C(12S)-C(13S)-H(13S)	120.3
C(8S)-C(14S)-H(14A)	109.5
C(8S)-C(14S)-H(14B)	109.5
H(14A)-C(14S)-H(14B)	109.5
C(8S)-C(14S)-H(14C)	109.5
H(14A)-C(14S)-H(14C)	109.5
H(14B)-C(14S)-H(14C)	109.5

Symmetry transformations used to generate equivalent atoms:

#1 x,y+1,z #2 x,y-1,z

Table 3: Anisotropic displacement parameters ($\text{\AA}^2 \times 10^3$) for Complex **2.8**. The anisotropic displacement factor exponent takes the form: $-2p^2 [h^2 a^{*2} U^{11} + \dots + 2 h k a^* b^* U^{12}]$.

	U ¹¹	U ²²	U ³³	U ²³	U ¹³	U ¹² ___
Fe(1)	54(1)	50(1)	59(1)	2(1)	25(1)	-5(1)
Fe(2)	56(1)	48(1)	57(1)	2(1)	24(1)	-5(1)
Cl(1)	55(1)	68(1)	71(1)	-3(1)	20(1)	-1(1)
Cl(2)	58(1)	60(1)	64(1)	2(1)	22(1)	-10(1)
O(3)	77(4)	57(4)	70(4)	-4(3)	37(3)	-3(3)
O(4)	61(3)	57(3)	61(3)	4(3)	29(3)	-3(3)

N(1)	56(3)	45(3)	56(3)	-1(3)	28(3)	-3(3)
N(2)	62(4)	57(4)	67(4)	8(3)	33(3)	-7(3)
N(3)	64(4)	62(5)	78(5)	14(4)	34(4)	-2(3)
N(4)	63(4)	47(3)	61(4)	1(3)	29(3)	0(3)
N(5)	62(4)	50(4)	56(4)	-1(3)	25(3)	-5(3)
N(6)	55(4)	65(4)	68(5)	4(3)	26(3)	-1(3)
O(1)	59(4)	72(4)	77(4)	8(3)	35(3)	1(3)
O(2)	86(5)	58(4)	75(4)	11(3)	44(4)	1(3)
C(1)	69(5)	64(5)	76(5)	8(4)	44(4)	-2(4)
C(2)	66(5)	72(6)	89(6)	16(5)	45(5)	-1(4)
C(3)	49(4)	49(4)	62(4)	2(3)	25(3)	-3(3)
C(4)	63(5)	50(5)	62(5)	3(4)	25(4)	-8(3)
C(5)	62(4)	49(4)	56(4)	-6(3)	25(4)	-11(3)
C(6)	130(10)	61(6)	108(9)	25(6)	85(8)	22(6)
C(7)	68(5)	56(5)	80(6)	5(4)	44(5)	-5(4)
C(8)	70(5)	65(5)	73(5)	7(4)	47(4)	1(4)
C(9)	99(8)	92(8)	79(6)	23(6)	44(5)	-9(6)
C(10)	108(8)	91(8)	87(7)	29(6)	48(5)	7(6)
C(11)	115(9)	101(8)	56(5)	7(5)	43(5)	7(6)
C(12)	108(9)	88(8)	59(5)	-3(5)	32(5)	-3(6)
C(13)	88(7)	73(7)	69(5)	4(5)	38(4)	-4(5)
C(14)	64(5)	51(5)	58(5)	-3(3)	25(4)	-5(3)
C(15)	81(5)	57(5)	58(5)	9(4)	29(4)	8(4)
C(16)	96(7)	45(7)	62(8)	25(6)	36(6)	2(5)
C(17)	126(14)	50(7)	59(10)	16(6)	35(9)	8(7)
C(18)	138(16)	72(8)	83(11)	19(6)	54(11)	29(9)
C(19)	119(13)	76(11)	91(9)	31(10)	51(9)	33(9)
C(20)	81(6)	73(11)	74(10)	18(8)	26(6)	18(6)
C(16X)	96(7)	45(7)	62(8)	25(6)	36(6)	2(5)
C(17X)	126(14)	50(7)	59(10)	16(6)	35(9)	8(7)
C(18X)	138(16)	72(8)	83(11)	19(6)	54(11)	29(9)
C(19X)	119(13)	76(11)	91(9)	31(10)	51(9)	33(9)
C(20X)	81(6)	73(11)	74(10)	18(8)	26(6)	18(6)
C(21)	59(5)	59(5)	76(6)	5(4)	30(4)	1(4)
C(22)	85(6)	42(4)	80(6)	5(4)	47(5)	5(4)

C(23)	59(4)	53(4)	47(4)	4(3)	18(3)	-3(3)
C(24)	64(5)	53(4)	53(5)	2(3)	22(4)	-5(4)
C(25)	41(4)	49(4)	57(4)	5(3)	17(3)	-5(3)
C(26)	70(5)	55(5)	62(5)	4(4)	34(4)	-3(4)
C(27)	60(5)	55(4)	65(4)	6(4)	31(4)	-1(4)
C(28)	55(4)	66(5)	59(5)	1(4)	23(4)	-5(4)
C(29)	65(5)	68(5)	54(5)	2(4)	26(4)	0(4)
C(30)	72(5)	70(6)	66(5)	14(4)	26(5)	3(5)
C(31)	74(5)	78(6)	57(5)	7(4)	23(4)	-16(4)
C(32)	44(4)	104(7)	60(5)	9(5)	22(4)	-7(4)
C(33)	60(5)	79(6)	70(6)	13(5)	26(4)	3(4)
C(34)	58(5)	57(4)	54(4)	5(3)	25(4)	-3(3)
C(35)	61(4)	58(4)	62(4)	5(3)	37(3)	-7(3)
C(36)	68(5)	68(6)	62(5)	-7(4)	30(4)	4(4)
C(37)	63(6)	94(7)	72(6)	-9(5)	26(4)	-1(5)
C(38)	78(6)	82(6)	62(5)	-10(4)	32(4)	-21(5)
C(39)	96(7)	65(6)	72(5)	-6(4)	46(5)	-12(5)
C(40)	80(6)	59(5)	67(5)	11(4)	39(4)	1(4)
C(1S)	100(20)	120(30)	110(30)	30(20)	80(20)	50(20)
C(2S)	67(17)	70(20)	100(30)	10(20)	55(17)	5(15)
C(3S)	60(20)	80(20)	90(30)	5(18)	52(17)	0(20)
C(4S)	70(20)	33(17)	130(30)	6(17)	50(20)	-3(14)
C(5S)	70(20)	170(60)	140(40)	60(50)	50(20)	30(30)
C(6S)	90(20)	190(60)	150(50)	90(50)	80(30)	60(30)
C(7S)	120(40)	160(50)	100(40)	50(40)	20(40)	0(40)
C(1T)	117(17)	65(10)	82(11)	-3(7)	25(11)	24(10)
C(2T)	96(15)	95(15)	66(10)	5(10)	32(10)	-3(13)
C(3T)	70(13)	110(16)	83(15)	24(12)	35(12)	21(11)
C(4T)	92(14)	99(16)	90(13)	11(10)	51(11)	13(11)
C(5T)	87(13)	85(14)	106(15)	-10(11)	19(10)	-4(11)
C(6T)	104(14)	92(14)	88(14)	-4(10)	27(10)	20(10)
C(7T)	140(30)	86(13)	65(11)	4(9)	6(15)	14(14)
C(8S)	81(12)	127(13)	116(11)	41(9)	45(9)	22(11)
C(9S)	58(10)	91(9)	119(9)	42(8)	47(8)	-1(8)
C(10S)	84(13)	103(11)	124(13)	36(9)	53(11)	25(10)

C(11S)	117(16)	120(13)	146(11)	54(11)	69(11)	43(13)
C(12S)	107(15)	103(12)	156(13)	63(10)	50(12)	10(13)
C(13S)	100(20)	118(12)	136(14)	60(9)	64(13)	10(11)
C(14S)	170(30)	135(16)	135(17)	15(13)	-6(17)	36(17)
C(8T)	53(18)	121(19)	123(13)	54(13)	53(15)	13(18)
C(9T)	58(10)	91(9)	119(9)	42(8)	47(8)	-1(8)
C(10T)	120(50)	95(16)	138(19)	16(16)	-20(30)	0(20)
C(11T)	117(16)	120(13)	146(11)	54(11)	69(11)	43(13)
C(12T)	100(40)	160(30)	146(14)	70(20)	60(20)	70(30)
C(13T)	90(30)	130(20)	116(17)	44(16)	20(20)	20(20)
C(14T)	170(30)	135(16)	135(17)	15(13)	-6(17)	36(17)

Appendix B.2 X-Ray Crystallography Data from Chapter 4

Appendix B.2.1 Crystallographic Data for 4.11

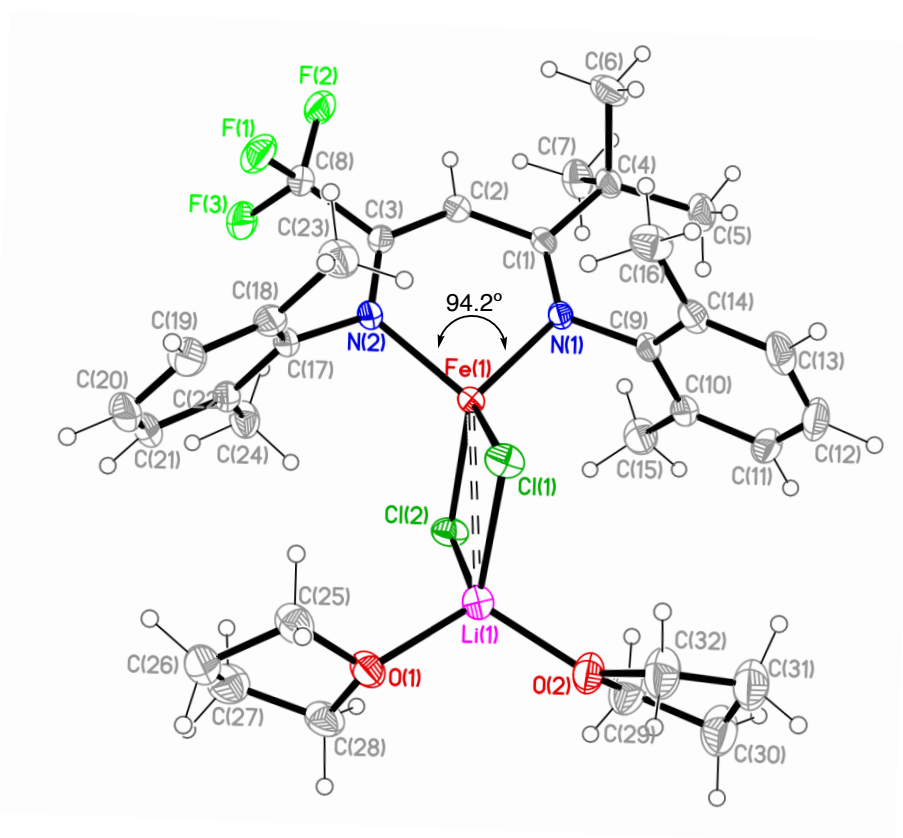


Figure 81: G: X-ray crystal structure of **X** with thermal ellipsoids represented at the 50% probability level.

Table 4: Crystal data and structure refinement for **4.11**.

Identification code	C32H44Cl2F3FeLiN2O2	
Empirical formula	C32 H44 Cl2 F3 Fe Li N2 O2	
Formula weight	679.38	
Temperature	173(2) K	
Wavelength	1.54178 \approx	
Crystal system	Triclinic	
Space group	P-1	
Unit cell dimensions	a = 12.6202(13) \approx	a = 73.374(4) ∞ .
	b = 12.6945(13) \approx	b = 89.943(4) ∞ .
	c = 12.7594(13) \approx	g = 62.708(4) ∞ .
Volume	1720.2(3) \approx^3	
Z	2	
Density (calculated)	1.312 Mg/m ³	
Absorption coefficient	5.330 mm ⁻¹	
F(000)	712	
Crystal size	0.260 x 0.120 x 0.080 mm ³	
Theta range for data collection	3.658 to 66.862 ∞ .	
Index ranges	-14 \leq h \leq 15, -15 \leq k \leq 15, -15 \leq l \leq 14	
Reflections collected	43995	
Independent reflections	6028 [R(int) = 0.0322]	
Completeness to theta = 66.862 ∞	98.6 %	
Absorption correction	Semi-empirical from equivalents	
Max. and min. transmission	0.7528 and 0.4924	
Refinement method	Full-matrix least-squares on F ²	
Data / restraints / parameters	6028 / 0 / 392	
Goodness-of-fit on F ²	1.040	

Final R indices [$I > 2\sigma(I)$]	R1 = 0.0273, wR2 = 0.0711
R indices (all data)	R1 = 0.0283, wR2 = 0.0718
Extinction coefficient	n/a
Largest diff. peak and hole	0.341 and -0.211 e. \approx ⁻³

Table 5. Bond lengths [\approx] and angles [∞] for (4.11).

Fe(1)-N(2)	1.9929(13)
Fe(1)-N(1)	2.0197(12)
Fe(1)-Cl(2)	2.3257(5)
Fe(1)-Cl(1)	2.3269(5)
Fe(1)-Li(1)	3.124(3)
Cl(1)-Li(1)	2.361(3)
Cl(2)-Li(1)	2.376(3)
F(1)-C(8)	1.3373(19)
F(2)-C(8)	1.341(2)
F(3)-C(8)	1.3354(19)
O(1)-C(28)	1.443(2)
O(1)-C(25)	1.450(2)
O(1)-Li(1)	1.909(3)
N(1)-C(1)	1.319(2)
N(1)-C(9)	1.4408(19)
O(2)-C(29)	1.436(2)
O(2)-C(32)	1.440(2)
O(2)-Li(1)	1.906(3)
N(2)-C(3)	1.334(2)
N(2)-C(17)	1.4480(19)
C(1)-C(2)	1.426(2)
C(1)-C(4)	1.562(2)
C(2)-C(3)	1.389(2)
C(2)-H(2)	0.9500
C(3)-C(8)	1.529(2)

C(4)-C(5)	1.535(2)
C(4)-C(6)	1.537(2)
C(4)-C(7)	1.537(2)
C(5)-H(5A)	0.9800
C(5)-H(5B)	0.9800
C(5)-H(5C)	0.9800
C(6)-H(6A)	0.9800
C(6)-H(6B)	0.9800
C(6)-H(6C)	0.9800
C(7)-H(7A)	0.9800
C(7)-H(7B)	0.9800
C(7)-H(7C)	0.9800
C(9)-C(10)	1.398(2)
C(9)-C(14)	1.399(2)
C(10)-C(11)	1.395(2)
C(10)-C(15)	1.502(2)
C(11)-C(12)	1.371(3)
C(11)-H(11)	0.9500
C(12)-C(13)	1.380(3)
C(12)-H(12)	0.9500
C(13)-C(14)	1.396(2)
C(13)-H(13)	0.9500
C(14)-C(16)	1.502(3)
C(15)-H(15A)	0.9800
C(15)-H(15B)	0.9800
C(15)-H(15C)	0.9800
C(16)-H(16A)	0.9800
C(16)-H(16B)	0.9800
C(16)-H(16C)	0.9800
C(17)-C(22)	1.402(2)
C(17)-C(18)	1.404(2)
C(18)-C(19)	1.399(2)
C(18)-C(23)	1.502(2)
C(19)-C(20)	1.379(3)
C(19)-H(19)	0.9500

C(20)-C(21)	1.379(3)
C(20)-H(20)	0.9500
C(21)-C(22)	1.399(2)
C(21)-H(21)	0.9500
C(22)-C(24)	1.504(2)
C(23)-H(23A)	0.9800
C(23)-H(23B)	0.9800
C(23)-H(23C)	0.9800
C(24)-H(24A)	0.9800
C(24)-H(24B)	0.9800
C(24)-H(24C)	0.9800
C(25)-C(26)	1.501(3)
C(25)-H(25A)	0.9900
C(25)-H(25B)	0.9900
C(26)-C(27)	1.510(3)
C(26)-H(26A)	0.9900
C(26)-H(26B)	0.9900
C(27)-C(28)	1.503(3)
C(27)-H(27A)	0.9900
C(27)-H(27B)	0.9900
C(28)-H(28A)	0.9900
C(28)-H(28B)	0.9900
C(29)-C(30)	1.494(3)
C(29)-H(29A)	0.9900
C(29)-H(29B)	0.9900
C(30)-C(31)	1.505(3)
C(30)-H(30A)	0.9900
C(30)-H(30B)	0.9900
C(31)-C(32)	1.484(3)
C(31)-H(31A)	0.9900
C(31)-H(31B)	0.9900
C(32)-H(32A)	0.9900
C(32)-H(32B)	0.9900
N(2)-Fe(1)-N(1)	94.16(5)

N(2)-Fe(1)-Cl(2)	114.27(4)
N(1)-Fe(1)-Cl(2)	118.88(4)
N(2)-Fe(1)-Cl(1)	117.83(4)
N(1)-Fe(1)-Cl(1)	115.55(4)
Cl(2)-Fe(1)-Cl(1)	97.708(18)
N(2)-Fe(1)-Li(1)	130.95(6)
N(1)-Fe(1)-Li(1)	134.90(6)
Cl(2)-Fe(1)-Li(1)	49.05(6)
Cl(1)-Fe(1)-Li(1)	48.67(6)
Fe(1)-Cl(1)-Li(1)	83.59(7)
Fe(1)-Cl(2)-Li(1)	83.27(7)
C(28)-O(1)-C(25)	108.96(13)
C(28)-O(1)-Li(1)	117.94(14)
C(25)-O(1)-Li(1)	118.85(13)
C(1)-N(1)-C(9)	125.01(12)
C(1)-N(1)-Fe(1)	126.76(10)
C(9)-N(1)-Fe(1)	107.83(9)
C(29)-O(2)-C(32)	109.05(14)
C(29)-O(2)-Li(1)	122.03(15)
C(32)-O(2)-Li(1)	122.40(15)
C(3)-N(2)-C(17)	124.32(13)
C(3)-N(2)-Fe(1)	121.55(10)
C(17)-N(2)-Fe(1)	113.92(10)
O(2)-Li(1)-O(1)	116.09(16)
O(2)-Li(1)-Cl(1)	110.22(13)
O(1)-Li(1)-Cl(1)	115.03(14)
O(2)-Li(1)-Cl(2)	110.87(14)
O(1)-Li(1)-Cl(2)	107.19(13)
Cl(1)-Li(1)-Cl(2)	95.40(10)
O(2)-Li(1)-Fe(1)	122.30(13)
O(1)-Li(1)-Fe(1)	121.41(13)
Cl(1)-Li(1)-Fe(1)	47.74(5)
Cl(2)-Li(1)-Fe(1)	47.67(5)
N(1)-C(1)-C(2)	119.90(13)
N(1)-C(1)-C(4)	126.69(13)

C(2)-C(1)-C(4)	113.41(13)
C(3)-C(2)-C(1)	129.81(14)
C(3)-C(2)-H(2)	115.1
C(1)-C(2)-H(2)	115.1
N(2)-C(3)-C(2)	126.86(14)
N(2)-C(3)-C(8)	118.34(13)
C(2)-C(3)-C(8)	114.79(13)
C(5)-C(4)-C(6)	107.10(14)
C(5)-C(4)-C(7)	106.29(14)
C(6)-C(4)-C(7)	108.56(15)
C(5)-C(4)-C(1)	117.72(13)
C(6)-C(4)-C(1)	109.22(13)
C(7)-C(4)-C(1)	107.64(12)
C(4)-C(5)-H(5A)	109.5
C(4)-C(5)-H(5B)	109.5
H(5A)-C(5)-H(5B)	109.5
C(4)-C(5)-H(5C)	109.5
H(5A)-C(5)-H(5C)	109.5
H(5B)-C(5)-H(5C)	109.5
C(4)-C(6)-H(6A)	109.5
C(4)-C(6)-H(6B)	109.5
H(6A)-C(6)-H(6B)	109.5
C(4)-C(6)-H(6C)	109.5
H(6A)-C(6)-H(6C)	109.5
H(6B)-C(6)-H(6C)	109.5
C(4)-C(7)-H(7A)	109.5
C(4)-C(7)-H(7B)	109.5
H(7A)-C(7)-H(7B)	109.5
C(4)-C(7)-H(7C)	109.5
H(7A)-C(7)-H(7C)	109.5
H(7B)-C(7)-H(7C)	109.5
F(3)-C(8)-F(1)	106.39(13)
F(3)-C(8)-F(2)	105.58(14)
F(1)-C(8)-F(2)	105.73(13)
F(3)-C(8)-C(3)	112.04(13)

F(1)-C(8)-C(3)	112.73(13)
F(2)-C(8)-C(3)	113.76(13)
C(10)-C(9)-C(14)	121.59(15)
C(10)-C(9)-N(1)	120.10(13)
C(14)-C(9)-N(1)	118.09(14)
C(11)-C(10)-C(9)	118.05(16)
C(11)-C(10)-C(15)	120.37(16)
C(9)-C(10)-C(15)	121.51(15)
C(12)-C(11)-C(10)	121.23(18)
C(12)-C(11)-H(11)	119.4
C(10)-C(11)-H(11)	119.4
C(11)-C(12)-C(13)	120.11(16)
C(11)-C(12)-H(12)	119.9
C(13)-C(12)-H(12)	119.9
C(12)-C(13)-C(14)	121.02(17)
C(12)-C(13)-H(13)	119.5
C(14)-C(13)-H(13)	119.5
C(13)-C(14)-C(9)	117.98(16)
C(13)-C(14)-C(16)	120.72(16)
C(9)-C(14)-C(16)	121.30(15)
C(10)-C(15)-H(15A)	109.5
C(10)-C(15)-H(15B)	109.5
H(15A)-C(15)-H(15B)	109.5
C(10)-C(15)-H(15C)	109.5
H(15A)-C(15)-H(15C)	109.5
H(15B)-C(15)-H(15C)	109.5
C(14)-C(16)-H(16A)	109.5
C(14)-C(16)-H(16B)	109.5
H(16A)-C(16)-H(16B)	109.5
C(14)-C(16)-H(16C)	109.5
H(16A)-C(16)-H(16C)	109.5
H(16B)-C(16)-H(16C)	109.5
C(22)-C(17)-C(18)	120.77(14)
C(22)-C(17)-N(2)	119.90(14)
C(18)-C(17)-N(2)	118.96(14)

C(19)-C(18)-C(17)	118.57(15)
C(19)-C(18)-C(23)	119.87(15)
C(17)-C(18)-C(23)	121.56(15)
C(20)-C(19)-C(18)	121.24(16)
C(20)-C(19)-H(19)	119.4
C(18)-C(19)-H(19)	119.4
C(21)-C(20)-C(19)	119.52(16)
C(21)-C(20)-H(20)	120.2
C(19)-C(20)-H(20)	120.2
C(20)-C(21)-C(22)	121.53(16)
C(20)-C(21)-H(21)	119.2
C(22)-C(21)-H(21)	119.2
C(21)-C(22)-C(17)	118.35(15)
C(21)-C(22)-C(24)	119.60(15)
C(17)-C(22)-C(24)	122.04(14)
C(18)-C(23)-H(23A)	109.5
C(18)-C(23)-H(23B)	109.5
H(23A)-C(23)-H(23B)	109.5
C(18)-C(23)-H(23C)	109.5
H(23A)-C(23)-H(23C)	109.5
H(23B)-C(23)-H(23C)	109.5
C(22)-C(24)-H(24A)	109.5
C(22)-C(24)-H(24B)	109.5
H(24A)-C(24)-H(24B)	109.5
C(22)-C(24)-H(24C)	109.5
H(24A)-C(24)-H(24C)	109.5
H(24B)-C(24)-H(24C)	109.5
O(1)-C(25)-C(26)	105.84(15)
O(1)-C(25)-H(25A)	110.6
C(26)-C(25)-H(25A)	110.6
O(1)-C(25)-H(25B)	110.6
C(26)-C(25)-H(25B)	110.6
H(25A)-C(25)-H(25B)	108.7
C(25)-C(26)-C(27)	101.85(16)
C(25)-C(26)-H(26A)	111.4

C(27)-C(26)-H(26A)	111.4
C(25)-C(26)-H(26B)	111.4
C(27)-C(26)-H(26B)	111.4
H(26A)-C(26)-H(26B)	109.3
C(28)-C(27)-C(26)	102.20(16)
C(28)-C(27)-H(27A)	111.3
C(26)-C(27)-H(27A)	111.3
C(28)-C(27)-H(27B)	111.3
C(26)-C(27)-H(27B)	111.3
H(27A)-C(27)-H(27B)	109.2
O(1)-C(28)-C(27)	105.18(14)
O(1)-C(28)-H(28A)	110.7
C(27)-C(28)-H(28A)	110.7
O(1)-C(28)-H(28B)	110.7
C(27)-C(28)-H(28B)	110.7
H(28A)-C(28)-H(28B)	108.8
O(2)-C(29)-C(30)	105.63(17)
O(2)-C(29)-H(29A)	110.6
C(30)-C(29)-H(29A)	110.6
O(2)-C(29)-H(29B)	110.6
C(30)-C(29)-H(29B)	110.6
H(29A)-C(29)-H(29B)	108.7
C(29)-C(30)-C(31)	103.06(17)
C(29)-C(30)-H(30A)	111.2
C(31)-C(30)-H(30A)	111.2
C(29)-C(30)-H(30B)	111.2
C(31)-C(30)-H(30B)	111.2
H(30A)-C(30)-H(30B)	109.1
C(32)-C(31)-C(30)	103.45(17)
C(32)-C(31)-H(31A)	111.1
C(30)-C(31)-H(31A)	111.1
C(32)-C(31)-H(31B)	111.1
C(30)-C(31)-H(31B)	111.1
H(31A)-C(31)-H(31B)	109.0
O(2)-C(32)-C(31)	107.06(17)

O(2)-C(32)-H(32A)	110.3
C(31)-C(32)-H(32A)	110.3
O(2)-C(32)-H(32B)	110.3
C(31)-C(32)-H(32B)	110.3
H(32A)-C(32)-H(32B)	108.6

Symmetry transformations used to generate equivalent atoms:

Table 6. Anisotropic displacement parameters ($\approx 2 \times 10^3$) for **4.11**. The anisotropic displacement factor exponent takes the form: $-2p^2 [h^2 a^* 2U^{11} + \dots + 2 h k a^* b^* U^{12}]$

	U ¹¹	U ²²	U ³³	U ²³	U ¹³	U ¹²
Fe(1)	18(1)	22(1)	30(1)	-10(1)	3(1)	-9(1)
Cl(1)	30(1)	38(1)	29(1)	-6(1)	4(1)	-17(1)
Cl(2)	29(1)	39(1)	31(1)	-5(1)	-2(1)	-18(1)
F(1)	54(1)	47(1)	50(1)	-32(1)	14(1)	-29(1)
F(2)	35(1)	39(1)	76(1)	-32(1)	18(1)	-24(1)
F(3)	47(1)	22(1)	61(1)	-7(1)	-6(1)	-12(1)
O(1)	27(1)	38(1)	39(1)	-16(1)	1(1)	-8(1)
N(1)	21(1)	18(1)	23(1)	-7(1)	1(1)	-6(1)
O(2)	45(1)	26(1)	43(1)	-11(1)	1(1)	-13(1)
N(2)	21(1)	21(1)	29(1)	-11(1)	3(1)	-6(1)
Li(1)	29(1)	29(1)	43(2)	-14(1)	4(1)	-12(1)
C(1)	18(1)	22(1)	21(1)	-6(1)	1(1)	-6(1)
C(2)	22(1)	24(1)	28(1)	-9(1)	4(1)	-11(1)
C(3)	24(1)	21(1)	26(1)	-8(1)	0(1)	-9(1)
C(4)	21(1)	25(1)	33(1)	-11(1)	7(1)	-8(1)
C(5)	28(1)	29(1)	63(1)	-20(1)	18(1)	-9(1)
C(6)	21(1)	47(1)	49(1)	-16(1)	0(1)	-10(1)
C(7)	39(1)	36(1)	40(1)	-14(1)	18(1)	-14(1)
C(8)	28(1)	25(1)	39(1)	-15(1)	4(1)	-10(1)
C(9)	18(1)	19(1)	32(1)	-8(1)	4(1)	-6(1)
C(10)	25(1)	28(1)	40(1)	-16(1)	4(1)	-9(1)
C(11)	37(1)	34(1)	63(1)	-28(1)	11(1)	-17(1)

C(12)	44(1)	23(1)	74(1)	-18(1)	20(1)	-15(1)
C(13)	33(1)	23(1)	50(1)	1(1)	9(1)	-7(1)
C(14)	22(1)	25(1)	34(1)	-4(1)	4(1)	-7(1)
C(15)	42(1)	41(1)	36(1)	-19(1)	-3(1)	-12(1)
C(16)	40(1)	44(1)	28(1)	0(1)	-3(1)	-20(1)
C(17)	21(1)	24(1)	32(1)	-14(1)	4(1)	-8(1)
C(18)	28(1)	33(1)	31(1)	-15(1)	1(1)	-13(1)
C(19)	37(1)	50(1)	34(1)	-25(1)	10(1)	-18(1)
C(20)	29(1)	46(1)	52(1)	-32(1)	12(1)	-10(1)
C(21)	24(1)	30(1)	48(1)	-18(1)	-1(1)	-3(1)
C(22)	26(1)	25(1)	33(1)	-13(1)	1(1)	-8(1)
C(23)	37(1)	42(1)	30(1)	-11(1)	-2(1)	-14(1)
C(24)	38(1)	28(1)	32(1)	-8(1)	-2(1)	-7(1)
C(25)	34(1)	47(1)	39(1)	-21(1)	3(1)	-12(1)
C(26)	35(1)	42(1)	59(1)	-24(1)	2(1)	-11(1)
C(27)	44(1)	43(1)	53(1)	-4(1)	-8(1)	-17(1)
C(28)	30(1)	50(1)	40(1)	-17(1)	-3(1)	-14(1)
C(29)	68(1)	40(1)	42(1)	-14(1)	-2(1)	-23(1)
C(30)	72(2)	40(1)	61(1)	-21(1)	-9(1)	-17(1)
C(31)	66(2)	34(1)	62(1)	-13(1)	-9(1)	-14(1)
C(32)	65(1)	32(1)	47(1)	-8(1)	-2(1)	-15(1)

Appendix B.2.2 Crystallographic Data for 4.5

Figure 82: G: X-ray crystal structure of **4.5** with thermal ellipsoids represented at the 50% probability level.

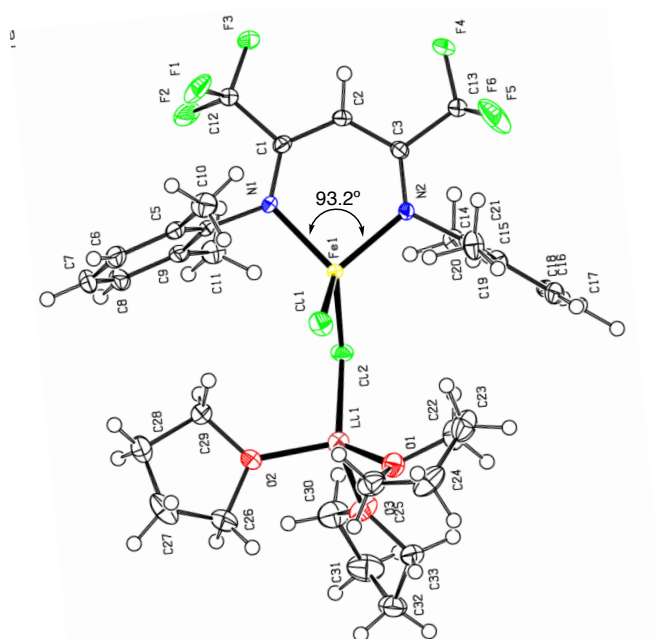


Table 7: Crystal data and structure refinement for **4.5**.

Identification code	Fe(C ₂₁ H ₁₉ N ₂ F ₆)Cl ₂ Li(THF) ₃	
Empirical formula	C ₃₃ H ₄₃ Cl ₂ F ₆ Fe Li N ₂ O ₃	
Formula weight	763.38	
Temperature	100(2) K	
Wavelength	1.54178 \approx	
Crystal system	Monoclinic	
Space group	P2 ₁ /n	
Unit cell dimensions	a = 12.1894(4) \approx	a = 90 ∞ .
	b = 13.4780(4) \approx	b = 95.839(2) ∞ .
	c = 21.8382(7) \approx	g = 90 ∞ .
Volume	3569.2(2) \approx ³	
Z	4	

Density (calculated)	1.421 Mg/m ³
Absorption coefficient	5.349 mm ⁻¹
F(000)	1584
Crystal size	0.440 x 0.230 x 0.100 mm ³
Theta range for data collection	3.859 to 68.396°.
Index ranges	-14 ≤ h ≤ 14, -16 ≤ k ≤ 16, -26 ≤ l ≤ 26
Reflections collected	42000
Independent reflections	6540 [R(int) = 0.0384]
Completeness to theta = 67.679°	100.0 %
Absorption correction	Semi-empirical from equivalents
Max. and min. transmission	0.7531 and 0.4776
Refinement method	Full-matrix least-squares on F ²
Data / restraints / parameters	6540 / 0 / 437
Goodness-of-fit on F ²	1.036
Final R indices [I > 2σ(I)]	R1 = 0.0312, wR2 = 0.0806
R indices (all data)	R1 = 0.0346, wR2 = 0.0829
Extinction coefficient	n/a
Largest diff. peak and hole	0.645 and -0.326 e. ⁻³

Table 8. Bond lengths [Å] and angles [°] for **4.5**.

Fe(1)-N(2)	2.0108(14)
Fe(1)-N(1)	2.0130(14)
Fe(1)-Cl(1)	2.2689(5)
Fe(1)-Cl(2)	2.3136(5)
Cl(2)-Li(1)	2.381(3)
F(1)-C(12)	1.329(2)
F(2)-C(12)	1.330(2)
F(3)-C(12)	1.337(2)
F(4)-C(13)	1.328(2)

F(5)-C(13)	1.324(2)
F(6)-C(13)	1.322(2)
N(1)-C(1)	1.322(2)
N(1)-C(4)	1.447(2)
N(2)-C(3)	1.320(2)
N(2)-C(14)	1.449(2)
C(1)-C(2)	1.399(2)
C(1)-C(12)	1.531(2)
C(2)-C(3)	1.404(2)
C(2)-H(2)	0.9500
C(3)-C(13)	1.531(2)
C(4)-C(9)	1.401(3)
C(4)-C(5)	1.402(3)
C(5)-C(6)	1.399(3)
C(5)-C(10)	1.504(3)
C(6)-C(7)	1.378(3)
C(6)-H(6)	0.9500
C(7)-C(8)	1.383(3)
C(7)-H(7)	0.9500
C(8)-C(9)	1.393(3)
C(8)-H(8)	0.9500
C(9)-C(11)	1.503(3)
C(10)-H(10A)	0.9800
C(10)-H(10B)	0.9800
C(10)-H(10C)	0.9800
C(11)-H(11A)	0.9800
C(11)-H(11B)	0.9800
C(11)-H(11C)	0.9800
C(14)-C(19)	1.401(2)
C(14)-C(15)	1.403(2)
C(15)-C(16)	1.393(2)
C(15)-C(20)	1.506(2)
C(16)-C(17)	1.387(3)
C(16)-H(16)	0.9500
C(17)-C(18)	1.381(3)

C(17)-H(17)	0.9500
C(18)-C(19)	1.393(3)
C(18)-H(18)	0.9500
C(19)-C(21)	1.506(3)
C(20)-H(20A)	0.9800
C(20)-H(20B)	0.9800
C(20)-H(20C)	0.9800
C(21)-H(21A)	0.9800
C(21)-H(21B)	0.9800
C(21)-H(21C)	0.9800
Li(1)-O(2)	1.921(4)
Li(1)-O(1)	1.933(4)
Li(1)-O(3)	1.951(4)
O(1)-C(25)	1.441(2)
O(1)-C(22)	1.447(2)
O(2)-C(26)	1.435(3)
O(2)-C(29)	1.442(2)
O(3)-C(33)	1.432(2)
O(3)-C(30)	1.444(3)
C(22)-C(23)	1.510(3)
C(22)-H(22A)	0.9900
C(22)-H(22B)	0.9900
C(23)-C(24)	1.519(4)
C(23)-H(23A)	0.9900
C(23)-H(23B)	0.9900
C(24)-C(25)	1.514(3)
C(24)-H(24A)	0.9900
C(24)-H(24B)	0.9900
C(25)-H(25A)	0.9900
C(25)-H(25B)	0.9900
C(26)-C(27)	1.492(3)
C(26)-H(26A)	0.9900
C(26)-H(26B)	0.9900
C(27)-C(28)	1.510(3)
C(27)-H(27A)	0.9900

C(27)-H(27B)	0.9900
C(28)-C(29)	1.514(3)
C(28)-H(28A)	0.9900
C(28)-H(28B)	0.9900
C(29)-H(29A)	0.9900
C(29)-H(29B)	0.9900
C(30)-C(31)	1.511(3)
C(30)-H(30A)	0.9900
C(30)-H(30B)	0.9900
C(31)-C(32)	1.516(3)
C(31)-H(31A)	0.9900
C(31)-H(31B)	0.9900
C(32)-C(33)	1.513(3)
C(32)-H(32A)	0.9900
C(32)-H(32B)	0.9900
C(33)-H(33A)	0.9900
C(33)-H(33B)	0.9900
N(2)-Fe(1)-N(1)	93.23(6)
N(2)-Fe(1)-Cl(1)	122.17(4)
N(1)-Fe(1)-Cl(1)	110.94(4)
N(2)-Fe(1)-Cl(2)	109.63(4)
N(1)-Fe(1)-Cl(2)	119.85(4)
Cl(1)-Fe(1)-Cl(2)	102.264(19)
Fe(1)-Cl(2)-Li(1)	102.15(9)
C(1)-N(1)-C(4)	122.66(14)
C(1)-N(1)-Fe(1)	124.21(12)
C(4)-N(1)-Fe(1)	113.12(10)
C(3)-N(2)-C(14)	122.31(14)
C(3)-N(2)-Fe(1)	124.18(12)
C(14)-N(2)-Fe(1)	113.47(10)
N(1)-C(1)-C(2)	125.46(16)
N(1)-C(1)-C(12)	119.94(15)
C(2)-C(1)-C(12)	114.58(15)
C(1)-C(2)-C(3)	127.11(16)

C(1)-C(2)-H(2)	116.4
C(3)-C(2)-H(2)	116.4
N(2)-C(3)-C(2)	125.41(16)
N(2)-C(3)-C(13)	119.83(15)
C(2)-C(3)-C(13)	114.75(15)
C(9)-C(4)-C(5)	121.67(17)
C(9)-C(4)-N(1)	118.38(16)
C(5)-C(4)-N(1)	119.73(16)
C(6)-C(5)-C(4)	117.71(18)
C(6)-C(5)-C(10)	119.83(18)
C(4)-C(5)-C(10)	122.46(17)
C(7)-C(6)-C(5)	121.44(19)
C(7)-C(6)-H(6)	119.3
C(5)-C(6)-H(6)	119.3
C(6)-C(7)-C(8)	119.83(18)
C(6)-C(7)-H(7)	120.1
C(8)-C(7)-H(7)	120.1
C(7)-C(8)-C(9)	121.14(19)
C(7)-C(8)-H(8)	119.4
C(9)-C(8)-H(8)	119.4
C(8)-C(9)-C(4)	118.18(18)
C(8)-C(9)-C(11)	120.62(18)
C(4)-C(9)-C(11)	121.19(17)
C(5)-C(10)-H(10A)	109.5
C(5)-C(10)-H(10B)	109.5
H(10A)-C(10)-H(10B)	109.5
C(5)-C(10)-H(10C)	109.5
H(10A)-C(10)-H(10C)	109.5
H(10B)-C(10)-H(10C)	109.5
C(9)-C(11)-H(11A)	109.5
C(9)-C(11)-H(11B)	109.5
H(11A)-C(11)-H(11B)	109.5
C(9)-C(11)-H(11C)	109.5
H(11A)-C(11)-H(11C)	109.5
H(11B)-C(11)-H(11C)	109.5

F(1)-C(12)-F(2)	106.72(15)
F(1)-C(12)-F(3)	106.19(16)
F(2)-C(12)-F(3)	105.71(16)
F(1)-C(12)-C(1)	111.92(15)
F(2)-C(12)-C(1)	112.93(15)
F(3)-C(12)-C(1)	112.85(15)
F(6)-C(13)-F(5)	105.93(16)
F(6)-C(13)-F(4)	107.30(17)
F(5)-C(13)-F(4)	104.50(17)
F(6)-C(13)-C(3)	112.11(16)
F(5)-C(13)-C(3)	113.17(16)
F(4)-C(13)-C(3)	113.22(15)
C(19)-C(14)-C(15)	121.86(16)
C(19)-C(14)-N(2)	119.45(15)
C(15)-C(14)-N(2)	118.47(15)
C(16)-C(15)-C(14)	117.97(16)
C(16)-C(15)-C(20)	120.22(16)
C(14)-C(15)-C(20)	121.79(15)
C(17)-C(16)-C(15)	121.06(17)
C(17)-C(16)-H(16)	119.5
C(15)-C(16)-H(16)	119.5
C(18)-C(17)-C(16)	119.85(17)
C(18)-C(17)-H(17)	120.1
C(16)-C(17)-H(17)	120.1
C(17)-C(18)-C(19)	121.35(17)
C(17)-C(18)-H(18)	119.3
C(19)-C(18)-H(18)	119.3
C(18)-C(19)-C(14)	117.87(17)
C(18)-C(19)-C(21)	120.26(17)
C(14)-C(19)-C(21)	121.87(16)
C(15)-C(20)-H(20A)	109.5
C(15)-C(20)-H(20B)	109.5
H(20A)-C(20)-H(20B)	109.5
C(15)-C(20)-H(20C)	109.5
H(20A)-C(20)-H(20C)	109.5

H(20B)-C(20)-H(20C)	109.5
C(19)-C(21)-H(21A)	109.5
C(19)-C(21)-H(21B)	109.5
H(21A)-C(21)-H(21B)	109.5
C(19)-C(21)-H(21C)	109.5
H(21A)-C(21)-H(21C)	109.5
H(21B)-C(21)-H(21C)	109.5
O(2)-Li(1)-O(1)	114.91(18)
O(2)-Li(1)-O(3)	103.23(17)
O(1)-Li(1)-O(3)	97.67(16)
O(2)-Li(1)-Cl(2)	106.18(15)
O(1)-Li(1)-Cl(2)	128.54(17)
O(3)-Li(1)-Cl(2)	101.81(15)
C(25)-O(1)-C(22)	109.38(16)
C(25)-O(1)-Li(1)	123.93(16)
C(22)-O(1)-Li(1)	119.72(16)
C(26)-O(2)-C(29)	108.79(16)
C(26)-O(2)-Li(1)	125.43(17)
C(29)-O(2)-Li(1)	125.56(15)
C(33)-O(3)-C(30)	109.10(16)
C(33)-O(3)-Li(1)	130.60(16)
C(30)-O(3)-Li(1)	120.13(16)
O(1)-C(22)-C(23)	105.75(17)
O(1)-C(22)-H(22A)	110.6
C(23)-C(22)-H(22A)	110.6
O(1)-C(22)-H(22B)	110.6
C(23)-C(22)-H(22B)	110.6
H(22A)-C(22)-H(22B)	108.7
C(22)-C(23)-C(24)	102.09(19)
C(22)-C(23)-H(23A)	111.4
C(24)-C(23)-H(23A)	111.4
C(22)-C(23)-H(23B)	111.4
C(24)-C(23)-H(23B)	111.4
H(23A)-C(23)-H(23B)	109.2
C(25)-C(24)-C(23)	101.48(17)

C(25)-C(24)-H(24A)	111.5
C(23)-C(24)-H(24A)	111.5
C(25)-C(24)-H(24B)	111.5
C(23)-C(24)-H(24B)	111.5
H(24A)-C(24)-H(24B)	109.3
O(1)-C(25)-C(24)	105.24(18)
O(1)-C(25)-H(25A)	110.7
C(24)-C(25)-H(25A)	110.7
O(1)-C(25)-H(25B)	110.7
C(24)-C(25)-H(25B)	110.7
H(25A)-C(25)-H(25B)	108.8
O(2)-C(26)-C(27)	104.93(19)
O(2)-C(26)-H(26A)	110.8
C(27)-C(26)-H(26A)	110.8
O(2)-C(26)-H(26B)	110.8
C(27)-C(26)-H(26B)	110.8
H(26A)-C(26)-H(26B)	108.8
C(26)-C(27)-C(28)	101.79(18)
C(26)-C(27)-H(27A)	111.4
C(28)-C(27)-H(27A)	111.4
C(26)-C(27)-H(27B)	111.4
C(28)-C(27)-H(27B)	111.4
H(27A)-C(27)-H(27B)	109.3
C(27)-C(28)-C(29)	103.75(18)
C(27)-C(28)-H(28A)	111.0
C(29)-C(28)-H(28A)	111.0
C(27)-C(28)-H(28B)	111.0
C(29)-C(28)-H(28B)	111.0
H(28A)-C(28)-H(28B)	109.0
O(2)-C(29)-C(28)	106.11(16)
O(2)-C(29)-H(29A)	110.5
C(28)-C(29)-H(29A)	110.5
O(2)-C(29)-H(29B)	110.5
C(28)-C(29)-H(29B)	110.5
H(29A)-C(29)-H(29B)	108.7

O(3)-C(30)-C(31)	106.59(18)
O(3)-C(30)-H(30A)	110.4
C(31)-C(30)-H(30A)	110.4
O(3)-C(30)-H(30B)	110.4
C(31)-C(30)-H(30B)	110.4
H(30A)-C(30)-H(30B)	108.6
C(30)-C(31)-C(32)	102.59(19)
C(30)-C(31)-H(31A)	111.2
C(32)-C(31)-H(31A)	111.2
C(30)-C(31)-H(31B)	111.2
C(32)-C(31)-H(31B)	111.2
H(31A)-C(31)-H(31B)	109.2
C(33)-C(32)-C(31)	101.53(17)
C(33)-C(32)-H(32A)	111.5
C(31)-C(32)-H(32A)	111.5
C(33)-C(32)-H(32B)	111.5
C(31)-C(32)-H(32B)	111.5
H(32A)-C(32)-H(32B)	109.3
O(3)-C(33)-C(32)	104.35(16)
O(3)-C(33)-H(33A)	110.9
C(32)-C(33)-H(33A)	110.9
O(3)-C(33)-H(33B)	110.9
C(32)-C(33)-H(33B)	110.9
H(33A)-C(33)-H(33B)	108.9

Symmetry transformations used to generate equivalent atoms:

Table 9. Anisotropic displacement parameters ($\approx 2 \times 10^3$) for **4.5**. The anisotropic displacement factor exponent takes the form: $-2p^2 [h^2 a^{*2} U_{11} + \dots + 2 h k a^* b^* U_{12}]$.

	U ₁₁	U ₂₂	U ₃₃	U ₂₃	U ₁₃	U ₁₂
Fe(1)	12(1)	16(1)	11(1)	-2(1)	2(1)	-2(1)
Cl(2)	24(1)	18(1)	21(1)	-5(1)	8(1)	-2(1)
Cl(1)	24(1)	28(1)	23(1)	10(1)	2(1)	-1(1)

F(1)	56(1)	33(1)	26(1)	-13(1)	-6(1)	-11(1)
F(2)	30(1)	64(1)	18(1)	-5(1)	-6(1)	12(1)
F(3)	31(1)	86(1)	13(1)	-8(1)	8(1)	-24(1)
F(4)	28(1)	100(1)	35(1)	-38(1)	21(1)	-27(1)
F(5)	32(1)	40(1)	64(1)	-18(1)	26(1)	-19(1)
F(6)	18(1)	77(1)	68(1)	26(1)	13(1)	14(1)
N(1)	14(1)	16(1)	11(1)	-2(1)	0(1)	-2(1)
N(2)	12(1)	15(1)	16(1)	-4(1)	1(1)	-2(1)
C(1)	18(1)	17(1)	14(1)	-3(1)	2(1)	-1(1)
C(2)	18(1)	21(1)	15(1)	-4(1)	6(1)	-2(1)
C(3)	14(1)	16(1)	19(1)	-3(1)	5(1)	-2(1)
C(4)	14(1)	25(1)	10(1)	-3(1)	1(1)	-4(1)
C(5)	23(1)	25(1)	14(1)	-3(1)	3(1)	-6(1)
C(6)	30(1)	36(1)	20(1)	-3(1)	4(1)	-17(1)
C(7)	16(1)	56(1)	24(1)	-1(1)	2(1)	-12(1)
C(8)	15(1)	48(1)	20(1)	2(1)	1(1)	3(1)
C(9)	19(1)	32(1)	12(1)	1(1)	2(1)	1(1)
C(10)	35(1)	18(1)	32(1)	-4(1)	7(1)	-4(1)
C(11)	25(1)	26(1)	25(1)	3(1)	0(1)	8(1)
C(12)	18(1)	32(1)	15(1)	-3(1)	4(1)	-5(1)
C(13)	18(1)	31(1)	20(1)	-8(1)	5(1)	-4(1)
C(14)	10(1)	18(1)	14(1)	-3(1)	3(1)	-2(1)
C(15)	12(1)	18(1)	14(1)	-1(1)	4(1)	-1(1)
C(16)	18(1)	18(1)	19(1)	-5(1)	6(1)	-3(1)
C(17)	18(1)	29(1)	16(1)	-7(1)	1(1)	-3(1)
C(18)	16(1)	28(1)	18(1)	2(1)	-2(1)	2(1)
C(19)	14(1)	18(1)	22(1)	0(1)	3(1)	1(1)
C(20)	20(1)	17(1)	21(1)	2(1)	2(1)	0(1)
C(21)	20(1)	19(1)	37(1)	2(1)	-4(1)	2(1)
Li(1)	24(2)	32(2)	21(2)	-2(1)	2(1)	-4(1)
O(1)	26(1)	23(1)	27(1)	-1(1)	1(1)	-1(1)
O(2)	24(1)	56(1)	23(1)	-10(1)	9(1)	-16(1)
O(3)	38(1)	35(1)	23(1)	-7(1)	-6(1)	13(1)
C(22)	25(1)	30(1)	41(1)	-3(1)	-3(1)	-3(1)
C(23)	35(1)	36(1)	38(1)	-7(1)	-11(1)	7(1)

C(24)	61(2)	31(1)	23(1)	1(1)	-10(1)	3(1)
C(25)	44(1)	28(1)	26(1)	0(1)	5(1)	-5(1)
C(26)	31(1)	71(2)	29(1)	-3(1)	14(1)	-12(1)
C(27)	25(1)	37(1)	56(2)	12(1)	14(1)	-2(1)
C(28)	21(1)	49(1)	43(1)	-14(1)	6(1)	-8(1)
C(29)	23(1)	37(1)	24(1)	-10(1)	4(1)	-5(1)
C(30)	40(1)	43(1)	32(1)	2(1)	1(1)	17(1)
C(31)	53(2)	38(1)	45(1)	1(1)	16(1)	16(1)
C(32)	36(1)	32(1)	32(1)	-6(1)	14(1)	-3(1)
C(33)	28(1)	30(1)	20(1)	-2(1)	5(1)	-3(1)

Appendix B.2.3 Crystallographic Data for 4.49

Figure 83: G: X-ray crystal structure of **4.49** with thermal ellipsoids represented at the 50% probability level.

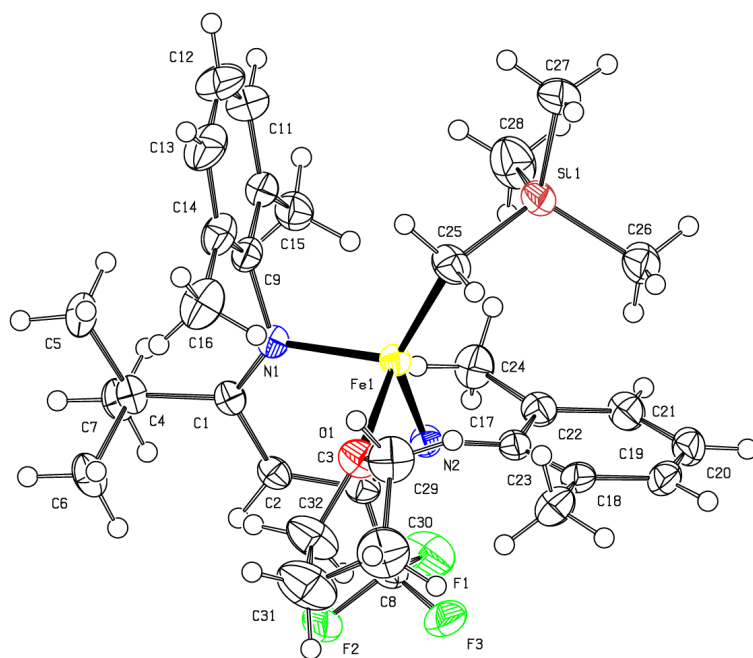


Table 9: Crystal data and structure refinement for **4.49**.

Identification code	C32H47F3FeN2OSi
Empirical formula	C32 H47 F3 Fe N2 O Si

Formula weight	616.65	
Temperature	173(2) K	
Wavelength	1.54178 \approx	
Crystal system	Monoclinic	
Space group	P2 ₁ /c	
Unit cell dimensions	a = 16.5833(10) \approx	a = 90 ∞ .
	b = 17.5731(11) \approx	b = 103.588(3) ∞ .
	c = 11.6434(7) \approx	g = 90 ∞ .
Volume	3298.1(4) \approx^3	
Z	4	
Density (calculated)	1.242 Mg/m ³	
Absorption coefficient	4.369 mm ⁻¹	
F(000)	1312	
Crystal size	0.220 x 0.160 x 0.120 mm ³	
Theta range for data collection	2.741 to 66.657 ∞ .	
Index ranges	-19 \leq h \leq 19, -20 \leq k \leq 20, -13 \leq l \leq 13	
Reflections collected	40460	
Independent reflections	5782 [R(int) = 0.0349]	
Completeness to theta = 66.657 ∞	99.2 %	
Absorption correction	Semi-empirical from equivalents	
Max. and min. transmission	0.7528 and 0.5813	
Refinement method	Full-matrix least-squares on F ²	
Data / restraints / parameters	5782 / 0 / 371	
Goodness-of-fit on F ²	1.057	
Final R indices [I > 2 σ (I)]	R1 = 0.0290, wR2 = 0.0772	
R indices (all data)	R1 = 0.0326, wR2 = 0.0795	
Extinction coefficient	n/a	
Largest diff. peak and hole	0.344 and -0.239 e. \approx^{-3}	

Table 10. Bond lengths [\approx] and angles [∞] for **4.49**.

Fe(1)-N(2)	2.0113(12)
Fe(1)-C(25)	2.0445(16)
Fe(1)-N(1)	2.0473(13)
Fe(1)-O(1)	2.2362(12)

Si(1)-C(25)	1.8383(18)
Si(1)-C(26)	1.872(2)
Si(1)-C(28)	1.875(2)
Si(1)-C(27)	1.8807(19)
F(1)-C(8)	1.335(2)
F(2)-C(8)	1.340(2)
F(3)-C(8)	1.341(2)
O(1)-C(32)	1.437(2)
O(1)-C(29)	1.447(2)
N(1)-C(1)	1.314(2)
N(1)-C(9)	1.436(2)
N(2)-C(3)	1.342(2)
N(2)-C(17)	1.437(2)
C(1)-C(2)	1.432(2)
C(1)-C(4)	1.553(2)
C(2)-C(3)	1.384(2)
C(2)-H(2)	0.9500
C(3)-C(8)	1.536(2)
C(4)-C(5)	1.533(2)
C(4)-C(7)	1.540(2)
C(4)-C(6)	1.547(2)
C(5)-H(5A)	0.9800
C(5)-H(5B)	0.9800
C(5)-H(5C)	0.9800
C(6)-H(6A)	0.9800
C(6)-H(6B)	0.9800
C(6)-H(6C)	0.9800
C(7)-H(7A)	0.9800
C(7)-H(7B)	0.9800
C(7)-H(7C)	0.9800
C(9)-C(10)	1.402(2)
C(9)-C(14)	1.402(2)
C(10)-C(11)	1.392(3)
C(10)-C(15)	1.500(3)
C(11)-C(12)	1.371(3)

C(11)-H(11)	0.9500
C(12)-C(13)	1.385(3)
C(12)-H(12)	0.9500
C(13)-C(14)	1.394(3)
C(13)-H(13)	0.9500
C(14)-C(16)	1.502(3)
C(15)-H(15A)	0.9800
C(15)-H(15B)	0.9800
C(15)-H(15C)	0.9800
C(16)-H(16A)	0.9800
C(16)-H(16B)	0.9800
C(16)-H(16C)	0.9800
C(17)-C(18)	1.407(2)
C(17)-C(22)	1.410(2)
C(18)-C(19)	1.395(2)
C(18)-C(23)	1.501(2)
C(19)-C(20)	1.379(3)
C(19)-H(19)	0.9500
C(20)-C(21)	1.381(3)
C(20)-H(20)	0.9500
C(21)-C(22)	1.396(2)
C(21)-H(21)	0.9500
C(22)-C(24)	1.506(2)
C(23)-H(23A)	0.9800
C(23)-H(23B)	0.9800
C(23)-H(23C)	0.9800
C(24)-H(24A)	0.9800
C(24)-H(24B)	0.9800
C(24)-H(24C)	0.9800
C(25)-H(25A)	0.9900
C(25)-H(25B)	0.9900
C(26)-H(26A)	0.9800
C(26)-H(26B)	0.9800
C(26)-H(26C)	0.9800
C(27)-H(27A)	0.9800

C(27)-H(27B)	0.9800
C(27)-H(27C)	0.9800
C(28)-H(28A)	0.9800
C(28)-H(28B)	0.9800
C(28)-H(28C)	0.9800
C(29)-C(30)	1.508(3)
C(29)-H(29A)	0.9900
C(29)-H(29B)	0.9900
C(30)-C(31)	1.496(4)
C(30)-H(30A)	0.9900
C(30)-H(30B)	0.9900
C(31)-C(32)	1.495(3)
C(31)-H(31A)	0.9900
C(31)-H(31B)	0.9900
C(32)-H(32A)	0.9900
C(32)-H(32B)	0.9900

N(2)-Fe(1)-C(25)	139.21(6)
N(2)-Fe(1)-N(1)	91.30(5)
C(25)-Fe(1)-N(1)	119.68(7)
N(2)-Fe(1)-O(1)	98.96(5)
C(25)-Fe(1)-O(1)	102.28(6)
N(1)-Fe(1)-O(1)	97.20(5)
C(25)-Si(1)-C(26)	109.78(9)
C(25)-Si(1)-C(28)	112.18(9)
C(26)-Si(1)-C(28)	107.28(11)
C(25)-Si(1)-C(27)	112.08(9)
C(26)-Si(1)-C(27)	108.75(9)
C(28)-Si(1)-C(27)	106.58(11)
C(32)-O(1)-C(29)	109.46(14)
C(32)-O(1)-Fe(1)	125.01(11)
C(29)-O(1)-Fe(1)	124.78(11)
C(1)-N(1)-C(9)	126.60(13)
C(1)-N(1)-Fe(1)	125.53(10)
C(9)-N(1)-Fe(1)	107.73(9)

C(3)-N(2)-C(17)	122.40(12)
C(3)-N(2)-Fe(1)	118.81(10)
C(17)-N(2)-Fe(1)	118.77(9)
N(1)-C(1)-C(2)	119.09(14)
N(1)-C(1)-C(4)	126.32(14)
C(2)-C(1)-C(4)	114.55(13)
C(3)-C(2)-C(1)	128.64(14)
C(3)-C(2)-H(2)	115.7
C(1)-C(2)-H(2)	115.7
N(2)-C(3)-C(2)	126.91(14)
N(2)-C(3)-C(8)	117.59(14)
C(2)-C(3)-C(8)	115.42(14)
C(5)-C(4)-C(7)	107.14(14)
C(5)-C(4)-C(6)	106.71(14)
C(7)-C(4)-C(6)	109.34(14)
C(5)-C(4)-C(1)	116.86(13)
C(7)-C(4)-C(1)	109.66(13)
C(6)-C(4)-C(1)	106.94(13)
C(4)-C(5)-H(5A)	109.5
C(4)-C(5)-H(5B)	109.5
H(5A)-C(5)-H(5B)	109.5
C(4)-C(5)-H(5C)	109.5
H(5A)-C(5)-H(5C)	109.5
H(5B)-C(5)-H(5C)	109.5
C(4)-C(6)-H(6A)	109.5
C(4)-C(6)-H(6B)	109.5
H(6A)-C(6)-H(6B)	109.5
C(4)-C(6)-H(6C)	109.5
H(6A)-C(6)-H(6C)	109.5
H(6B)-C(6)-H(6C)	109.5
C(4)-C(7)-H(7A)	109.5
C(4)-C(7)-H(7B)	109.5
H(7A)-C(7)-H(7B)	109.5
C(4)-C(7)-H(7C)	109.5
H(7A)-C(7)-H(7C)	109.5

H(7B)-C(7)-H(7C)	109.5
F(1)-C(8)-F(2)	106.02(14)
F(1)-C(8)-F(3)	106.40(15)
F(2)-C(8)-F(3)	106.00(14)
F(1)-C(8)-C(3)	113.77(14)
F(2)-C(8)-C(3)	112.84(14)
F(3)-C(8)-C(3)	111.26(14)
C(10)-C(9)-C(14)	121.57(15)
C(10)-C(9)-N(1)	118.01(14)
C(14)-C(9)-N(1)	119.80(15)
C(11)-C(10)-C(9)	118.45(17)
C(11)-C(10)-C(15)	120.22(17)
C(9)-C(10)-C(15)	121.33(15)
C(12)-C(11)-C(10)	120.9(2)
C(12)-C(11)-H(11)	119.5
C(10)-C(11)-H(11)	119.5
C(11)-C(12)-C(13)	120.12(18)
C(11)-C(12)-H(12)	119.9
C(13)-C(12)-H(12)	119.9
C(12)-C(13)-C(14)	121.43(18)
C(12)-C(13)-H(13)	119.3
C(14)-C(13)-H(13)	119.3
C(13)-C(14)-C(9)	117.53(17)
C(13)-C(14)-C(16)	120.58(17)
C(9)-C(14)-C(16)	121.89(16)
C(10)-C(15)-H(15A)	109.5
C(10)-C(15)-H(15B)	109.5
H(15A)-C(15)-H(15B)	109.5
C(10)-C(15)-H(15C)	109.5
H(15A)-C(15)-H(15C)	109.5
H(15B)-C(15)-H(15C)	109.5
C(14)-C(16)-H(16A)	109.5
C(14)-C(16)-H(16B)	109.5
H(16A)-C(16)-H(16B)	109.5
C(14)-C(16)-H(16C)	109.5

H(16A)-C(16)-H(16C)	109.5
H(16B)-C(16)-H(16C)	109.5
C(18)-C(17)-C(22)	120.24(15)
C(18)-C(17)-N(2)	119.00(14)
C(22)-C(17)-N(2)	120.49(14)
C(19)-C(18)-C(17)	118.85(15)
C(19)-C(18)-C(23)	119.91(15)
C(17)-C(18)-C(23)	121.17(15)
C(20)-C(19)-C(18)	121.20(16)
C(20)-C(19)-H(19)	119.4
C(18)-C(19)-H(19)	119.4
C(19)-C(20)-C(21)	119.69(16)
C(19)-C(20)-H(20)	120.2
C(21)-C(20)-H(20)	120.2
C(20)-C(21)-C(22)	121.38(16)
C(20)-C(21)-H(21)	119.3
C(22)-C(21)-H(21)	119.3
C(21)-C(22)-C(17)	118.52(16)
C(21)-C(22)-C(24)	119.28(15)
C(17)-C(22)-C(24)	122.17(15)
C(18)-C(23)-H(23A)	109.5
C(18)-C(23)-H(23B)	109.5
H(23A)-C(23)-H(23B)	109.5
C(18)-C(23)-H(23C)	109.5
H(23A)-C(23)-H(23C)	109.5
H(23B)-C(23)-H(23C)	109.5
C(22)-C(24)-H(24A)	109.5
C(22)-C(24)-H(24B)	109.5
H(24A)-C(24)-H(24B)	109.5
C(22)-C(24)-H(24C)	109.5
H(24A)-C(24)-H(24C)	109.5
H(24B)-C(24)-H(24C)	109.5
Si(1)-C(25)-Fe(1)	119.43(9)
Si(1)-C(25)-H(25A)	107.5
Fe(1)-C(25)-H(25A)	107.5

Si(1)-C(25)-H(25B)	107.5
Fe(1)-C(25)-H(25B)	107.5
H(25A)-C(25)-H(25B)	107.0
Si(1)-C(26)-H(26A)	109.5
Si(1)-C(26)-H(26B)	109.5
H(26A)-C(26)-H(26B)	109.5
Si(1)-C(26)-H(26C)	109.5
H(26A)-C(26)-H(26C)	109.5
H(26B)-C(26)-H(26C)	109.5
Si(1)-C(27)-H(27A)	109.5
Si(1)-C(27)-H(27B)	109.5
H(27A)-C(27)-H(27B)	109.5
Si(1)-C(27)-H(27C)	109.5
H(27A)-C(27)-H(27C)	109.5
H(27B)-C(27)-H(27C)	109.5
Si(1)-C(28)-H(28A)	109.5
Si(1)-C(28)-H(28B)	109.5
H(28A)-C(28)-H(28B)	109.5
Si(1)-C(28)-H(28C)	109.5
H(28A)-C(28)-H(28C)	109.5
H(28B)-C(28)-H(28C)	109.5
O(1)-C(29)-C(30)	105.38(17)
O(1)-C(29)-H(29A)	110.7
C(30)-C(29)-H(29A)	110.7
O(1)-C(29)-H(29B)	110.7
C(30)-C(29)-H(29B)	110.7
H(29A)-C(29)-H(29B)	108.8
C(31)-C(30)-C(29)	103.16(18)
C(31)-C(30)-H(30A)	111.1
C(29)-C(30)-H(30A)	111.1
C(31)-C(30)-H(30B)	111.1
C(29)-C(30)-H(30B)	111.1
H(30A)-C(30)-H(30B)	109.1
C(32)-C(31)-C(30)	103.93(18)
C(32)-C(31)-H(31A)	111.0

C(30)-C(31)-H(31A)	111.0
C(32)-C(31)-H(31B)	111.0
C(30)-C(31)-H(31B)	111.0
H(31A)-C(31)-H(31B)	109.0
O(1)-C(32)-C(31)	106.68(17)
O(1)-C(32)-H(32A)	110.4
C(31)-C(32)-H(32A)	110.4
O(1)-C(32)-H(32B)	110.4
C(31)-C(32)-H(32B)	110.4
H(32A)-C(32)-H(32B)	108.6

Symmetry transformations used to generate equivalent atoms:

Table 11. Anisotropic displacement parameters ($\approx 2 \times 10^3$) for C₃₂H₄₇F₃FeN₂O₂Si. The anisotropic displacement factor exponent takes the form: $-2p^2 [h^2 a^{*2} U^{11} + \dots + 2 h k a^* b^* U^{12}]$

	U ¹¹	U ²²	U ³³	U ²³	U ¹³	U ¹²
Fe(1)	19(1)	24(1)	27(1)	-1(1)	4(1)	1(1)
Si(1)	30(1)	31(1)	40(1)	-2(1)	13(1)	3(1)
F(1)	28(1)	75(1)	64(1)	-24(1)	10(1)	-16(1)
F(2)	34(1)	42(1)	79(1)	-8(1)	31(1)	1(1)
F(3)	46(1)	42(1)	72(1)	10(1)	33(1)	-3(1)
O(1)	36(1)	43(1)	25(1)	1(1)	3(1)	4(1)
N(1)	23(1)	24(1)	25(1)	0(1)	4(1)	-1(1)
N(2)	22(1)	25(1)	27(1)	-1(1)	5(1)	-2(1)
C(1)	25(1)	26(1)	20(1)	-4(1)	0(1)	0(1)
C(2)	23(1)	31(1)	29(1)	-3(1)	6(1)	3(1)
C(3)	21(1)	31(1)	26(1)	-2(1)	6(1)	-2(1)
C(4)	30(1)	25(1)	29(1)	-4(1)	3(1)	4(1)
C(5)	40(1)	24(1)	47(1)	0(1)	6(1)	0(1)
C(6)	50(1)	34(1)	37(1)	-11(1)	9(1)	4(1)
C(7)	34(1)	33(1)	36(1)	1(1)	2(1)	9(1)
C(8)	27(1)	36(1)	47(1)	-8(1)	14(1)	-2(1)

C(9)	26(1)	22(1)	37(1)	4(1)	8(1)	0(1)
C(10)	38(1)	26(1)	38(1)	3(1)	15(1)	2(1)
C(11)	54(1)	44(1)	53(1)	4(1)	29(1)	-5(1)
C(12)	47(1)	57(1)	77(2)	7(1)	33(1)	-12(1)
C(13)	28(1)	43(1)	75(2)	7(1)	9(1)	-10(1)
C(14)	29(1)	29(1)	47(1)	5(1)	3(1)	-3(1)
C(15)	47(1)	37(1)	30(1)	-2(1)	10(1)	1(1)
C(16)	38(1)	46(1)	47(1)	3(1)	-9(1)	-11(1)
C(17)	20(1)	26(1)	33(1)	-3(1)	10(1)	-2(1)
C(18)	24(1)	30(1)	36(1)	1(1)	12(1)	-2(1)
C(19)	31(1)	27(1)	48(1)	4(1)	16(1)	-2(1)
C(20)	33(1)	28(1)	54(1)	-9(1)	16(1)	-6(1)
C(21)	28(1)	36(1)	40(1)	-10(1)	7(1)	-5(1)
C(22)	23(1)	32(1)	34(1)	-4(1)	7(1)	-2(1)
C(23)	41(1)	37(1)	35(1)	7(1)	7(1)	-4(1)
C(24)	40(1)	38(1)	34(1)	-2(1)	1(1)	-3(1)
C(25)	24(1)	40(1)	44(1)	-7(1)	7(1)	4(1)
C(26)	33(1)	36(1)	66(1)	-3(1)	19(1)	2(1)
C(27)	48(1)	48(1)	78(2)	-6(1)	40(1)	-3(1)
C(28)	73(2)	54(1)	44(1)	-2(1)	8(1)	12(1)
C(29)	42(1)	52(1)	32(1)	4(1)	-4(1)	3(1)
C(30)	78(2)	68(2)	32(1)	8(1)	5(1)	7(1)
C(31)	76(2)	96(2)	37(1)	-8(1)	14(1)	16(1)
C(32)	55(1)	72(2)	36(1)	-6(1)	14(1)	18(1)

Appendix B.2.4 Crystallographic Data for 4.55

Figure 83: G: X-ray crystal structure of **4.55** with thermal ellipsoids represented at the 50% probability level.

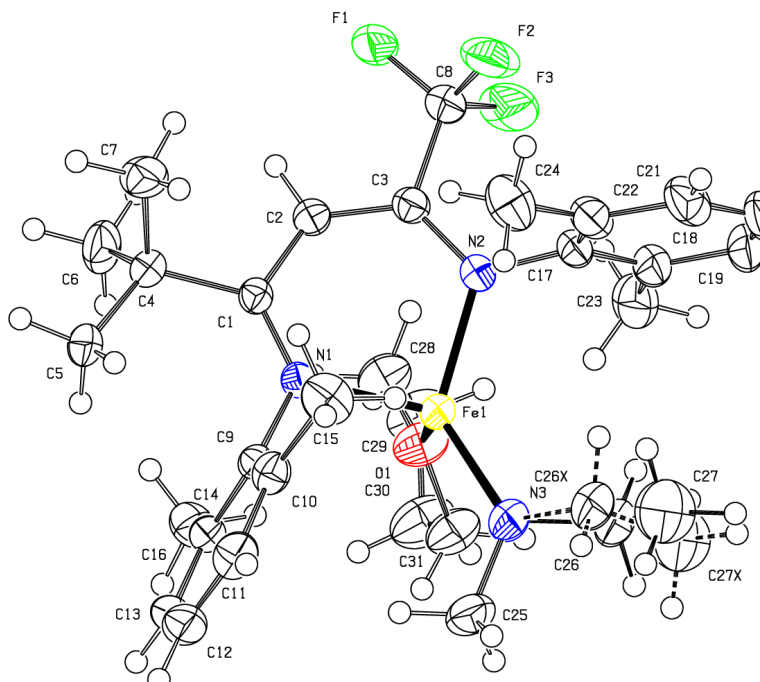


Table 12: Crystal data and structure refinement for **4.55**.

Identification code	C31H44F3FeN3O	
Empirical formula	C31 H44 F3 Fe N3 O	
Formula weight	587.54	
Temperature	100(2) K	
Wavelength	0.71073 \approx	
Crystal system	Monoclinic	
Space group	P2 ₁ /n	
Unit cell dimensions	a = 11.3578(7) \approx	a = 90 ∞ .
	b = 23.4795(13) \approx	b = 90.895(2) ∞ .
	c = 11.5123(6) \approx	g = 90 ∞ .
Volume	3069.7(3) \approx ³	
Z	4	
Density (calculated)	1.271 Mg/m ³	
Absorption coefficient	0.537 mm ⁻¹	

F(000)	1248
Crystal size	0.420 x 0.180 x 0.160 mm ³
Theta range for data collection	1.735 to 28.307°.
Index ranges	-15 ≤ h ≤ 15, -31 ≤ k ≤ 31, -15 ≤ l ≤ 15
Reflections collected	82221
Independent reflections	7619 [R(int) = 0.0617]
Completeness to theta = 25.242°	99.9 %
Absorption correction	Semi-empirical from equivalents
Max. and min. transmission	0.7457 and 0.6745
Refinement method	Full-matrix least-squares on F ²
Data / restraints / parameters	7619 / 2 / 373
Goodness-of-fit on F ²	1.068
Final R indices [I > 2σ(I)]	R1 = 0.0394, wR2 = 0.0974
R indices (all data)	R1 = 0.0627, wR2 = 0.1145
Extinction coefficient	n/a
Largest diff. peak and hole	0.358 and -0.335 e. ⁻³

Table 13. Bond lengths [Å] and angles [°] for **4.55**.

Fe(1)-N(3)	1.8832(17)
Fe(1)-N(2)	1.9982(15)
Fe(1)-N(1)	2.0221(14)
Fe(1)-O(1)	2.1990(15)
F(1)-C(8)	1.334(2)
F(2)-C(8)	1.334(2)
F(3)-C(8)	1.331(2)
O(1)-C(31)	1.430(3)
O(1)-C(28)	1.441(3)
N(1)-C(1)	1.319(2)
N(1)-C(9)	1.436(2)
N(2)-C(3)	1.340(2)
N(2)-C(17)	1.437(2)
N(3)-C(25)	1.434(3)
N(3)-C(26)	1.471(3)
C(1)-C(2)	1.432(2)

C(1)-C(4)	1.554(2)
C(2)-C(3)	1.381(3)
C(2)-H(2)	0.9500
C(3)-C(8)	1.525(3)
C(4)-C(5)	1.536(3)
C(4)-C(6)	1.539(3)
C(4)-C(7)	1.540(3)
C(5)-H(5A)	0.9800
C(5)-H(5B)	0.9800
C(5)-H(5C)	0.9800
C(6)-H(6A)	0.9800
C(6)-H(6B)	0.9800
C(6)-H(6C)	0.9800
C(7)-H(7A)	0.9800
C(7)-H(7B)	0.9800
C(7)-H(7C)	0.9800
C(9)-C(14)	1.400(2)
C(9)-C(10)	1.404(2)
C(10)-C(11)	1.392(3)
C(10)-C(15)	1.504(3)
C(11)-C(12)	1.375(3)
C(11)-H(11)	0.9500
C(12)-C(13)	1.380(3)
C(12)-H(12)	0.9500
C(13)-C(14)	1.391(3)
C(13)-H(13)	0.9500
C(14)-C(16)	1.505(3)
C(15)-H(15A)	0.9800
C(15)-H(15B)	0.9800
C(15)-H(15C)	0.9800
C(16)-H(16A)	0.9800
C(16)-H(16B)	0.9800
C(16)-H(16C)	0.9800
C(17)-C(22)	1.400(3)
C(17)-C(18)	1.410(3)

C(18)-C(19)	1.394(3)
C(18)-C(23)	1.499(3)
C(19)-C(20)	1.370(4)
C(19)-H(19)	0.9500
C(20)-C(21)	1.376(4)
C(20)-H(20)	0.9500
C(21)-C(22)	1.401(3)
C(21)-H(21)	0.9500
C(22)-C(24)	1.503(3)
C(23)-H(23A)	0.9800
C(23)-H(23B)	0.9800
C(23)-H(23C)	0.9800
C(24)-H(24A)	0.9800
C(24)-H(24B)	0.9800
C(24)-H(24C)	0.9800
C(25)-H(25A)	0.9800
C(25)-H(25B)	0.9800
C(25)-H(25C)	0.9800
C(26)-C(27)	1.506(6)
C(26)-H(26A)	0.9900
C(26)-H(26B)	0.9900
C(27)-H(27A)	0.9800
C(27)-H(27B)	0.9800
C(27)-H(27C)	0.9800
C(28)-C(29)	1.504(3)
C(28)-H(28A)	0.9900
C(28)-H(28B)	0.9900
C(29)-C(30)	1.498(4)
C(29)-H(29A)	0.9900
C(29)-H(29B)	0.9900
C(30)-C(31)	1.520(3)
C(30)-H(30A)	0.9900
C(30)-H(30B)	0.9900
C(31)-H(31A)	0.9900
C(31)-H(31B)	0.9900

N(3)-Fe(1)-N(2)	129.32(7)
N(3)-Fe(1)-N(1)	127.55(7)
N(2)-Fe(1)-N(1)	93.91(6)
N(3)-Fe(1)-O(1)	101.15(8)
N(2)-Fe(1)-O(1)	99.94(6)
N(1)-Fe(1)-O(1)	98.03(6)
C(31)-O(1)-C(28)	110.32(16)
C(31)-O(1)-Fe(1)	124.29(13)
C(28)-O(1)-Fe(1)	125.13(13)
C(1)-N(1)-C(9)	126.34(15)
C(1)-N(1)-Fe(1)	125.18(12)
C(9)-N(1)-Fe(1)	108.35(10)
C(3)-N(2)-C(17)	122.22(15)
C(3)-N(2)-Fe(1)	119.23(12)
C(17)-N(2)-Fe(1)	117.90(12)
C(25)-N(3)-C(26)	111.35(19)
C(25)-N(3)-Fe(1)	126.07(15)
C(26)-N(3)-Fe(1)	120.67(17)
N(1)-C(1)-C(2)	119.63(15)
N(1)-C(1)-C(4)	127.44(16)
C(2)-C(1)-C(4)	112.93(15)
C(3)-C(2)-C(1)	129.19(16)
C(3)-C(2)-H(2)	115.4
C(1)-C(2)-H(2)	115.4
N(2)-C(3)-C(2)	126.72(17)
N(2)-C(3)-C(8)	118.16(16)
C(2)-C(3)-C(8)	115.11(16)
C(5)-C(4)-C(6)	107.41(17)
C(5)-C(4)-C(7)	106.49(16)
C(6)-C(4)-C(7)	109.62(18)
C(5)-C(4)-C(1)	116.50(15)
C(6)-C(4)-C(1)	107.89(15)
C(7)-C(4)-C(1)	108.82(16)
C(4)-C(5)-H(5A)	109.5

C(4)-C(5)-H(5B)	109.5
H(5A)-C(5)-H(5B)	109.5
C(4)-C(5)-H(5C)	109.5
H(5A)-C(5)-H(5C)	109.5
H(5B)-C(5)-H(5C)	109.5
C(4)-C(6)-H(6A)	109.5
C(4)-C(6)-H(6B)	109.5
H(6A)-C(6)-H(6B)	109.5
C(4)-C(6)-H(6C)	109.5
H(6A)-C(6)-H(6C)	109.5
H(6B)-C(6)-H(6C)	109.5
C(4)-C(7)-H(7A)	109.5
C(4)-C(7)-H(7B)	109.5
H(7A)-C(7)-H(7B)	109.5
C(4)-C(7)-H(7C)	109.5
H(7A)-C(7)-H(7C)	109.5
H(7B)-C(7)-H(7C)	109.5
F(3)-C(8)-F(1)	106.05(18)
F(3)-C(8)-F(2)	105.88(18)
F(1)-C(8)-F(2)	105.09(17)
F(3)-C(8)-C(3)	111.78(17)
F(1)-C(8)-C(3)	114.06(16)
F(2)-C(8)-C(3)	113.30(17)
C(14)-C(9)-C(10)	120.51(17)
C(14)-C(9)-N(1)	120.74(15)
C(10)-C(9)-N(1)	118.37(16)
C(11)-C(10)-C(9)	118.55(18)
C(11)-C(10)-C(15)	120.07(18)
C(9)-C(10)-C(15)	121.37(17)
C(12)-C(11)-C(10)	121.40(19)
C(12)-C(11)-H(11)	119.3
C(10)-C(11)-H(11)	119.3
C(11)-C(12)-C(13)	119.47(19)
C(11)-C(12)-H(12)	120.3
C(13)-C(12)-H(12)	120.3

C(12)-C(13)-C(14)	121.36(19)
C(12)-C(13)-H(13)	119.3
C(14)-C(13)-H(13)	119.3
C(13)-C(14)-C(9)	118.56(17)
C(13)-C(14)-C(16)	119.94(17)
C(9)-C(14)-C(16)	121.47(17)
C(10)-C(15)-H(15A)	109.5
C(10)-C(15)-H(15B)	109.5
H(15A)-C(15)-H(15B)	109.5
C(10)-C(15)-H(15C)	109.5
H(15A)-C(15)-H(15C)	109.5
H(15B)-C(15)-H(15C)	109.5
C(14)-C(16)-H(16A)	109.5
C(14)-C(16)-H(16B)	109.5
H(16A)-C(16)-H(16B)	109.5
C(14)-C(16)-H(16C)	109.5
H(16A)-C(16)-H(16C)	109.5
H(16B)-C(16)-H(16C)	109.5
C(22)-C(17)-C(18)	121.18(19)
C(22)-C(17)-N(2)	119.07(18)
C(18)-C(17)-N(2)	119.45(18)
C(19)-C(18)-C(17)	117.8(2)
C(19)-C(18)-C(23)	120.5(2)
C(17)-C(18)-C(23)	121.73(19)
C(20)-C(19)-C(18)	121.7(2)
C(20)-C(19)-H(19)	119.2
C(18)-C(19)-H(19)	119.2
C(19)-C(20)-C(21)	120.1(2)
C(19)-C(20)-H(20)	119.9
C(21)-C(20)-H(20)	119.9
C(20)-C(21)-C(22)	121.0(2)
C(20)-C(21)-H(21)	119.5
C(22)-C(21)-H(21)	119.5
C(17)-C(22)-C(21)	118.2(2)
C(17)-C(22)-C(24)	122.04(19)

C(21)-C(22)-C(24)	119.7(2)
C(18)-C(23)-H(23A)	109.5
C(18)-C(23)-H(23B)	109.5
H(23A)-C(23)-H(23B)	109.5
C(18)-C(23)-H(23C)	109.5
H(23A)-C(23)-H(23C)	109.5
H(23B)-C(23)-H(23C)	109.5
C(22)-C(24)-H(24A)	109.5
C(22)-C(24)-H(24B)	109.5
H(24A)-C(24)-H(24B)	109.5
C(22)-C(24)-H(24C)	109.5
H(24A)-C(24)-H(24C)	109.5
H(24B)-C(24)-H(24C)	109.5
N(3)-C(25)-H(25A)	109.5
N(3)-C(25)-H(25B)	109.5
H(25A)-C(25)-H(25B)	109.5
N(3)-C(25)-H(25C)	109.5
H(25A)-C(25)-H(25C)	109.5
H(25B)-C(25)-H(25C)	109.5
N(3)-C(26)-C(27)	111.8(3)
N(3)-C(26)-H(26A)	109.3
C(27)-C(26)-H(26A)	109.3
N(3)-C(26)-H(26B)	109.3
C(27)-C(26)-H(26B)	109.3
H(26A)-C(26)-H(26B)	107.9
C(26)-C(27)-H(27A)	109.5
C(26)-C(27)-H(27B)	109.5
H(27A)-C(27)-H(27B)	109.5
C(26)-C(27)-H(27C)	109.5
H(27A)-C(27)-H(27C)	109.5
H(27B)-C(27)-H(27C)	109.5
O(1)-C(28)-C(29)	106.13(18)
O(1)-C(28)-H(28A)	110.5
C(29)-C(28)-H(28A)	110.5
O(1)-C(28)-H(28B)	110.5

C(29)-C(28)-H(28B)	110.5
H(28A)-C(28)-H(28B)	108.7
C(30)-C(29)-C(28)	102.0(2)
C(30)-C(29)-H(29A)	111.4
C(28)-C(29)-H(29A)	111.4
C(30)-C(29)-H(29B)	111.4
C(28)-C(29)-H(29B)	111.4
H(29A)-C(29)-H(29B)	109.2
C(29)-C(30)-C(31)	104.4(2)
C(29)-C(30)-H(30A)	110.9
C(31)-C(30)-H(30A)	110.9
C(29)-C(30)-H(30B)	110.9
C(31)-C(30)-H(30B)	110.9
H(30A)-C(30)-H(30B)	108.9
O(1)-C(31)-C(30)	104.93(19)
O(1)-C(31)-H(31A)	110.8
C(30)-C(31)-H(31A)	110.8
O(1)-C(31)-H(31B)	110.8
C(30)-C(31)-H(31B)	110.8
H(31A)-C(31)-H(31B)	108.8

Symmetry transformations used to generate equivalent atoms:

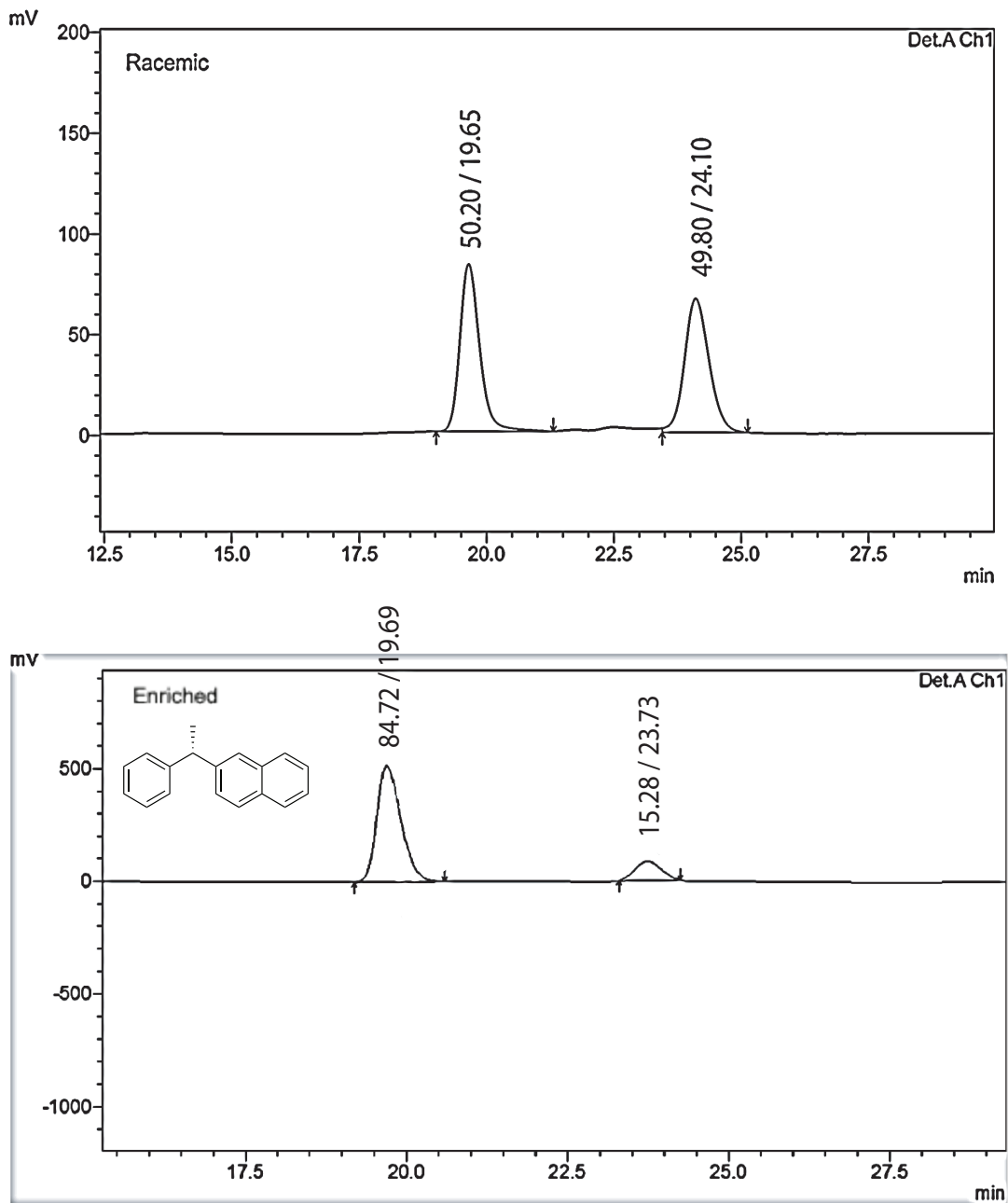
Table 14. Anisotropic displacement parameters ($\approx 2 \times 10^3$) for **4.55**. The anisotropic displacement factor exponent takes the form: $-2p^2 [h^2 a^* U_{11} + \dots + 2 h k a^* b^* U_{12}]$

	U11	U22	U33	U23	U13	U12
Fe(1)	23(1)	26(1)	36(1)	-1(1)	0(1)	0(1)
F(1)	34(1)	34(1)	100(1)	0(1)	17(1)	8(1)
F(2)	57(1)	44(1)	83(1)	27(1)	13(1)	18(1)
F(3)	67(1)	48(1)	87(1)	-34(1)	-14(1)	19(1)
O(1)	40(1)	60(1)	35(1)	1(1)	0(1)	9(1)
N(1)	25(1)	23(1)	26(1)	-1(1)	1(1)	-1(1)

N(2)	28(1)	24(1)	36(1)	1(1)	1(1)	-1(1)
N(3)	26(1)	39(1)	72(1)	-1(1)	7(1)	-1(1)
C(1)	25(1)	26(1)	23(1)	3(1)	0(1)	-2(1)
C(2)	26(1)	28(1)	32(1)	0(1)	3(1)	1(1)
C(3)	29(1)	26(1)	31(1)	1(1)	2(1)	2(1)
C(4)	24(1)	31(1)	37(1)	-1(1)	-2(1)	-1(1)
C(5)	31(1)	31(1)	53(1)	-6(1)	-8(1)	-6(1)
C(6)	36(1)	46(1)	57(1)	-2(1)	13(1)	-13(1)
C(7)	46(1)	41(1)	54(1)	-6(1)	-21(1)	6(1)
C(8)	33(1)	29(1)	51(1)	0(1)	2(1)	3(1)
C(9)	21(1)	26(1)	30(1)	-4(1)	-1(1)	0(1)
C(10)	30(1)	35(1)	29(1)	-4(1)	1(1)	-3(1)
C(11)	36(1)	46(1)	38(1)	-15(1)	6(1)	0(1)
C(12)	36(1)	35(1)	58(1)	-15(1)	0(1)	6(1)
C(13)	36(1)	27(1)	51(1)	0(1)	-7(1)	4(1)
C(14)	27(1)	28(1)	33(1)	1(1)	-4(1)	-1(1)
C(15)	58(1)	49(1)	32(1)	6(1)	8(1)	1(1)
C(16)	51(1)	36(1)	34(1)	7(1)	-2(1)	0(1)
C(17)	30(1)	23(1)	48(1)	-1(1)	5(1)	0(1)
C(18)	34(1)	30(1)	61(1)	-6(1)	3(1)	-1(1)
C(19)	38(1)	31(1)	85(2)	-10(1)	5(1)	-7(1)
C(20)	42(1)	30(1)	95(2)	2(1)	25(1)	-7(1)
C(21)	52(1)	35(1)	66(2)	10(1)	23(1)	0(1)
C(22)	40(1)	29(1)	53(1)	4(1)	10(1)	2(1)
C(23)	60(2)	44(1)	58(2)	-12(1)	-10(1)	-7(1)
C(24)	71(2)	44(1)	42(1)	8(1)	6(1)	-5(1)
C(25)	31(1)	50(1)	64(2)	-12(1)	-3(1)	8(1)
C(26)	31(2)	46(2)	70(2)	-7(2)	1(1)	-6(1)
C(27)	64(3)	84(3)	128(5)	41(4)	37(3)	-7(2)
C(26X)	32(5)	48(6)	79(8)	1(5)	7(4)	-5(4)
C(27X)	64(3)	84(3)	128(5)	41(4)	37(3)	-7(2)
C(28)	41(1)	61(2)	40(1)	-2(1)	4(1)	4(1)
C(29)	49(1)	86(2)	43(1)	-5(1)	0(1)	12(1)
C(30)	51(2)	93(2)	48(1)	10(1)	-3(1)	9(1)
C(31)	38(1)	68(2)	42(1)	4(1)	-9(1)	4(1)

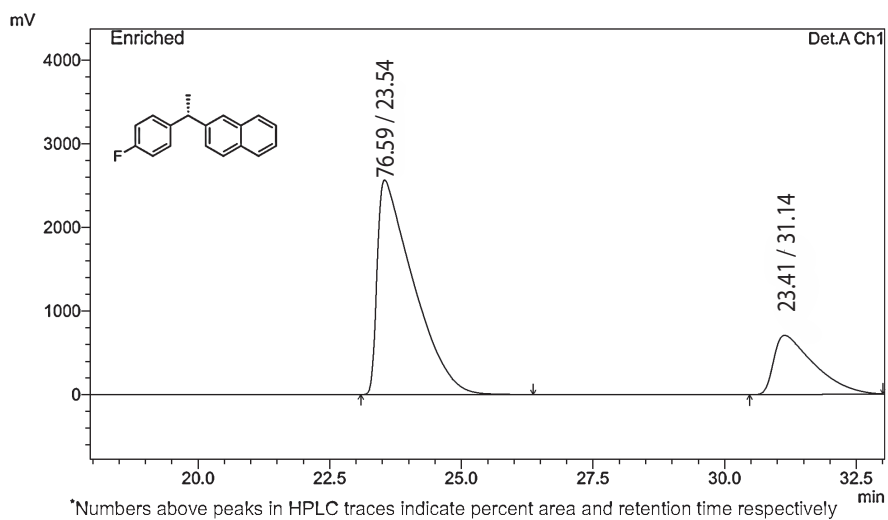
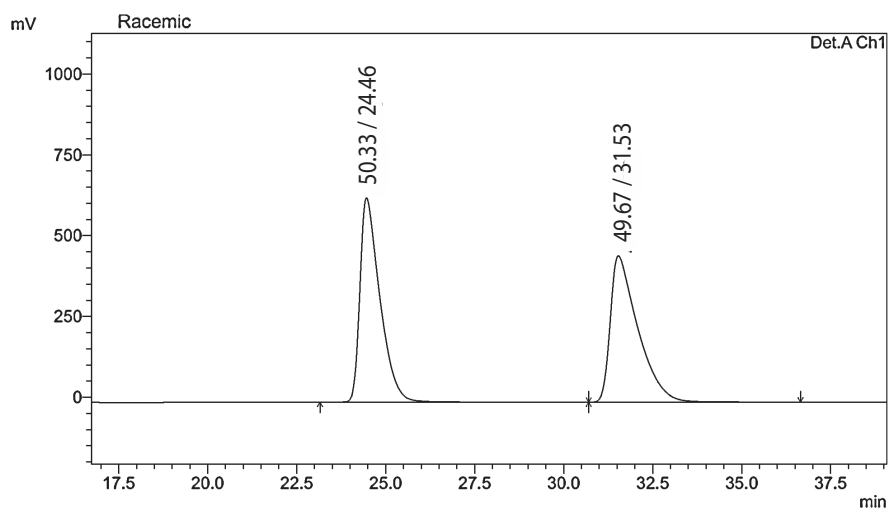
Appendix C. HPLC data for Chapter 3

Figure 77 – HPLC trace for 3.6.



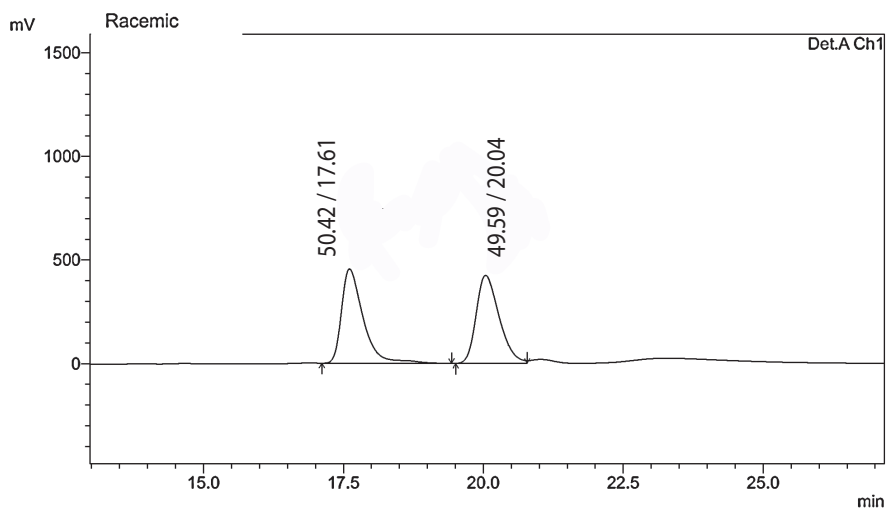
*Numbers above peaks in HPLC trace indicate retention time and percent area respectively

Figure 78 – HPLC trace for **3.17**.

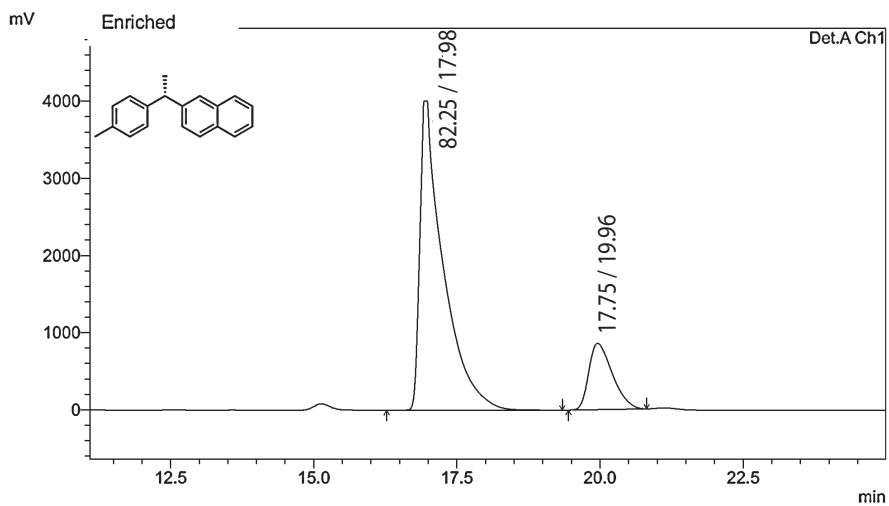


*Numbers above peaks in HPLC traces indicate percent area and retention time respectively

Figure 78 – HPLC trace for 3.18.

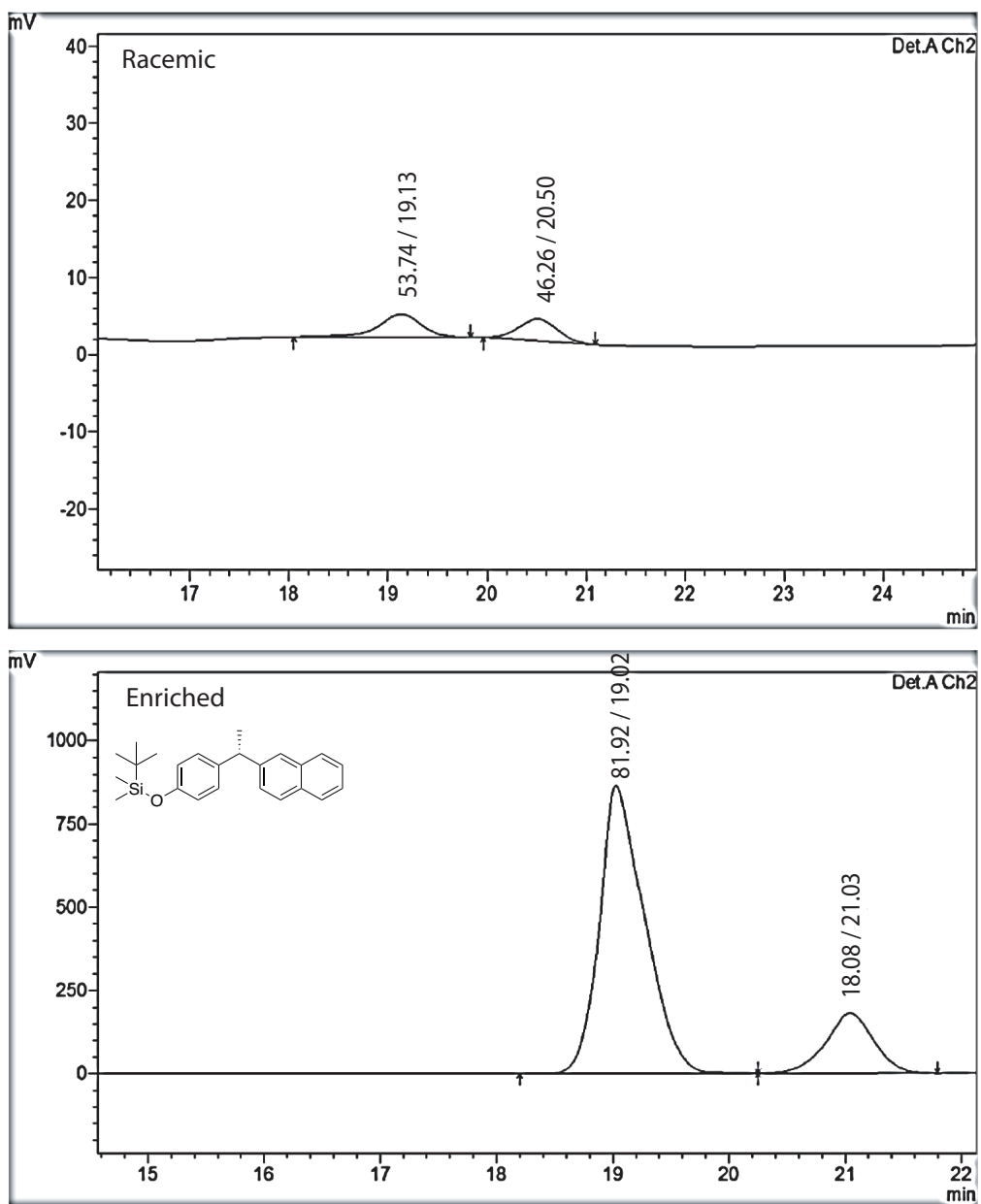


Numbers above peaks in HPLC traces indicate percent area and retention time respectively



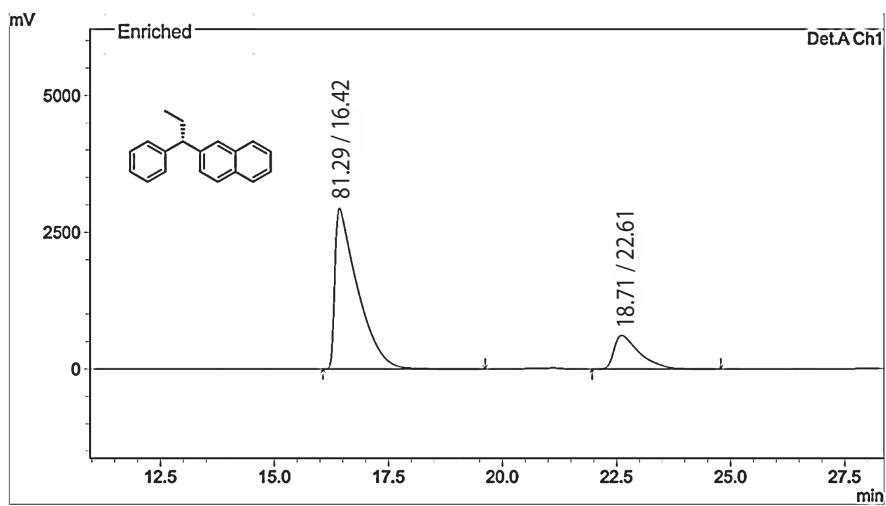
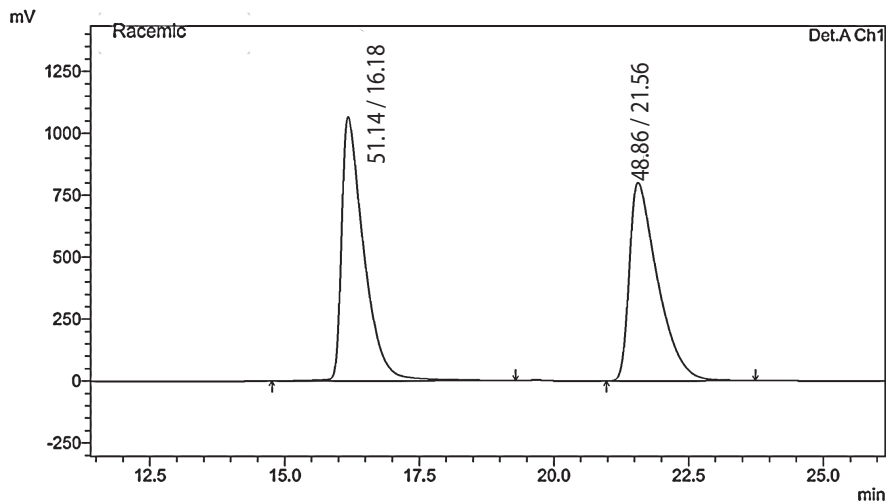
Numbers above peaks in HPLC traces indicate percent area and retention time respectively

Figure 79 – HPLC trace for **3.19**.



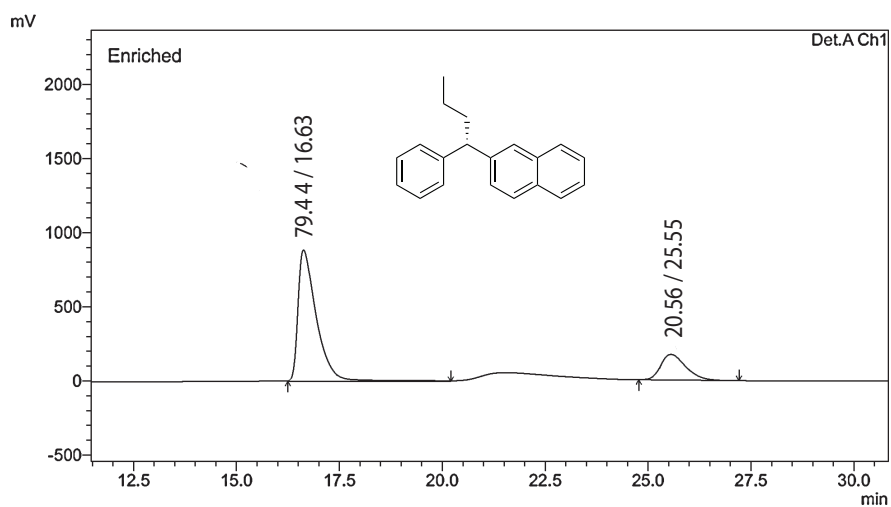
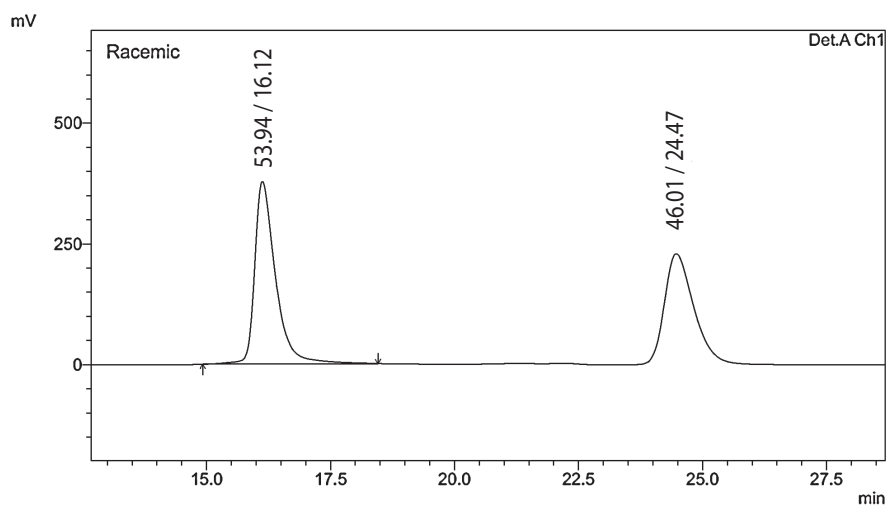
*Numbers above peaks in HPLC trace indicate retention time and percent area respectively

Figure 77 – HPLC trace for 3.20.



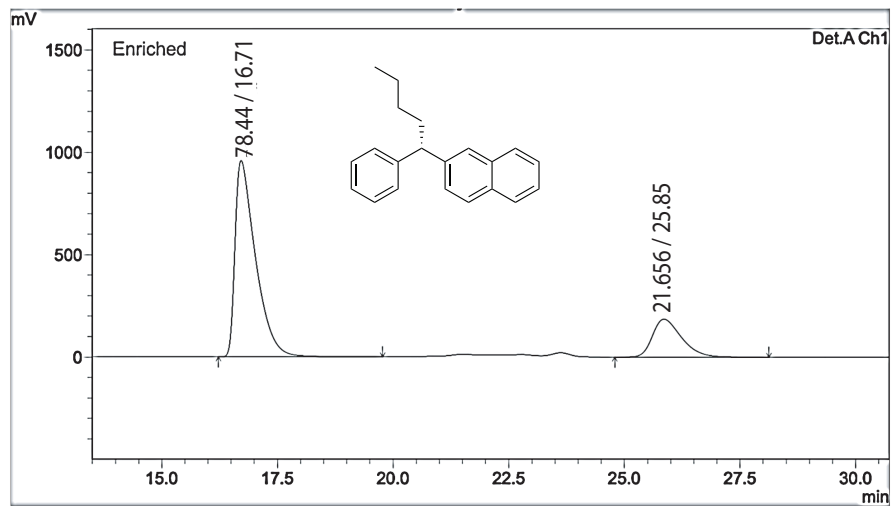
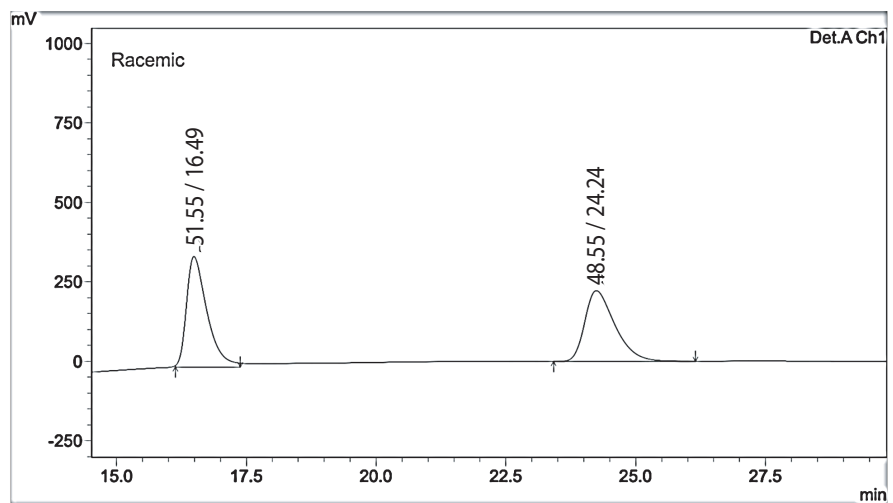
*Numbers above peaks in HPLC traces indicate percent area and retention time respectively

Figure 80 – HPLC trace for **3.21**.



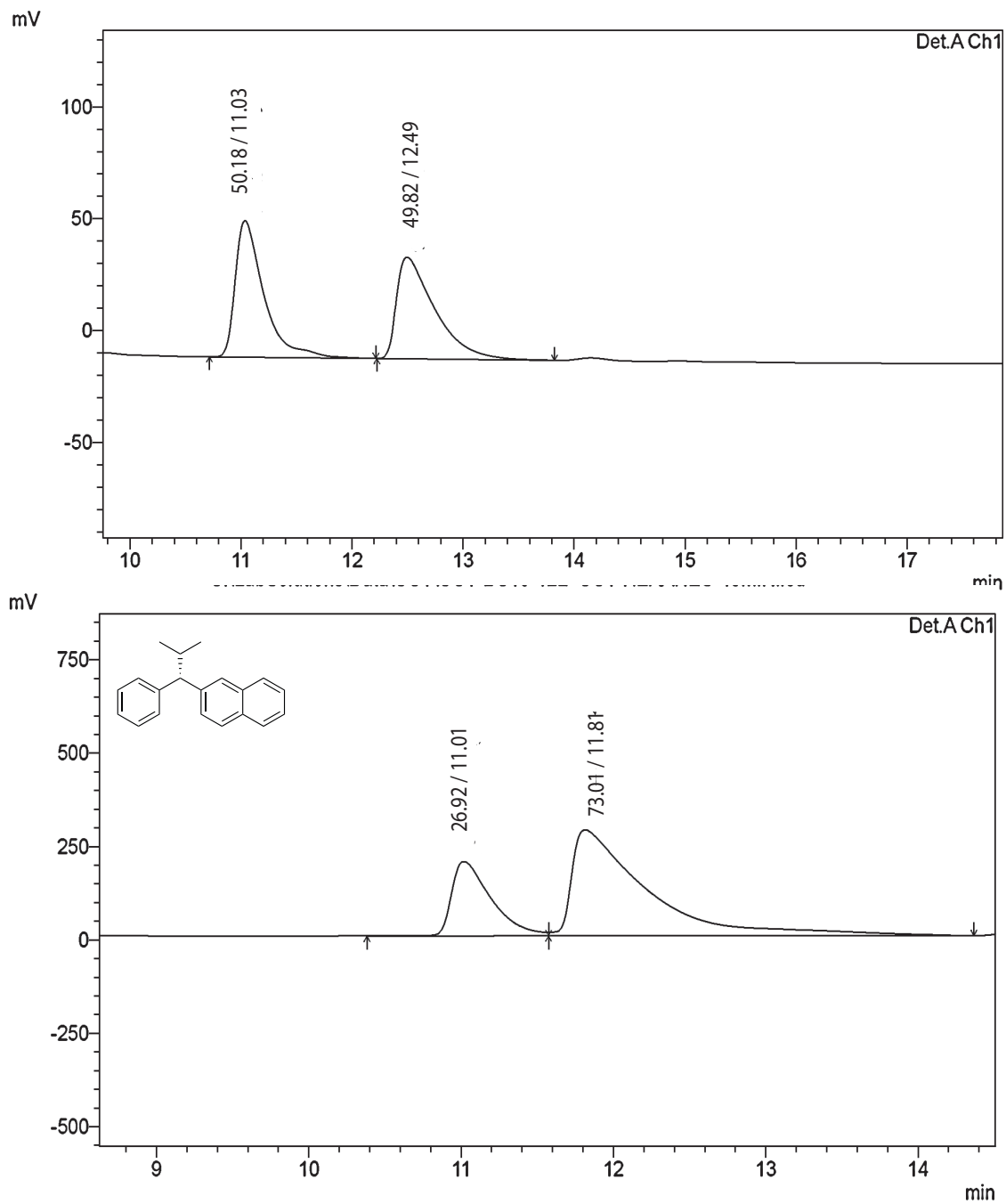
*Numbers above peaks in HPLC traces indicate percent area and retention time respectively

Figure 81 – HPLC trace for 3.22.



Numbers above peaks in HPLC traces indicate percent area and retention time respectively

Figure 82– HPLC trace for 3.23.



*Numbers above peaks in HPLC traces indicate percent area and retention time respectively

Figure 83– HPLC trace for **3.24**.

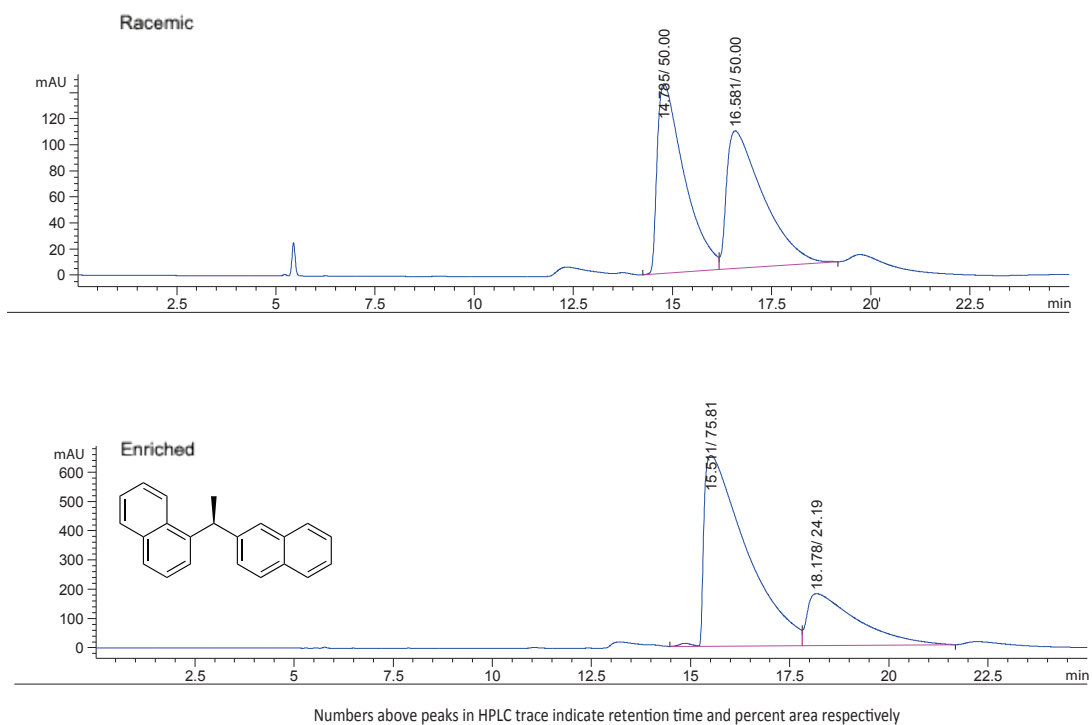
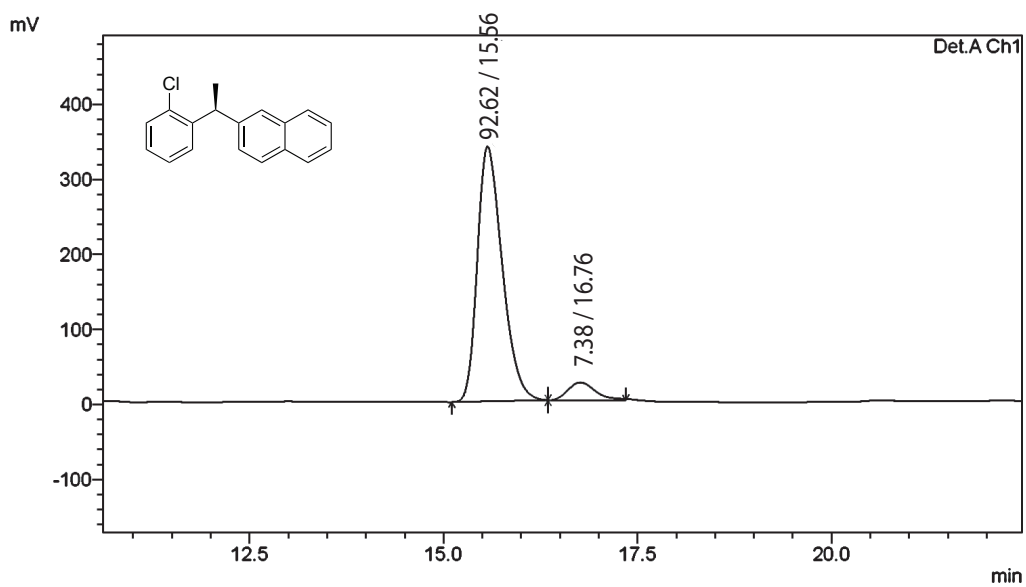
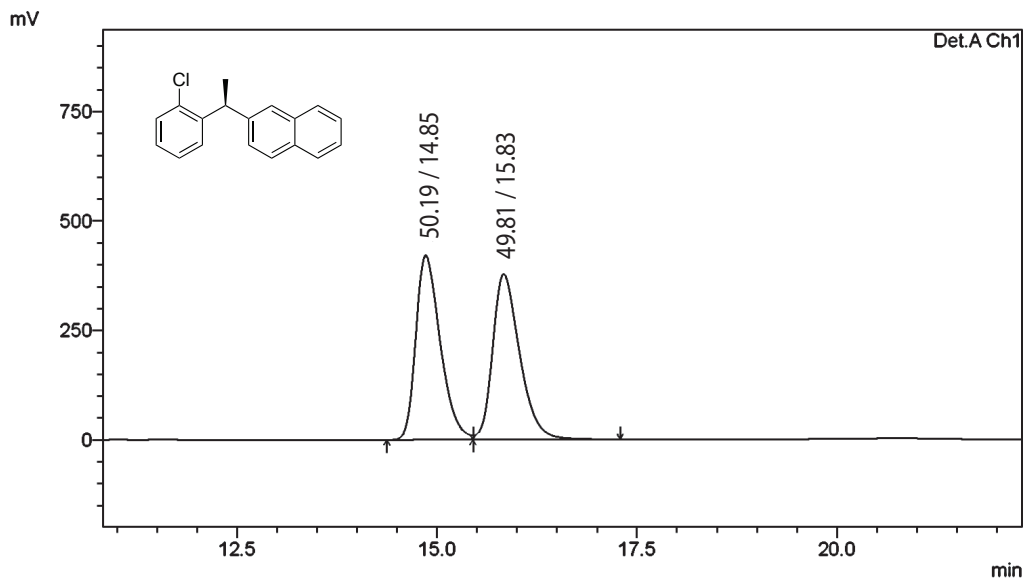
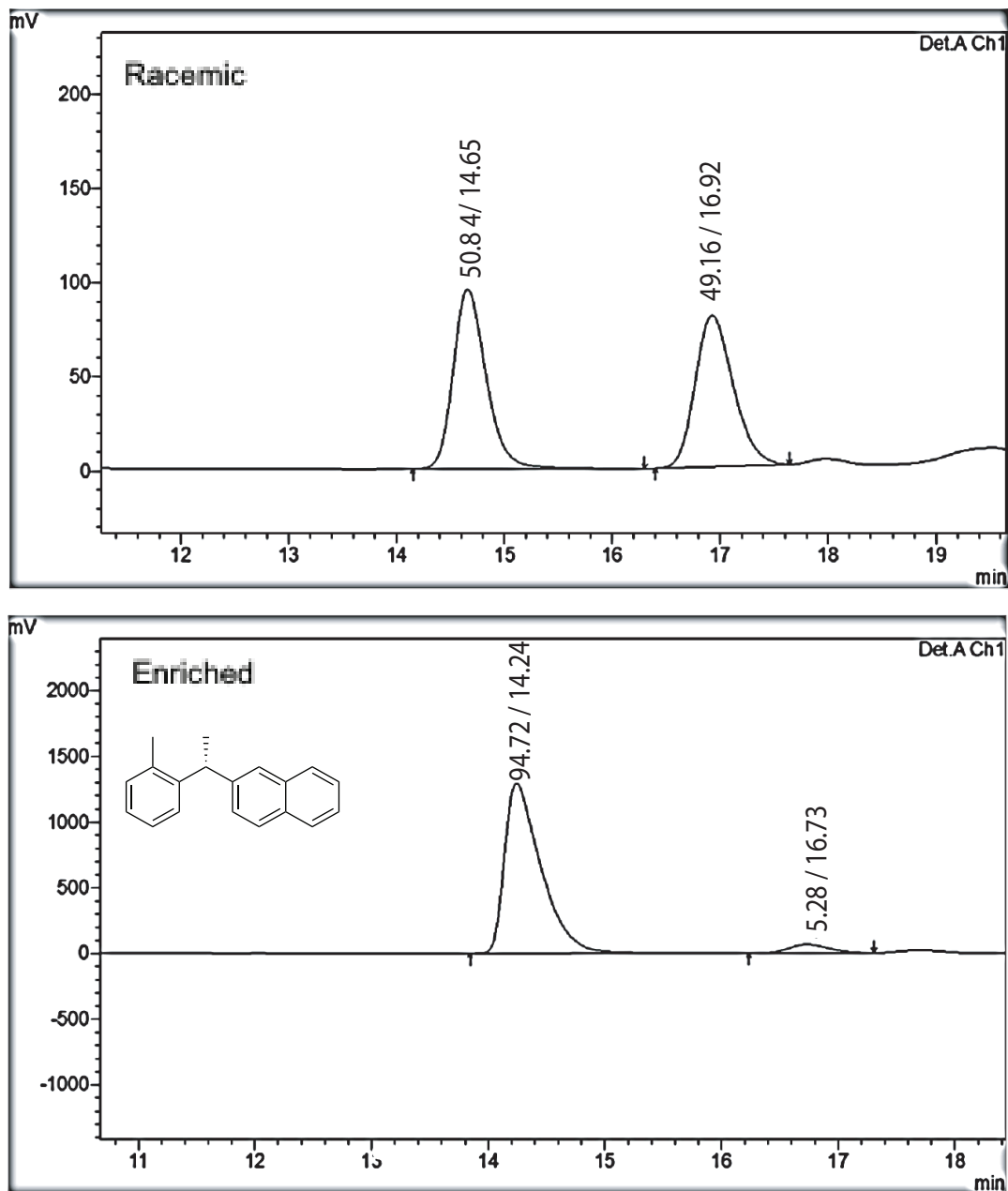


Figure 84 – HPLC trace for **3.25**.



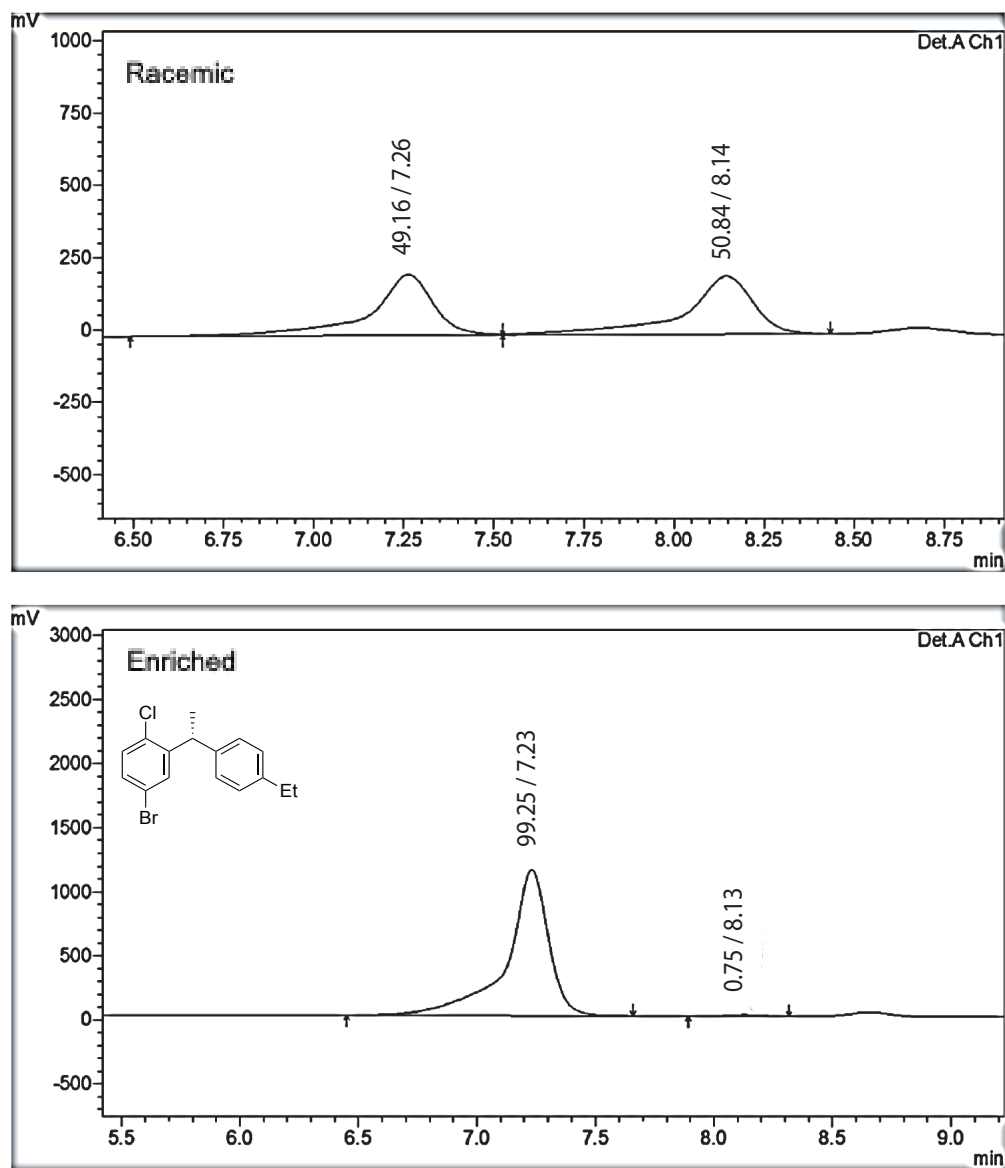
*Numbers above peaks in HPLC trace indicate percent area and retention time respectively

Figure 85 – HPLC trace for 3.26.



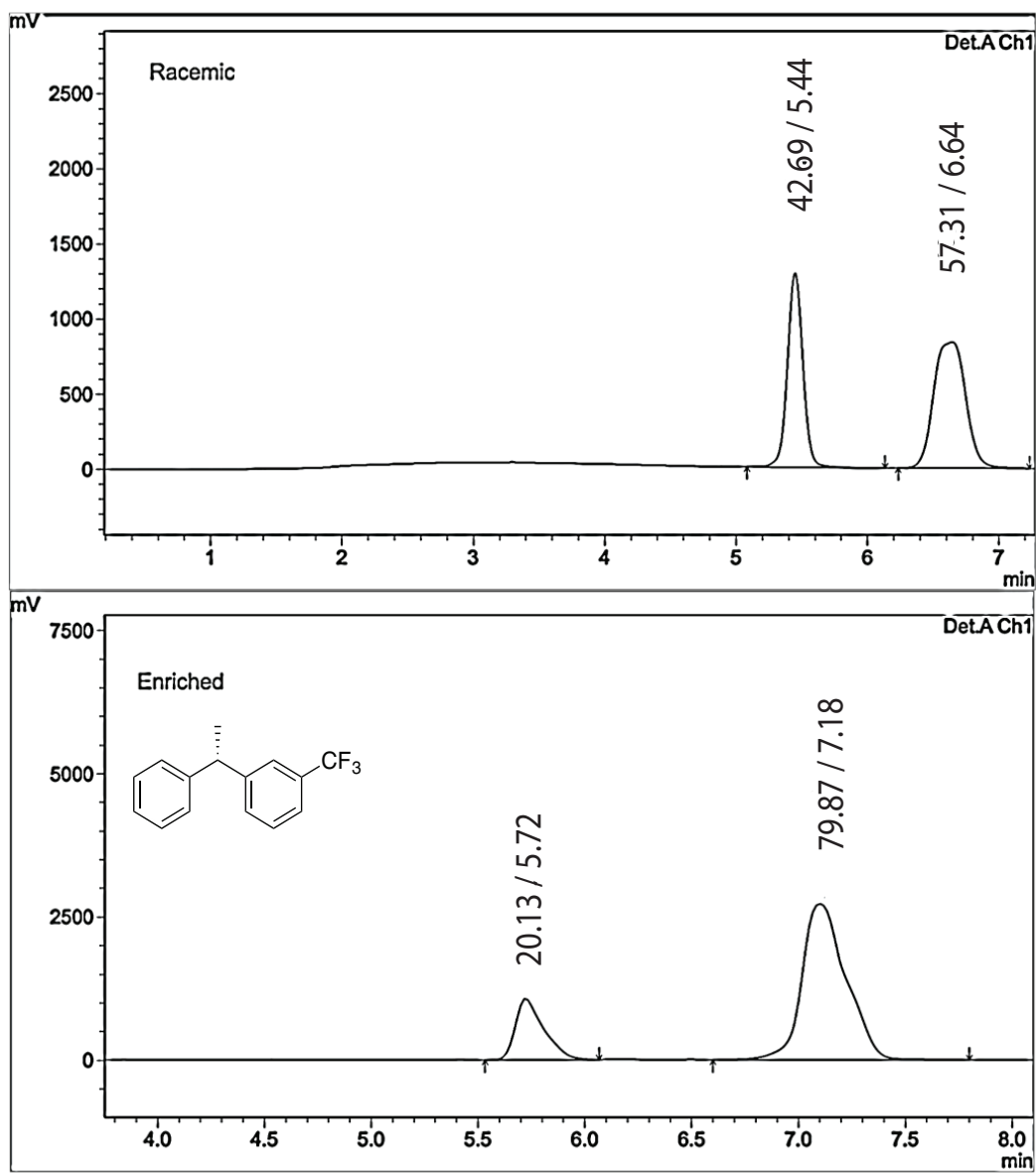
*Numbers above peaks in HPLC trace indicate retention time and percent area respectively

Figure 86 – HPLC trace for 3.27.



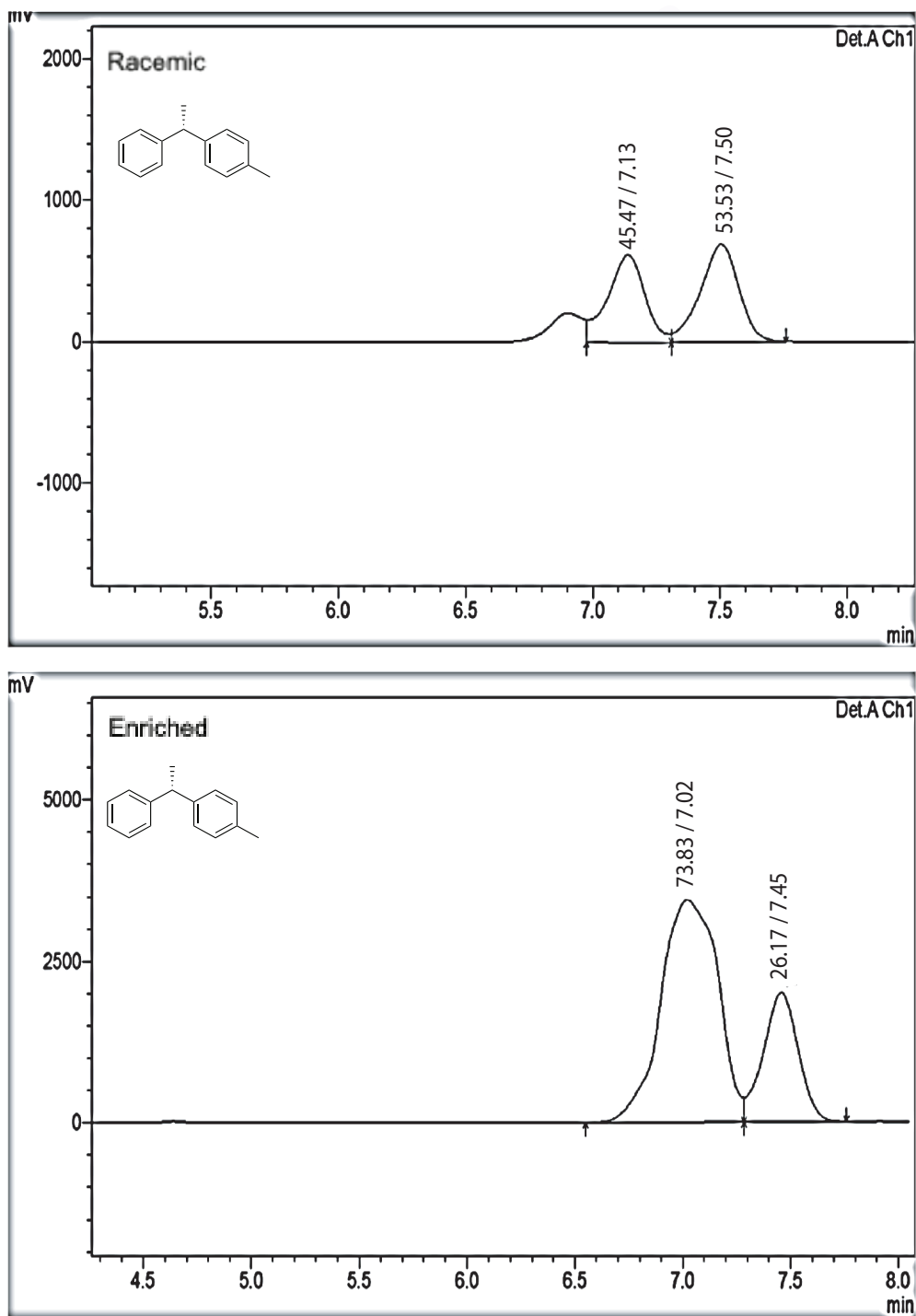
*Numbers above peaks indicate percent area and retention time respectively

Figure 87 – HPLC trace for 3.28.



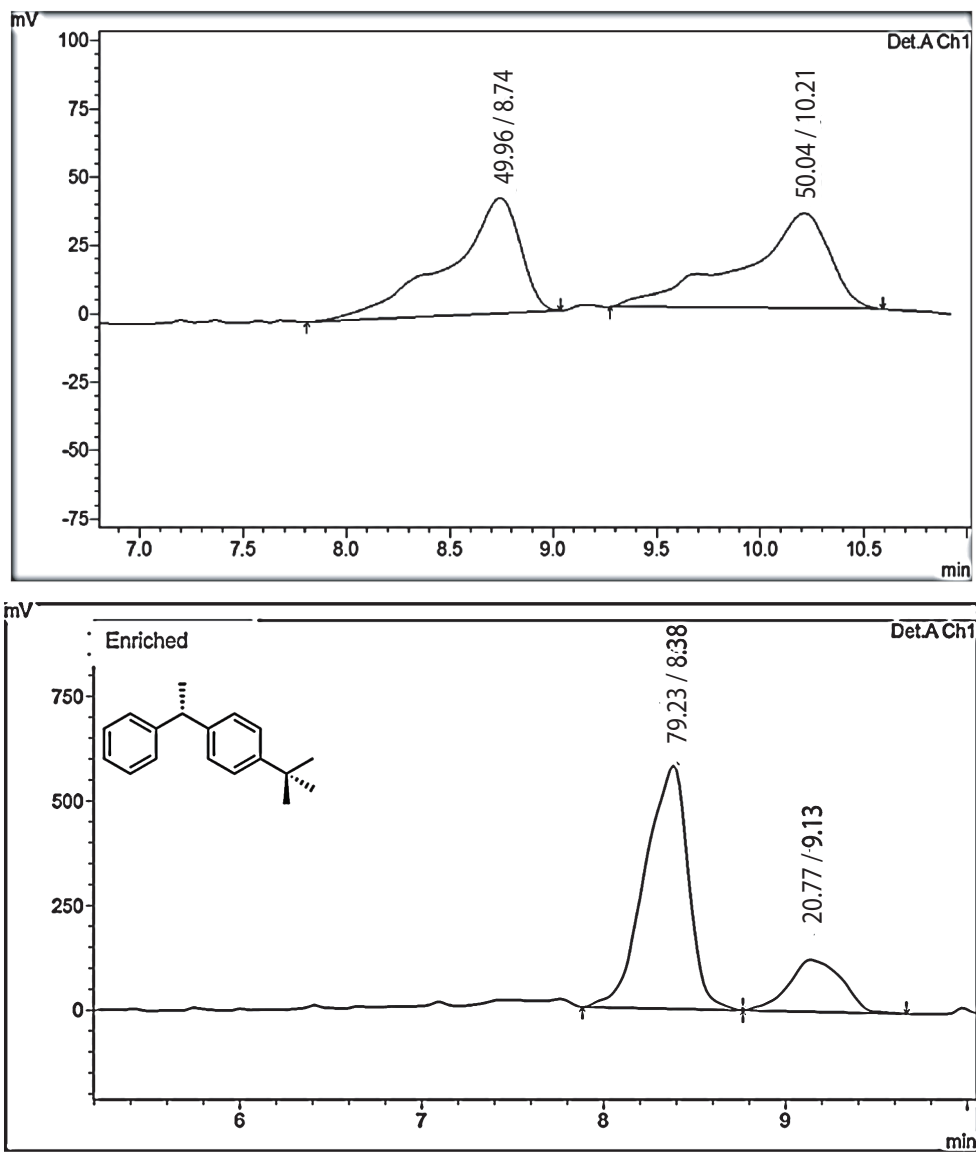
*Numbers above peaks in HPLC traces indicate percent area and retention time respectively

Figure 88 – HPLC trace for 3.29.



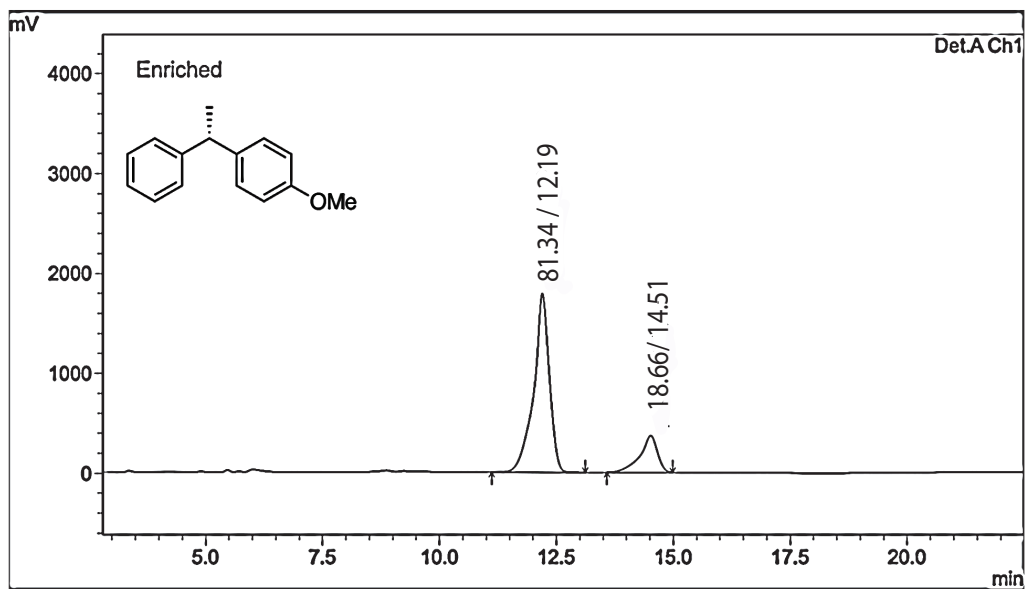
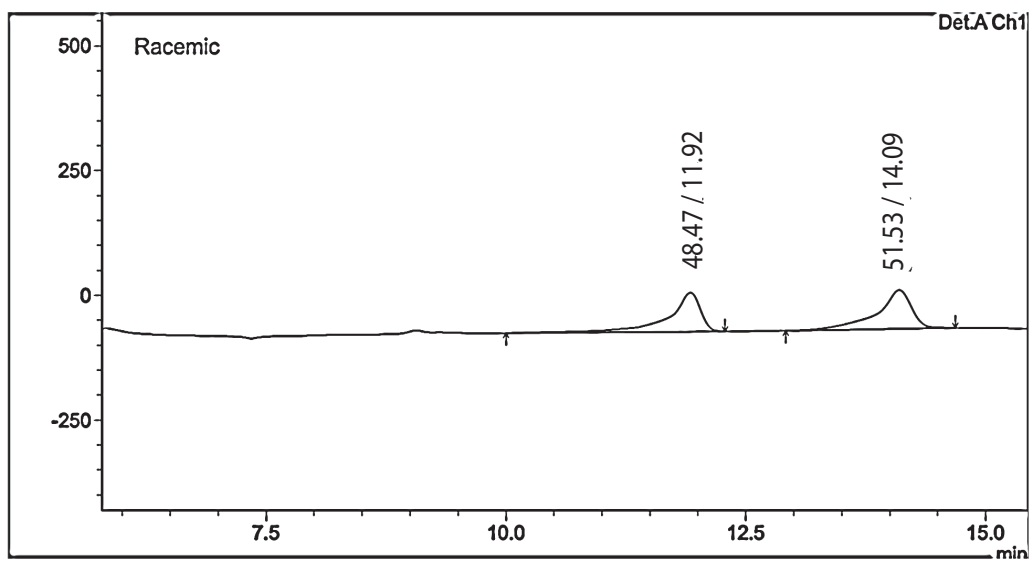
*Numbers above peaks in HPLC trace indicate retention time and percent area respectively

Figure 89 – HPLC trace for 3.30.



Numbers above peaks in HPLC traces indicate percent area and retention time respectively

Figure 90 – HPLC trace for 3.2.



*Numbers above peaks in HPLC traces indicate percent area and retention time respectively